

GEOLOGICAL EVOLUTION OF THE GEDİZ GRABEN, SW TURKEY:
TEMPORAL AND SPATIAL VARIATION OF THE GRABEN

A THESIS SUBMITTED TO
THE GRADUATE SCHOOL OF NATURAL AND APPLIED SCIENCES
OF
MIDDLE EAST TECHNICAL UNIVERSITY

BY
BOZKURT N. ÇİFTÇİ

IN PARTIAL FULFILLMENT OF THE REQUIREMENTS
FOR
THE DEGREE OF DOCTOR OF PHILOSOPHY
IN
GEOLOGICAL ENGINEERING

MARCH 2007

Approval of the Graduate School of Natural and Applied Sciences

Prof. Dr. Canan Özgen
Director

I certify that this thesis satisfies all the requirements as a thesis for the degree of Doctor of Philosophy.

Prof. Dr. Vedat Doyuran
Head of Department

This is to certify that we have read this thesis and that in our opinion its fully adequate, in scope and quality, as a thesis for the degree of Doctor of Philosophy.

Prof. Dr. Erdin Bozkurt
Supervisor

Examining Committee Members

Prof. Dr. Ali Koçyiğit (METU, GEOE) _____

Prof. Dr. Erdin Bozkurt (METU, GEOE) _____

Prof. Dr. Orhan Tatar (Cumhuriyet Unv., GEOE) _____

Assoc. Prof. Dr. Kadir Dirik (Hacettepe Unv., GEOE) _____

Assoc. Prof. Dr. Hasan Sözbilir (Dokuz Eylül Unv., GEOE) _____

I hereby declare that all the information in this document has been obtained and presented in accordance with academic rules and ethical conduct. I also declare that, as required by these rules and conduct, I have fully cited and referenced all material and results that are not original to this work.

Name, Last name:

Signature:

ABSTRACT

GEOLOGICAL EVOLUTION OF THE GEDİZ GRABEN, SW TURKEY: TEMPORAL AND SPATIAL VARIATION OF THE GRABEN

Çiftçi, Bozkurt N.

Ph.D., Department of Geological Engineering

Supervisor: Prof. Dr. Erdin Bozkurt

March 2007, 290 pages

Gediz Graben is a continental extensional basin filled with Neogene sediments. Its margins are controlled by active ~E–W-trending fault systems with major system, in terms of total offset and duration of activity, located along the southern margin. The graben evolved as a half graben by the activity of the southern margin during the entire Miocene. Then, the northern margin-bounding structure initiated by Plio–Quaternary to form the current configuration of the graben with an inherited asymmetry.

The southern margin-bounding fault system forms a graben-facing step-like pattern from the horst block (~2000 m) down to the graben floor (~200 m). The faults become younger towards the graben and the structural maturity decreases in the same direction. Fault plane data suggest ~N–S-oriented regional crustal extension through the entire graben history with no evidence of temporal change in the regional extension direction. Minor spatial variations are attributed to poorly defined σ_3 -axis or local stress field anomalies caused by fault interactions.

Evolution of the Gediz Graben is a dynamic process as indicated by pronounced changes in the geometry and lateral extend of the southern margin-bounding structures along strike and dip directions. This also influenced the

lithofacies, depositional pattern and thickness of the graben fill units. The western Anatolian extension is episodic with earlier (Miocene) and later (Plio–Quaternary) phases of extension and intervening short phase of contraction (Late Miocene–Early Pliocene). Despite of this fact, evidence for the short-term intervening contractional phase throughout the Gediz Graben is scarce and there is local observation of folds and thrust/reverse faults affecting the Alaşehir formation. These structures suggest that the short-term phase of contraction might have existed but most probably been absorbed by the high rates of extension. This data may further imply that graben evolution from half-graben phase (Miocene configuration) to full graben phase (present day configuration) might be a discontinuous process accompanied by a short-time break in-between.

Keywords: Southwestern Turkey, Gediz Graben, continental extension, graben, normal fault, stress analysis

ÖZ

GEDİZ GRABENİ' NİN JEOLJİK EVRİMİ (GB TÜRKİYE): GRABENİN ZAMANSAL VE ALANSAL DEĞİŞİMİ

Çiftçi, Bozkurt N.

Doktora, Jeoloji Mühendisliği Bölümü

Tez Yöneticisi: Prof. Dr. Erdin Bozkurt

Mart 2007, 290 sayfa

Gediz Grabeni, Neojen yaşlı karasal sedimanları içeren gerilmeli bir havzadır. Graben kenarları, yaklaşık D–B uzanımlı aktif fay sistemleri tarafından denetlenmektedir. Toplam atım ve aktivite süresi dikkate alındığında grabenin güney kenarı kuzey kenardan daha etkin ve baskındır. Havza Miyosen boyunca sadece güney kenarın aktif olduğu yarım graben olarak gelişmiş, Pliyo–Kuvaterner’de kuzey kenar fay sisteminin faaliyete geçmesi ile bugünkü görünümünü Miyosen döneminden kalan asimetriyi koruyarak kazanmıştır.

Güney kenar fay sistemi, graben merkezine doğru kuzeye eğimli fayların oluşturduğu, tavan bloğundan taban bloğuna doğru giden basamaklı bir yapıya sahiptir. Faylar graben merkezine doğru gençleşirlerken yapısal olgunluk aynı yönde azalmaktadır. Fay düzlemi verileri, bölgesel gerilme yönünün havza evrimi boyunca değişmeden yaklaşık K–G doğrultusunda sabit kaldığına işaret etmektedir. Alansal olarak gözlenen gerilme yönü değişimleri ise σ_3 ekseninin iyi tanımlı olmaması ve yersel gerilme alanı anormallikleri ile ilişkilidir.

Gediz Grabeni’nin evrimi güney kenar fay sisteminin grabene paralel ve dik yönde sürekli bir değişim içerisinde olduğu dinamik bir süreç ile kontrol edilmiştir. Bu

süreçte gözlenen değişimler kaya türlerini, çökelim dokusunu ve sedimenter birimlerin kalınlığını da kontrol etmiştir. Batı Anadolu'nun evrimi, erken gerilme (Miyosen) ve geç gerilme (Pliyo–Kuvaterner) fazları ile bu fazları birbirinden ayıran kısa sıkışma dönemini (Geç Miyosen–Erken Pliyosen) içeren episodik bir özellik taşımaktadır. Bu gerçeğe rağmen Gediz Grabeni'nde kısa sıkışma fazına yönelik veriler son derece kısıtlı ve yersel alanlarda, sadece Alaşehir formasyonu içerisinde gözlenen kıvrımlar ve ters fay/bindirmeler ile sınırlıdır. Bu yapılar kısa sıkışma döneminin mevcut olabileceğini fakat büyük olasılıkla grabendeki yüksek gerilme oranı nedeniyle doğrulduğunu göstermektedir. Ayrıca bu veri, yarım graben evresi (Miyosen konumu) ile tam graben evresinin (bugünkü konum) kısa bir dönem ile ayrılmış olabileceği süreksiz bir evrime de işaret etmektedir.

Anahtar sözcükler: Güneybatı Türkiye, Gediz Grabeni, kıtasal gerilme, graben, normal fay, gerilim analizi

ACKNOWLEDGMENTS

I would like to express gratitude to Erdin Bozkurt for his invaluable contributions to this study not only as a formal supervisor but also as a teacher, a colleague and a friend. I have benefited greatly from his enthusiasm and insight to the geological problems. Sincere appreciation is also expressed to committee members Ali Koçyiğit and Kadir Dirik for the guidance they have provided and for being excellent teachers. Special thanks to thesis referees Orhan Tatar and Hasan Sözbilir for reading and commenting on this dissertation.

I also benefited greatly from discussions with various individuals at different stages of my study. Many sincere thanks to Halit Alkan, Sami Derman, Mustafa Ali Engin, John Shaw, Chris Guzovski, Nuri Terzioğlu, Hasan Sarıkaya, Özgür Temel, Ömür M. Nohut and İsmet Sincer for sharing their expertise and insights. I appreciate the financial support provided by METU Research Foundation grants BAP-2004-03-09-04 and BAP-2006-03-09-01, TÜBİTAK grant 1004Y154 and TPAO. TPAO is also acknowledged for providing the subsurface data.

I would like to dedicate this study to my wife Reyhan and to my son Bartu. May this small effort acknowledge the blessing of a family that they provided to me?

TABLE OF CONTENTS

ABSTRACT.....	iv
ÖZ.....	vi
ACKNOWLEDGEMENTS.....	viii
TABLE OF CONTENTS.....	ix
LIST OF TABLES.....	xii
LIST OF FIGURES.....	xiii
CHAPTER	
1. INTRODUCTION.....	1
1.1. Current Problems.....	2
1.2. Research Objectives.....	3
1.3. Research Contributions.....	3
1.4. Study Area.....	4
1.5. Methodology.....	4
1.6. Tectonic Setting.....	8
1.6.1. Origin of Neotectonic Regime.....	10
1.7. Regional Geology.....	15
1.7.1. Stratigraphy.....	18
1.7.2. Structural Geology.....	19
2. STRATIGRAPHIC FRAMEWORK AND DEPOSITIONAL SYSTEM OF THE NEOGENE DEPOSITS.....	22
2.1. Lithostratigraphic Framework of the Graben Fill.....	24
2.1.1. Alaşehir Formation.....	27
2.1.2. Toygarlı Andesite.....	37
2.1.3. Çaltılık Formation.....	38
2.1.4. Gediz Formation.....	40
2.1.5. Bintepeleler Formation.....	47
2.1.6. Kaletepe Formation.....	48
2.1.7. Quaternary Alluvium.....	52

2.2. Subsurface Correlation of Lithostratigraphic Units.....	53
2.2.1. Boreholes.....	54
2.2.2. Depositional Geometries from Seismic Data.....	59
3. PATTERNS OF NORMAL FAULTING IN THE	
GEDIZ GRABEN.....	66
3.1. Geometry of Normal Faulting.....	69
3.1.1. Fault Pattern in Plio-Quaternary Strata.....	70
3.1.2. Fault Pattern in Neogene Strata.....	89
3.2. The Stress Field.....	98
3.2.1. The Stress Field of Faulting in Plio-Quaternary Strata.....	99
3.2.2. Stress Field of Faulting in Neogene Strata.....	107
3.3. Discussion.....	109
4. RELAY RAMPS AND FAULT SEGMENT LINKAGE.....	114
4.1. Background on Relay Ramps.....	114
4.2. Stratigraphy of the Field Station.....	119
4.3. Structural Geology.....	123
4.4. The Relay Ramp.....	125
4.4.1. Stress Field at the Ramp Area.....	130
4.4.2. Cluster Analysis.....	134
4.5. Discussion.....	137
5. INTERPRETATION OF SUBSURFACE	
DATA AND SURFACE TO SUBSURFACE CORRELATION.....	140
5.1. Time to Depth Conversion of Seismic Data.....	142
5.1.1. The Velocity Model.....	143
5.1.2. Time to Depth Conversion.....	146
5.2. Fault Pattern from Seismic Data.....	149
5.2.1. Graben Bounding Structures.....	152
5.2.2. Fault Pattern of the Graben Fill.....	162
5.2.3. Stress Field of Faulting.....	170
5.3. Graben Fill.....	174
5.3.1. Alaşehir Formation.....	178
5.3.2. Çaltılık Formation.....	181
5.3.3. Gediz Formation.....	184
5.3.4. Pliocene to Quaternary Deposits.....	187

5.4. Correlation of Surface to Subsurface Data.....	190
6. FOLDING IN THE GRABEN FILL.....	201
6.1. Folds and Process of Folding: A Review.....	202
6.2. Outcrop Observations: Actual Data.....	210
6.3. Subsurface Interpretations.....	221
6.3.1. Forward Modeling of Transverse Folding.....	227
6.4. Discussion.....	231
7. CONCLUSIONS: GEOLOGICAL EVOLUTION OF THE GEDIZ GRABEN.....	233
7.1. Structural Evolution.....	233
7.2. Stratigraphic Evolution.....	236
6.3. Basin Evolution.....	241
REFERENCES.....	245
APPENDICES.....	259
Appendix I: Measured Stratigraphic Sections.....	261
Appendix II: Principals of Gamma Ray (GR) Logs.....	267
Appendix III: Theory of Palaeostress Reconstruction.....	274
Appendix IV: Curriculum Vitae.....	290

LIST OF TABLES

TABLES

Table 2.1. Dominant facies, facies descriptions and interpretations of the Alaşehir formation	29
Table 2.2. Facies associations of the Alaşehir formation.....	30
Table 2.3. Dominant facies, facies descriptions and interpretations of the Çaltılık formation.....	39
Table 2.4. Facies associations of the Çaltılık formation.....	39
Table 2.5. Dominant facies, facies descriptions and interpretations of the Gediz formation	44
Table 2.6. Facies association of the Gediz formation.....	44
Table 2.7. Description and interpretation of the lithofacies observed in the Bintepeleler formation.....	49
Table 2.8. Description and interpretation of the lithofacies observed in the Kaletepe formation.....	49

LIST OF FIGURES

FIGURES

Figure 1.1. Location of the Gediz graben and the other major southwest Anatolian grabens.....	5
Figure 1.2. General view of the Gediz Graben illustrating locations of the field station, 2-D seismic data and boreholes.....	6
Figure 1.3. Map illustrating the major neotectonic provinces and related structures in Turkey and surrounding area.....	9
Figure 1.4. Simplified tectonic map illustrating the main Tethyan sutures and neighboring tectonic units of western Turkey.....	11
Figure 1.5. Simplified geological map of SW Turkey showing the distribution of ~E–W-trending and NE–SW-trending neotectonic basins.....	16
Figure 2.1. Neogene stratigraphy of the Gediz Graben documented by various researchers.....	23
Figure 2.2. Neogene stratigraphy of the Gediz Graben around Alaşehir.....	25
Figure 2.3. Geological map of the study area around Alaşehir showing major structures and mapped geological units.....	26
Figure 2.4. A block diagram illustrating conceptual schematic palaeogeography of the depositional period of the Alaşehir formation.....	31
Figure 2.5. Field photographs illustrating the fault contact between the Alaşehir formation and the underlying metamorphic rocks (schists) near Kayadibi village.....	32
Figure 2.6. A block diagram depicting conceptual schematic paleogeography of the depositional period of the Çaltılık formation.....	41
Figure 2.7. Field photographs taken near Soğukyurt village to illustrate lithofacies in the Çaltılık formation.....	42
Figure 2.8. A block diagram depicting conceptual schematic palaeogeography of the depositional period of the Gediz formation.....	45
Figure 2.9. Field photographs of lithofacies in the Gediz formation taken near Çıkrıkçı village, Akçapınar.....	46

Figure 2.10. A block diagram depicting conceptual schematic paleogeography of Bintepeleler and Kaletepe formations and the Quaternary deposits of the Gediz Graben.....	50
Figure 2.11. A summary section correlating the boreholes drilled in the Gediz graben.....	55
Figure 2.12. Figure illustrating lithologies of the formations and corresponding GR responses in BH-1	56
Figure 2.13. Schematic cross-section illustrating the facies distribution of Alaşehir and Çaltılık formations within the fault controlled basin.....	58
Figure 2.14. 2-D seismic section (S-12) oriented transverse to the Gediz Graben...	61
Figure 2.15. A transverse seismic section (S-10) with basic interpretations and Borehole 1 (BH-1).....	64
Figure 3.1. Elevation model of the Gediz Graben showing the locations of the field stations, and the available subsurface data including 2-D seismic profiles and boreholes.....	68
Figure 3.2. General characteristics of faults influencing the Plio-Quaternary deposits.....	71
Figure 3.3. A field photograph and its sketch at the St-1.....	73
Figure 3.4. Field photograph and sketch of an outcrop surface in St-2.....	74
Figure 3.5. Field photo and sketch of an outcrop surface in St-2.....	75
Figure 3.6. Field photograph and sketch of an outcrop surface in St-3.....	77
Figure 3.7. Fault data depicting examples of conjugate fault systems in the Quaternary deposits.....	78
Figure 3.8. Simultaneous slip on crossing conjugate normal faults produces a compatibility problem requiring area gain or lost in cross-section.....	80
Figure 3.9. Sequential slip on crossing conjugate normal faults eliminates the compatibility problem at the intersection zone.....	81
Figure 3.10. Sequential restoration of conjugate fault systems of St-3.....	83
Figure 3.11. Geological map of the St-2.....	84
Figure 3.12. Three separate conjugate fault systems identified in the St-2.....	86
Figure 3.13. Fault data of the St-2.....	88
Figure 3.14. Fault data observed across the Neogene deposits.....	90
Figure 3.15. Profile based field station St-8 within the Çaltılık formation.....	91

Figure 3.16. Field photographs and their sketched drawings depicting faulting in Neogene deposits at St-9.....	92
Figure 3.17. Normal (σ_n) and shear (τ) components of stress σ on a fault plane.....	94
Figure 3.18. Sketched field photograph illustrating the cross-cutting relationship between the detachment fault and high angle normal faults.....	95
Figure 3.19. Stress analyses carried out within the Plio-Quaternary deposits.....	100
Figure 3.20. Multiple inverse method applied to all Quaternary faulting.....	104
Figure 3.21. Results of the stress inversion method that require only fault slip senses applied to all Quaternary faulting.....	106
Figure 3.22. Stress analyses carried out within the Neogene deposits.....	108
Figure 3.23. Solution of the fault slip data acquired from Neogene deposits according to multiple inverse method.....	110
Figure 3.24. Summary of the stress inversion results carried out along the southern margin of the Gediz Graben.....	113
Figure 3.25. Spatial variation of the stress field at St-10.....	114
Figure 4.1. Block diagram of two overstepping normal fault segments dipping in the same direction.....	115
Figure 4.2. Schematic diagram showing evolutionary stages of a relay ramp.....	117
Figure 4.3. Block diagram illustrating deformation mechanisms at a relay ramp...	118
Figure 4.4. Simplified stratigraphic column of the area-based field station St-15...	120
Figure 4.5. Geological map of the field station St-15.....	121
Figure 4.6. Geological cross-sections through I-I', II-II' and III-III' on Figure 4.5.....	124
Figure 4.7. Digital Elevation Model depicting the topographical manifestations of the normal faults and the breaching Akçapınar relay ramp.....	126
Figure 4.8. Map showing the seismicity of western Turkey, available fault plane solutions and extension directions around the Gediz Graben.....	127
Figure 4.9. Stereoplots illustrating fault slip data of the Akçapınar area.....	128
Figure 4.10. Schematic diagram showing the cross-cutting relationship between the N–S-oriented ramp-related faults and E–W-oriented older faults.....	131
Figure 4.11. Stages of distinct deformation styles at the ramp area.....	132
Figure 4.12. Fault-slip data and computed principle stress direction in the study area.....	133

Figure 4.13. Fault-slip data and principal stress directions for the two subsets differentiated by applying cluster analysis to the heterogenous fault data at the Akçapınar relay ramp.....	136
Figure 5.1. Surface to subsurface correlation was carried out using 2-D seismic sections, three boreholes (BH-1, BH-2 and BH-3), a surface geological map and digital elevation model (DEM) of the region.....	141
Figure 5.2. The 3-D base grid of the intended velocity model.....	144
Figure 5.3. Interval velocity versus two-way travel time plot of BH-1 with a seismic section.....	145
Figure 5.4. The graph showing interval velocities obtained from the stacking velocities versus two way travel time.....	147
Figure 5.5. Final velocity model based on check-shot and stacking velocities.....	148
Figure 5.6. An example of a seismic section in the time domain and in depth domain.....	150
Figure 5.7. Identification of faults in seismic sections.....	151
Figure 5.8. Direct fault plane reflections acquired from southern margin structure of the Gediz Graben.....	154
Figure 5.9. Extensional fault-bend folding or roll-over folding.....	155
Figure 5.10. Formation of multiple rollover panels due to multiple bends on the fault plane.	157
Figure 5.11. Models of inclined collapse of hanging wall can be applied to seismic section in the Gediz Graben.....	158
Figure 5.12. Similar geometrical construction as in Figure 5.10, also reveals a fault bend for this seismic section.....	159
Figure 5.13. 3-D geometry of the southern margin-bounding structure of the Gediz Graben.....	161
Figure 5.14. Northern margin bounding structure of the Gediz Graben imaged by the seismic sections S-5 and S-6.....	163
Figure 5.15. 3-D geometry of the northern margin-bounding structure of the Gediz Graben.....	164
Figure 5.16. Seismic section S-12 showing general deformation characteristics of the graben fill.....	166
Figure 5.17. Seismic section S-6 showing general deformation characteristics of the graben fill.....	167

Figure 5.18. 3-D fault model of the Gediz Graben.....	168
Figure 5.19. Backward rotation of hanging-wall structures within the rollover panel.....	169
Figure 5.20. Stereoplots illustrating poles to the fault planes in Figure 5.18.....	172
Figure 5.21. Fault data extracted from Figure 5.20 and used in the stress analysis.	173
Figure 5.22. Isopack map showing the thickness distribution of the fill of the Gediz Graben.....	175
Figure 5.23. Longitudinal seismic section S-4 and its interpreted cross section extending from Salihli to Alaşehir.....	179
Figure 5.24. Geological map of the area around Alaşehir.....	180
Figure 5.25. Model showing the graben-bounding structures and top of the Alaşehir formation.....	179
Figure 5.26. Structural map of the top of the Alaşehir formation.....	182
Figure 5.27. Model showing the graben-bounding structures and top of the Çaltılık formation.....	183
Figure 5.28. Structural map of the top of the Çaltılık formation.....	185
Figure 5.29. Model showing the graben-bounding structures and top of the Gediz formation.....	186
Figure 5.30. Structural map of the top of the Gediz formation.....	188
Figure 5.31. Model showing the graben bounding structures and the modern graben floor.....	189
Figure 5.32. Transverse cross-sections depicting the geology of the Gediz Graben in Alaşehir subbasin.....	191
Figure 5.33. Transverse cross-sections depicting the geology of the Gediz Graben in Alaşehir subbasin.....	192
Figure 5.34. Forward model illustrating simultaneous activity of two structures that are linked to the same detachment at depth.....	195
Figure 5.35. Schematic diagram illustrating the structural evolution of the southern margin of the Gediz Graben in the continuum of deformation.....	196
Figure 5.36. Longitudinal cross section passing along the Alaşehir subbasin.....	192
Figure 5.37. Longitudinal cross section passing along the Alaşehir subbasin.....	200
Figure 6.1. Folding is commonly achieved by two major mechanisms: flexural folding and passive folding.....	203

Figure 6.2. Contractional fault-related folding is achieved by means of three major processes.....	205
Figure 6.3. More than a dozen mechanisms were described as the cause of folding in extensional settings.....	207
Figure 6.4. Typical displacement profile across a normal fault.....	209
Figure 6.5. Location map of the road cut that is mapped for contractional folds and faults in detail.....	211
Figure 6.6. Road cut cross-section that illustrate the deformation pattern of the Alaşehir formation to the SW of Osmaniye.....	212
Figure 6.7. Outcrop photograph and basic interpretation to illustrate complex deformation patterns observed along the road-cut cross-section.....	213
Figure 6.8. Stereoplot illustrating bedding and fault data along the road-cut section.....	214
Figure 6.9. Stereoplot depicting hinge-line orientations of folds.....	216
Figure 6.10. Outcrop photograph and its sketch showing an asymmetrical anticline that exposed along the road-cut section.....	217
Figure 6.11. Outcrop photograph (A) and basic interpretation (B) showing a broad symmetrical syncline that form on the hanging wall of a reverse fault.....	218
Figure 6.12. Outcrop photograph (A) and basic interpretation (B) showing a tight chevron syncline with plunge direction to the observer.....	219
Figure 6.13. Outcrop photograph illustrating the slump features within the Alaşehir formation.....	220
Figure 6.14. Part of seismic section S-10 illustrating small-scale longitudinal folds forming in association to normal faults.....	222
Figure 6.15. Figure depicting the transverse anticlines and synclines in the Gediz Graben.....	224
Figure 6.16. Two different ways of folding in contractional fault related folds.....	225
Figure 6.17. Interpretation of the seismic section S-16 in the Gediz Graben.....	226
Figure 6.18. The extracted subsidence profiles.....	228
Figure 6.19. Modeling of the transverse anticlines in the Gediz Graben.....	230
Figure 7.1. Schematic diagrams depicting geological evolution of the Alaşehir subbasin of the Gediz graben.....	237

Figure 7.2. Computer-based model of continental rift stratigraphy controlled by segmented bounding structure.....	239
Figure 7.3. Geological evolution of the Gediz Graben.....	243

CHAPTER 1

INTRODUCTION

Continental rifts and overlying sag basins form one of the most common tectonic settings that world's giant hydrocarbon reserves have discovered. Because of this economical significance, graben basins became the subject of main interest for oil industry and earth sciences community for the last few decades (e.g., Harding, 1984; Morley *et al.*, 1990; Morley, 1995; McClay *et al.*, 2002). Efforts were intensified to improve the geological understanding of the graben basins, which eventually lead to more efficient exploration, and exploitation of the hydrocarbon reserves in these basins. This led to the improved understanding of the graben-bounding structures and rift sequences deposited during the evolution of grabens. In relation to this, field observations, numerical modeling and experimental studies focusing on the normal fault systems revealed many aspects of extensional deformation such as basic fault dimensions, fault propagation and fault tip processes and simultaneous evolution of numerous faults by linkage (e.g. Walsh and Watterson, 1988; Peacock and Sanderson, 1991; Cowie and Scholz, 1992; Cartwright *et al.*, 1995; Dawers and Anders, 1995; Morley, 2002). Accordingly, influence of normal fault evolution on the depositional patterns of the graben fill sediments has been investigated by numerous studies as well (e.g. Schlische, 1991; Schlische, 1992; Prosser, 1993; Schlische and Anders, 1996; Morley, 2002). All these efforts have brought along the modern understanding of graben basins, which is more advanced now than a decade ago.

Parallel to all these advances, hydrocarbon potential of the western Anatolian grabens started to attract our national oil company, TPAO, by the mid 90s. Few exploration projects were conducted in the region until the first well drilled in Alaşehir in 1999. Discovery of oil in this well accelerates the exploration efforts in the region and each graben in western Anatolia was covered by a separate

exploration project. Unfortunately, that was followed by unsuccessful drill results coming from Gediz, Büyük Menderes and Edremit grabens. Although, the apparent cause of the poor results are predominantly attributed to the flaws of region's hydrocarbon system, it was mostly ignored that the geological predictions also failed in these wells. This is a very clear indication of poorly developed geological model suggesting that our understanding of western Anatolian grabens were still immature and further geological studies were needed to improve this understanding.

Motivated by the poor geological results coming from drilling activities, this study was initiated in 2001 with an ultimate aim to improve the geological understanding of the western Anatolian grabens. Gediz Graben was selected as the study area for multiple reasons: (1) it is the best-developed western Anatolian graben probably hosting the thickest sedimentary fill among the others; (2) surface geological observations can be supported by subsurface data including drilled wells and a 2-D reflection seismic survey. Efforts based on the analysis of these data provided with a new perspective to the evolution of the Gediz Graben. This evolution, which is characterized by temporal and spatial variation of the graben basin, has certain implications to evaluate the hydrocarbon potential of the western Anatolian grabens. Results may also apply to similar geological settings around the world.

1.1. Current Problems

During the last two decades, intensive research were carried out across the western Anatolia (see sections 1.5 and 1.6 for summary). Despite these studies, there remain many controversial issues awaiting a solution to complete our understanding of the region. These issues includes but not limited to:

- The driving mechanism and initiation time of extension in the southwestern Anatolia.
- The age and evolution of the southwestern Anatolian grabens.
- Continuous versus episodic evolution of the extensional regime.
- The relationship among the presently inactive low-angle normal fault(s) and active high-angle normal faults.
- Folds as the evidence of short phase of compression.

1.2. Research Objectives

This study intends to improve the geological understanding of the Gediz Graben that may serve as a model for the western Anatolian extension. The main objectives of the dissertation are:

- To revise the established stratigraphy of the Gediz Graben in order to construct a framework that can serve to reconstruct the basin geometry and to correlate surface and subsurface geology.
- To investigate different normal fault systems and governing stress fields in the Gediz Graben and to assess their nature, interrelation and modes of formation.
- To investigate evolutionary path of normal faults from the segmented immature stage to the single large-scale mature stage.
- To jointly interpret subsurface data coming from boreholes and a 2-D reflection seismic survey. To establish a correlation between surface and subsurface to portray the geometry of the Gediz Graben and to observe the temporal and spatial distribution of the related geological phenomenon.
- To assess the origin of folding in the Gediz Graben.
- To reconstruct the spatial and temporal geological evolution of the Gediz Graben.

1.3. Research Contributions

Efforts to meet the above-mentioned objectives have developed a perspective to the spatial and temporal evolution of the Gediz Graben. This perspective comes along with:

- Improved understanding of normal fault systems and controlling stress regimes that deformed or actively deforming the Gediz Graben.
- More accurate insight to graben's geometry that is achieved by integrated utilization of surface and subsurface data.
- More accurate understanding of spatial and temporal distribution of the related geological phenomenon in the Gediz Graben benefited from both surface and subsurface data.

1.4. Study Area

Numbers of neotectonic graben basins are available in the western Anatolia with a potential of shedding light to the tectonic evolution of the region (Figure 1.1). These grabens are best developed across southwestern Anatolia in relation to Menderes Massif and suggest that graben formation and rapid exhumation of metamorphic core complex are somehow related. Accordingly, the Gediz Graben was selected as the focus of this study as it is the best-developed graben basin and includes multiple styles of deformations, which needs to be evaluated to understand the graben evolution.

The Gediz Graben is an ~E–W-trending geomorphologic feature with a strong topographical manifestation. It starts SE of Alaşehir to the east and extends westward to the west of Turgutlu along more than 100 km-long plain of the Gediz River (Figure 1.1). Several-medium scale towns including but not limited to Alaşehir, Salihli, Karataş, Ahmetli, and Turgutlu are partly or completely contained by the graben and have been exposed related seismic activities in historic and recent years. The southern margin of the Gediz Graben is better defined with a broad, convex-northward outline and separates almost flat graben floor from the rugged topography of the Bozdağ Mountains, reaching up to 2000 m elevation (Figure 1.1). The graben is relatively narrow to the east (~7 km) where the northern margin is closer to the southern margin. To the west, however, the two margins gradually become separated as the northern margins experiences several northward steps to form a 25-km-wide plain around Salihli. Further westward, the graben is splayed into two branches and merges with the Manisa graben (Figure 1.1).

1.5. Methodology

This study intends to benefit from both surface and subsurface data to meet with the stated objectives. In relation to this intention, outcrop studies were initially carried out in the Gediz Graben, particularly along its southern margin structure (Figure 1.2). Fieldwork was conducted by field stations approach in order to obtain data and observations that can objectively account for the spatial variations. Thus, 15 field stations were set which can be classified as point-based and area-based field stations. Point-based field stations are selected among very good exposures that can provide information on the deformation characteristics. They served as locations of geological cross-sections, which portray deformation characteristics in the dip

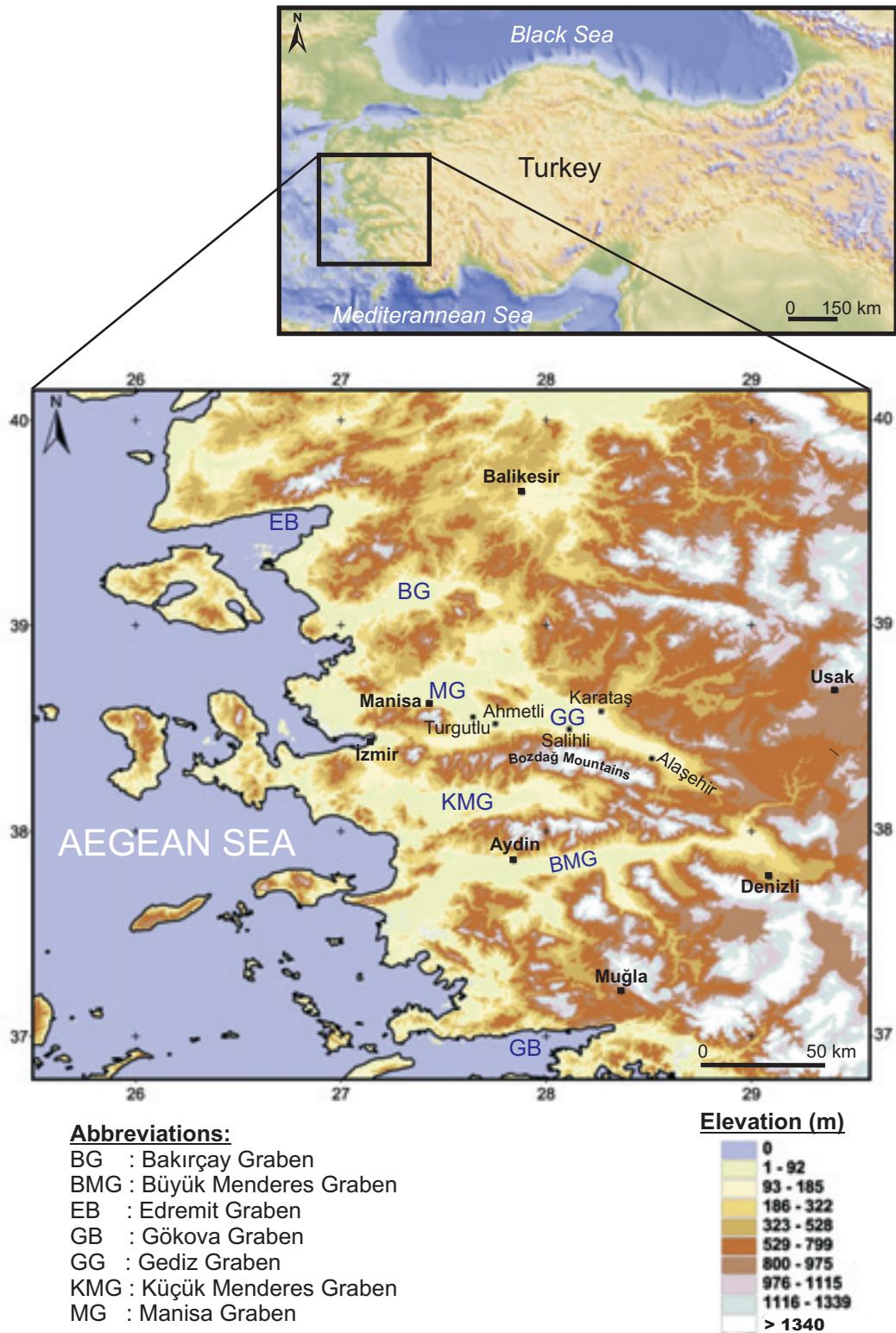


Figure 1.1. Location of the Gediz Graben and the other major southwestern Anatolian grabens. Color code on the map depicts the elevation.

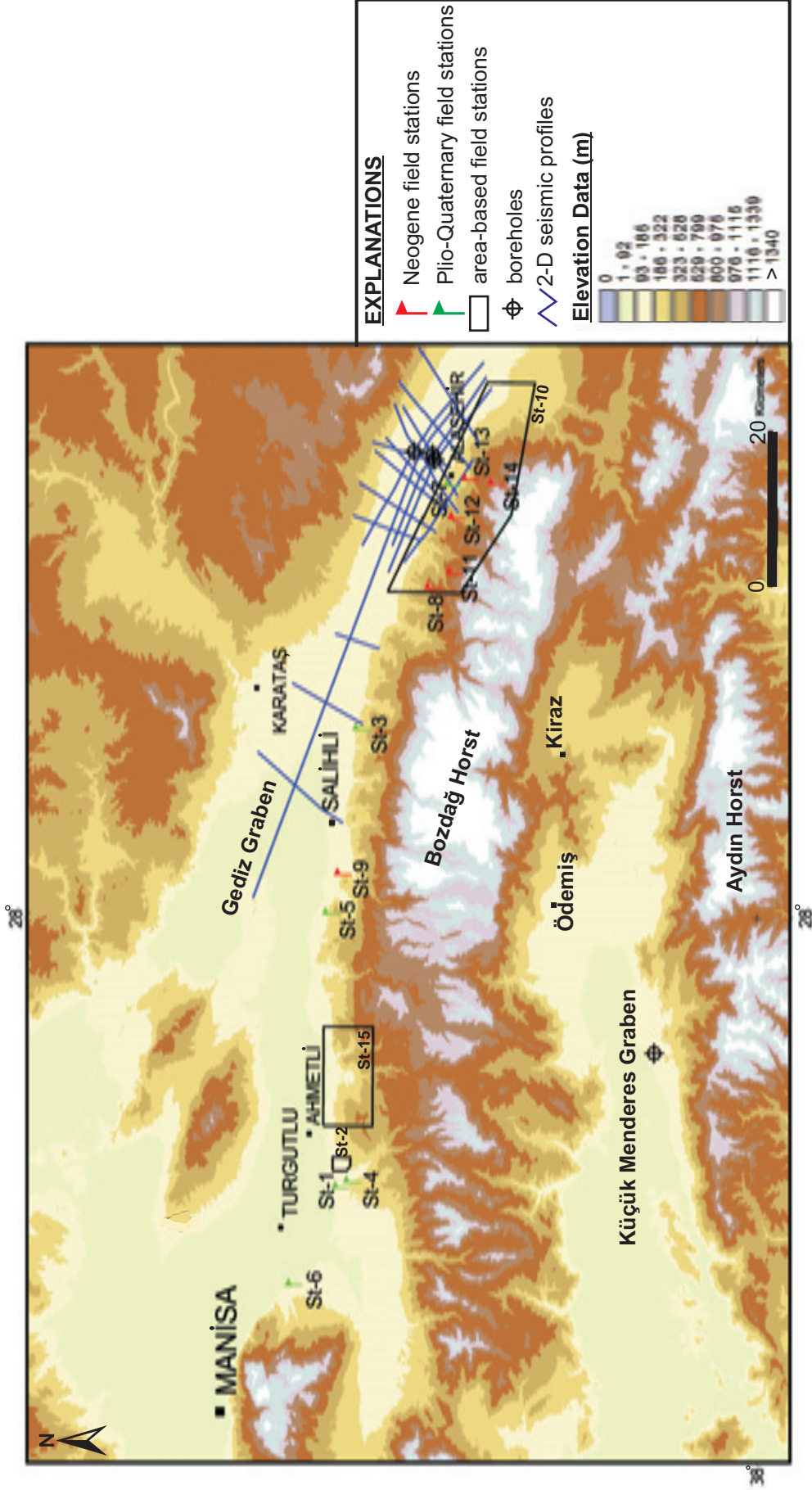


Figure 1.2. General view of the Gediz Graben illustrating locations of the field station, 2-D seismic data and boreholes. Color code on the map depicts elevation. See Figure 1.1 for the location of the Gediz Graben.

directions of the structures. These stations aid to improve the understanding of deformation pattern in the graben. Fault slip data was acquired from the point-based stations including strike and dip of the fault plane and the rake of slickenside lineation. Palaeostress inversion was carried out with this data set to assess the governing stress fields of deformation.

Three different localities are selected for the area-based field stations (Figure 1.2). These stations intend to document spatial variation of deformation and lithofacies characteristics of the stratigraphic units. Conventional geological mapping was carried out at the area-based field stations at various scales. Mapping effort at these stations is also accompanied by; (1) stratigraphic section measurement to document facies characteristics of each defined stratigraphic units, (2) fault-slip data acquisition to improve the coverage of palaeostress analysis and (3) sketch cross-section construction and structural data acquisition to document deformation characteristics of each stratigraphic unit. All these field-oriented efforts improved the understanding of deformational and depositional mechanisms that have taken place along the margins of the Gediz Graben.

In the next step, subsurface data including three boreholes and 270 km 2-D seismic reflection data were interpreted by strictly based on the geological understanding acquired during the outcrop studies. For the most proper integration of surface and subsurface data, 2-D seismic sections, which are in time domain, were converted into depth domain by building a velocity model that is based on the velocity data coming from the boreholes and seismic processing. Then, surface and subsurface data were correlated by building geological cross-sections, which start from the southern horst block, cut through the graben basin and end at the northern horst block. These transverse cross-sections (perpendicular to graben trend) were also correlated with the longitudinal seismic sections (parallel to graben trend) to build longitudinal geological cross-sections as well. These efforts led to understand the basin geometry and spatial variation of its geological aspects. In other words, surface observations, which are strictly limited to basin margins, were projected into and compared with the entire basin. Forward modeling efforts, which are based on extensional fault-bend-fold theories (Xiao and Suppe, 1992; Shaw *et al.*, 1997), aid to improve the understanding of some of the geological relations, geometries and patterns of the Gediz Graben.

1.6. Tectonic Setting

Turkey constitutes an important sector on the western segment of Alpine-Himalayan orogenic belt. Hellenides and Carpathians branches of Alpine system cross Turkey in the form of complex Tauride and Pontide blocks and connect with Bitlis-Zagros zone to the east (Şengör and Yılmaz, 1981). Compressional, strike-slip and local extensional deformations are observable along the entire Alpine-Himalayan belt driven by complicated convergence of Africa and Eurasia. Several major structures control the neotectonic configuration of Turkey driven by this continental convergence (Figure 1.3). The Aegean-Cyprian subduction zone constitutes the plate boundary where African plate to the south is subducting N-NW beneath the Anatolian microplate and Eurasia to the north. This subduction is accompanied by two intra-continental transform fault systems to accommodate the movement of the overriding Anatolian wedge: dextral North Anatolian Fault System (NAFS) and sinistral East Anatolian Fault System (EAFS). These fault systems bound the Anatolian microplate and guide its westward extrusion from the zone of continental collision between the Eurasian and Arabian plates, marked by the Bitlis-Zagros suture zone (Şengör, 1979; Dewey and Şengör, 1979; Şengör *et al.*, 1985). The Dead Sea Fault System (DSFS) accommodates the differential northward motions among the southern plates; i.e. the African and Arabian plates.

Controlled by NAFS and EAFS, WSW escape of the Anatolian microplate onto the easily subductable eastern Mediterranean lithosphere is accompanied by counterclockwise rotation (Rotstein, 1984). Unavoidably, all these processes of rigid body movements brings along internal strain that is relieved by various deformation mechanisms at different parts of Turkey. As a result, Turkey can be separated into four major neotectonic provinces each of which is characterized by unique deformation style and specific sedimentary basin formation (Koçyiğit and Özacar, 2003) (Figure 1.3). An extensional regime dominates across southwestern Anatolia with consequential deformation pattern that is characterized by neotectonic graben formation. In fact, this extensional region is part of a well-known Aegean Extensional Province (AEP), which includes western Turkey, Aegean Sea and southern Balkan region comprising Greece, Macedonia, Bulgaria and Albania.

The Anatolian microplate is composed of amalgamated continental fragments separated by several suture zones. These continental fragments constitute the basement rocks to the neotectonic sedimentary basins of the Anatolia. Amalgamation

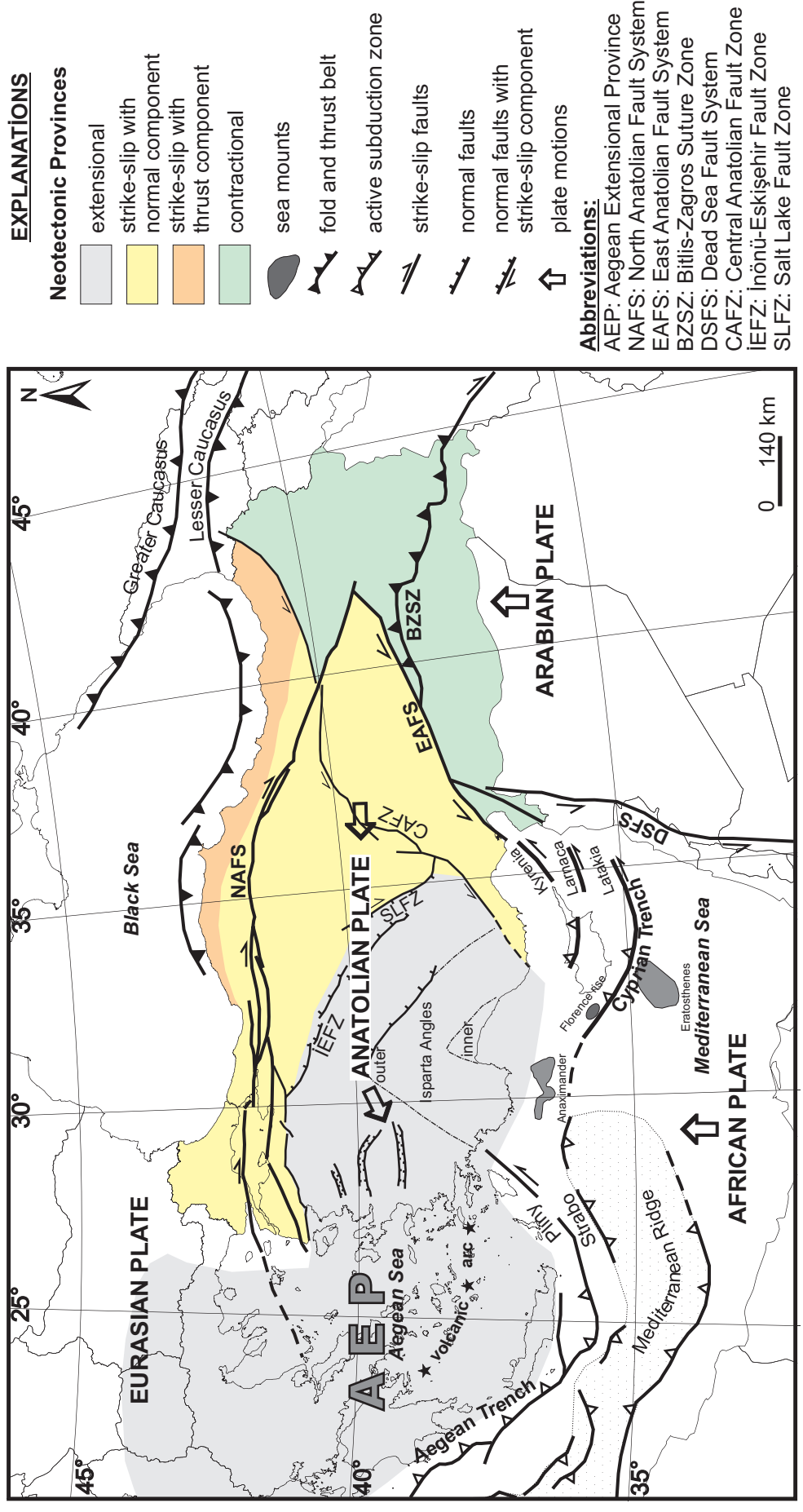


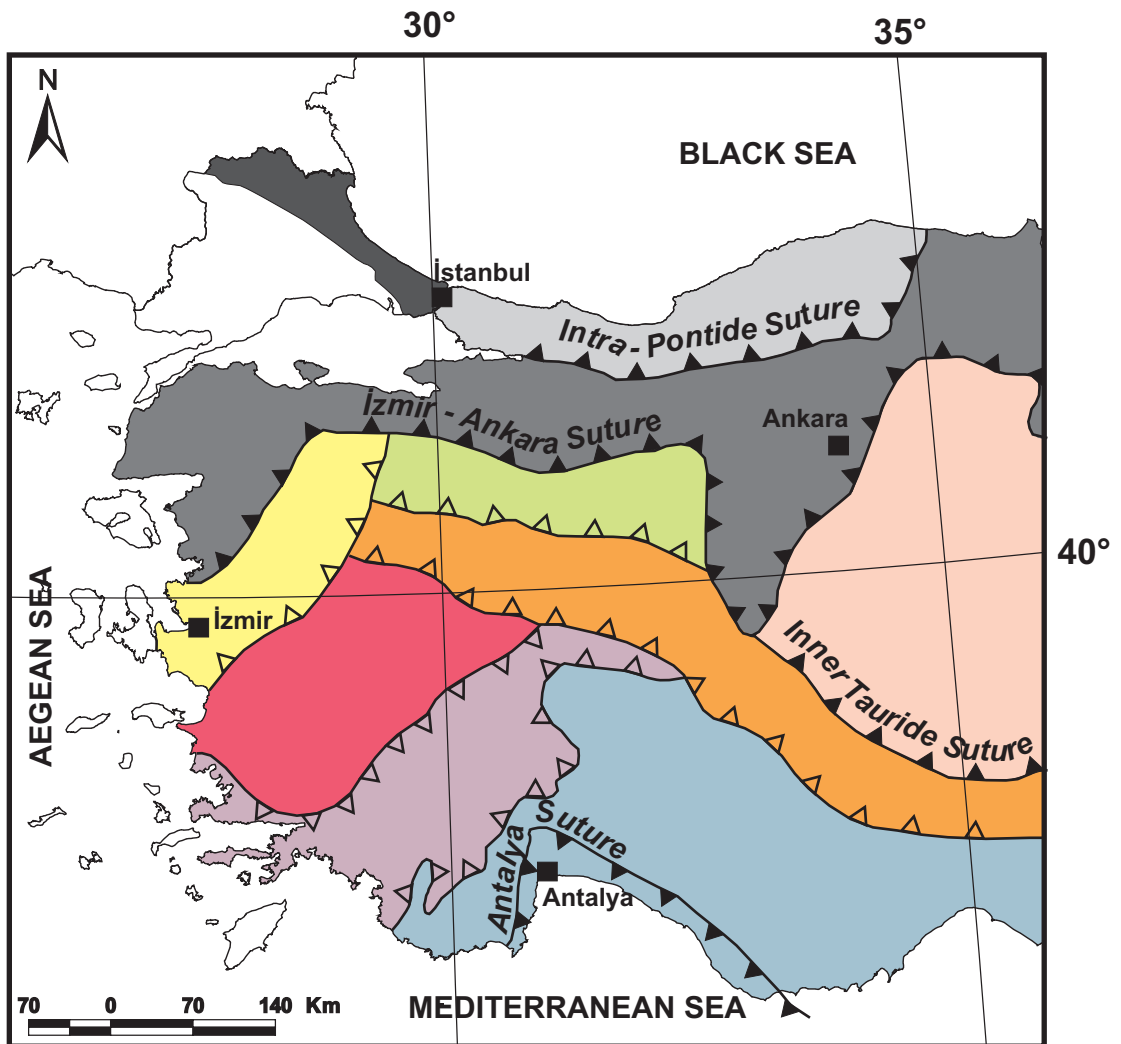
Figure 1.3. Map illustrating the major neotectonic provinces and related structures in Turkey and surrounding area. Color code in Turkey illustrates major neotectonic provinces each of which is characterized by unique deformation style and sedimentary basin formation. Modified from Koyuğit and Özacar (2003), Woodside *et al.* (2002) and Zitter *et al.* (2005).

of these continental fragments took place by means of continent-continent collisions across the northern and southern branches of Neotethys during the Early Tertiary (Şengör and Yılmaz, 1981). Deformation fabric resulted from this collision played an important role in directing the superimposed neotectonic structures.

Two suture zones bound the major continental fragments of western Anatolia (Figure 1.4). The Intra-Pontide Suture separates İstanbul Zone to the north from the Sakarya Zone to the south. The İzmir-Ankara Suture bounds the southern margin of Sakarya Continent and separates it from the Anatolide-Tauride platform. This platform made up of several tectonic units bounded by major faults. These units include a blueschist belt of Tavşanlı Zone, the Bornova Flysch Zone, which consists of large Mesozoic limestone blocks within a matrix of Maastrichtian–Paleocene greywacke-shale; the Afyon zone which is made up of a Paleozoic–Mesozoic sedimentary sequence metamorphosed into the greenschist facies; the Menderes Massif which includes a Precambrian gneissic basement and the structurally overlying Paleozoic–Paleocene sediments metamorphosed at greenschist to amphibolite-facies conditions; and Lycian Nappes which consist of Mesozoic sedimentary sequences and a peridotite thrust sheet (Piper *et al.*, 2002; Bozkurt and Oberhänsli, 2001 and references therein).

1.6.1. Origin of the Neotectonic Regime

Aegean Extensional Province (AEP) is a typical locality of an extensional deformation associated with the vast orogenic Alpine-Himalayan belt (Figure 1.3). Many studies have been conducted in this province for more than two decades focusing on the cause of tensional stress field and the consequential seismic activity (e.g. Jackson and McKenzie, 1984; Eyidoğan and Jackson, 1985; Ambrasseys, 1988; Taymaz *et al.*, 1991; Seyitoğlu and Scott, 1991, 1992; Taymaz, 1993; Le Pichon *et al.*, 1995; Reilinger *et al.*, 1997; Ambrasseys and Jackson, 1998; Altunel, 1999; Koçyiğit *et al.*, 1999a, b; McClusky *et al.*, 2000; Bozkurt, 2001; Koçyiğit, 2005; Bozkurt and Mittwede, 2005 and the references therein). Consensus is well established on the fact that western Anatolia is currently extending in ~N-S direction at a rate of ~30-40 mm/year (Oral *et al.*, 1995; Le Pichon *et al.*, 1995). However, what causes this extension and when this extension started has remained as controversial issues for many years now despite the large number of studies carried



EXPLANATIONS













- | | | | |
|-------------------------------------------------------------------------------------|---------------------------------------|--------------------------------------------------------------------------------------|-----------------|
|  | Central Anatolian Crystalline Complex |  | İSTANBUL ZONE |
|  | Menderes Massif |  | SAKARYA ZONE |
|  | Bornova Flysch Zone |  | STRANDJA MASSIF |
|  | Tavşanlı Zone |  | suture zone |
|  | Afyon Zone |  | thrust belt |
|  | Elmalı Nappes | | |
|  | Beydağı Autochthone | | |
- TAURIDE ANATOLIDE PLATFORM**

Figure 1.4. Simplified tectonic map illustrating the main Tethyan sutures and neighboring tectonic units of western Turkey. Modified from Okay and Tüysüz (1999).

out in the region. Available literature addresses several different models as the cause of Aegean extension.

The first model suggested that the subduction process along the Aegean-Cyprian subduction zone is the main control on the Aegean extension. Roll-back process of the subducting African Plate and resulting south-southwestward migration of the Aegean arc given rise to an extensional regime in the back-arc region (Figure 1.3). This led to general subsidence of Aegean Sea and the formation of present day AEP (McKenzie, 1978b; Le Pichon and Angelier, 1979, 1981; Jackson and McKenzie, 1988; Meulenkamp *et al.*, 1988, 1994). Nevertheless, proposals about the inception date of subduction, rollback process and the consequential extension are controversial. Proposed timing for initiation of the subduction includes 5 Ma – 10 Ma (McKenzie, 1978a; Mercier, 1981), 13 Ma (Le Pichon and Angelier, 1979), 29-36 Ma (Thomson *et al.*, 1998) and 60 Ma. It is a fact that, the initiation of extensional regime has to postdate the initiation of subduction because back-arc extension has followed roll-back of subducting slab and south-southwestward migration of the Aegean arc. Hassani *et al.* (1997) numerically modeled that minimum slab length of 300 km is required to provide sufficient forces to drive roll-back process and the resulting back-arc extension. Conformable with this requirement, Meulenkamp *et al.* (1988) suggested 26 Ma for the initiation of subduction and 12 Ma for the onset of extension across the AEP. Beyond all these arguments regarding to timing, there is still not a single, widely accepted model explaining the mechanisms of back-arc extension (Mantovani *et al.*, 2001).

In another model, Dewey and Şengör (1979) proposed that AEP formed as a consequence of the westward motion or escape of the Anatolian microplate from the east Anatolian convergence zone by dextral NAFS and sinistral EAFS (Figure 1.3). The westward escape of the Anatolian wedge is being obstructed by southwesterly bend in the course of the NAFS system in Aegean Sea and Greece (Şengör *et al.*, 1985). This obstruction results in E–W shortening, which can be relieved in the form of N–S extension by lateral spreading (N–S in this case) of the continental material onto the oceanic lithosphere of the eastern Mediterranean (Şengör *et al.*, 1985). As a critical guide in the westward extrusion of the Anatolian microplate, formation of NAFS in late Serravallian (~12 Ma) is probably coincident with the initiation of the tectonic escape and the consequential extension of AEP (Barka and Hancock, 1984; Şengör *et al.*, 1985). On the other hand, recent work on the NAFS proposed that age

of the fault system is Pliocene and much younger than the ~12 Ma (Barka and Kadinsky-Cade, 1988; Koçyiğit, 1988, 1989; Westaway, 1994; Koçyiğit *et al.*, 2000). This age assignments together with the evidence of extensional strain before ~12 Ma limits the plausibility of the escape model for the AEP, since NAFS postdates the initiation age of extension (Le Pichon and Angelier, 1979; Jolivet *et al.*, 1994; Le Pichon *et al.*, 1995). Mantovani *et al.* (2002) contradicts this argument and supports the tectonic escape model by suggesting that Anatolian microplate and Pontides were migrating as a single block during the Early–Middle Miocene period. NAFS formed as a right-lateral guide of the tectonic escape in Late Miocene due to decreased mobility of Pontides with respect to Anatolian microplate following to collision of Carpathian arc with Eurasia (Şengör, 1993; Mantovani *et al.*, 2002).

Because of the limitations that the back-arc extension and the tectonic-escape models hold, the post orogenic collapse model was erected by Dewey (1988) as the cause of extension in AEP. The post orogenic model requires an orogenic belt with an over-thickened crust where body forces resulting from isostatically compensated elevation exceeds the compressional tectonic forces forming the orogenic belt (Dewey, 1988). This crustal thickening, further supported by structural inhomogeneities and thermal anomaly of the lithosphere, creates an extensional stress field and promotes rifting (Dewey, 1988). In other word, orogen starts to collapse under its own weight. Şengör *et al.* (1985) suggested that, following the Paleocene–Eocene collision across the northern branch of Neotethys, a crustal thickness of 65–70 km was probably reached in western Turkey. This crustal configuration could be the potential trigger of the extension in the region. Consequently, post orogenic collapse model, encouraged by field evidence in western Anatolia, supported by many researchers following the first proposal by Dewey (1988) (e.g., Seyitoğlu and Scott, 1991; Bozkurt and Park, 1994; Collins and Robertson, 1998; Ring *et al.*, 1999; Koçyiğit *et al.*, 1999a, b; Yılmaz *et al.*, 2000).

Most recent researches focusing on western Anatolia employs episodic extensional models as none of the models described above explain the cause and timing of the extension in a satisfactory manner. These models based on combination of the two or more of the above-mentioned models that operate during separate time intervals. The pioneering work of Koçyiğit *et al.* (1999a, b) defined a two stage extensional model with an intervening phase of short-term contraction in the region. According to this model, the first phase of extension started with Early Miocene and

was driven by orogenic collapse along the İzmir-Ankara suture (Figure 1.4). Then, it was substituted by a short phase of ~N–S contraction in Late Miocene–Early Pliocene interval, possibly related to a change in the plate kinematics of the Eurasian and African plates (Koçyiğit *et al.*, 1999a, b). In Late-Early Pliocene, Anatolian micro-plate and its boundary structures, NAFS and EAFS formed and the westward escape initiated (Figure 1.3). This brought along the second phase of N–S extension, which might further enhanced by the subduction roll-back process at Mediterranean-Cyprian arc (Koçyiğit *et al.*, 1999a, b). Following to this initial proposal, field evidence provided by multiple studies supported this episodic model (Bozkurt, 2000, 2001, 2003, 2004; Yılmaz *et al.*, 2000; Sözbilir, 2001, 2002; Cihan *et al.*, 2003; Bozkurt and Sözbilir, 2004, 2006; Purvis and Robertson, 2004, 2005; Kaya *et al.*, 2004; Bozkurt and Rojay, 2005; Beccaletto and Stenier, 2005; Westaway *et al.*, 2005).

Yılmaz *et al.* (2000) proposed a slightly different insight for the episodic evolution of western Anatolia. According to this view, Early–Middle Miocene period in western Anatolia is characterized by N–S oriented contractional regime that is related to the continuing convergence of continental fragments along the İzmir-Ankara suture zone (Figure 1.4). Following to this period of convergence, N–S extension began during Late Miocene time, possibly with the contribution of post orogenic collapse processes. The N–S extensional regime was interrupted by Late Miocene–Early Pliocene (?) quiescent period. Then, N–S extensional regime was rejuvenated again by Pliocene to establish the present day neotectonic configuration (Figure 1.3). Tectonic escape of the Anatolian microplate, which began during Late Miocene–Early Pliocene period may be responsible for the beginning of neotectonic period (Yılmaz *et al.*, 2000).

There is also a model claiming that the current extension in the AEP is related to the differential rate of convergence between the subducting African Plate and the overriding plate. Faster southwestward movement of Greece compared to Anatolian microplate causes extension in AEP (Doglioni *et al.*, 2002). Furthermore, modeling of the block rotations that are based on the palaeomagnetic studies provide important clues to the evolution of the Neotectonic regime in the Aegean region (Gürsoy *et al.*, 2003; Kissel *et al.*, 2003) and any viable model should satisfy the results of these studies as well.

Although earlier studies emphasized 30° longitude as the easternmost limit of the AEP in western Anatolia (Şengör et al., 1985), recent studies documented field evidence for more extensive area, which is influenced by the Neotectonic extensional deformation (Koçyiğit and Özacar, 2003; Koçyiğit, 2005) (Figure 1.3). İnönü–Eskişehir Fault Zone (İEFZ), Salt Lake Fault Zone (SLFZ) and Central Anatolian Fault Zone (CAFZ) apparently bound the eastern margin of the AEP (Koçyiğit and Özacar, 2003) (Figure 1.3).

1.7. Regional Geology

As usual response to continental extension, graben basins and intervening horst blocks are widespread neotectonic elements of western Anatolia. While the graben basins are filled with Neogene to recent strata, horst blocks expose lithologies belonging to amalgamated continental fragments of the Anatolian microplate (Figure 1.5). This horst-graben architecture manifest itself at two dominant structural direction as ~E–W-trending grabens and NE–SW-trending basins and intervening horst blocks (Figure 1.5). ~E–W-trending grabens are more prominent geological features than the other and include Bakırçay, Gediz, Kütahya, Simav, Küçük Menderes and Büyük Menderes grabens. These grabens are site of continental deposition by currently active alluvial and fluvial processes (e.g., Koçyiğit *et al.*, 1999a, b; Yılmaz *et al.*, 2000; Bozkurt, 2004; Koçyiğit, 2005). On the other hand, rising sea level of Aegean about 120 m during last 21.5 Ka (Perissoratis and Conispoliatis, 2003) probably resulted in marine flooding of gulfs of Edremit, Çandarlı, and Gökova, which are currently sites of shallow marine clastic deposition. The boundary structures of the ~E–W-trending grabens are seismically active and are associated with many historical and recent earthquakes with magnitudes reaching up to 7.1 (Ambraseys and Jackson, 1998; Altunel, 1999; Bozkurt, 2004; Koçyiğit, 2005). Although approximately E–W-oriented extension can be inferred for the Gediz Graben, extensive studies on the fault kinematics suggest variation of the extension direction along the graben (e.g., Zanchi et al., 1993; Temiz et al., 1998).

The age of ~E–W-trending grabens are controversial. Earlier studies suggest Tortonian age in relation to initiation age of NAFS (Şengör and Yılmaz, 1981; Şengör *et al.*, 1985; Şengör, 1987). Based on the oldest Neogene sediments exposed along the margins of the Gediz and Büyük Menderes grabens, a group of researchers claims Early Miocene as the onset age of the graben formation (Seyitoğlu and Scott,

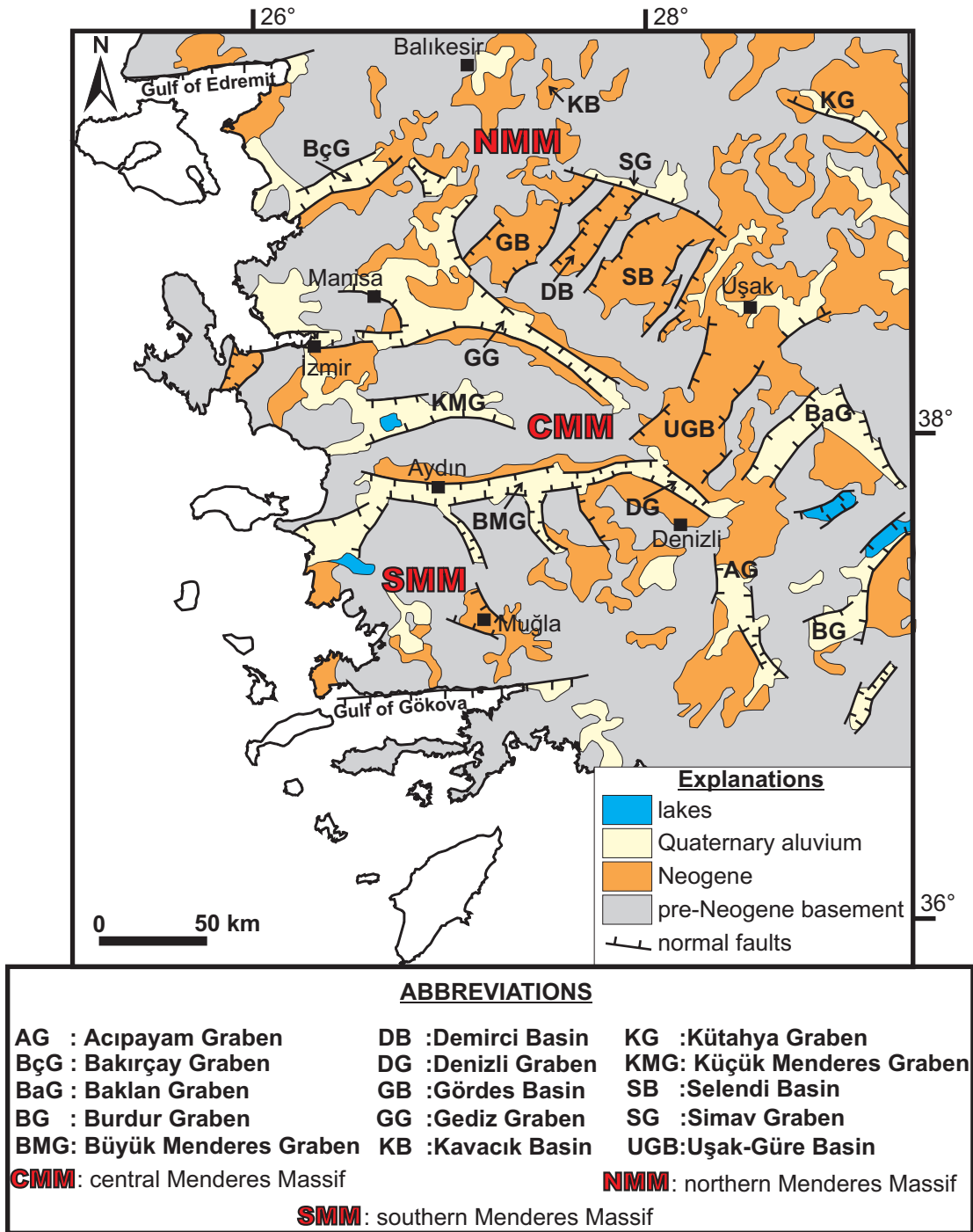


Figure 1.5. Simplified geological map of SW Turkey showing the distribution of ~E–W-trending and NE–SW-trending neotectonic basins. Subdivisions of Menderes Massif are also illustrated. From Bozkurt (2000).

1991, 1992, 1996; Seyitoğlu *et al.*, 2002; Gessner *et al.*, 2001). The other group proposed that these sediments are not genetically related to the ~E–W-trending modern grabens, which started in or later than 5 Ma (Koçyiğit *et al.*, 1999a, 1999b, 2000; Bozkurt, 2000; Sarıca, 2000; Yılmaz *et al.*, 2000; Koçyiğit, 2005).

The NE–SW-trending basins are recognizable on the geological maps as NE–SW oriented stripes of Neogene/Quaternary sediments separated by intervening highlands exposing pre-Neogene basement (Figure 1.5). These basins preserve strong parallelism among each other and are oriented at high angle (~ 60-70°) to the ~E–W-trending grabens. They seem to be concentrated immediately north of the Gediz Graben and south of the Büyük Menderes Graben. The best developed of these includes Gördes, Demirci, Selendi and Uşak-Güre basins immediately north of the Gediz Graben (Figure 1.5). Seismic activities associated with the bounding structures of these grabens are not as pronounced as compared to ~E–W-trending grabens (McKenzie, 1978b; Eyidoğan and Jackson, 1985). Kaya (1979, 1981) identified numerous NNE-trending blocks south of Bakırçay Graben separated by steep oblique slip faults. These faults have both normal and reverse separation associated with considerable left lateral strike slip component. Similarly, NW–SE-trending right-lateral strike slip fault zone was recently documented at the northwestern continuation of the Gediz graben as the further evidence of wrenching in the region (Kaya *et al.*, 2004). Similar strike-slip faulting is also well-documented along the Manisa Fault (Bozkurt and Sözbilir, 2006).

The origin of NE–SW-trending basins has been a subject of controversy for many years. By some researchers, these basins are regarded as palaeotectonic Tibet-type grabens that formed under N–S compression following the closure of Northern branch of the Neotethys (Şengör *et al.*, 1985; Şengör, 1987; Yılmaz *et al.*, 2000). Others claim that NE–SW-trending basins are synchronous with the ~E–W-trending grabens and are the product of neotectonic N–S extension of the AEP (Seyitoğlu and Scott, 1991, 1992; Collins and Robertson, 1998). In another view, these grabens were described as basins controlled by cross accommodation faults on the hanging wall of presently low-angle, north-dipping normal fault (detachment fault) bounding the southern margin of the Gediz Graben (Şengör, 1987; Bozkurt, 2003).

1.7.1. Straigraphy

The rock units exposing in the western Anatolia can simply be classified into two groups as basement and cover units. For most grabens, metamorphic rocks belonging to Menderes Massif constitutes the pre-Neogene basement and exposes extensively over the horst blocks rising up to ~2000 m elevation between the graben basins. Within the graben basins, pre-Neogene basement lies unconformably underneath the graben-fill. This fill varies in age from Miocene to Recent and forms the cover units.

Menderes Massif forms a NE–SW-trending, large, elongate (300x200 km), crustal-scale metamorphic culmination and represents the Alpidic orogen in western Turkey (Bozkurt and Oberhänsli, 2001 and references therein). The massif is separated into three portions as northern, central and southern submassifs, by means of Gediz and Büyük Menderes grabens (Figure 1.5). It consists of core and cover lithologies which can be analyzed in a broad tripartite lithological succession (Bozkurt and Oberhänsli, 2001). The gneiss core at the base is composed of augen gneisses, metagranites, high-grade schists, and metagabbros with eclogite relics (e.g., Gessner *et al.*, 2001; Bozkurt and Oberhänsli, 2001). The cover rocks includes schist and marble envelopes. The schist envelope includes quartzo-feldspathic gneisses, psammitic gneisses, mica schists, quartzites, garnet amphibolites, ‘augen’ schist, phyllites and limestone intercalations (e.g., Bozkurt and Oberhänsli, 2001 and references therein). Above the schist envelope, marble envelope starts with basal conglomerates and includes following rock types: (1) Upper Triassic–Liassic marbles intercalated with schist and metavolcanics; (2) a Jurassic–Lower Cretaceous thick massive marble unit with metabauxite lenses; (3) Upper Cretaceous rudist-bearing marbles intercalated locally with thin mica schists. The Menderes Massif has complex, polyphase metamorphic history; it was generated by contractional deformation and is currently experiencing N–S-oriented continental extension of the AEP (Bozkurt and Oberhänsli, 2001). The massif was also intruded by syn-extensional granites in the footwall of detachment fault (Hetzl *et al.*, 1995; Bozkurt 2004).

Neogene cover units of the western Anatolia has been studied extensively by many workers both in the ~E–W-trending grabens and in the NE–SW-trending basins (e.g. İztan and Yazman, 1991; Cohen *et al.*, 1995; Yazman *et al.*, 1998; Koçyiğit *et al.*, 1999a, b; Yılmaz *et al.*, 2000; Genç *et al.*, 2001; Seyitoğlu *et al.*, 2002; Purvis and Robertson, 2005; Koçyiğit, 2005). Although, these studies have

produced many debates about the ages of lithostratigraphic units, number of intervening unconformities and the correlation of formations, it was understood that these basins are sites of Miocene–Recent continental deposition. Laterally gradational fluvial and alluvial activities and consequential conglomerates, sandstones and mudstones constitute the predominant lithologies of the basin fills. These lithologies are commonly poorly lithified and clast/grain population points out Menderes Massif as the sediment source. Occasionally, lacustrine systems intercalates in the form of carbonaceous lithologies to indicate activities of ephemeral or short-lived lakes at distal settings to the basin margins. At some localities, the lowermost part of the basin fill is characterized by thick section of bituminous shales and coals and suggest that earlier phases of basin development has taken place under swamp to lacustrine conditions.

Along the southern margin of Gediz Graben and northern margin of Büyük Menderes Graben, presently inactive, low-angle normal faults (detachments) constitutes the contact between the cover and basement lithologies. These structures controlled the exhumation of Menderes Massif and had important implications on the formation of the grabens. The cover units of the Gediz Graben exposing on the hanging-wall of the presently inactive, low-angle normal fault(s) will be discussed in detail in Chapter 2.

1.7.2. Structural Geology

Various (different) geological structures can be recognized within the deformation pattern of the western Anatolia. Nevertheless, the most striking structure is the major, low-angle (0-20°), north dipping, normal fault(s) bounding the southern margin of the Gediz graben. The fault separates metamorphic rocks in the footwall from continental sediments over the hanging wall and imply that it has played a significant role in the rapid exhumation of the Menderes Massif (e.g., Hetzel *et al.*, 1995; Emre, 1996; Koçyiğit *et al.*, 1999a, b; Bozkurt, 2000; Yılmaz *et al.*, 2000; Bozkurt and Oberhansli, 2001; Işık *et al.*, 2003; Bozkurt, 2004; Bozkurt and Sözbilir, 2004). The footwall rocks exhibits a structural sequence typical of extensional shear zones. In an ascending order, a sequence of mylonite, brecciated mylonite and cataclasites are observable (e.g., Hetzel *et al.*, 1995; Emre, 1996; Bozkurt and Oberhansli, 2001; Işık *et al.*, 2003; Bozkurt and Sözbilir, 2004). The hanging wall is dominated by coarse clastics derived directly from the underlying metamorphics of the footwall.

Controversy arises for the original attitude of the low-angle normal fault whether it was originally a low-angle structure (Hetzl *et al.*, 1995) or a high-angle normal fault (48–53°), which progressively rotated to lower angles in response to the flexural response of the footwall (Bozkurt, 2000; Gessner *et al.*, 2001; Seyitoğlu *et al.*, 2002). In a different view, it was suggested that this structure was originally a thrust fault and then reactivated as normal fault with the emergence of neotectonic extensional regime (Lips *et al.*, 2001; Bozkurt, 2001). Studies carried out in the region have documented presence of similar low-angle normal faults along the northern margin of Büyük Menderes Graben, in the southern and northern Menderes Massifs (Bozkurt and Park, 1994, 1997; Emre and Sözbilir, 1997; Bozkurt, 2000, 2001; Gessner *et al.*, 2001; Özer and Sözbilir, 2003).

Based on the character of seismic events and large and diffuse area of epicenter distribution in western Anatolia, particularly to the north of Gediz Graben, Şengör (1987) has reasoned the existence and activity of low-angle, major normal fault underlying most of the region. However, most recent studies in the Gediz Graben emphasized the inactivity of the exposed low-angle normal fault, which is cut and displaced by younger, high-angle normal faults of the present day grabens (Emre, 1996; Koçyiğit *et al.*, 1999a, b; Yılmaz *et al.*, 2000; Bozkurt, 2004; Bozkurt and Sözbilir, 2004). Yet, this does not rule out the possibility of and it can be still a valid approach to consider an active deeper detachment fault to the north of the Gediz Graben, which is kinematically not connected with the exposed detachment to the south of the Gediz Graben.

Fault systems bounding the ~E–W-trending grabens are observable at approximately E–W to WNW–ESE or ENE–WSW-orientations (Figure 1.5). They either occur as single faults with lengths varying from sub-kilometers to tens of kilometers, or as sets composed of discontinuous, mostly synthetic, and parallel to sub-parallel segments. Graben-facing step-like pattern is very common by first order major- and second-order synthetic and antithetic faults, with younging direction towards the graben floor (Cohen *et al.*, 1995; Koçyiğit *et al.*, 1999a, b; Seyitoğlu *et al.*, 2002; Bozkurt and Sözbilir, 2004). Well-preserved slip planes indicate the activity of the fault system in which predominantly normal-slip with usually minor strike-slip component is observable. Linear coalesced alluvial fan aprons are commonly associated with this fault system as an indication of their accommodation creation potential. Actively growing travertines, hot water springs, shifting/bending

of river courses and ground ruptures of historical earthquakes (e.g., 1969 Alaşehir Earthquake, Eyidoğan and Jackson, 1985) were illustrated as further evidence of fault activity (Koçyiğit *et al.*, 1999a, b). This fault system cuts and displaces the low-angle normal fault, which is interpreted as the superimposition of the neotectonic style of deformation over the older style related to exhumation of the Menderes Massif (Bozkurt and Sözbilir, 2004).

The NE–SW-trending fault system bounds the NE–SW-oriented basins and strikes at high angle to major, low-angle normal fault and the ~E–W-trending, steep normal faults (Figure 1.5). Best developed ones of these are observable immediately north of the Gediz Graben up to the Bakırçay and Simav grabens to the north. They divide the area into NNE-trending basins with intervening high blocks having less prominent basin margins compared to ~E–W-trending grabens. Preserved slip-planes are relatively rare in this system and commonly indicates oblique-slip movement (Şengör, 1987). Limited fault data from Demirci and Çubukludağ basins illustrate predominantly strike-slip movement with minor normal component (Yılmaz *et al.*, 2000; Genç *et al.*, 2001). The faults of the system also lack major earthquakes (Şengör, 1987). It was suggested that, these faults were formed over the hanging-wall of the low-angle normal fault as cross-accommodation faults in order to compensate the differential stretching within the hanging wall (Şengör, 1987; Bozkurt, 2003).

Folds are common structures reported for some parts of the Neogene deposits of western Anatolia (Koçyiğit *et al.*, 1999a, 1999b, 2000; Seyitoğlu *et al.*, 2000; Sözbilir, 2001, 2002; Koçyiğit and Özacar, 2003; Bozkurt, 2003; Bozkurt and Sözbilir, 2004; Koçyiğit, 2005). Koçyiğit *et al.* (1999a, b) showed that Miocene–Lower Pliocene sedimentary units is folded in the Gediz Graben. A series of plunging to non-plunging anticlines and synclines with parallel to sub-parallel curvilinear axes occur in the graben with lengths ranging from few km to 30 km. They commonly trend sub-parallel to the graben-bounding marginal faults although those of oblique relation do exists (Koçyiğit *et al.*, 1999a, b; Seyitoğlu *et al.*, 2000). The origin of the folds in the Gediz Graben is debated whether they represent a short phase of N–S contraction or they were the products of normal fault-related folding mechanisms (Koçyiğit *et al.*, 1999a, b; Seyitoğlu *et al.*, 2000, 2002; Bozkurt, 2002; Yusufoglu, 2002). Bozkurt (2003) also documented folds within Neogene fill of the NE–SW-trending basins with fold axis trending parallel to the basin margins.

CHAPTER 2

STRATIGRAPHIC FRAMEWORK AND DEPOSITIONAL SYSTEM OF THE NEOGENE DEPOSITS

Neogene stratigraphy of the Gediz Graben has been the focus of many studies since the early 90's (İztan and Yazman, 1991; Cohen *et al.*, 1995; Yazman *et al.*, 1998; Koçyiğit *et al.*, 1999a; Yılmaz *et al.*, 2000; Seyitoğlu *et al.*, 2002; Purvis and Robertson, 2005). These studies have produced number of formation names, controversial age assignments and different facies models for the same deposit, devising the need for major refinement of the established stratigraphy. Figure 2.1 illustrates correlated summary of the stratigraphic units defined by various researchers in the Gediz Graben. The main reason for the inconsistency among the stratigraphic columns is the fact that the graben fill shows important lateral variations in facies and age along the graben. Unfortunately, most workers underestimated the relationship between the lateral variation of the graben fill and spatiotemporal evolution of the graben. Consequently, other mechanisms such as multiple stages of basin formations (e.g., İztan and Yazman, 1991; Yılmaz *et al.*, 2000) were invoked to explain the observed lateral variations of the graben fill. However, dynamics of the graben formation and graben evolution certainly had some implications on the spatial variations of the Neogene strata. Such variations need to be assessed carefully and may provide useful clues to the temporal and spatial evolution of the graben and particularly the graben-bounding fault system(s). It is therefore indispensable to establish the mutual relationship between basin margin evolution and resultant stratigraphic architecture. Although it is not the main focus of this dissertation to address all problems of stratigraphic framework of the graben fill, this study needs a working stratigraphic model to understand the tectonic evolution of the basin. Thus, it depends on geological mapping, measured stratigraphic sections, borehole data (rock cuttings and Gamma Ray logs) from three exploration wells and 2-D seismic

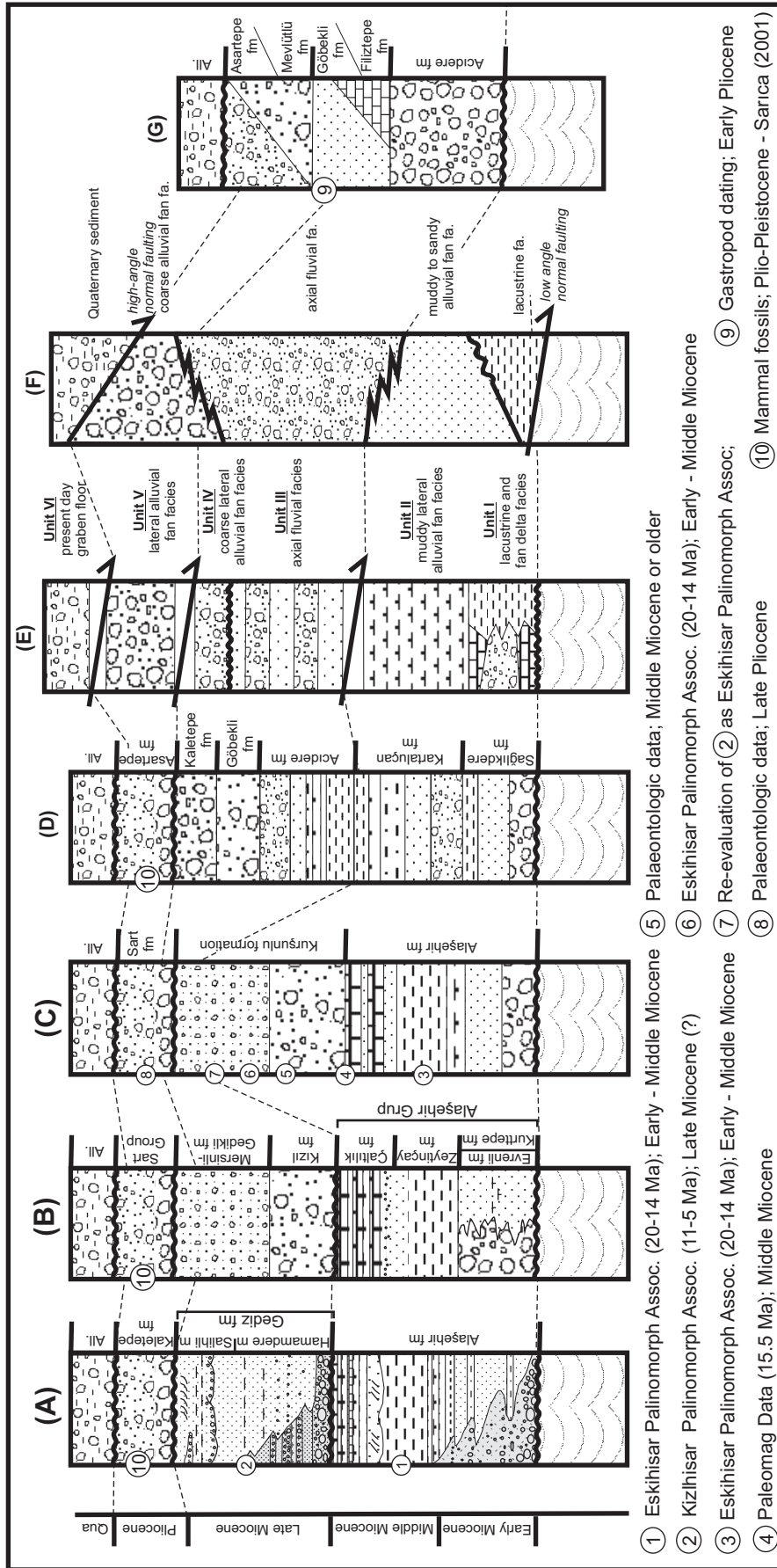


Figure 2.1. Neogene stratigraphy of the Gediz Graben documented by various researchers. Available age data are also illustrated on each column. Age data were derived from the associated study. Note the controversy among the stratigraphic columns and given ages. Dashed lines depict approximate correlations. Abbreviations - fm: formation; fa.: facies association. (A) Yazman et al., 1998, (B) Yilmaz et al., 2000, (C) Seyitoğlu et al., 2002 (D) Koçyiğit et al., 1999a, (E) Cohen et al., 1995, (F) Purvis and Robertson, 2005. (G) Emre, 1996. Note that stratigraphic columns (A) to (F) represents Alaşehir area whereas (G) is based on the data from Salihli area. Arrows in (E) and (F) illustrates fault contacts.

reflection profiles in order to refine the available stratigraphic models of the graben, particularly for the Alaşehir area. Following this initial focus on the stratigraphy by this chapter, stratigraphic architecture of the graben fill will be related to the evolution of the margin bounding structure(s) of the graben in the following chapters.

The rock units exposed in the Gediz Graben can be divided into two groups as the basement and the cover units (Figure 2.2). The basement is composed completely of crystalline metamorphic rocks and predates the Neogene evolution of the graben. The graben evolution has been associated with the sedimentary Neogene cover that was deposited under the control of active normal faulting during the graben formation. As a result, this chapter focuses only on the stratigraphic framework of the cover units.

2.1. Lithostratigraphic Framework of the Graben Fill

The cover units of the Gediz Graben around the Alaşehir area comprise Miocene to Recent continental clastic rocks that were accumulated in lacustrine, alluvial and fluvial depositional environments (Figure 2.2). These clastic rocks either lie unconformably over or they have faulted contact with the basement rocks (Figures 2.2 and 2.3). The faulted contacts have variable dip amounts (as high as 60° for younger structures to as low as 10° for older structures) implying some degree of fault rotation. The cover unit is predominantly exposed along the southern margin of the graben where the most active master graben-bounding normal fault (e.g., MGBF) is located (Figure 2.3). The exposures along the northern margin exhibit much less lithological variations and shorter period of deposition compared to the southern margin (Figure 2.3). Volcanic rocks are also exposed in a small area along the northern margin. As a representation of the Neogen volcanism, this exposure suggests a relatively minor volcanic activity in the Gediz graben compared to the extensive Neogene volcanic activity observed to the north of the Gediz Graben in north western Anatolia (e.g., Çiftçi et al., 2004).

Ten different lithostratigraphic units were mapped in the study area around Alaşehir (Figure 2.3). These units include metamorphic basement, five Neogene lithostratigraphic formations, a Neogene subvolcanic body and various types of Quaternary deposits. The lithological characteristics of the Neogene formations were documented by means of 9 stratigraphic sections logged at various locations along the southern margin (Appendix I). Basic facies analysis was carried out to define

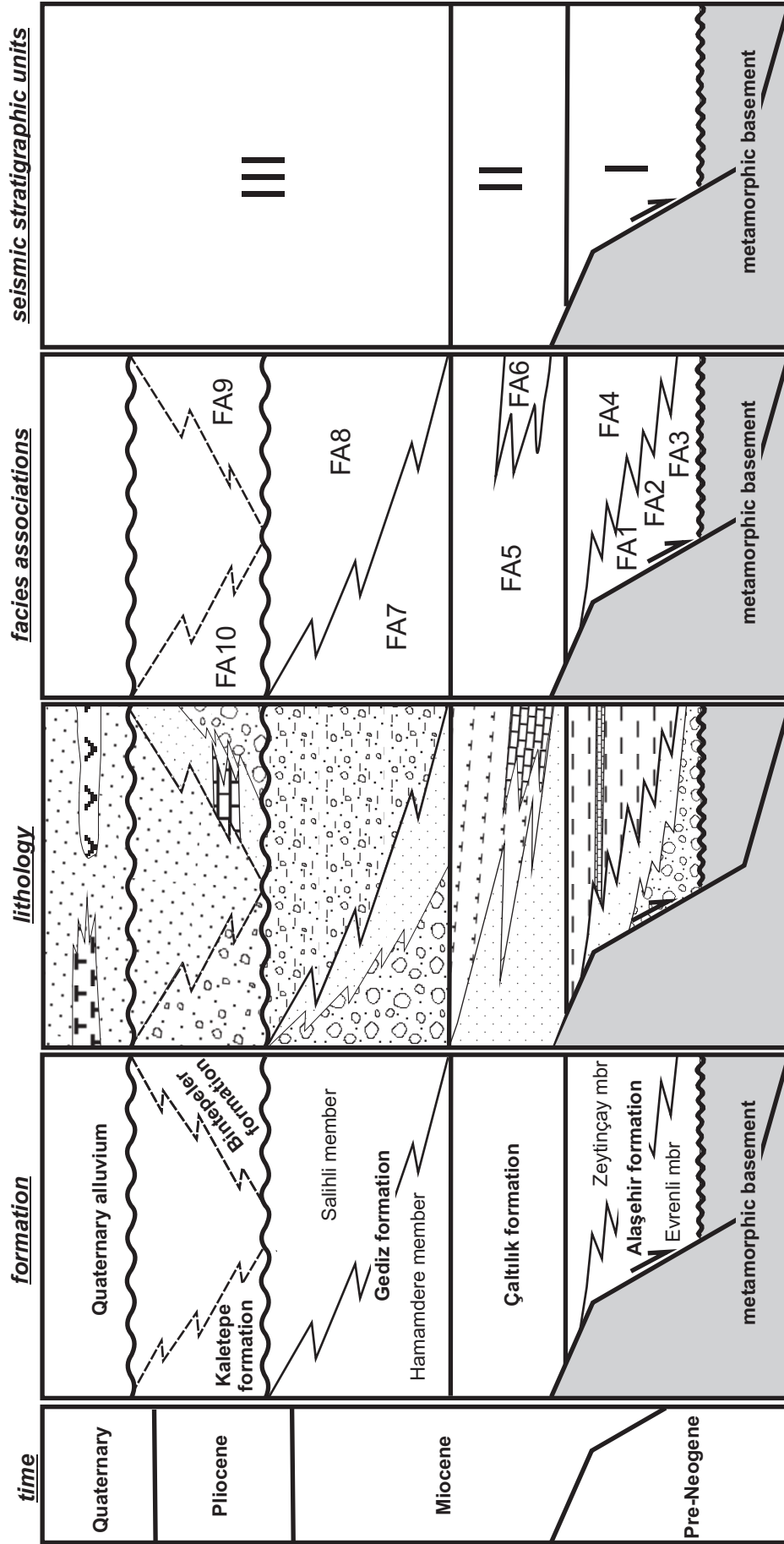


Figure 2.2. Neogene stratigraphy of the Gediz Graben based on the geological data around Alaşehir. Figure briefly depicts the relationship between the lithostratigraphic units, associated lithologies, governing depositional environments and interpreted seismic stratigraphic units. See text for detailed discussion on the figure. Description of facies associations and constituent facies are given through Table 2.1 to Table 2.8.

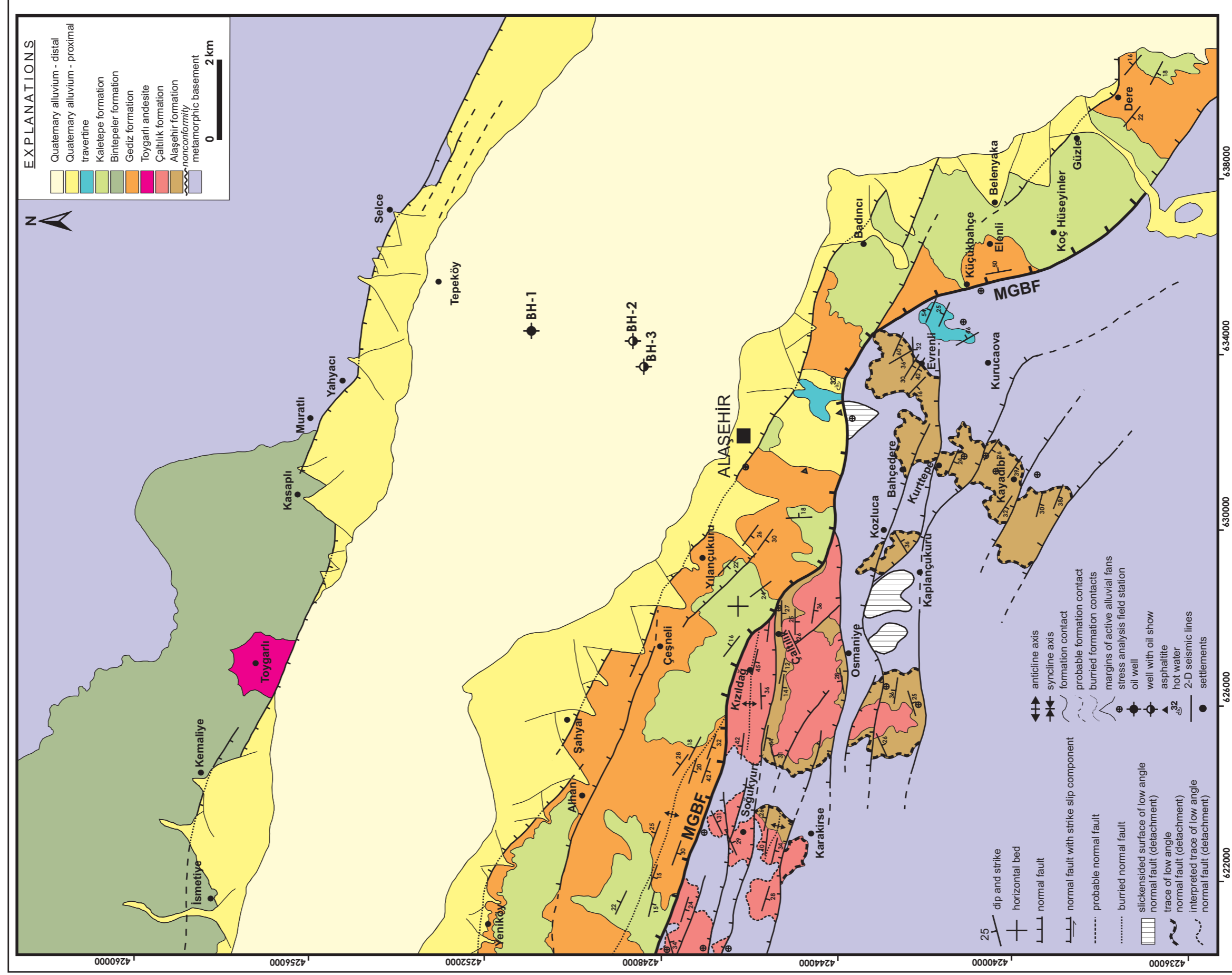


Figure 2.3. Geological map of the study area around Alaşehir showing major structures and mapped geological units. Abbreviations: MGBF, master graben bounding fault; BH: borehole.

facies associations and governing depositional environments of different lithologies. It should be kept in mind that the graben fill may show some along-strike variations in terms of lithostratigraphic units and their ages. For example, stratigraphic framework documented in Figure 2.2 for the Alaşehir area may not be identical to that of Salihli area (Figure 2.1G). This variation is related to the segmented evolution of the Gediz Graben, which will be further discussed in Chapter 5 and Chapter 7.

2.1.1. Alaşehir Formation

The Alaşehir formation is the oldest Neogene unit exposed along the southern margin of the Gediz Graben (Figures 2.2 and 2.3). The formation is only locally exposed in the vicinity of the Alaşehir. Therefore, the name Alaşehir formation is properly assigned to the unit by Yazman and İztan (1990). Later, the name Alaşehir group was adapted by Yılmaz *et al.* (2000).

Traditionally, the Alaşehir formation is defined as a fining upward succession, which starts with cobble pebble conglomerates at the base (Figure 2.1A, B and C). These basal conglomeratic facies, which were interpreted as fault scree and alluvial fan deposit (cf. Yazman *et al.*, 1998; Yılmaz *et al.*, 2000), is differentiated as a lithostratigraphic member of the Alaşehir formation and named as Hacíveliler member (Yazman and İztan, 1990), Kayadibi member (Yazman *et al.*, 1998) and Evrenli formation of the Alaşehir group (Yılmaz *et al.*, 2000). Laterally, these coarse conglomerates display rapid gradual transition to sand-rich facies and then to shale-marl-dominated facies (Figure 2.2). The sand-rich and shale-marl-rich deposits were differentiated in the formation rank by Yılmaz *et al.* (2000) and named as Kurtepe formation and Zeytinçay formation of the Alaşehir group, respectively. Yazman and İztan (1990) defined these two formations as a single unit in the member rank, comprising monotonous alternation of sandstones, siltstones and shales that are rich in organic content. These finer detrital deposits were interpreted as lacustrine facies (Yazman and İztan, 1990; İztan *et al.*, 1991; Cohen *et al.*, 1995; Yazman *et al.*, 1998; Purvis and Robertson, 2005) and named as the Evrenli member of the Alaşehir formation (Yazman and İztan, 1990).

This study favors Yazman and İztan (1990) definition of the Alaşehir formation. The main reason for this simplified approach is the fact that the exposures of the Alaşehir formation has limited spatial extend and defining more than one formation out of this limited exposure will only contribute to the confusion on the

available stratigraphy of the region (Figure 2.1). As a result, the lithological variations within the Alaşehir formation are treated in the member rank as coarser-grained Evrenli and finer-grained Zeytinçayı members after their best exposures around Evrenli village and Zeytinçayı creek, respectively (Figure 2.2).

Four geological sections were measured through the Alaşehir formation to document its lithological characteristics (Appendix I). The sections are located in the Zeytinçayı creek around Osmaniye (MS-I), along the Alaşehir–Evrenli road near Evrenli (MS-II), near Kayadibi village (MS-III) and along the Soğukyurt-Karakirse road (MS-V) (Appendix I). In each section, sedimentary facies were defined based on lithology, primary sedimentary structures and grain size (Table 2.1 and Appendix I). The lithofacies diversity, which is defined by 19 different facies, was grouped into 4 main facies associations (Tables 2.1 and 2.2). These facies associations are directly linked to the depositional environment of the Alaşehir formation (Figure 2.4). The lithological variations reflected by these four different facies associations are used to define two members of the Alaşehir formation.

Alluvial Fan Facies Association (FAI)

This facies association is characterized by the relative abundance of facies Cm, Sp, Gms, Stl and Gtx (See Table 2.1 for detailed description of the facies). The association is best observed along the MS-II where the lower 60 meters of the section is characterized by conglomerates that are intercalated with pebbly sandstones (Appendix I). The conglomerates are thick bedded to massive, poorly sorted, generally internally chaotic and structureless, have sharp and erosive base with irregular tops suggesting debris flow processes for the deposition of the facies (cf. Nilsen, 1982; Miall, 1996; Collinson, 1996). The clasts are derived from basement metamorphic rocks and range in size from coarse sand in the matrix to 5-meter-large blocks as clast. Polimictic clast population includes gneiss, phyllite, schist, marble and chert. Crude clast imbrication is indicative of N–NE-directed palaeocurrents. Intercalated pebbly sandstones and laminated siltstones may indicate water laid deposits that may have formed during the flood flows (cf. Nemeč and Steel, 1984; Nilsen, 1982). Similar conglomerate-rich facies were also observed at the lowermost 30–40 meters of the MS-III. At the base of the section, these conglomerates directly overly the metamorphic basement rocks along a north dipping, slickensided, low-angle fault plane (Figure 2.5).

Table 2.1. Dominant facies, facies descriptions and interpretations of the Alaşehir formation. Some of the lithofacies and interpretations are modified from Miall (1985). See Appendix I for the related measured stratigraphic sections.

	Description	Interpretation
Cm, massive conglomerates	massive and chaotic, polymictic, sandy to gravelly matrix supported, angular granule to cobble size clasts, sharp (and locally sheared) base, irregular top, poorly sorted, locally inversely graded, locally contains sandstone lenses	debris flow
Gtx, trough cross-bedded conglomerates	moderate to poorly medium bedded, generally lensoidal, moderately rounded and poorly sorted, moderate to poorly cemented, polymictic, coarse sand to gravel matrix supported, generally fining upward with erosive base with or without lag, trough cross bedded	channel fill
Gms, matrix-supported gravelstones	thick to massive and poorly bedded, sandy matrix supported, angular granule to pebble size clasts, poorly sorted	debris flow to hyper-concentrated flow deposits
Gr, rippled gravelly sandstones	medium bedded, sandy matrix supported, poorly sorted and rounded, rippled at the top, locally pebbly, erosive base	deposits from channelized flows
Sp, pebbly sandstones	medium and poorly bedded, moderately cemented, coarse grained, pebbly, locally FeCO ₃ nodules bearing, slightly erosive base	deposits of flash flow - sand dominated hyperconcentrated flow
Se, erosive-based sandstones	medium bedded, locally red colored, coarse sand grained, moderate to poorly sorted, cross bedded (crude), erosive base, fining upward	scour-fills
Ss, stratified sandstones	medium to thin bedded, medium-fine grained, moderately cemented, moderately sorted, FeCO ₃ nodules bearing, locally laminated,	subaqueous deposits at lower flow regime
Sfu, fining-upward sandstones	thick to massive, usually formed as a single bed, medium grained, locally laminated, fining upward, ripples at top	subaqueous deposits at lower flow regime - waning flows
Sr, rippled sandstones	medium-thin bedded, medium-fine grained, generally laminated at the lower parts of the bed and rippled at the top (wave ripples?)	subaqueous deposits at lower flow regime-oscillation
Sng, normally-graded sandstone	medium-fine grained, thin bedded, normally graded, well cemented, locally occurring in fining upward cycles	unchannelized turbidites (Hyperpycnal flows)
Sst, alternation of sandstone-siltstone	thin bedded, laminated, moderately cemented, locally sandstones with graded bedding, locally rippled and FeCO ₃ nodules bearing	deposition from turbulent flow
Ssh, alternation of sandstone-shale	thin bedded, laminated, locally convolute laminated, moderately cemented	deposition from suspension with episodic turbulent flows
Stl, laminated siltstones	thin bedded, laminated, locally sandy	deposition from suspension
Fst, alternation of shale/marl and siltstone	thin bedded, laminated, bitumous, abundant plant remnants, calcareous	deposition from suspension; generally low energy environment
Fps, paper shales	thin bedded, wavy laminated, very bitumous, abundant plant remnants	deposition from suspension; low energy environment
Fm, mudstone	laminated	channel overbank deposits – waning currents in channel
Fsm, siliceous mudstone	red colored, thin bedded, siliceous	deposition from precipitation and suspension under sediment starvation (hydrothermal source?)
C, coal-coaly mudstone	brown colored, laminated	subaerial low energy, channel overbanks – coastal plain
L, limestone	beige colored, very hard, clayey, poorly bedded	low energy

Table 2.2. Facies associations of the Alaşehir formation. See Appendix I for the related measured stratigraphic sections.

Facies Association	Constituent Lithofacies
FA1, alluvial fan facies associations	Cm, Gms, Sp, Stl, Gtx
FA2, lacustrine fan delta/delta front facies association	Ss, Sfu, Sng, Sst, Cm, Gms, Fps, Sr, Stl, Sp, Se
FA3, coastal plain marsh facies association	Fm, C, Sr, Sst, Se, Ss, Sp, Gr
FA4, lacustrine basin facies association	Fps, Fst, Sng, Ss, Ssh, Fsm, L

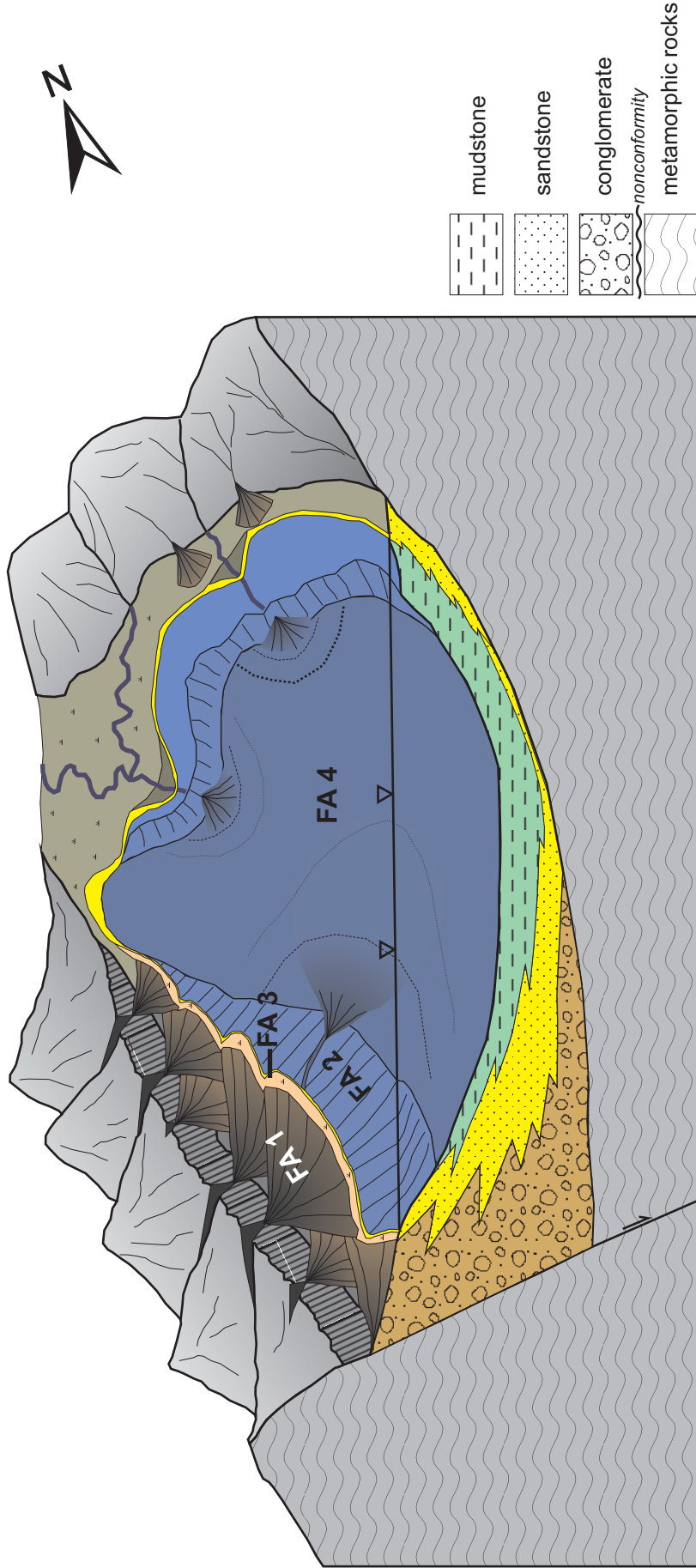


Figure 2.4. A block diagram illustrating conceptual palaeogeography of the depositional period of the Alaçehir formation (Miocene). FA 1: alluvial fan facies association; FA 2: lacustrine fan delta/delta front facies association; FA 3: coastal plain marsh facies association; FA 4: lacustrine basin facies association. See Tables 2.2 and 2.1 for the definition of facies and facies associations.

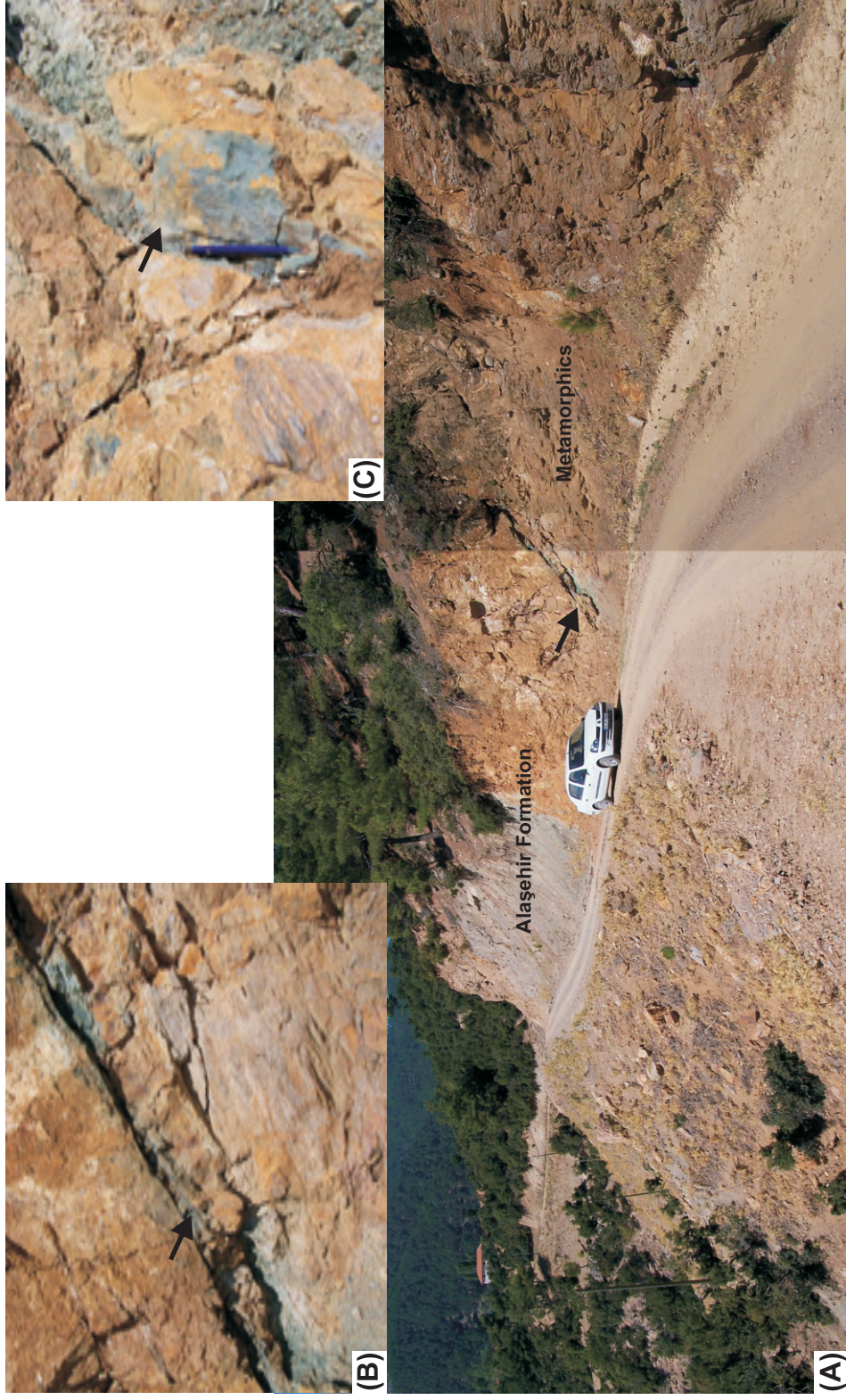


Figure 2.5. (A) Field photographs illustrating the fault contact between the Alaşehir formation and the underlying metamorphic rocks (schists) near Kayadibi village. Note that fault dips gently to the south almost paralleling the bedding plane of the overlying Alaşehir formation. (B) Close-up view of the fault zone. Note the green (chloritic) recoloration and polished surface. (C) Slickensided planes are also observable within the fault zone. Note the cataclastic deformation under the slip plane. Arrow illustrates the location of the fault zone and is located at the same place in all pictures.

The conglomeratic facies of FA1 were probably deposited on an alluvial fan in front of a highland fed from metamorphic source area. The large clast size, textural immaturity and the lack of permanent channel facies probably indicate that the distance of sediment transportation is very limited, the slope is steep and the gravity is the main agent of transportation. It can be inferred from the foregoing evidence that the relief provoking the deposition of FA1 is probably fault controlled. Considering the N–NE-directed crude palaeocurrent indicators, an orthogonal trend to the palaeocurrent direction is suspected for the controlling structure, which is approximately E–W-oriented.

Lacustrine Fan Delta / Delta Front Facies Association (FA2)

This facies association is composed of Ss, Sfu, Sng, Sst, Cm, Gms, Fps, Sr, Stl, Sp, Se facies (Tables 2.1 and 2.2). The facies association and the constituent facies are best observed in the MS-II although the facies association can also be recognized in MS-I and MS-III (Appendix I). Despite the large variation of facies; Ss, Sfu, Sng and Sst are the dominant types in this association. Intercalation of debris flow facies Cm and Gms within the FA2 probably indicates that FA1 and FA2 were in close proximity due to relatively narrow facies belts resulting in lateral gradation and interfingering among each association.

Various physical sedimentary structures are observed within the sandy facies of FA2. Horizontal lamination, convolute lamination, ripples, graded bedding and flame structures occur at various levels (Appendix I). Steady flow of currents may produce horizontal lamination under three types of condition: (1) during the plane bed phase of upper flow regime (Harms and Fahnestock, 1965); (2) under shallow flow conditions in lower flow regime by migration of low relief ripples which lack avalanche faces to prevent the formation of cross laminae (McBride *et al.*, 1975); (3) at low velocities from suspension below the critical velocity of ripple formation for particles >0.7 mm (Guy *et al.*, 1966). Simultaneous occurrence of parallel lamination and ripples in sandy facies such as Ss, Sfu and Sr probably indicates that the lower flow regime was the controlling agent of deposition in FA2 (c.f., Collinson, 1992). Graded bedding and fining-upward strata packages suggest that there were fluctuations in the hydraulic energy of the system that resulted in deposition from waning flows (e.g., Boggs, 1987; Walker, 1992; Stow, et al., 1996). Fast sedimentation rate is indicated by flame structures and convolute lamination.

Therefore, the sandy FA2 is probably deposited in fan delta/delta front environment that formed in standing body of water immediately adjacent to an alluvial fan system of FA1 (Figure 2.4).

Considering the steep slope and short distance of transportation, and very coarse grain size distribution within FA1, it is reasonable to consider that running water entering into the lacustrine basin from the high land would have been rich in coarse grained bed load and have been relatively poor in fine-grained suspended load. This normally results in formation of homopycnal flows as the running water and the standing water has close densities (Bates, 1953). Yet, hyperpycnal flows can also develop in such settings particularly during the floods and flash flows during which the running surface water became saturated by suspended load to increase its density (Bates, 1953; Walker, 1992; Stow, et al., 1996). These hyperpycnal flows may carry sediments down into the basin in the form of density flows (turbidites) given that the basin margin is steep and fault controlled (Figure 2.4).

Coastal Plain Marsh Facies Association (FA3)

The association is composed of Fm, C, Sr, Sst, Se, Ss, Sp and Gr facies varieties that are observed in the MS-II (Tables 2.1, 2.2 and Appendix I). The association is characterized by alternation of low-energy (Fm, C) and high-energy (Gr, Se) facies, indicating periodic variations of the depositional energy. Deposition of laminated mudstones (Fm) and coal (turba) probably represent marshy settings located at the low relief areas or lower reaches of the alluvial fan marginal to lacustrine basin. Periodic flooding of the vegetated wetlands or marshes by running surface waters during the high discharge periods of the alluvial system was probably responsible for the deposition of the coarser grained, high energy erosive facies such as Gr and Se by temporarily channelized flows. Fluctuations in the lake level, on the other hand, probably stabilized the marshes and expedited the deposition of coaly facies. Facies Sst, Ss and Sp probably formed as marginal facies to the temporary channels as overbank flows spreads over the interchannel marshes.

Facies observed within this association suggest that deposition probably took place at a low-relief and marshy coastal plane environment through which the subaerial coarse-grained alluvial system meets with the subaqueous deposits of the lacustrine basin.

Lacustrine basin facies associations (FA4)

FA4 is defined by Fps, Fst, Sng, Ss, Ssh, Fsm and L facies (Table 2.1 and 2.2). Fine-grained facies (Fps, Fst and Fsm) are very bitumous, tabular and horizontally laminated (warve-like). This may indicate low-energy conditions and deposition from suspension at relatively deeper parts of the basin distal to marginal fan delta complex (Figure 2.5). Disseminated and nodular pyrite occurrences probably indicate anaerobic environmental conditions (Talbot and Allen, 1996; Fouch and Dean, 1982). Occasional intercalations of facies Sng with these finer fractions may indicate peaks in the energy of the environment. Graded bedding and Bouma (1962) successions indicate the activity of turbidity currents in the deeper parts of the system. These turbidity currents can be caused by hyperpycnal flows that form during the flood stages. Alternatively, periodic activity of the margin-bounding fault system may trigger the turbidity currents by provoking the sediments that are already deposited at the steep basin margins. All these basic reasoning suggest that, FA4 indicates a deposition within the lacustrine basin generally under low-energy conditions with occasional contributions of the turbidity currents.

FA1, FA2 and FA3 described above can be grouped into a fan delta complex representing the course-grained deposits marginal to the lacustrine basin. The exposure of the fan delta complex is predominantly constraint to the E–SE of the outcrops of the Alaşehir formation (Figure 2.3). To the E–NE, deposits of the fan delta complex display obvious grain size reduction into the fine-grained facies of FA4 representing the deposits of the lacustrine basin. In this study, the fan delta complex comprising of FA1, FA2 and FA3 is named as the Evrenli member and lacustrine deposits characterized by FA4 is named as the Zeytinçay member of the Alaşehir formation, respectively (Figure 2.2).

The order of facies associations observed through the Alaşehir formation provides clues about the base level changes in the basin. Stratigraphically, the lowermost part of the formation is characterized by FA1, which represent earlier subaerial phase of deposition in the basin (MS-II and MS-III in Appendix I). The FA1 is overlain by FA2 on MS-II and MS-III that indicates deepening of the basin with transgression of the lacustrine system. Then, deposition in the basin has continued by some fluctuations in the base level that is reflected by intercalation of FA2 and FA3 in MS-II, which probably located at a close setting to the basin margin. In deeper part of the basin, same base level fluctuations have probably included in

the stratigraphic record in the form of local concentration of turbiditic Sng facies within the FA4 (e.g., MS-I in Appendix I). Following to this period of fluctuation, basin-filling phase was probably initiated in a progradational pattern. This can be inferred by FA2 and overlying alluvial deposits of Çaltılık formation observed above FA4 in MS-I. The basin filling phase is also distinguished in the upper meters of MS-II in which FA2 is overlain by FA1.

The lower contact of the Alaşehir formation with the underlying metamorphic rocks was considered as nonconformable (İztan and Yazman, 1991; Yılmaz *et al.*, 2000, Seyitoğlu *et al.*, 2002). Although originally a nonconformable relation is anticipated, outcrop observations revealed a slickensided, low-angle fault plane between the Alaşehir formation and the metamorphic basement as first discussed by Deniz *et al.* (2002) (Figures 2.3 and 2.5). This suggests that the Alaşehir formation to the south of the MGBF is not in place but it is rafted on the hanging-wall of the low-angle fault plane. The total displacement of the Alaşehir formation in the hanging-wall is not possible to estimate because of the lack of observations to identify in-situ exposures of the formation in the footwall.

Based on the studies of palynological biostratigraphy, Alaşehir formation was assigned an Early-Middle Miocene age (İztan and Yazman, 1990; Ediger *et al.*, 1996; Seyitoğlu and Scott, 1992). Palynomorphs identified in samples from the Alaşehir formation, particularly from the Zeytinçay member, correspond to Eskişehir spore-pollen biozone (20–14 Ma) (Benda, 1971; Benda and Meulenkamp, 1979). However, the palynological age data does not provide enough resolution to determine whether the Alaşehir formation was deposited during Early, Middle or through the entire Early-Middle Miocene period. Coal beds observed in the Evrenli member also sampled during this study for age determination. Although, no index palynomorph groups were identified in these samples, palynomorph facies were found very similar to those of Eskişehir spore-pollen biozone (personal communication with Hayrettin Sancay).

Early–Middle Miocene lacustrine deposits are observed at various localities across the western Anatolia. Küçükuyu formation around Gulf of Edremit (Yılmaz *et al.*, 2000; Yılmaz and Karacık, 2001; Çiftçi *et al.*, 2004), Soma formation in Bakırçay Graben (İnci, 1998, 2002), Köprübaşı and Demirci formations in Demirci Basin (Yılmaz *et al.*, 2000) and Hasköy formation (Emre and Sözbilir, 1997) in

Büyük Menderes Graben can be correlated with the Alaşehir formation in terms of age and depositional environments.

2.1.2. Toygarlı Andesite

Toygarlı andesite represents the only volcanic rock exposed in the study area (Figure 2.3). With its subcircular geometry and a radius of approximately 1 km, the unit is intruded into the metamorphic basement. The Bintepeleler formation nonconformably overlies the Toygarlı andesite.

Toygarlı andesite has typical andesitic purple color and feldspar porphyritic texture. Thin section examination of the samples indicated that the rock has hyaloporphyratic texture with glassy matrix and phenocrystal populations with predominant (in the order of relative abundance) plagioclase (oligoclase-andesine), bitotite, basaltic hornblend, augite and orthopyroxene. The rock also includes minor amounts of quartz and sanidine (thin section examination was carried out by Nuri Terzioğlu). The observed mineral paragenesis suggests that the rock possesses trachyandesitic composition. On the other hand, textural and geometrical aspects of the unit indicate a subvolcanic (hypabysal) origin possibly in the form of shallow andesitic dome. Yılmaz *et al.* (2000) comment that the Toygarlı andesite is petrochemically similar to the widespread lower-middle Miocene volcanic associations of the northwestern Anatolia. In fact, mineral paragenesis and textural aspects of the Toygarlı andesite are similar to the 3rd stage volcanic activity observed around the gulf of Edremit (Çiftçi *et al.*, 2004 and also Nuri Terzioğlu, personal communication).

The available age data for the unit clusters around Middle Miocene: 14.4±1 Ma (Ercan *et al.*, 1997), 14.65±0.06 to 16.08±0.91 Ma (Purvis *et al.*, 2005), 12-16 Ma (TPAO unpublished data) and 15 Ma (Yılmaz *et al.*, 2000). This age assignment partially overlaps with the depositional period of the Alaşehir formation. In fact, available borehole data provides some evidence for the thin tuff layers characterized by high gamma ray (GR) responses within the lower portions of the Alaşehir formation. Although, the Toygarlı andesite is rather in a subintrusive character, extrusive equivalents of the unit to the north might be the source of the volcanic inclusion within the Alaşehir formation probably in the form of ash fall deposits.

2.1.3. Çaltılık Formation

Çaltılık formation conformably overlies the Alaşehir formation through a gradational contact from the Alaşehir formation to sandstones, channelized gravelstones and rare limestone lenses of the Çaltılık formation (Figure 2.2 and MS-1 in Appendix II). Although, earlier studies consider this formation as part of the Alaşehir formation (Yazman and İztan, 1990; Yazman *et al.*, 1998), the Çaltılık formation is a very distinctive lithostratigraphic unit exposed along the southern margin of the Gediz Graben. The formation is first described by Yılmaz *et al.* (2000) from the exposures near the Çaltılık village. Seyitoğlu *et al.* (2002) also recognized the formation with its conformable superimposition over the Alaşehir formation and named it as Kurşunlu formation. However, the definition of the Kurşunlu formation in Seyitoğlu *et al.* (2002) also includes two other formations overlying the Çaltılık formation. Therefore, the name Çaltılık formation was adopted in this study as proposed by Yılmaz *et al.* (2000). Çaltılık formation also correlates with Unit II of Cohen *et al.* (1995) and with muddy to sandy alluvial fan facies associations of the Purvis and Robertson (2005) (Figure 2.1).

As the Alaşehir formation, Çaltılık formation is also observed at spatially limited areas along the Gediz Graben (Figure 2.3) but it exhibits relatively extensive exposures along the Alaşehir-Salihli segment. Wherever the Alaşehir formation exists, Çaltılık formation conformably overlies the Alaşehir formation. In areas outside the depositional realm of the Alaşehir formation, Çaltılık formation juxtaposes with the metamorphic rocks of Menderes Massif by means of a low-angle fault plane (Figure 2.3).

Three stratigraphic sections were measured through the Çaltılık formation in the study area (MS-I, MS-IV and MS-V in Appendix I). These sections are located in Zeytinli creek between Çaltılık and Osmaniye villages and along the Alaşehir-Gökçealan road near Gökçealan village. At the Zeytinli creek section, the gradation between the Alaşehir and Çaltılık formations can be clearly observed (MS-I in Appendix I). Faulted contact of the formation with the metamorphic basement is well-exposed near Karakirse (Figure 2.3).

Table 2.3 lists the main facies types observed in the Çaltılık formation with brief descriptions and interpretation. The observed Gt, Gp, Sp, Sl, Se, Ssc, Sh S, Fl, Fm and L facies of the formation can be classified into two groups: (i) alluvial fan facies association (FA5) in proximal to distal fan setting and (ii) small lake or pond

Table 2.3. Dominant facies, facies descriptions and interpretations of the Çaltık formation. Some of the lithofacies and interpretations are modified from Miall (1985). See Appendix I for the related measured stratigraphic sections.

Facies	Description	Interpretation
Gt, troughy cross-bedded gravelstones and conglomerates	medium bedded, moderately rounded and poorly sorted, moderately cemented, polymictic, matrix supported with coarse sandy matrix, scoured based with lag, fining upward	channel fills
Gp, planar cross-bedded gravelstones and conglomerates	medium bedded, moderately rounded and poorly sorted, poorly cemented, polymictic, matrix supported with coarse sand matrix, base is non-erosive, foreset cross bedding	mid-channel bars
Sp, planar cross-bedded sandstone	similar to Gp, but finer grained	mid-channel sand bars
Sl, low angle cross-bedded sandstones	red colored, medium bedded, medium grained, moderate to poorly sorted, with low angle planar cross-bedding	crevasse splays
Se, erosive-based sandstones	red colored, medium bedded, coarse grained, moderate to poorly sorted, crude cross bedding, erosive based, fining upward	scour-fills
Ssc, scoured-based sandstones	red colored, medium bedded, coarse grained, moderate to poorly sorted, broad scoured based with lag, fining upward	scour-fills
Sh, horizontally laminated sandstones	medium bedded, well sorted, coarse grained, horizontally laminated	deposits from planar bed flow
S, sandstone	others	
Fl, sand, silt, mud	red colored, thin bedded, laminated to faintly rippled, well cemented, locally fist size nodules bearing	overbank or waning flood deposits
Fm, mud, silt	red colored, thin bedded, desiccation (?)	overbank or muddy channel fill (drape) deposits
L, limestone	very hard and carbonaceous, clayey, poorly bedded, lensoidal	deposition at ponds during draught

Table 2.4. Facies associations of the Çaltık formation. See Appendix I for the related measured stratigraphic sections.

Facies Association	Constituent Lithofacies
FA5, alluvial fan facies associations	Gt, Gp, Sp, Sl, Se, Ssc, Sh, S, Fl, Fm, L
FA6, small lake or pond facies associations	L, S

facies association (FA6) (Table 2.4; Figure 2.6). The formation is predominantly composed of poorly-sorted, moderate- to well-cemented sandstones interbedded with conglomerates and siltstones (Figure 2.7). Mud is a constituent of the matrix both in the sandstones and in the conglomerates together with sand. The clast population is polymictic and derived directly from various metamorphic lithologies of Menderes Massive. Beside, rip-up clasts are also observed in the formation in relation to scour surfaces (Figure 2.7). In general terms, the facies of the formation, especially the muddy facies, are strongly reddened. Greenish gray color is usually observed for the gravel and coarse sand dominated facies. Yet, red staining of the outcrop surface, which is derived from muddy facies, always hides the true color of the sand-gravel rich facies and result in general red colored appearance of the formation. Clast imbrication, cross bedding and channel orientations indicate dominant sediment transport direction from south to north varying in the range of SSW–NNE to SSE–NNW. Occasionally, limestone lenses are also present, probably indicating deposition in pod-like depressions during the seasonal drought periods. Purvis and Robertson (2005) have carried out intensive paleocurrent analysis for their muddy-to-sandy alluvial fan facies association along to southern margin of the Gediz Graben. The overlapping part of their study with this study area indicates a strong N–NE directed palaeocurrent for the formation (Figure 8 in Purvis and Robertson, 2005), which is in agreement with the data presented in this work.

No palaeontological age date has been acquired from the Çaltılık formation. Mudstone samples collected during this study for palinologic assessment were also failed due to lack of dateable palinomorph associations. The only age data available for the formation is the magnetostratigraphic work, which depict that the transition from the Alaşehir formation to the Çaltılık formation occurred around 15.5 Ma (unpublished data of Şen and Seyitoğlu in Seyitoğlu *et al.*, 2002). This data is in agreement with the Eskişehir sporomorph association (20–14 Ma) of Benda and Meulenkamp (1979, 1990) and suggest that no significant time gap exists between the Alaşehir and Çaltılık formations.

2.1.4. Gediz Formation

Gediz formation is exposed along NW–SE trending fault-controlled belt at the immediate margin of the modern graben floor (Figure 2.3). The exposure of the formation is bounded by two northward-dipping normal faults that bring the unit in

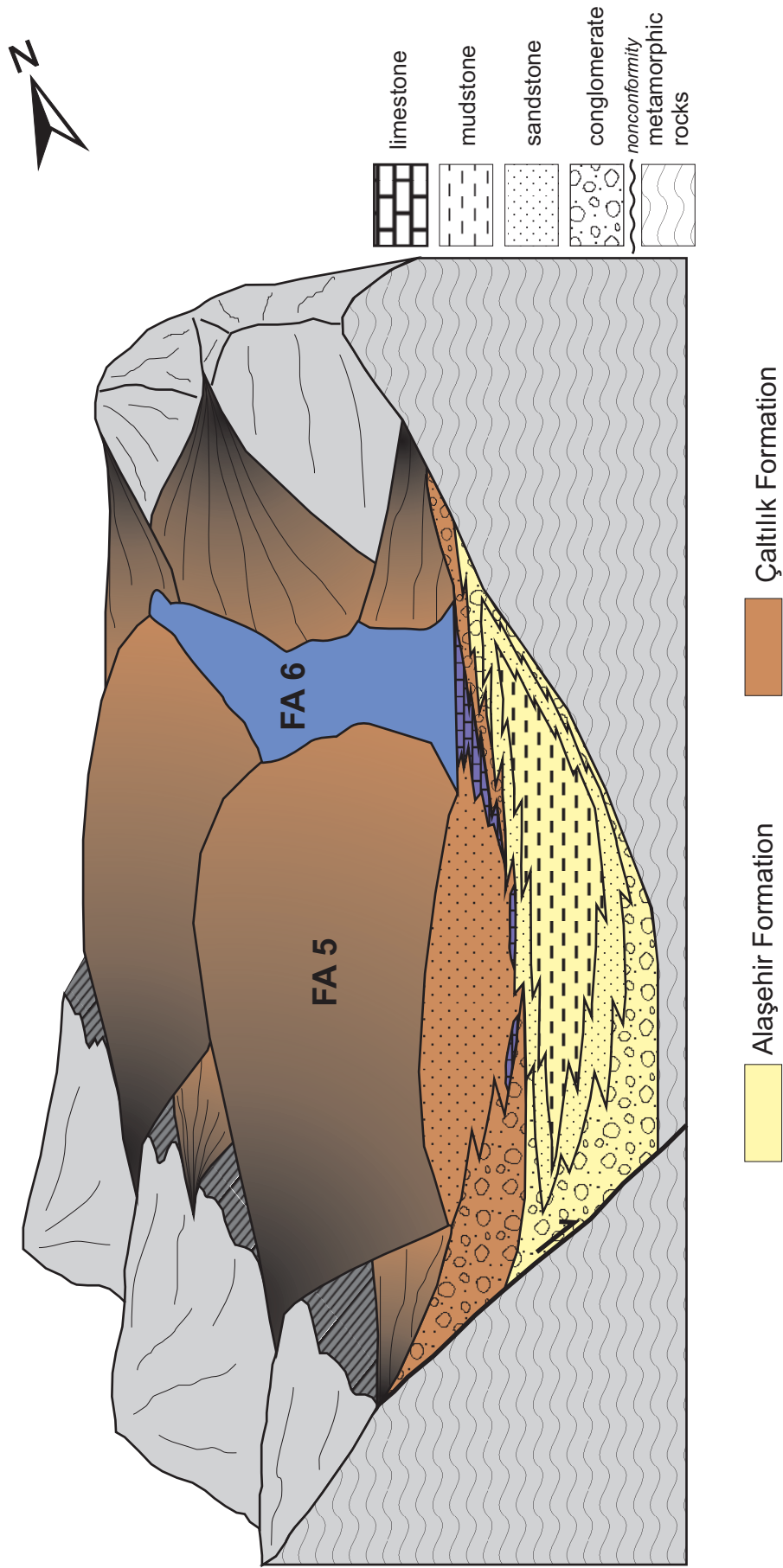


Figure 2.6. A block diagram depicting conceptual paleogeography of the depositional period of the Çaltılık formation (Miocene). FA 5: alluvial fan facies associations; FA 6: small lake or pond facies associations. See Tables 2.3 and 2.4 for description of facies and facies associations.



(A)



(B)



(C)

Figure 2.7. Field photographs taken near Soğukyurt village to illustrate lithofacies in the Çaltılık formation. (A) General appearance of the unit comprising sandstone and conglomerate beds and intervening sandstones and siltstones. (B) Mudstone rip-up clasts that were scoured and included by sandstone or conglomerate lenses. (C) Cross bedding in sandstones. The field notebook is 21x15 cm.

contact with the metamorphic basement, Alaşehir and Çaltılık formations to the south and with the Quaternary graben floor sediments to the north (Figure 2.3). Stratigraphically, the unit overlies the Çaltılık formation although no clear contact relationship was observed between these formations (Figure 2.2). On the surface exposures, the unit is tilted and generally dips towards south to the master graben bounding fault (MGBF on Figure 2.3).

Gediz formation is first named by Yazman and İztan (1990) as Gediz group including Hamamdere and Salihli formations. These formations are composed of conglomeratic deposits of alluvial fan system and sandy deposits of a fluvial system, respectively. Yılmaz *et al.* (2000) proposed the name Kızıldağ grup for these lithologies including Kızıl and Mersinligedik formations. These two formations refer to Hamamdere and Salihli formations of the Yazman and İztan (1990), respectively. On the other hand, Koçyiğit *et al.* (1999a) adopted Sağlıkdere, Kartaluçan, Acidere, Göbekli and Kaletepe formations to refer proximal alluvial fan to distal braided river deposits. Seyitoğlu *et al.* (2002) treated the Gediz formation as part of the Kurşunlu formation; the Kurşunlu formation includes both Çaltılık and Gediz formations although subsurface data reveals a very pronounced distinction between these formations (see section 2.2). Gediz formation also correlates to Unit III – axial fluvial facies and Unit IV coarse lateral alluvial fan facies of Cohen *et al.* (1995). Purvis and Robertson (2005) defined the axial fluvial facies associations to refer the Gediz formation (Figure 2.2).

Three stratigraphic sections were measured within the Gediz formation. These sections are located west of the study area, between Salihli and Turgutlu, where best exposures of the formations are present in this region (MS-VI, MS-VII and MS-IX in Appendix I). Seven different lithofacies were identified and logged within the Gediz formation (Table 2.5). The lower part of the formation is composed predominantly of red colored, coarse grained, texturally immature, polymictic conglomerates derived from the various lithologies of basement metamorphics. This lower coarse-grained part is named as Hamamdere member of the Gediz formation (Yazman and İztan, 1990). The Hamamdere member mainly includes lithofacies Cm, Sp and Sh (Table 2.5 and Figure 2.9). These lithofacies were interpreted to represent proximal alluvial fan facies associations (Collinson, 1996; Miall, 1985, 1992, 1996; Nilsen, 1982) (Table 2.6 and FA7 in Figure 2.8). Upward in the formation, textural maturity of the formation increases and grain size decreases, as red color gradually

Table 2.5. Dominant facies, facies descriptions and interpretations of the Gediz formation. Facies nomenclature and interpretations are modified from Miall (1985). See Appendix I for the related measured stratigraphic sections.

Facies	Description	Interpretation
Cm, massive conglomerates	massive and chaotic, polymictic, sandy to gravelly matrix supported, angular granule to cobble size clasts, sharp base, irregular top, locally inversely graded, locally sandstone lenses bearing	debris flow deposits
Gt, troughy cross-bedded gravelstones and conglomerates	medium bedded, moderately rounded and sorted, polymictic, trough cross bedded, generally fining upward, scoured based with lag	channel fills
St, trough cross-bedded sandstones	medium bedded, coarse grained – locally pebbly, moderately sorted, trough cross bedded, scoured based with lag, fining upward	channel fills
Sp, planar cross-bedded sandstones	medium-thick bedded, moderately sorted, well cemented, tabular cross bedded	sand bars
Sh, horizontally laminated sandstones	thin bedded, fine to coarse grained, pebbly to silty, horizontally laminated	planar bed flow deposits
S, sandstones	others	
Fl, sand, silt, mud	thin bedded intercalation dominated by silt and mud, locally laminated	overbank or muddy channel fill

Table 2.6. Facies associations of the Gediz formation. See Appendix I for the related measured stratigraphic sections.

Facies Association	Constituent Lithofacies
FA7, proximal alluvial fan facies association	Cm, Sp and Sh
FA8, distal alluvial fan and fluvial facies association	Gt, Sh, Sp, S, Fl and Cm

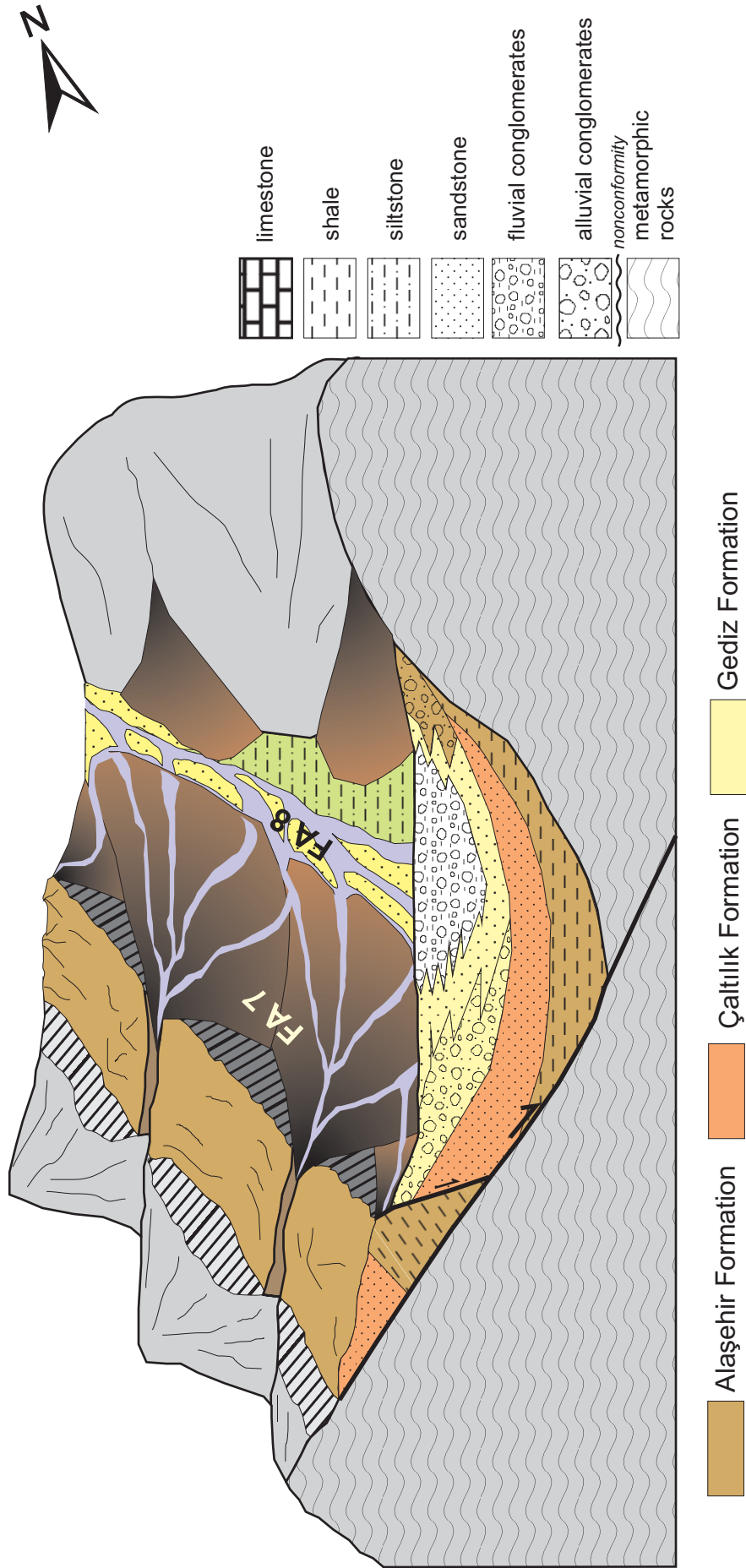


Figure 2.8. A block diagram depicting conceptual palaeogeography of the depositional period for the Gediz formation (Miocene). Alaşehir and Çaltılık formations are represented by most typical lithology of the formation. FA 7: proximal alluvial fan facies associations; FA 8: distal alluvial fan and fluvial facies associations. See Tables 2.5 and 2.6 for description of facies and facies associations.

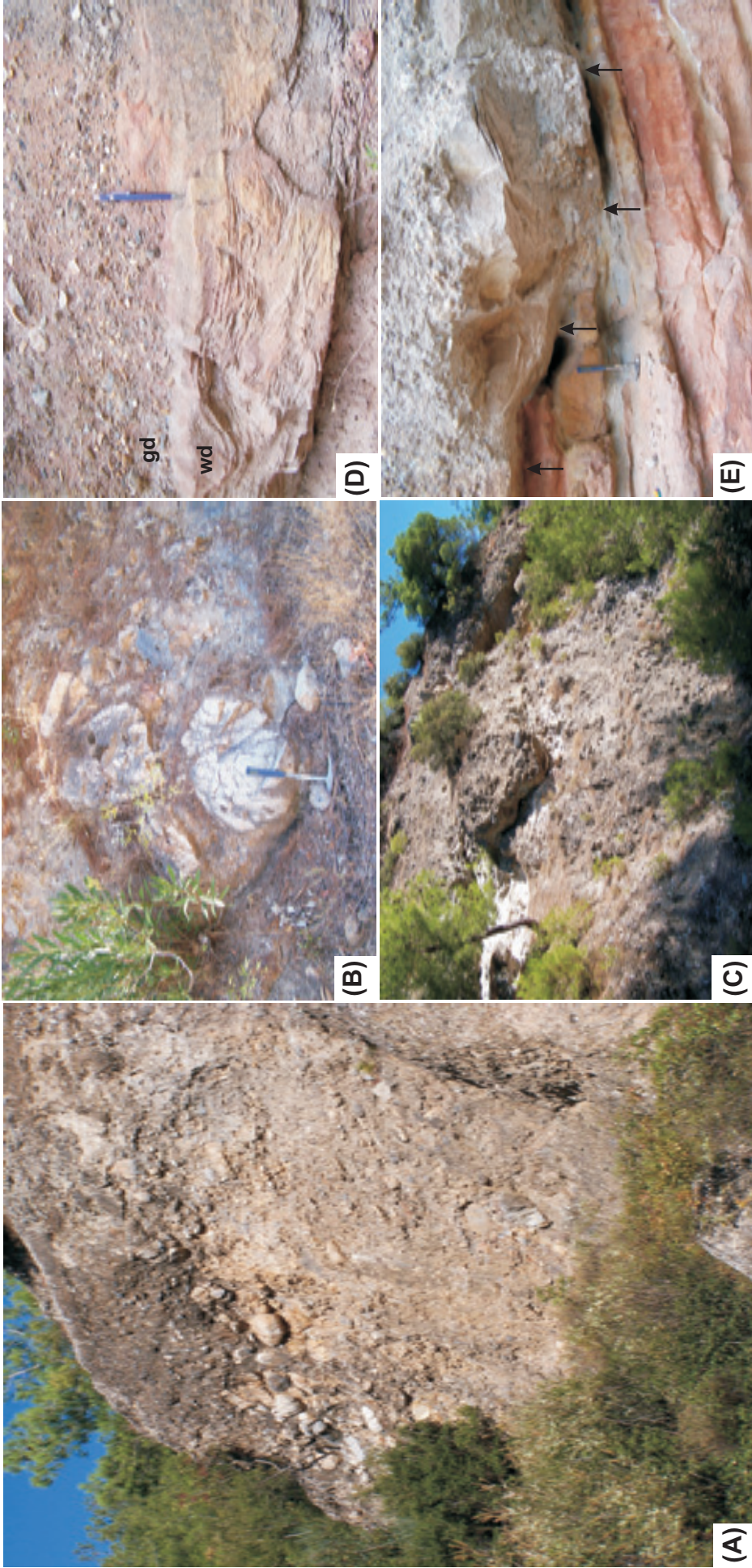


Figure 2.9. Field photographs of lithofacies in the Gediz formation taken near Çıkırıkcı village, Akçapınar. (A) Lithofacies Cm (Table 2.5). Note the crude inverse grading. (B) Close-up view from the metamorphic clasts locally reaching up to 0.5 m in diameter. (C) Lensoidal geometry locally observed for the facies Cm. (D) Note the intercalation of the water driven(wd) and gravity driven (gd) deposits. (E) Scouring of the fine-grained deposits by overlying coarse-grained pulses is a common phenomenon in the Gediz formation. Hammer in the figure is 40 cm and pencil is 15cm.

turns into beige-green. The dominant lithofacies observed in the upper part includes Gt, Sh, Sp, S and Fl with occasional intercalation of the Cm. Facies associations become more fluvial-dominated in the upper part of the formation as textural maturity increases. Therefore, these lithofacies are grouped into distal alluvial fan and fluvial facies associations (FA8) and named as Salihli member of the Gediz formation.

First order observation indicates a NE–NW-directed sediment transport for the Hamamdere member and W–NW-directed sediment transport for the Salihli member. These observations are in agreement with that of Cohen et al. (1995). There is also some degree of match between Salihli member and intensive palaeocurrent analysis conducted on axial-fluvial facies association of Purvis and Robertson (2005). Seismic data, on the other hand, clearly illustrates thinning of the formation from south to north (see section 2.2), which indicates that major sediment transportation is from south to north as well. This change in thickness implies that the formation is an alluvial system marginal to southern boundary of the Gediz Graben (Figure 2.8).

The Gediz formation, as the other formations defined so far, lacks reliable age data. Emre (1996) defined Acıdere, Göbekli and Filiztepe formations in the Salihli area, which probably correlates with the Gediz formation. In Emre (1996), Dacian (Miocene–Pliocene boundary) was assigned to the Göbekli formation based on Gastropod fossils as. As Göbekli formation is comparable to the upper parts of the Gediz formation (Figure 2.1), Late Miocene–Pliocene can tentatively be assigned to the Gediz formation.

2.1.5. Bintepeleler Formation

Bintepeleler formation is the only sedimentary unit mapped along the northern margin of the Gediz Graben around Alaşehir area. First named and mapped by Yazman and İztan (1990), the formation nonconformably overlies the metamorphic rocks of the Menderes Massif. In the Salihli segment, the Mevlütlü formation is probably the lateral equivalent of the Bintepeleler formation.

The Bintepeleler formation starts with very coarse grained, texturally immature conglomerate that is predominantly composed of limestone clasts, locally up to boulder size (Figure 2.2). Large clast sizes, textural immaturity, internally chaotic and scour-based conglomerate cycles are observable at the base of the formation to

indicate deposition at a close proximity to the source area (Collinson, 1996; Miall, 1985, 1992, 1996; Nilsen, 1982). Stratigraphically upward in the formation, the grain size decreases and the lacustrine limestone beds become distinct. The amount of lacustrine limestone further increases upward and the formation become limestone dominated. There is a complete lateral gradation and interfingering between the conglomeratic facies and the lacustrine limestone. Sandstones, intercalated with marls and channelized conglomerates are the dominant lithologies at the uppermost part of the formation. Pebble imbrication and crude cross-bedding suggest NE to SW sediment transport. The unit indicates depositional environment dominated by southward prograding alluvial fans and interfingering lacustrine basins formed at toe of the fans (cf. İnci, 2002; Miall, 1996).

There is no stratigraphic section logged for the Bintepeleler formation. Facies defined by basic field observations includes Cm, Gt, St, S, F and L (Table 2.7). These facies are grouped into alluvial fan and lacustrine facies associations (FA9). As the only formation sourced by northern horst block of the Gediz Graben, Bintepeleler formation has an importance to constraint the timing of the northern margin boundary structure of the Gediz Graben (Figure 2.10). Yusufoglu (1996) defined Balçıkdere, Ulubey and Asartepe formations at the northern margin of the Gediz Graben deposited from Early Pliocene to Early–Middle Pleistocene period (Yusufoglu, 1996). These formations correlate with the Bintepeleler formation. Thus, Plio–Pleistocene is tentatively assigned to the Bintepeleler formation.

2.1.6. Kaletepe Formation

Kaletepe formation is exposed extensively along the southern horst block of the Gediz graben (Figure 2.3). The formation is named by Yazman and İztan (1990) and is subsequently called as Sart group (Yılmaz *et al.*, 2000), Sart formation (Seyitoğlu *et al.*, 2002) and Asartepe formation (Emre, 1996; Koçyiğit *et al.*, 1999a) (Figure 2.1). Based on its sedimentological aspects, Cohen *et al.* (1995) defined the unit as lateral alluvial fan facies while Purvis and Robertson (2005) used coarse alluvial fan facies association definition for the same unit (Figure 2.1).

In general, the unit is earth colored, thick and poorly bedded, poorly lithified and composed of polymictic conglomerates with relatively minor sandstone and mudstone intercalations. Nevertheless, sand and mud are important constituent of the matrix of conglomerates. It rests over the Gediz formation with pronounced change

Table 2.7. Description and interpretation of the lithofacies observed in the Bintepeler formation. Some of the lithofacies descriptions are modified from Miall (1985).

Facies	Description	Interpretation
Cm, massive conglomerates	massive and chaotic, polymictic, sandy to gravelly matrix supported, angular granule to cobble size clasts,	debris flow deposits
Gt, troughy cross-bedded conglomerates	medium bedded, poorly rounded and sorted, polymictic, trough cross bedded, scoured base	channel fills (Temporary?)
St, trough cross-bedded sandstones	medium bedded, coarse grained – locally pebbly, poorly cemented, moderately sorted, trough cross bedded, scoured based with lag, fining upward	channel fills
S, sandstones	others	
F, silt and clay	thin bedded with wavy lamination and calcereous	overbank or muddy channel fill
L, limestone	beige colored, medium-thick bedded, gastropod shells bearing	small lake

Table 2.8. Description and interpretation of the lithofacies observed in the Kaletepe formation. Some of the lithofacies descriptions are modified from Miall (1985). See Appendix I for the related measured stratigraphic sections.

Facies	Description	Interpretation
Cm, massive conglomerates	massive and chaotic, polymictic, sandy to gravelly matrix supported, angular granule to cobble size clasts,	debris flow deposits
Gt, troughy cross-bedded conglomerates	medium bedded, poorly rounded and sorted, polymictic, trough cross bedded, scoured base	channel fills (temporary?)
Sp, pebbly sandstone	medium bedded, coarse grained – locally pebbly, poorly cemented, moderately sorted, trough cross bedded, scoured based with lag, fining upward	channel fills
Fm, mudstone	others	

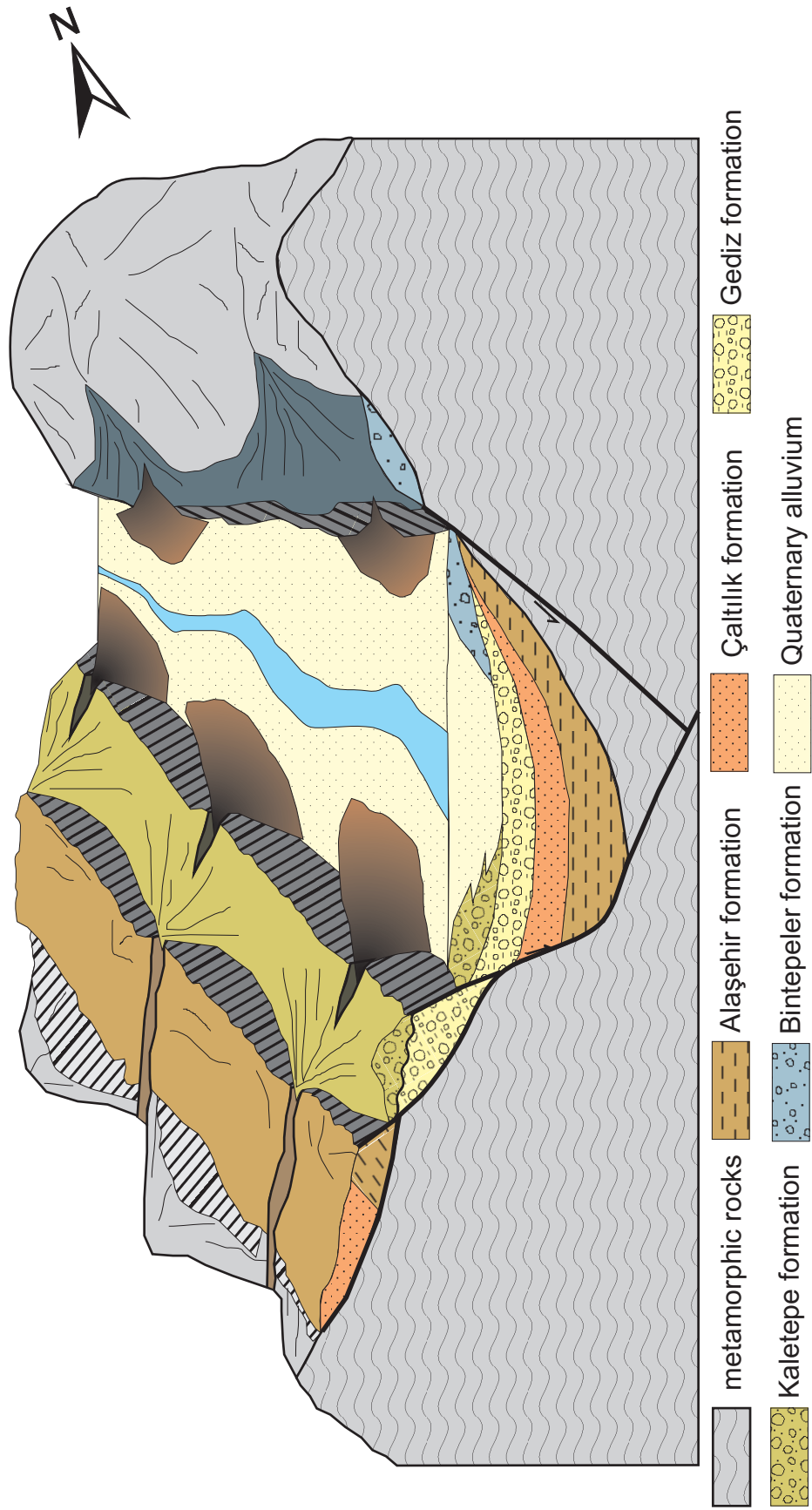


Figure 2.10. A block diagram depicting conceptual paleogeography of Bintepele and Kaletepe formations and the Quaternary deposits of the Gediz Graben (Pliocene-Quaternary).

in dip angle implying an unconformable relationship between the two formations (Figure 2.2). In some places the unit directly overlies the metamorphic rocks. The outcrops of the Kaletepe formation are morphologically distinct where they form steep linear hills due to deep river incision.

Together with the Gediz formation, Kaletepe formation borders the modern graben floor of the Gediz Graben (Figure 2.3). Along this border zone, both formations usually dip to the south towards the master graben-bounding fault (MGBF) (Figure 2.3). The dominant dip direction is the result of back rotation of the strata in the hanging-wall of north dipping graben-bounding normal faults (Yılmaz *et al.*, 2000).

Kaletepe formation does not show much facies variation both vertically and laterally along its exposures. Hence, only a single stratigraphic section was logged for the formation (MS VIII in Appendix I). The main lithofacies observed along the section includes Cm and Gt with minor amounts of Sp and Fm (Table 2.8). The dominant coarse-grained facies Cm and Gt are composed of subangular to subrounded clasts with grain size ranging from gravel to boulder. The matrix is variably clast to matrix supported. Earth color is very typical for the unit although weak reddening is locally observable. Clasts population is polymictic, mostly derived from Menderes massif and includes schist, quartzite, limestone, chert and gneiss. Beside, both sedimentary and metamorphic clasts derived from older sedimentary units of the graben fill are also included within the formation through a cannibalization process. Coarse facies are usually lenticular, having erosive bases. Weak trough cross-bedding and faint grading are locally observable with well-developed pebble imbrications, indicating northward sediment transport. The observed facies Cm, Gt, Sp and Fm (Table 2.8) can be grouped into alluvial fan facies associations (FA10) that represent a very coarse-grained and texturally immature proximal facies to the sediment source area. Purvis and Robertson (2005) have documented more vertical and lateral facies variation for their coarse alluvial fan facies association that correlates with the Kaletepe formation. Their study area is located to the west of this study area with a little overlap around Şahyar (Figure 2.3). Intensive palaeocurrent analysis carried out by Purvis and Robertson (2005) indicates a strong south to north component of sediment transport direction for the formation. Cohen *et al.* (1995) also documents evidence for south to north sediment transportation for the Kaletepe formation.

The contact relation of the Kaletepe formation with the underlying Gediz formation is an angular unconformity observed clearly along the southern margin of the Gediz Graben (Figure 2.3). Yet, this contact may be a basin margin unconformity and extend to the buried graben block as a correlative conformity. Indeed, interpretations of subsurface data suggest continuous deposition for the buried graben block from the Gediz formation to Recent, as represented by seismic stratigraphic units III (Figure 2.2 – see also Section 2.2.2 and Chapter 5). There is no outcrop observation regarding to the contact relation between the Kaletepe and Bintepeleler formations in this study. However, as seismic stratigraphic unit III includes both of the formation, there should be a gradation among the Kaletepe and Bintepeleler formations within the buried graben block.

The available age assignments for the Kaletepe formation are not precise. Based on the mammal fossils, Sarıca (2000) dated some sediments exposing along the margins of Gediz and Büyük Menderes grabens as Plio–Pleistocene. Some of these Plio–Pleistocene sediments can be correlated with the Kaletepe formation based on the definition of Sarıca (2000). The other literature generally assigns Pliocene age for the unit (Figure 2.1) (Yazman and İztan, 1990; Cohen *et al.*, 1995; Yazman *et al.*, 1998; Koçyiğit *et al.*, 1999a; Yılmaz *et al.*, 2000; Seyitoğlu *et al.*, 2002; Purvis and Robertson, 2005). Therefore, Plio–Pleistocene is tentatively accepted for the Kaletepe formation in the present study.

2.1.7. Quaternary Alluvium

The Quaternary deposits in the Gediz graben is dominated by fluvial sediments of the modern Gediz River. However, alluvial systems also coexist in the graben floor along the northern and southern margins of the graben. As a result, Quaternary fill of the Gediz Graben in the study area is differentiated into two units as proximal and distal alluviums to refer; (i) the relative positions with respect to margin-bounding faults and (ii) dominance of the gravitational mass flow versus fluvial processes (Figure 2.3). Proximal Quaternary alluvium is characterized by coalesced alluvial fans of diverse sizes. They are fed from the horst blocks uplifted in the footwall of graben-bounding normal faults. Larger alluvial fans form at the reaches of the horst block drainage, which roughly displays linear pattern and oriented orthogonal to the graben bounding faults. Proximal alluvial deposits are dominated by debris flow and channel-fill conglomerates, sands and fine-grained overbank deposits. Towards the

center of the graben, proximal alluvium facies grades into and interfingers with finer-grained axial fluvial system of the graben. Meandering channel system of the Alaşehir River controls the axial fluvial system. Together with distal alluvial fan sediments, the deposits of fluvial system were mapped as the distal Quaternary alluvium (Figure 2.3). This unit refers to distal location with respect to graben-bounding faults and the dominance of fluvial processes with respect to gravitational processes. Distal Quaternary alluvium is probably composed of channel fill sands and fine-grained overbank sediments.

Quaternary travertines are also observable in the study area. They occur in a close proximity to the MGBF, controlling the southern margin of the Gediz Graben (Figure 2.3). They either intercalate with the Quaternary alluvium or overlie the metamorphic basement. There are active hot-springs in close proximity to the travertine accumulations (Figure 2.3).

2.2. Subsurface Correlation of the Lithostratigraphic Units

Previous studies conducted in the Gediz Graben have focused on the outcrop exposures mainly along the southern margin and to some extent along the northern margin of the graben (Figure 2.1). These exposures are very important since they delineate the stratigraphic units (lithofacies and their distribution) and deformation characteristics of the margin-bounding fault systems of the graben. However, as the loci of most intense deformation, margins of graben are very sensitive to tilting, erosion due to base level changes, and formation of consequent basin-margin unconformities. It is of critical importance to know how surface stratigraphic units continue into subsurface. Unfortunately, available subsurface data is under-utilized to address this critical issue of correlating the surface geology to the subsurface in the Gediz Graben. Without a concrete subsurface correlation, which extends from the margin to the depocenter of a basin, a basin's stratigraphy can only be constructed to a limited extent.

This section intends to tie the surface observation to the subsurface data in order to assess the depositional geometries and the governing depositional system of the Gediz Graben. The starting point of such an analysis is the evaluation of the available borehole data to identify the depth of formations and stratigraphic units in the boreholes. Correlation of the lithofacies observed on the surface with that of interpreted in the boreholes, also provides information on the lateral variation of the

stratigraphic units. Then, the borehole data are tied to 2-D seismic sections to relate the seismic stratigraphic units to the actual lithostratigraphic units. Calibration of the seismic sections in this way helps to define the lateral extent and geometries of stratigraphic units, their stratal patterns, contact relationships and deformation characteristics. In this way, high resolution but laterally discontinuous surface data will be supported by relatively low resolution but laterally continuous seismic data.

2.2.1. Boreholes

Three hydrocarbon exploration wells have been drilled in the Gediz Graben near Alaşehir by TPAO (Figure 2.3). These boreholes penetrated thick sections of Neogene sediments with one reaching to the basement metamorphic rocks (Figure 2.11). The thickest section of the graben fill sediments is encountered in BH-1 which is 2464 m. However, thicker sections are expected in BH-2 and BH-3, which were drilled in closer proximity to the basin's depocenter and didn't reach the basement.

All three boreholes intersect the Alaşehir formation. Only the northernmost BH-1 reached to the base of the Alaşehir formation by cutting through the entire formation (Figure 2.11). At the base of the BH-1, polymictic conglomerates with interbeds of sandstones and pebbly sandstones characterize the Evrenli member of the Alaşehir formation. Gamma Ray (GR) response of the unit is usually low, representing the coarse-grained, clay free nature of the unit with rare and thin GR picks (Figure 2.1 – see Appendix II for background on gamma ray logs). These GR pick are higher than the normal shale responses of the Alaşehir formation. They may therefore indicate a volcanic input to the system in the form of thin ash layer intercalations. This volcanic content might be related to the regional Early–Middle Miocene volcanism of the western Anatolia represented by Toygarlı andesite along the northern margin of the Gediz Graben (see Section 2.1.2).

Evrenli member overlies the basement with a nonconformity. The unit displays a general fining-upward character as indicated by increasing sand content. (Figure 2.12). Within this overall fining-upward pattern, 20–30-m-thick coarsening-upward cycles are easily distinguishable in GR patterns probably indicating periods of progradation in overall retrogradation (Figure 2.12). These data are in close agreement with the outcrop observations of the Evrenli member and fits well with the fan delta complex interpretation of the unit. Above the Evrenli member, Zeytinçayı member of the Alaşehir formation is marked by a very sharp change in the GR

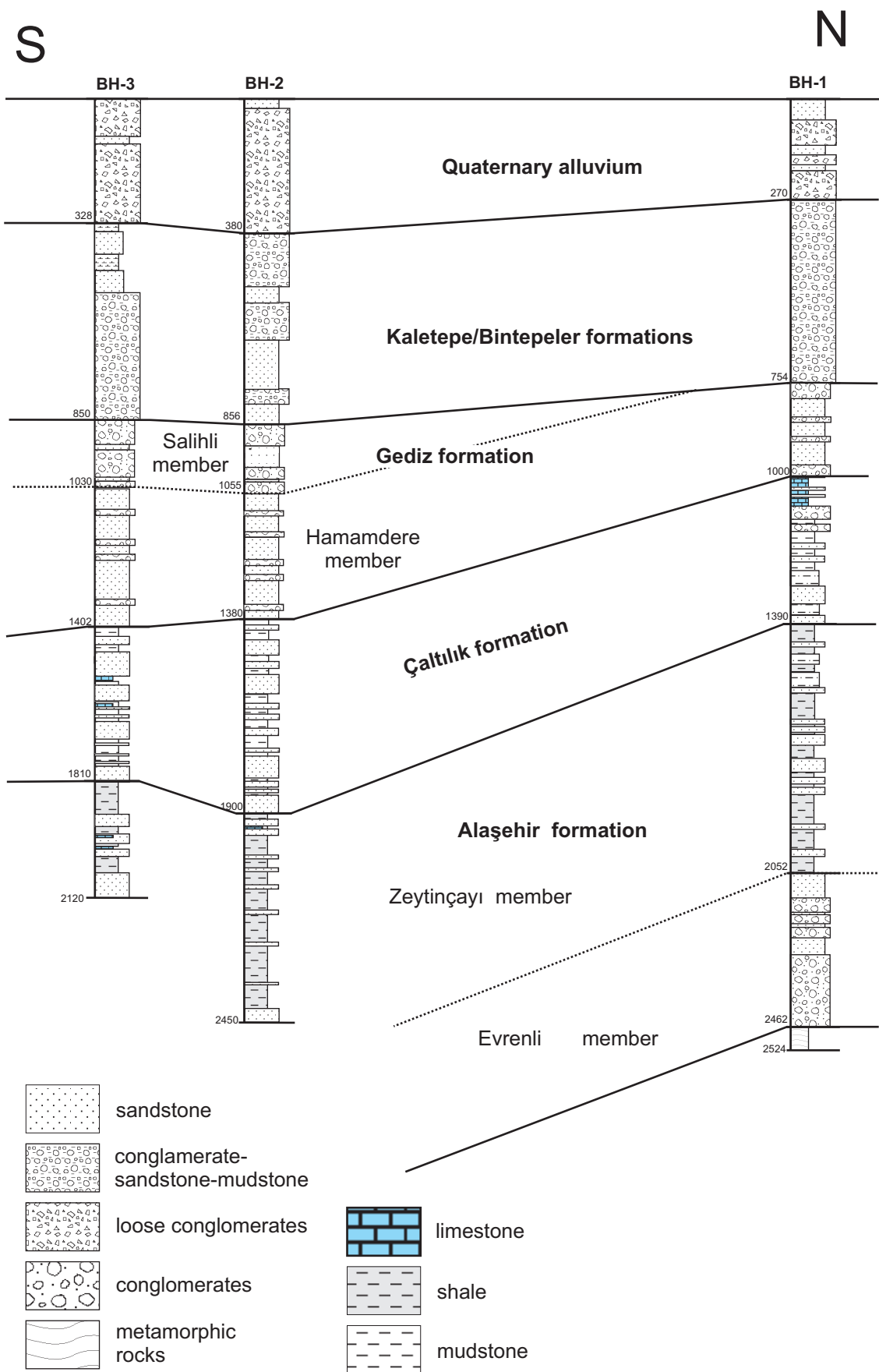


Figure 2.11. A summary section correlating the boreholes drilled in the Gediz graben. See Figure 2.3 for the location of boreholes.

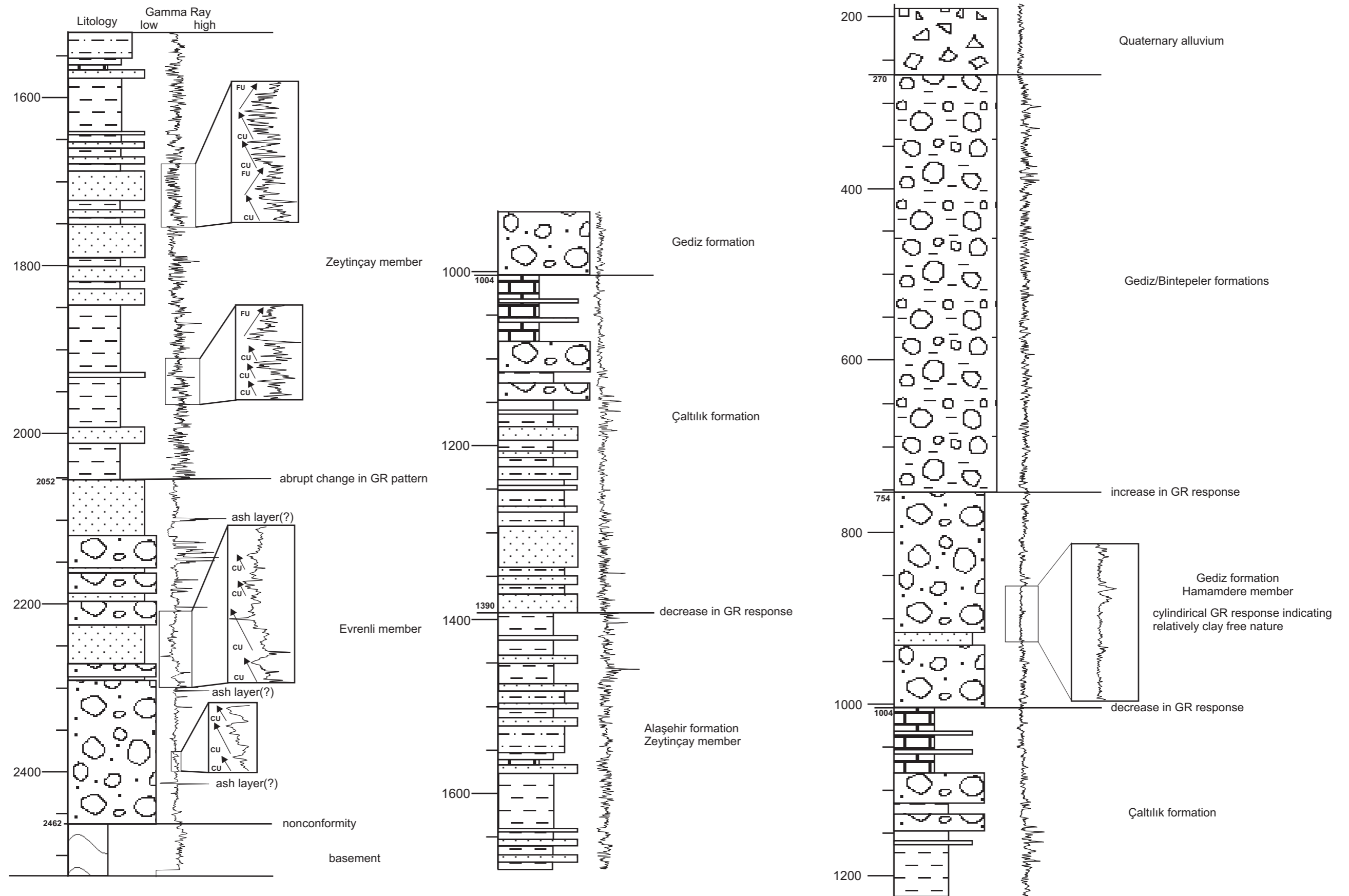


Figure 2.12. Figure illustrating lithologies of the formations and corresponding GR responses in BH-1. Exaggerated GR logs depicts the internal character of the deposits that includes coarsening-upward (CU) / fining-upward (FU) cycles or cylindrical log responses. See Appendix II for background information on GR logs.

pattern (Figure 2.12). The unit is characterized by relatively higher and erratic GR response and comprises dark brown to green colored, laminated, bituminous and locally carbonaceous shales intercalating with brown to beige colored, quartz- and mica-bearing and well-cemented sandstones (Figure 2.12). GR log response indicates coarsening- and fining- upward cycles in 10–30 m thickness range as evidence of variations in the energy of the system. Zeytinçay member correlates well among the three boreholes by its distinctive lithology and GR pattern (Figures 2.11, 2.12).

From the examination of well cuttings Çaltılık formation is recognized by its green to yellow colored, quartz and mica-bearing sandstones and polyimictic conglomerates with distinctive brick red colored mudstones intercalations. The log pattern of the formation is characterized by erratic but lowered GR response compared to Alaşehir formation. This indicates increased amount of sand in the formation (Figure 2.12). Thus, the well data is in confirmation with the surface observations that the Çaltılık formation is sandstone-dominated deposit with mudstone intercalations and belongs to an alluvial fan system. Thin limestone lenses occur occasionally within the clastic rocks as observed in borehole cuttings and outcrop exposures, indicating presence of small, temporary fresh water lakes or ponds within the system. However, BH-1 indicates that the amount of limestone is significantly increased in the formation and reached up to 70 m thickness towards the northern margin of the basin (Figures 2.11, 2.12 and 2.13). If facies distribution of the Alaşehir and Çaltılık formations evaluated together, one can recognize that the sediment was derived mainly from the southern margin of the governing basin (Figure 2.13). This confirms the field observations that the active margin of the basin is located in the southern side and the basin geometry mimics a half graben as schematically constructed in Figure 2.13. The Çaltılık formation is identified and correlated across all three boreholes above the Alaşehir formation (Figure 2.11).

Dominantly conglomerates and sandstones represent Gediz formation in the boreholes. Although lithological descriptions based on rock cuttings cannot separate two members of the formation, Hamamdere and Salihli can be recognized based on the GR readings. The lower Hamamdere member is characterized by cylindrical log pattern and low GR response, which indicates clean sand dominated nature of the unit, representing alluvial fan setting (Figure 2.13). Above the Hamamdere member, the Salihli member is recognized by generally low, sandstone dominated but erratic GR response. High GR picks of the formation are probably related to the thin

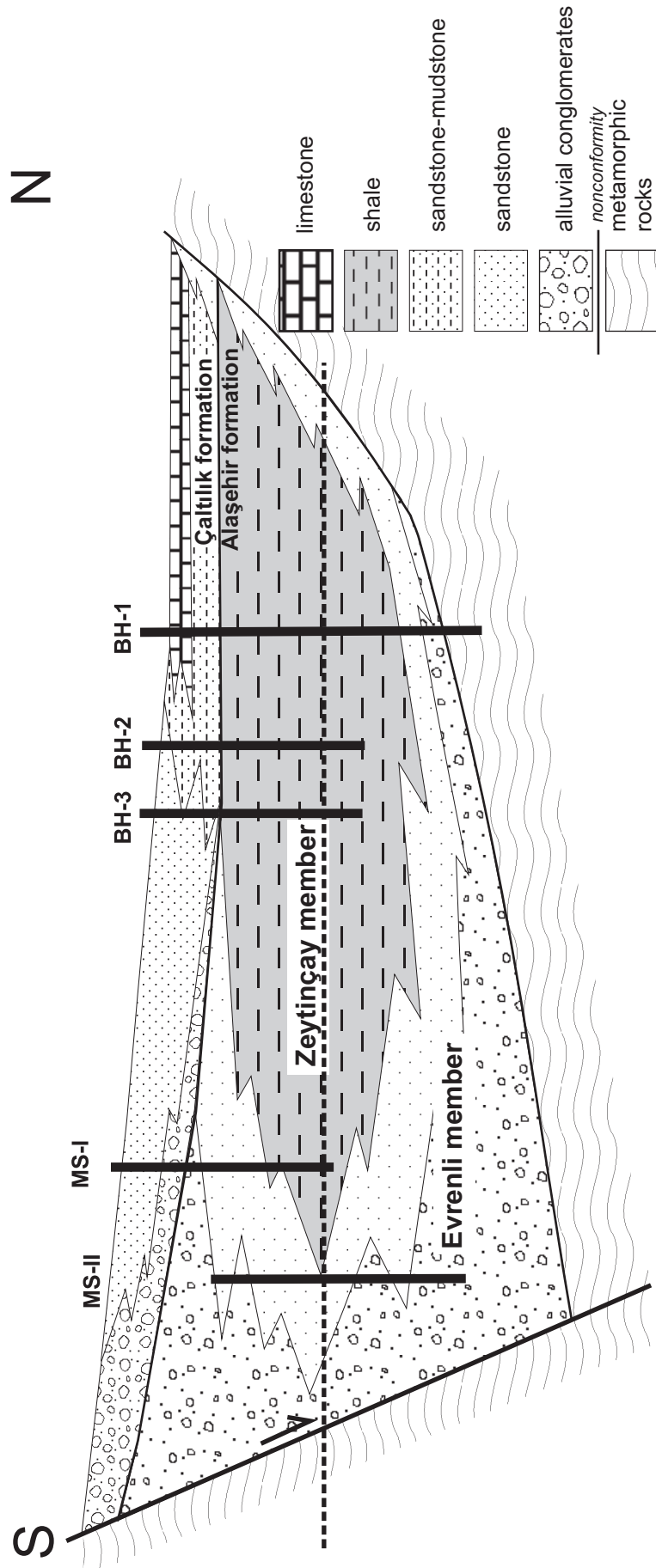


Figure 2.13. Schematic cross-section illustrating the facies distribution of Alaşehir and Çaltılık formations within the fault controlled basin. Related measured sections and boreholes are approximately located on the cross-section to refer encountered lithologies. Dashed line separates retrogradational or basin-deepening phase from progradational or basin-fill phase. Note the vertical repetition of lithostratigraphic Evrenli member and wedging of the Zeytinçayı member to the south. The contact between the Alaşehir and Çaltılık formations is conformable and gradational.

mudstone intercalations and clay content of the matrix in conglomerates, which can be expected in fluvial depositional systems (Collinson, 1996; Miall, 1992; Cant, 1982). The Gediz formation is recognized in all three boreholes above the Çaltılık formation with a distinct thickness change from south to north (See Figure 2.11). This thickness change suggests that the southern margin of the graben is still the most active one during the deposition of the formation. Therefore, the active basin margin probably was not changed during the deposition of Alaşehir, Çaltılık and Gediz formations.

Kaletepe/Bintepeler formations overlies the Gediz formation and composed predominantly of conglomerates. Discrimination of the Kaletepe/Bintepeler formations from the Gediz formation is difficult by borehole data due to lithological similarity of the formations. Yet, slightly increased GR response and relatively weak cementation may help to identify these formations. Compared to the underlying formations, thickness change of the Kaletepe/Bintepeler formations is minor from south to north and probably indicates more symmetrical subsidence of the basin during the depositional period of the formations. This uniform subsidence is most likely related to the initiated activity of the northern margin structure, which brings along the deposition of the Bintepeler formation. As a result, the Kaletepe and Bintepeler formations are interpreted as partly age equivalents sourced by southern and northern margins, respectively. Similar symmetrical subsidence can also be inferred for the overlying Quaternary alluviums of loose conglomerates and sands.

2.2.2. Depositional Geometries from Seismic Data

Interpretation of 2-D seismic sections provide unique opportunity to understand the geometries, lateral variations, contact relations, depositional patterns and deformation characteristics of the stratigraphic units by providing continuous images of less deformed and unexposed sections of a sedimentary basin's deposits. This is extremely important to assess the subsurface continuations of the stratigraphic units that are mainly observed, if exposed, along the tectonically active margins of a basin. Basin margin exposures are very important to draw the outlines of a depositional system by providing opportunity of working with high-resolution outcrop data. However, they are limited to depict the entire picture of a depositional system if their basinward continuations are not assessed carefully by means of a subsurface methodology. Understanding the depositional system will inevitably

enlighten the tectonic evolution of a basin. Seismic data serve as a perfect tool for this purpose if calibrated by boreholes.

The available seismic data from the Gediz Graben was interpreted to identify the seismic stratigraphic units and depositional geometries of the graben fill. If figure 2.14 is examined, one can easily identify the metamorphic basement rocks of the by their acoustic transparency (i.e. zone of no prominent reflectors). Above the basement, *seismic unit I* has characteristic continuous parallel reflector pattern which dips towards the bounding fault in the south of the basin and becomes almost horizontal toward the north of the basin. This geometry is in confirmation with the extensional fault bend fold models having a concave upward bend in the dip of the fault (see Chapter 5 for further discussion and relevant literature). The thickness of the unit is apparently influenced by secondary hanging-wall faults that created basement highs and lows across the depositional realm of the *unit I*. This resulted in thickness variation within the unit that was controlled by syn-depositional faulting.

Seismic unit II overlies the *seismic unit I* with a distinct change in the stratal pattern and a downlap surface (Figure 2.14). In general, the unit displays a tangential reflector pattern, which has steep dips toward the bounding fault, but dips gradually become tangential onto the underlying seismic unit to the north. Northward dipping reflectors of the unit observed across the southern side of the graben gradually changes dip direction towards the north and become southward dipping around the north side of the basin. This change in the dip direction is related to the differential subsidence within the basin, which may be caused by both more active southern margin and more pronounced compaction at the depocenter of the basin. The above-mentioned reflector pattern of the *seismic unit II*, together with a clear decrease in thickness from south to north, probably indicating that the unit was progradational and sourced by southern margin of the graben. Reflector character of the *seismic unit II* also changes from south to north. Towards the southern margin-bounding fault, unit displays hummocky reflector pattern characterized by irregular, subparallel and discontinuous reflections. To the north, the reflectors become more distinct and parallel. Although, some of this change may be attributable to the change in the imaging quality in the vicinity of the master fault, there must also be a lateral facies change from north to south. Disorganized conglomerates dominates the proximal (southern) parts of the *seismic unit II*, resulting in hummocky reflector pattern. To

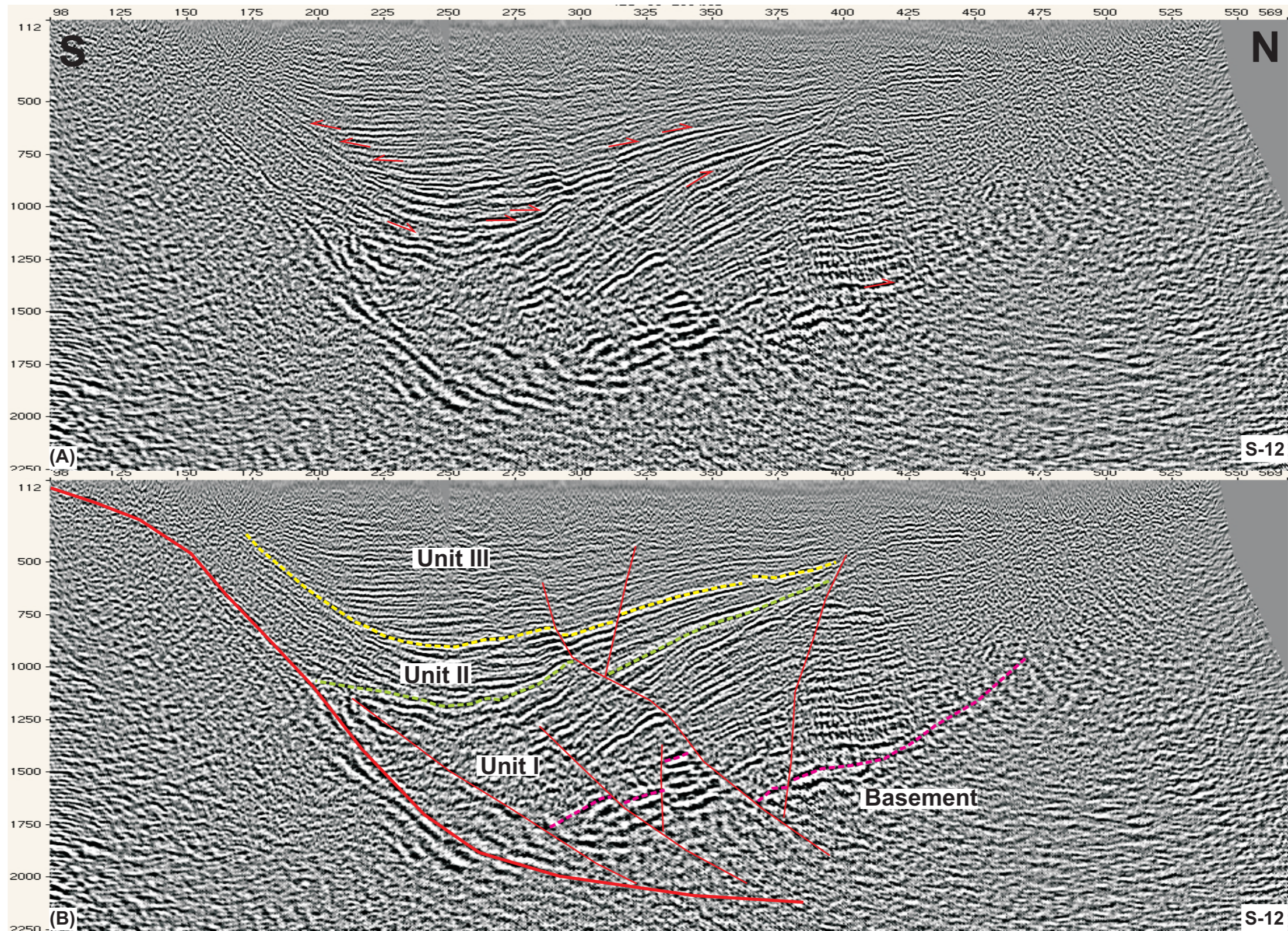


Figure 2.14. 2-D seismic section (S-12) oriented transverse to the Gediz Graben. Vertical scale is in milliseconds. The distance between the horizontal thick marks is 625 m. Note that there is nonlinear vertical exaggeration associated with the seismic sections. **(A)** Uninterpreted section. Small arrows point out the stratal terminations. **(B)** Section with basic interpretation. Basement metamorphic rocks can be differentiated by their acoustic transparency. Three seismic units can be recognized based on stratal terminations and change in the reflector dips. Thick red line depicts the main graben bounding fault and thinner red lines illustrate some secondary hanging-wall faults offsetting the stratigraphic units. See Chapter 5 for location and detailed interpretation of the seismic sections.

the distal (northern) parts of the unit, more organized and water driven deposition is expected to produce more parallel and continuous reflection responses.

Seismic Unit III overlies the *unit II* by almost horizontal reflector dips with a onlapping relation (Figure 2.14). The *unit III* is composed of parallel and subcontinuous reflectors that have a tendency of thickening towards the central thickest part of the unit. The reflectors also appear more continuous towards the southern and northern sides of the *unit III* but become relatively discontinuous at the central part of the unit. This may suggest that a lateral alluvial system, which carries sediment from the horst block to the graben parallel to the section orientation, may be influential at the northern and southern margins of the graben. Contrarily, more axial system with an orthogonal sediment transport direction with respect to section orientation governs the central part of the basin. The axial and lateral depositional systems are probably synchronous and interfingers at all stratigraphic levels.

In contrast to the *unit II*, thickness variation of the *unit III* is more symmetrical with respect to underlying graben fill. This suggests that subsidence rate is probably distributed more equally to the northern and southern margins of the graben. However, the thickest section of the *unit III* is still closer to the southern margin possibly indicating more activity for the southern margin-bounding fault. Differential compaction of the basin fill may also result in more accommodation creation at the depocenter of the underlying unit. This could also be influential on the development of the thickest section of *unit III* closer to the southern margin due to preceding asymmetrical development.

All the seismic stratigraphic units defined in Figure 2.14 indicates a some kind of changes in the depositional system, which result in stratal reorientation and the formation of the bounding surfaces between the seismic stratigraphic units. These bounding surfaces are not significant erosional surfaces or unconformities that are sites of major time gaps. Although, local and minor erosion may incorporate with these surfaces particularly towards the margins of the graben, there is no evidence of major erosion or lost section with in the graben fill. Towards the active southern margin, however, these surfaces can correlate to unconformities recognized on the surface exposures. In rift basins, minor and local unconformities tend to develop with block rotation and shift in the locus of extension yet they rarely represent major hiatus (Moretti and Colleta, 1987, 1988; Coletta *et al.*, 1988). The main cause of the discrete seismic stratigraphic units and intervening bounding surfaces is probably

more related to the activity of the graben-bounding faults. Change in the rate of subsidence and/or deposition, change in the geometry of the graben-bounding structures and/or spatiotemporal evolution of the graben can easily influence the depositional patterns and lead to formation of discrete sediment packages and intervening surfaces. The main question at this point is how the seismic stratigraphic units correlate with the lithostratigraphic units that are mapped and differentiated on the surface. If these lithostratigraphic units can be correlated to the seismic stratigraphic units of genetical importance, their surface distribution can provide further clues to the origin of the graben.

Figure 2.15 illustrates a transverse seismic section with BH-1 plotted on the profile. As in Figure 2.14, seismic stratigraphic units can be clearly differentiated on this section based on changes in reflection character and stratal terminations (Figure 2.15). When the lithostratigraphic formations are transferred on to the section by means of the BH-1, it is become evident that there is a strong correlation and good match between the seismic stratigraphic and the lithostratigraphic units. *Unit I* and *unit II* correlate very well with the Alaşehir and Çaltılık formations respectively. Both units display decrease of thickness from south to north as clearly depicted by Figure 2.15. Unit III, on the other hand, corresponds more than one formation and includes Gediz formation, Kaletepe formation and Quaternary alluvium, which are characterized by alluvial to fluvial facies. The contact between the Gediz and Kaletepe formations correspond to a prominent single reflector that can be traced along the entire section in Figure 2.15. However, there is no stratal reorientation across this contact as in the case of bounding surfaces of the seismic units I and II. This suggests that no significant changes took place in the manner of deposition between Gediz and overlying Kaletepe/Bintepeler formations.

If we refer to geological map in Figure 2.3 based on seismic units and formation correlations in Figure 2.15, one can easily observe that the Gediz and Kaletepe formations corresponding to the *unit III* forms an exposure belt and is separated by the MGBF from the Alaşehir and Çaltılık formations corresponding to *Unit I and Unit II*, respectively. Alaşehir and Çaltılık formations, on the other hand, expose along the same belt south of the MGBF but within different spatial domains having an overlapping region. All these basic observations suggest distinct stages during the evolution of the graben, which is discussed in detail in Chapter 5.

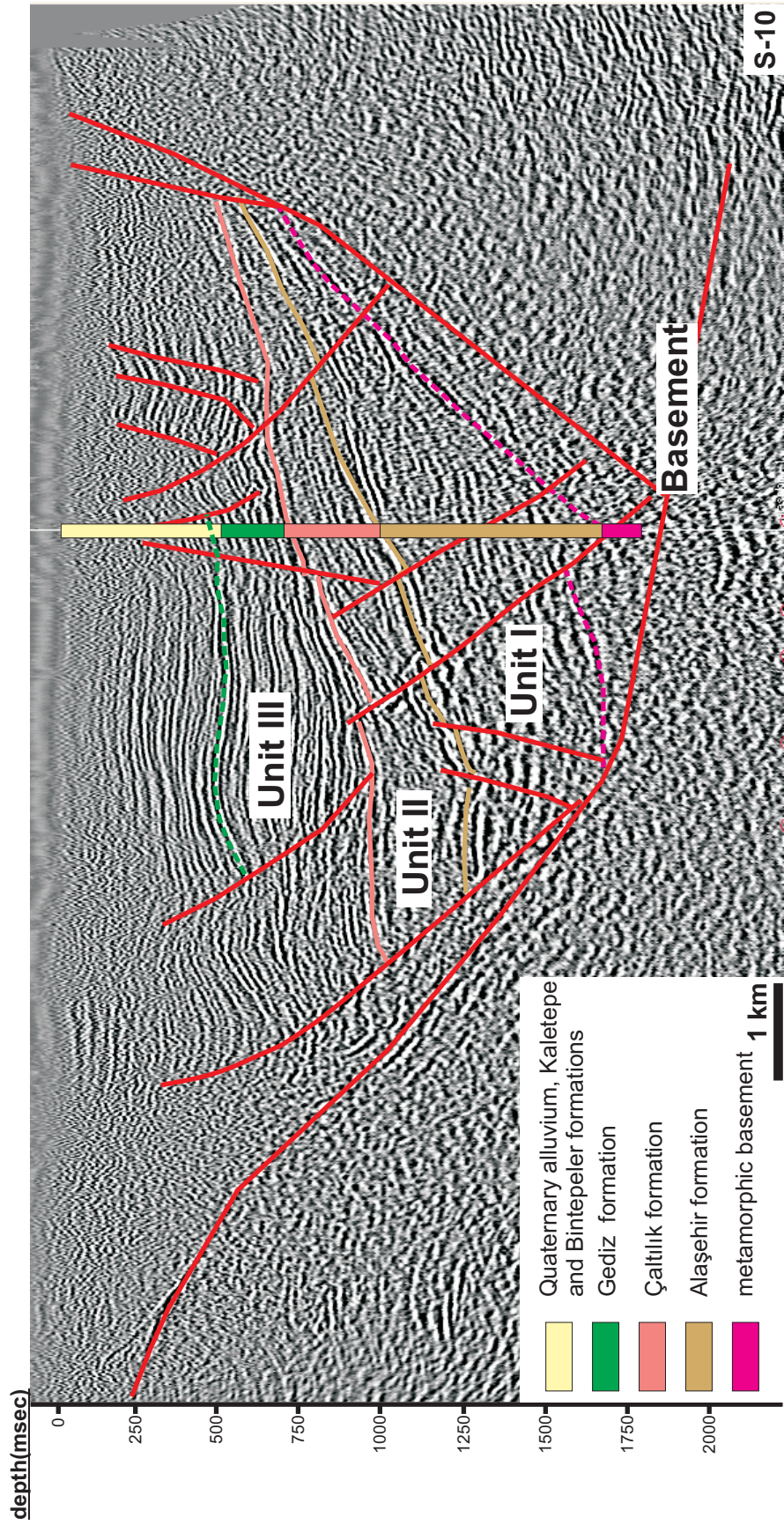


Figure 2.15. A transverse seismic section (S-10) with basic interpretations and Borehole 1 (BH-1). The vertical axis is in time (msec) and the horizontal scale is as illustrated. There is a good correlation between lithostratigraphic formation(s) identified in the BH-1 and seismic stratigraphic units. Although Gediz formation and overlying Kaletepe formation and Quaternary alluvium appear as a single seismic stratigraphic unit, a prominent reflector marks the boundary between Gediz and overlying Kaletepe/Bintepeleer formations. The boundary between Kaletepe/Bintepeleer formations and Quaternary alluvium is not very distinct on the seismic sections. See Chapter 5 for location and detailed interpretations of the seismic sections.

The contact relation between the Alaşehir and Çaltılık formations (i.e. the seismic *unit I* and *unit II*) were defined as conformable and gradual when discussing the lithostratigraphy of the graben at the beginning of this chapter. The question here is if this observation contradicts with the differentiation of the *unit I* and *unit II* based intervening bounding surface, which is defined as downlap surface in Figure 2.14. Although, the two units are separated by a downlap surface of an alluvial system prograding from south to north over the underlying lacustrine system, the lithofacies change between these units shouldn't be very sharp at this contact. Some degree of interaction is inevitable between the two systems resulting in gradual lithofacies change unless there is an unconformity in between for which no surface or subsurface evidence was identified. The angular relation (change in dip) between the two units is minor and variable across the seismic profiles with almost no dip differences observed at some sections (e.g. Figure 2.15). Such a low angular relations are difficult to observe at the exposures, especially if the exposure quality is not perfect.

CHAPTER 3

PATTERNS OF NORMAL FAULTING IN THE GEDIZ GRABEN

Gediz Graben is part of a well-known Aegean Extensional Province (AEP), which includes western Turkey, Aegean Sea and southern Balkan region (Figure 1.3). This province is a typical locality of an extensional deformation within the vast orogenic Alpine-Himalayan belt. Rate and mechanism of extensional deformation as well as the consequential seismic activity in AEP and in western Turkey has been the focus of many studies for last 20 years (e.g., Jackson and McKenzie, 1984; Eyidođan and Jackson, 1985; Ambrasseys, 1988; Taymaz *et al.*, 1991; Taymaz, 1993; Le Pichon *et al.*, 1995; Reilinger *et al.*, 1997; Ambrasseys and Jackson, 1998; Altunel, 1999; McClusky *et al.*, 2000; Bozkurt, 2001 and the references therein). These studies agree on the fact that western Anatolia is currently experiencing ~N–S-oriented extension. The rate of this extension is estimated around 30-40 mm/year (Oral *et al.*, 1995; Westaway, 1994; Le Pichon *et al.*, 1995).

As usual response to continental extension, grabens and associated normal fault systems constitute the most important structural elements in the geology of western Turkey (e.g., Hetzel *et al.*, 1995; Emre, 1996; Koçyiđit *et al.*, 1999a; Seyitođlu *et al.*, 2000, 2002; Yılmaz *et al.*, 2000; Lips *et al.*, 2001; Bozkurt, 2001, 2002, 2003; Sözbilir, 2001, 2002; Bozkurt and Sözbilir, 2004, 2006; Kaya *et al.*, 2004; Bozkurt and Mittwede, 2005). Among the several morphologically well-defined grabens, Gediz Graben is the most prominent and best-developed structural element of the region. Its asymmetry, with the most seismically active and largest faults located along the southern margin, manifested by numerous earthquakes during the last century (Arpat and Bingöl, 1969; Eyidođan and Jackson, 1985).

Associated normal faults of the Gediz Graben occurs at various scales from the largest graben-bounding faults extending hundreds of kilometers to mesoscopic

faults with offsets in centimeters scale. Formed synchronously with the sedimentation, these faults influence many aspects of the Gediz Graben, including basin geometry, distribution and variation of the lithofacies within the graben fill, surface geomorphology, drainage, and exposure of the rock units. As a result, understanding of the Gediz basin has a prerequisite to deduce the geometry and the characteristics of the normal faults dynamically shaping and changing the graben geometry. This also requires understanding of the stress regime governing the faulting, which is not addressed adequately so far in the Gediz Graben. Changes in the regional stress field during the course of graben evolution inevitably influence fault patterns and lead to a change in structural style. This not only influences the basin's geometry but also impact the depositional geometries and patterns. Furthermore, lateral variation of the stress field may lead to lateral changes of structural style as further contribution to the complexity of the system. Therefore, any change in structural style needs to be identified and assessed on the basis of controlling active stresses, stratigraphic occurrences and regional extend.

This chapter focuses on the geometrical properties of the normal faults and the nature of the controlling stress fields within the stratigraphic framework for the Gediz Graben. The analyses are initially based on the outcrop observations at numerous field stations in this chapter and then extended to the subsurface analyses including 2-D seismic and borehole data in the Chapter 5 (Figure 3.1).

Outcrop observations were carried out at 15 field stations along the southern margin of the graben. The field stations investigated can be separated into two groups: (i) section-based field stations and (ii) area-based field stations. Section-based field stations are characterized by an exposure surface along a road cut, quarry wall or canyon wall that allow 2-D examination of fault systems by means of a section oriented roughly parallel to the dominant dip direction of the faults. These field stations are suitable to observe the nature of stress field controlling the faulting, geometrical aspects of faults in the dip direction and characteristics of the hanging-wall deformation.

Area-based field stations are selected areas that include many profile-based exposures. The main function of area-based stations is to check the spatial variation of the prominent faults and the stress field in the strike direction of the faulting. By studying both profile-based and area-based field stations, geometrical properties of

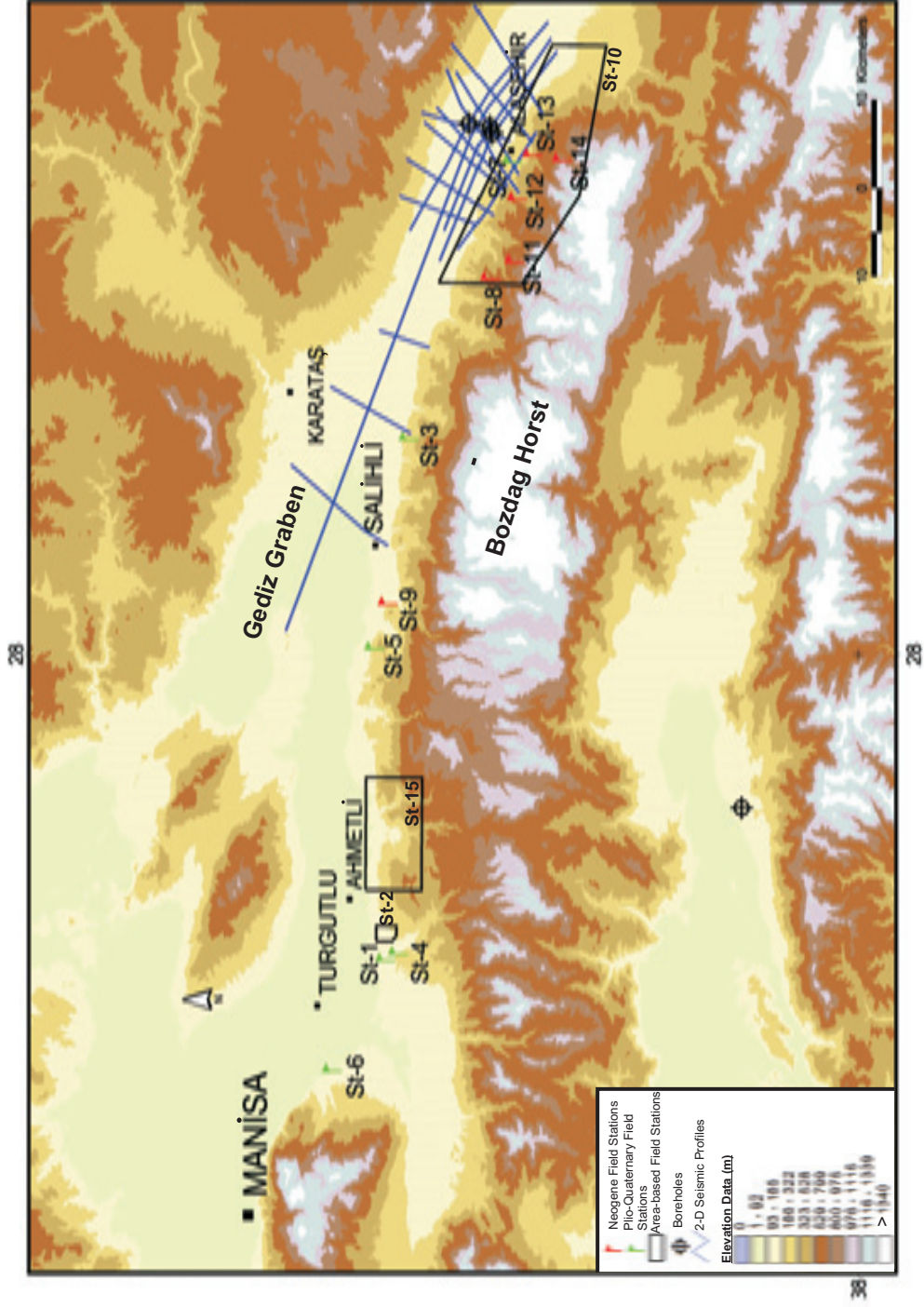


Figure 3.1. Elevation model of the Gediz Graben showing the locations of the field stations, and the available subsurface data including 2-D seismic profiles and boreholes.

the faults both in dip and strike direction were documented together with the spatial variation of the controlling active stresses.

3.1. Geometry of Normal Faulting

Normal faults are observable in the Gediz Graben at wide range of scales with displacements ranging from kilometers to millimeters and even smaller. Studies carried out in the graben refers two different structural styles for the observed faulting that are manifested by two groups of normal faults: (1) Large scale, low angle ($\sim 10^\circ$) normal fault (the detachment) that is observed along the southern margin of the Gediz Graben. (2) Approximately E–W-trending high-angle normal-slip faults that locally cut and offset the detachment fault (Hetzl *et al.*, 1995; Emre, 1996; Koçyiğit *et al.*, 1999a; Seyitoğlu *et al.*, 2000, 2002; Yılmaz *et al.*, 2000; Lips *et al.*, 2001; Bozkurt, 2001, 2002, 2003; Sözbilir, 2001, 2002; Bozkurt and Sözbilir, 2004; Kaya *et al.*, 2004; Bozkurt and Mittwede, 2005). The most recent literature agrees to relate these two different structural styles with episodic, multiphase extensional model of the region having earlier phase of N–S extension during Miocene and later phase of N–S extension during Plio-Quaternary (Koçyiğit *et al.*, 1999a; Bozkurt, 2003; Bozkurt and Sözbilir, 2004; Purvis and Robertson, 2004 and 2005; Bozkurt and Rojay, 2005). Some studies further divide the Miocene extension into two separate phases as Early-Middle Miocene E–W extension and Late Miocene N–S extension (Yılmaz *et al.*, 2000).

Analyses of faulting in areas of multiphase deformation require use of stratigraphy as a controlling agent to assess the faulting of different sedimentary packages. Based on stratigraphic occurrences of different structural styles a chronology of faulting can be established. In areas of single-phase deformation, this approach aids to understand the original structural style and predicts probable modification of older faults during the continuum of deformation. In accordance with the proposed multiphase extensional models of the region, faulting in the exposed fill of the Gediz Graben were investigated; (1) throughout the Plio-Quaternary strata and (2) throughout the Neogene strata.

The youngest faults of the Gediz Graben can be observed extensively within the Plio-Quaternary deposits. Because of the unconsolidated nature, these deposits are exposed to severe erosion, making it difficult to observe major fault planes. However, hanging-wall deformation of major faults is locally exposed by

excavations in clay pits, agricultural fields and along road-cuts. These exposures provide opportunity to study the nature of faulting that influence the Plio-Quaternary strata. Investigation of fault patterns in Neogene strata, particularly in Miocene strata, may lead to the identification of different structural styles that does not exist within the Plio-Quaternary section(s). If identified, this provides important evidence for the existence of multiphase deformation history in western Turkey.

3.1.1. Fault Pattern in Plio-Quaternary Deposits

Numerous mesoscale normal faults having cm-scale to m-scale displacements, were investigated within the Plio-Quaternary sediments (Figure 3.2). The majority of the faulting examined by field stations trends ENE–WSW with dips to the south and north, respectively (Figure 3.2A and B). Fault dips are usually steeper exceeding 45° and clustering around 60° (Figure 3.2C). Movements on the fault planes are predominantly dip-slip with minor strike-slip component, rarely exceeding 30° deviation from pure dip slip (Figure 3.2-D). However, small number of strike-slip faults does also exist (Figure 3.2E and F). Although very saddle, some relations can be defined between slip component and dip/dip azimuth of the fault planes. Figure 3.2E illustrates the relation between the fault dip and the measured rake of the slickenside lineations. In this plot, the rake varies between 0° and 180° , which emphasizes the type of strike slip component (sinistral for rake $< 90^\circ$; dextral for rake $> 90^\circ$). Representing the angle between the strike and the slickenside lineation on the fault plane, the rake is measured from the right hand side of the fault plane in a clockwise sense as the fault plane dips towards the observer (right hand rule; Angelier, 1994). The rake versus dip plot depicts that faults with predominantly dip-slip motion mostly have dips in the range of 50° to 70° (Figure 3.2E). This dip range is in good confirmation with the mechanical theory of faulting (c.f., Anderson, 1951; Davis, 1984). Above and below this dip amount, there is a relative increase in strike-slip component. Yet, there is no relative preference for sinistral or dextral component in relation to fault dip (Figure 3.2E). In a similar way, Figure 3.2F illustrates the relation between the dip azimuth and the rake of the faults. Strike-slip component is relatively higher for faults that dips towards SSE (dip azimuth: $\sim 165^\circ$), WSW (dip azimuth: $\sim 240^\circ$), and NNW (dip azimuth: $\sim 330^\circ$) in a way that WSW-dipping faults have sinistral whereas SSE- and NNW- dipping faults have dextral components

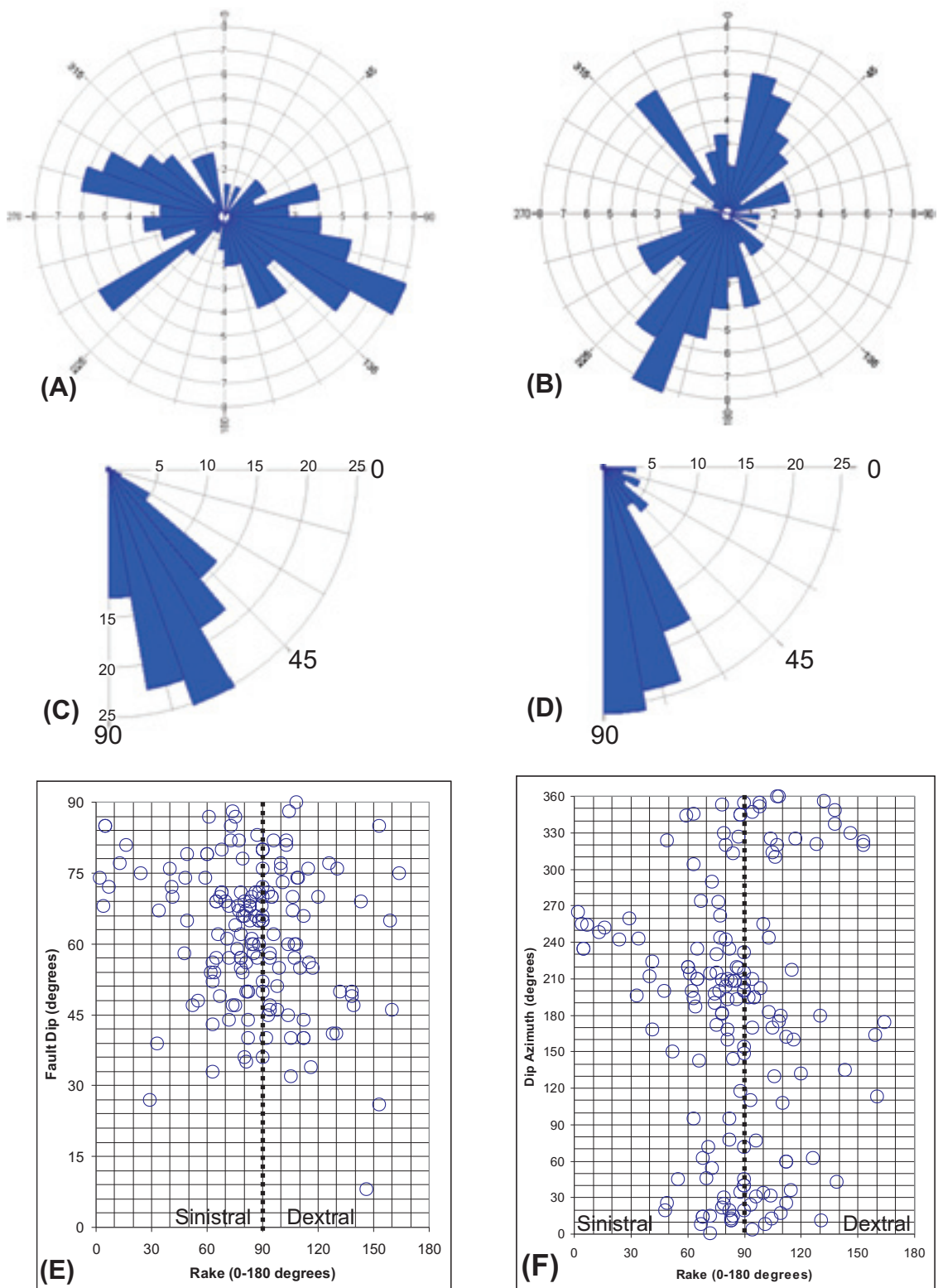


Figure 3.2. General characteristics of faults influencing the Plio-Quaternary deposits (N=161). (A) Rose diagram for strike of faults (right hand rule); (B) dip azimuths of the faults; (C) fault dips; (D) measured rake of the slickenside lineations on the fault plane (0° to 90°); (E) binary plot showing the fault dips vs rake of the slickenside lineations; (F) binary plot showing the azimuth of fault dips vs rake of the slickenside lineations. In (E) and (F) dashed lines separate sinistral and dextral components of motion. The rake is measured from 0° to 180° starting from right hand side of the fault plane as fault plane is dipping towards the observer.

(Figure 3.2-F). These orientations are oblique to dominant trend of the faults with predominant dip-slip component.

The observations at the field stations are dominantly concentrated around a relatively larger fault, referred as the master fault, cutting the entire section of observation. Secondary faults, or parasitic faults (c.f., Fossen and Gabrielsen, 1996), form extensively in the vicinity of the master fault (e.g. Figure 3.3). As the master fault is a discontinuity, which results from slip on a narrow zone, it results in some degree of mismatch in layering across the fault plane. In Figure 3.3 (St-1), for example, detailed observations on the sedimentary layering found out that, point A in the hanging-wall was cut and offset from point B in the footwall, resulting in 11.5 m separation associated with the normal fault plane. This separation is not the total displacement or net separation but only the apparent relative movement along the observed section (c.f., Angelier, 1994). The fabric developed within the fault gauge also confirms the normal separation of the fault plane (Figure 3.3B). The actual slip vector can be inferred from slickenside lineations.

The deformation around the master fault is always dominated by secondary synthetic and antithetic faults, having same and opposite dip direction to the master fault, respectively (Figures 3.3, 3.4, and 3.5). Analog physical modeling efforts has shown that relative abundance of antithetic and synthetic faults is directly related to the master fault's geometry. While, concave upward bends in the fault plane facilitates formation of antithetic structures, convex upward bends is characterized by the dominance of synthetic structures (Withjack *et al.*, 1995). The underlying cause of this match is the fact that antithetic inclined simple shear arises in concave upward fault bends and synthetic inclined simple shear is influential in convex upward bends (White *et al.*, 1986; Dula, 1991; Xiao and Suppe, 1992; Withjack *et al.*, 1995). In the scale of outcrop observations carried out in this study, faults are mostly planar and the relative abundance is not an issue for the observed antithetic and synthetic faults. They seem to be formed at equal amounts in most sections (Figures 3.3, 3.4, 3.5 and 3.6). However, the intensity of deformation accommodated by the secondary faults is more pronounced within the hanging-wall compared to the footwall as also modeled by Fossen and Gabrielsen (1996) (Figure 3.3). This provides with graben blocks that are more intensely deformed than the horst blocks (Figure 3.4)

Figure 3.5 illustrates a typical example of a master fault with a well-developed hanging-wall deformation. The deformation influences a sedimentary

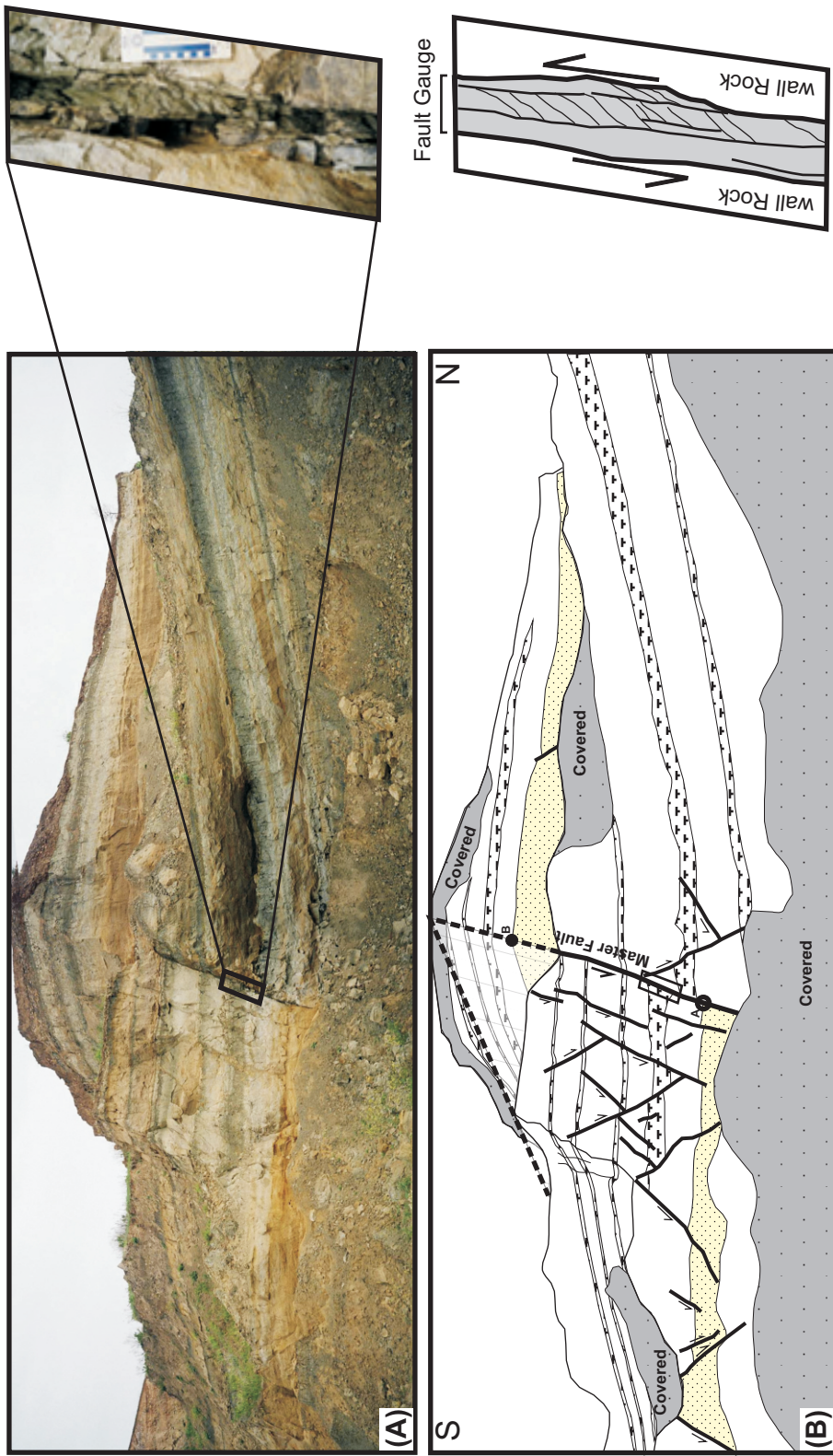


Figure 3.3. A field photograph (A) and its sketch (B) at the St-1. The photograph and the sketch illustrate the surface of the outcrop exposure. Master fault cut and offset the sedimentary layering with associated hanging-wall deformation. Yellow layer is a key bed correlated across the master fault. Fault slip data acquired from the main fault and secondary faults were analyzed to compute the stress field responsible for the observed deformation. Inset picture show close up view of the fault gauge illustrating the fabric developed within the fault zone. The fabric confirms the normal slip on the fault plane.

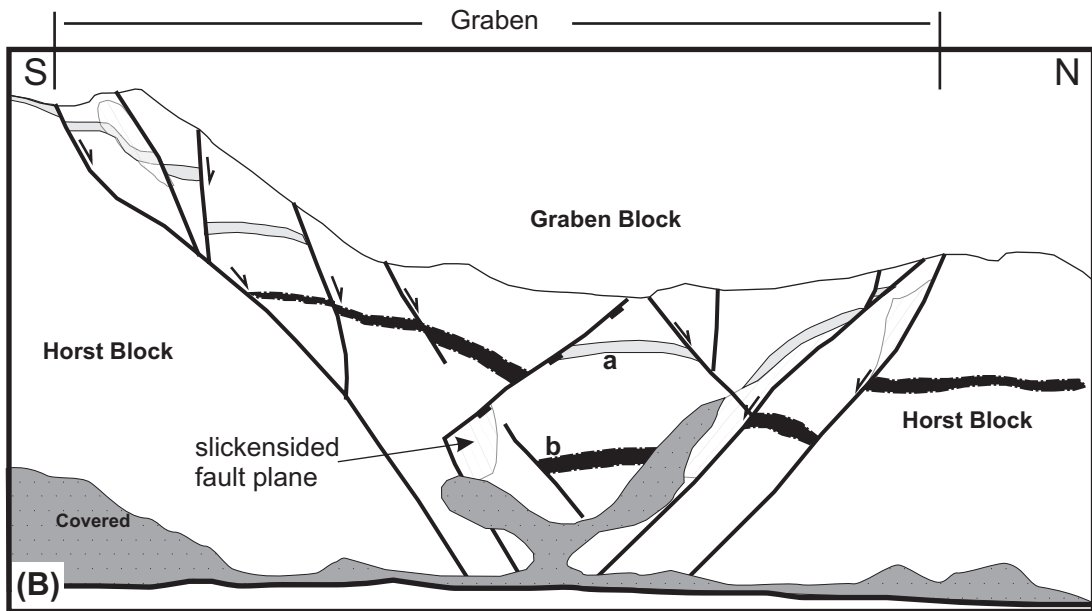


Figure 3.4. Field photograph (A) and sketch (B) of an outcrop surface in St-2. See Figure 3.1 for the location of the station. A pair of conjugate normal faults form a graben block between two horst blocks. Deformation is more pronounced in the graben block compared to the horst blocks. a and b illustrates the location of key layers in the picture. The truck in the picture is 2 m high.

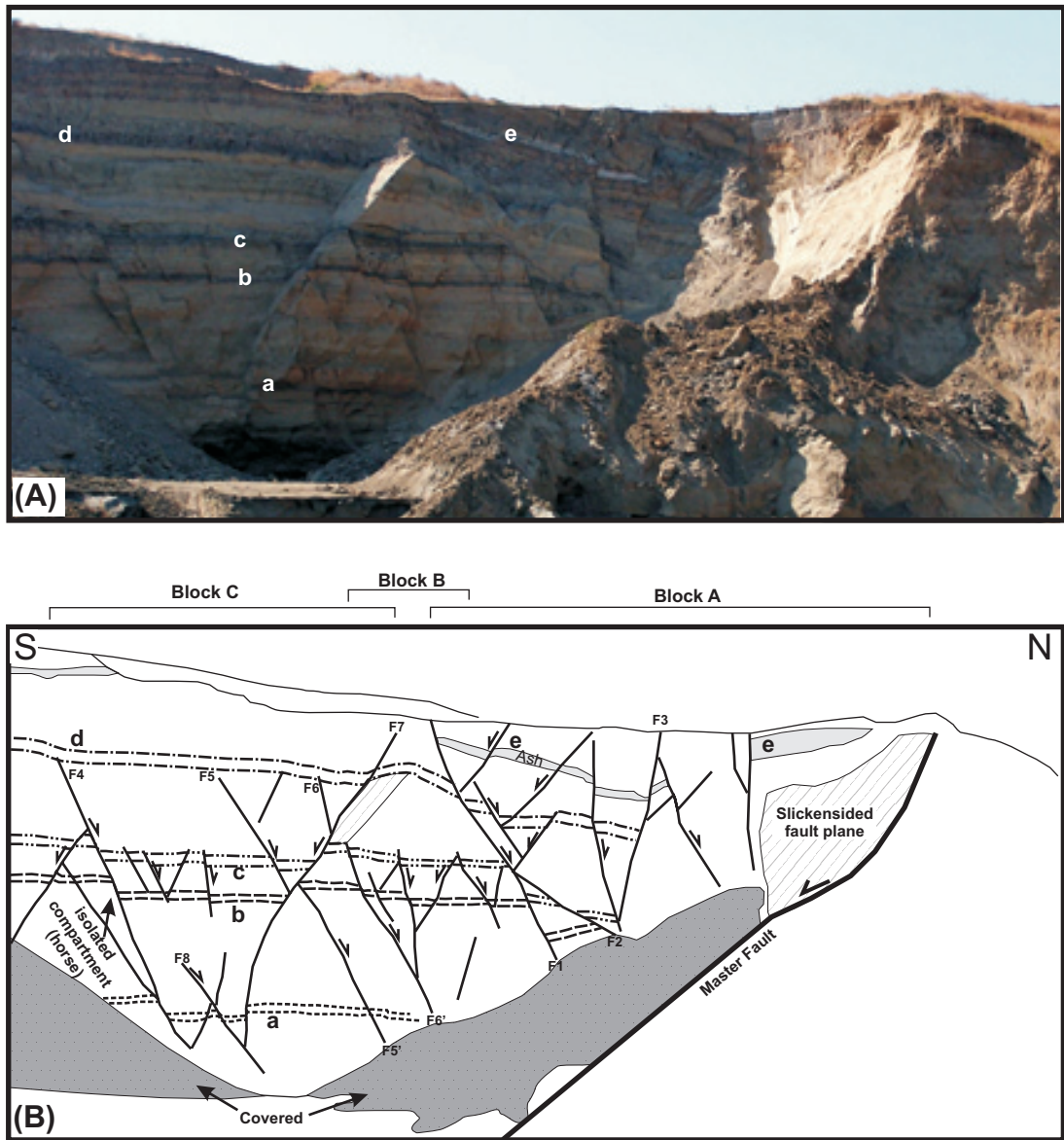


Figure 3.5. Field photo (A) and sketch (B) of an outcrop surface in St-2. See Figure 3.1 for the location of the station. The faulted sedimentary section is composed of claystone beds (dark-gray colored), siltstone-fine sandstone beds (yellowish colored) and a layer of ash (white colored). Note the interrelation of conjugate faults and the intensity of the hanging-wall deformation of the main fault. a through e illustrates location of the key beds on the picture. Slickensided fault plane surface is 2.5 m high.

section comprising alternation of clay beds (dark-gray colored) and siltstone-fine sandstone beds (yellowish colored) with a layer of ash (white colored). It is clear in the figure that the intensity of deformation in the hanging-wall accommodated by the secondary faults increases towards the master fault. This increase not only includes the number of faults dissecting the volume of hanging-wall but also counts for the amount of displacement accrued on the secondary faults. Based on the most prominent secondary faults, the hanging-wall of the master fault can be separated into three main blocks as Block A to C respectively (Figure 3.5). The Block A forms a graben bounded between the master fault and the F1. The Block B defines a horst block bounded by F1 and F7. The Block C is another graben constraint by F7 and F4. It is evident on the figure that internal deformation in each block is accommodated by secondary faults and it varies among the adjacent blocks. For example, the most intense deformation occurs in Block A, which is manifested by relatively larger rotation of key beds from subhorizontal and large amount of offsets associated with the second order faults. Comparatively, smaller offsets are distributed among many secondary faults in block B that is free of significant tilting of key beds from subhorizontal. Block C, on the other hand, is characterized by minor amount of offsets, along smaller number of secondary faults as an evidence of least deformation among the blocks observed on the figure.

As it is stated, hanging-wall deformation of the master fault is usually dominated by two sets of oppositely dipping faults (Figures 3.3, 3.4, 3.5 and 3.6). Collectively, these sets are referred as conjugate normal faults having dihedral angle of approximately 60° (c.f., Anderson, 1951). Several requirements constraint conjugate faults systems to be identified (Angelier, 1994). There should be at least two families of faults among which each family is defined, based on common geometry in terms of dip, strike and the pitch of slickenside lineation. Furthermore, slickenside lineation of faults in each family should be perpendicular to the line of intersection of the conjugate counterparts (β -axis). Last but not least, rotation couples implied by the slip on the conjugate faults should be in opposite sense. Faulting observed in the Plio-Quaternary sediments of the Gediz Graben commonly satisfies these requirements within the range of uncertainties and natural variations (Figure 3.7).

Intersecting and crossing conjugate normal faults are common structures in extensional terrains and have received some attention in the literature (Horsfield,

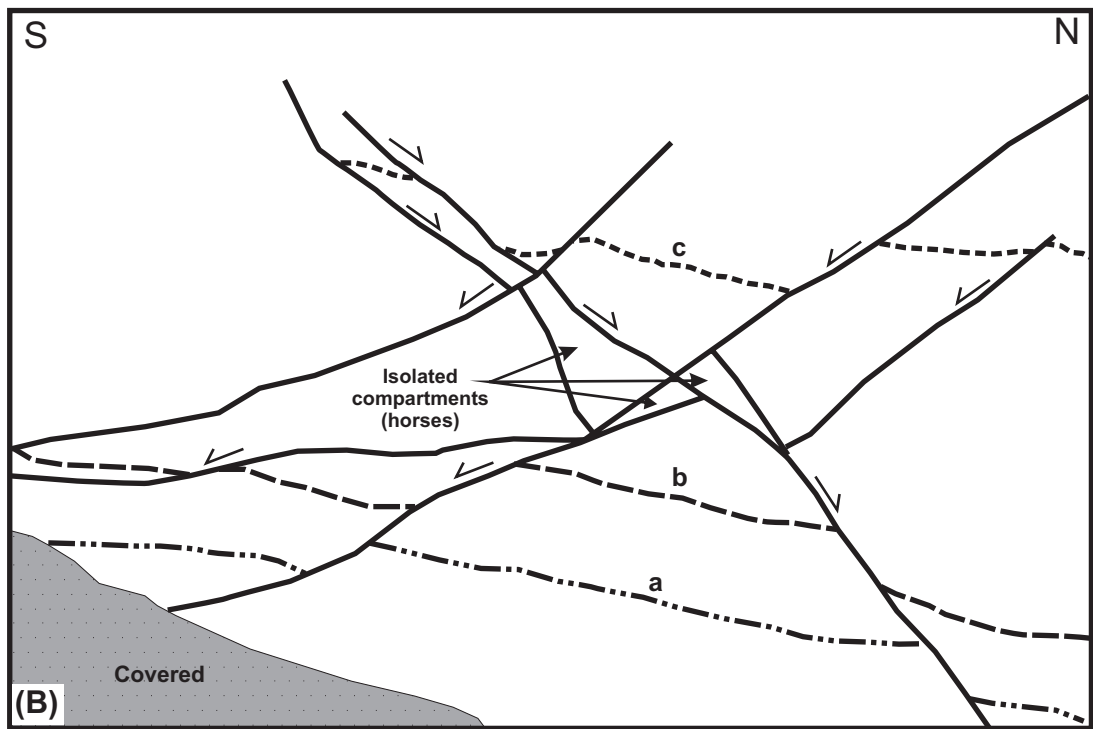
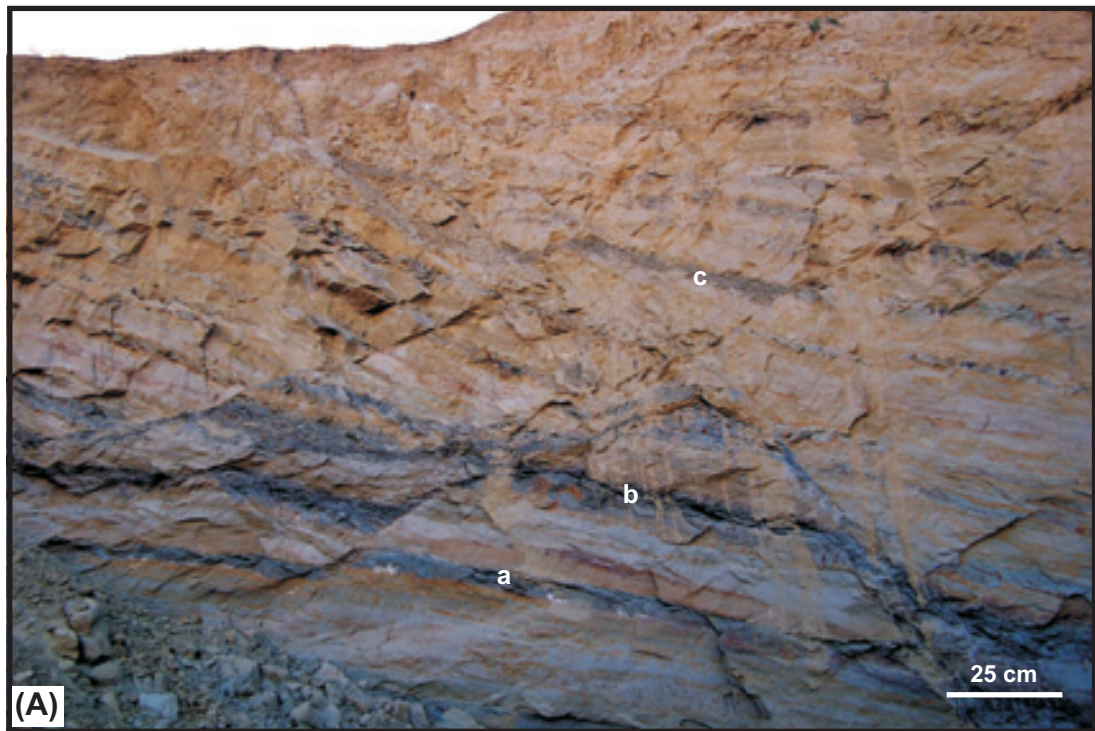


Figure 3.6. Field photograph (A) and sketch (B) of an outcrop surface in St-3. See Figure 3.1 for the location of the station. Note the complex deformation at the zone of intersection of crossing conjugate faults. a through c illustrates location of the key horizons in the photo.

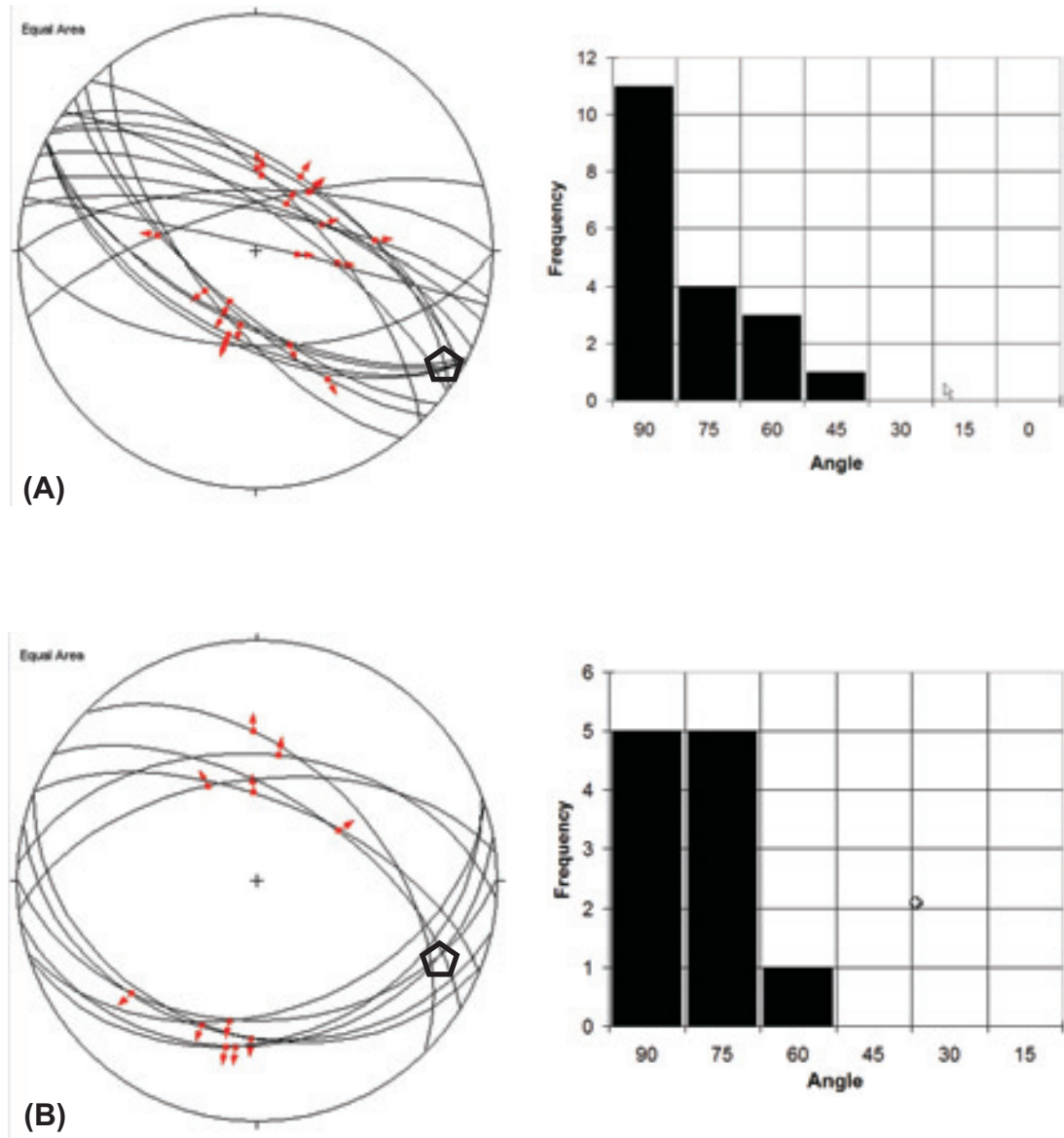


Figure 3.7. Fault data depicting examples of conjugate fault systems in the Quaternary deposits. Left column illustrates stereographic projections of fault data including slickenside lineation. Pentagon symbol is for the average position of intersection line of conjugate fault families (β -axis). Right column shows the frequency of angle between the slickenside lineation of the fault plane and the β -axis. This angle is expected to be 90° for conjugate faults. **(A)** Station 1 with n (number of measurements)=19 (Figure 3.2). **(B)** Station 3 with $n=11$ (Figure 3.5).

1980; Nicol *et al.*, 1995; Watterson *et al.*, 1998; Castagna, 1996; Ferrill *et al.*, 2000). Conjugate normal faults also named as “X-pattern” or hour-glass based on its cross-sectional appearance in seismic sections (Castagna, 1995; Woods, 1992). Slip on crossing conjugate normal faults are usually considered as simultaneous (or synchronous) (Horsfield, 1980; Oddone and Massonnat, 1992; Watterson *et al.*, 1998). Although, X-pattern produced by crossing conjugate faults do not impose a geometric problem, simultaneous operation of the crossing pair imposes a compatibility problem requiring gain, loss or redistribution of the cross-sectional area (Figure 3.8) (c.f., Ramsey and Hubber, 1987; Ferrill *et al.*, 2000). Watterson *et al.* (1998) showed that strain within the intersection zone of conjugate faults is accommodated by several mechanisms such as intergrain slip and layer thinning at constant volume. Yet, if the slip on the conjugate pairs occur in alternating sequential manner rather than simultaneous, there is no need left for the area change eliminating the compatibility problem (Ramsey and Huber, 1987; Ferrill *et al.*, 2000). In the classical sequential model, a new fault forms in each stage of the sequence to cut and offset the earlier faults (Figure 3.9A) (Ramsey and Hubber, 1987). However, reactivation of existing fault segment may sometimes be a case after T2 in Figure 3.9A because earlier zone of weaknesses are easier to break than a new fault (Morris *et al.*, 1996). The reactivation may take place in four different ways (Ferrill *et al.*, 2000) (Figure 3.9B). (1) Reactivation and downward propagation (1 in Figure 3.9B); (2) Reactivation and upward propagation (2 in Figure 3.9B); (3) Linkage of offset segments (3 in Figure 3.9B) (4) Reactivation with juxtaposed segment (Figure 3.9C) (Ferrill *et al.*, 2000). These processes may form complex geometries at the intersection zone of the conjugate sets (Figure 3.6). Isolated fault bounded compartments and/or wedges may generally form near intersection zones (Figures 3.5 and 3.6). These compartments may introduce significant reservoir heterogeneities in oil fields of similar structural style.

The field observations are in good confirmation with the sequential activity model (Figure 3.5). For example, F_5 and F_6 in Figure 3.5 is cut and displaced by their conjugate counterpart F_7 . F_7 , on the other hand, is cut by F_8 which is synthetic to F_5 and F_6 . Therefore, among the pair of conjugate faults, neither set consistently cut and offset the other set. This eliminates the probability of superimposition of one set over the other as a succeeding style and proves that conjugate faults form within the same time frame in which slip on conjugate pairs occur sequentially one after another. To

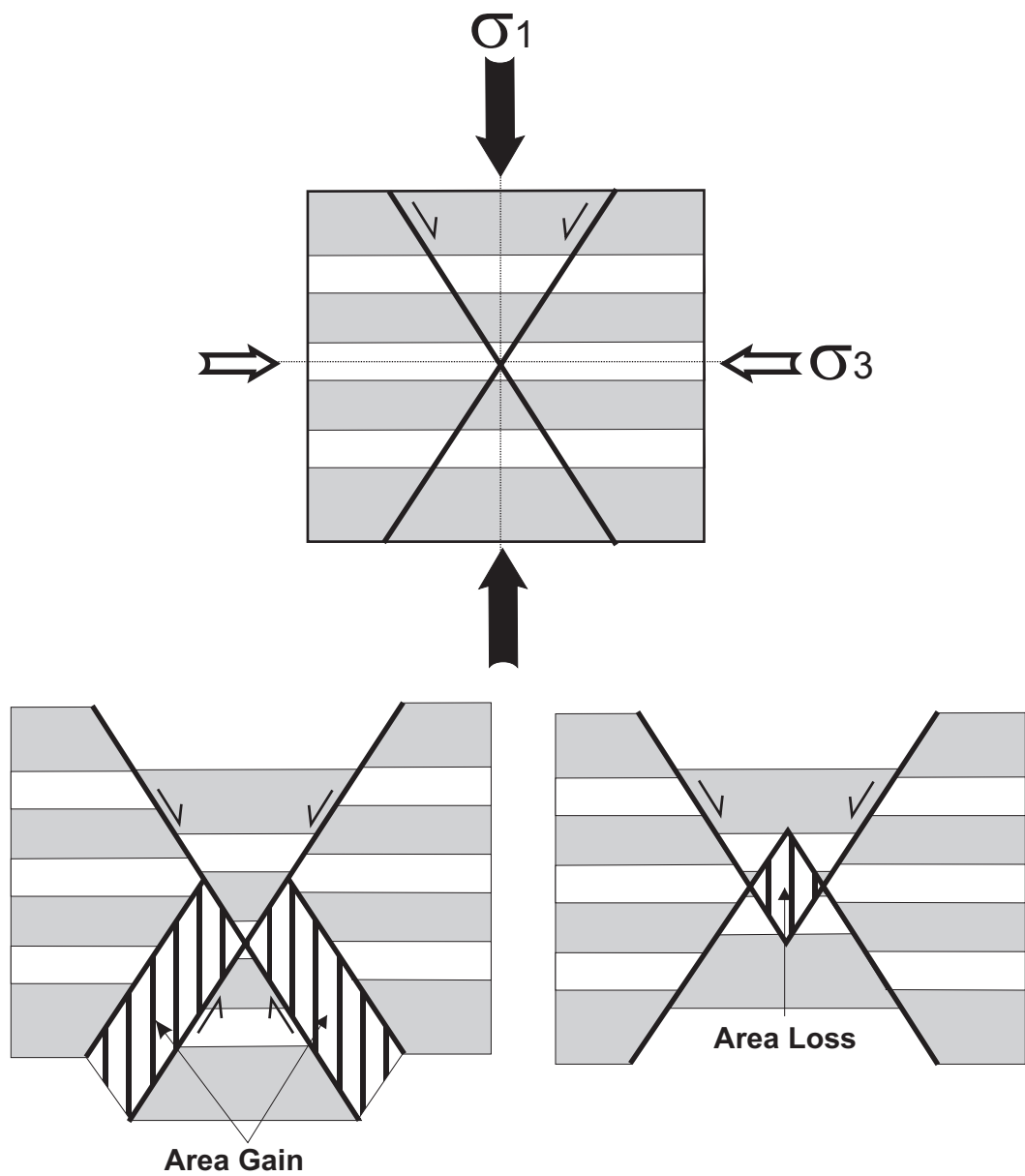


Figure 3.8. Simultaneous slip on crossing conjugate normal faults produces a compatibility problem requiring area gain or lost in cross-section (Ferrill *et al.*, 2000).

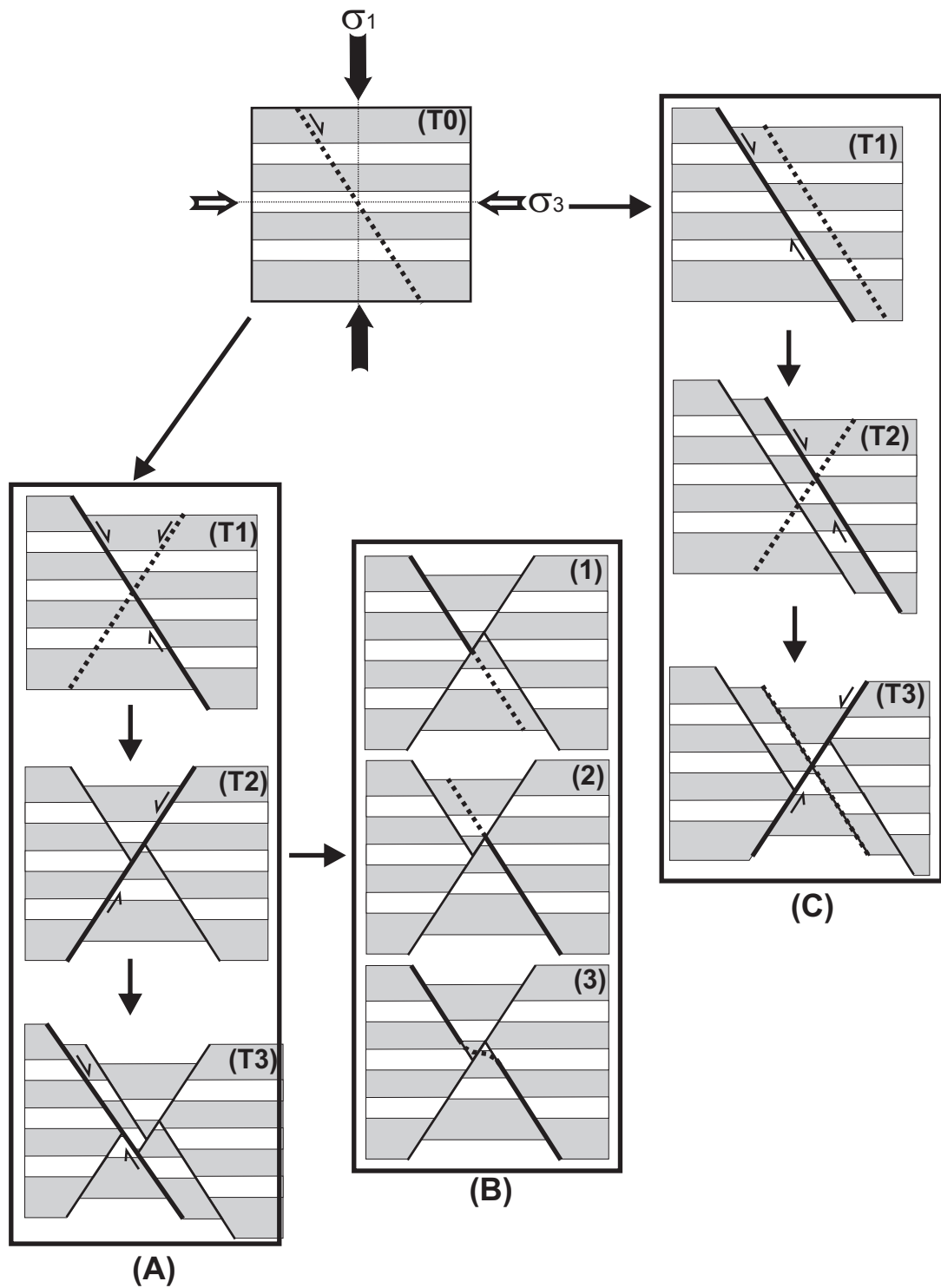


Figure 3.9. Sequential slip on crossing conjugate normal faults eliminates the compatibility problem at the intersection zone. **(A)** New faults form in each stage of sequence and cut and offset the earlier fault; **(B)** Reactivation of the earlier fault instead of forming a completely new fault. Reactivation can take place in three different ways: (1) Reactivation and downward propagation, (2) Reactivation and upward propagation, (3) Linkage of offset segments. **(C)** Reactivation with juxtaposed segment. T0, T1, T2 and T3 represents progress in time (modified from Ferrill *et al.*, 2000; Ramsey and Hubber, 1987).

further test this model, basic restoration of the conjugate fault systems given in Figure 3.6 was carried out in a sequential manner in Figure 3.10. Fault activities were restored one after another starting from the current stage to reach pre-deformed stage (T_4 to T_0 in Figure 3.10). Restoration of the sequential activities provided with a reasonable solution at first order leading to pre-deformed stage successfully (T_0 in Figure 3.10). Yet, there seems to be minor amount of ductile strain associated with the fault slips resulting in layer thinning and slight mismatches in the pre-deformed stage T_0 . It is likely that amount of ductile strain accompanying fault slip is a function of lithology in our case which is dominated by ductile claystones. On the other hand, simultaneous slip on conjugate pairs may remain a possibility in the case of faults with vertical displacement gradients towards the conjugate intersection that is characterized by ductile strain (Watterson *et al.*, 1998).

Outcrop observations (e.g., Figures 3.3, 3.4 and 3.5) suggest that partial development of the conjugate pairs is also a possibility. In these cases, one of the faults in the conjugate pair will preferentially form either on the hanging-wall or footwall of the other fault. This results in “Y” or upside down “Y” type of geometry in the cross section for the conjugate faults that are not crossing each other but one abutting against the other (Figures 3.3, 3.4 and 3.5). In Figure 3.5, for example, this geometry is commonly associated with faults having relatively larger amount of offsets, such as F_1 , F_4 and F_6 . This suggests that relatively large amount of slip on the fault may affect formation of crossing conjugate counterpart, and an incomplete conjugate forms to accommodate strain only on the hanging-wall or footwall block.

It is also important to assess the strike-wise geometries of the fault planes observed so far in dip section. In order to serve for this purpose, field mapping were carried out at the St-2 to document spatial geometries of the fault systems (Figure 3.11). The mapped area is a clay pit excavated extensively to provide raw material for the brick industry. It is very probable during the mapping effort that observed fault density is biased by the location of the most recent and more intense excavations as they provide fresh exposures of fault planes that are hidden otherwise. The mapped area includes field photos discussed in Figures 3.4, 3.5 and 3.6. Five different units were differentiated in the map area all of which correlates to the proximal Quaternary alluvium in Figure 2.3 (Figure 3.11):

Unit A is predominantly composed of thick and poorly bedded, weakly consolidated, laterally continuous, locally cross bedded and rippled, medium to very

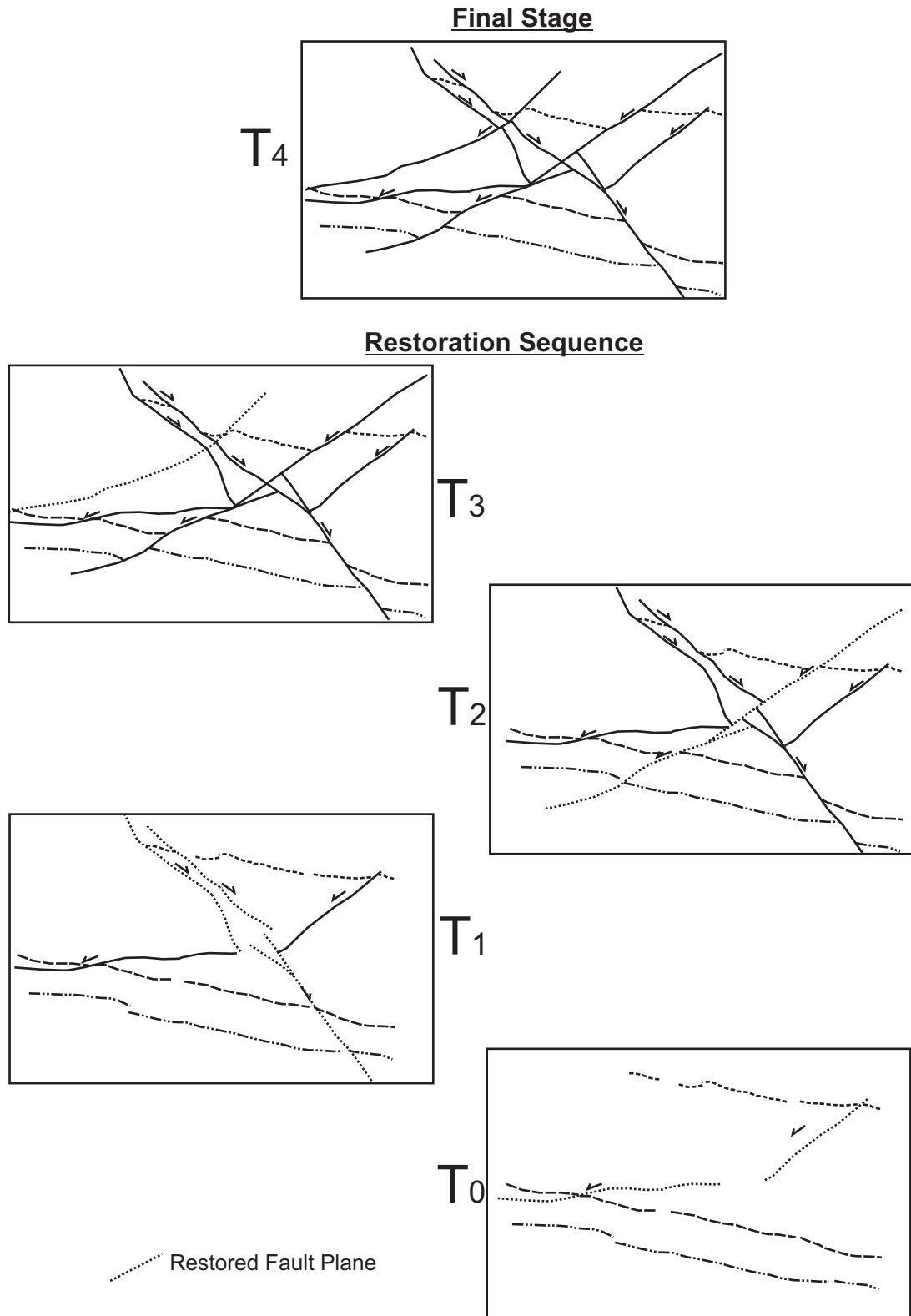


Figure 3.10. Sequential restoration of conjugate fault systems of St-3 (Figure 3.6). T₀ to T₄ represents stages of deformation from pre-deformed state to final state respectively. Sequential restoration based on the sequential activity of conjugate faults provides with acceptable restoration at first order. However, there is also evidence of minor amount of ductile strain which results in layer thinning and slight mismatches at the pre-deformed stage T₀. Contribution of ductile strain is probably a function of lithology which is claystone dominated in our case.

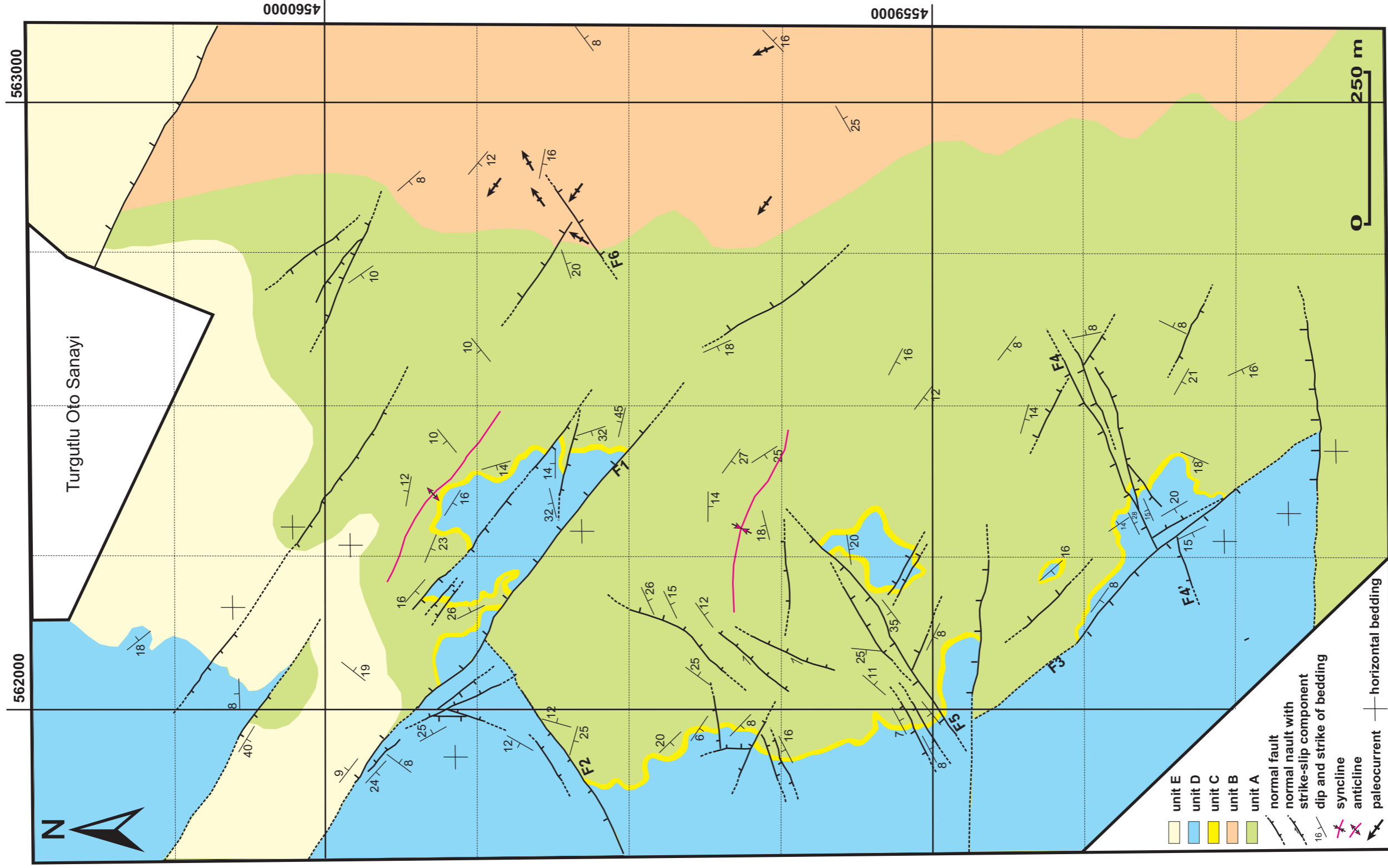


Figure 3.11. Geological map of the St-2. See Figure 3.1 for the location of the station. The mapped units A through E can be correlated with proximal Quaternary alluvium deposits in Figure 2.3. The differentiation of the units is based on the lithological differences which is discussed in the text. Note that the map view pattern of the faults is similar to that of cross-sectional view. This pattern is caused by the nature of active stresses that is discussed in section 3.2.

fine grained sandstones and intercalating siltstones that are rich in mica content. The unit also includes lenses of polymictic conglomerates that are composed of well-rounded and poorly sorted metamorphic clasts. Base of conglomerate lenses are scoured and throughy cross bedding is very common. In a very general sense, Unit A fines upward into dark gray colored clay stones by means of numerous fining-upward cycles.

Unit B is composed of polymictic, gravelly matrix-supported, and moderate to well-rounded conglomerates, showing well developed pebble imbrications. Laterally, the unit B grades into the unit A.

Unit C is a key horizon overlying units A and B in the mapped area. It is a single bed of white colored, 15-30-cm-thick, very fine-grained ash layer observed in Figures 3.4 and 3.5.

Unit D is very similar to the unit A, except that it is relatively finer grained and lacking conglomerate lenses. Unit C separates units A and D with a very sharp boundary.

Unit E is the recent soil covering the exposures.

All units described above probably deposited in an alluvial fan environment that is having permanent channel system characterized by the Unit B. Palaeocurrent indicators in the unit B suggest SE- to NW-directed flow for the channel (Figure 3.11). Unit A and unit D probably represent overbank deposits of the main channel system having complete lateral gradation with the unit B (e.g., Miall, 1992, 1996; Cant, 1992). A Quaternary volcanic activity perhaps related to Kula volcanics (Richardson-Bunburry, 1996) or volcanism in Aegean islands (e.g., volcanic caldera of Santorini) may relate to the Unit C.

It is interesting that, similar “X” and “Y” patterns formed by conjugate pairs in cross-sectional view are also observable in the map view in larger scale (Figure 3.11). As Anderson’s theory of faulting predicts that conjugate pairs observed in the dip sections are essentially parallel in their strike orientations, the observed fault systems having angular relation in the map view can not be regarded as conjugate pairs (Figure 3.11). In fact, three separate conjugate systems were identified at St-2 satisfying the conjugate requirements (Figure 3.12). These systems have an approximate trend of NW–SE, E–W and NE–SW.

As a general observation in the map, NE–SW-striking faults seem to abut to the NW-SE striking ones. Examples to this are documented by the cases of F₁-F₂ and

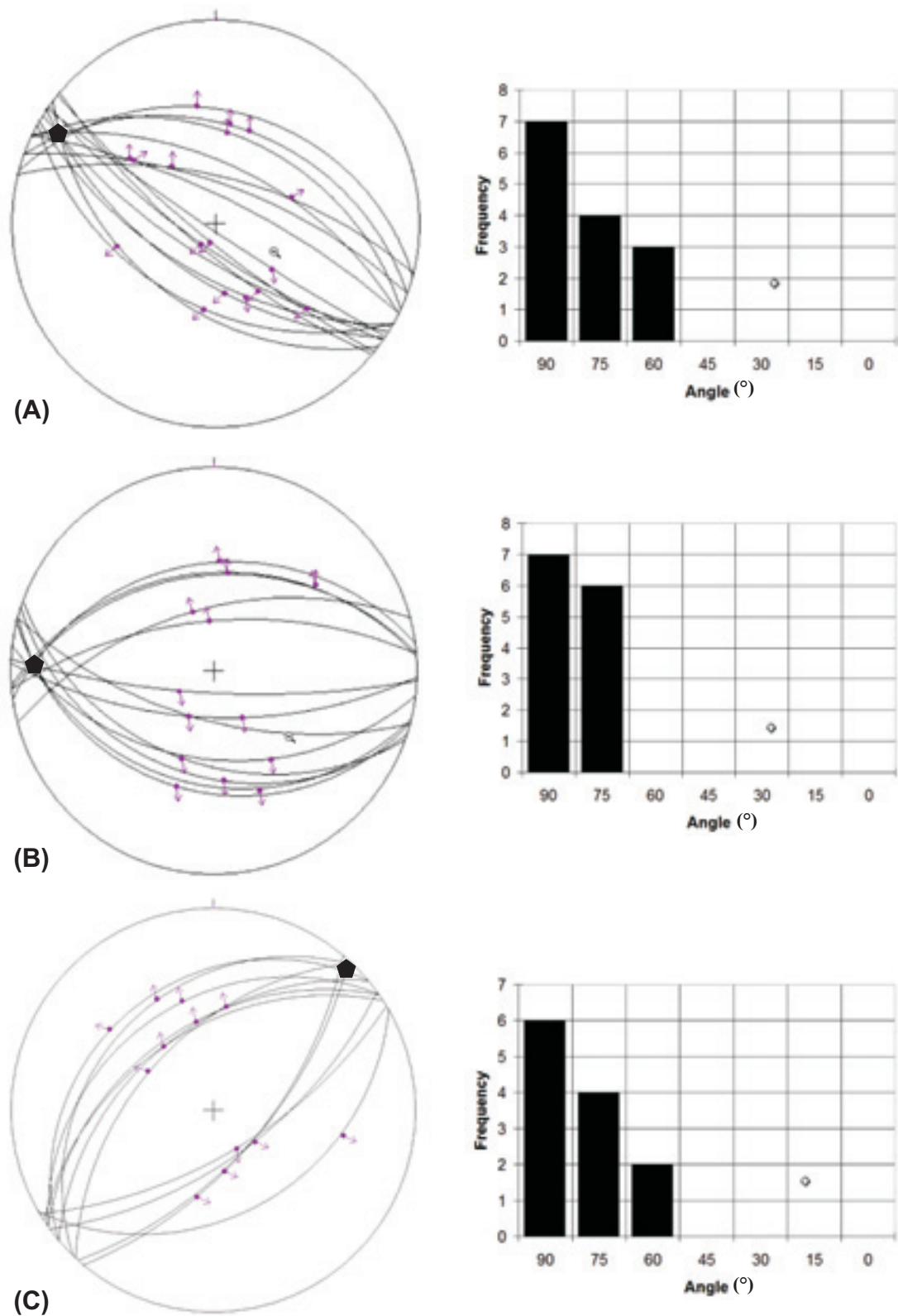


Figure 3.12. Three separate conjugate fault systems identified in the St-2 (Figure 3.11). Left column documents fault data for each conjugate system with pentagon depicting the average position of the line of intersection of the two sets (β -axis). Right column illustrates the angle between the line of intersection and the β axis. This angle is expected to be 90° for the conjugate faults.

F₃-F₄ pairs (Figure 3.11). However, more focused observations on the map can easily reveal the cases that are vice versa. Around the F₅ and F₆, for example, NW–SE-oriented faults seem to abut to the NE–SW-oriented faults. Similarly, E–W-oriented faults also lack consistency of cutting to or being cut by the other systems. This suggests that all three conjugate fault systems form in the same time frame without a distinct cross-cutting relationship that one cannot put into a chronology. It can also be inferred that the abutting faults generally form on the footwall of the corresponding fault (Figure 3.11). Therefore, angular relation between the different conjugate fault systems is not a complexity caused by hanging-wall deformation either. If there is a cross-cutting relationship due to successive phases of deformation, one should expect the continuation of the abutting fault on the other side of the cutting fault. Most of the time, this is not the case. The only exception to this occurs for the F₃ where a small segment of NE–SW-striking fault (F₄) is observable in the hanging-wall and in the footwall (F₄). This unique exception can easily be regarded as a local complexity related to the hanging-wall deformation of F₃ because there is not enough constraint to correlate F₄' and F₄ across the F₃.

If the fault data in Figure 3.11 is illustrated graphically, strike orientations of the fault planes clusters around three main directions confirming three main conjugate systems of NW-SE, E-W and NE-SW (Figure 3.13-A and B). Dips are roughly to the north and south in the range of 45° to 90° (Figure 3.13-B and C). Rake of slickenside lineations indicate dominance of dip-slip motion on the fault planes with minor amounts of sinistral and dextral strike-slip component (Figure 3.13D, E and F).

Based on these pure geometrical observations emphasized in the previous section, it is not possible to assess the deformation mechanism resulting the observed fault pattern of multi-direction fault orientations. Yet, it is clear that multiple phases of normal faulting is not a case for the Figure 3.11 as there is no consistent superimposition of one fault system to the other. This may suggest that observed fault pattern might be related to the lack of well-defined direction of extension over the history of faulting. This may result in multi-directional extension to cause fault pattern of multi-directional strike orientations related to poorly constraint σ_3 axis (Angelier, 1994).

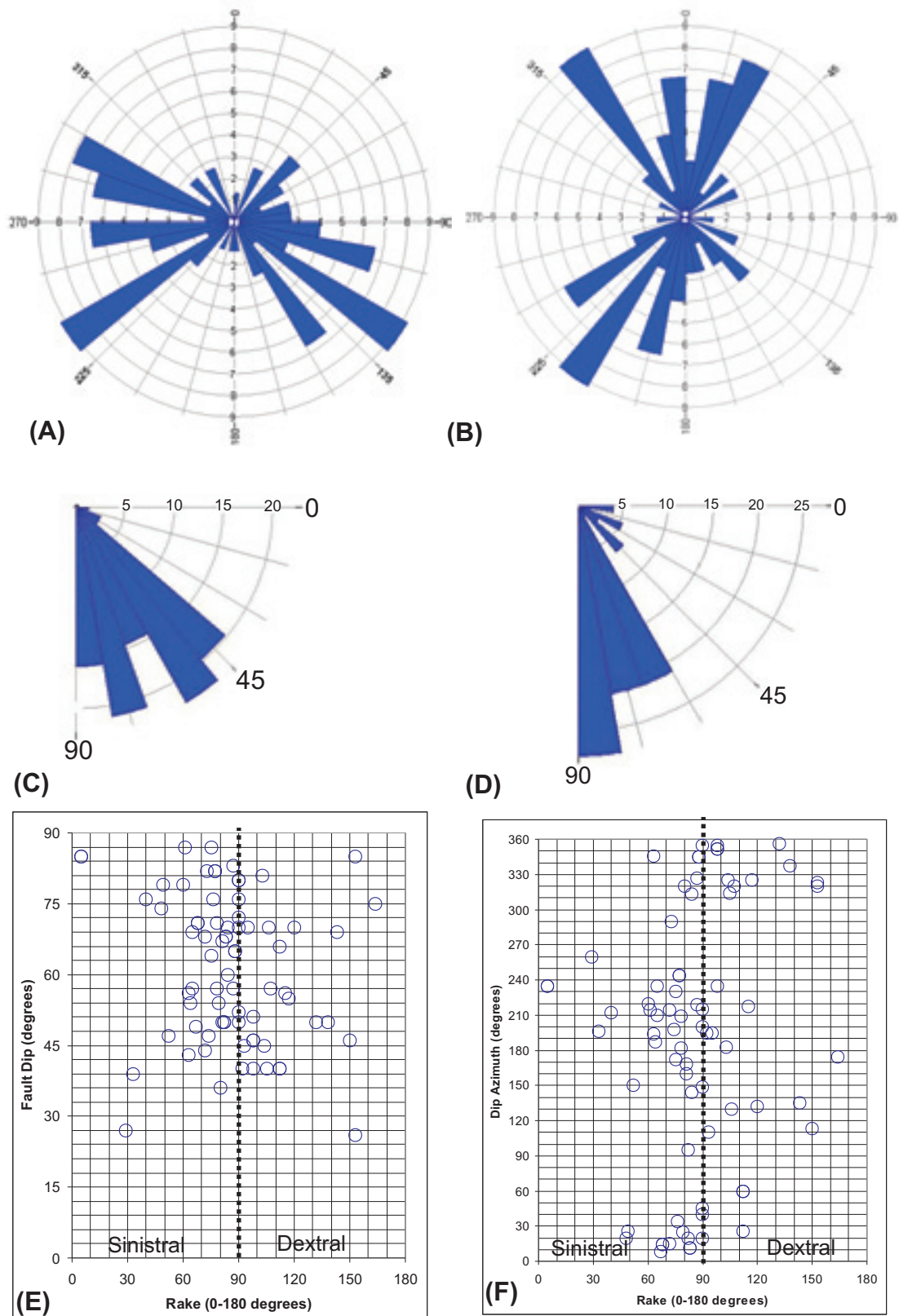


Figure 3.13. Fault data (N=75) of the St-2. See Figure 3.11 for the geological map of the station. (A) Fault strikes (right hand rule); (B) dip azimuths of the faults, (C) fault dips; (D) measured rake of the slickenside lineations on the fault plane; (E) plot showing the fault dips vs rake of the slickenside lineations; and (F) plot showing the azimuth of fault dips vs rake of the slickenside lineations

3.1.2. Fault Patterns in Neogene Deposits

Normal faulting is extensively observable within the Neogene sedimentary units of the Gediz Graben as well. In a similar analyses approach, several profile-based and an area-based field stations were examined within the Neogene strata to understand the deformation pattern (Figure 3.1). In the bulk analysis of the fault data, it has been observed that faults trend predominantly WNW–ESE with dips to the N and S, respectively (Figure 3.14A and B). This is in good confirmation with faulting observed in Plio-Quaternary strata (Figure 3.2A and B). However, when fault dips are examined within the Neogene strata, one can observe tri-modal distribution of the fault dips concentrated around subvertical, around 60° , and less than 45° (Figure 3.14C). Similar multi-modal distribution is also recognized for measured rake of the faults which clusters around subvertical, $60\text{-}70^\circ$ range, and less than 45° (Figure 3.14D). These distributions observed for fault dips and measured rake is clearly different than that of Quaternary strata showing unimodal distribution around 60° for the fault dips and subvertical for the measured rake (Figure 3.2C and D). Fault dip and dip azimuth versus rake plots shows similar clustering to that of Quaternary strata with slightly more scattering (compare Figure 3.13E and F and Figure 3.2E and F).

Profile-based field stations revealed that normal faulting including conjugate sets is also a prominent hanging-wall deformation style of the Neogene deposits (Figure 3.15). If the faulted strata are subhorizontal, the fault pattern is almost identical to that of Quaternary deposits (compare Figures 3.5 and 3.15). However, in places of tilted strata some complications were imposed on to this basic pattern by variable degree of fault block rotation, fault deactivation and new fault formation or fault reactivation. The field evidence of this is illustrated by Figure 3.16 in which some of the northward dipping faults were rotated into shallower dips as low as 20° (e.g., faults 1, 2 and 6). In the mean time, faults of antithetic orientations, which were originally conjugate counterparts of the shallower faults, were become steeper by approaching to subvertical dips (e.g., faults 4, 5, 7, 8 and 9). This rotation is probably the cause of tri-modal distribution of fault dips in Neogene strata introducing shallowly dipping and subvertical faults into the system of normal faults dipping around 60° (Figure 3.14C).

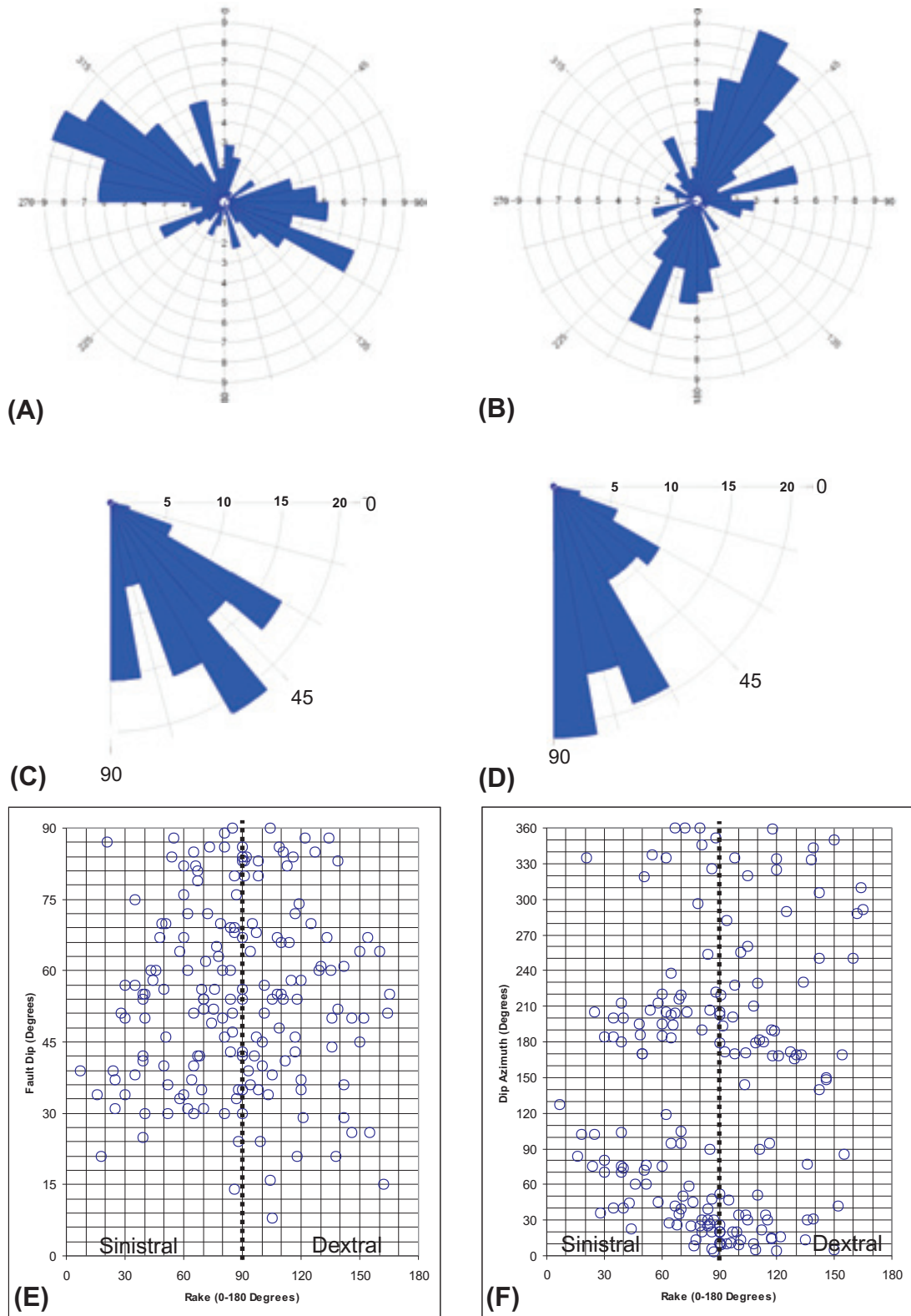


Figure 3.14. Fault data (N=174) observed across the Neogene deposits. **(A)** Fault strikes (right hand rule); **(B)** dip azimuths of the faults; **(C)** fault dips; **(D)** measured rake of the slickenside lineations on the fault plane; **(E)** plot showing the fault dips vs rake of the slickenside lineations; and **(F)** plot showing dip direction of the fault planes vs rake of the slickenside lineations.

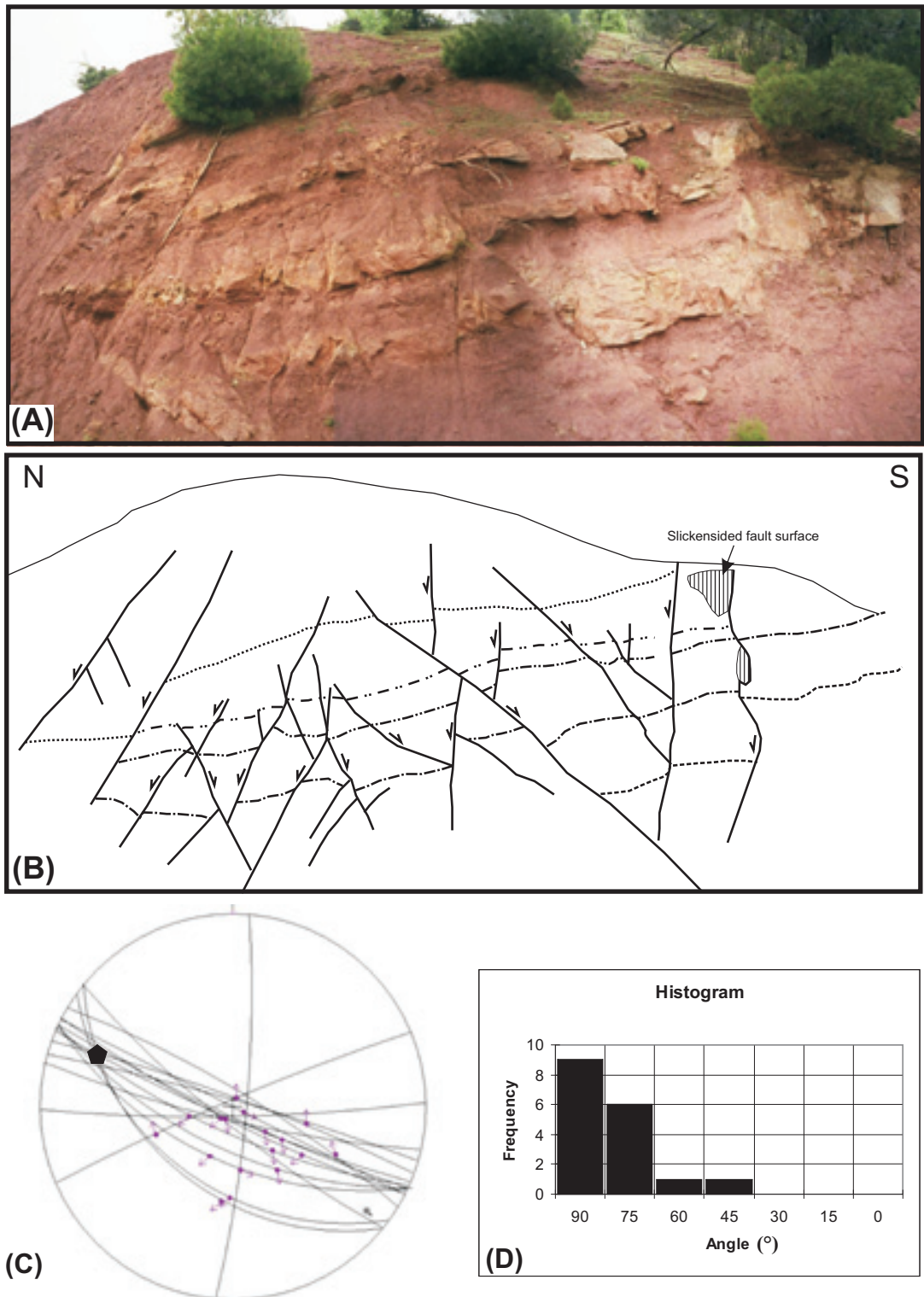


Figure 3.15. Profile based field station St-8 within the Çaltılık formation. See Figure 3.1 for the location of the station. (A) Photograph illustrates the deformation style at the station; (B) sketch of the photograph that shows the observed fault planes and the correlation of the hanging-wall and footwall blocks. Conjugate pattern of faulting is also observable within the Neogene deposits; (C) stereoplot illustrates the fault data with pentagon depicting the average attitude of the line of intersection of the two conjugate sets (β axis); (D) histogram documents the distribution of the angle between the slickenside lineation and the β axis. This angle is expected to be 90° for the conjugate faults.

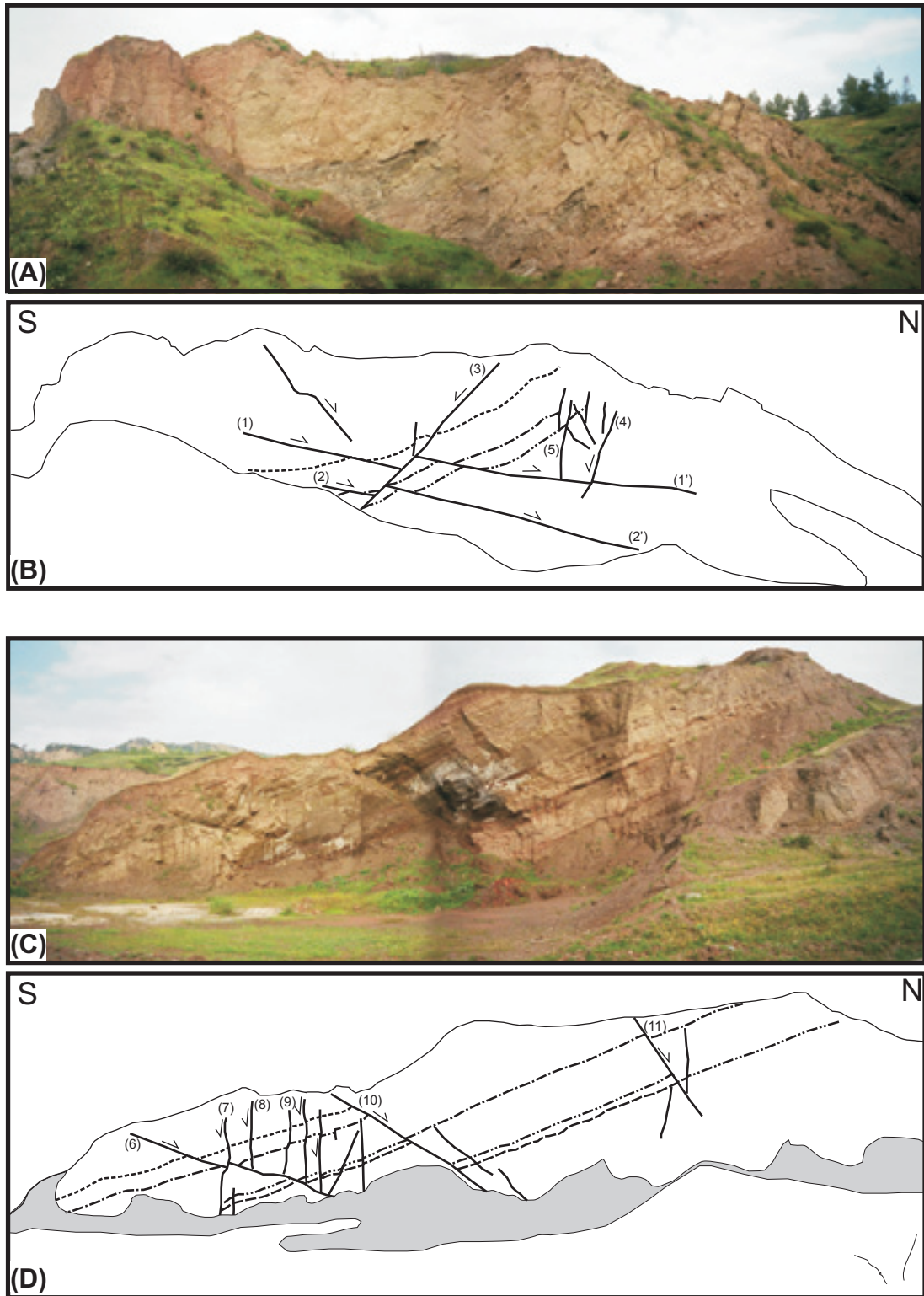
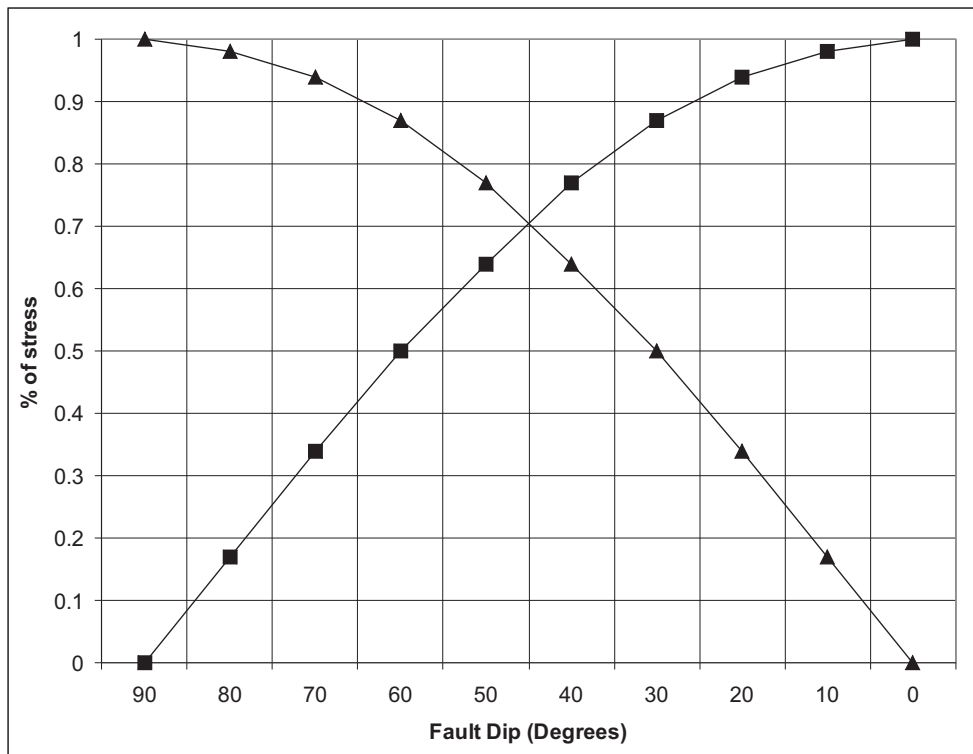
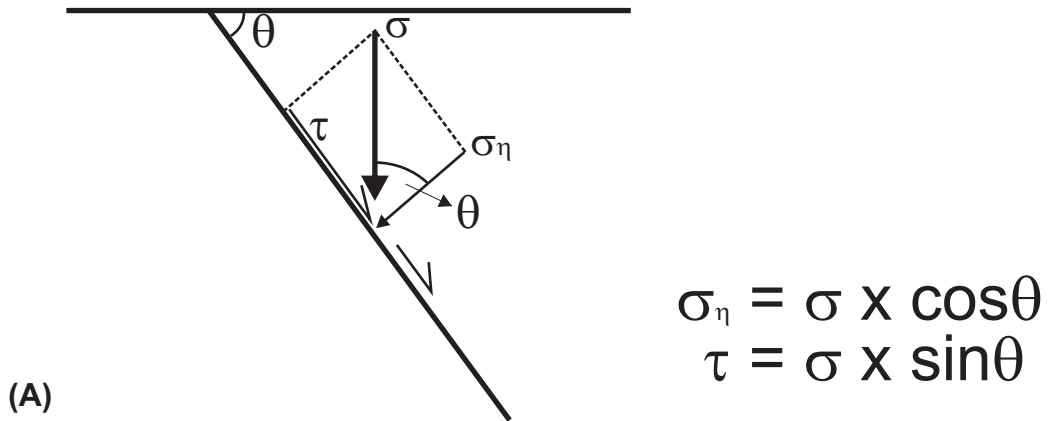


Figure 3.16. Field photographs (A, C) and their sketched drawings (B, D) depicting faulting in Neogene deposits at St-9. See Figure 3.1 for the location of the station. Faults 1 and 2 were rotated into shallow dips to lock up (A, B); a new fault 3 cuts and offsets faults 1 and 2 (A, B); as fault 6 rotates to shallower dips and locks up its conjugate counterparts faults 7 still remain active and offset the fault 6 (C, D); note the increase in rotation from north to south as illustrated by dips of faults 11, 10 and 6, respectively (C, D).

Behavior of the fault that rotates into a shallower dip is predictable. If you consider a stress σ on the fault plane shown in Figure 3.17A, mutual magnitudes of two components of σ , normal component (σ_n) and shear component (τ), determines the movement on the fault plane. This occurs in a way that (τ) facilitates and drives the motion along the fault plane and (σ_n) resists the movement by increasing the friction on the fault surface. The graph on Figure 3.17B illustrates the relative magnitudes of (σ_n) and (τ) with respect to (σ) for fault planes having different amount of dips. It is clear on the figure that as fault dip becomes shallower (σ_n) increases and (τ) decreases to deactivate the fault plane. Conversely, increasing fault dip reduces (σ_n) and increases (τ) to facilitate movement of the fault plane. Outcrop observations in Figure 3.16 are in confirmation with this relation. Faults (1) and (2) that rotated into as low as 20° dip have been deactivated and new faults, such as (3) form to accommodate the extension. Therefore, the new fault cut and offset the older low-angle fault (Figure 3.16). Alternatively, as rotated fault locked up at low dip angles, its conjugate counterparts may still remain active at their rotated subvertical dips (e.g., faults 4, 5, 7, 8 and 9 in Figure 3.16). This result in subvertical faults, which were originally conjugates of the low-angle fault, cut and offset the low-angle fault (e.g., faults 1'-4 and 6-7). The amount of rotation is probably controlled by multiple factors such as distance to major structures, the geometry of the major faults, etc. However, it is generally observed that the amount of rotation increases from N to S as a function of distance from the controlling structure of the graben. Figure 3.16-B mimics this variation by exhibiting that fault rotation increases from north to south considering the faults 11, 10 and 6, respectively.

Deformation is a dynamic phenomenon including gradual changes in the geometry of faults. These changes may bring in mechanically unfavorable conditions for some fault sets to sustain their activity. Yet, the deformation keeps going by forming the new fault sets having cross-cutting relationships with the former deactivated faults. Although, there are certain cross-cutting relationships and age differences between these fault sets, this does not necessarily require different and successive phases of deformation. The observed fault pattern can be produced during a single phase of deformation but may represent successive increments (Figure 3.16).

Area-based field-station St-10 illustrates spatial characteristics of the fault pattern influencing the Neogene strata (Figure 3.18). Master graben-bounding fault



(B) ■ σ_n ▲ τ

Figure 3.17. Normal (σ_n) and shear (τ) components of stress σ on a fault plane. (A) τ drives the motion along the fault plane and (σ_n) resist movement by increasing the friction along the fault plane; (B) relative magnitudes of (σ_n) and (τ) for faults of variable dips under a constant stress σ . The relative magnitudes of (σ_n) and (τ) are shown as percentage of applied stress σ . Note that with decreasing fault dip (σ_n) increases and (τ) decreases both of which are unfavorable to sustain the movement along the fault plane.

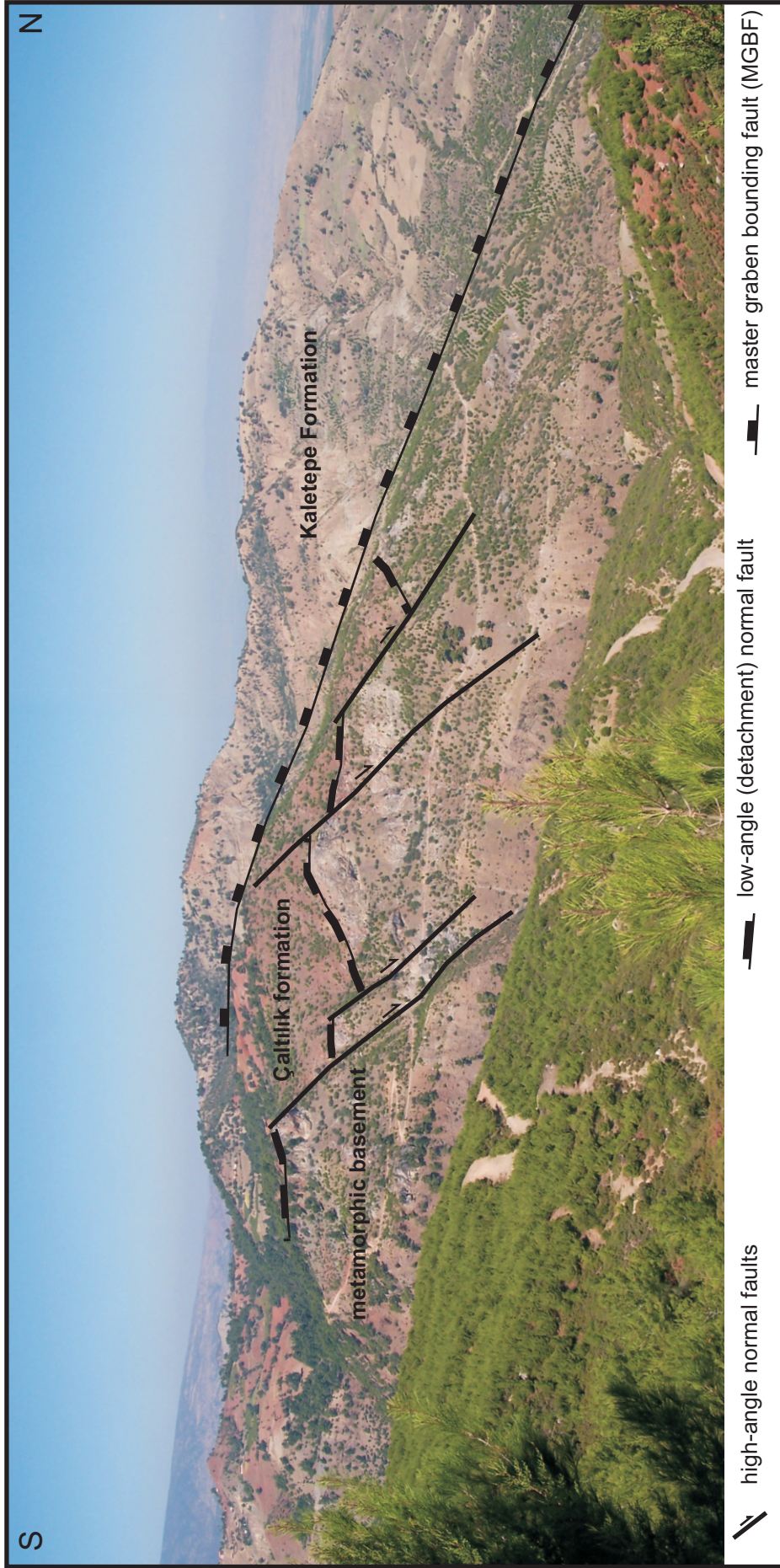


Figure 3.18. Sketched field photograph illustrating the cross-cutting relationship between the detachment fault and high angle normal faults. MGBF follows the creek and juxtaposes Kaletepe formation with Çaltılık formation and metamorphic basement.

(MGBF) is the most prominent structure on the map that is bounding the southern margin of the Gediz Graben. Although it is not as pronounced, the northern margin structure of the graben can still be traced and mapped on the surface (Figure 3.18).

Step-like pattern formed by graben-facing normal faults characterizes the geomorphology of the southern margin of the graben (e.g., Kocyigit *et al.*, 1999a; Bozkurt and Sözbilir, 2004). From south to north, topographical elevation gradually diminishes by means of WNW–ESE-oriented normal faults and finally reaches to almost flat graben floor (Figure 3.18). The most severe elevation decrease is caused by MGBF. Although, MGBF is a prominent and continuous structure having bends along strike direction across the St-10, faults located north of MGBF are segmented in nature and comprises planar and short segments that are overstepping in map view (Figure 2.3). This geometry is very clearly depicted by the northernmost fault set extending from Yeniköy to Dere and passing immediately south of the Alaşehir (Figure 2.3). In fact, this fault set bounds the southern margin of the modern graben floor and marked by coalesced Quaternary alluvial fans. In a similar way, a series of coalesced Quaternary alluvial fans mark northern margin structure of the graben, which is also discontinuous and segmented. With time and progressive deformation, these isolated fault segments are expected to join and form a single fault with along strike bends corresponding to former overlapping zones (e.g., McDonald 1957; Larsen 1988; Morley *et al.*, 1990; Peacock, 1991; Peacock and Sanderson, 1991, 1994; Childs *et al.*, 1995; Coşkun, 1997; Peacock *et al.*, 2000; Lezzar *et al.*, 2002; McLead *et al.*, 2002; Mauk and Burruss, 2002; Trudgill, 2002; Younes and McClay 2002; Young *et al.*, 2002; Soliva and Benedicto, 2004, 2005; Acocella *et al.*, 2005; Bozkurt and Sözbilir, 2006). The segmented geometry and the age of lithostratigraphic units that the faults influenced suggest that these faults are younger and geometrically more immature than the MGBF (Figure 2.3). Interaction of the fault segments and their connection with progressive deformation is dealt in Chapter 4 based on a field example.

To the south of the MGBF in Figure 2.3, the observed field relations are more complicated. At this part of the St-10, the contact between the exposed Miocene sediments (Alaşehir or Caltılık formations) and the metamorphic basement is a low-angle normal fault which is traditionally called as the detachment fault (Hetzl *et al.*, 1995; Emre, 1996; Koçyiğit *et al.*, 1999a; Seyitoğlu *et al.*, 2000, 2002; Yılmaz *et al.*,

2000; Lips *et al.*, 2001; Bozkurt, 2001, 2002, 2003; Sözbilir, 2001, 2002; Bozkurt and Sözbilir, 2004; Kaya *et al.*, 2004). Due to low dip amount of the detachment fault, it is sometimes difficult to accurately identify the fault zone unless careful outcrop observations are carried out. The difficulty is especially pronounced for the cases where conglomeratic facies of the Miocene deposits overlie the metamorphic basement via the detachment fault. Under these circumstances, the low angle normal fault between the Miocene deposits and the metamorphic basement can easily be misidentified as an unconformity (e.g., Cohen *et al.*, 1995; Dart *et al.*, 1995; Yılmaz *et al.*, 2000; Seyitoğlu *et al.*, 2002). Accurate delineation of the fault requires observations on the slickensided and polished nature of the contact as well as the texture of the underlying metamorphic rocks (Figure 2.5). Cases of paper shales overlying the metamorphic basement or remnants of Neogene deposits sitting at the top of the exposed slickensided fault surface do also exist as an evidence of the faulted contact. This relation was first documented by Deniz *et al.* (2002) in the Gediz graben.

Presently low-angle and inactive detachment fault exposing south of the MGBF is cut and displaced by more steeply-dipping normal faults that offset the Miocene strata as well (Figure 2.3 and 3.18). This relation is already documented by Bozkurt and Sözbilir (2004) at west of Soğukyurt village (Figure 2.3). The observed cross-cutting relation constitutes the main foundation of the models suggesting a two-stage extension for the western Turkey (Kocyigit *et al.*, 1999a; Bozkurt and Sozbilir, 2004): (1) Earlier stage of extension related to core complex formation in the footwall of low angle normal fault during the Miocene; (2) late stage extension producing E–W-grabens with high-angle normal faults during Plio-Quaternary times. This relation mimics the outcrop observation between shallow dipping faults and steep dipping faults in the St-9 (Figure 3.15). As already discussed, rotation of a fault into lower dip amounts gradually works against the movement on the fault plane by increasing the normal component and decreasing the shear component of the stress (Figure 3.17). This inevitably stops the activity along the rotated fault plane and necessitates formation of new fault planes or reactivation of older fault planes that possess more favorable dip amounts. These new fault planes are therefore may cut and offset the fault rotated to shallower dip amounts as in the cases of St-9 and St-10 (Figures 3.16 and 3.17). Although, the cross-cutting relationship can be a product of multiphase deformation history, similar geometries can also be created during

continuum of deformation with in a single phase. St-9 in Figure 3.16 is probably an example of this. Further data is required to assess if the cross-cutting relationship between the detachment fault and the steep normal faults represent a multiphase-deformation history. Analyses of subsurface data in Chapter 5 provide further evidence to constraint this argument.

Beds of Miocene strata exposing south of the MGBF are predominantly back tilted with dips to the south towards the intersecting steeper normal faults (Yılmaz *et al.*, 2000). Although, the detachment fault usually dips towards the north in the range of 40° - 10° , there are places where the detachment fault is also back tilted with dips to the south (Figure 2.5).

Several studies suggest that there is a basinward migration of the southern boundary structure of the Gediz Graben (Dart *et al.*, 1995; Koçyigit *et al.*, 1999a). This implies that the northern faults are younger than the southern faults along the southern margin of the Gediz Graben. Although this is correct for north of the MGBF as already discussed above, there is not enough constraint to suggest that the steeper normal faults exposing south of the MGBF and cutting and offsetting the detachment fault is older than the MGBF (Figure 2.3). Subsurface evidence from 2-D seismic profiles and 2-D forward modeling of the extension indicate that the presently low-angle detachment fault may be the rotated continuation of the MGBF (see Chapter 5). If this is the case, steeper normal faults cutting and offsetting the detachment could be younger than the MGBF.

3.2. The Stress Field

Identification of the stress field that drives the deformation in an area is one of the basic questions that methods of fault analyses are intended to solve. Driving the deformation, deviatoric stresses can be inferred from field observations on the orientation of fault plane striations of exposed faults. Numerical palaeostress reconstructions based on fault-slip data have been a useful tool for decades (e.g., Carey and Brunier, 1974; Angelier, 1979, 1994; Etcheopar *et al.*, 1981; Gephart and Forsyth, 1984; Yamaji, 2000). These reconstruction methods are based on the theories of stress-shear relationship proposed first by Wallace (1951) and Bott (1959). Determination of the stress tensor based on the fault data, that includes direction and sense of slip measured on numerous faults, is known as stress inversion (Angelier, 1990, 1994). In the absence of rupture-friction data, the complete stress

tensor can not be determined but the reduced stress tensor which constrains the orientation of three principal stress axes and the ratio of Φ can be solved (Bishop, 1966; Angelier, 1984).

$$\Phi = (\sigma_2 - \sigma_3) / (\sigma_1 - \sigma_3) \quad 0 \leq \Phi \leq 1 \text{ (Bishop, 1966) [1]}$$

Various methods and improvements have been published for the solution of inverse problem since the early 70s (Carey and Brunier, 1974; Angelier, 1975, 1990, 1994; Etchecopar *et al.*, 1981; Angelier *et al.*, 1982; Reches, 1987). These methods are based on two basic assumptions: (1) the stress is uniform and invariant over the history of faulting; (2) the slip on each fault surface has the same direction and sense as the maximum shear stress resolved on the fault surface from the regional stress field (The Wallace – Bott Hypothesis). Validity of these assumptions has been questioned by various studies (e.g., Pollard and Segal, 1987; Pollard *et al.*, (1993). Based on empirical observations and theoretical analysis, Angelier (1994) concludes that discrepancy caused by invalidation of basic assumptions remains statistically minor compared to error in data collection. Furthermore, Twiss and Unruh (1998) proved that the assumption (2) is valid in cases where fault block rotations are negligible and there is linear relationship between stress and strain. Appendix III documents the theory of stress inversion methods in detail.

The techniques of basic inversion methods are problematic if the observed deformation is a product of multiphase deformation history. Fault data of this character is commonly called as heterogeneous. If faults belonging to individual deformation phases can be classified based on field observations, the basic inversion methods can easily be applied to heterogeneous data sets. Although, such classifications can be done on a regional scale, it is difficult to classify slip measurements of meso-scale faults in this way through field observations. There are several methods presented to address the analyses of heterogeneous fault slip data (Reches, 1987; Arminjo *et al.*, 1982; Huang, 1988; Angelier, 1994; Yamaji, 2000).

3.2.1. Stress Field of Faulting in Plio-Quaternary Deposits

Inversion of fault-slip data from Plio-Quaternary field stations constrained the reduced stress tensor successfully (Figure 3.19). Figure 3.19 not only illustrates the fault data with the governing principal stress direction but also two important values,

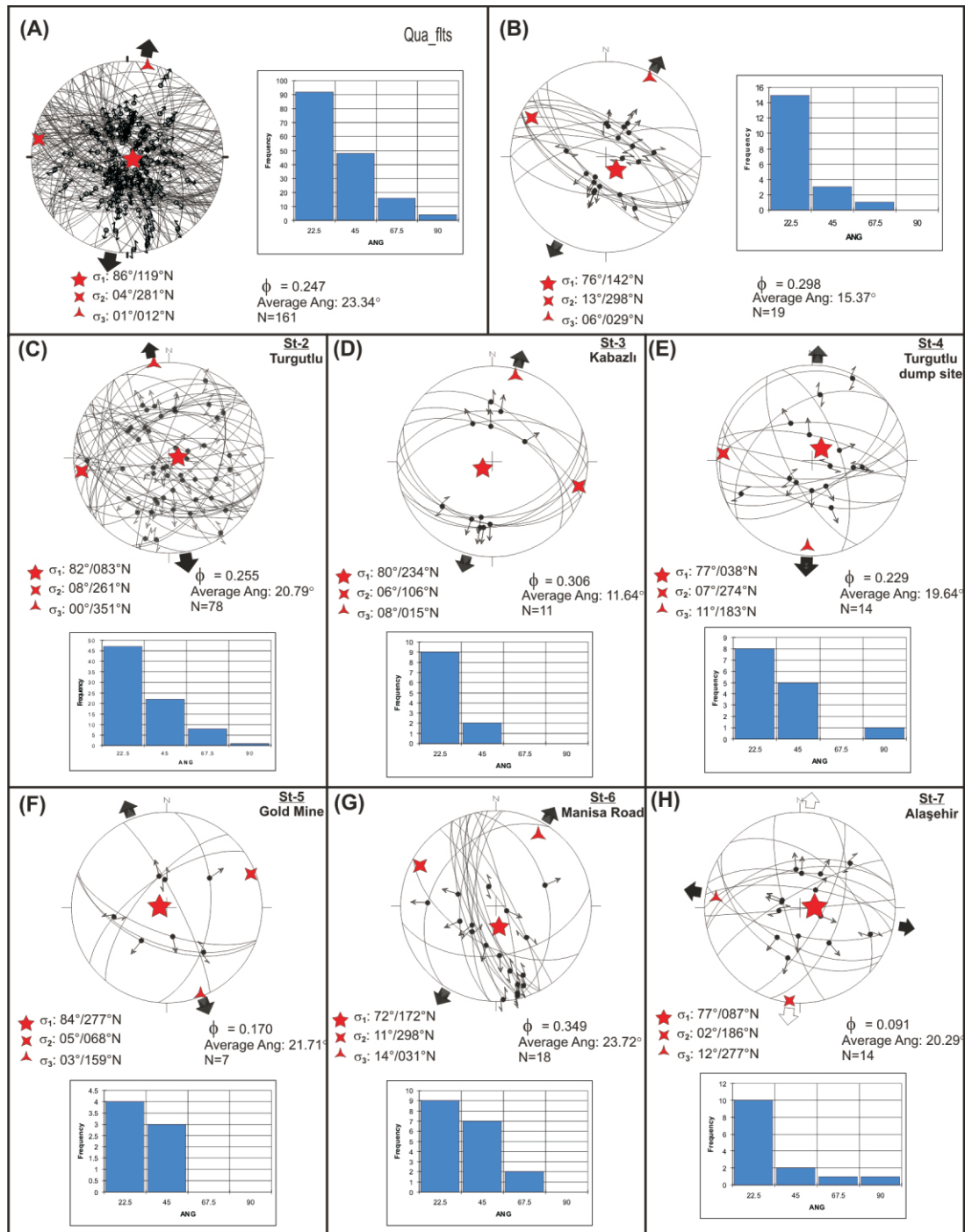


Figure 3.19. Stress analyses carried out within the Plio-Quaternary deposits. Stereoplots illustrate fault data and the position of principle stress axes. Histogram depicts distribution of ANG value as a measure of fit. **(A)** All the Quaternary fault data acquired from profile based field stations. Fault data acquired from field station **(B)** St-1; **(C)** St-2; **(D)** St-3; **(E)** St-4; **(F)** St-5; **(G)** St-6; and **(H)** St-7. See Figure 3.1 for the location of the field stations.

the ϕ ratio and the quality estimator ANG. Referring the relative magnitudes of principle stresses, the ϕ ratio in formula [1] conveniently describes the shape of the stress ellipsoid (Angelier, 1994). Ranging between two extreme values of 0 and 1, the ϕ ratio constraints all-possible cases between uniaxial compression ($\sigma_2=\sigma_3$; $\phi=0$) and uniaxial extension ($\sigma_1=\sigma_2$; $\phi=1$) respectively (Angelier, 1994). In extensional tectonic settings, simple (uniaxial) extension is generally represented by relatively elevated values of ϕ (e.g., 0.5) implying that there is a well-defined σ_3 axis having considerable difference from σ_1 and σ_2 in magnitudes (Angelier, 1994). On the other hand, lower values of ϕ indicates closeness of σ_2 and σ_3 in magnitude which facilitates (σ_2) / (σ_3) permutations (Angelier, 1994). In another words, magnitudes of σ_2 and σ_3 are close to each other that these two axes may swap positions during the deformation phase and result in multidirectional extension and related complex fault patterns similar to St-2 in Figure 3.11.

The quality estimator ANG defines the angle between the measured slip on the fault plane and the theoretical shear vector resolved on the fault plane from the computed stress axes (Angelier, 1994). If one remembers the assumption (2) of slip inversion methodology, it states that measured slip and the resolved shear vector on the fault plane are essentially parallel, i.e. ANG equals to zero. Therefore, smaller values of ANG indicate a better fit of the computed stress axes to the measured fault slip. As a rule of thumb, ANG values smaller than $22,5^\circ$ are considered as good fit and those between $22,5^\circ$ - 45° represents poor fit. Anything larger than 45° indicates a bad consistency between the measured slip and the computed stress tensor. Solutions that yields ANG values smaller than 45° are usually considered as acceptable (Angelier, 1984). See Appendix III for detailed discussion on the ϕ and the ANG values.

It is clear on the Figure 3.19A and C that Plio-Quaternary faulting examined in the profile based field stations and St-2 respectively indicates an almost N-S-oriented extension with sub-vertical σ_1 and N-S-oriented sub-horizontal σ_3 axes. Being perpendicular to both σ_1 and σ_3 , σ_2 axis trends almost E-W with a shallow dip. The ϕ ratio is low, around 0,25 (Figure 3.19A and C). Quality estimator ANG clusters within the good fit threshold of $22,5^\circ$ with most of the deviation being less than 45° . Therefore, average ANG value suggests an acceptable fit for the slip data

and the computed stress tensor (Figure 3.19A and C). However, histograms in the figure indicate that despite the reasonable fit suggested by the average ANG, there are also individual misfits that are much higher than the average. The potential causes for the inconsistent measurements could be variable: (1) the stress field may vary spatially with local stress field anomalies that are caused by fault interactions and linkage (Çiftçi and Bozkurt, 2007); (2) poorly defined σ_3 axis may result in variation of extension direction leading to multi-directional extension (Angelier, 1994); (3) fault interaction may invalidate basic assumptions of the slip inversion methodology yielding poor solutions (Pollard and Segal, 1987; Pollard *et al.*, 1993); (4) instrumental and measurement errors during data collection.

Slip inversion carried out at the individual profile based field stations also confirms N–S-oriented extension in general although some variations do exist (Figure 3.19C to H). Compared to cumulative analyses carried out at Figure 3.19-A, analyses of individual stations have sometimes yielded better fit between the slip-shear angle, i.e. the ANG value (Figure 3.13). The better fit is especially pronounced in the cases of fault pattern that is characterized by conjugate fault systems of St-1 and St-3 (Figure 3.19B and D). In these stations most of the ANG values fall into the 22,5° class with a relatively small average ANG. The relatively elevated ϕ ratio and the observed conjugate fault pattern probably suggest a better-defined direction of extension for these stations (Figure 3.19B and D). The other stations are characterized by multiple orientations of fault strikes (St-4 to St-7), and therefore the fit is comparable to that of cumulative analyses.

The ϕ ratio varies from 0,091 to 0,349 for all the stations (Figure 3.19). This low value of ϕ suggest that σ_2 is close to σ_3 in magnitude and $(\sigma_2)/(\sigma_3)$ permutations are likely. Indeed, Figure 3.19H depicts a situation where the σ_3 -axis is almost E–W-oriented in contrast to the general N–S-oriented extension. As a potential example of $(\sigma_2)/(\sigma_3)$ permutations, the lowest computed ϕ value and the observed fault pattern of St-7 clearly indicates a multi-directional extension.

Although, the computed stress tensor and the acquired fault data are in good confirmation as illustrated by Figure 3.19, it still worth to test the fault data for heterogeneity. The heterogeneity of the fault data can be caused not only by polyphase deformation history but also incremental deformation and spatial variation of the stress state. Several methods and improvements have been published for the

analyses of heterogenous fault data (e.g., Angelier, 1979; Armijo *et al.*, 1982; Huang, 1988; Yamaji, 2000). In this part of the study the multiple inverse method, which based on the classical slip inversion methodology, is employed to test the heterogeneity of fault data (Yamaji, 2000). The method is a numerical technique to separate stresses from heterogenous data without a priori knowledge on the stresses or the classification of the faults (Yamaji, 2000; Yamaji *et al.*, 2005). The method is basically an adaptation of Hough transformation to stress inversion (Ballard, 1981; Yamaji, 2000; Yamaji *et al.*, 2005). The theoretical background of the multiple inverse method is also discussed in Appendix III together with the slip inversion methodology.

Figure 3.20 illustrates the results of the multiple inverse method applied to the area based field station St-2 (Figure 3.20A) and all the Plio-Quaternary fault data acquired at the profile based field stations (Figure 3.20B). The stereoplots on the left depicts the orientation of the σ_1 axes while those on the right illustrates that of σ_3 . The colour of axis indicates a ϕ ratio that is classified based 10% intervals in the colour scale varying between 0 and 1. It is clearly emphasized on the figure that the attitude of σ_1 axis is very well constraint (Figure 3.20). Average σ_1 orientation in Figure 3.20A and B is very close to the slip inversion solution illustrated in Figure 3.19-A and C having mere differences of 2,9° for all the quaternary faults and 4,0° for the St-2. Similarly, the ϕ ratio also possesses similar low values in both analyses to support the argument of σ_2 is being close to σ_3 in magnitude to result in poorly defined direction of extension.

Three main clusters can be identified on the σ_3 distribution plots given on the right column. These clusters, named as I, II and III, correlate very well in both Figure 3.20A and B. In a general sense, clusters I and II, are probably related and represents rough N–S-oriented extension which was already interpreted based on stress inversion results shown in Figure 3.19. The distribution range of clusters varies between N–S to NW–SE for the cluster A and N-S to NE-SW for the cluster II (Figure 3.20). This suggests that the rough N–S extension is generally constraint and variable between NW–SE to NE–SW. Similarly, the slip inversion methodology have also computed extensional axes generally varying between NW–SE to NE–SW (Figure 3.19). The cluster III, on the other hand, is different than I and II and indicates an almost E–W-oriented extension (Figure 3.20). If the ϕ values of cluster

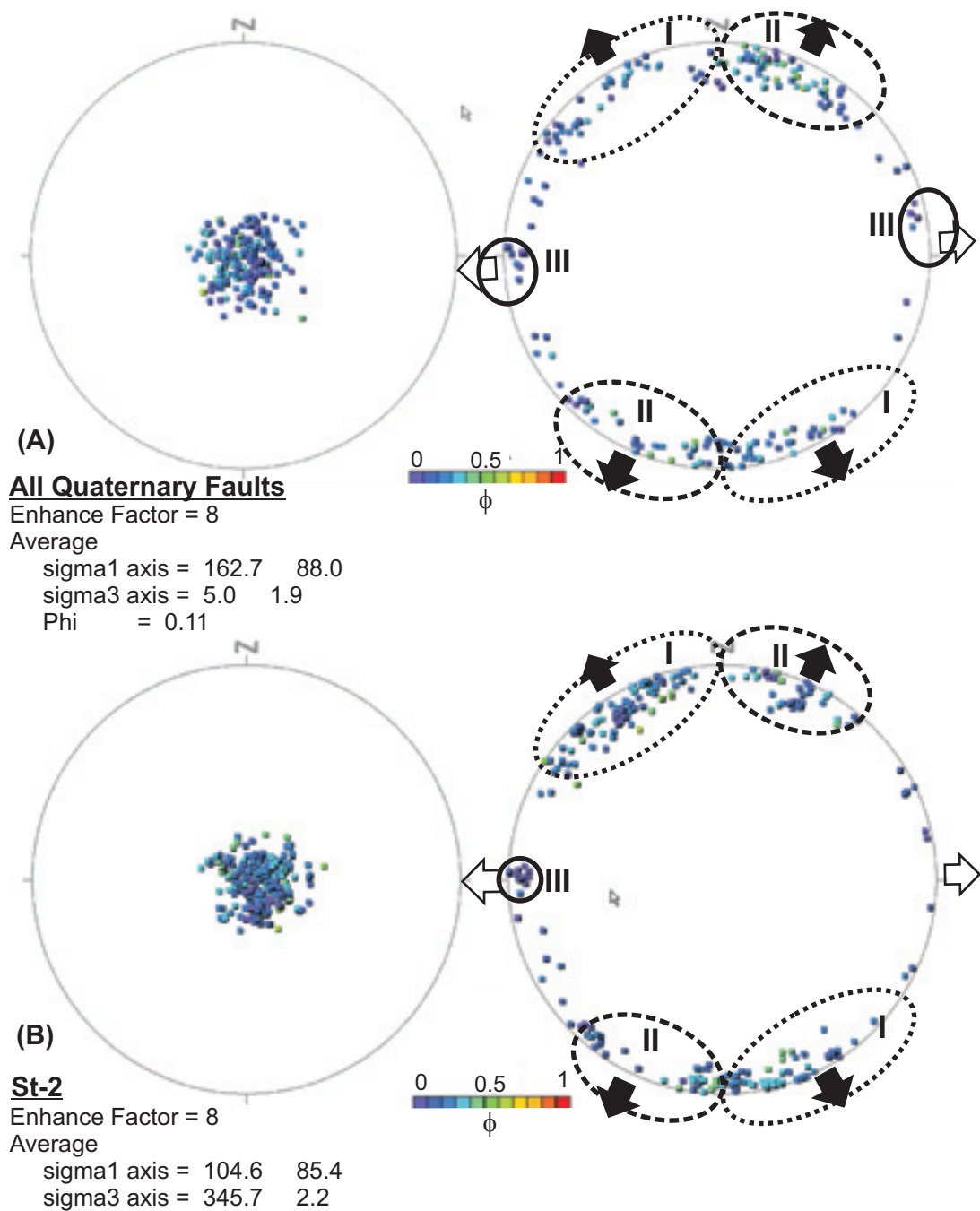


Figure 3.20. Multiple inverse method (Yamaji, 2000) applied to: **(A)** All Quaternary faulting from profile based field stations; **(B)** area based field station St-2. See Figure 2.3 for the location of the stations. Stereoplots on the left column indicate orientation of σ_1 axes and that on the right indicates σ_3 axes. There is a good consistency in the attitudes of σ_1 axes. Three main clusters I, II and III can be identified based on the σ_3 axes. The clusters do not represent successive phases but multi-directional character of the extension as also supported by observed fault pattern.

III is referred based on the colour scale for the cluster III, one can also see that the ϕ ratio is very low for the cluster varying in the range of 0,0 to 0,1. All these aspects of the cluster III is very similar to the slip inversion result for the St-7 and probably indicates an episodes of $(\sigma_2)/(\sigma_3)$ stress permutations.

Although, stress inversion methods offer potential of computing four of the six component of the stress tensor (called as the reduced stress tensor), it requires the slip vector to be measured. The slip vector can be approximated by slickenside lineation on the fault plane, which requires measurement of the attitude of the fault surface as well as the rake of the slickenside lineation. This is an easy field task to accomplish unless the faults cut lithologies lacking well-defined slickensided fault surfaces. Further limitations arise for the cases of faults defined based on subsurface data such as borehole logs and seismic reflection data. Lisle *et al.* (2001) have proposed a method of stress inversion that can be applied to fault populations avoiding measurement of the slip vector. This method only requires the sense of fault's dip-slip component to be known (i.e. the normal or reverse). Appendix III documents the theoretical background of the methodology.

The stress inversion method requiring only the fault slip sense was applied to all Quaternary faulting and area based field station St-2 (Figure 3.21). The main aim of this effort is to check the slip inversions of slip-vector based Angelier (1990) method and slip-sense based method of Lisle *et al.* (2001) mutually. Similarity of the obtained results from both methods will not only improve the validity of computed stress axes for Plio-Quaternary faulting but also test the slip-sense based method before applying to subsurface data in Chapter 5. Although the slip-vector based method can compute a unique stress tensor with orientation of stress axes and ϕ ratio, the slip-sense based method allows computation of numerous compatible tensors (Figure 3.21). Therefore, the selection of stress axes and the ϕ ratio in the slip-sense based method needs to be done using frequency distribution plots (Figure 3.21). It is clear on the Figure 3.19A and C and Figure 3.21A and B that stress axes of both slip-vector and slip-sense based methods are in good confirmation with each other having subvertical σ_1 and subhorizontal σ_3 -axis trending roughly in N-S direction. Compared to ϕ ratios of 0.25 in slip-vector based method, ϕ values are clustered in the range of 0 – 0.20 for the slip-sense based method (Figure 3.19A and C and Figure

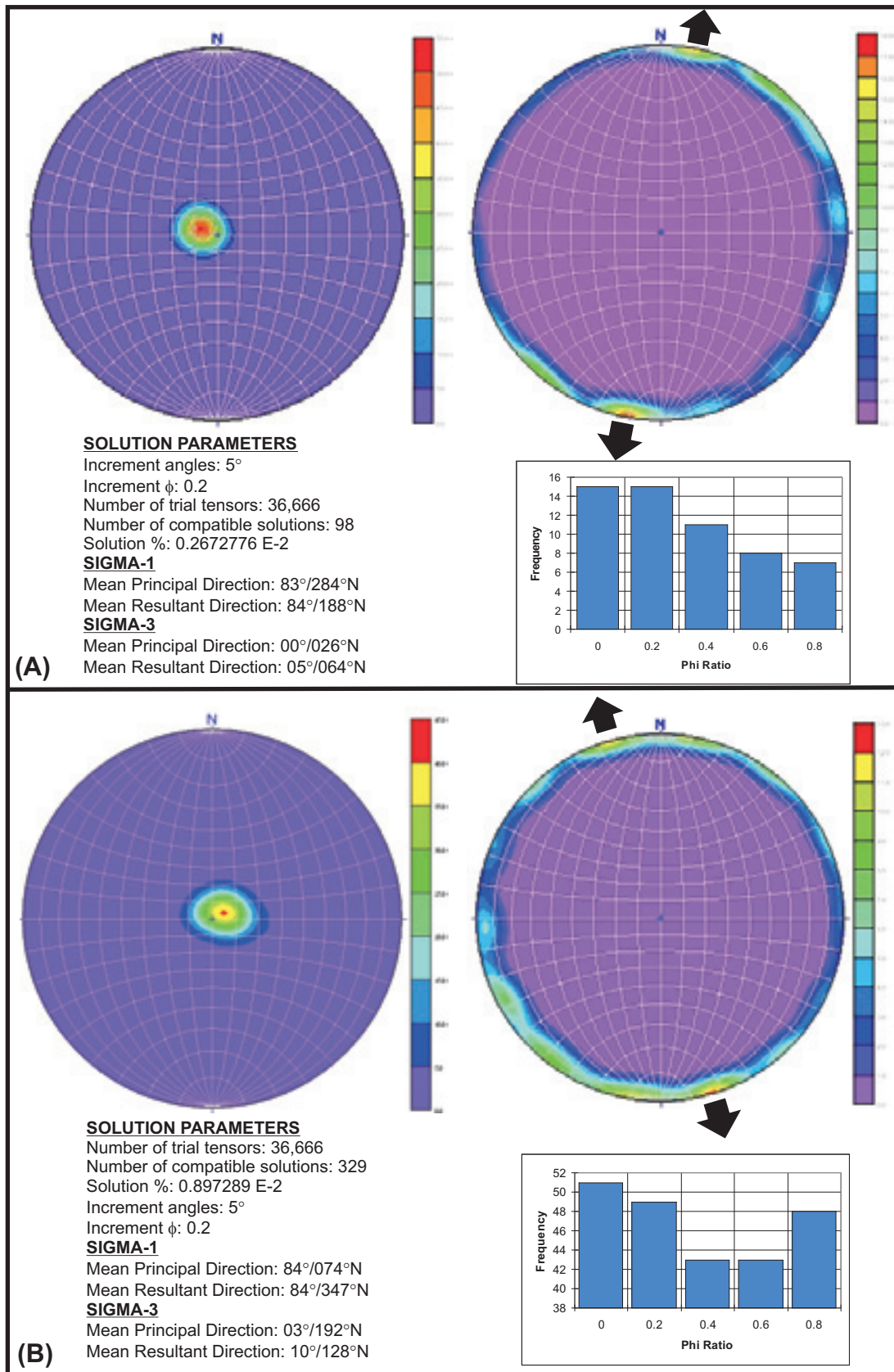


Figure 3.21. Results of the stress inversion method that require only fault slip sense applied to **(A)** all Quaternary faulting; **(B)** area based St-2. The column on the right shows location of σ_1 axes and column on the left illustrates location of σ_3 axes. Φ ratio is given as an histogram with 0.2 increments.

3.21). Despite this difference, the computed ϕ ratios are still close to each other and are in conformation of the fact that σ_2 is close σ_3 in magnitude.

3.2.2. Stress Field of Faulting in Neogene Deposits

Stress inversion methodology was also applied to fault data acquired from Neogene sedimentary units of the Gediz Graben. The solution of the inverse problem suggests that bulk of the fault data confirms the NNE–SSW-oriented extension with subvertical σ_1 , WNW-ESE trending σ_2 and NNE-SSW trending σ_3 axes (Figure 3.22A). ϕ ratio is low around 0.25 and similar to that of Plio-Quaternary strata. Although, the average ANG value is slightly higher than the good-fit threshold of 22.5° , frequency distribution clearly indicates that most of the measured slip is in good confirmation ($ANG < 22.5$) with the theoretical slip vector computed based on the inverted stress tensor (Figure 3.22). Therefore, the inverse problem also yields satisfactory solution for the case of Neogene strata by constraining the reduced stress tensor, which is composed of three principal stress axes and the ratio of ϕ (Figure 3.22A).

When the solution of individual field stations are examined and compared with that of the bulk analysis, one can observe that results yielding similar direction of extension were generally obtained from the individual field stations (Figure 3.22). However, some minor variations can still be observed among the field stations, which might be important to understand the nature of extension. These variations can particularly be observed at stations 8, 9 and 11. Stations 8 and 11, for example, are characterized by almost N–S-oriented extension and are good candidates of $(\sigma_2) / (\sigma_3)$ axes permutations (Figure 3.22B and E). In fact, close examination of fault data at these stations can recognize some fault slips that fit to almost E–W-oriented extension as well. Evidence of E–W-extension is not only limited to fault slips but also the fault orientations. Although general fault pattern at these stations suggest a NNE–SSW-oriented extension with WNW–ESE-oriented conjugate faults, there are also couple of N–S-striking faults granting with the E–W-oriented extension. All these fault plane evidence together with low ratio of ϕ on the order of 0.1 propose that $(\sigma_2) \setminus (\sigma_3)$ axes swapping were probably the case for these stations. Because the solution of the inverse problem averages between the two components of multi-

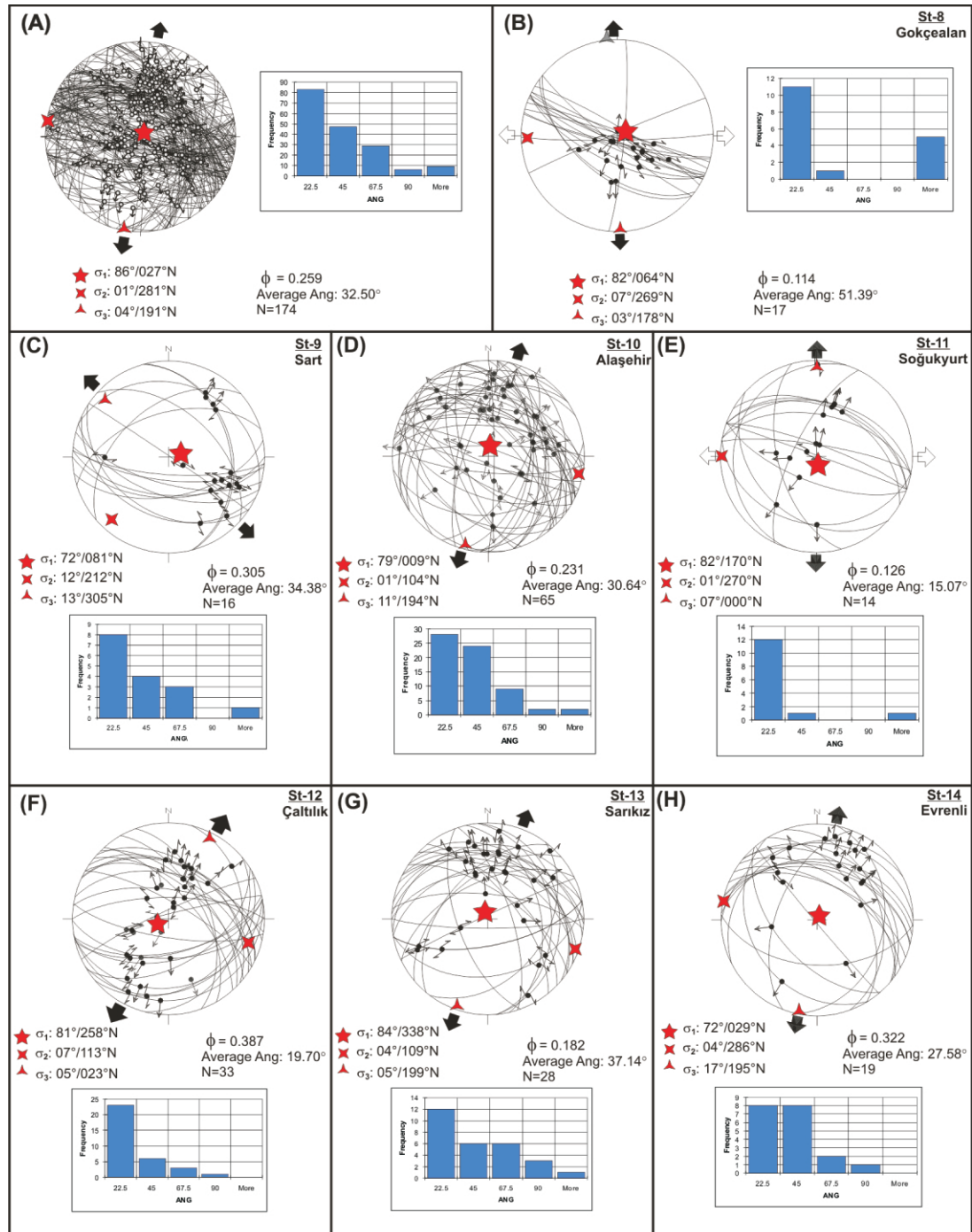


Figure 3.22. Stress analyses carried out within the Neogene deposits. Stereoplots illustrate fault data and the position of principal stress axes. Histogram depicts the distribution of ANG value as a measure of fit. (A) All fault data acquired within the Miocene strata. Fault data acquired from (B) St-8; (C) St-9; (D) St-10; (E) St-11; (F) St-12; (G) St-13 and (H) St-14. See Figure 3.1 for the location of the stations.

directional extension, the computed stress axes and inferred direction of extension slightly deviates from the solution of bulk analysis and the other field stations.

A slightly different scenario can be drawn for St-9 having NW–SE-oriented extension (Figure 3.22C). If you examine fault orientation and neglect the slip data at this station for a second, the observed fault pattern seems to mimic the conjugate fault system forming under NNE–SSW-oriented extension (e.g., similar to St-12). In fact, there are some slip data at St-9, which is conformable with NNE–SSW-oriented direction of extension. It is likely for this station that the original fault pattern have probably formed under NNE–SSW-oriented regional extension but subsequently exposed to a local stress field anomaly. Therefore, original faults have started to slip in accordance with the local stress field of NW–SE-oriented extension. The local stress field not only changes the slip direction of former faults but also change the structural style by breaking new faults striking NE–SW. Local stress field anomaly can developed due to fault interaction and/or during the fault segment linkage process (Çiftçi and Bozkurt, 2007). An example of this with detailed analysis of the stress field is discussed in the next chapter.

Multiple inverse method of Yamaji (2000) was also applied to this data set to check the data for heterogeneity (Figure 3.23). The actual σ_1 axis is again well constrain at subvertical attitude based on the distribution of computed σ_1 axes. σ_3 axis, however, requires some evaluation of compatible orientations having distinct clustering. Indeed, NNW–SSE-oriented solutions form a very strong cluster suggesting that most of the solutions are compatible with the NNW–SSE-oriented extension. Named as cluster I, this orientation is similar to classical slip inversion solution given in Figure 3.22A. Although not as distinct, cluster II can also be differentiated based on the σ_3 solutions (Figure 3.23). This cluster probably represents the axis-swapping phenomenon for the Neogene strata that results in multi-directional extension as in the cases of St-8 and St-11. Solutions falling out of these clusters are not significant and probably represent natural variation, local anomalies or invalidation of the methodology.

3.3. Discussion

Detailed analyses of fault systems carried out through Plio-Quaternary and Neogene deposits find out that fault systems investigated in both sedimentary

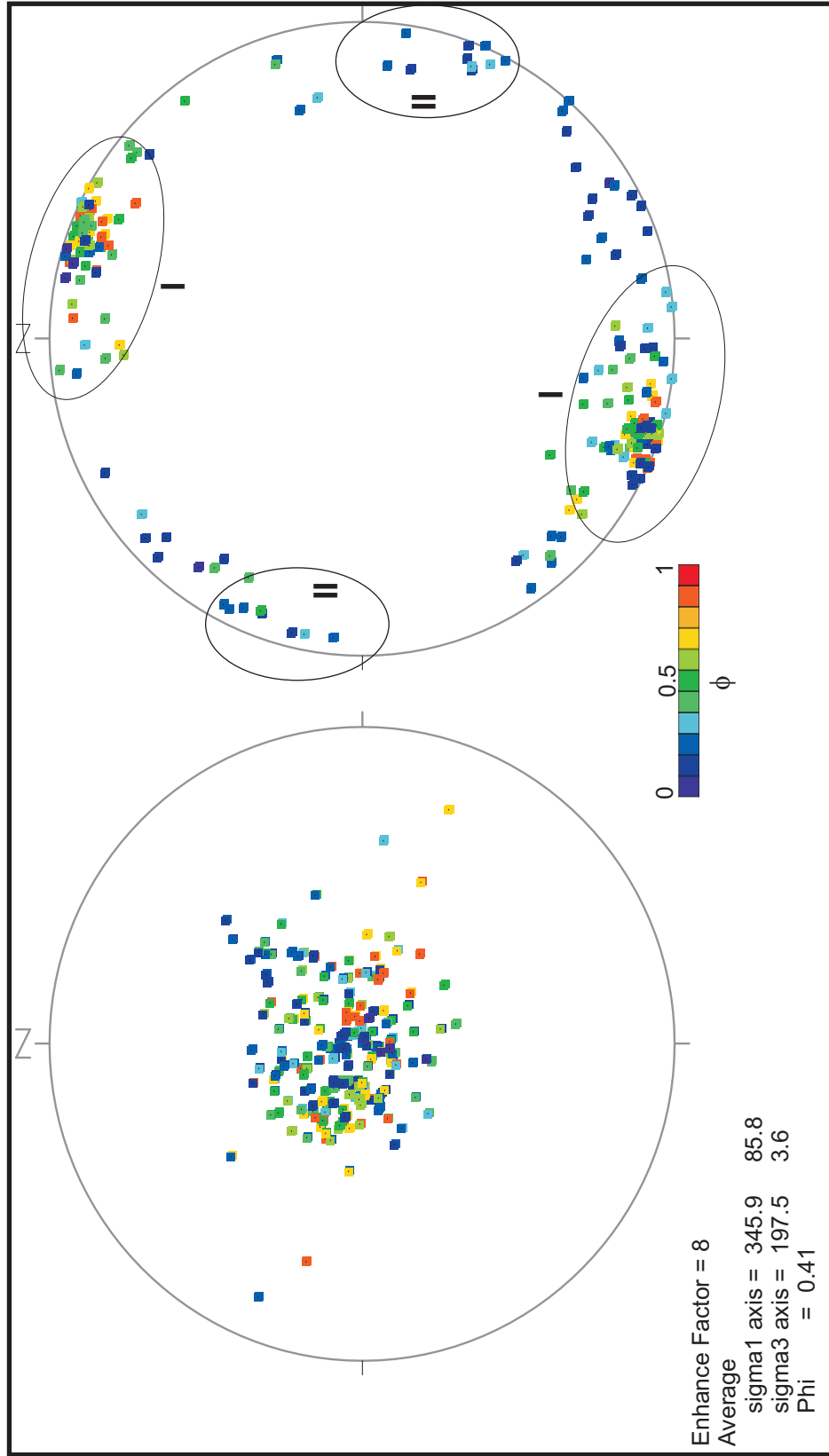


Figure 3.23. Solution of the fault slip data acquired from Neogene deposits according to multiple inverse method (Yamaji, 2000). Stereoplot on the left depicts the σ_1 orientations and the one on the right σ_3 orientations. The color of dots reflects the Φ ratio which is quantified in the color bar. A dominant single cluster can be inferred from the distribution of σ_3 axes indicating NNE-SSW-directed extension that is in agreement with the solution of slip inversion methods. Fault data falling out of the cluster are probably related to local variations.

packages share many similarities (Figures 3.2 and 3.14). These similarities are not limited to fault patterns but also cover the governing stress field controlling the deformation. Dip-frequency and rake-frequency diagrams showing uni-modal distribution for the plio-Quaternary package and tri-modal distribution for the Neogene package portray the most important distinction between the fault populations (Figures 3.2 and 3.14). However, the observed evidence of rotation at St-9 in Figure 3.16 may explain the three-modal distribution of the fault dips by forming shallowly dipping and subvertical faults for the Neogene population. The inferred rotation can also influence the slip measurements if the rotation axis deviates from the strike of the faults. This changes the rake of the lineation with respect to strike of the fault plane.

Based on the similarity of fault patterns observed in Plio-Quaternary and Neogene populations, no clear evidence of change in structural style was observed. The exception to this is depicted by the low-angle detachment fault and the high-angle normal faults having cross-cutting relationship at the St-10. Referred as two distinct structural styles of extension by the recent literature (Bozkurt and Rojay, 2005; Bozkurt and Mittwede, 2005 and references therein), there is not enough constraint to separate these styles into two distinct phases of extension. Associated with large amount of offset, it is likely that the detachment fault has undergone significant amount of change in its geometry related to wide range of factors from crustal scale isostasy to gravitational collapse (Wernicke and Axen, 1988; Buck, 1988; Graue, 1992; Fossen and Gabrielsen, 1996). In a similar way to St-9, both styles can form in the continuum of deformation. Rotating a structures to shallow dips in the course of deformation will naturally stops its activity and necessitate new structures to form that potentially have cross-cutting relation with the former.

Before the conclusion on this issue another hesitation arises due to the fact that the outcrop observations were desperately concentrated along the southern margin of the Gediz Graben due to the availability of the exposures. Although this margin provides invaluable information to the geology of the graben, fault systems here are likely to expose later modifications in their geometry (e.g. rotation, bending etc.) more than anywhere else in the basin as the most intense and active site of deformation. Subsurface studies are required to provide more concrete and conclusive evidence on this issue by providing data from the entire basin.

Slip inversion methodology applied to fault data has yielded satisfactory solutions both for Plio-Quaternary and Neogene populations (Figures 3.19 and 3.22). Based on these data, it can be stated that graben is experiencing roughly N–S-oriented extension during the deposition of the graben fill (Figure 3.24). Most field stations including bulk analysis of Plio-Quaternary and Neogene fault populations yielded a reduced stress tensor that is conformable with the NNE–SSW-oriented extension. As a result, this is accepted as the main direction of extension for the southern margin of the Gediz Graben (Figure 3.24). Variation from this direction does exist and probably represents local stress field anomalies and stress axes permutations. Indeed, observation on the spatial variation of the stress field in the structural framework of the St-10 clearly illustrates that variation in the general trend of extension is commonly associated with bends in the strike of faults or zones of potential fault interaction (Figure 3.25).

Two different methods were tested to compute the principal stress axes of deformation for the Plio-Quaternary fault population. Angelier's (1990, 1994) direct inversion method based on measurement of slip vector and Lisle's (2001) method requiring only fault slip sense have produce very close solutions to constrain the principal stress directions. Furthermore, the computed stress directions are conformable with the observed fault patterns. This suggests that despite the hesitation on the validity of stress inversion methods (Reches, 1987; Marrett and Allmendinger, 1990; Pollard *et al.*, 1993), the applied methodology produced acceptable solutions.

The fault slip data were also tested for heterogeneity using the multiple inverse method (Yamaji, 2000). Assessment of the method's solution together with the observed field relations lead to conclusion that the fault populations of Plio-Quaternary and Neogene strata are not heterogeneous. Yet, multi-directional extension inferred from fault patterns and value of ϕ -ratio has introduced some complexity to the observed fault patterns. Furthermore, no major differences were detected between Plio-Quaternary and Neogene fault populations to state that there are multiple phases of deformation. This doesn't necessarily exclude the validity of two-stage extension model of the region. If both stages are characterized by similar orientations of stress axes, the applied analyses may fail to reveal the distinction.

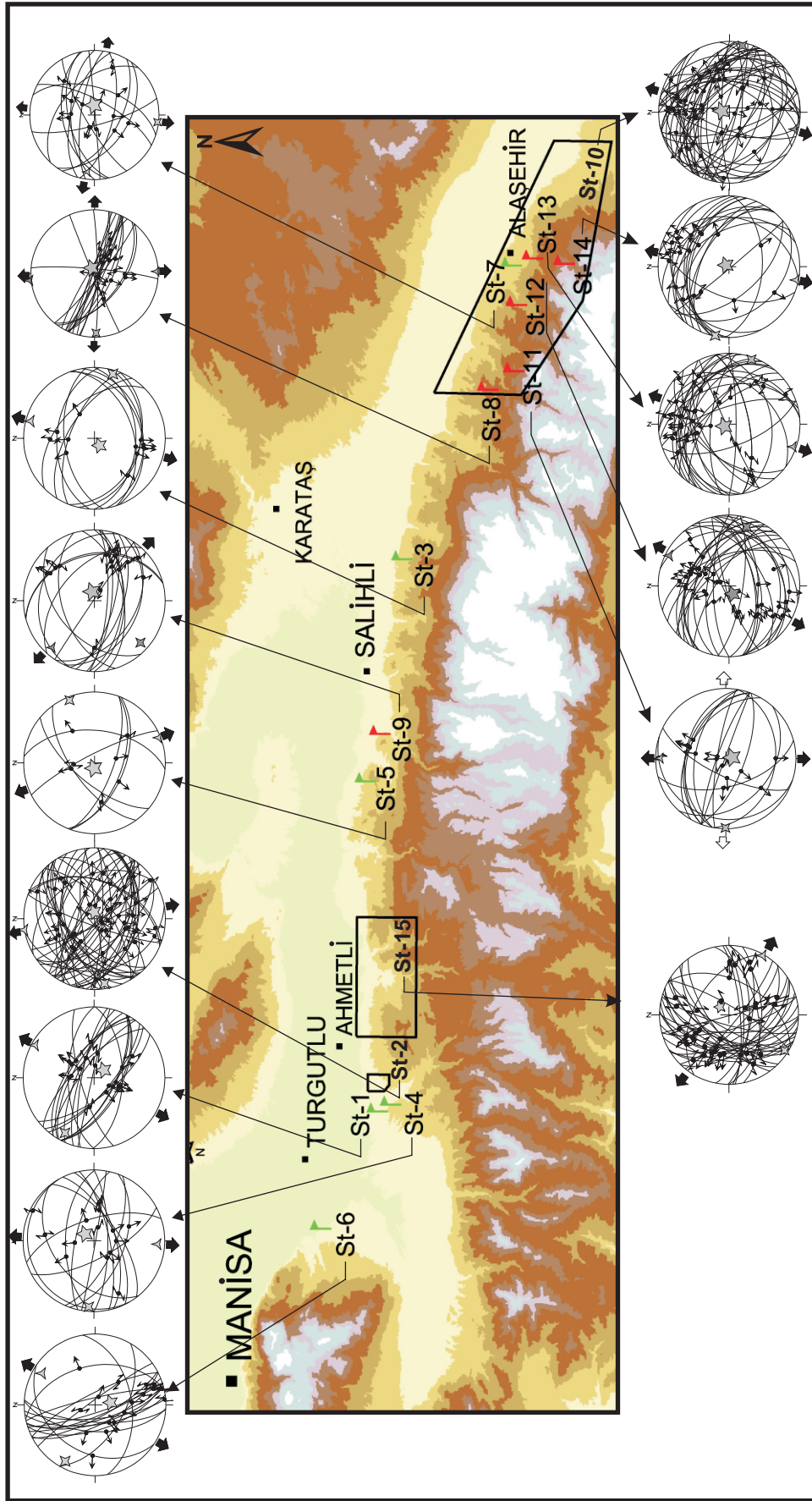


Figure 3.24. Summary of the stress inversion results carried out along the southern margin of the Gediz Graben. See Figures 3.13 and 3.16 for detailed information on the individual stations. The inverted stress tensor suggests that the graben is currently experiencing ~N-S oriented extension ranging from NNW-SSE to NNE-SSW. NNE-SSW-directed extension is probably more common and regional.

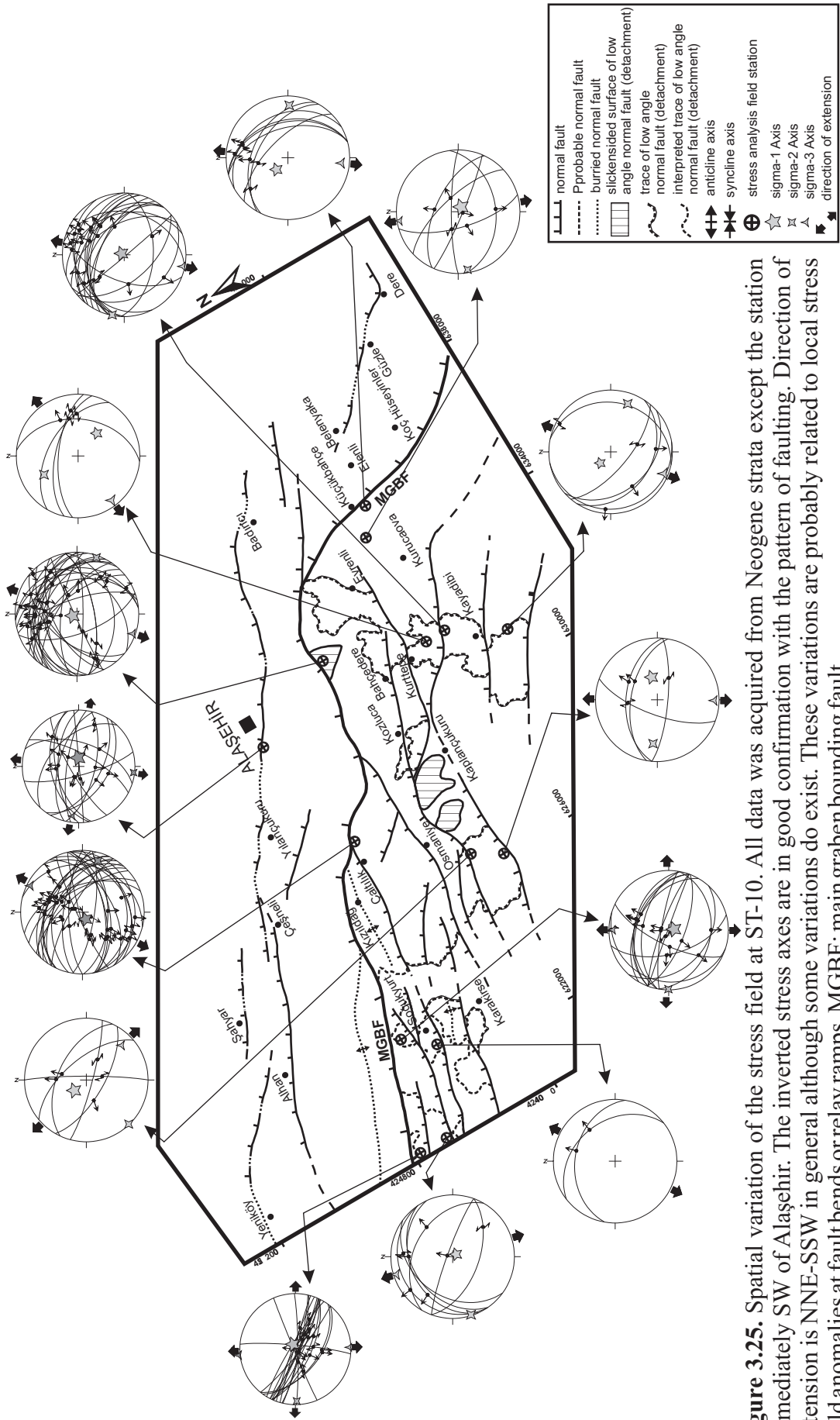


Figure 3.25. Spatial variation of the stress field at ST-10. All data was acquired from Neogene strata except the station immediately SW of Alaşehir. The inverted stress axes are in good confirmation with the pattern of faulting. Direction of extension is NNE-SSW in general although some variations do exist. These variations are probably related to local stress field anomalies at fault bends or relay ramps. MGBF: main graben bounding fault.

CHAPTER 4

RELAY RAMPS AND FAULT SEGMENT LINKAGE

This chapter documents the geological characteristics of a relay ramp currently evolving along the southern margin of the Gediz Graben. The analyses are based on the geological field mapping carried out at field station St-15 (Figure 3.1). At the field station, the relay ramp is identified based on morphological and structural criteria. The ramp area represents a local anomaly of deformation, which is characterized by variation of the structures from the regional style. The observed variations at the ramp area include variation of dip direction and orientation and intensity of faulting as well as variation of the governing stress regime. The change of structural style takes place both in spatial and temporal context in relation to the change of stress field during ramp evolution.

4.1. Background on Relay Ramps

Normal faults and associated deformation zones are common structures in regions experiencing extension. Although normal fault zones typically extend in excess of 100 km, they commonly comprise an array of overstepping and linked fault segments. The volume of rock that is deformed and tilted between two normal fault segments that overstep in map view is called a transfer zone (e.g., Peacock *et al.*, 2000). If two segments dip in the same direction, the transfer zone is called a synthetic transfer zone (Morley *et al.*, 1990) or a relay ramp (Larsen, 1988; Peacock and Sanderson, 1991, 1994) (Figure 4.1). Widths of relay ramps between overstepping normal faults follow a power-law (fractal) relation from millimetre scales to tens or hundreds of kilometers (e.g., Peacock and Sanderson, 1994; Schlische *et al.*, 1996; Peacock, 2003).

Although a range of specific geometries can developed between the overstepping fault segments, the terms ‘*soft-linked*’ and ‘*hard-linked*’ represent the

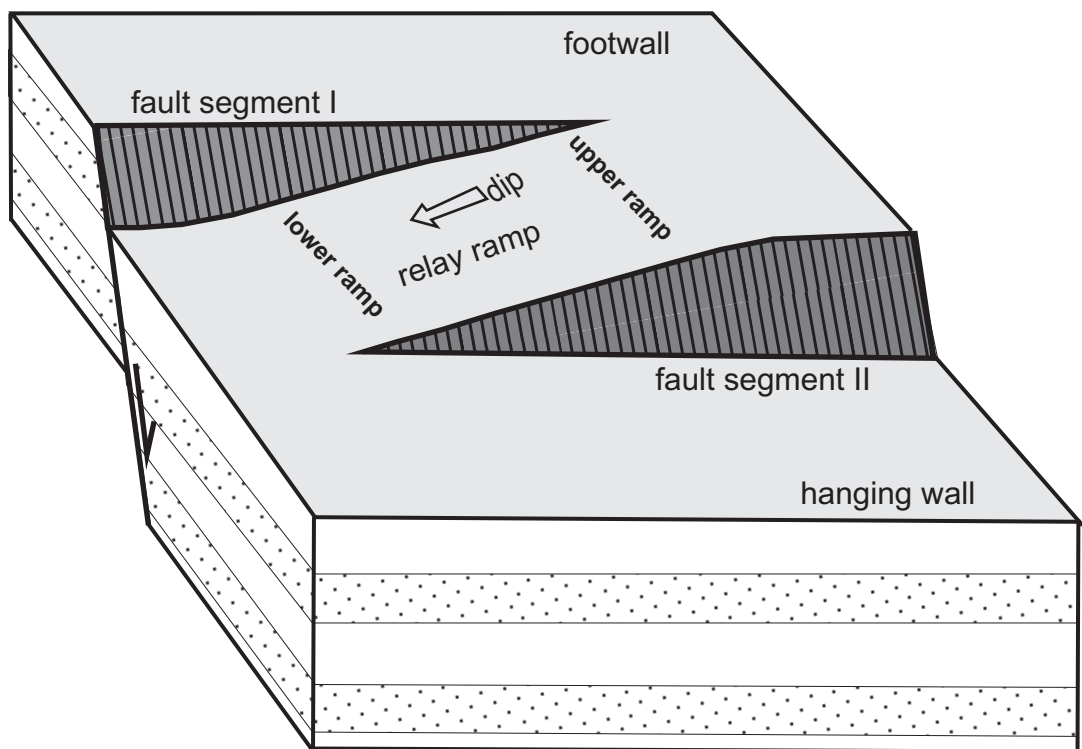


Figure 4.1. Block diagram of two overstepping normal fault segments dipping in the same direction. Displacement among the fault segments is transferred by formation of a relay ramp. From Larsen (1988), Peacock and Sanderson (1991, 1994).

two end-member geometries (Gibbs, 1984; Walsh and Watterson, 1991). Soft-linked segments are those that are characterized by a distributed deformation of a relay ramp without a breaching fault (Figures 4.1, 4.2A and B). On the other hand, hard-linked segments contain a fault surface (a breaching fault) that cuts through the relay ramp and links the individual segments (Figure 4.2D and E). Soft-linked segments may become hard-linked segments through time in an evolutionary manner (Peacock and Sanderson, 1994). Four different stages were described through soft-linked to hard-linked evolution (Figure 4.2; Peacock and Sanderson, 1991, 1994). In stage 1, fault segments are isolated with little or no interaction between the segments. In stage 2, segment interaction initiates as faults propagate toward each other and overlaps. At this stage a relay ramp connects the footwall of one fault with the hanging-wall of the other. Displacement is transferred from one segment to the other by deformation of the relay ramp. Transfer of displacement at a relay ramp is achieved in three ways (Figure 4.3): (1) rotation about a vertical axis to accommodate heave gradients on bounding faults; (2) rotation about one or more horizontal or low inclination axes to accommodate vertical throw gradients on bounding faults, i.e. tilting; (3) transverse faulting and fracturing to accommodate fault-parallel extension (Ferrill and Morris, 2001). With stage 3, fracturing initiates at the relay ramp in response to accumulated tilting, vertical axis rotation and cut-off parallel elongation prevailing in the ramp area.

Finally in stage 4, the relay ramp is broken by a composite fault or a breaching fault and consequently two overstepping segments join with an along-strike bend (Figure 4.2E). The primary factors controlling the breaching of a relay ramp can be underlined as slip vectors and displacement gradients of overlapping faults that bound the ramp area (Ferrill and Morris, 2001). Depending on the stress conditions at the overlap area, breaching may take place either at the upper ramp or at the lower ramp with abandonment of the other.

The interpretation of relay ramps in complex deformation zones is difficult, yet indispensable in hydrocarbon prone basins. They play an important role in hydrocarbon migration and structural trapping mechanisms (Morley *et al.*, 1990; Peacock and Sanderson, 1994, Ferrill and Morris, 2001). As they link the hanging-wall and footwall of fault systems, relay ramps can be important loci of hydrocarbon migration (Larsen, 1988, Ferrill and Morris, 2001). Migration can occur from the basin, which is the hanging-wall, up to the ramp and to the footwall (Peacock and

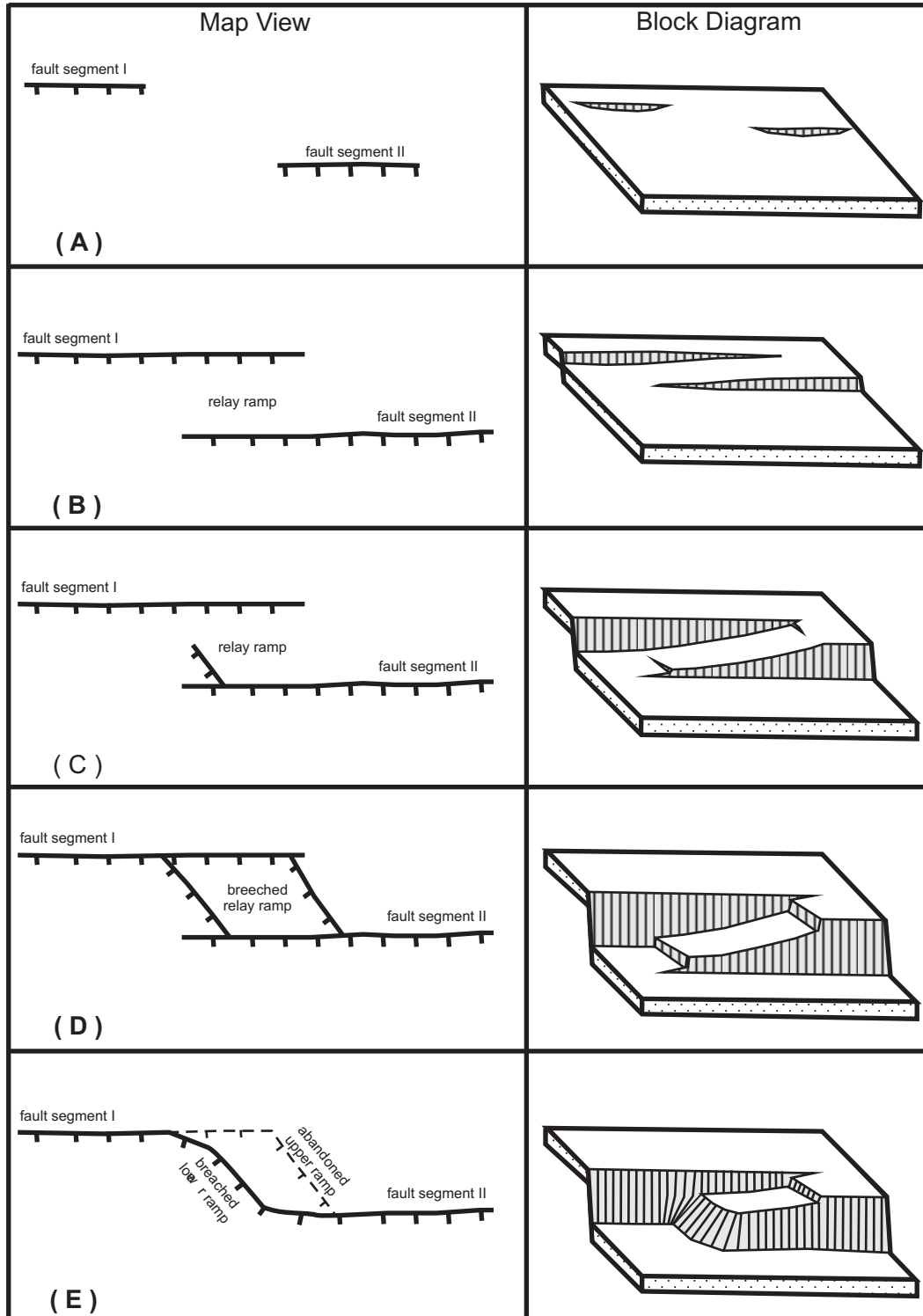


Figure 4.2. Schematic diagram showing evolutionary stages of a relay ramp. Tick marks on the map view depict the down thrown block of normal faults. (A) Stage I: The faults do not interact; (B) Stage II: The faults have started to interact and a relay ramp developed to transfer the displacement among the segments; (C) Stage III: Accumulated strain in the relay ramp resulted in initiation of fracturing; (D) Stage IV: The relay ramp is broken by a breaching fault to form a single fault zone with strike irregularity; (E) Upper bench is abandoned and two segments joined through breaching of lower ramp that form an along strike bend on the course of the main fault. Modified from Peacock and Sanderson (1994).

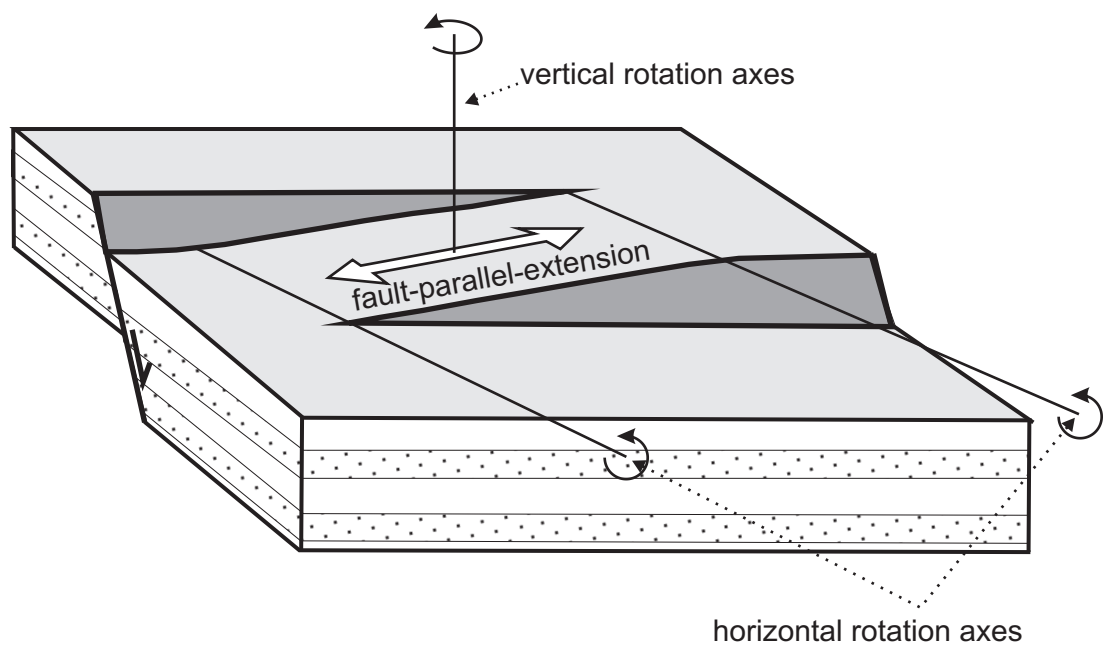


Figure 4.3. Block diagram illustrating deformation mechanisms at a relay ramp. Rotation about horizontal axes and vertical axis and fault-parallel-extension is predominantly controlled by slip vectors and displacement gradients of the bounding faults. From Ferrill and Morris (2001).

Sanderson, 1994; Ferrill and Morris, 2001). Mechanical interaction of fault segments and resulting variation of local stress field leads to a change of structural style at relay ramps. A relay ramp also represents an upgrade from approximately two-dimensional extension to three-dimensional (triaxial) extension with oblique-slip fault systems (Morley, 1988). These changes in structural style are manifested in the form of changes in fault dip direction, variation in the orientation and intensity of faulting (Morley *et al.*, 1990). Therefore, greater chance arises at a relay ramp to form oil and gas traps of different structural styles, which are greater in concentration than anywhere else in an extensional basin (Morley *et al.*, 1990; Ferrill and Morris, 2001). Furthermore, relay ramps can significantly influence drainage, erosion and sedimentation to create favourable depositional patterns for exploration (Morley *et al.*, 1990; Grawthorpe and Hurst, 1993). Examples of relay ramp associated oil and gas fields in North Sea, Sirte Basin and the other hydrocarbon prone extensional basins of the world are discussed in the recent literature (e.g., Morley *et al.*, 1990; Peacock and Sanderson, 1994; Larsen, 1988).

Formation and evolution of relay ramp of various scales has been the focus of numerous studies that are based on analogue and numeric modelling and natural examples at different locations around the world (e.g., McDonald 1957; Larsen 1988; Morley *et al.*, 1990; Peacock, 1991; Peacock and Sanderson, 1991, 1994; Childs *et al.*, 1995; Coşkun, 1997; Peacock *et al.*, 2000; Lezzar *et al.*, 2002; McLead *et al.*, 2002; Mauk and Burruss, 2002; Trudgill, 2002; Younes and McClay 2002; Young *et al.*, 2002; Imber *et al.*, 2004; Soliva and Benedicto, 2004, 2005; Acocella *et al.*, 2005). These studies established a reasonable consensus on the evolutionary stages of relay ramp formation, as first suggested by Peacock and Sanderson (1991, 1994). However, how the stress field changes around a relay ramp during this evolution has not been documented clearly. It is the main theme of this chapter.

4.2. Stratigraphy of the Field Station

The field station is located along the southern margin of the Gediz Graben between towns of Akçapınar and Turgutlu (Figure 3.1). Six different lithostratigraphic units were differentiated during geological mapping in this particular station (Figures 4.4 and 4.5). The lowermost unit named as the basement comprises metamorphic rocks of the Menderes Massif, which includes schists,

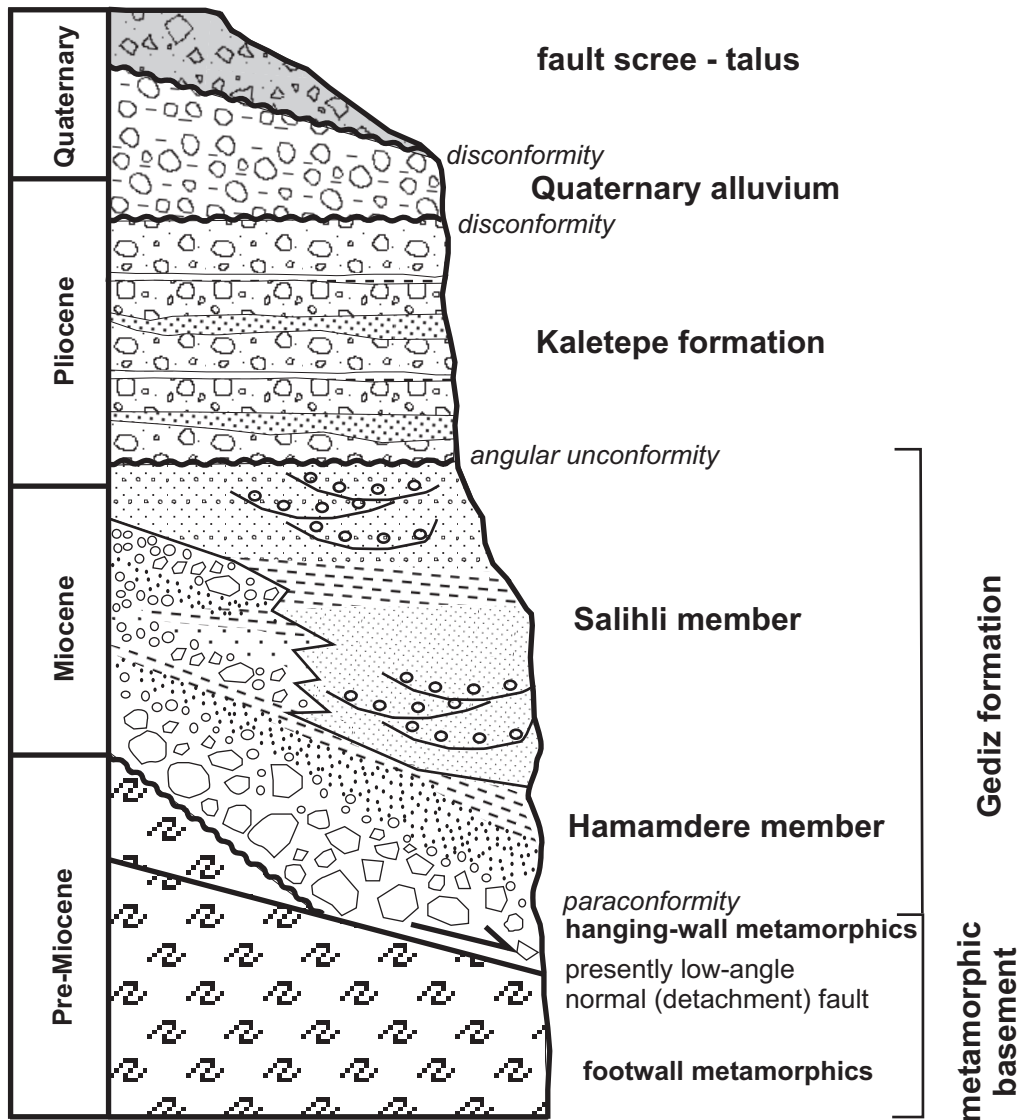


Figure 4.4. Simplified stratigraphical columnar section of the area-based field station St-15. See Figure 3.1 for the location of the station.

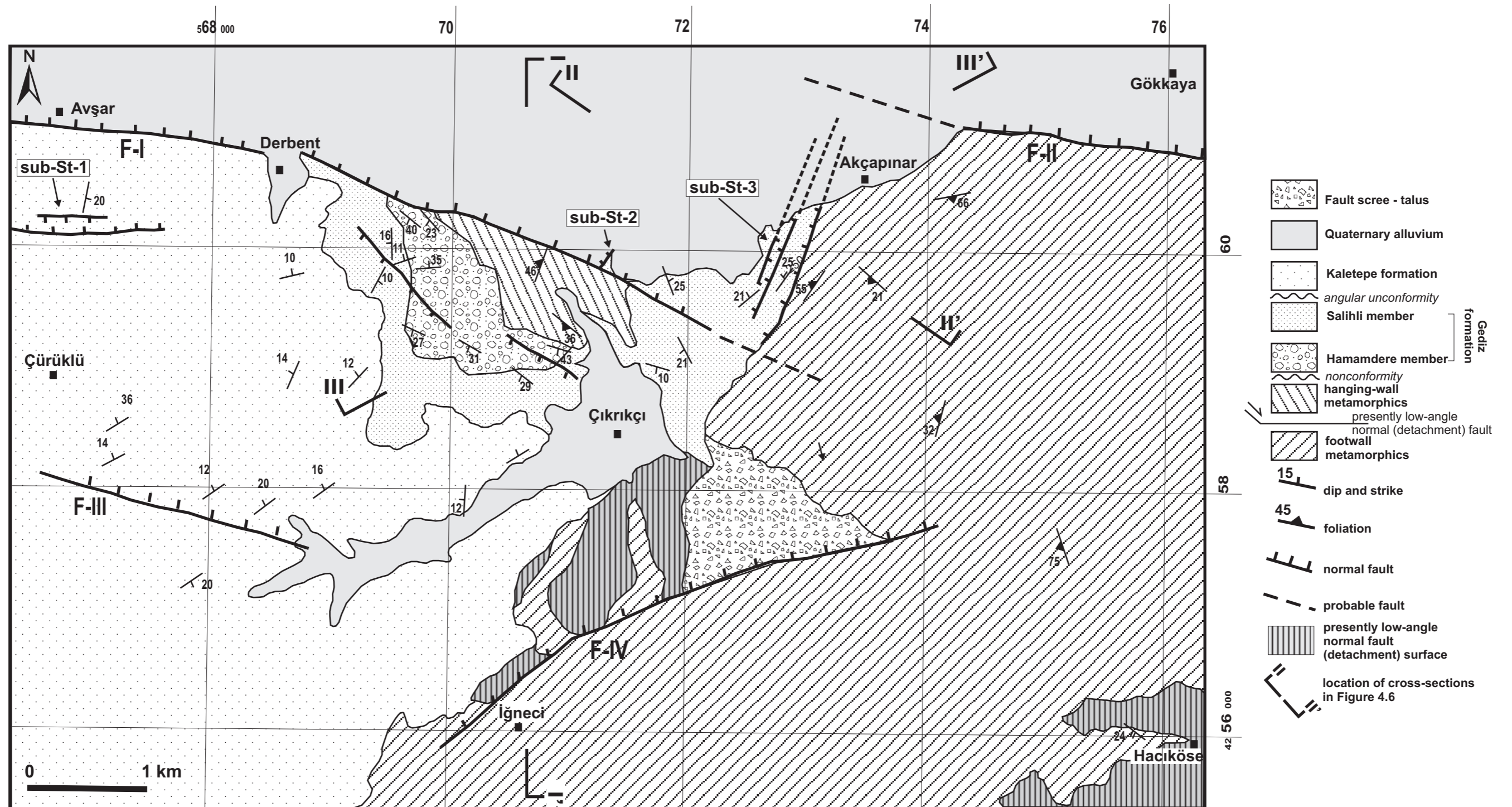


Figure 4.5. Geological map of the field station St-15. The low-angle normal fault is illustrated as an area representing the exposed slickensided surface of the fault. Major high-angle normal faults are labeled on the map as F-I, F-II, F-III and F-IV. Five different lithostratigraphic units comprising continental clastics overlie the metamorphic rocks of the Menderes massif. Akçapınar relay ramp is located between F-I and F-II. Sub-St-1 to 3 illustrates the substations where fault slip data was acquired.

quartzites and phyllites. The unit exposes extensively across the field station. Unconformably above the basement and/or the presently low-angle normal fault, Neogene clastic rocks were differentiated, based on lithological characters, and mapped as five different lithostratigraphic units (Figures 4.4 and 4.5). Although, simple descriptions of the lithostratigraphic units are given below, they are described in Chapter 2 in more detail.

At the field station St-15, Hamamdere member of the Gediz formation is composed predominantly of conglomerates with intervening sandstones. Conglomerates are massive to very thick bedded, poorly sorted, coarse-grained (cobbles and boulders), usually matrix-supported with sandy matrix and polymictic by clasts of underlying metamorphics. Hamamdere member laterally grades into Salihli member of the Gediz formation, which is composed of sandstones and conglomerates with minor siltstone and mudstones. The channel formed sandstones and conglomerates with roughly E-W-trending channel orientation suggest a dominance of fluvial processes in the deposition of the unit. Trough cross-bedded conglomerates and sandstones occasionally intercalate with chaotic conglomerates of the Hamamdere member, representing the lateral gradation between the two members. In general, both units dip towards SW.

Kaletepe formation unconformably overlies the Gediz formation with an angular unconformity and is composed of conglomerates and pebbly sandstones with sandstone and mudstone intercalations. Conglomerates are beige to yellow colored, massive and poorly bedded, poorly sorted, semi-consolidated and polymictic with various metamorphic clasts. Sand is an important constituent of conglomerates as matrix. The unit dips in the NW direction with relatively shallow angles and is influenced by river incision severely exposing thick sections of the unit as canyon walls. Quaternary alluvium is deposited in the hanging wall of the graben-bounding normal faults and in the footwall as modern river deposits. In the hanging wall along the bounding faults, the unit includes diverse size of coalesced alluvial fans that grade into finer fractions towards the centre of the graben where they interfinger with modern fluvial system of the Gediz River. The uppermost unit represents unconsolidated talus of metamorphic clasts and deposited in front of a relief that is created by active fault zones.

4.3. Structural Geology

The two types of structures that are peculiar to the southern margin of the Gediz Graben are both observable in the study area. The presently low-angle normal fault (detachment) has surface exposures of slickensided fault plane that trends 230° to 240°N and dips 08° to 10° to the NW (Figure 4.5). The low-angle normal fault (detachment) generally constitutes to contact between the Neogene sedimentary fill and the basement metamorphic rocks by constraining the metamorphic rocks into the footwall and exposing the sedimentary rocks on its hanging-wall (Figures 4.5 and 4.6). Exception to this is observable to the northwest of Çıkırıkçı, where metamorphic rocks also expose in the hanging-wall block, called as extensional allochthons (Sözbilir, 2002). As a result, metamorphic rocks of the basement were differentiated into two distinct units as hanging-wall and footwall metamorphics to refer whether they expose on the hanging-wall or footwall of the presently low-angle normal fault, respectively (Figures 4.4, 4.5 and 4.6).

High-angle normal faults, which are the second group of structures in the Gediz Graben, exposes with approximately E-W-oriented surface traces in the study area (Figures 4.5). Forming the southern margin of the Gediz Graben, these faults normally occur in a graben-facing step-like pattern with a younging direction towards the graben; i.e. to the north (Bozkurt and Sözbilir, 2004). Thus, F-I and F-II forms the northernmost and youngest fault zone immediately adjacent to the graben floor. To the south, two other major faults (F-III and F-IV) exposes in a subparallel configuration to the northern fault zone (Figures 4.5 and 4.6). Various smaller-scale faults are also observable between the northern and southern zones. Observed field relations suggest that high-angle normal faults cut and offset the presently low-angle normal fault (Figures 4.5 and 4.6).

The northern fault zone, which is composed of F-I and F-II in the study area, is part of a more extensive fault zone currently bounding the southern margin of the modern floor of the Gediz Graben (Figure 4.5). The geological map of the field station clearly illustrates an example of the fact that this fault zone does not comprise a single and continuous fault but is composed of overlapping segments. As representation of this major structure, two faults (F-I and F-II) trending 275° to 285° N with a northward overstep were identified and mapped in field station (Figure 4.5). These faults form 350 to 400 m elevation difference between the almost flat graben floor and the rugged horst block with strong topographical manifestation of the fault

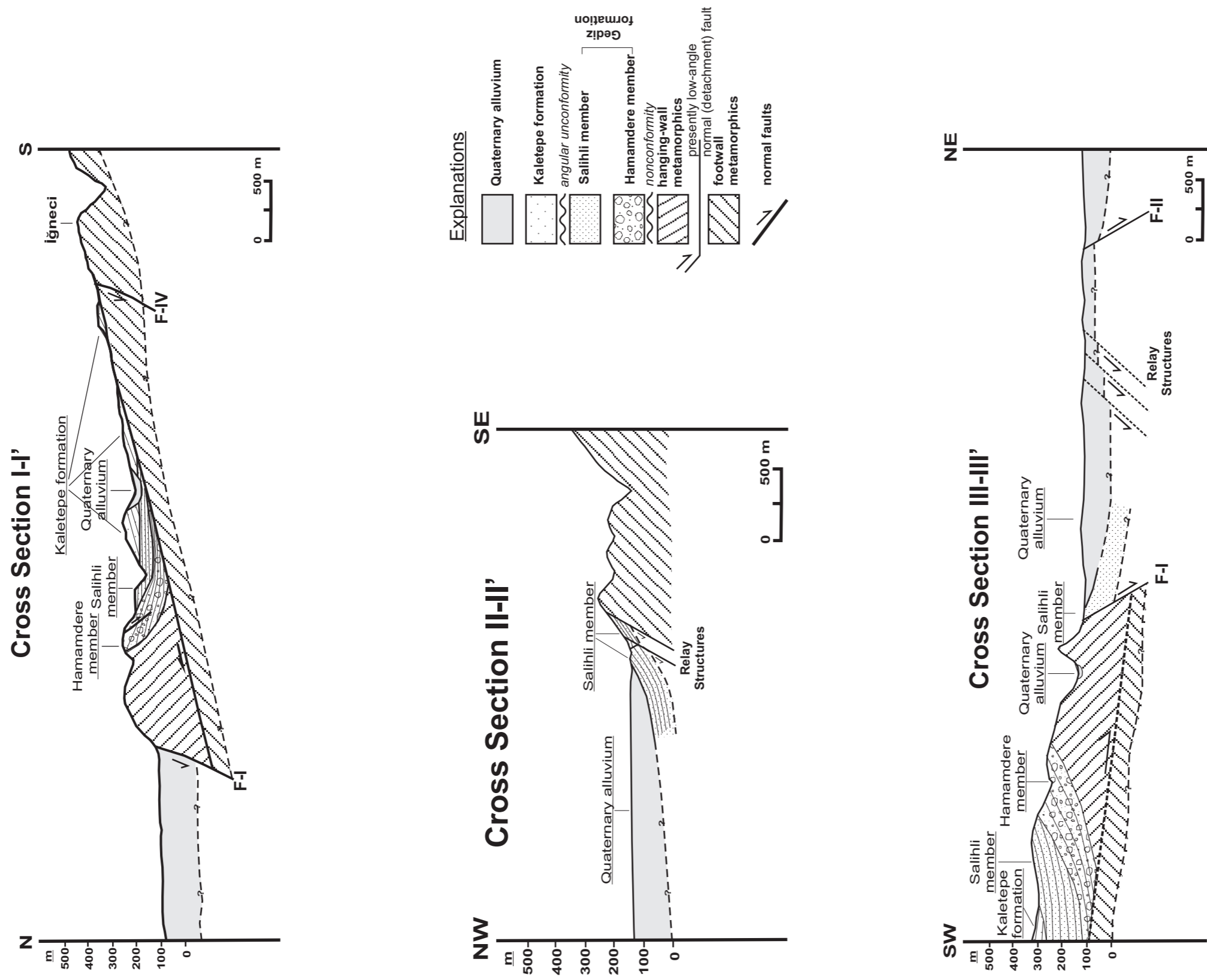


Figure 4.6. Geological cross-sections through I-I', II-II' and III-III' on Figure 4.5. (A) Cross-section I-I' illustrates general relations in the study area. Note the cross-cutting relationship between the high-angle and low-angle normal faults. A small basin filled with continental clastics formed above the detachment. (B) Cross-section II-II' is parallel to the bounding faults and cut through the relay ramp. Salihli member is tilted towards the common hanging-wall to NW at the relay ramp in contrast to its SW regional dip. (C) Cross section III-III' is oriented obliquely to the relay bounding faults. As relay structures are syn-depositional with respect to Quaternary alluvium, they probably result in thickening of the unit downdip the relay ramp.

zone (Figure 4.7). The available literature suggests more than 2.0 km offset associated with the southern margin structure of the Gediz Graben (Bozkurt and Sözbilir, 2004). However, it is important to emphasize that this cumulative offset is probably partitioned among sub-parallel fault zones forming the graben facing step-like pattern of the southern margin.

F-I and F-II are active with predominantly normal dip-slip component and controlled the deposition of the Quaternary alluvium in the modern graben floor. In addition to available earthquake data, GPS measurements (e.g., Eyidoğan and Jackson 1985; McClusky *et al.*, 2000; Lenk *et al.*, 2003) and the fault data documented by various studies along the main bounding faults of the Gediz Graben (e.g., Koçyiğit *et al.*, 1999; Seyitoğlu *et al.*, 2002; Bozkurt and Sözbilir, 2004; Bozkurt and Mittwede, 2005; Bozkurt and Rojay, 2005 and references therein), intensive fault data analyzed in Chapter 3 agreed on the general trend and slip on the southern margin structures of the Gediz Graben, which is conformable with the ~N-S-oriented extension in the region (Figure 4.8 and 3.25). Although limited due to exposure quality, fault data acquired in the vicinity of F-I in St-15 also confirms the general ~N-S-oriented extension (Figure 4.9A). However, the fault data acquired within the relay area has heterogeneous appearance that cannot be explained by only ~N-S-oriented extension (Figure 4.9B).

4.4. The Relay Ramp

Between the overlapping segments around Akçapınar, a relay ramp can be defined based on predominantly geometrical criteria (Figure 4.5). Named as Akçapınar relay ramp, the overlap zone between the bounding F-I and F-II slopes westward towards the common hanging-wall with an overlap separation of approximately 2 km. Although, detailed kinematic analysis are desirable to eliminate the possibility of non-relay overlap at Akçapınar (e.g., Childs *et al.*, 1995), difficulty of constraining precise displacement on bounding faults is an issue due to the quality of the surface exposures. However, it is clearly observed during the field studies that, topographical manifestation of FI and FII diminishes and the associated fault zones become poorly defined towards the relay ramp probably as an indication of increased displacement gradients on bounding faults (cf. Peacock and Sanderson, 1991; Walsh and Watterson, 1991). It is also evident on the geological map that in the ramp area, the Salihli member dips obliquely towards the common hanging-wall of the bounding

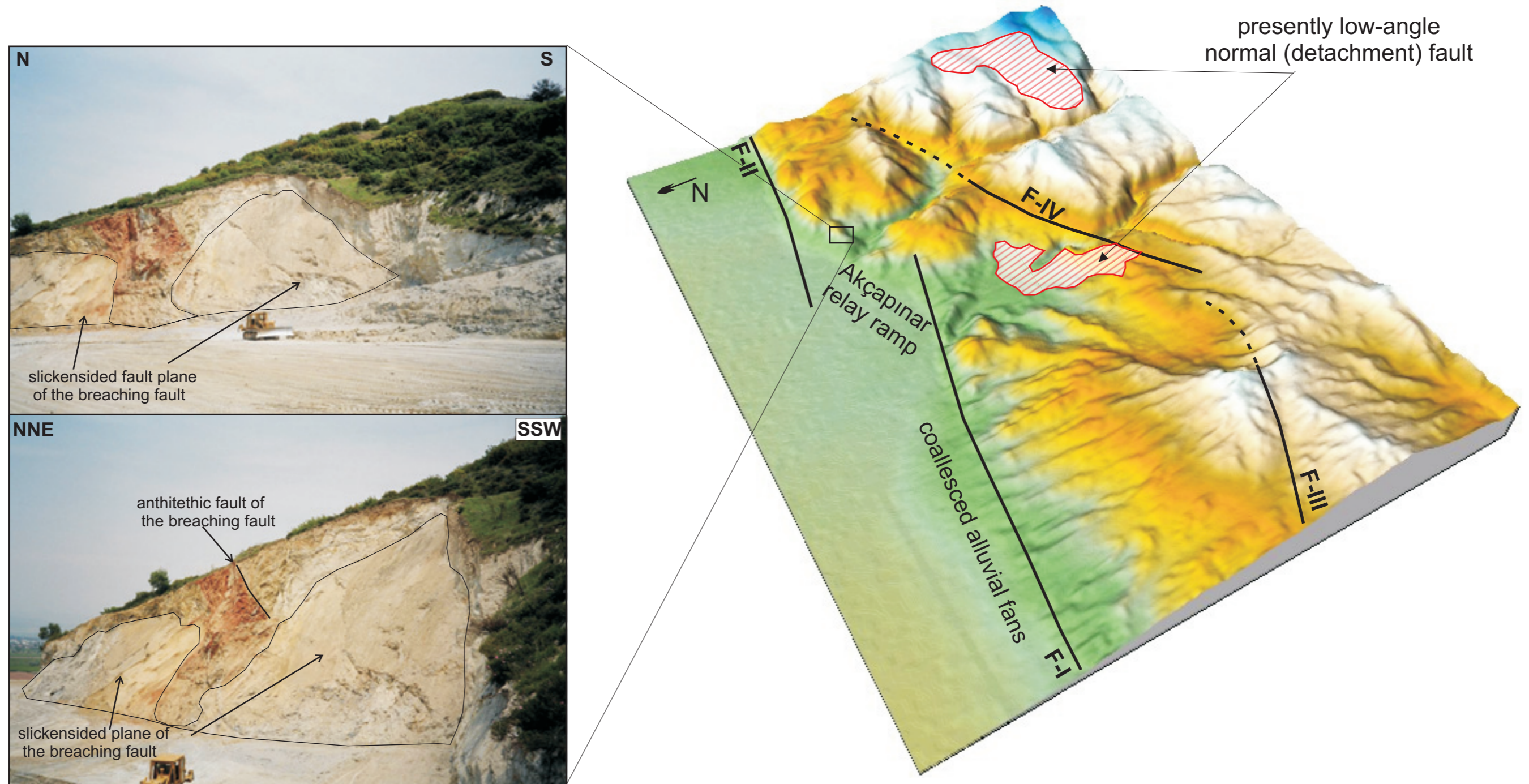


Figure 4.7. Digital Elevation Model depicting the topographical manifestations of the normal faults and the breaching Akçapınar relay ramp. The raw elevation data is based on 90 m grid spacing on which smoothing was performed. Notice on the elevation model that alluvial fans formed adjacent to F-I diminishes topographical manifestation of the fault. Dotted lines are the possible extensions of the faults inferred from the elevation model. Areas encircled by red lines corresponds to presently low-angle normal (detachment) fault surfaces. On the pictures taken at the ramp area, breaching is clearly evident in the form of obliquely oriented faults to the main E-W trend of the graben-bounding faults. The bulldozer in the figure is 5-m-high.

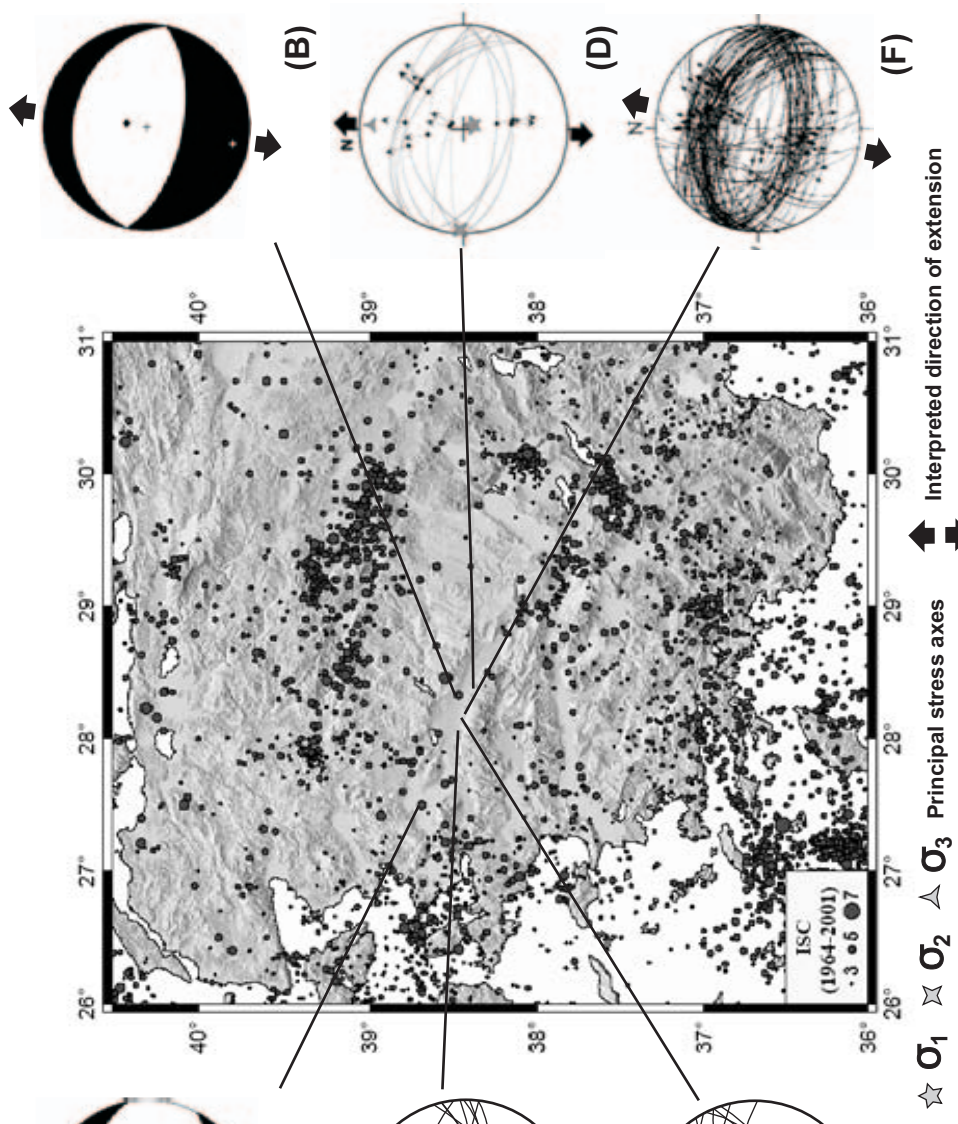


Figure 4.8. Map showing the seismicity of western Turkey, available fault plane solutions and extension directions around the Gediz Graben (black arrows). See also Figure 3.25 where extensive fault data and extension directions are illustrated in the Gediz Graben. (A) Fault plane solution of 1994 Manisa earthquake by Taymaz *et al.* (2004); (B) Fault plane solution of 1969 Alaşehir earthquake by McKenzie (1978); (C) and (E) Fault slip analyses by Barka (1996); (D) Fault slip analyses by Bozkurt and Sözbilir (2004); (F) Fault data by Koçyiğit *et al.* (1999).

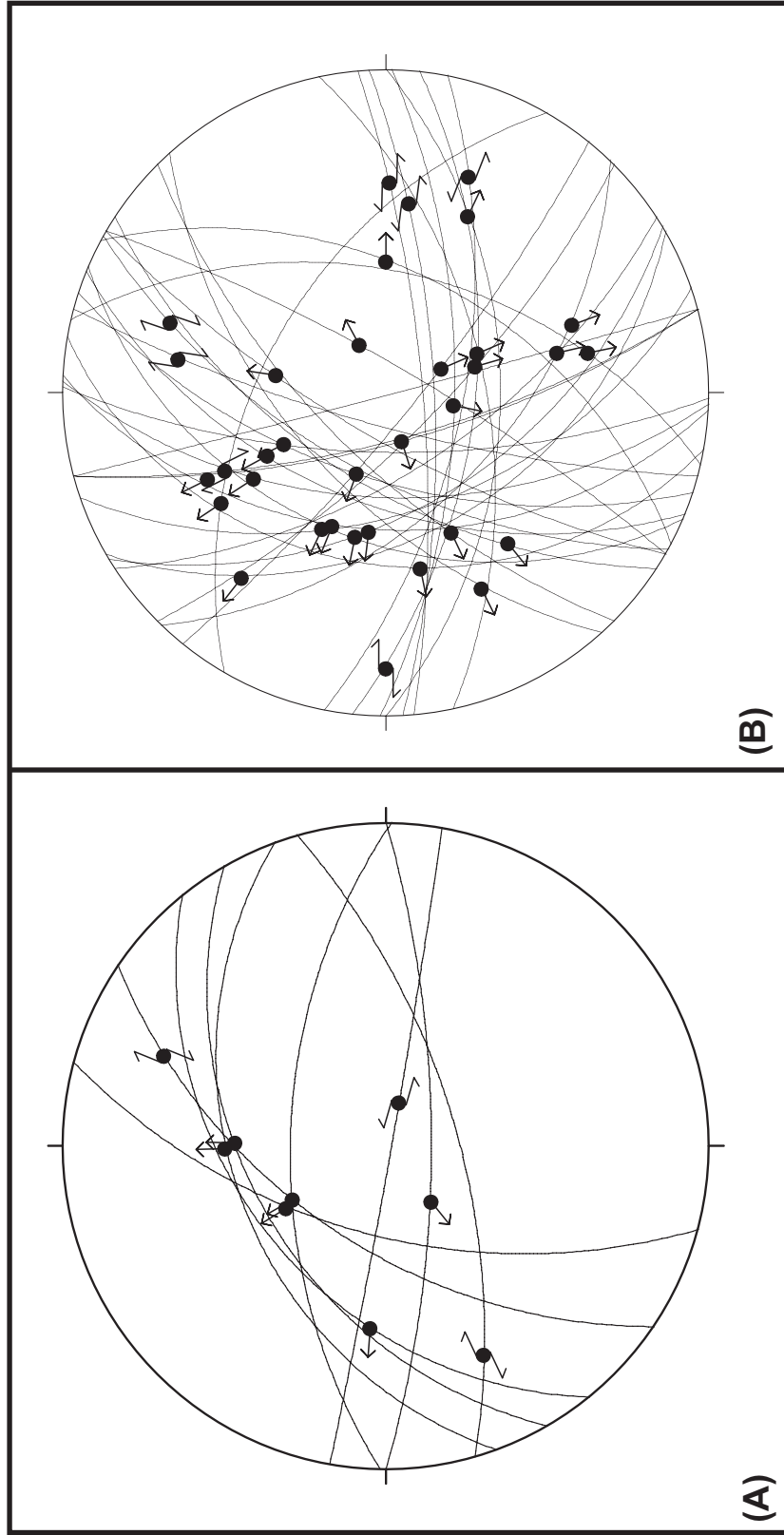


Figure 4.9. Stereoplots illustrating fault slip data of the Akçapınar area. **(A)** Fault data was acquired in the vicinity of F-I out of the relay ramp (N=9). The observed fault pattern is conformable with the regional N-S oriented extension summarized in Figure 4.8. Unfortunately, poor exposure quality limiting exposure of fault planes avoid acquisition of extensive data from F-I and F-II. **(B)** Fault data acquired at the Akçapınar relay ramp (N= 34). Construction-related excavation revealed fresh exposures of numerous fault planes at the ramp area. The fault data dominated by N-S-oriented faults clearly illustrates that the manner of deformation is different at the ramp area.

faults in contrast to its regional southward dip (Figures 4.5, 4.6). This indicates rotation of bedding about sub-vertical and sub-horizontal axes at the ramp area to accommodate heave and throw gradients on bounding faults, respectively. Furthermore, distributed brittle deformation characterized by faulting at transverse orientation to the bounding faults implies that fault-parallel extension is taking place at the at the ramp area together with the rotation (Figures 4.5 and 4.6). All these observations suggest that F-I and F-II are probably coherent, i.e. the two faults are kinematically interdependent with displacement of transfer from one segment to the other (cf. Walsh and Watterson, 1991). In fact, kinematically independent faults forming non-relay overlaps are considered as the products of temporal or spatial separation of the bounding faults (Childs *et al.*, 1995). As F-I and F-II are both syn-depositional with respect to the Quaternary alluvium, the possibility of temporal separation is probably not the case. Relatively small overlap separation of the Akçapınar relay ramp compared to lateral extend and the offset of the bounding faults invalidate the possibility of spatial separation as well.

Akçapınar relay ramp is characterized by various ramp-related faults and fracture zones that exhibit significant orientation shifts from general E–W-trend of the bounding fault segments (Figures 4.5 and 4.9B). Based on regional synthesis and limited fault data acquired from the F-I, the bounding faults can be considered as roughly E–W-oriented structures conformable with the ~N–S-oriented extension (Figures 4.9A). However, as an evidence of clear change in structural style, ~N–S-oriented faults are observed at the ramp area with dip directions predominantly towards NW and W (Figures 4.5 and 4.9B). Indeed, this fault pattern is conformable with the fault parallel ~E–W-oriented extension predicted for the ramp area. Analogous to the bounding faults; ramp-related faults are also active although it is difficult to trace them through the Quaternary alluvium due to unconsolidated nature of the unit. The relief created by the ramp related faults feeds few small-scale active alluvial fans representing the basin margin facies of the Quaternary alluvium.

Although poor exposure quality limits the acquisition of the fault data at the bounding faults, construction related excavation fortunately revealed fresh exposures of numerous pristine fault surfaces. These exposures allow observations on many mesoscale faults and acquisition of relatively extensive fault data characterizing the distributed deformation of the ramp area. This data introduced that the trend of faults in this zone is bimodal including both ~E–W-oriented and ~N–S-oriented structures,

the latter being more dominant (Figure 4.9B). Interestingly, a clear cross-cutting relationship is observed on some of the mesoscale faults in a way that N–S-oriented faults are cut and offset the E–W-oriented faults (Figure 4.10). This suggests that the current fault-parallel extension characterized by N–S-oriented normal faults is superimposed onto the regional N–S-oriented extension characterized by the E–W-oriented structures. When this fact is assessed in the framework of relay-ramp evolution illustrated in the Figure 4.2 (Peacock and Sanderson, 1994), earlier stages of ramp evolution during which bounding faults are kinematically independent were governed by ~N–S-oriented extension at the Akçapınar relay ramp. As coherency of bounding faults was established and relay ramp formed, a local stress field anomaly arose at the ramp area by fault parallel ~E–W-extension that result in superimposition of relay-related structures onto the former regional style (Figure 4.11). The former structures at the ramp area were probably rotated and deviated slightly from the regional style due to ductile accommodation of throw and heave gradients on the bounding faults until the onset of brittle deformation at the ramp area (Figure 4.11).

4.4.1. Stress Field at the Ramp Area

Fault slip data were acquired at three separate substations (sub-St-1, sub-St-2 and sub-St-3 in Figure 4.5) in the study area along the southern boundary structure of the Gediz Graben. The data were limited and inaccessible most of the time due to steep topography, resulting severe erosion, coalesced alluvial fans lean against the fault zone and unconsolidated to semi-consolidated nature of the deposits. However, we were able to collect numerous slip data that are sufficient to solve the inverse problem at the stations using Angelier’s methodology (Angelier, 1990).

Principal stress directions calculated at the sub-St-1 approximate the stress regime associated with the main bounding faults (i.e. F-I and F-II) in the study area (Figure 4.12A). Computed stress directions at this site indicate ~N–S-oriented extension. If you move along the boundary structure towards Akçapınar relay ramp and examine the stress state at the sub-St-2, NNW–SSE-oriented extension is encountered (Figure 4.12B). This suggests a counter-clockwise rotation of the direction of extension compared to the sub-St-1. However, the computations at these two sub-stations are based only on very few fault data and one should be cautious not to over interpret computations based on such a limited data set. The only inference

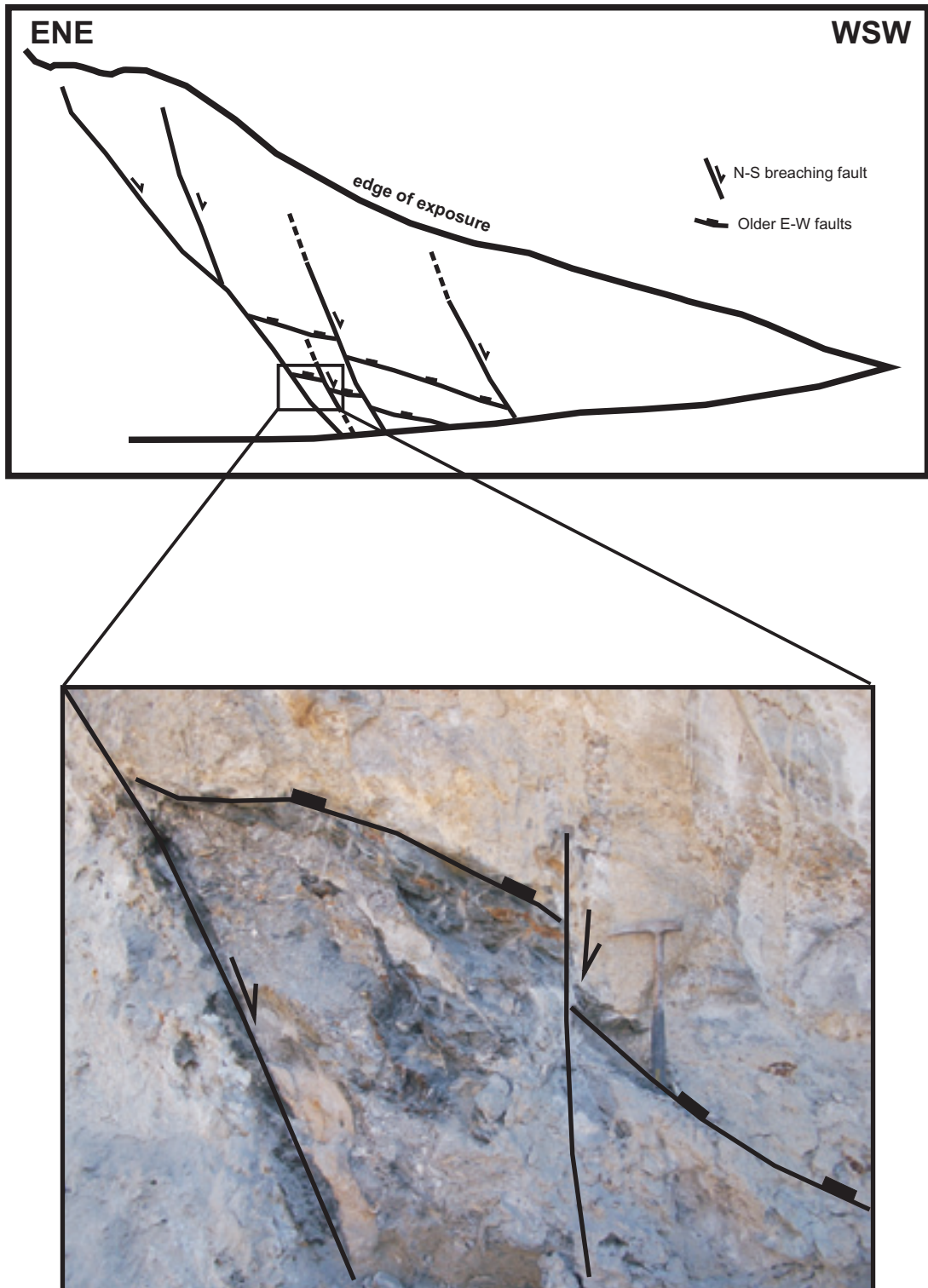


Figure 4.10. Schematic diagram showing the cross-cutting relationship between the N–S-oriented ramp-related faults and E–W-oriented older faults on a subvertical exposure surface. The hammer on the photograph is 41-cm-long.

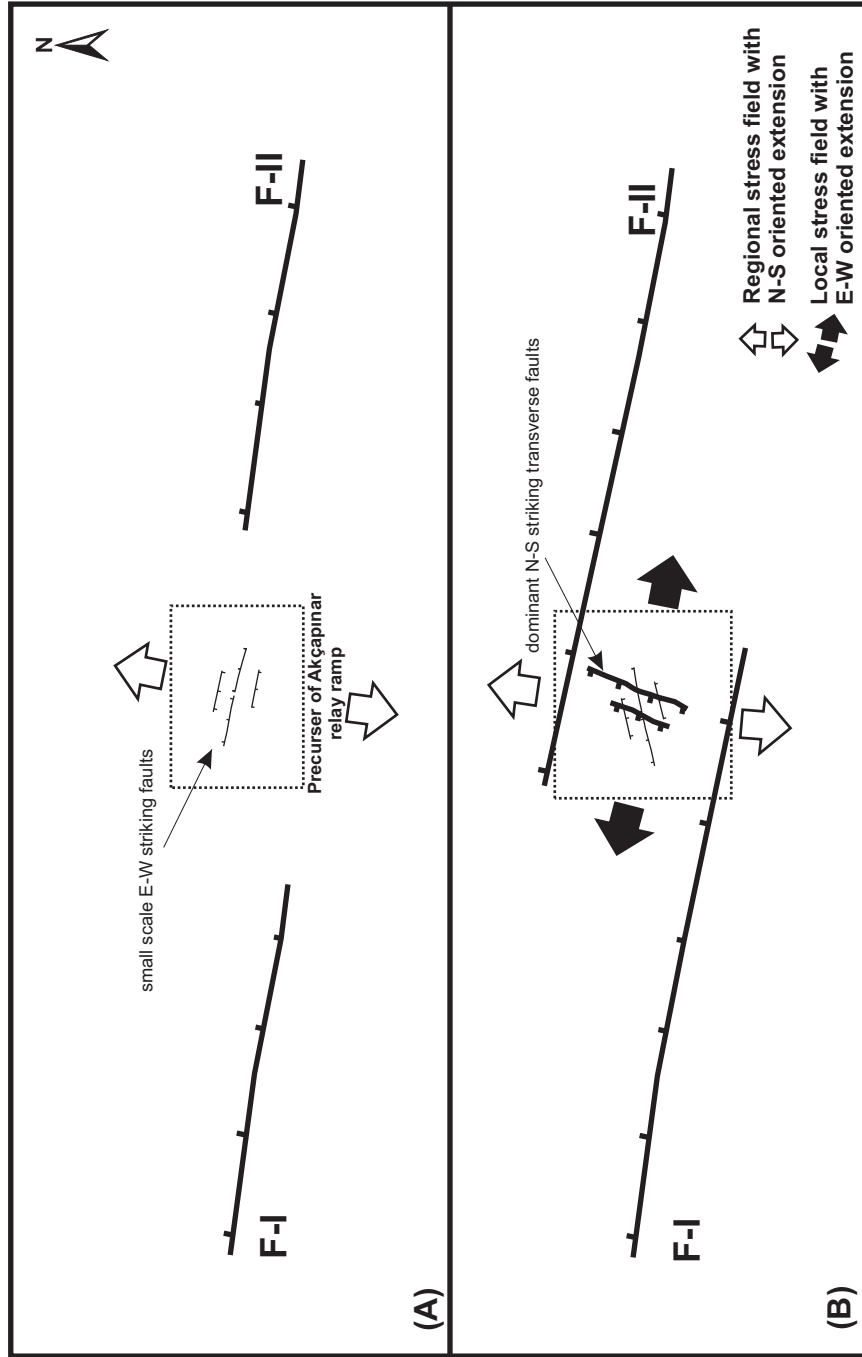


Figure 4.11. Stages of distinct deformation styles at the ramp area. **(A)** Earlier stage is characterized by kinematically independent bounding faults. At this stage deformation at the precursor ramp area is characterized by small-scale normal faulting that is conformable with the regional N–S-oriented extension. **(B)** As displacement accrues on bounding faults, the fault tips propagate to form the overlap zone through which displacement is transferred from one segment to the other. At this stage, fault-parallel extension arose at the ramp area and conformable transfer faulting is superimposed on to the earlier style of deformation at the ramp area. Earlier E–W-oriented faults were probably rotated during the ductile stages of ramp evolution. Note the difference of structural style at the ramp area between **(A)** and **(B)**.

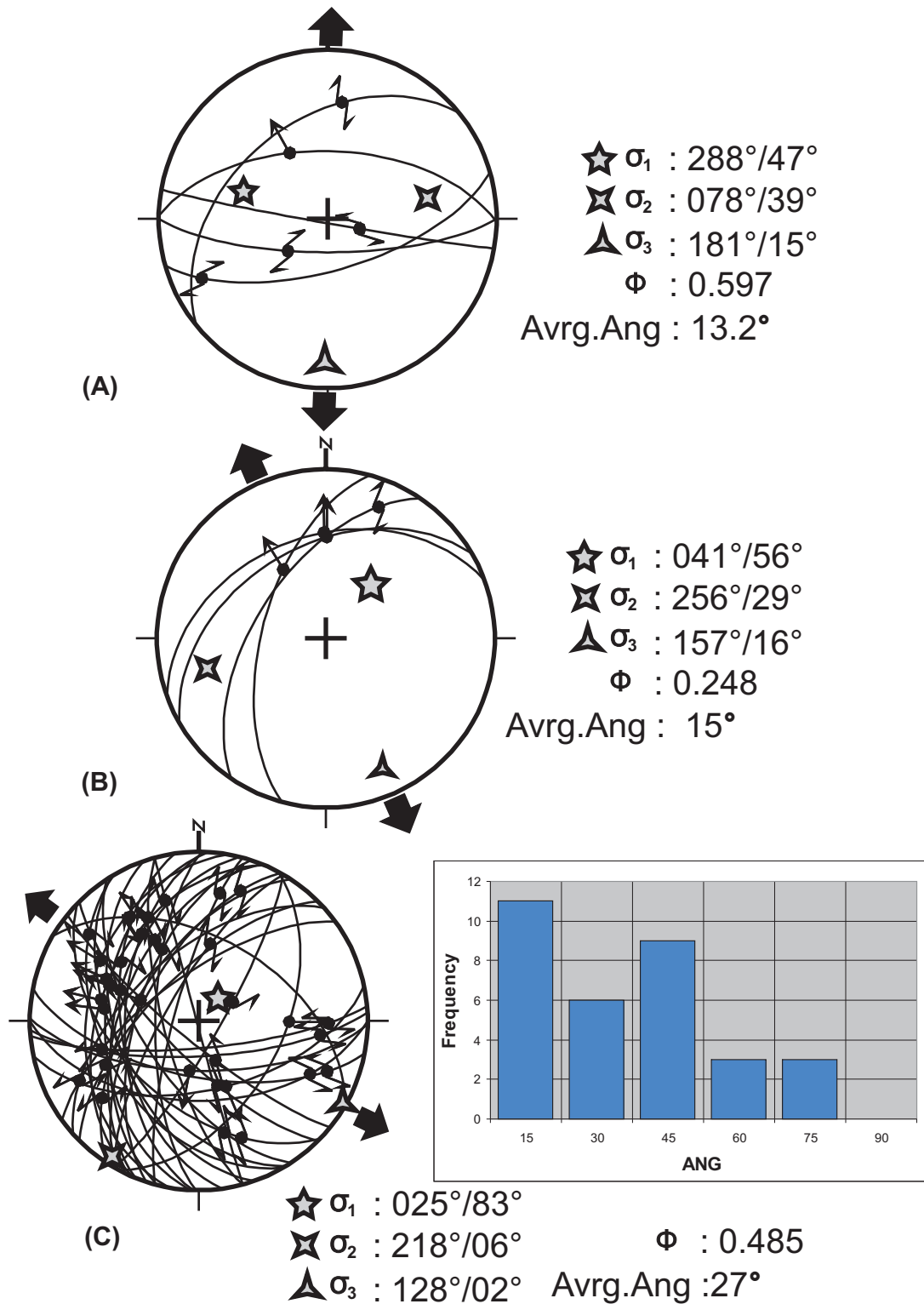


Figure 4.12. Fault-slip data and computed principle stress direction in the study area. (A) Data from sub-St-1 (see Figure 4.5 for location) indicate N–S-oriented extension. This data probably represent the stress regime associated with the main segments of the bounding faults; (B) Data from sub-St-2 (see Figure 4.5 for location) indicate NNW–SSE-oriented extension. Although the stress state here is close to regional N–S-oriented extension, it still exhibits some degree of deviation probably as an indication of local stress field perturbation; (C) Data from sub-St-3 (see Figure 4.5 for location) indicate NW–SE-oriented extension. Histogram illustrates the heterogenous nature of data having bimodal ANG distribution.

that we can draw from these sub-stations is that the regional direction of extension is probably prevails along the main segments away from the relay area.

At the Akçapınar relay ramp relatively extensive data acquisition was carried out at sub-St-3. However, solution of the inverse problem at the Akçapınar relay ramp is controversial as this zone is characterized by fault interaction. Pollard *et al.* (1993) has shown that slip direction along small faults near the end of larger faults invalidates the assumption 2, i.e. resolved shear stress on the fault plane is parallel to the slip vector. However, due to the asymmetric nature of the interaction, one fault may be consistent with the assumption 2 whereas the other fault may be less consistent (cf. Angelier, 1994). Depending on the orientation of the faults with respect to stress field, discrepancy may remain minor (cf. Angelier, 1994).

Leaving this discussion aside and solving the principal stresses for the sake of data, NE–SW-oriented extension was obtained at the Akçapınar relay ramp (Figure 4.12C). However, this solution clearly indicates a heterogeneous stress field that is not consistent with a single set of stress axes as suggested by obvious cross-cutting relation (Figures 4.10 and 4.11). The computed quality estimators also indicate a poor fit between the shear stress and slip for more than half of the faults with bimodal distribution (Figure 4.12C). Therefore, we utilize dynamic cluster analysis (Huang, 1988) to separate heterogeneous fault slip data into relatively homogenous subsets.

4.4.2. Cluster Analysis

Field observations revealed a distinct cross-cutting relationship between some of the E–W and N–S-oriented faults at the ramp area, suggesting that earlier stage of ~N–S-oriented extension was substituted by later stage of ~E–W-oriented extension (Figure 4.11). However, based purely on field observations, we were unable to classify the entire fault data in Figure 4.9B into two classes that represent earlier and later stages of extension at the ramp area. The main reason of this is the fact that most of the measured fault planes represent small-scale faults (smaller than the scale of mapping) of the relay area and therefore lacking to overlap all the times to portray the cross-cutting relationship. Therefore, we applied dynamic cluster analysis (c.f., Huang, 1988) in order to resolve the fault data of each phase out of the heterogeneous data, which represents the earlier and later phases of deformation at

the ramp area. Slip-inversion methodology is also utilized together with the cluster analysis.

Huang's (1988) methodology of cluster analysis is based on the minimization of the cumulative angular distance between σ_1 , σ_2 , σ_3 axes of potential subsets and P_0 , β and T_0 axes of individual fault planes, respectively (Huang and Angelier, 1987). A fault plane is assigned to a subset that producing minimum angular distance with the fault. It is an iterative process requiring computation of stress axes of each subset until the classification of faults are stabilized. At each iteration, stress axes were computed by using slip inversion methodology of Angelier (1975, 1990, 1994).

Application of the Huang's (1988) methodology of clustering to the data set at sub-St-3 lead to the recognition of two subsets. The fault slip data and stress tensors computed for the two subsets, named subset A and subset B are illustrated on 5.14. Subset A is characterized by NNW–SSE-oriented extension (Figure 4.13A), which is in close agreement with the regional direction of extension (Figures 3.24 and 4.8). Fault trends in the subset vary from E–W to NE–SW and NW–SE with dips both towards north and south. Faults carry both dip-slip and strike-slip components. The Φ value of 0.532 indicates simple unidirectional extension for the subset, i.e. the magnitude of σ_2 is closer to σ_1 rather than the σ_3 with well-defined direction of extension.

Subset B is characterized by WNW–ESE-directed extension (Figure 4.13B). As an average, faults of the subset strikes NNE–SSW with dips predominantly to the W. Dip-slip component dominates the fault movements with very high Φ value of 0.804. This suggests that σ_1 and σ_2 axes are rather poorly defined whereas σ_3 axis is very well defined. The strong component of extension parallel to the bounding faults of the Akçapınar relay ramp is unconcealed evidence that the breaching phase and fault-parallel extension has already begun at the ramp area. In fact, subset B represents a local stress field anomaly compared to the other subsets and the regional state of stress (Figures 3.24 and 4.7).

It is important to evaluate whether the heterogeneous stress field defined by the two subsets at the ramp area is real and based on natural causes or they are only artefacts produced by fault interaction and invalidation of the basic assumptions that the applied stress analysis relied on. As a matter of fact, computed subsets are conformable with the observed field relation suggesting that earlier ~E–W-oriented

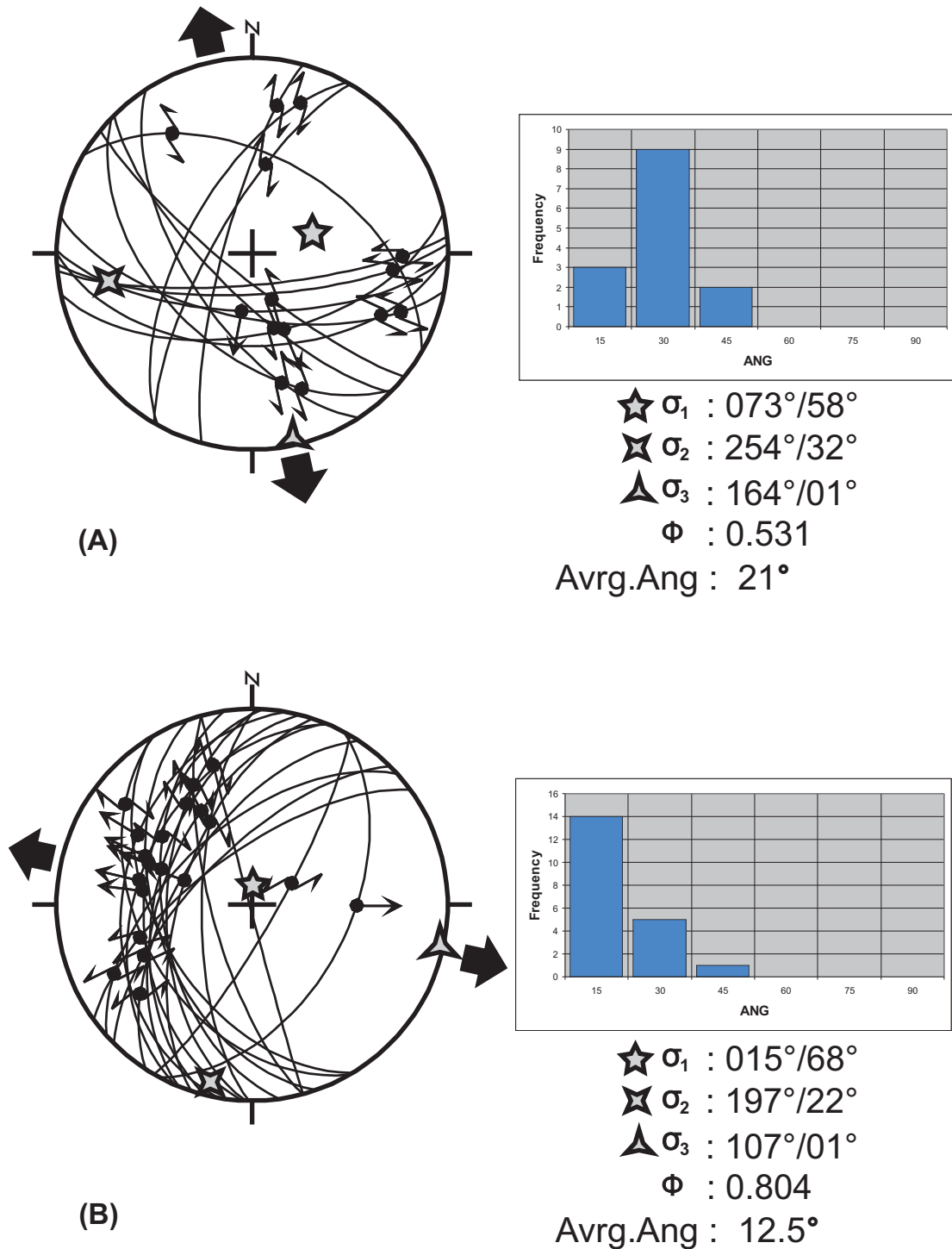


Figure 4.13. Fault-slip data and principal stress directions for the two subsets differentiated by applying cluster analysis to the heterogenous fault data at the Akçapınar relay ramp. Distribution of ANG values are improved significantly in each subset compared to that of Figure 4.12C. **(A)** Subset A representing early phase of deformation (N= 14); **(B)** Subset B representing later phase of deformation (N= 20). Histograms illustrates the ANG value as a measure of fit of the inverted solution to the actual slip data.

faults are cut by later ~N–S-oriented faults (Figure 4.11). Based on this basic observation, it can be argued that the applied cluster analysis, which clearly separates subset A from subset B, represents an actual change of the stress field. This brings up a time sequence in which subset A dominated by approximately E–W-oriented faults are older than the subsets B that is dominated by N–S-oriented breaching faults. Therefore, the stress field at the ramp area has evidently rotated from almost N–S-directed extension, confirming to regional stress field to anomalous almost E–W-directed current extension through time.

It is likely that the rotation of the stress field at the ramp area could be related to the ramp evolution in which the subset A is probably representing the earlier stages (Figure 4.2A). At these stages, lack of significant interaction among the main fault segments may result in ~N–S-oriented field of extension, which is in confirmation with the regional direction of extension. However, it needs to be emphasized that the computed principal stress axes and inferred direction of extension for the subset A structures probably do not represent the original style of deformation but a slightly modified version because of the rotation during the ductile evolution stages of the relay ramp (Figure 4.11). As interaction among the segments grows, strain accumulated at the ramp area and lead to the initiation of fracturing and faulting under an extensional setting that is parallel to the bounding faults of the relay ramp (Figure 4.2C, D). Representing this fault-parallel extension, the anomalous almost ~E–W-oriented extension of subset B, which is superimposed on subset A, probably indicates that the breaching phase has already initiated at the ramp area (Figure 4.11). However, lack of a single, well-defined breaching structure that connects the overlapping main segments suggests that the breaching is currently an ongoing process at the ramp area.

4.5. Discussion

Southern margin boundary structures of the graben floor constitute a major fault zone parallel to the trend of Gediz Graben. In a strike-wise direction, this zone does not comprise a single and continuous structure but is composed of discrete fault segments among which displacement transfer mechanisms operate. Akçapınar relay ramp is a typical example of these zones formed between two overstepping fault segments dipping in the same direction.

Various small-scale faults are observable in the Akçapınar relay ramp. However, there is no indication of a single fault that cuts through the entire ramp area and joining the overlapping segments. Therefore, this configuration of the Akçapınar relay ramp probably exemplifies the transition stage from predominantly ductile deformation to brittle deformation of the breaching process (between stages III and IV in Figure 4.2). At this level, progressive fracturing and faulting that has already initiated in the ramp area will advance with time to form a single, irregular fault by connecting the two-isolated segment. Laterally more extensive faults such as the main graben-bounding fault in Figure 2.3, have probably go through these stages during its evolution to form a single fault. Yet, the evidence of these processes can be observed on the resulting fault surface and the fill of the graben (Chapter 5).

The Akçapınar relay ramp is a site of local stress field anomaly characterized by E–W-oriented fault-parallel extension. Although the relay bounding main faults confirms the N–S-oriented regional direction of extension out of the relay zone, an anomalous almost E–W-directed extension arises at the Akçapınar relay ramp. The similar variation of the stress field is also observed in a temporal context at the ramp area. Earlier phase of deformation confirming the regional N–S-oriented extension is superimposed by E–W-oriented anomalous phase of extension portrayed by subsets A and B, respectively. As relay ramp evolution is considered (Figure 4.2), it is probable that the subset A exemplifies an earlier stage in ramp evolution (between stages I and II in Figure 4.2) in which fault interaction is either limited or absent and the stress field confirms the regional. Subset B, on the other hand, exemplifies more advanced stages in the ramp evolution (between stages III and IV in Figure 4.2). At this stage breaching of the relay ramp probably initiates by approximately N–S-oriented normal slip faults and local stress field anomaly caused by the interaction among the fault segments is relieved in the form of extension almost transverse to the regional extension direction. Therefore, progressive evolution of stress field anomaly at the ramp area probably follows the ramp evolution stages as suggested by Peacock and Sanderson (1991, 1994).

The observed field relations in the study area clearly show that the stress field at the relay ramp displays temporal and spatial variations. The resulting deformation accommodates differential displacements, which is the manifestation of both local and regional strain.

CHAPTER 5

INTERPRETATION OF THE SUBSURFACE DATA AND SURFACE TO SUBSURFACE CORRELATION

Southern margin of the Gediz Graben provides excellent opportunity to investigate the nature of graben-fill deposits as well as the characteristics of the deformation concentrated along the graben-bounding structures. However, as this margin is the most active site of deformation, it is prone to local variations of geological phenomenon more than anywhere else in the graben. This brings along the risk of ascribing some local features to be the general characteristics of the graben unless the basin margin observations are extended towards the rest of the basin. Subsurface data provide unique opportunity to accomplish this correlation.

Approximately 270 km 2-D seismic reflection data and data from three boreholes were utilized together with a surface geological map and digital elevation model of the region in order to establish a correlation between the surface and subsurface (Figure 5.1). The correlation effort has required several stages. As an initial step, 2-D seismic sections were interpreted in the time domain. Then, the sections and the interpretations were converted from the time domain to the depth domain. Well data are utilized to tie the seismic lines with the actual geology and to check the validity of the time to depth conversion. Finally, geological cross-sections starting from the southern horst block, cutting across the entire graben floor and extending to the northern horst block were constructed. This is achieved by using the surface data across the exposed horst blocks and by benefiting from the interpretation of seismic data for the buried graben block. These cross-sections portray the entire geometry and deformation characteristics of the graben in a spatially more continuous manner.

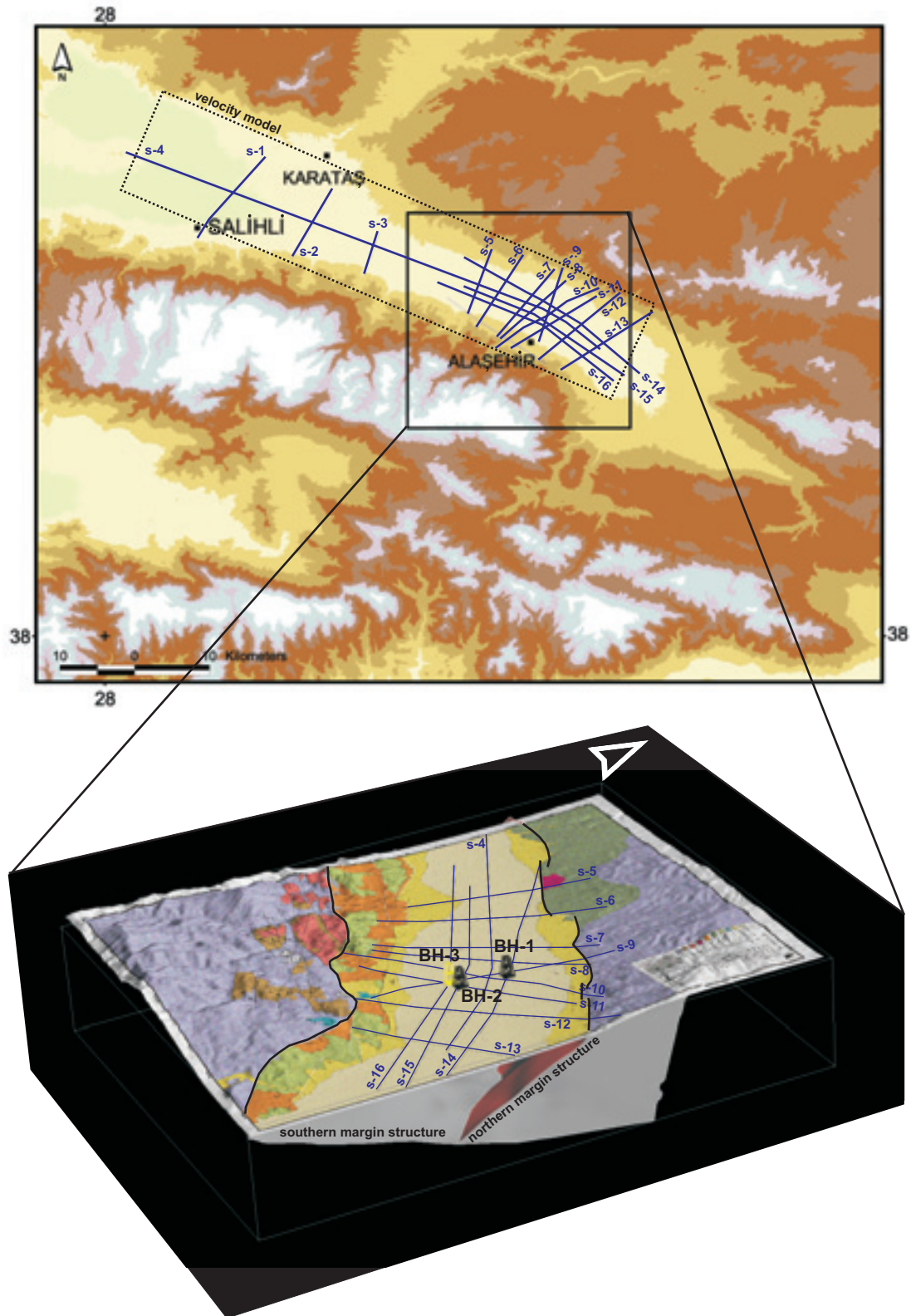


Figure 5.1. Surface to subsurface correlation was carried out using 2-D seismic sections, three boreholes (BH-1, BH-2 and BH-3), a surface geological map and digital elevation model (DEM) of the region. Derrick symbol depicts the location of boreholes and blue lines illustrates the available 2-D seismic sections. The geological map draped onto the DEM is given in Figure 2.3. For time to depth conversion of seismic sections, a velocity model was constructed within the area shown by dotted rectangle in the inset map.

5.1. Time to Depth Conversion of the Seismic Data

Time domain seismic imaging is the most common and most efficient processing method applied to seismic data (e.g., Yilmaz, 2001). Although the subsurface geology exists in depth, traditional processing portrays this geology in two-way travel time (TWT) that represent the time passed for a signal to travel from surface to geological reflectors and back to the surface again. Working in the time domain usually does not cause any problem for stratigraphic applications, such as seismic facies and sequence stratigraphic analysis, as their interpretations are predominantly independent of the changing structure. However, structural interpretations in the time domain have some pitfalls. The main concern arises due to the fact that you are dealing with different vertical and horizontal scales when looking at the time-domain seismic sections. Therefore, the observed angles, such as dip of the strata or fault plane, are incorrect. This is a major problem, for example, in the application of contractional and extensional fault-related folding models to seismic data (e.g., Suppe, 1983; Suppe and Medwedeff, 1990; Xiao and Suppe, 1992). Furthermore, false structures can be generated or real structures can be obscured due to lateral variation of the velocity even in the case of very simple geology.

Another limitation of time sections arises when interpretations and seismically derived rock properties are intended to be integrated with geological and engineering data, which are always in the depth domain. Thus, time to depth conversion of seismic data become a critical issue in attempts to integrate the data obtained from multiple sources. In this study, for example, the effort is to integrate seismic data in the time domain with the surface geological data in elevation (height above sea level) to portray the entire geometry of the Gediz basin from horst to graben block (Figure 5.1).

Depth conversion methods can broadly be separated into two categories as *direct time-depth conversion* and *velocity modeling for depth conversion* (Etris *et al.*, 2001). Direct time to depth conversion is simple approach to convert a time horizon directly into depth by a applying a fixed translation equation or a spatially oriented function. On the other hand, velocity modeling initially intends to predict the velocity structure of the subsurface by using velocity values from different sources (e.g., stacking velocities, sonic logs, check-shot surveys, etc.). After a reliable velocity model is established, time to depth conversion can be carried out.

This study employs the second approach by building the velocity model of the Gediz Graben, based on available velocity data (Figure 5.1). There are two types of velocities utilized in this effort: (1) The true vertical propagation velocities obtained from check-shot survey in BH-1 (Figure 5.1); and (2) the imaging velocities or pro-velocities obtained from the seismic processing and utilized during the stacking (Al-Challabi, 1994). Check-shot survey simply measures the travel times of a signal from surface to various depths in a borehole. This allows computation of accurate velocities in each stratigraphic units encountered in the borehole. Stacking velocities, on the other hand, is the parameter that produces optimum alignment of the primary reflection on the traces of the CMP gather (Yılmaz, 2001). It is tentatively related to the actual velocity in the ground (Al-Chalabi, 1994).

5.1.1. The Velocity Model

The velocity-modeling module of the GOCAD is utilized for the velocity modeling implementation. GOCAD (Geological Object Computer Aided Design) is integrated and geologically oriented CAD software to construct a wide-range of earth models, for application in geology, geophysics and reservoir engineering. A 3-D grid composed of 3,369,600 grid cells (234 x 48 x 300) was constructed in time domain as an initial step to velocity modeling. The grid covers the area illustrated in Figure 5.1 and extends from -300 msec to 3000 msec. By interpreting the seismic lines, the metamorphic basement was differentiated from the graben fill, and the 3-D grid was separated into two volumes representing the basement metamorphic rocks (the basement volume) and the sedimentary fill of the graben (the graben fill volume) (Figure 5.2). A constant velocity of 5000 m/sec was assigned to each grid cell in the basement volume for two reasons: (1) The available data can not constraint the velocity field of the basement volume accurately; (2) The velocity field of the basement volume doesn't influence the depth conversion of the graben fill volume which is the main focus of this study. The velocity-modeling effort is therefore concentrated onto the graben fill volume.

The most reliable velocity data for the graben fill volume comes from BH-1 in which a check-shot survey was conducted through the sedimentary fill of the Gediz Graben. Plotting of check-shot derived interval velocities (V_{int}) versus two-way-travel-time (TWT) from check shot survey suggest that an approximate linear relationship can be established between these two parameters (Figure 5.3A).

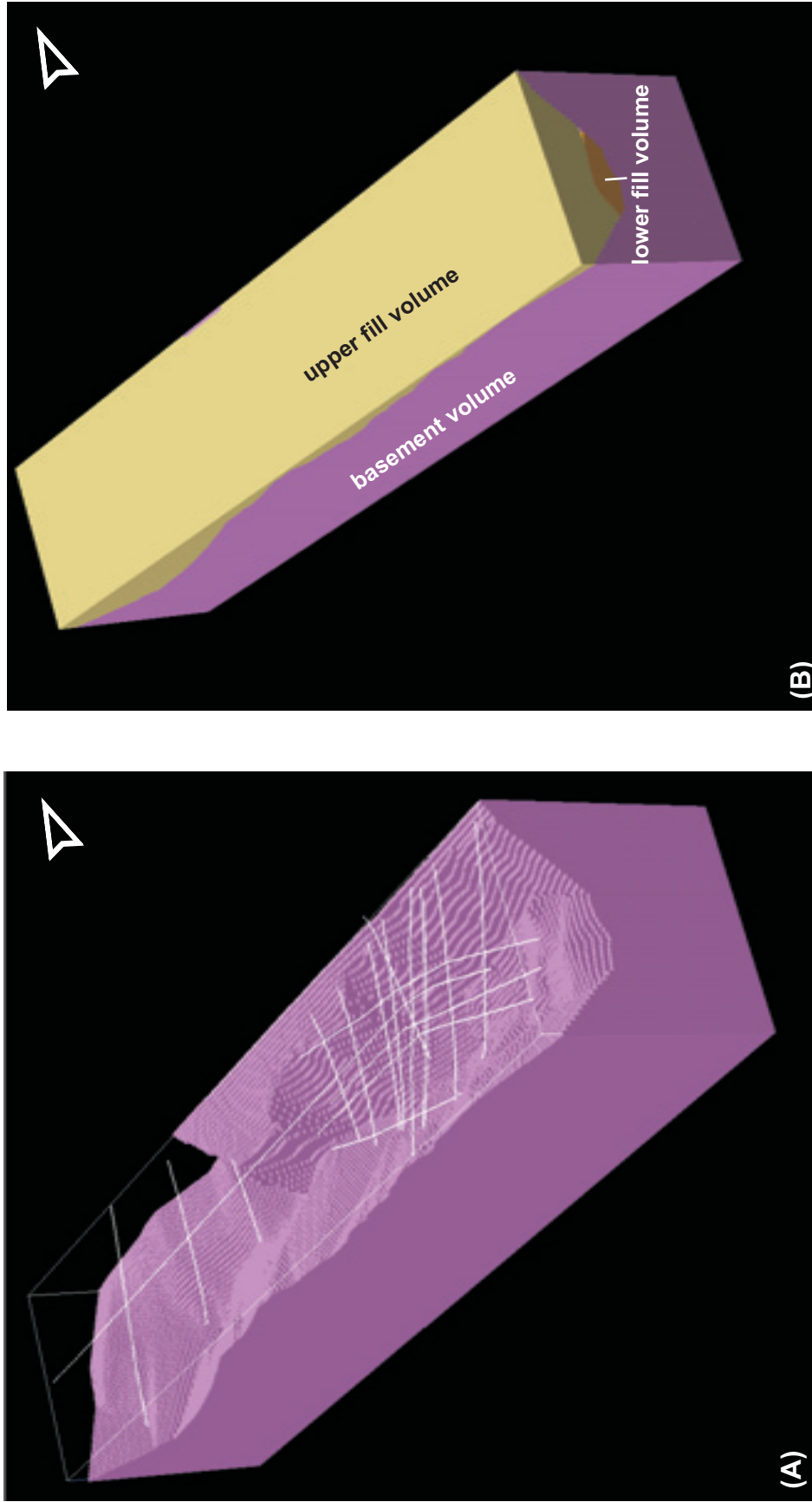
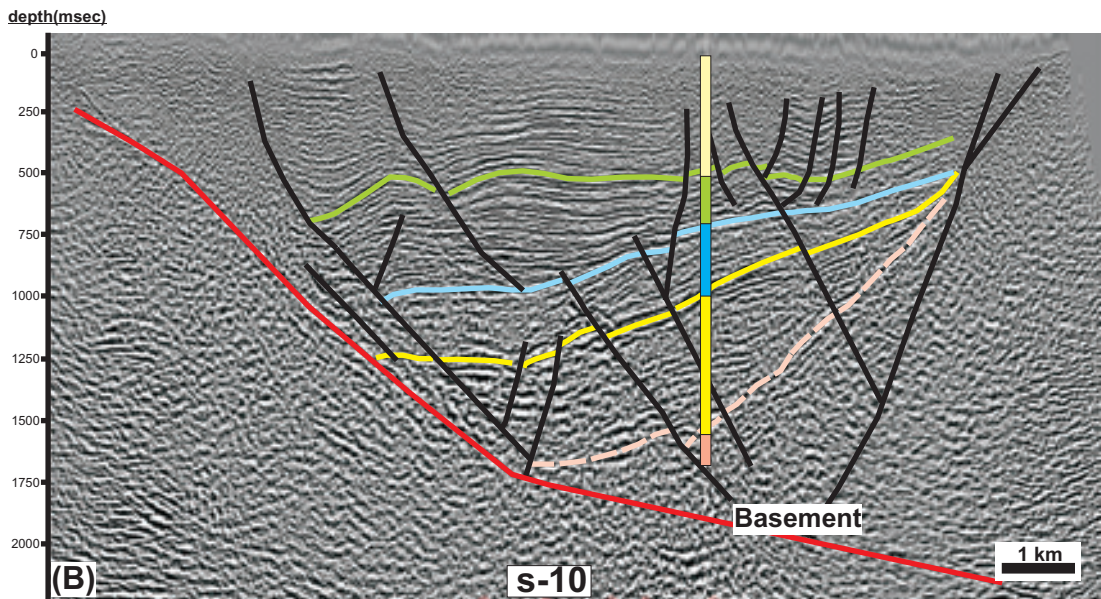
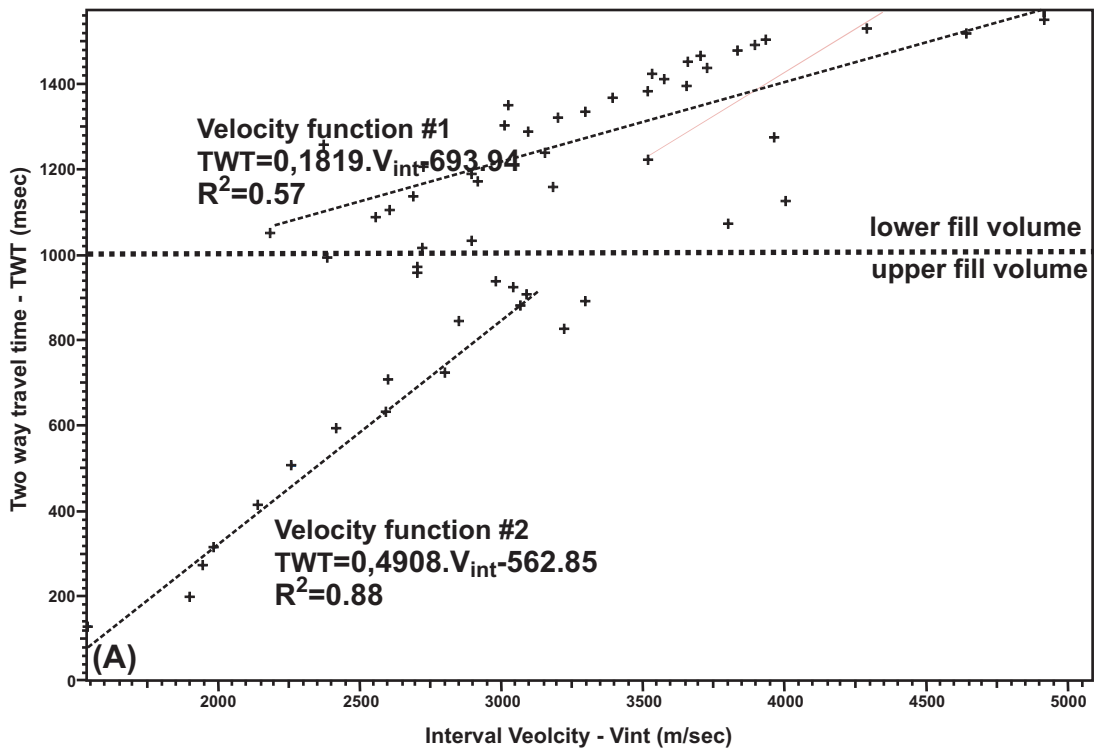


Figure 5.2. The 3-D base grid of the intended velocity model. (A) illustrates the basement volume in which a constant velocity value is assigned to each grid cell. White lines represent the available seismic lines. (B) depicts the graben fill volume, including upper and lower fill volumes above the basement volume. The lower fill volume is populated by velocity function #1 and the upper fill volume is populated by velocity function #2 (Figure 5.3).



- | | |
|------------------------------------------------------------------------------------------------------------------------------------------------------------------------------------------|---------------------------------------------------------------------------------------------------------------------------------------------------------------------|
| Quaternary alluvium and Kaletep formation | Çaltılık formation |
| Gediz formation | Alaşehir formation |
| | Metamorphic basement |

Figure 5.3. (A) Interval velocity (V_{int}) versus two way travel time (TWT) plot of BH-1. Notice the sharp change in the trend of data which is observable at 1000 msec. Two separate functions, velocity function #1 and velocity function #2, are defined for below and above 1000 msec. (B) The change of data trend at 1000 msec in (A) reasonably corresponds to Alaşehir formation and Çaltılık formation contact.

However, a sharp change in V_{int} - TWT relation can easily be identified at 1000 msec depth, which reasonably corresponds to the contact between the Alaşehir and Çaltılık formations (Figure 5.3B). Therefore, two separate linear velocity functions can be established to represent velocity structure of the Neogene to Quaternary fill of the Gediz graben (Figure 5.3A). While the first function (velocity function #1) can define a relation for the Alaşehir formation, the second function can be applied to the rest of the graben fill from Çaltılık formation to Quaternary alluvium (Figure 5.3). Accordingly, the graben fill volume was separated into two sub-volumes as lower fill and upper fill, which were populated with velocity values based on the velocity function #1 and velocity function #2, respectively (Figure 5.3A). Consequently, an initial velocity model composed of three main domains including the basement volume, the lower fill volume and the upper fill volume, were constructed.

Although their estimations are influenced by many factors, stacking velocities constitute a significant data set of velocity available for the Gediz Graben (Figure 5.4A). As a result, they are also incorporated within the velocity model by means of pseudo-wells designed at corresponding points in the seismic sections (Figure 5.4B). Then, the associated velocities of the wells were superimposed onto the background velocity model based on the linear velocity functions (Figure 5.3A). The resulting grid was interpolated and the velocity modeling was finalized (Figure 5.5).

Although accurate depthing requires true vertical propagation velocities (e.g. check shot surveys) obtained from wells, stacking velocities were also utilized in this case due to limited amount of well derived velocity data. Remember that check-shot survey is available for only one well in the graben and utilized for estimation of the background velocity for the model. Consequently, the obtained velocity model may not be perfect due to uncertainties inherited from the stacking velocities. On the other hand, the constructed model is still useful and within the range of acceptable accuracy for depth conversion onto which structural methods can be applied (Personal communication; John Shaw, Chris Guzovski)

5.1.2. Time to Depth Conversion

Velocity modeling is an important step to the depth conversion. The modeling effort not only allows visual examination of the velocity structure for reasonableness but also enables to make use of velocity information from both seismic and well data. When the velocity model comprising velocity values for all the grid points of the

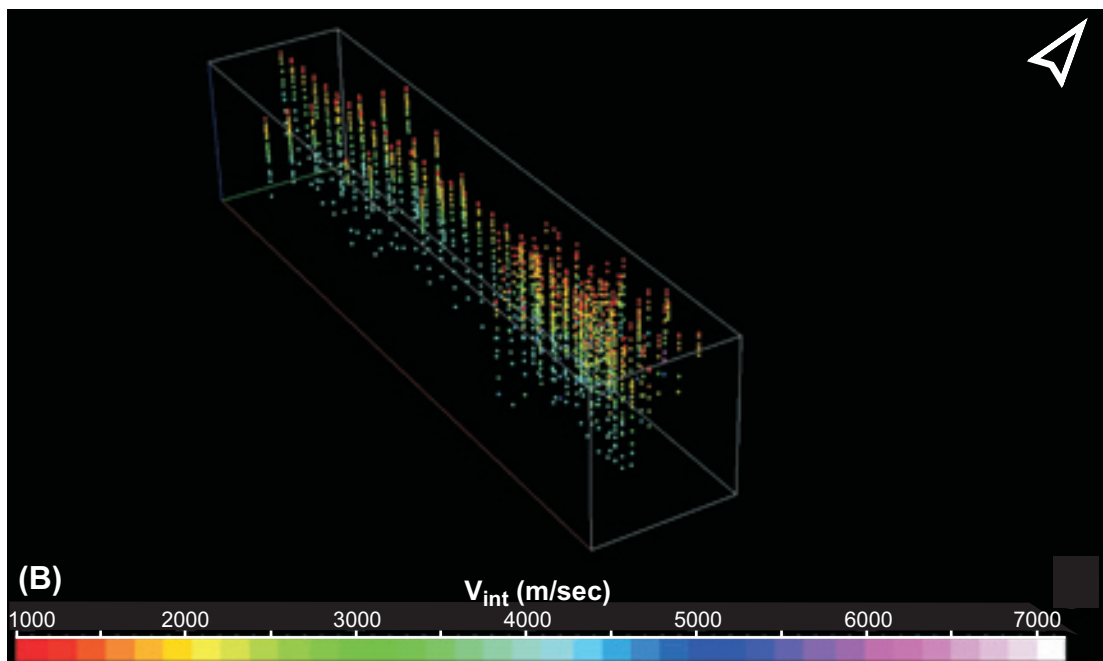
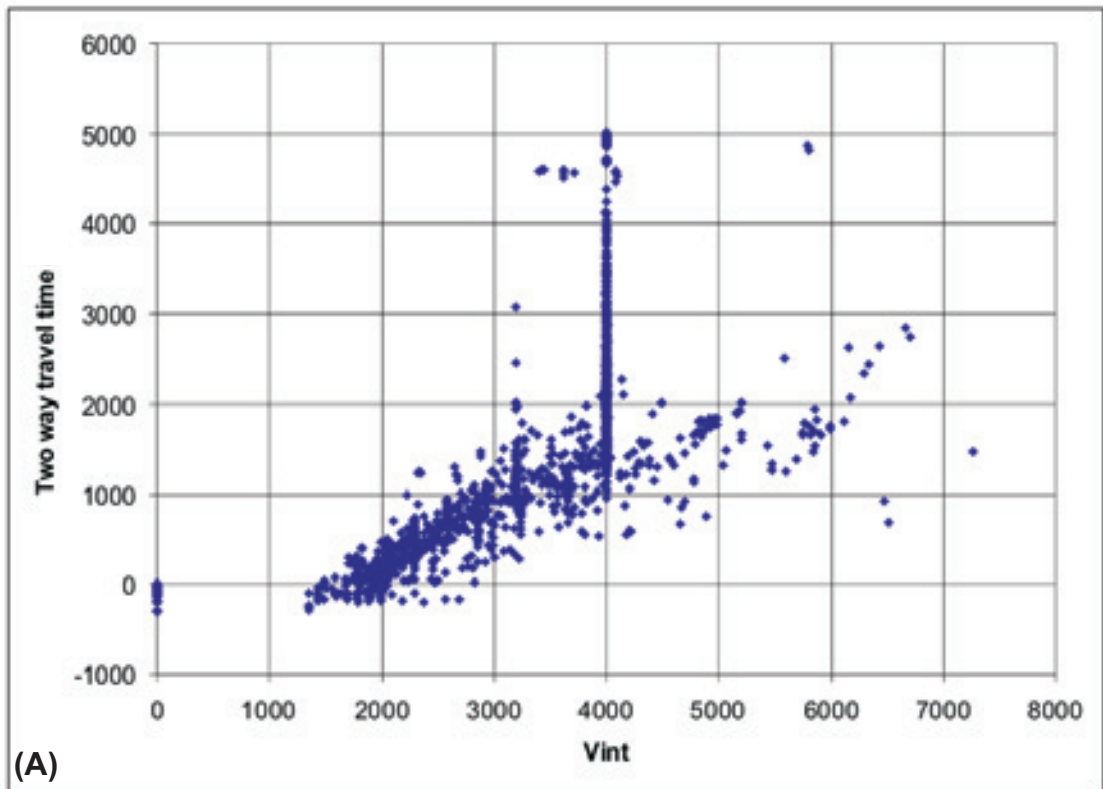


Figure 5.4. (A) The graph showing interval velocities obtained from the stacking velocities versus two way travel time. Compared to Figure 5.3A, it is more difficult to define a simple relation between V_{int} and TWT. (B) V_{int} values falling within the basement volume was removed from the data set and the rest of the data was introduced to the model in the form of pseudo-wells.

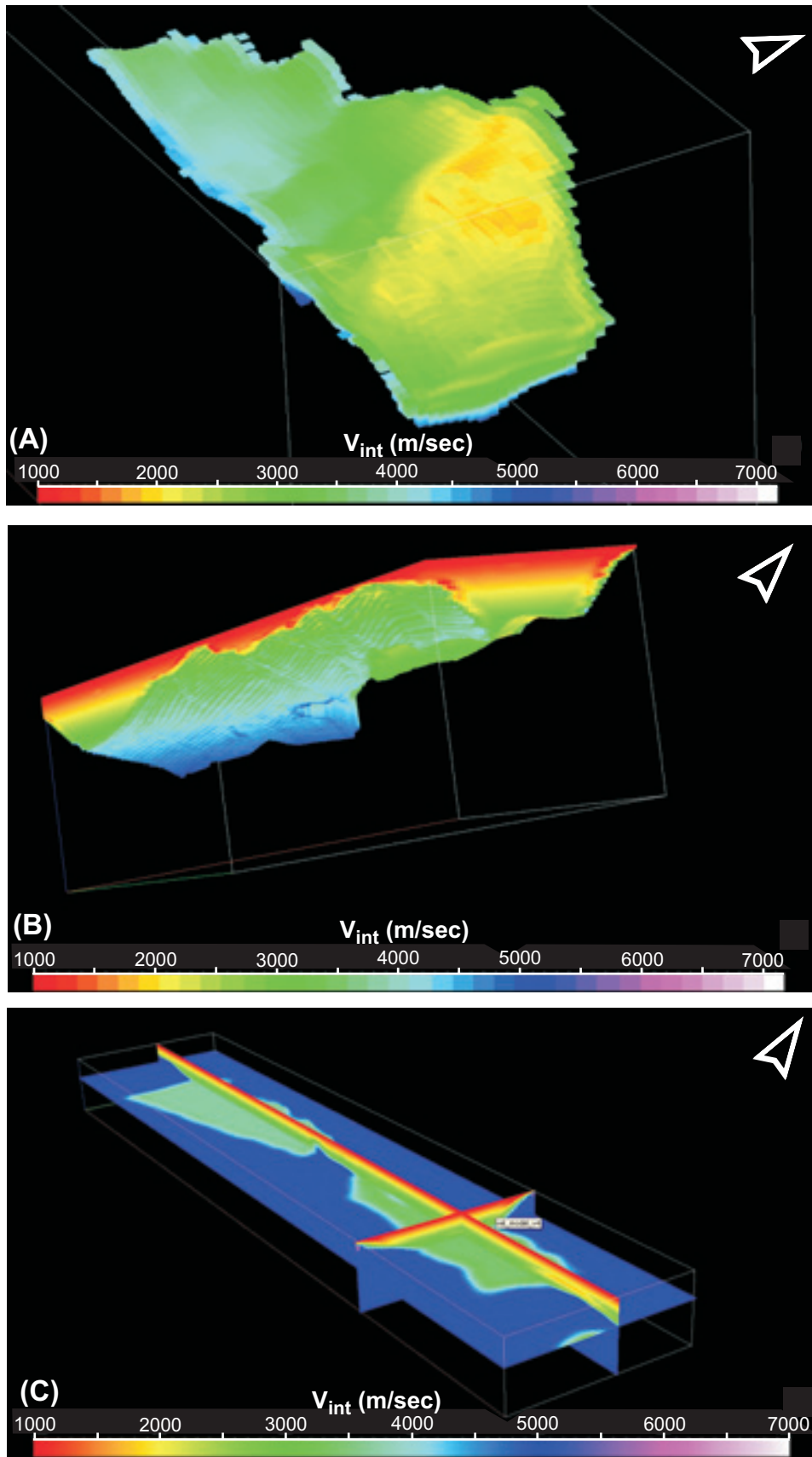


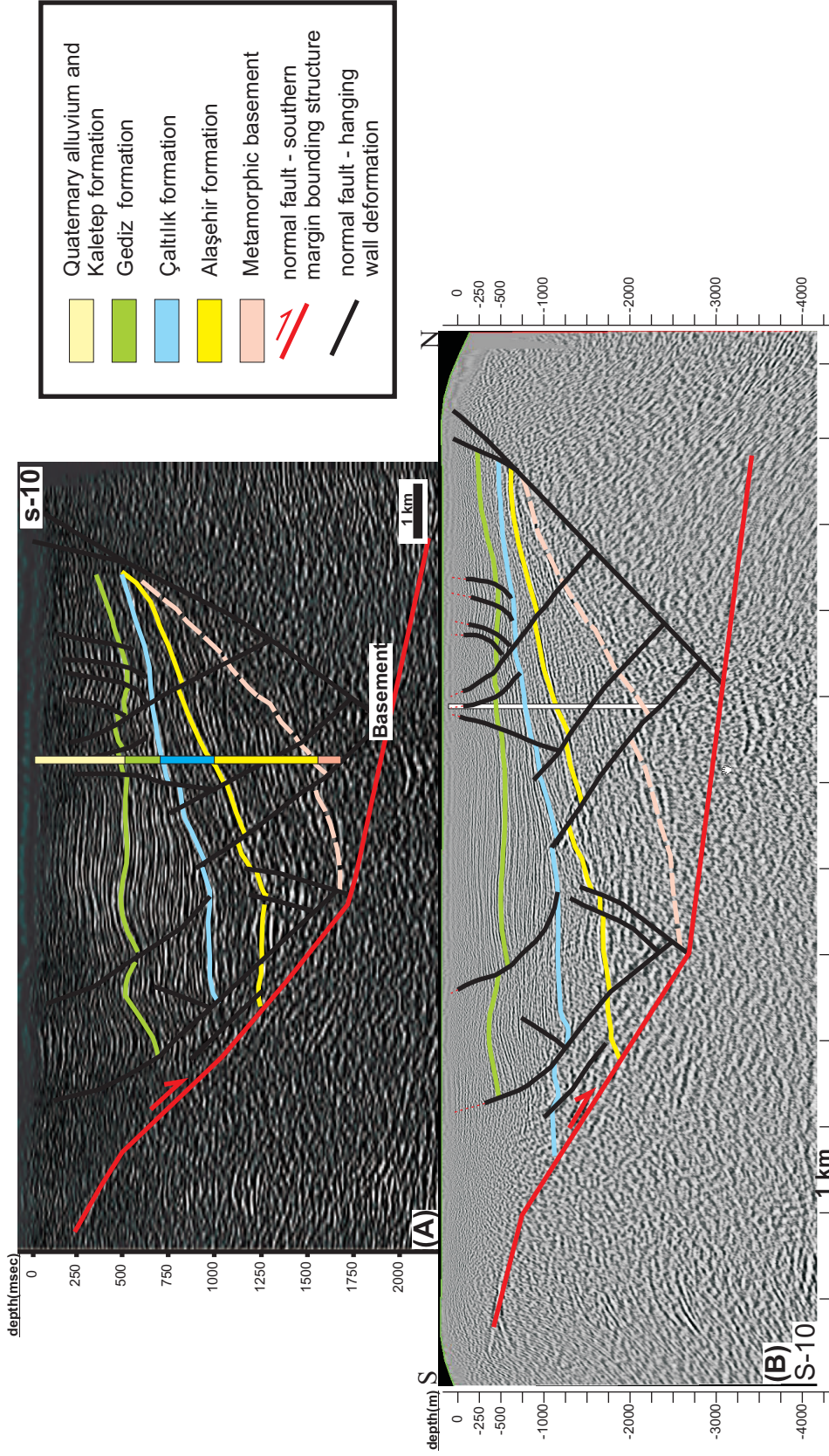
Figure 5.5. Final velocity model based on check-shot and stacking velocities. **(A)** The velocity structure of the lower fill volume. **(B)** The velocity structure of the upper fill volume. **(C)** 2-D sections and time slice from the entire velocity model. Note the constant velocity of the basement.

intended resolution is constructed, depth to time conversion can quickly be carried out. Workstation softwares and all the related algorithms in the industry employ Dix formulation almost unexceptionally (Dix, 1955). Indeed, same formulation is used by GOCAD for the depth conversion.

The first step in the depth conversion is to extract the velocity values corresponding to surface of interest from the 3-D model. This surface could be a fault plane, a stratigraphic horizon or a seismic section that is intended to be depth converted. When the extraction process is completed, time to depth conversion module of the software automatically performs the depth conversion based on Dix equation (Dix, 1955). In this way, all the interpretations, including stratigraphic surfaces and fault planes were converted to depth domain as well as the seismic sections. This constructed geometrically more accurate image of the graben and provided with foundation for improved surface to subsurface correlation (Figure 5.6). The reliability and the consistency of the conversions were checked by means of the available boreholes for the match of interpreted seismic stratigraphic horizons and well picks. Based on this correlation, it is concluded that a satisfactory depth conversion was achieved within the acceptable accuracy range for the purpose of this study.

5.2. Fault Pattern From Seismic Data

Faults can be identified on seismic sections based on several criteria. Fault cutoffs, which are the abrupt termination of reflectors or changes of reflection attributes (e.g., amplitude, polarity) at fault surfaces, are the most common evidence for the existence of a fault surface (Figure 5.7A). In some cases, reflection signals can be acquired directly from a fault plane given that there is sufficient velocity and density change across the fault plane and the dip of the fault plane is shallow enough to acquire the reflection signals with the employed receiver spread of the survey (Figure 5.7B). Once the fault planes are identified on individual 2-D sections, correlation between the adjacent sections can be carried out to construct the 3-D geometry of the fault planes. The accuracy of the constructed fault models is directly related with the intensity of the seismic grid. As the adjacent seismic sections get closer to each other, smaller faults can be correlated. Consequently, more detailed fault models can be built.



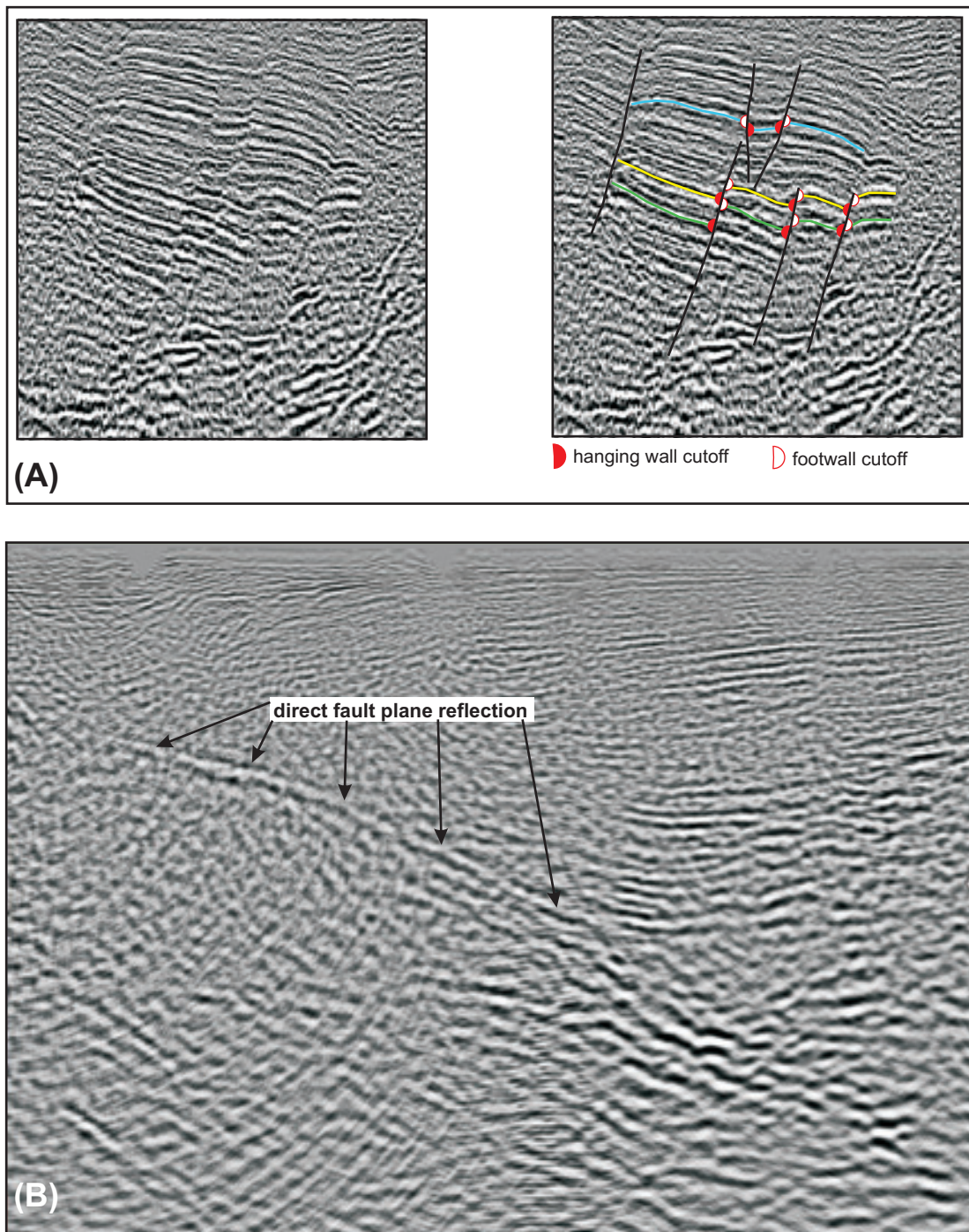


Figure 5.7. Identification of faults in seismic sections. **(A)** Faults can be identified predominantly based on truncation and offset of seismic reflectors along planar features. Hanging-wall and footwall cutoffs mark the position of the fault plane. **(B)** In some cases direct reflections can be acquired from fault planes given that there is a difference in acoustic parameters across the fault plane and fault plane has suitable dip for the acquisition of reflection signals.

In contrast to outcrop data, seismic data have resolution issues. Even faults of centimeter scale can be studied properly in outcrops; offsets of tens of meters are commonly required for a fault to be identified in a 2-D seismic section. This problem further deteriorates with depth. Although, 3-D seismic surveys offer significant improvement of resolution over conventional 2-D data, they are usually not available for initial geological analysis as their acquisition usually follows discoveries of the oil fields. High resolution 2-D seismic, on the other hand, brings along some improvement on this problem but it suffers from reduced depth of penetration compared to conventional 2-D seismic.

Available 2-D seismic data set in the Gediz Graben has unique significance beyond its above-mentioned limitations. This data set is the only data with potential of portraying subsurface geology in the grabens of western Anatolia. Although the data quality and spacing of seismic grid are not very favorable, they serve well to construct the general geometry of the graben and graben bounding structures. They also aid to delineate the nature of hanging-wall deformation and to evaluate the thickness distribution of discrete sedimentary packages sum of which forms the entire graben fill. Geological analyses were also benefited from the surface to subsurface correlation following to depth conversion of the seismic data. This effort allowed accurate matching of the surface observations with the subsurface. In this way, deformation pattern observed along the graben margins were compared with the entire basin to assess whether this pattern is spatially consistent or represent only basin margin configuration. Furthermore, lateral distribution and thickness variation of the exposed sedimentary units were examined across the buried graben block. All these efforts improved the understanding of the spatial variation of geological phenomenon in the Gediz graben.

5.2.1. Graben Bounding Structures

The Gediz Graben is bounded by two major structures possessing characteristics of normal faults. Both of these structures are observable and traceable on the surface exposures (see Chapter 3). Seismic expression of these structures is also strong and allows subsurface correlation between the seismic sections along the entire graben basin. The geometry of these structures are controlled by the evolutionary path of the Gediz graben and exerts strong control onto the distribution of sedimentary unit and the style of hanging-wall deformation.

The Southern Margin-Bounding Structure

The southern margin-bounding structure of the Gediz Graben can clearly be identified on the seismic sections (Figure 5.8). Juxtaposing the metamorphic basement with sedimentary fill of the graben, this structure marks an interface for obvious change in acoustic parameters of the rock units (i.e. the velocity and density) and provides direct fault plane reflections through the graben fill (Figure 5.8). Thus, the southern margin of the graben can be constrained relatively easily. However, if the structure is traced towards the deeper parts of the graben, the fault plane reflection demises. The reason for that is probably the reduced difference of the acoustic parameters between the footwall and the hanging-wall below the graben fill where the fault plane juxtaposes metamorphic rocks both in the hanging-wall and in the footwall. However, the geometry of the rollover that formed within the hanging-wall allows estimation of the downward continuation of the fault plane (Figure 5.9).

Hanging-wall collapse above a listric normal fault results in formation of rollovers or folding within the hanging-wall strata (Figure 5.9) (Xiao and Suppe, 1992). If the hanging-wall is a rigid body free of internal deformation, a void would inevitably form between the hanging-wall and footwall in response to slip on the fault plane (Figure 5.9A). In reality, a hanging-wall cannot be that strong and collapses due to gravity to fill the void (Figure 5.9B). There are vertical and inclined collapse models to explain this process (Gibbs, 1983; Jackson and Galloway, 1984; White *et al.*, 1986). However, the latter researches abandoned the vertical collapse and favor the inclined collapse model in which collapse takes place in the direction of antithetic normal faulting (White *et al.*, 1986; Xiao and Suppe, 1988, 1992; Dula, 1991). Since the collapse is in the Coulomb shear direction dipping $65 - 70^\circ$, it is called as Coulomb collapse (Xiao and Suppe, 1988, 1989 and 1992). The theory of Xiao and Suppe (1992) illustrates that active fold hinges or active axial surfaces of the hanging-wall structure are pinned to fault bends at depth and extend upward from pre-growth (prerift) to growth (synrift) strata (Figure 5.9B). With accumulating slip on the fault plane, the hanging-wall strata passes through the active axial surface, deforms and becomes incorporated into the kink bend or roll-over panel (Figure 5.9B). The inactive axial surface marks the other margin of the rollover panel and separates the strata that passed from the fault bend and that never did (Figure 5.9B). The width of rollover panel is therefore related to the total slip on the fault plane. As

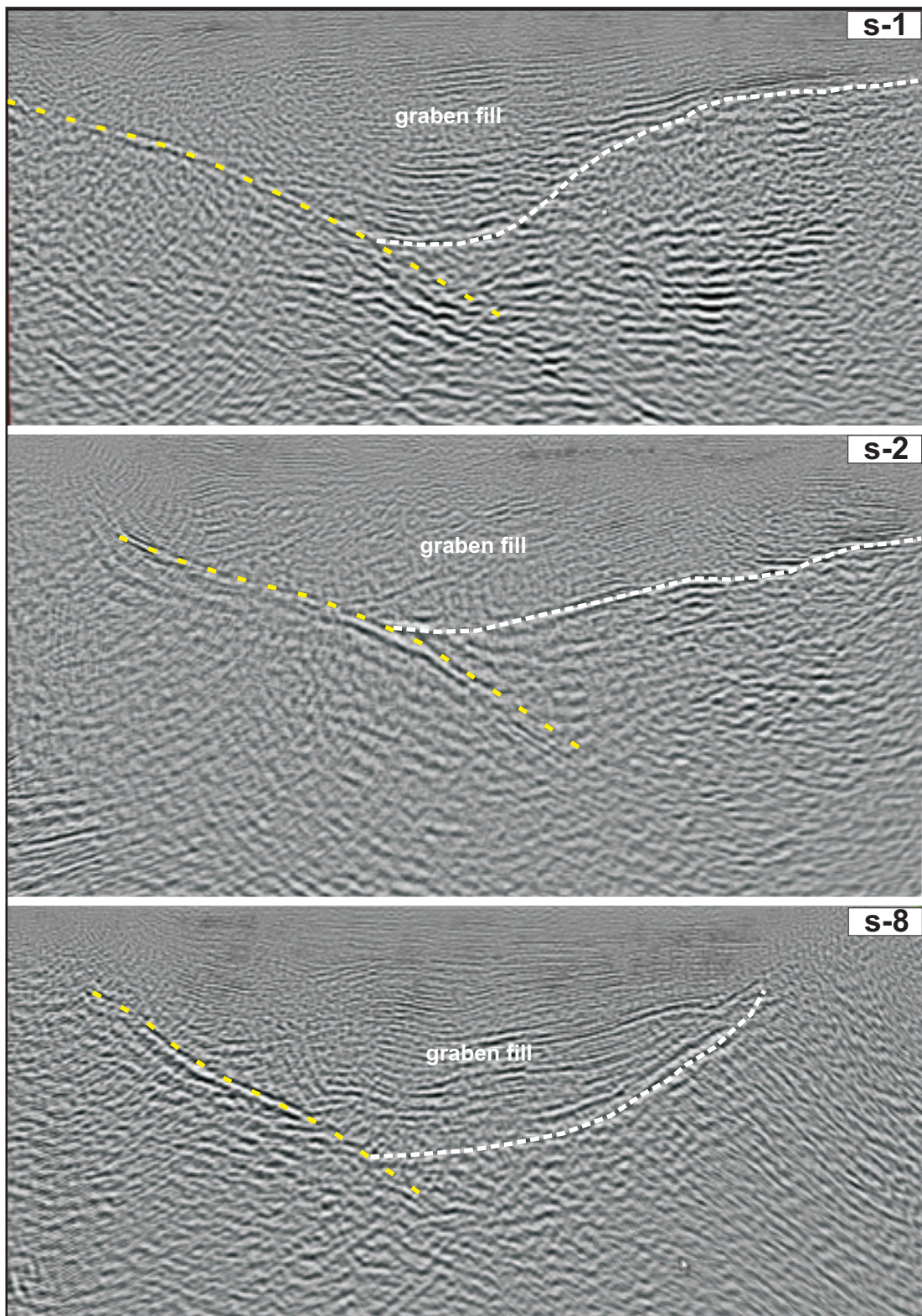


Figure 5.8. Direct fault plane reflections acquired from southern margin structure of the Gediz Graben. Note that fault plane reflection demises down-dip the fault plane below the graben fill where fault plane juxtaposes metamorphic rocks both in the hangingwall and in the footwall. Dashed white line marks the interpreted boundary between metamorphic basement and the graben fill. See Figure 5.1 for the location of the seismic lines.

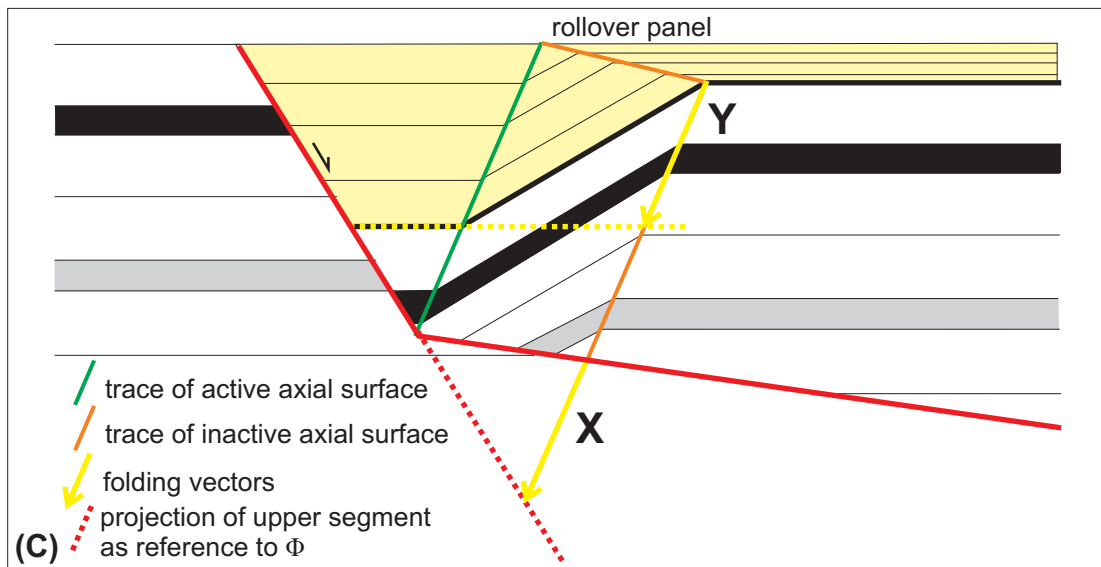
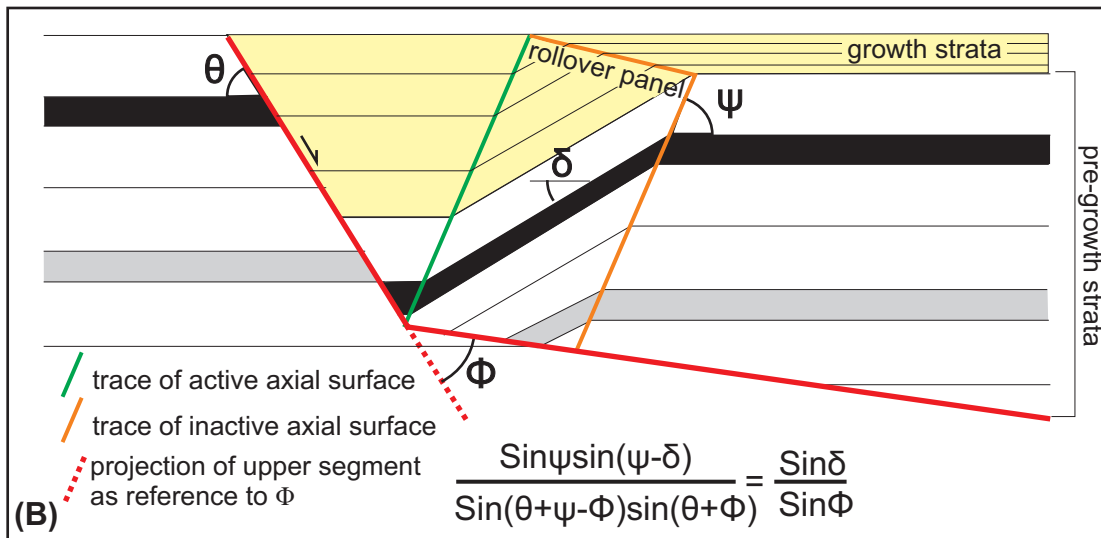
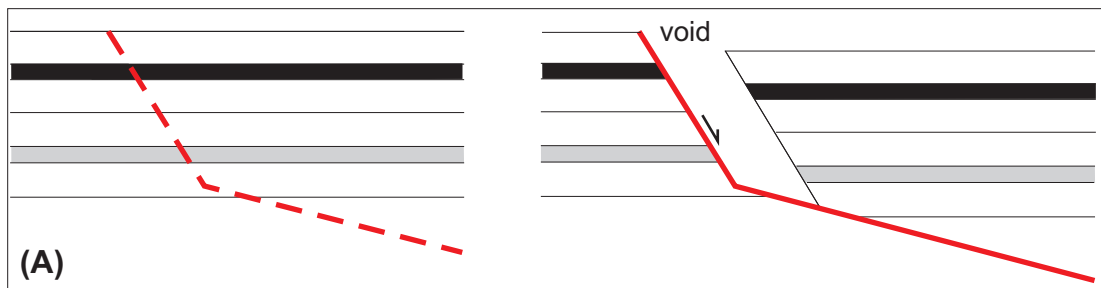


Figure 5.9. Extensional fault-bend folding or roll-over folding. **(A)** Slip along a fault plane that become shallower with depth creates a void if the hanging-wall is free of internal deformation. **(B)** Hanging-wall block is never that strong and collapses to fill in the void. Collapse takes place parallel to the axial surfaces. Based on the preservation of cross-section area, a relationship can be established among the dip of the fault (θ), dip of the rollover panel (δ), dip of the axial surfaces (ψ) and the angle between upper and lower segments of the fault plane (Φ). **(C)** This relation can also be solved geometrically using folding vectors. From Xiao and Suppe (1992), Shaw *et al.* (1997) and Shaw *et al.* (2005).

formation of the rollovers are directly related to the bend at the fault plane, these structures are also called as extensional fault-bend folds analogous to their contractional counterparts (Shaw et al., 1997). Faults having multiple fault-bends will form multiple rollover panels (Figure 5.10A). Broadly curved fault bends can be described by using numerous axial surfaces (Figure 5.10B).

Based on the preservation of the cross-section area, Xiao and Suppe (1992) derived a quantitative relationship among the dip of axial surfaces (ψ), the dip of upper segment of the fault plane (θ), the dip of strata within the rollover panel (δ) and the angle between the upper and lower segments of the fault plane (ϕ) (Figure 5.9B). This relation allows estimation of the fault plane's position in poorly imaged deeper parts of the basin by computing ϕ angle, as the other angles ψ , θ and δ can easily be measured on seismic sections. This can be achieved either by solving the equation in Figure 5.9B, or by using folding vectors in Figure 5.9C (Shaw et al., 2005). Folding vectors are measured parallel to axial surfaces and represent the amount of deflection of strata or fault across an axial surface. In Figure 5.9C, let's say that the folding vector X at the inactive axial surface describes deflection of fault plane at the fault bend. On the same axial surface, the folding or deflection of the strata in the rollover panel can be described by folding vector Y that is identical to the folding vector X. In this way, the dip of the lower segment of the fault can be determined if the folding vector in the rollover panel can be estimated (Figure 5.9C).

The fault bend and rollover relation were constructed successfully for the southern margin structure of the Gediz graben on some of the seismic sections (Figures 5.11 and 5.12). The observed rollover geometry in the hanging-wall is conformable with Coulomb collapse models indicating that the southern margin structure becomes shallower with depth across one or two fault bends. Traces of active axial surfaces were identified on the sections based on changes in dip domains and the folding vectors were resolved geometrically on the rollover panels (Figures 5.11 and 5.12). Then, the same folding vectors were applied to the master fault and the downward continuation of the structure was estimated below the graben (Figures 5.11 and 5.12).

Observations on the fault plane reflection and geometrical construction of the hanging-wall collapse reveal that southern margin-bounding structure of the Gediz Graben become shallower both in the up-dip and down-dip directions (Figures 5.8,

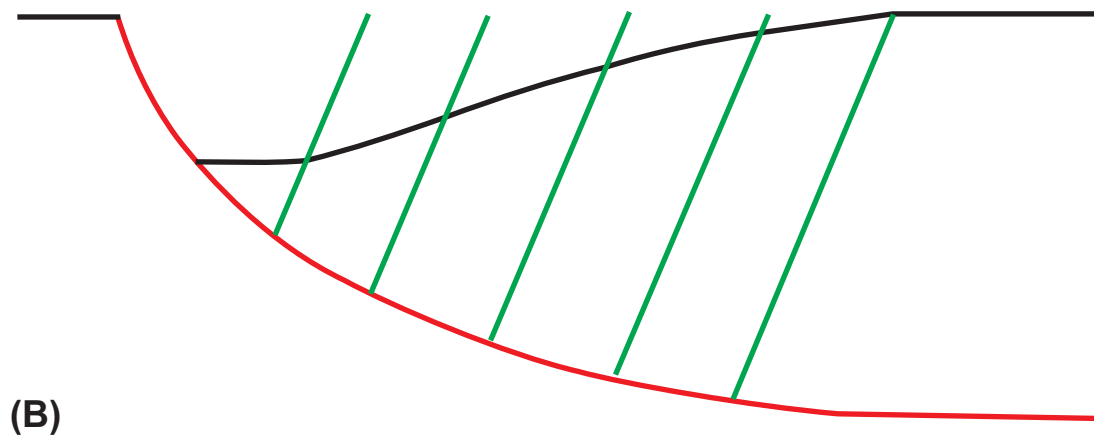
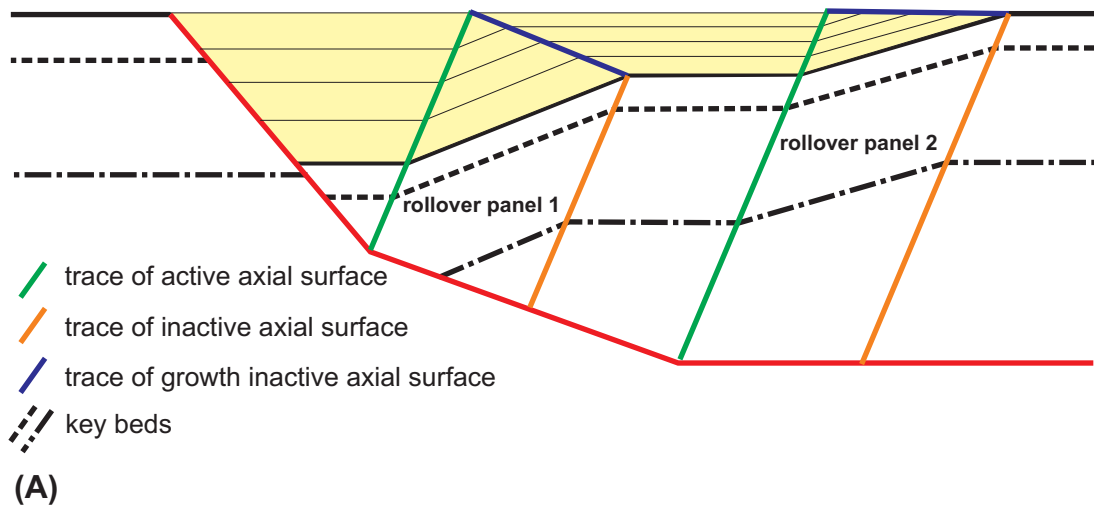


Figure 5.10. (A) Formation of multiple rollover panels due to multiple bends on the fault plane. With accumulating slip on the fault these panels can overlap. (B) Curved fault geometry can be model by using numerous axial planes. From Shaw *et al.* (1997).

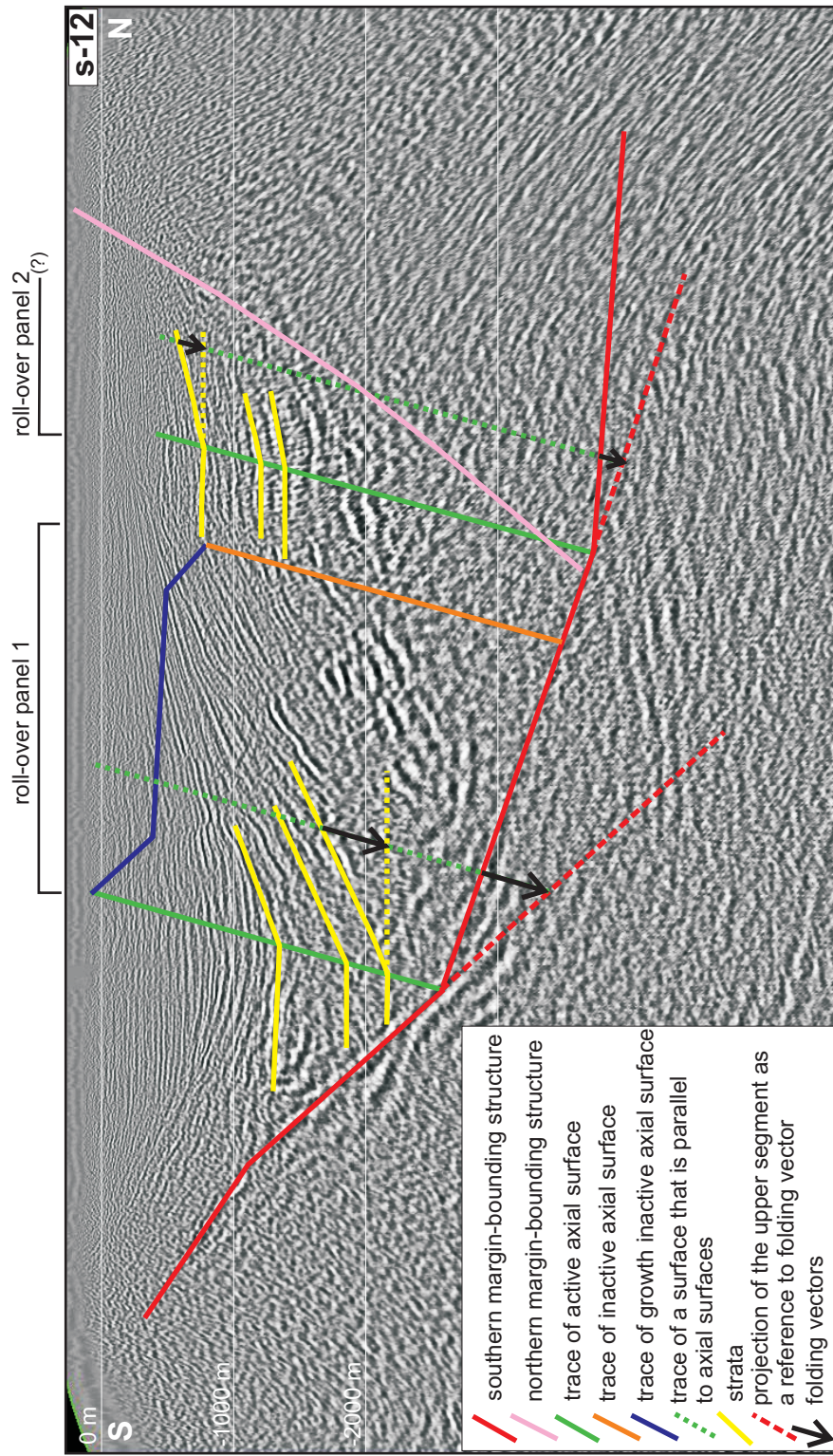


Figure 5.11. Models of inclined collapse of hanging wall can be applied to seismic section in the Gediz Graben. In seismic sections, traces of axial surfaces can be located. Active axial surfaces correspond to fault bends and bounds the rollover panel from one side. The other margin of the rollover panel is marked by the passive axial surface. At the onset of slip in the fault plane, the active and passive axial surfaces are both located at the fault bend. With accumulating slip, passive axial surface become separated from the active and the rollover panel widens. Folding vectors geometrically resolve the amount of deflection of the fault plane at the fault bends. There is an evidence of two different fault bends in this section. See Figure 5.1 for location of the seismic line.

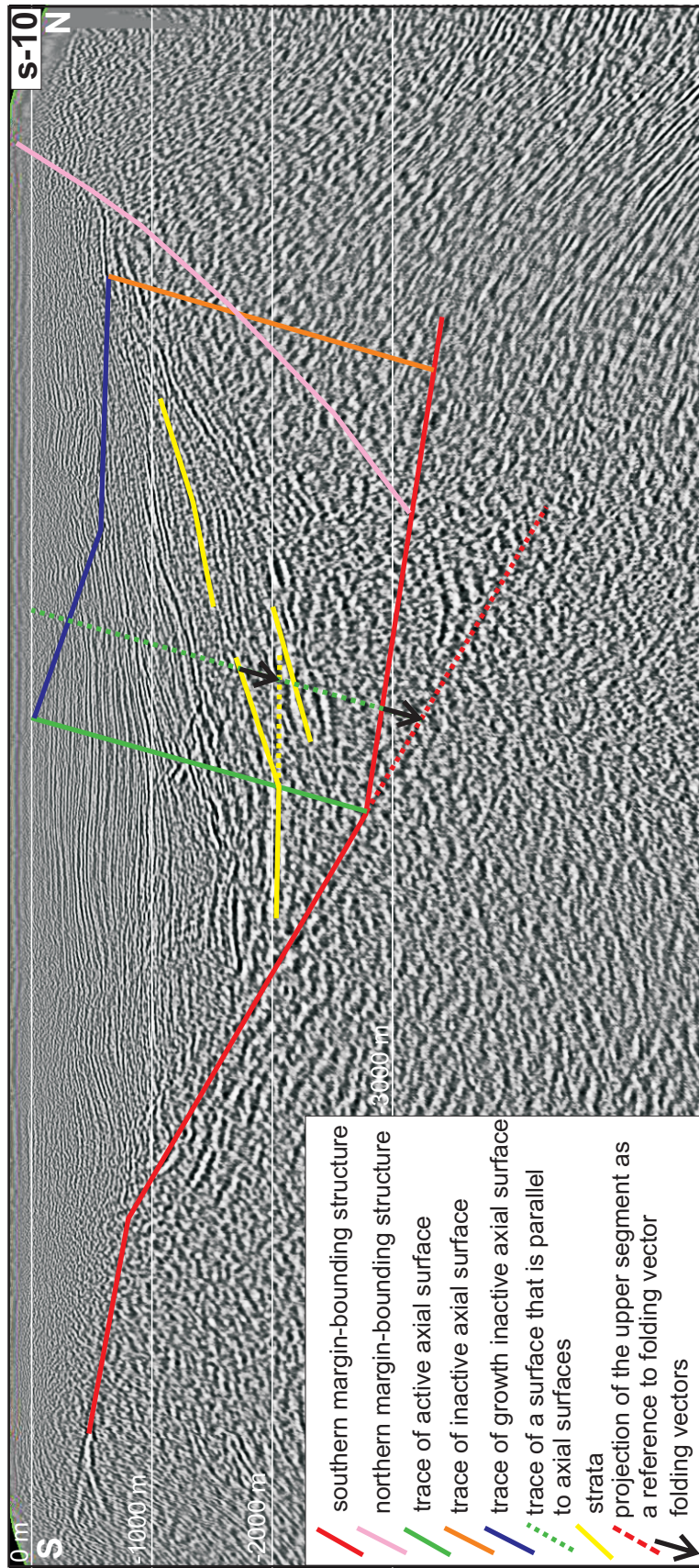


Figure 5.12. Similar geometrical construction as in Figure 5.10, also reveals a fault bend for this seismic section. In both sections southern margin structure of the Gediz Graben become shallower below the graben fill at a fault bend around 2600m. It is also evident in these sections that fault plane also become shallower in the upper parts. See Figure 5.1 for location of the seismic section.

5.11 and 5.12). If the entire fault surface is constructed based on the data coming from the seismic sections, this geometry of the fault plane can be perceived more clearly (Figure 5.13A). The fault plane can be divided into three segments based on the fault dip. The steeply dipping middle segment of the fault plane can be differentiated from shallowly dipping upper and lower segments with dips in the range of 35° to more than 50° (Figure 5.13A). The upper segment, on the other hand, possesses relatively lowered dip values, around 20° . However, at some locations, particularly towards the ground surface, the upper segment becomes steeper again by exceeding 30° . An abrupt shallowing of the fault plane with depth as geometrically constructed in Figures 5.11 and 5.12 marks the lower segment of the fault. In this segment, the dip of the fault plane quickly diminishes to dips approaching to 10° and extrapolation extends the surface further downward with approximately the same dip (Figure 5.13A). Thus, the overall geometry of the structure can be described as flat and ramp geometry made up of shallowly dipping and steeply dipping segments. This ramp–flat geometry was also predicted by Sözbilir (2002).

The southern margin-bounding structure is not very uniform in strike-wise direction as well (Figure 5.13B). Within the general WNW–ESE trend, the structure possesses broad undulations and related strike variations. Named as fault plane corrugations, undulations on the normal fault planes are attributed to originally segmented and en echelon arrangement of the fault (e.g., Andres and Schlische, 1994; Childs *et al.*, 1995; Dawers and Anders, 1995; Ferrill *et al.*, 1999). Two mechanisms were suggested for the formation of corrugated normal fault planes which start as segmented en echelon fault system and eventually breakthrough to produces a single, corrugated fault surface: (1) Lateral curved propagation and linkage of individual segments; (2) formation and breaching of relay ramps by segment interaction (Peacock and Sanderson, 1994; Trudgill and Cartwright, 1994; Ferrill *et al.*, 1999). Anticlines that observed at transverse orientation to the southern margin structure of the graben provide further evidence for originally segmented nature of the structure (see Chapter 6). Sometimes tectonic stresses operating parallel or subparallel to fault strike may result in folding of the fault plane into broad synclines and anticlines as reported by Bozkurt and Sözbilir (2006) from western Anatolia.

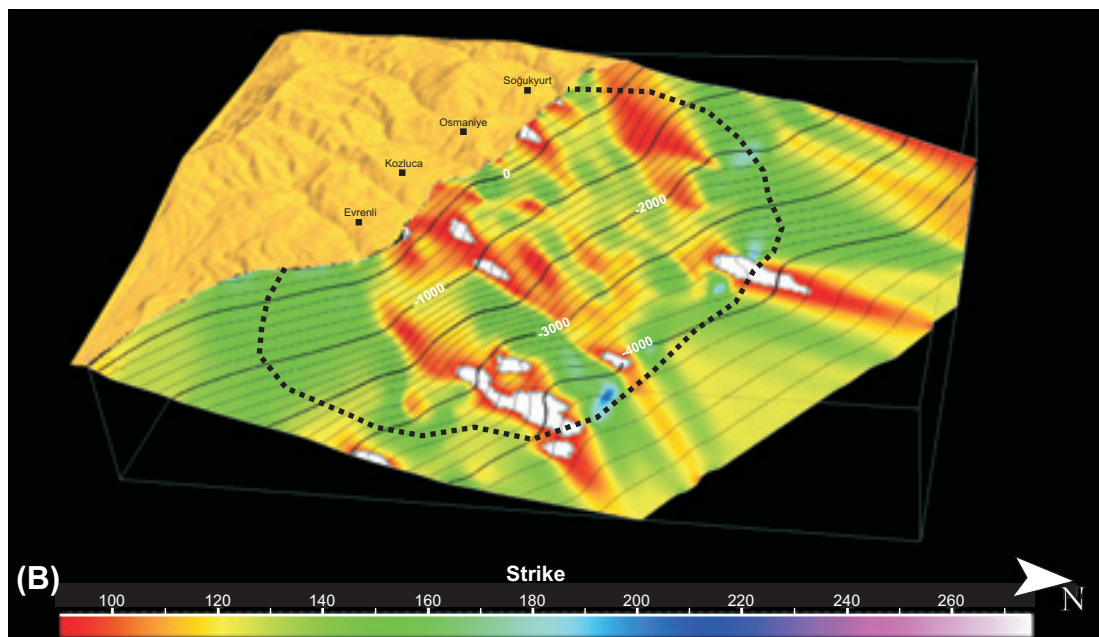
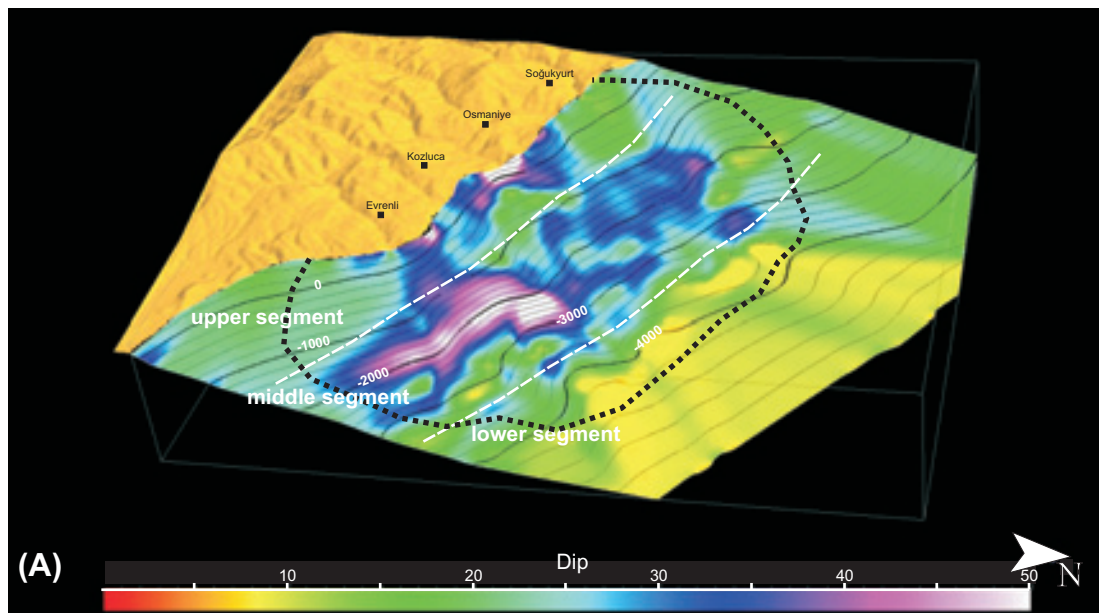


Figure 5.13. 3-D geometry of the southern margin-bounding structure of the Gediz Graben. Contour lines on the surfaces represent elevation below sea level. The dotted line bounds the area of good data coverage out of which were constructed by extrapolation. **(A)** Distribution of fault dips depicts the flat and ramp geometry of the fault plane. **(B)** Distribution of the fault strikes reveals the ondulations or corrugations of the fault surface.

b. The Northern margin structure

The northern margin-bounding structure of the Gediz Graben is not prominent structure as the southern margin-bounding structure. This is clearly evident on some of the seismic sections, which portray a general half-graben geometry for the Gediz Graben (Figure 5.8). However, surface observations (Figure 2.3) and some of the seismic section (Figures 5.11, 5.12 and 5.14) clearly demonstrate a normal fault bounding the northern margin of the graben. Indeed, surface observations reveal the trace of a distinct fault system, composed of discontinuous segments along the northern margin of the graben (Figure 2.3). Marking a zone of sudden shift in surface topography, this trace correlates very well with the northern margin-bounding structure identified on the seismic sections (Figures 5.11, 5.12 and 5.14).

The northern margin structure is an antithetic to the southern margin-bounding structure and lean against it (Figure 5.15). The structure is steeper with dips commonly greater than 35° , typically around 45 to 50° (Figure 5.15A). It generally trends in the NW–SE direction with some variations in strike (Figure 5.15B). These strike variations can also be attributed to segmented nature of the fault as observed from the surface traces of these faults. Although the fault plane was modeled as a single and continuous surface, it constitutes numerous fault segments, which may or may not be linked at depth.

Observations on the seismic sections suggest that displacement accrued on the southern margin-bounding structure is much more significant than that of northern margin-bounding structure. This is also supported by the asymmetrical nature of the graben fill since more accommodation space was created closer to the southern margin. This, in turn, controlled the thickness of the growth strata with distinct thickening towards the southern margin (Figure 5.6). The northern margin-bounding structure was probably become active during the Plio–Quaternary. This is manifested in the thickness of the uppermost stratigraphic unit, where relatively symmetrical thickness distribution is evident within the graben fill (Figure 5.6). Yusufoglu (1996) suggest early Pliocene for the initiation of subsidence at the northern margin of the Gediz graben.

5.2.2. Fault Pattern of the Graben Fill

The fill of the Gediz graben is deformed by numerous second-order faults that form in association with the master graben-bounding faults, particularly with the southern

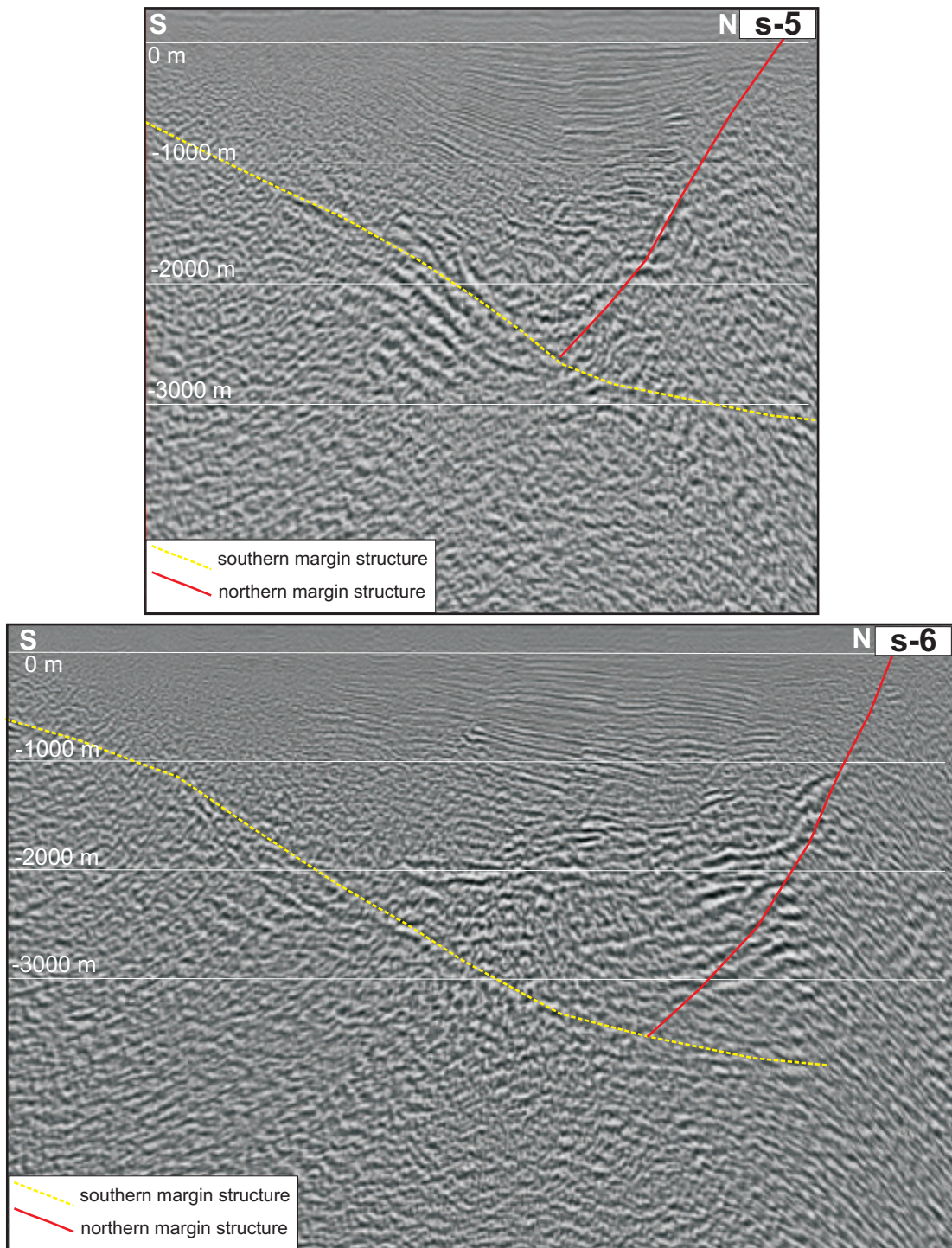


Figure 5.14. Northern margin bounding structure of the Gediz Graben imaged by the seismic sections S-5 and S-6. This structure is antithetic to the southern margin-bounding structure with dips around 45-50°.

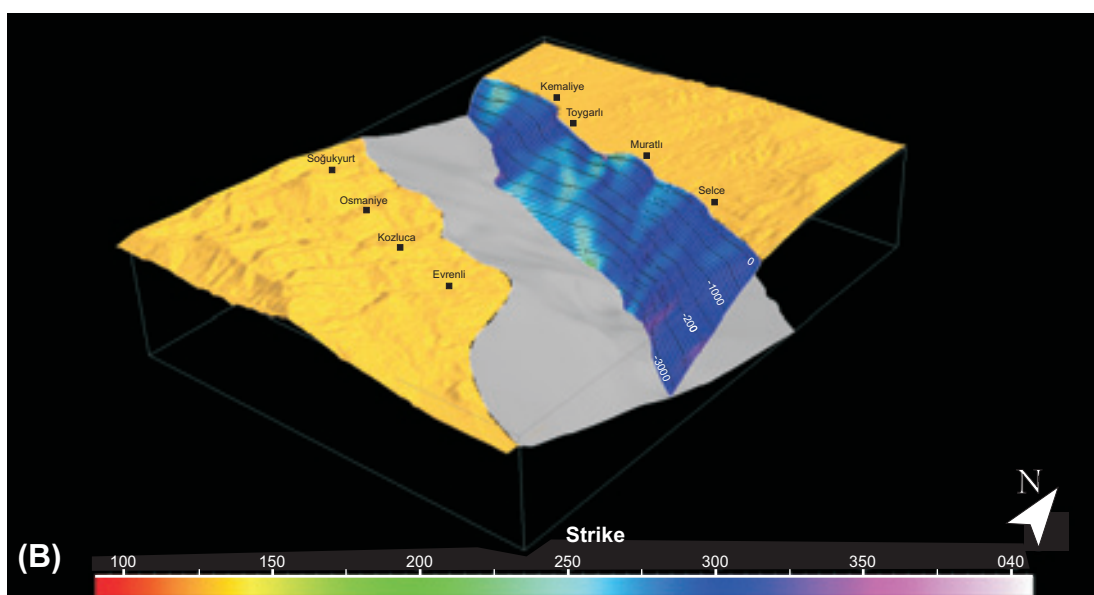
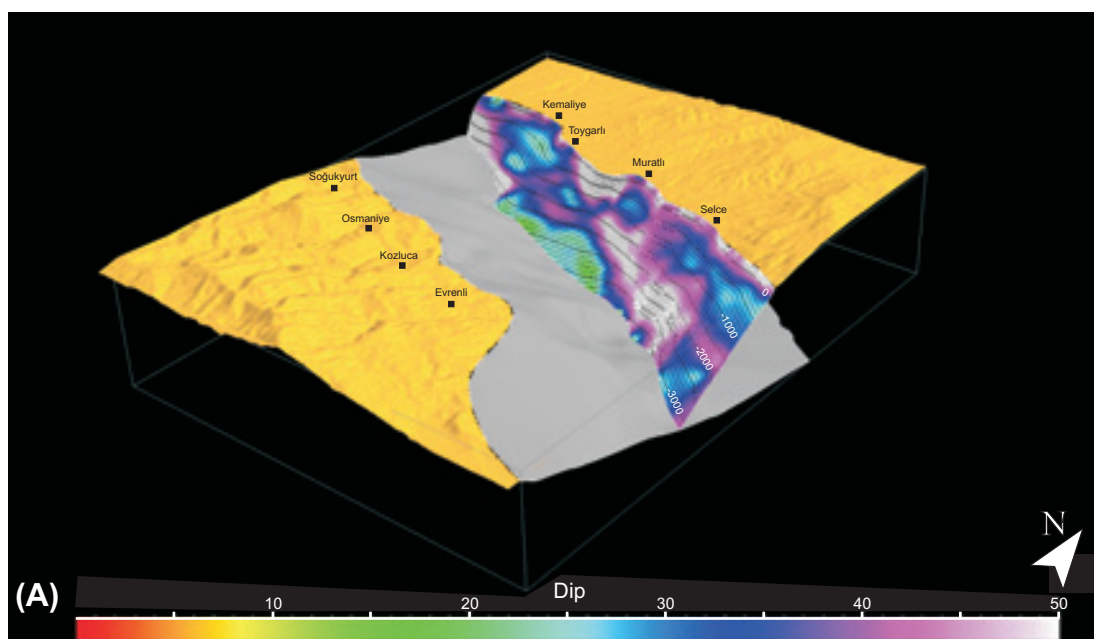


Figure 5.15. 3-D geometry of the northern margin-bounding structure of the Gediz Graben. Contour lines on the surfaces represent elevation below sea level. The dotted line bounds the area of good data coverage out of which were constructed by extrapolation. **(A)** Distribution of fault dips depicts the flat and ramp geometry of the fault plane. **(B)** Distribution of the fault strikes reveals the ondulations or corrugations of the fault surface.

margin-bounding structure (Figures 5.16, 5.17 and 5.18). The secondary faults are both synthetic and antithetic structures to the southern margin-bounding structure. The displacement accrued along these structures commonly varies from few tens of meters to several hundreds of meters (Figures 5.16 and 5.17). It is very clear on the seismic sections that, the displacements diminishes upward in the fault planes and fall below the imaging resolution through the uppermost strata (Figures 5.16 and 5.17). This emphasizes the syndepositional nature of the faulting, and that the faults gradually become influential on younger and younger strata as they deposited. In this way, deformation keeps up with the sedimentation. This also suggests that the deeper portion of the same fault is older than the shallower portion. Generally, the observed faults of the graben fill have smaller dips at depth and become steeper towards the surface. The reason for this is due to the fact that the lower segment, which form earlier, experiences more extension (and consequently back rotation/back tilting) than the upper segment, which forms later. Moreover, parts of the faults that fall within the rollover panel of the master fault become further rotated during the rollover formation (Figure 5.19). The lower rotated portion of the fault seed the upward continuation, which forms in accordance with the Andersonian faulting with, dips around 60° (Figure 5.19D).

The observed style of deformation in the seismic sections mimics the outcrop-scale deformations observed in the exposures (Figures 3.3, 3.4 and 3.5). While the seismic data portray the basin scale structures, outcrop observations were mostly concentrated on the mesoscopic scale structures. In both cases, sub-order faults of antithetic and synthetic orientations dominate the hanging-wall deformation above the master fault that is defined at the scale of observation. The amount of deformation increases significantly towards the master structures in both cases with a distinct increase in the amount of offsets and rotation. In other words, crust responses to the extension in similar ways at different scales. Yet, there are some style differences observed between surface and subsurface data. Distinct crosscutting relation observed in the outcrop exposures is the most obvious differences between the two data sets.

Crosscutting relationship between shallowly- and steeply-dipping faults in outcrops was presented in Figure 3.16. In the same Chapter 3, rotation of a fault to low-angle dips was assessed to lead to eventual lock-up of the fault plane under small confining pressure, close to ground surface (Figure 3.17). As the locked-up low

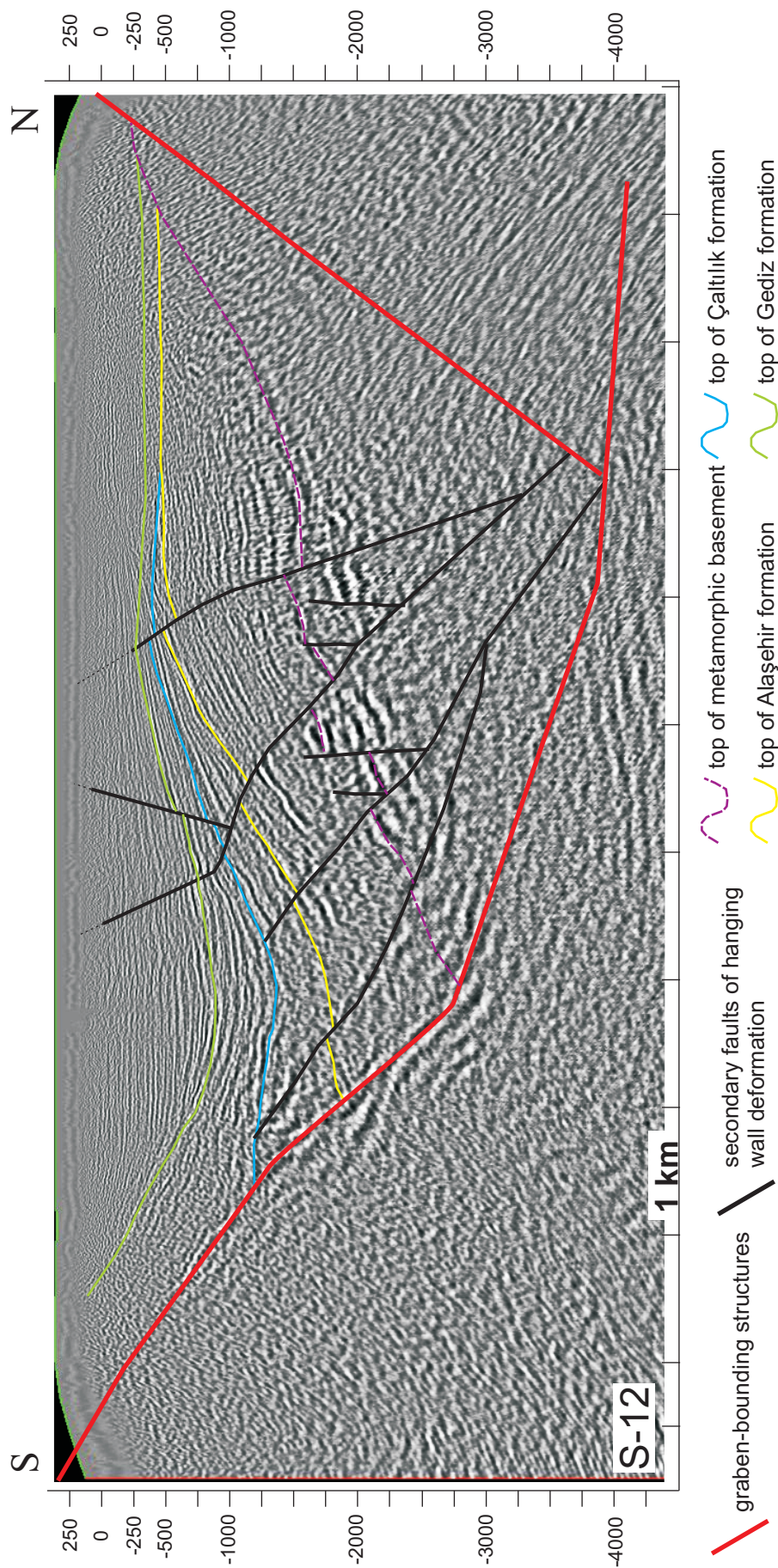


Figure 5.16. Seismic section S-12 showing general deformation characteristics of the graben fill. Antithetic and synthetic faults dominate the hanging-wall deformation above the main fault. Note the well-defined rollover formed above the fault bend of the main fault. In the rollover panel, faults are evidently rotated backward towards the main fault together with the strata. Upward in the stratigraphic section these faults become steeper towards the youngest sedimentary unit. See Figure 5.1 for the location of the section.

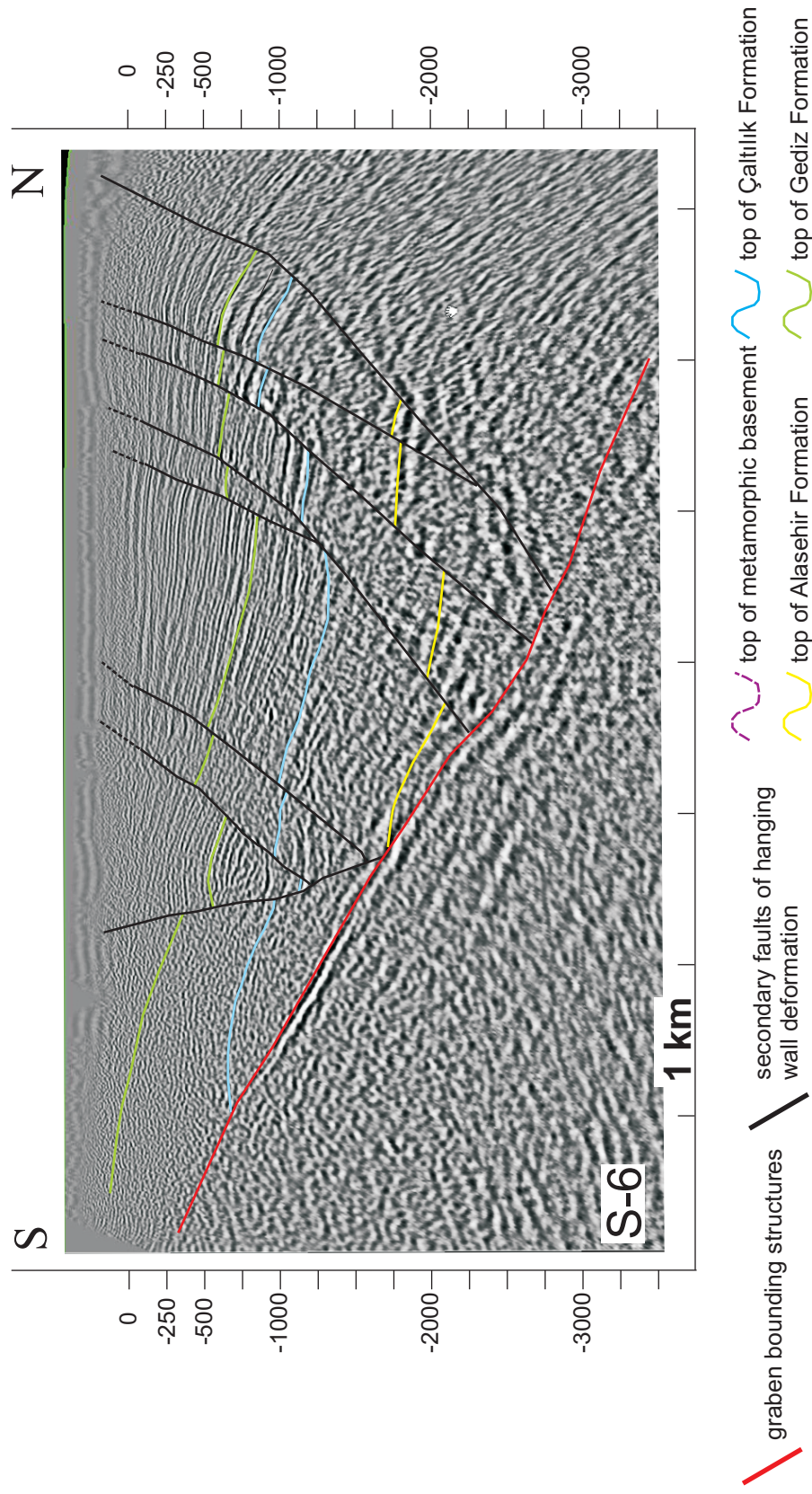


Figure 5.17. Seismic section S-6 showing general deformation characteristics of the graben fill. Antithetic faults commonly dominate the hanging-wall deformation towards west of the study area. These faults form roughly parallel to the inclined shear direction that is antithetic to the southern margin structure. Rollover formation in the hanging wall probably hindered by the formation of these antithetic structures. See Figure 5.1 for the location of the section.

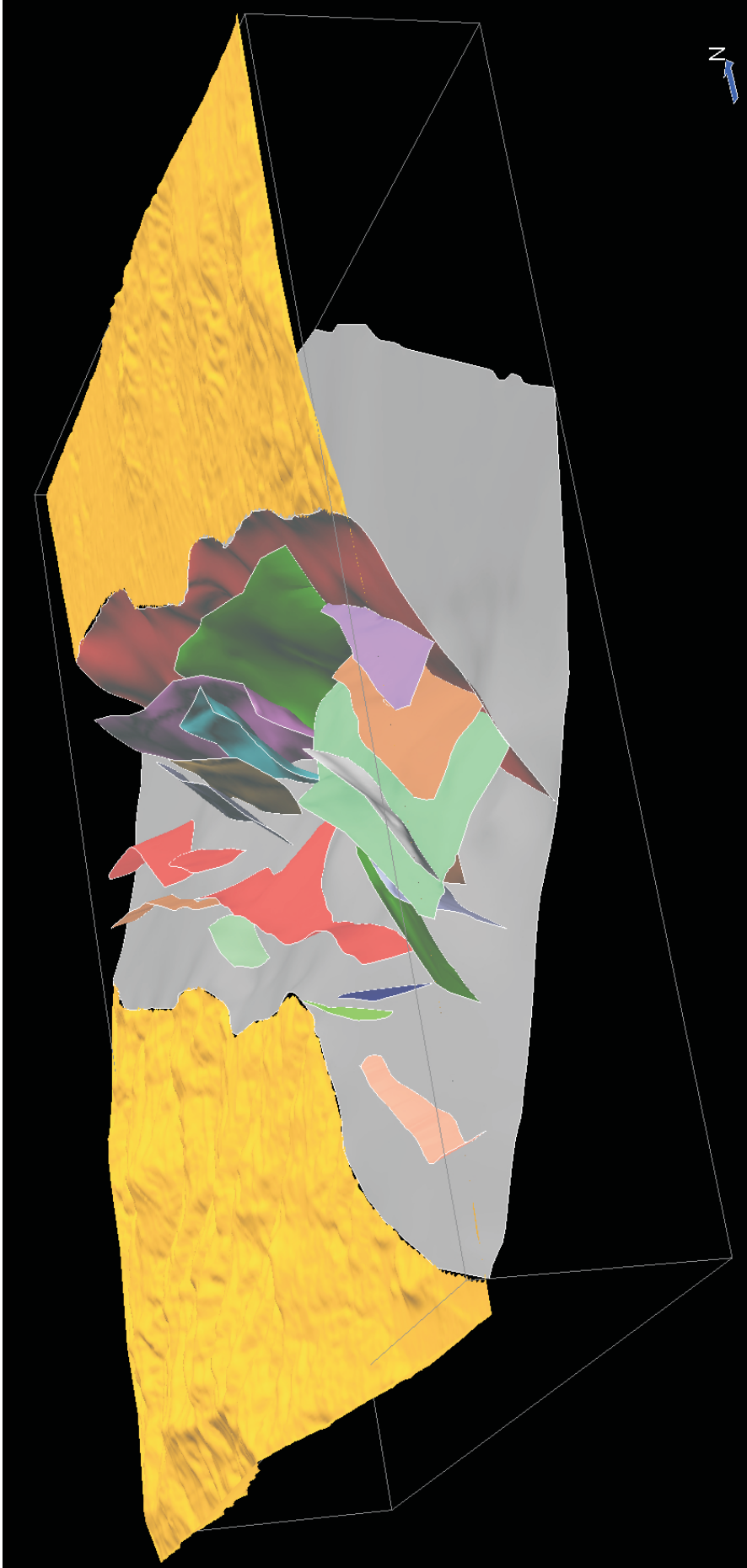
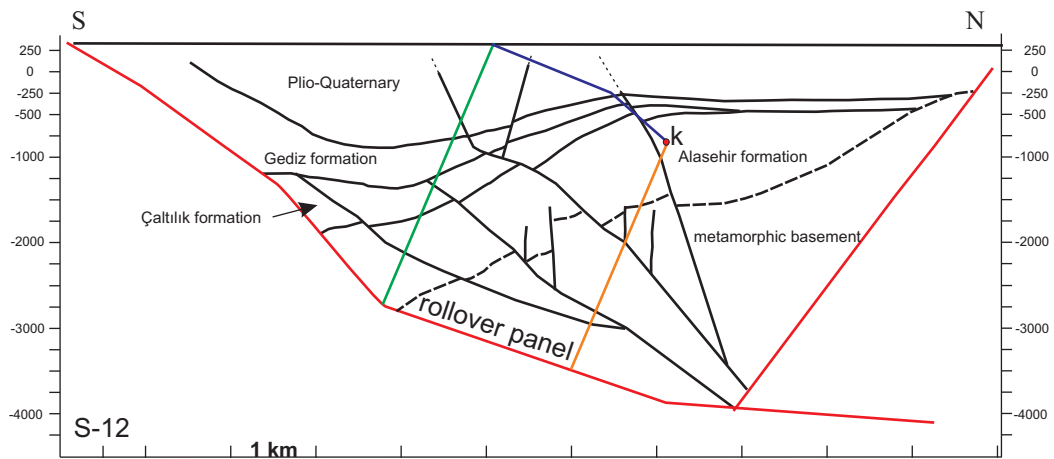


Figure 5.18. 3-D fault model of the Gediz Graben. The eastern part of the graben is characterized by dominantly synthetic faults to the southern margin-bounding structure and well-developed rollover. Contrarily, the western side is dominated by antithetic faults to the southern margin-bounding structure which impeded formation of rollover. This lateral change in structural style could also indicate slightly different structural evolution for the eastern and western parts. This difference may be related to the originally segmented nature of the southern margin structure.

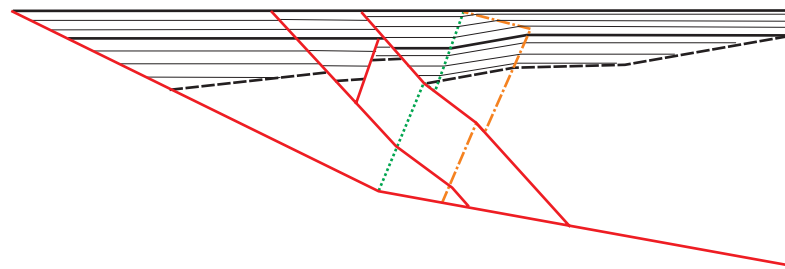


- / trace of active axial surface
- / trace of inactive axial surface
- / trace of growth axial surface
- / graben bounding structures
- / secondary faults of hanging wall deformation

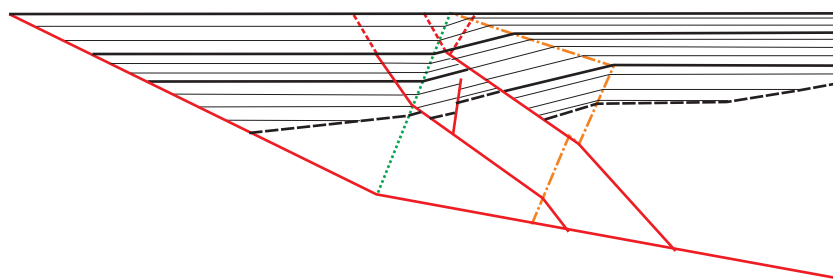
(A)



(B)



(C)



(D)

Figure 5.19. Backward rotation of hanging-wall structures within the rollover panel. (A) Basic interpretation of seismic section S-12 in Figure 5.16. The rollover panel is also illustrated. Point 'k' on the inactive axial surface marks the stratigraphic level separating the pre-growth and growth strata. (B), (C) and (D) illustrates simplified evolution of the rollover panel with accumulating slip. Fault rotation takes place within the rollover panel during this evolution. Faults gradually become influential in younger sedimentary units with more steeper dip (dashed faults in D).

angle structures cannot accommodate the extension anymore, new faults of more favorable dip form. This results in cross cutting relationship between the locked-up, shallowly dipping structure and the new-formed steeper structures (Figure 3.16). However, no crosscutting relationship similar to those observed in outcrops was interpreted in the seismic data. Instead, individual fault planes generally display variation of dip having relatively low angles at depth and become steep towards the surface (Figures 5.16 and 5.17). Although rotation of the fault to low-dip angles lead to fault lock-up under small confining pressure close to surface, low angle faults are more likely to sustain their activity under increased confining pressure at depth. In fact, confining pressure contributes to resolved shear stress on the low-angle fault plane significantly. As a result, relatively low angle portions of the faults including the southern margin-bounding structure can still stay active at depth (Figure 5.16 and 5.17). In this way, the extension that the grabens fill experiences is accommodated by low angle portion of the faults deeper in the basin and relatively younger high angle portions close to surface.

5.2.3. Stress Field of Faulting

The striations analyses of the faults observed through surface exposures along the southern margin of the Gediz graben are discussed in Chapter 3. Through these analyses the principal stress axes controlling the faulting were computed by using stress inversion methodology (Angelier, 1990, 1994). Based on these analyses, it is concluded that Gediz Graben experiences general N-S oriented extension with minor spatial but no temporal variations in the stress field.

Both 2-D and 3-D seismic surveys provide significant amount of fault data to construct the fault geometries. Indeed, there is a need for a new method that employ the fault geometries to infer the stress regime that drives the deformation. Unfortunately, traditional stress inversion methodologies require measured slickenside lineations to represent the slip vectors on the fault planes (e.g., Carey and Brunier, 1974; Angelier, 1979, 1994; Etcheopar *et al.*, 1981; Gephart and Forsyth, 1984; Yamaji, 2000). As a result, these approaches cannot be applied to seismically constructed fault geometries because no clear indication of slip vector can be interpreted out of the seismic data sets. Recently, Lisle *et al.* (2001) proposed a method of stress inversion that can be applied to fault populations in which slip vector cannot be determined but sense of dip-slip could be inferred. The way to

estimate the slip sense is to relate the dip-slip with the dip-separation. Although the relation between separation and slip is not always straightforward, sense of dip separation mimics sense of dip slip under certain circumstances. These circumstances include: (1) faults offsetting the horizontal markers, (2) faults having horizontal cut of lines and (3) the fault and offset strata have the same strike (Lisle *et al.*, 2001, Orife *et al.*, 2002). Fortunately, these conditions can be validated in our case. Stratigraphically up in the section the strata are relatively horizontal. If not, cut off lines can be approximated as roughly horizontal. Furthermore, as the bed tilting is directly related with normal faulting and rollover formation, the bed strike and the fault strike should be close to each other. Consequently, the proposed methodology is applicable and may produce a viable solution with the constructed fault geometries (Figure 5.18). This methodology has already been tested and compared with slip vector-based inversion in Chapter 3. In this test drive, both methodologies produced almost identical solutions (Figures 3.22 and 3.20A).

In order to compute the stress regime related to fault model in Figure 5.18, dip and strike values were extracted from the modeled fault surfaces as a first step. As the employed methodology (Lisle *et al.*, 2001) depends only on fault attitude and the sense of slip, this data will constitute the main input of the computation. As the observed sense of separation is normal for all the interpreted faults, sense of the dip-slip is assigned as normal. The extracted data set is large and includes a total of 33,610 dip and strike values out of 18 major fault planes (Figure 5.18). Because the employed software is based on a grid-search algorithm, this large data set is difficult to solve if it is ever possible. The approach to this problem is to plot the poles of extracted fault plane attitudes separately as shown in the Figure 5.20. Each plot represents the individual fault planes and is characterized by generally unimodal and sometimes bimodal distribution of poles to the fault planes. A single fault plane is assigned for those of unimodal distribution and two fault planes were assigned for bimodal distributions in a way to honour the plotted data. A total of 20 fault planes were then input into the software DIPSLIP (Orife *et al.*, 2002) to compute the stress axes (Figure 5.21A). The computed result includes numerous compatible principal stress axes to the input fault data. The distribution of compatible σ_1 axes (Figure 5.21B) concentrates around vertical, which is conformable with the outcrop based slip inversion efforts documented in Chapter 3 (Figures 3.20 and 3.23). The concentration of σ_3 axes, on the other hand, indicates a NE–SW-oriented extension

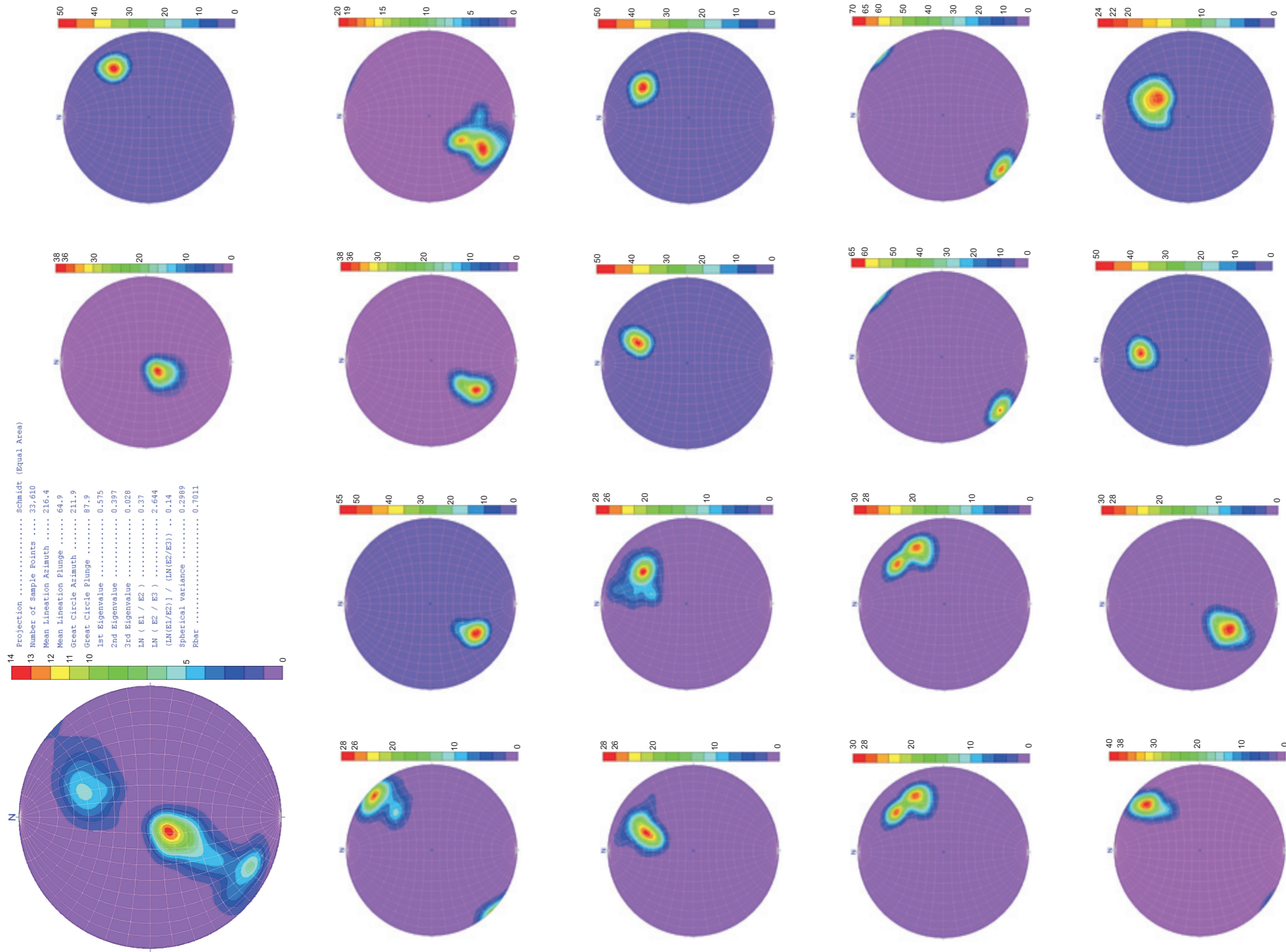


Figure 5.20. Stereoplots illustrating poles to the fault planes in Figure 5.18. A total of 33,610 dip and strike data were extracted from the fault model. The first stereoplot illustrates the entire data set with basic statistical analysis. The other stereoplots belong to individual fault planes modeled in Figure 5.18. In these individual stereoplots, a fault plane was assigned to each cluster to be used in stress analysis. Those illustrating bimodal distribution was represented by two fault planes. A total of 20 fault planes were input to the stress analysis program (Figure 5.21).

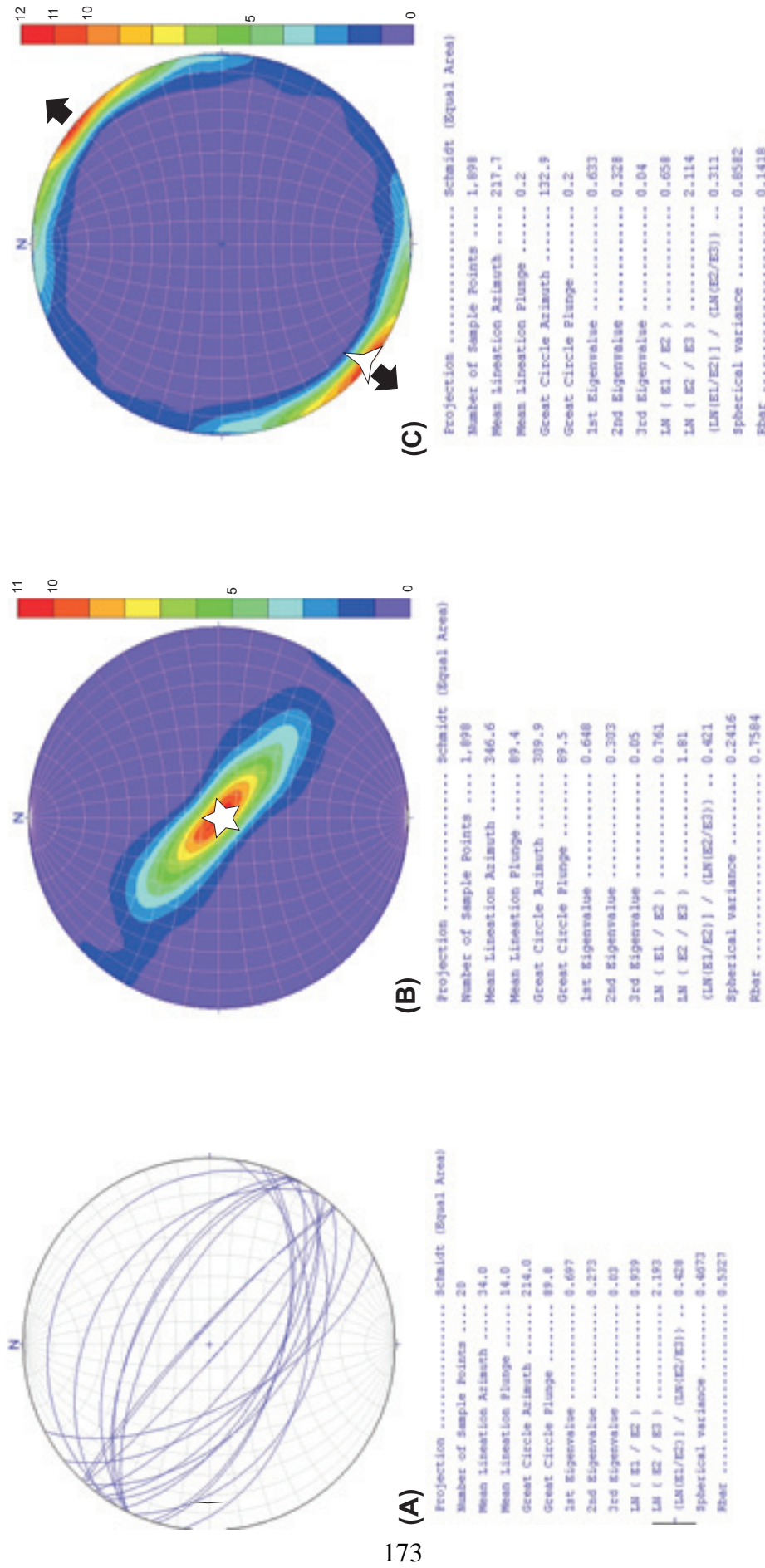


Figure 5.21. (A) Fault data extracted from Figure 5.20 and used in the stress analysis. (B) Stereoplot showing the distribution of s_1 stress axes according to the stress analyses. Almost vertical σ_1 orientation correlates very well with stress analyses in Chapter 3 which is completely based on the surface exposures. (C) Stereoplots showing the distribution of σ_3 axes. This distribution suggests a NE-SW-oriented direction of extension. This result is conformable with surface-based analyses around Alaşehir as summarized in Figure 3.2.5.

(Figure 5.21C). Although this deviates from general N–S-oriented extension computed in Chapter 3 for the Gediz graben, it still falls very close to NNE–SSW-oriented extension direction inverted around Alaşehir (Figure 3.25). Conclusively, the result of slip-sense-based methodology of Lisle *et al.* (2001), which employs seismically derived fault data, are in close agreement with that of slip vector based methodology of Angelier (1994) that employs outcrop data.

5.3. Graben Fill

Lithofacies characteristics of the sedimentary fill of the Gediz Graben were described in detail in Chapter 2. The same chapter also addresses the facies models and the governing depositional systems of the graben fill. Although the seismic data evaluated in this chapter are far from providing detailed lithological information, they portray the lateral distribution of the sedimentary units within the graben more accurately than any other available data source. Indeed, this distribution may provide significant clues to the evolution of the graben.

The distribution of the graben fill in the Gediz Graben is conformable with the graben's geometry that suggest the thickest sedimentary section located in the middle of the basin (Figure 5.22). Exceeding 3000 m vertical thickness, the depocenter is limited both in perpendicular and parallel to the graben strike in a way that the thickness of the fill gradually diminishes in these directions. It is conceivable and expected that the thickness of the graben fill decreases towards the northern and southern bounding structures perpendicular to the graben strike. However, the thickness variation parallel to the graben strike is more genetically related to the graben evolution as this suggests lateral variation of the accommodation space generation. These variations are mostly related to the originally segmented nature of the graben-bounding structures (e.g., Morley, 2002; Schlische, 1995; Morley *et al.*, 1990).

Lateral thickness variation of the graben fill is a significant fact for the Gediz Graben and has been overlooked by the available literature. It is really not very realistic to expect that the entire Gediz Graben extending more than 150 km in strike-wise direction subsided as a single intact piece with a constant rate of subsidence. Temporarily and spatially, the subsidence rate of the basin must vary along the graben. The available studies on normal fault systems clearly illustrated how large normal faults are evolved by amalgamation of discrete fault segments (Griffiths,

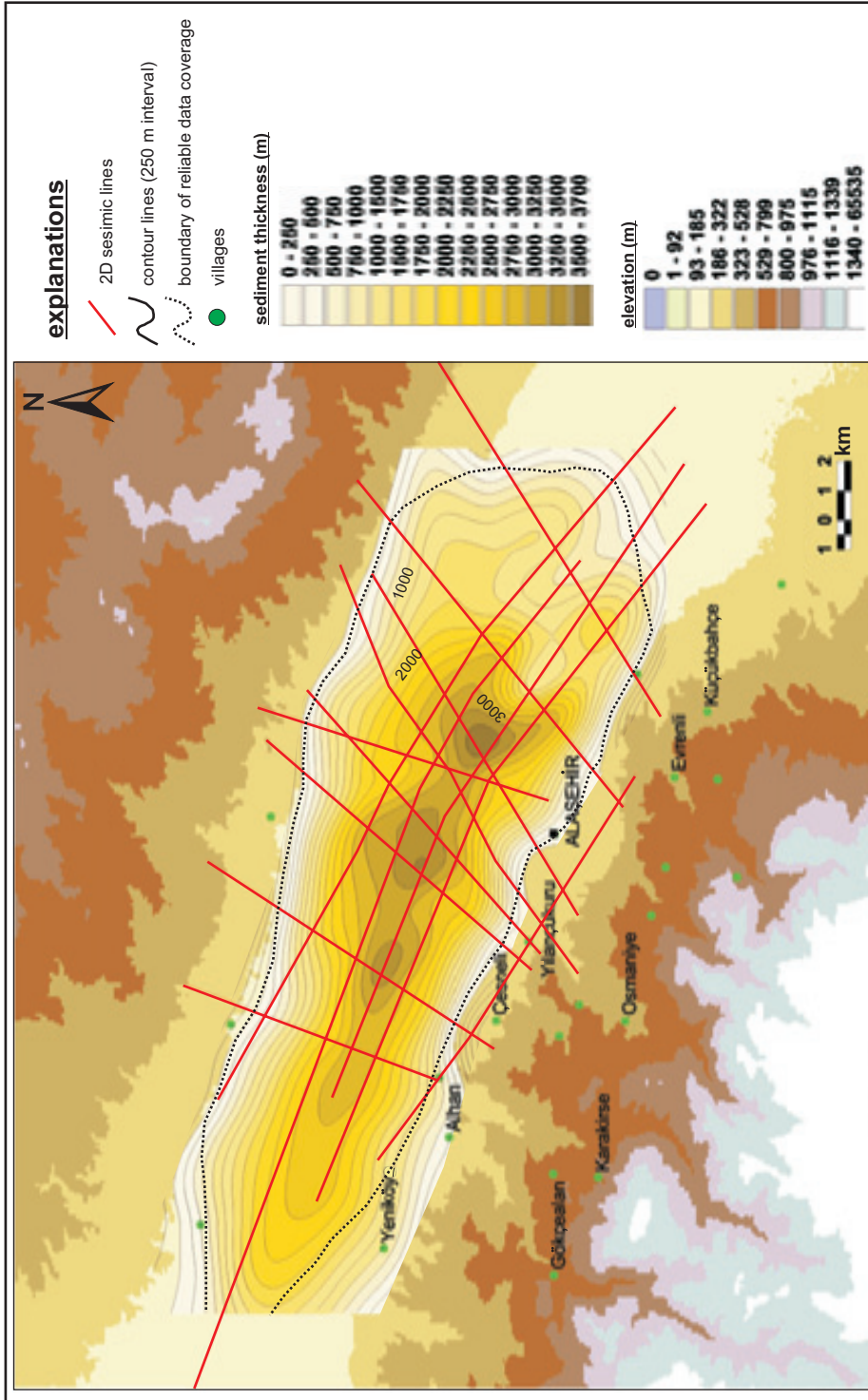


Figure 5.22. Isopack map showing the thickness distribution of the fill of the Gediz Graben. The thickest section is located somewhere in the middle of the graben and exceeds 3000m. If the thickness distribution is examined parallel to graben strike, the thickest portion is located from N of Çeşneli to NE of Alaşehir. Towards NE and SW from this thickest portion, the thickness decreases parallel to graben strike.

1980; Morley *et al.*, 1990; Peacock and Sanderson, 1991; Cartwright *et al.*, 1995; Morley, 2002; Bozkurt and Sözbilir, 2006; Çiftçi and Bozkurt, 2007). Indeed, similar mechanisms are observed to currently take place in the Gediz Graben as described in Chapter 4. It is a prerequisite that identical processes have taken place in the geological history of the graben. Such an evolutionary path for the graben-bounding structures has certain implications to the graben fill, the most striking one being the lateral variation of the graben fill in thickness, lithofacies and ages.

If the longitudinal seismic section S-4 extending from Salihli to Alaşehir is examined, a clear lateral thickness variation of the graben fill can be observed (Figure 5.23). In fact, the Gediz Graben can be differentiated into two subbasins as Salihli and Alaşehir subbasins with a distinct sediment minima and basement high located in between. There are some differences among the two subbasins such as thickness and ages of the sedimentary units. While the deposition in the Alaşehir subbasin started with the Alaşehir formation, deposition in the Salihli subbasin started later with the Çaltılık formation (Figure 5.23). Considering thickness of the sediments in two subbasins, which are close to each other, Salihli subbasin has probably experienced higher rate of subsidence for a relatively shorter period compared to the Alaşehir subbasin. This inarguably suggests that two subbasins have partially independent evolution. A probable transfer fault between the two subbasins may accommodate the consequential kinematic differences among them (Figure 5.23).

Other interesting structural features observed in Figure 5.23 are the folds oriented transverse to the trend of the graben. Indeed, these structures are common in the Gediz Graben and observed in all the longitudinal seismic sections. It is interesting with these transverse structures that anticlines are associated with the thinning of the stratigraphic units whereas synclines are associated with the thickening of the stratigraphic units. This clearly indicates the syndepositional nature of the transverse folds. Schlicshe (1993 and 1995) illustrated that transverse folds form in association with segmented normal fault systems to accommodate the displacement gradients within and in-between the discrete fault segments. Called as displacement gradient folding, transverse folds form in a way that synclines are associated with displacement maximum and anticlines are associated with displacement minimums. This pairing, in turn, explains the stratigraphic thickening in synclines and thinning in anticlines.

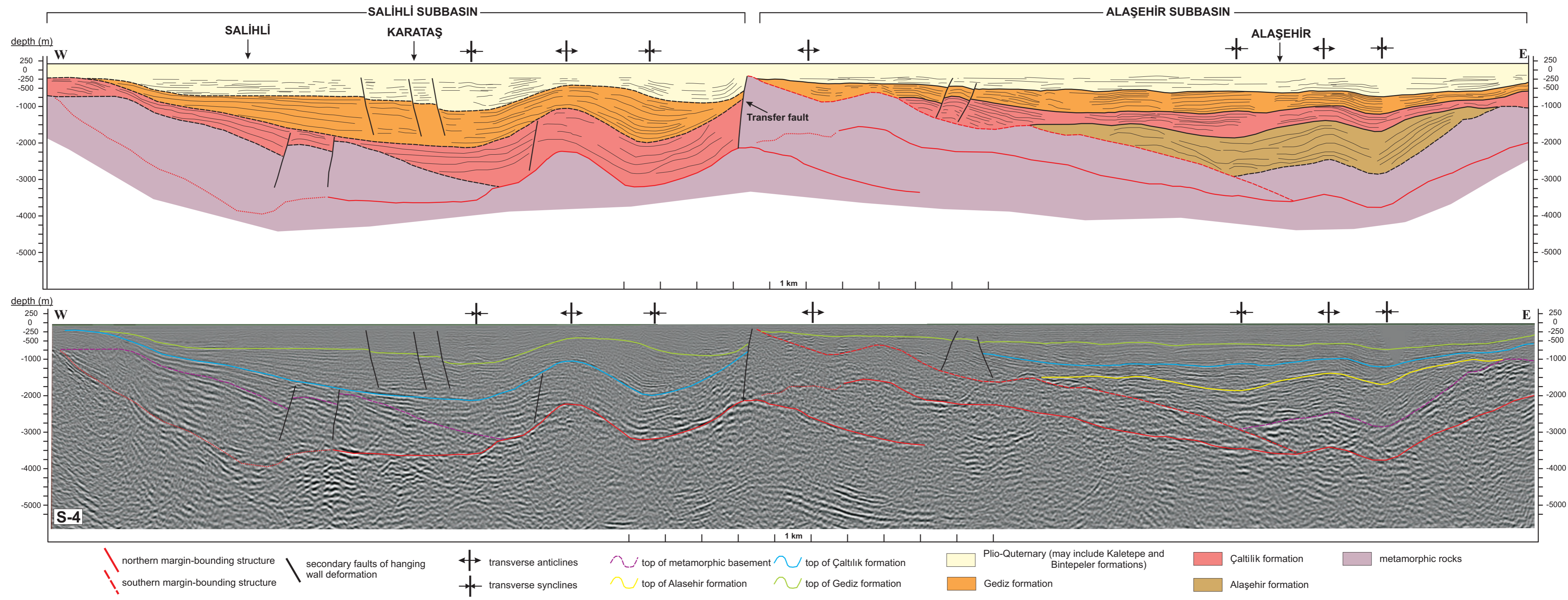


Figure 5.23. Longitudinal seismic section S-4 and its interpreted cross section extending from Salihli to Alaşehir. Lateral thickness variation of the graben fill is clearly evident in these sections. Two separate subbasins were differentiated based on the distribution of depocenters. Named as Salihli and Alaşehir subbasins, a basement high with sediment minima clearly separates these subbasins. Transverse synclines and anticlines are observable in each subbasins. See figure 5.1 for the location of the seismic section.

5.3.1. Alaşehir Formation

Alaşehir formation has limited spatial distribution along the southern margin of the Gediz Graben. Indeed, the formation's only exposures are observable S–SW of the Alaşehir immediately south of the MGBF (Figure 5.24). There is no reported exposures of the formation exists along the southern horst block of the graben around Salihli region (Yazman *et al.*, 1998; E. Bozkurt, oral communication). Seismic interpretations also agrees with the outcrop distribution in a way that Alaşehir formation were not interpreted to exist within the Salihli subbasin (Figure 5.23). Transverse seismic sections also support this interpretation. Figure 5.19A illustrates that the Alaşehir formation, which is proved by boreholes to exist within the Alaşehir subbasin, constitutes partly growth and partly pre-growth strata with respect to modern Gediz Graben. This inference is based on the stratigraphic level indicated by point 'k' in Figure 5.19A, where inactive axial surface diverted into growth axial surface to mark the boundary between the growth and pre-growth strata (e.g., Xiao and Suppe, 1992; Shaw *et al.*, 1997). When seismic sections S-1 and S-2 in Figure 5.8 are examined from Salihli subbasin, no stratigraphic unit sharing the above-mentioned characteristics of the Alaşehir formation can be observed. While the rollover in S-1 forms along basement-sediment contact, the entire graben fill appears as the growth strata (Figure 5.8). Furthermore, no seismic stratigraphic unit that shares the seismic facies characteristics of the Alaşehir formation exists in the Salihli segment. Top of the Alaşehir formation, which is a distinct stratigraphic surface characterized by reflection truncations under the surface and onlaps above the surface, is identified only within the Alaşehir subbasin (Figure 2.14).

If the thickness distribution of the Alaşehir formation is examined within the Alaşehir subbasins, it can be observed that the formation reaches to maximum vertical thickness around 1400 m at its depocenter. The location of this depocenter in the graben correlates very well with the formation's exposures on the horst block (Figure 5.25). The formation gets thinner laterally from the depocenter along the graben strike, and finally wedges off towards the west of the graben. To the east, the formation gets thinner as well and probably wedges off out of the area of seismic coverage. This indicates that compared to today's configuration, the graben was probably very limited in strike-wise extend during the deposition of the Alaşehir formation as representation of the earlier increments of extension. With time and

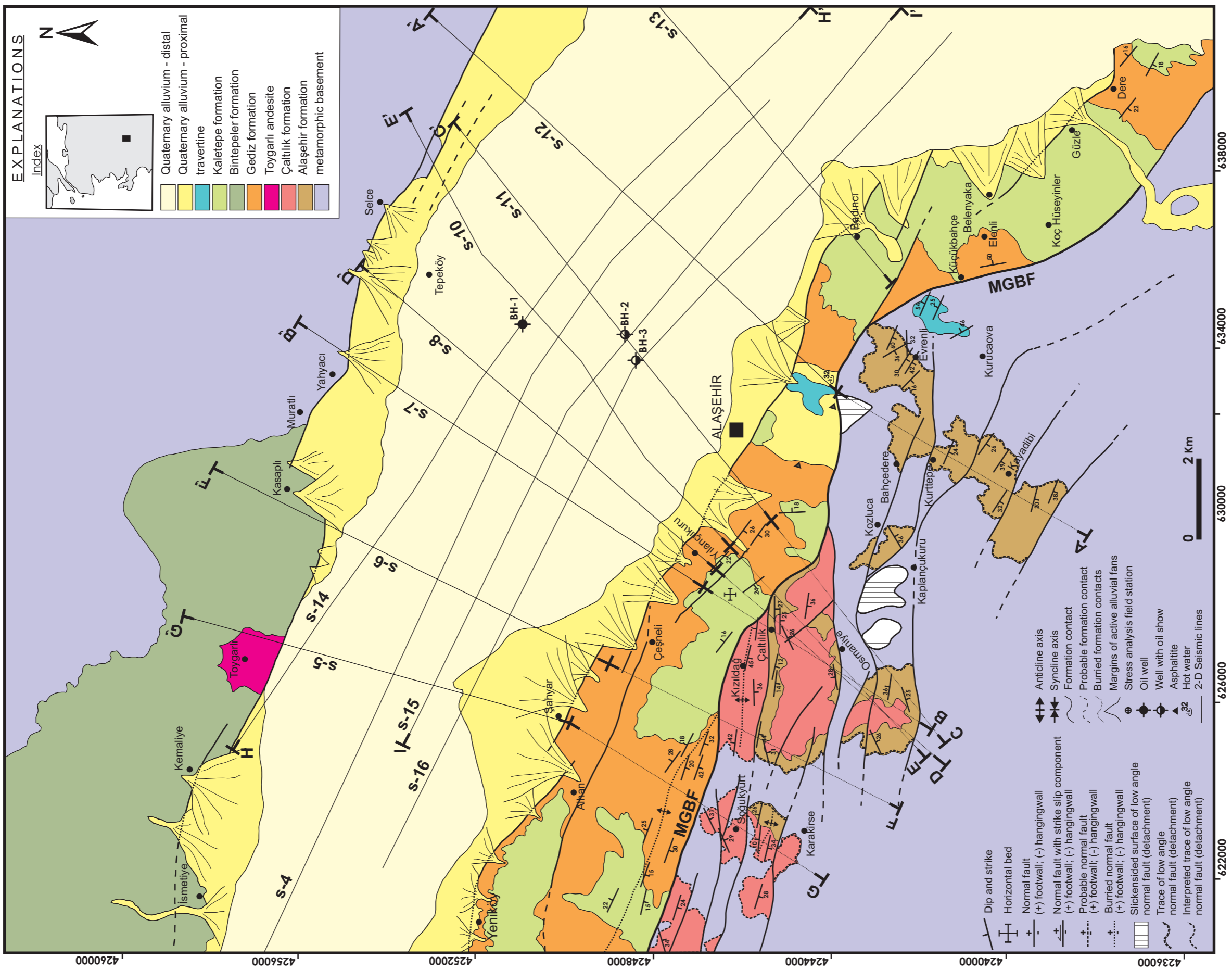


Figure 5.24. Geological map of the area around Alaşehir. A-A' to I-I' illustrates the location of the cross sections drawn in Figures 5.27 to 5.30. Solid lines represent the part of cross sections that is based on 2-D seismic sections. Dashed lines represent part of cross sections that is based on surface geology. MGBF: Master graben bounding fault.

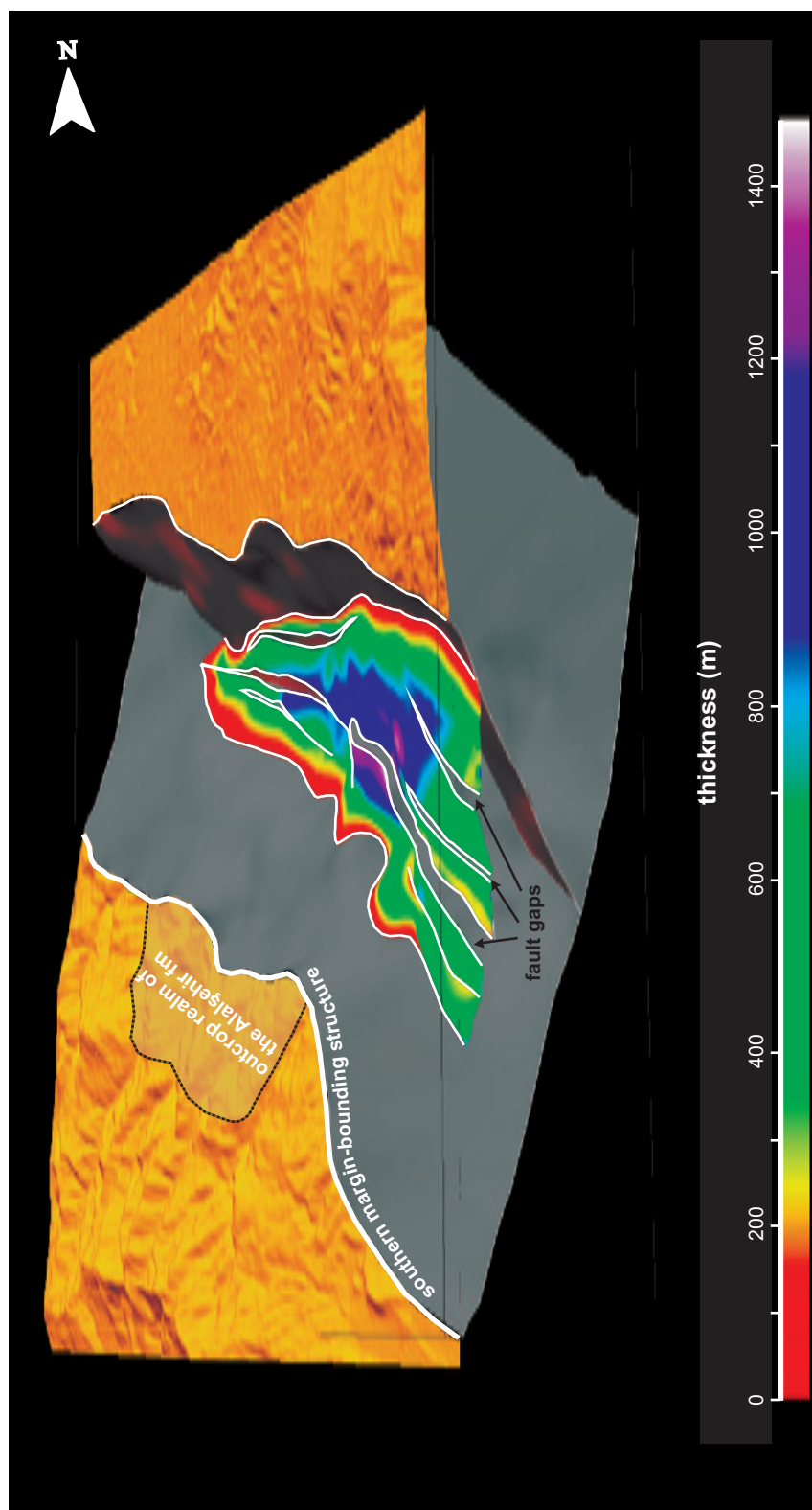


Figure 5.25. Model showing the graben-bounding structures and top of the Alaşehir formation (yellow horizon in Figure 5.16). Fault gaps created by modeled faults in Figure 5.18 are also illustrated. The color code on the stratigraphic surface depicts thickness distribution of the Alaşehir formation projected onto this surface. White lines illustrates fault cutoffs.

accumulated extension, Gediz Graben extended beyond the limits of the Alaşehir formation and finally reached to today's configuration. This, in turn, explains the limited distribution of the formation within the graben.

Transverse folds are clearly depicted by the structural contour map of the top of the Alaşehir formation (Figure 5.26). These folds are oriented almost orthogonal to the southern margin structure of the graben. Although, axial surface traces of the folds are truncated by secondary normal faults of the graben fill, the axial traces can be matched well across the footwall and hanging-wall of these faults. Generally, folds are more pronounced closer to the southern margin structure with steeper limb dips and higher amplitudes. As you go away from the southern margin structure towards north, limb dips get gentler and fold amplitude diminishes. This inarguably shows the relationship between the southern margin-bounding structure and transverse folding in the graben.

5.3.2. Çaltılık Formation

Çaltılık formation overlies the Alaşehir formation in the Gediz Graben. In contrast to Alaşehir formation, which is only limited to Alaşehir subbasin, Çaltılık formation is interpreted to exist within both the Salihli and Alaşehir subbasins (Figure 5.23). Although the formation is probably thicker in the Salihli subbasin (Figure 5.23), it reaches over 1000 m thickness within two separate depocenters across the Alaşehir subbasin (Figure 5.27). One of these depocenters spatially correlates well with the depocenter of the Alaşehir formation. However, the other depocenter, which is located further west, corresponds those parts of the graben where Alaşehir formation was never deposited (Figure 5.27). This clearly suggests that accommodation space creation was gradually extended westward during this period. In other words, the initial graben in which the Alaşehir formation was deposited, propagated towards west during the deposition of the Çaltılık formation. At the mean time, subsidence was probably initiated within the Salihli subbasin as well, although the two subbasins were probably still unconnected, which is reflected by the significant thickness variation of the Çaltılık formation among the subbasins (Figure 5.23). Thus, the graben configuration was modified significantly from its initial phase and the graben was extended spatially to the west during this period as natural response to accumulating extension in the region. On the other hand, the Çaltılık formation wedges off onto the Alaşehir formation to the east, which indicates that eastward

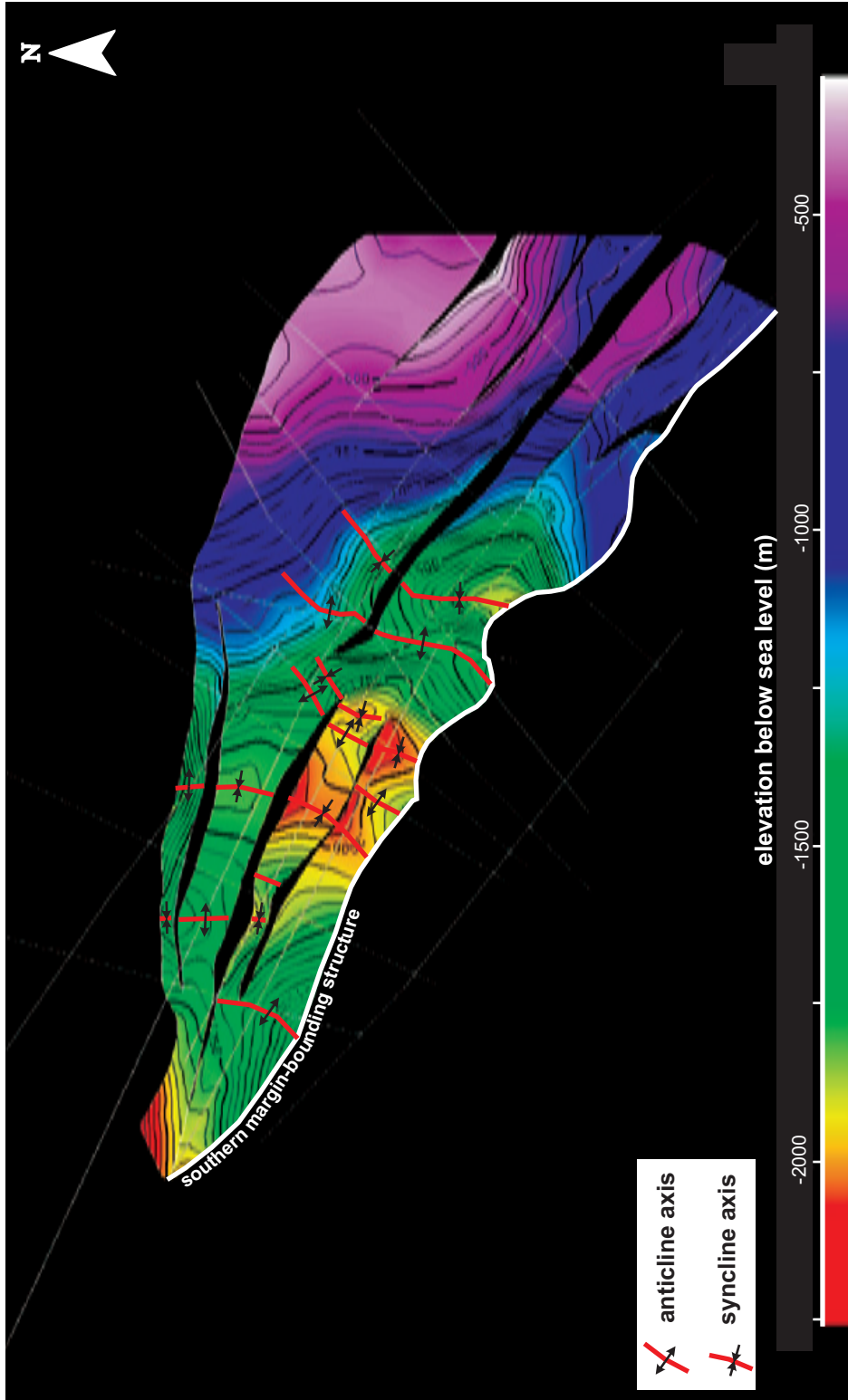


Figure 5.26. Structural map of the top of the Alaşehir formation. Contour interval is 50 m. Note that impression of transverse anticlines and synclines decline gradually as one go away from the southern margin structure.

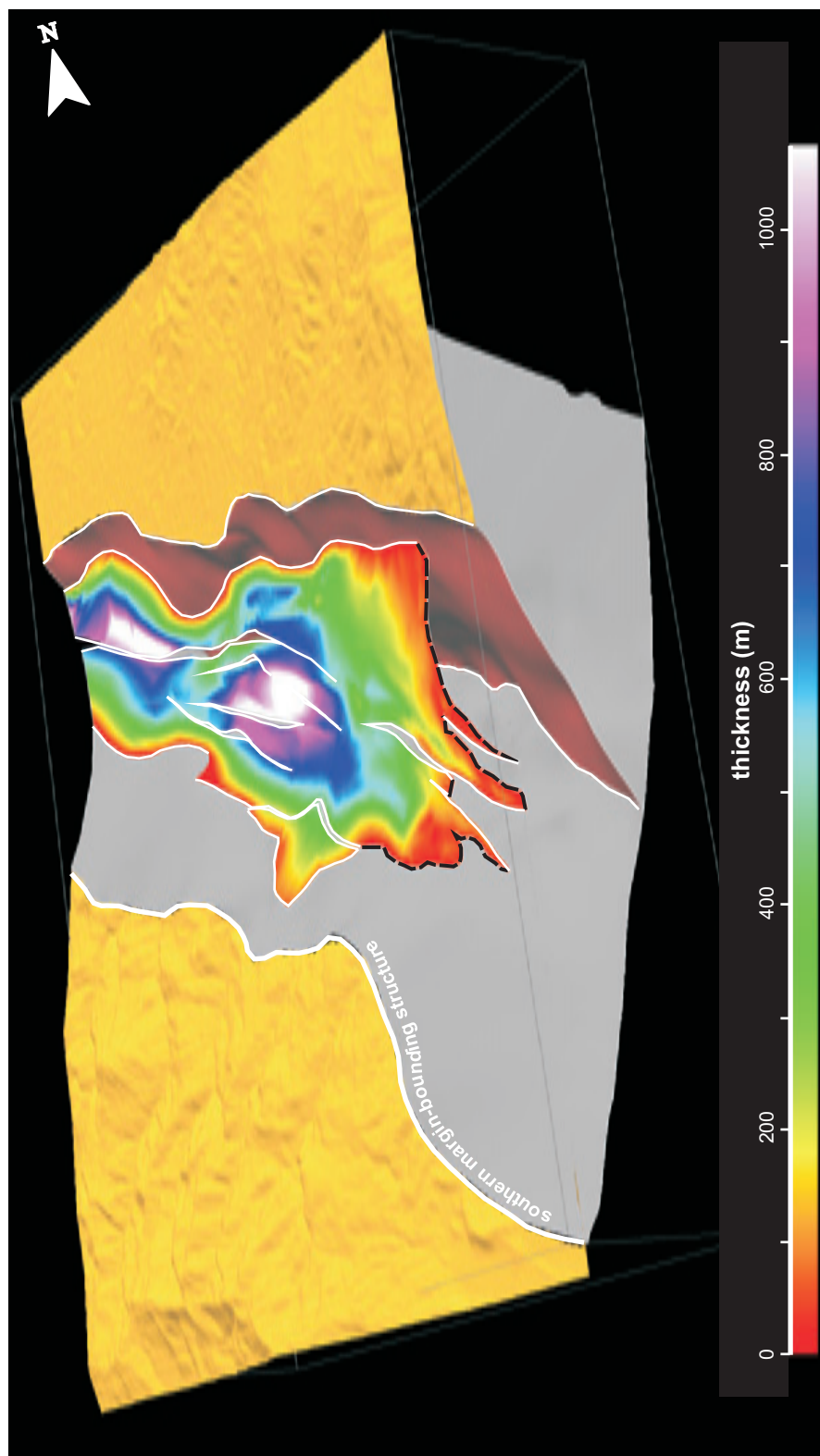


Figure 5.27. Model showing the graben-bounding structures and top of the Çaltılık formation (blue horizon in Figure 5.16). White lines represent fault cutoffs with intervening fault gaps. The color code on the stratigraphic surface depicts thickness distribution of the Çaltılık formation projected onto this surface. To the east, Çaltılık formation wedges off onto the Alaşehir formation along the dashed-black lines where Alaşehir formation forms a structural high (Figure 5.26). In contrast to Alaşehir formation Çaltılık formation has two separate depocenters, one of which matches with the Alaşehir formation and the other is located further west.

propagation of the graben was probably not the case during this period of deposition (Figure 5.27).

Structural map of the top of the Çaltılık formation also reveals the transverse folds formed within the graben (Figure 5.28). In general, axial traces of these folds correlate well with that of Alaşehir formation as illustrated in Figure 5.26. However, small differences do exist which probably resulted in due to the syn-depositional nature of the folding. As this process controls the distribution of the accommodation space in a way to result in more deposition in synclines compared to anticlines, traces of axial planes may vary at different stratigraphic levels. Secondary hanging-wall faults of the southern margin-bounding structure may complicate the folding pattern further as these small-scale faults also follow individual spatio-temporal evolution similar to master graben-bounding structures. In fact, some of the smaller folds may appear as structures specific to certain fault block within the graben fill (Figures 5.26 and 5.28).

5.3.3. Gediz Formation

Gediz formation overlies the Çaltılık formation with a vertical thickness locally reaching up to 700 m (Figure 5.29). In contrast to Alaşehir and Çaltılık formations, there is no well-defined depocenter exist for the Gediz formation. The thickness distribution of the formation is relatively uniform around 400 m, with local and distributed peaks around 700 m. The formation thins towards east in the same way of Çaltılık formation. Yet, the relatively uniform thickness distribution clearly suggests that accommodation space creation is much uniform during the deposition of the Gediz formation compared to the underlying Alaşehir and Çaltılık formations. This may suggest that the Alaşehir subbasin of the Gediz graben was experiencing uniform rates of subsidence in the strike-wise direction during this period. This uniform subsidence may indicate that originally segmented graben bounding faults, which controlled to deposition of Alaşehir and Çaltılık formations, were already amalgamated to form a single and continuous bounding fault during the deposition of the Gediz formation. At the mean time, Salihli subbasin was also subsiding independent of the Alaşehir subbasin. Lateral thickness variation together with transverse folding observed in the Gediz formation in Salihli subbasin may suggest that this basin, as well, were not acting as a single basin but composed of a number of interdependent smaller subbasins (Figure 5.23).

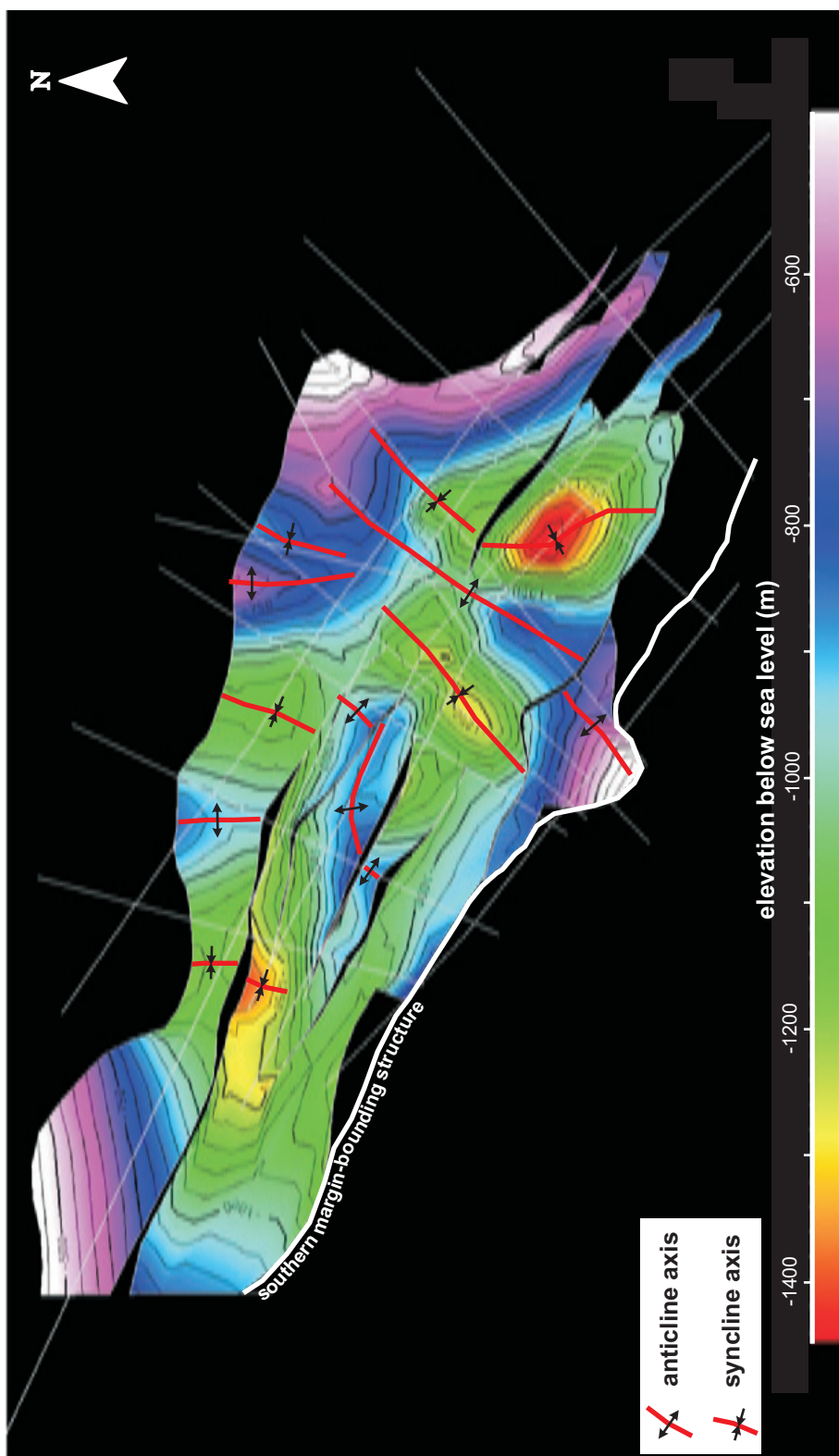


Figure 5.28. Structural map of the top of the Çaltılık formation. Contour interval is 50 m. Transverse anticlines and synclines are observable on this surface as well. In general, folds observed on this surface correlate with that of Alaşehir formation in Figure 5.26. However, there are some differences of axial traces among the Alaşehir and Çaltılık formations due to the fact that folding is syn-depositional and the position of axial planes are modified in each separate stratigraphic units.

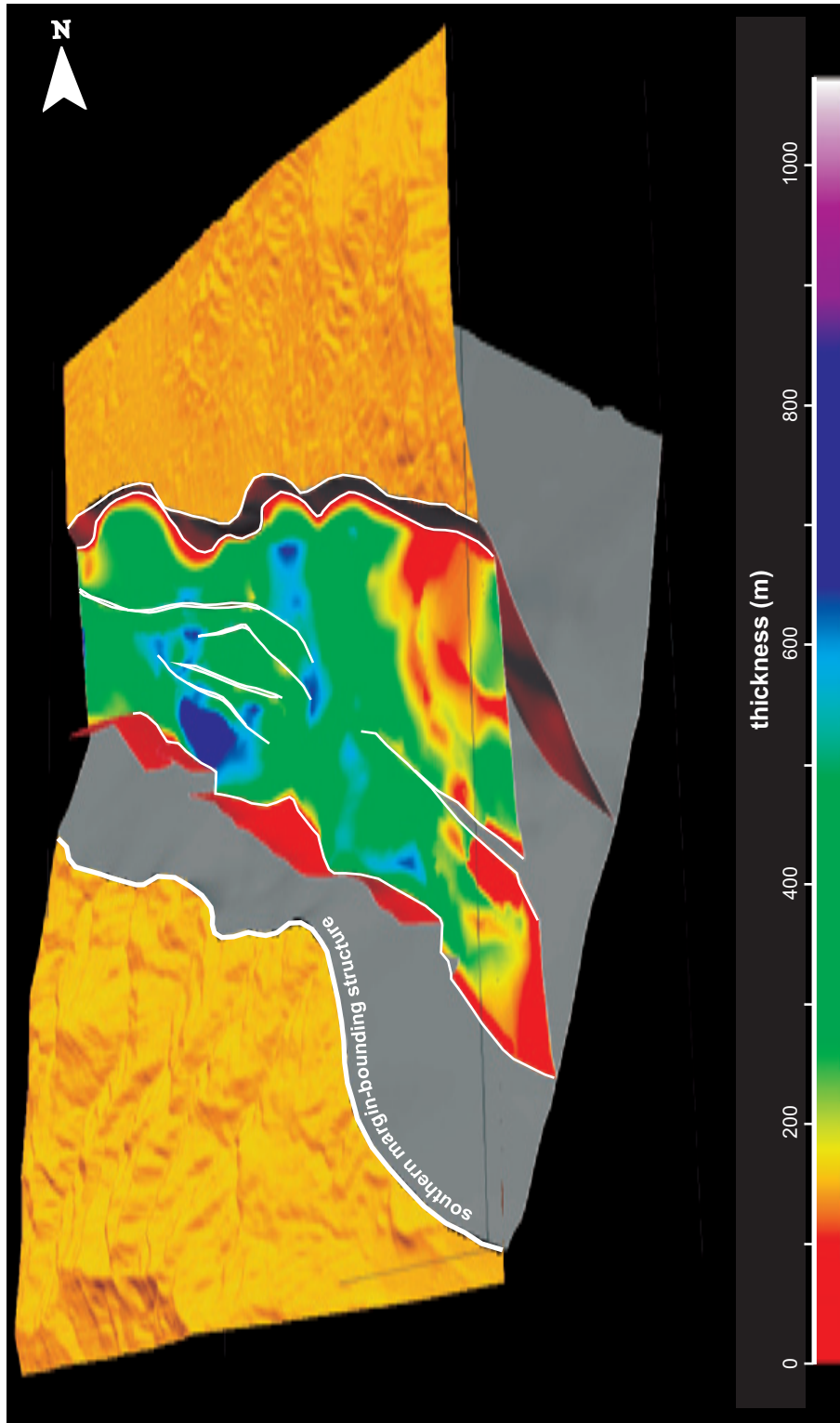


Figure 5.29. Model showing the graben-bounding structures and top of the Gediz formation (green horizon in Figure 5.16). White lines represent fault cutoffs with intervening fault gaps. The color code on the stratigraphic surface depicts thickness distribution of the Gediz formation projected onto this surface. Between the southern margin-bounding structure and the pink fault, the Gediz formation exposes, therefore this surface is eroded. In contrast to Alaşehir and Çaltılık formations, the Gediz formation displays more uniform thickness distribution without a well-defined depocenter(s). Formation gradually thins towards east.

Structural contour map of the top of the Gediz formation also discloses transverse folds of the graben. Among these transverse folds, the major ones still correlates reasonably with that of underlying Alaşehir and Çaltılık formations. However, this structural map also reveals some longitudinal folds (Schlische, 1995) that formed in close association to the normal faults. These folds trend parallel/subparallel to the second-order normal faults within the graben fill and probably formed by drag or rollover processes (see top of Gediz formation in Figure 5.17). Competing interaction between the transverse folding and longitudinal folding may create doubly plunging dome-like or bowl-like structures, which can be locally observed in the structural contour maps (Figures 5.26, 5.28 and 5.30).

5.3.4. Pliocene to Quaternary Deposits

Pliocene to Quaternary deposits include Kaletepe formation, Bintepeleler formation and the distal and proximal Quaternary alluvium of the modern graben floor (Figure 5.24). There is not enough evidence on seismic sections to differentiate these units properly. Therefore, they were treated as a single seismic stratigraphic unit that overlies the Gediz formation and reaches up to the modern graben floor.

Thickness distribution of these deposits is interesting with multiple depocenters exceeding 1000 m vertical thicknesses. These depocenters correlates very well with the synclines identified on the top of the Gediz formation (Figure 5.31). Hence, normal-fault related folding in the underlying units including both transverse and longitudinal folding controlled the distribution of the accommodation space during the Pliocene / Quaternary depositional period and resulted in thickening of the unit in synclines and thinning of the units in anticlines. This period is also important for the connection of Salihli and Alaşehir subbasins. The two subbasins, which were independent during most of the graben's evolution, finally merged together and started to subside jointly (Figure 5.23).

Data from the Gediz Graben revealed that the distribution of Neogene sedimentary units within the basin is a function of evolutionary path of the graben. Evidently, the basin experiences variable rate of subsidence in strike-wise direction. This not only controlled the thickness distribution of the sedimentary units but also initiation time of the sedimentation at different parts of the basin (e.g., Alaşehir and Salihli subbasins in Figure 5.23). Expecting a uniform distribution of sedimentary units in thickness and age along the graben strike is an unrealistic approach for

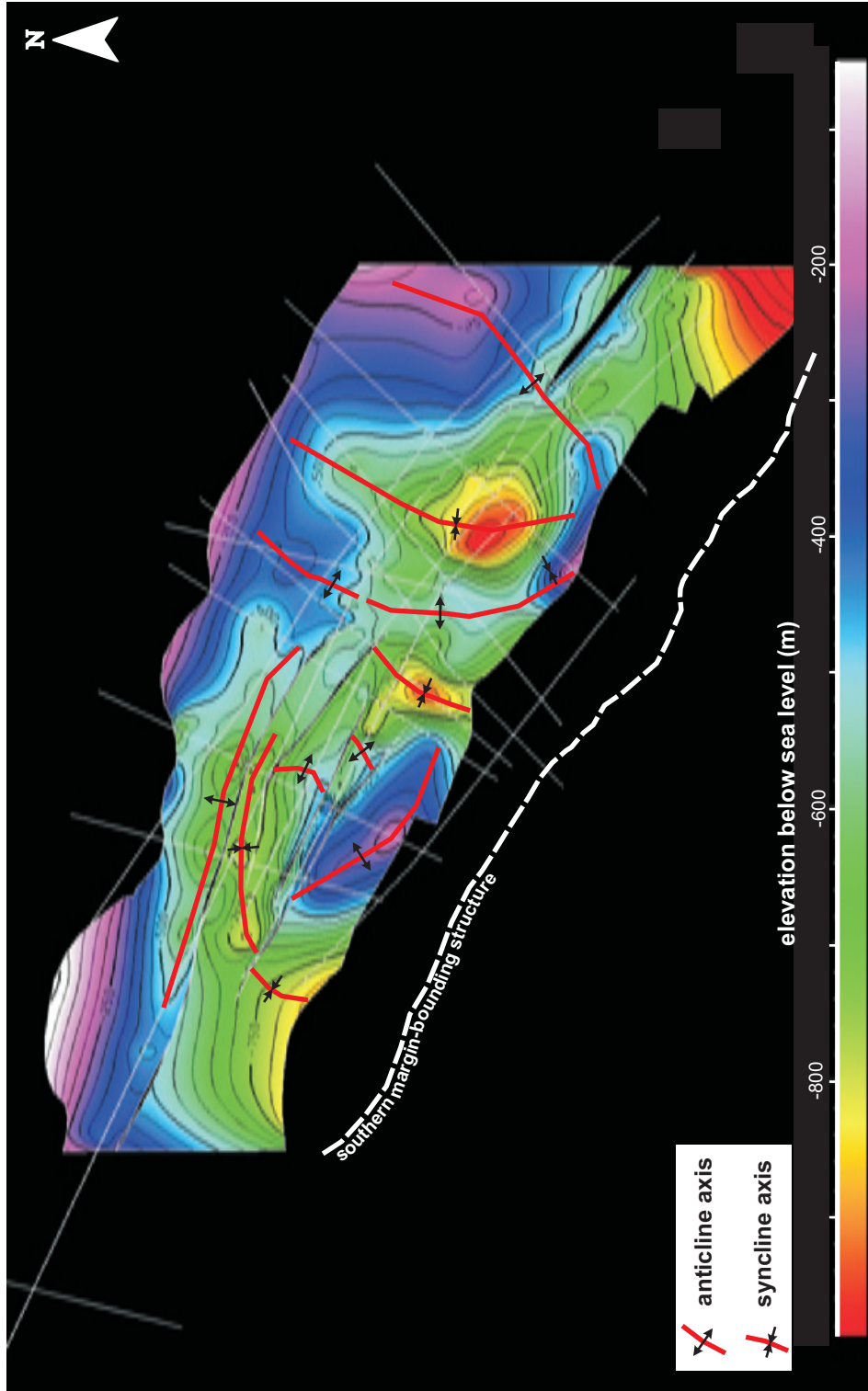


Figure 5.30. Structural map of the top of the Gediz formation. Contour interval is 50 m. Transverse anticlines and synclines are observable on this surface as well.

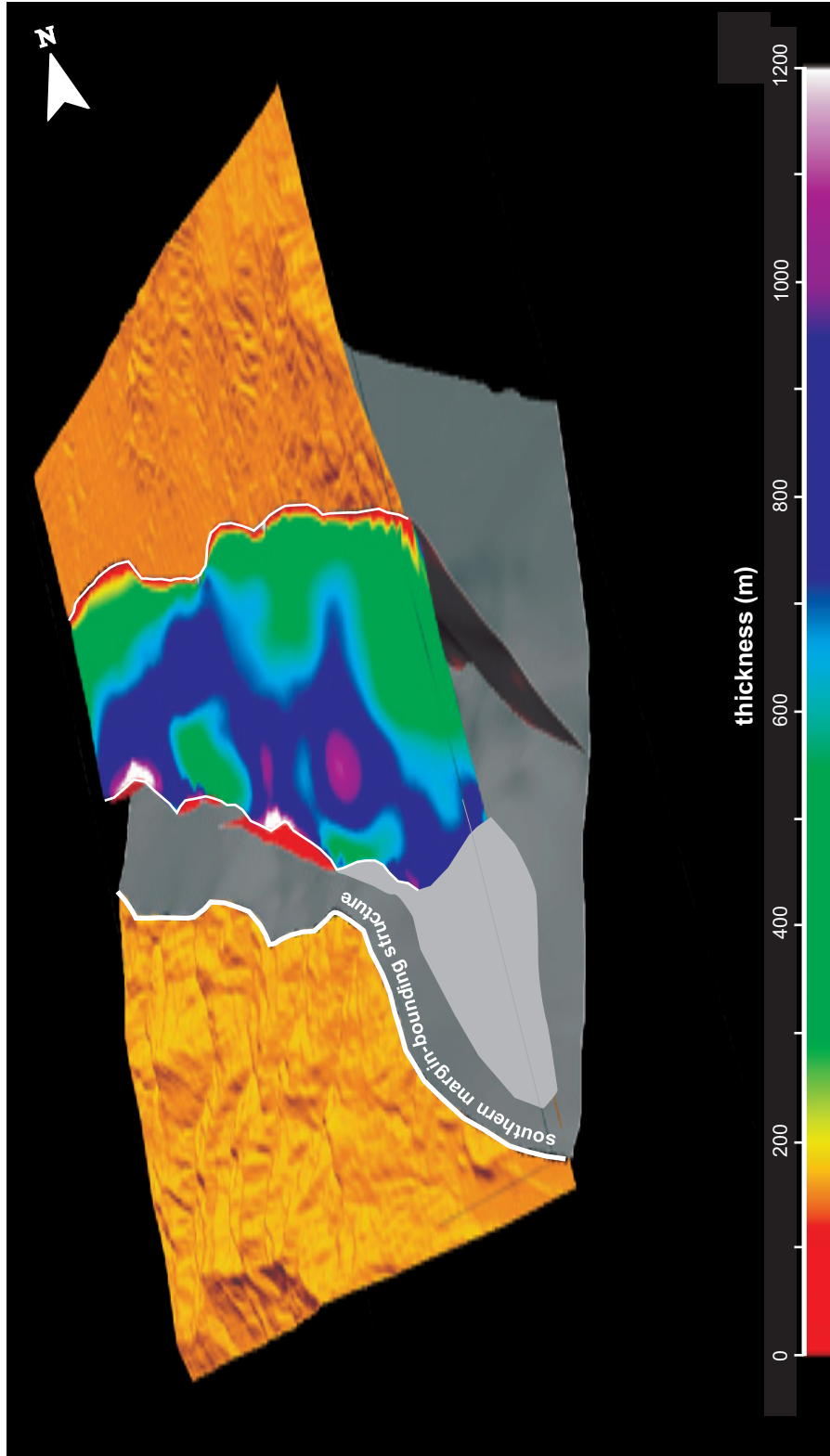


Figure 5.31. Model showing the graben bounding structures and the modern graben floor. White lines represent fault cutoffs with intervening fault gaps. The color code on the stratigraphic surface depicts thickness distribution of the Pliocene to Quaternary deposits projected onto the graben floor. The location of depocenters correlates very well with the synclines identified on the top of Gediz formation (Figure 5.30).

grabens. Continental setting of the Gediz Graben further complicates the graben fill by imposing lateral facies variation and interfingering in short distances as described in detail in Chapter 2. Although all these factors make it difficult to understand continental graben basins, efforts benefit significantly from accurate understanding of the controlling deformation and boundary structures (e.g. Chapters 3 and 4).

5.4. Correlation of Surface and Subsurface Data

One of the aims of this study is to correlate the surface and subsurface data in a most convenient way to draw the complete picture of the graben basin. Surface and subsurface data benefits mutually from this effort. Geological understanding acquired through high resolution but discontinuous surface data undeniably improves the interpretation of the subsurface data. On the other hand, low resolution but continuous subsurface data reveals the spatial distribution of the geologic phenomenon more accurately than the surface data. Furthermore, this effort tests the surface observations, which are limited to basin margins, with the subsurface for their basin-wide distribution.

Several transverse cross-sections were constructed starting from southern horst block of the graben, passing across the graben basin and finalizing at the northern horst block (Figures 5.32 and 5.33). These cross-sections served very well to depict the entire geometry of the graben basin. As defined by surface observations, the graben has an asymmetric geometry in general with most active site being the southern margin. Cross sections A-A' to E-E' in Figures 5.32 and 5.33 clearly illustrates this fact. In all these sections, the depocenter of the graben is located closer to southern margin-bounding structure indicating that more accommodation space is created on this site compared to the northern margin. This inevitably influenced the thickness distribution of the units with a distinct general thinning towards north (Figures 5.32 and 5.33). However, the uppermost stratigraphic unit including Pliocene to Quaternary deposits fails to follow this general trend with more uniformly distributed thickness on both margins. This suggests that subsidence of the graben block was rather equally partitioned among the northern and southern margin structures during this period and the activity of the northern margin structure is mostly limited with the uppermost unit.

Cross-sections F-F' and G-G' in Figure 5.33 are slightly different than the rest of the cross-sections with relatively symmetrical appearance of the graben fill. In

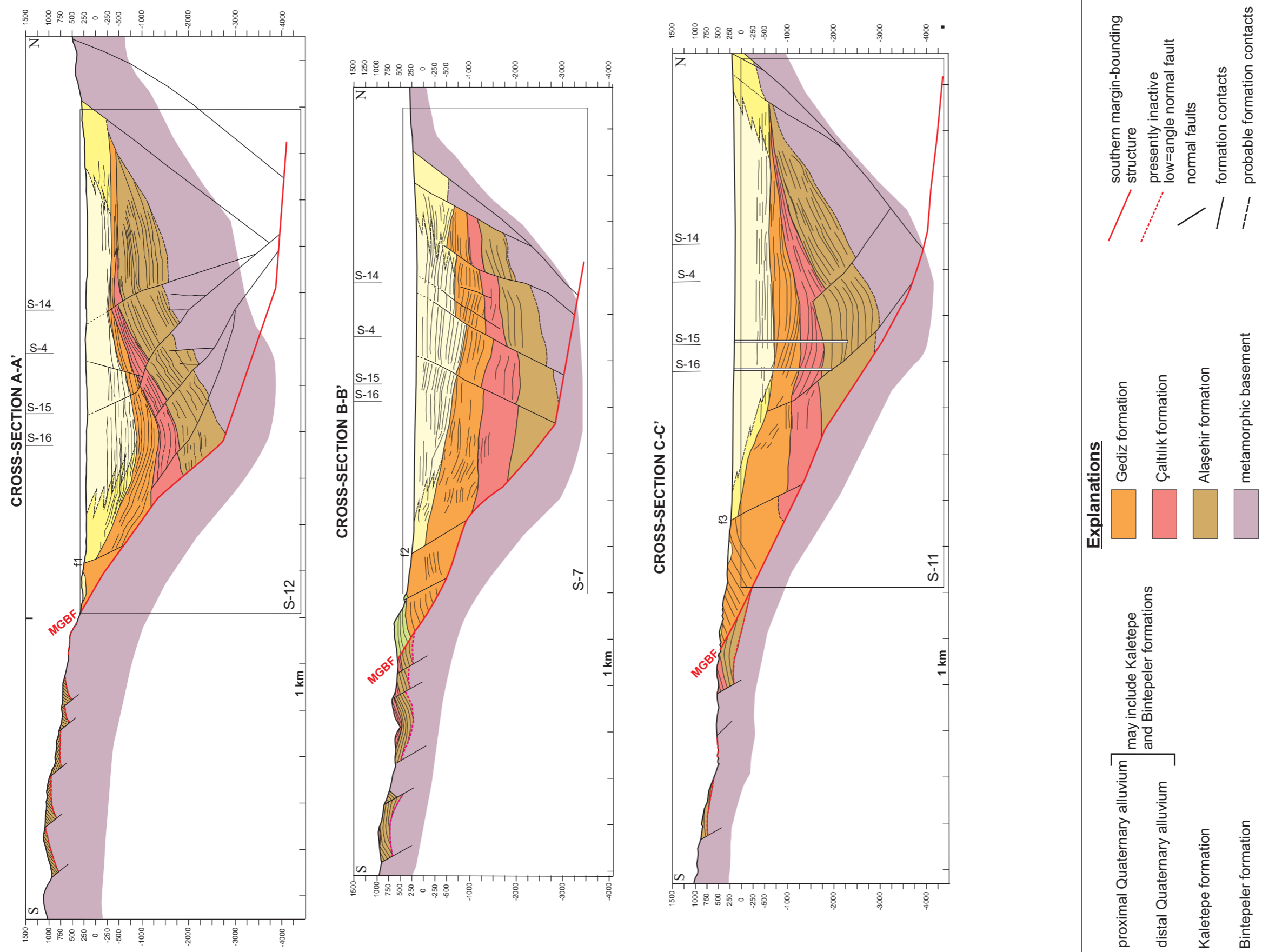


Figure 5.32. Transverse cross-sections depicting the geology of the Gediz Graben in Alaşehir subbasin. See Figure 2.8 for the color coding of the formations. Section locations are illustrated in Figure 5.24. Rectangular box in cross-sections illustrates the coverage of the labeled seismic section. Uninterpreted seismic sections are given in Appendix VI. Rest of the sections are based on surface geology given in Figure 5.23. Surface topography was extracted from 1/25,000 scale topographical maps. MGBF stands for master graben bounding fault in Figure 5.24 which represent surface trace of the southern margin-bounding structure.

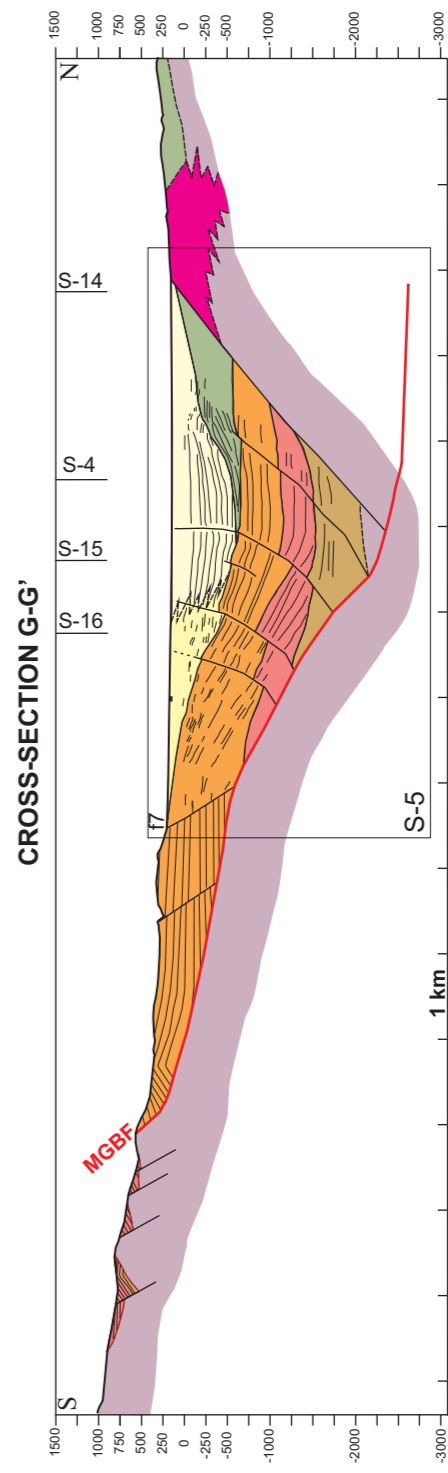
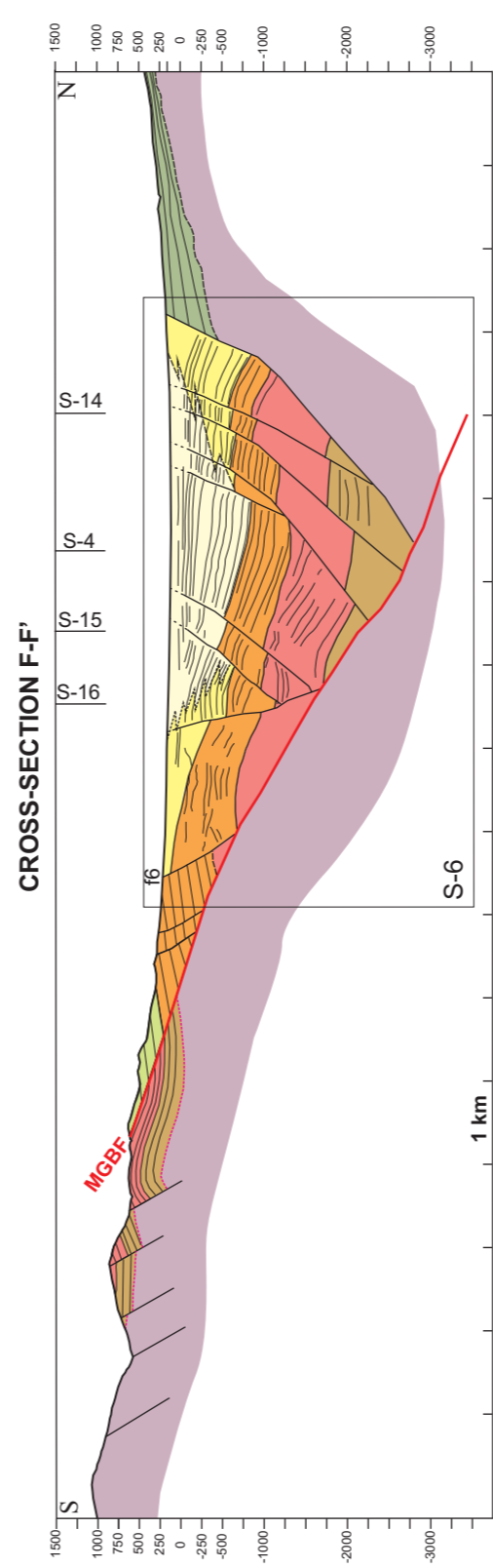
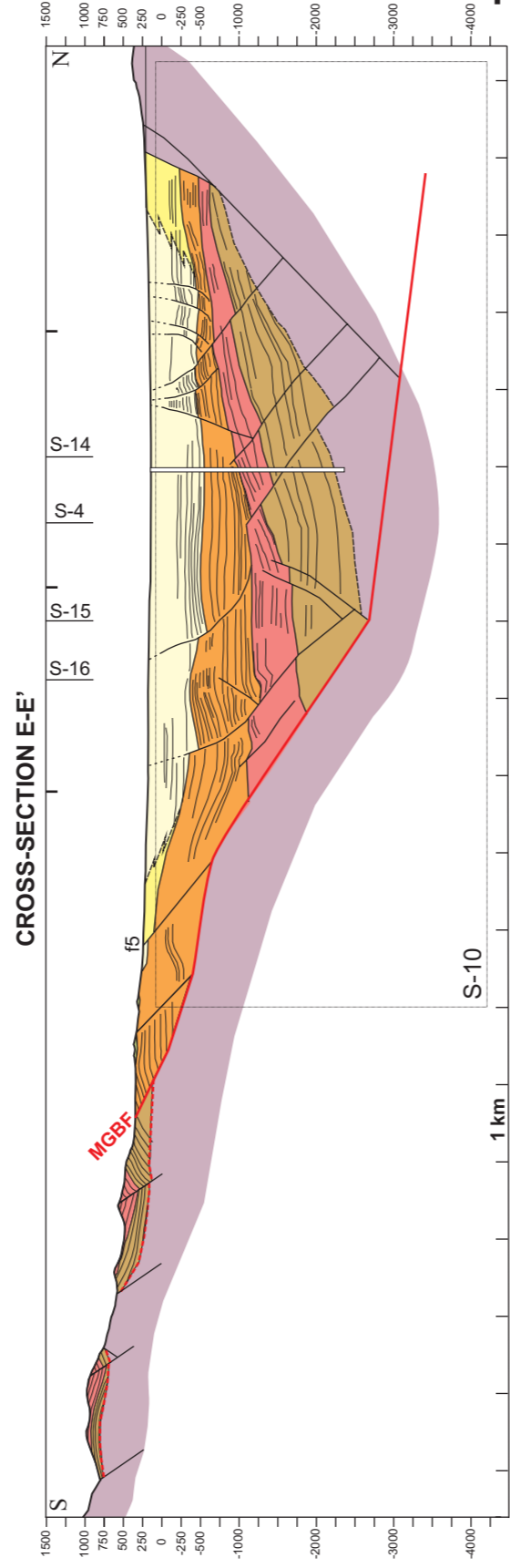
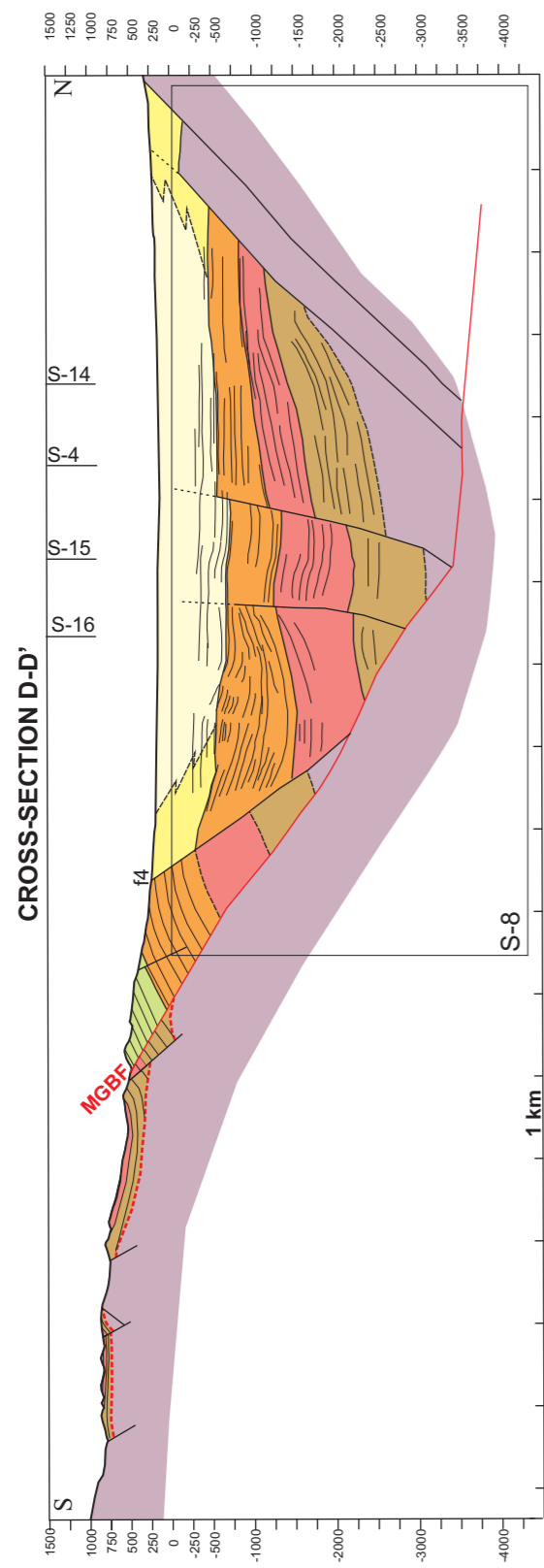


Figure 5.33. Transverse cross-sections depicting the geology of the Gediz Graben in Alaşehir subbasin. See Figure 2.8 for the color coding of the formations. Section locations are illustrated in Figure 5.24. Rectangular box in cross-sections illustrates the coverage of the labeled seismic section. Uninterpreted seismic sections are given in Appendix VI. Rest of the sections are based on surface geology given in Figure 5.23. Surface topography was extracted from 1/25,000 scale topographical maps. See Figure 5.32 for explanations.

these sections, no distinct trend can be observed in formation thickness except for the Gediz formation, which thins towards north as in the most of the sections. Lack of northward-thinning trend for Alaşehir and Çaltılık formations in these sections can be attributed to either limited inclusion of these formations in cross-sectional area or unfavorable orientation of the sections with respect to paleo-basin geometry in this part of the graben. In fact, these sections are located very close to the margins of the depositional realm of the Alaşehir formation and can also be influenced by basin margin complications (Figures 5.24, 5.25 and 5.26). Another specific feature of the cross-sections F-F' and G-G' is that they are located next to the exposures of the Bintepeleler formation to the north. This formation is only observable NW of the Alaşehir subbasin. Fortunately, cross-section G-G' resolves a wedge-like sedimentary package lying against to northern margin structure immediately adjacent to the exposure realm of the Bintepeleler formation. The geometry and internal stratification of this wedge suggests that it is a southward-prograding unit, sourced by northern margin of the graben. Consequently, this wedge correlates well with the exposures and depositional characteristics of the Bintepeleler formation and most probably it is the continuation of this formation within the graben. This unit cannot be resolved in cross-section F-F' and is probably included within the uppermost unit of Pliocene to Quaternary deposits.

In cross-section G-G', genetic relation is obvious between the northern margin structure and the Bintepeleler formation as represented by the depositional wedge. This relation is key to estimate the age of northern margin structure, as increased rate of deposition on this margin indicates the initiated activity of the structure. Because the wedge directly overlies the Gediz formation and underlies the Quaternary alluvium, its deposition should postdate Gediz formation and predates Quaternary alluvium. From this stratigraphic position, Bintepeleler formation can be correlated with the Kaletepe formation of the southern margin (see Chapter 2). Unfortunately, Kaletepe formation cannot be resolved in the seismic sections. However, surface observation clearly determines stratigraphic position of this formation above the Gediz formation and below the Quaternary alluvium (Figure 5.24).

An obvious observation made across the surface exposures is the distinct cross-cutting relationship between the low-angle normal fault and the high-angle normal faults to the south of the master graben-bounding fault (Figures 3.19, 5.24,

5.32 and 5.33). When this observation was extended towards the subsurface through the constructed cross-sections, it is become evident that no such relation exist basinward. The imaged southern margin-bounding structure of the graben extend without any offset, evidently become shallower towards the south in some sections and finally disappear in the poorly imaged southern edge of the sections (Figures 5.8, 5.11, 5.12, 5.14, 5.16, 5.17). When the southernmost limit of the imaged fault is extended with approximately same dip amount, it correlates very well with the master graben-bounding fault in Figure 5.24. Consequently, the imaged southern margin-bounding structure in the seismic sections is correlated with the master graben-bounding fault mapped in the outcrop exposures (Figures 5.32 and 5.33). Although they are not imaged very well in the seismic sections, second-order faults exposing immediately north of the MGBF in Figure 5.24 probably merges into the master structure because there is no evidence of offset on the master structure imposed by the second-order faults at this part (Figures 5.32 and 5.33). The observed cross-cutting relationship between the low-angle and high-angle normal faults is specific to the south of the MGBF in Alaşehir subbasin (Figure 5.24).

The MGBF is probably a dynamic structure changing its geometry with accumulating extension. This change in large scale may be controlled by rolling hinge process that developed in response to footwall rebound (Figure 5.35A) (Buck, 1988, 1991). As the rolling model predicts, MGBF is composed of steeply- and shallowly-dipping segments to form flat and ramp geometry (Figure 5.13A). This geometry is not static but alters in terms of segment lengths and fault dips, as the locus of incremental uplift migrates through the footwall with rolling hinges (Spencer, 1994; Buck, 1988; Wernicke and Axen, 1988). However, activity of a potential deeper structure will also influences the geometry of the southern margin-bounding structure (i.e., the MGBF) as well. Although, no concrete evidence of a deeper structure below the southern margin-bounding structure is available from surface and subsurface data, existence of such a structure is not beyond the possibility. In fact, the high-angle normal faults, which cut and offset the low-angle normal fault south of the MGBF, could be linked to the almost flat lowermost segment of the southern margin-bounding structure by means of a deeper structure (Figures 5.32 and 5.33). A forward model constructed in Figure 5.34 deals with the operation of two structures that are linked to the same deeper detachment in a similar way speculated above (Figure 5.34). The forward model is based on extensional

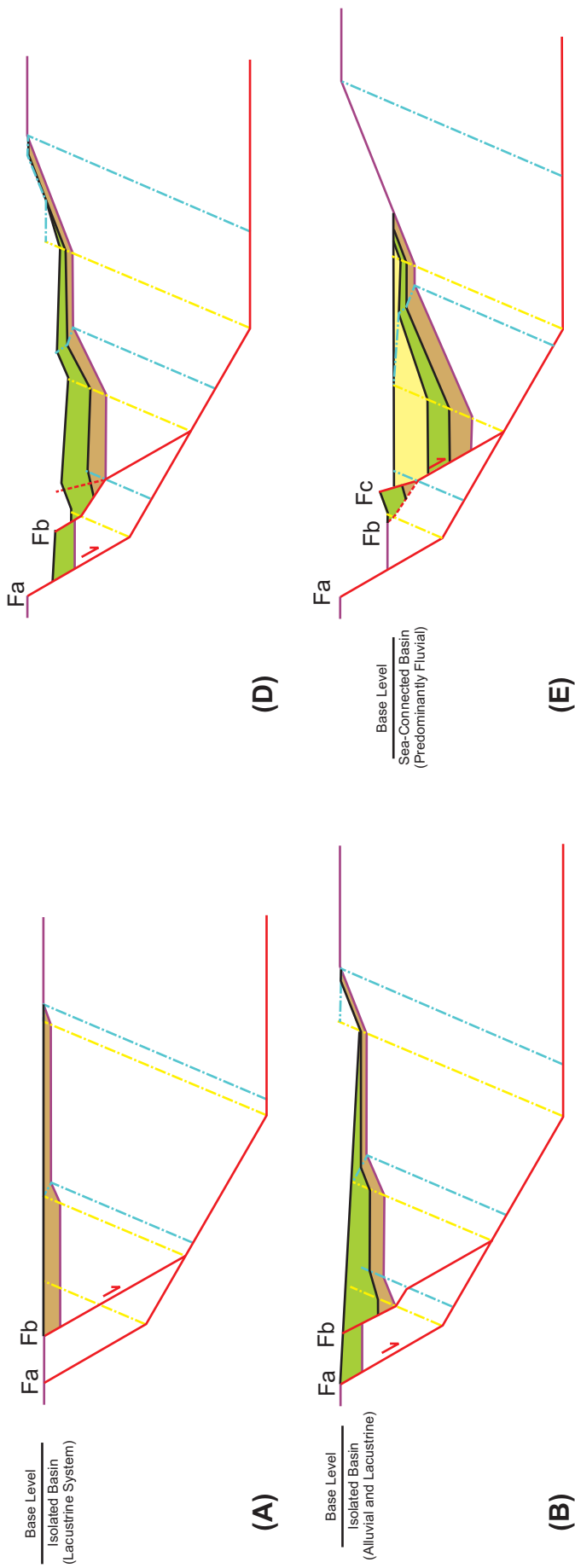


Figure 5.34. Forward model illustrating simultaneous activity of two structures that are linked to the same detachment at depth. A through E represent progressive stages. Arrow on the fault plane indicates the active fault at this stage. Sediment accumulates simultaneously in the graben. At the final stage E, base level drops due to accumulated extension and the upper segment of Fb become flattened. As this segment doesn't have favorable dip amount to sustain its activity, it is become abandoned and Fc forms to keep up with the extension. The constructed models are based on extensional fault bend folding theory (Figure 5.9).

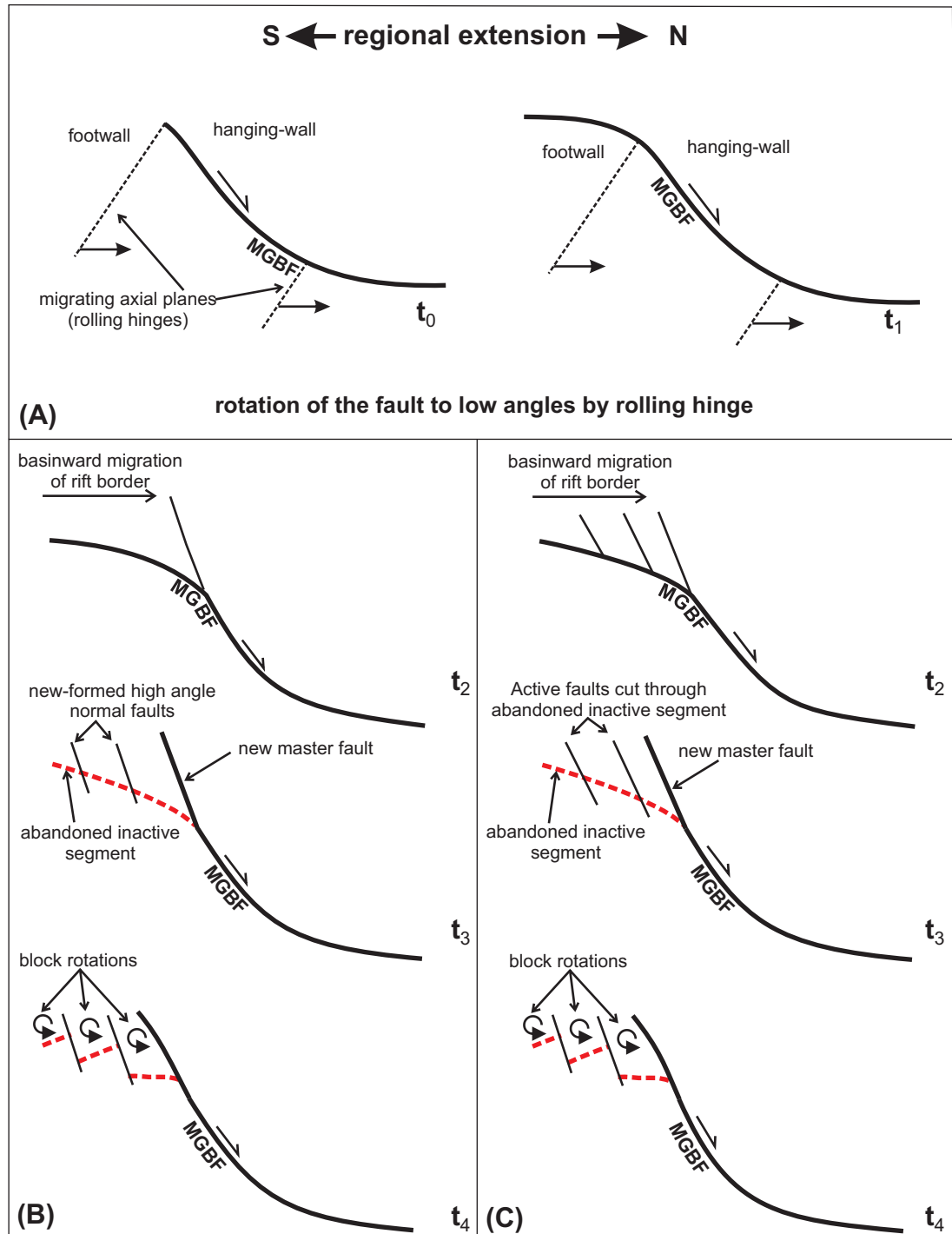


Figure 5.35. Schematic diagram illustrating the structural evolution of the southern margin of the Gediz Graben in the continuum of deformation. **(A)** The MGBF rotates to low angles by rolling hinge process due to footwall rebound (e.g., Buck, 1988; Axen and Bartley, 1997). The uppermost segment of the MGBF become inactive when it is easier for the system to break a new fault of favorable dip. Two alternative paths **(B)** and **(C)** were proposed to explain the observed cross cutting relationship between the inactive low angle fault and new-formed high angle faults. See text for the discussion of the two scenarios. t_0 , t_1 , t_2 , t_3 and t_4 illustrates the sequential evolution in time.

fault-bend folding theories of Xiao and Suppe (1992) and Shaw *et al.* (1997) (Figure 5.9). Note in the model that, activity of the deeper structure (Fa) influences geometry of the upper structure (Fb) and results in flattening of the segment of Fb falling into rollover panel of the Fa (Figure 5.34). With dropping base level of erosion, this flattened segment may become exposed on the graben margin. Because lower dip amounts that the upper segment of Fb reached is not favorable to sustain its activity, Fc forms after some point and the flattened segment of Fb is become abandoned (Figure 5.34). Similar geometric relations to this simplified model can be observed in most of the transverse cross-sections in Figures 5.32 and 5.33 in which MGBF represents the Fc and the presently inactive low-angle normal faults south of the MGBF represents the Fb. Therefore, similar processes predicted by the forward model might be taking place along the southern margin of the Gediz Graben.

Whether controlled by the rolling-hinge process (Figure 5.35A) or simultaneous activity of a deeper structure (Figure 5.34), the segment of the southern margin-bounding structure that is rotated to shallower dip amount will be abandoned by forming a new fault to the north (Figure 5.35B and C). This is also conformable with the basinward migration of the rift borders. MGBF located north of the presently inactive low-angle normal fault is probably a current example to this process (Figures 5.24, 5.32 and 5.33). Once the MGBF invaded the system and start to operate as the master fault, the low-angle segment of the southern margin-bounding structure that is left behind became the presently low-angle, inactive normal fault, i.e., the detachment fault. With time and accumulating extension, it is likely that this process will probably repeat itself by second order faults (f1, f2, f3, f4, f5, f6 and f7 in Figures 5.32 and 5.33) located north of the MGBF, and the uppermost low-angle segment of the southern margin-bounding structure will be chopped off again and abandoned (Figures 5.32 and 5.33). Although, these candidate faults (f1 through f7) that bounds the graben floor is not a single fault but comprises overlapping segments (Figure 5.24), they will probably amalgamate into a single fault with time before they start to operate as the master fault.

At this point, it is critical to assess the cross-cutting relationship between the low-angle and high-angle faults south of the MGBF because this relationship is not defined by the available rolling hinge models (Spencer, 1984; Buck, 1988, 1991; Wernicke and Axen, 1988). Nevertheless, simple reasoning can integrate the cross-cutting relationship with the rolling-hinge model (Figure 5.35B and C). As the

inactive low-angle normal fault is unfavorable to keep up with the extension, faults of more favorable dip is needed because the region south of the MGBF is still exposed to the extension. These high-angle faults with more favorable dip to accommodate the extension can form shortly after the new master fault in order to cut and offset the low-angle fault (Figure 5.35B). Alternatively, these high angle faults can form before the new master fault conformable to basinward migration. Once the low angle fault is abandoned by the new master fault, the high-angle faults cut and offset the low-angle fault (Figure 5.35C). Whatever the sequence of formation, these high-angle faults will also result in rotation and back tilting of the low angle fault cut into pieces and produce geometries similar to those observed to the south of MGBF in constructed cross-sections (Figures 5.32 and 5.33). The entire process with two alternatives is schematically illustrated in Figure 5.35.

As transverse cross-sections provide significant clues to the character and evolution of the graben-bounding structures, longitudinal cross-sections in Figures 5.36 and 5.37 illustrates how subsidence rate vary laterally along the graben basin. Thickness variations of the sedimentary units are clearly evident in these longitudinal sections, which is already discussed in Figure 5.23. Lithostratigraphic formations thin to the east and/or to the west and finally wedges out, although the morphologic expression of the graben on the surface is continuous (Figure 5.1). As discussed earlier in this chapter, transverse folds forming approximately at orthogonal orientation to graben trend are also observable as an indication of displacement gradients arose along the graben-bounding structures. It should be emphasized that progressive evolution of the graben in time is a spatial phenomenon, which needs assessments not only in transverse direction to the graben trend but also along strike direction.

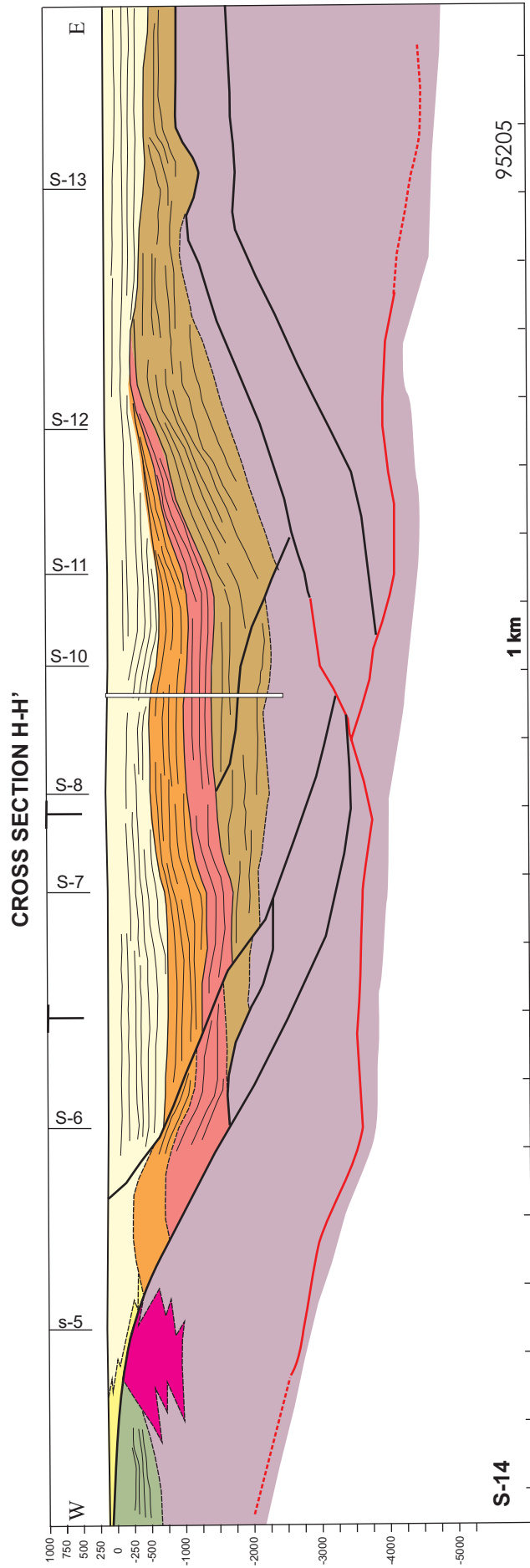


Figure 5.36. Longitudinal cross section passing along the Alaşehir subbasin. See Figure 5.24 for location of the cross section and Figure 5.32 for the explanations. As this cross-section is the most distant one to the MGBF, impression of transverse folds are diminished although they can still be observed.

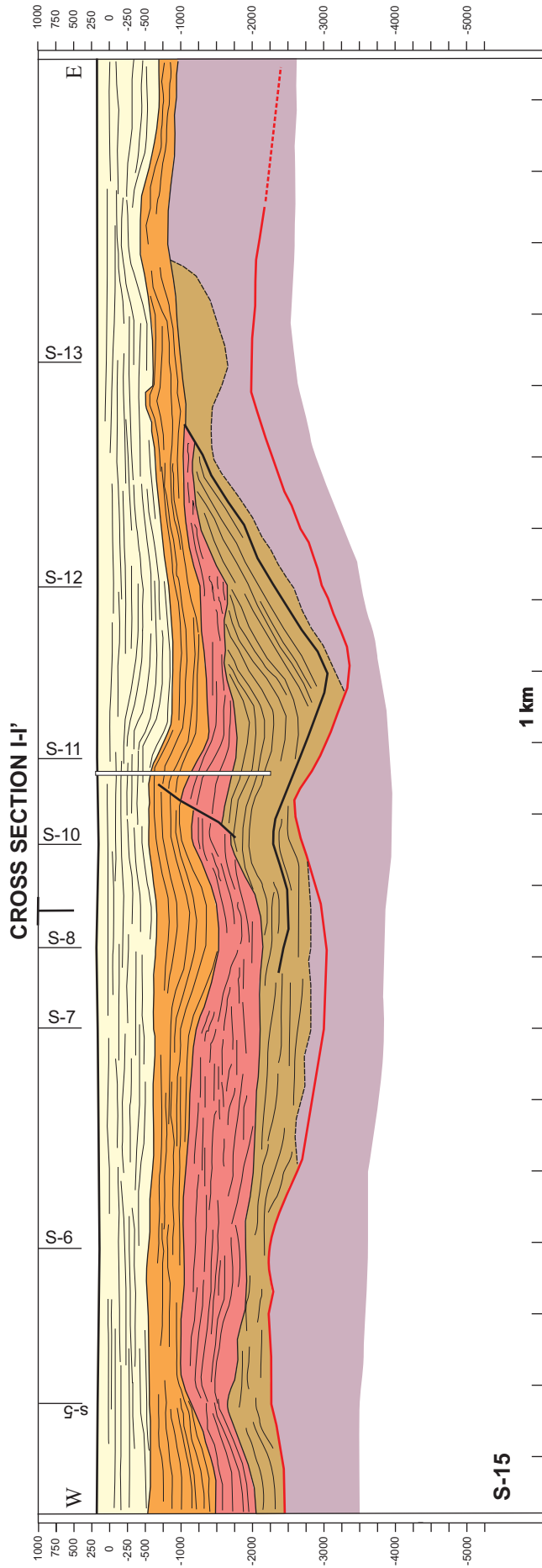


Figure 5.37. Longitudinal cross section passing along the Alaşehir subbasin. See Figure 5.24 for location of the cross section and Figure 5.32 for the explanations. Transverse folds can be easily observed on the cross-section.

CHAPTER 6

FOLDING IN THE GRABEN FILL

Folds are extraordinary displays of strain and illustrate how the original shapes of rock bodies may change during the course of deformation. They occur in almost limitless geometries in response to competing folding mechanisms controlled not only by nature of active stress field but also by mean ductility and mechanical influence of layering during the deformation. Traditionally, folded strata and process of folding have been regarded as the products of contractional deformation arising under compressive stresses (Davis, 1984; Twiss and Moores, 1992; Davis and Reynolds, 1996). Rollover folds are considered as an exception to this because they form due to slip above listric normal faults in extensional settings (e.g., Dula, 1991; Xiao and Suppe, 1992; Shaw *et al.*, 1997). Nevertheless, studies carried out during the last few decades revealed the fact that folding in extensional settings is not limited with the rollover folds and it is a more common phenomenon than previously thought. Consequently, numerous recent studies documented the occurrences of folds and their modes of formation in extensional tectonic settings (e.g., Schlische, 1995; Janecke *et al.*, 1998; Khalil and McClay, 2002;).

Folds constitute a part within dominantly extension-related deformation pattern of the Gediz Graben. They occur at various styles and attitudes. Although surface observations usually recognize folds oriented parallel or slightly oblique to the graben trend, seismic data are able to depict the existence of folds oriented transverse to the graben strike as well. Observed folds vary in shape from broad non-plunging folds to tight and overturned plunging folds. Sometimes, surface observations can recognize very complicated deformation patterns associated with the folded zones. Intensity of folding varies apparently among the lithostratigraphic units and even spatially within the same unit.

Folds reported from the Gediz Graben became a subject of debate if these folds are extensional in origin or they represent a period of compression during the evolution of the Gediz Graben (Koçyiğit *et al.*, 1999a; Seyitoğlu *et al.*, 2000; Sözbilir, 2001, 2002; Bozkurt, 2002; Yusufoglu, 2002; Seyitoğlu *et al.*, 2002). Unfortunately, answer to this question is not simple, as some of the folds in the Gediz Graben appear completely to be extensional in origin. These folds are associated with the movements on normal fault planes and form in response to fault geometry and lateral displacement gradients on the fault surfaces (e.g. Schlische, 1995). On the other hand, increasing number of recent studies in the western Anatolia reports a N–S-oriented short phase of compression that potentially relates some of the observed folding (Koçyiğit *et al.*, 1999a; Bozkurt, 2003; Bozkurt and Rojay, 2005; Bozkurt and Mittweide, 2005).

This chapter investigates folds of the Gediz Graben, using surface and subsurface data in order to assess their mode of formation. Data acquired from outcrop exposures are analyzed by statistical methods of stereographic projection to document the general attitude characteristics. Field photos and schematic cross-sections depict the fold geometries and associated deformation features. Interpretation of seismic data depicts folding of stratigraphic horizons by 2-D geological cross-sections and by structural contour maps. Modeling efforts intend to explain the origin of transverse folding observed in seismic sections.

6.1. Folds and Process of Folding: A Review

Folds can simply be described as wave-like undulations emphasized by bedding, foliation or any other originally planar surface. They have been classified in many different ways from purely descriptive classifications to those honoring the fold-forming mechanisms (e.g., Fleuty, 1964; Ramsay, 1967; Hudleston, 1973; Donath and Parker 1964). Unfortunately, every classification has defects inherited from its specific point of view and no one is ideal. Perhaps, the best classification is the one that best suits the main aim of the intended geological study.

Two mechanisms are influential during folding process, namely flexural folding and passive folding (Donath and Parker 1964). Flexural folding takes place when the mechanical influence of layering is strong and the mean ductility of the rock volume is moderate to low (Figure 6.1). It may take place in two different ways and represents the two end-member processes: flexural-slip and flexural-flow (Figure

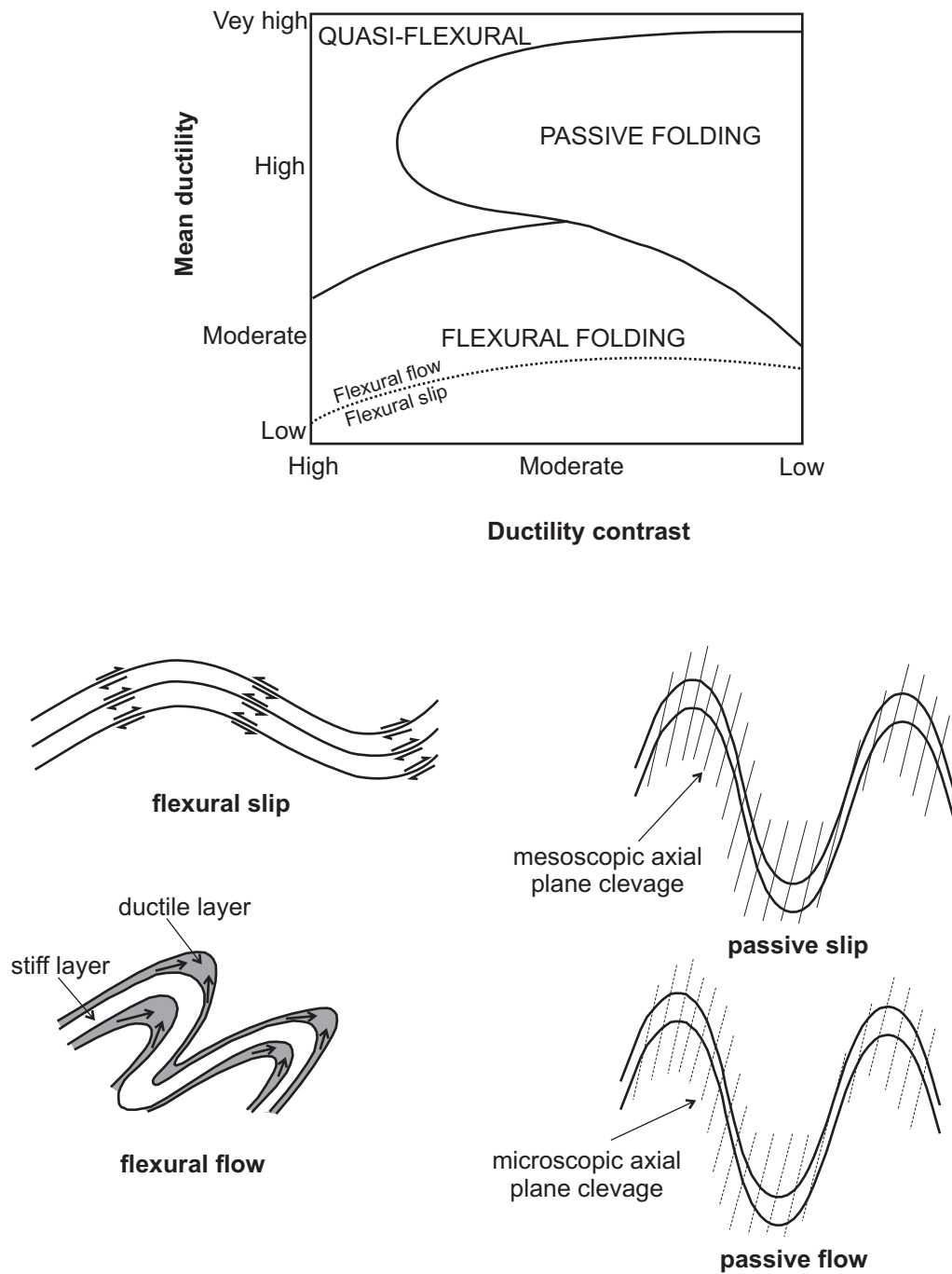


Figure 6.1. Folding is commonly achieved by two major mechanisms: flexural folding and passive folding. Flexural folding includes flexural-slip and flexural-flow processes under the mechanical influence of layering. Passive folding can be considered as fake folding in which layer become folded by means of mesoscopic or microscopic axial plane cleavages without really being flexed or bent. Folds falling out of these two groups do exist and are considered to form by quasi-flexural processes. Modified from Hatcher (1990).

6.1). Flexural-slip folds form by buckling, bending and slip parallel to layering. Strong and stiff layers with contacts having low cohesive strength are good candidates for this process. Individual layers that are folded by flexural slip tend to retain their original thickness to form parallel folds (or concentric folds). Layered rocks with strong ductility contrast are prone to flexural-flow process with bending and flexing but without slip parallel to layering (Figure 6.1). In this process strong and stiff layers maintain constant thickness while ductile layers flow to result in thickening across axial zones and thinning along the limbs (Donath and Parker, 1964). The resulting geometry mostly includes non-parallel folds (or similar folds) but may also include some parallel folds. Layered rocks in the upper crust are mostly folded by flexural folding mechanism.

In passive folding mechanism the mechanical influence of layering is very weak or absent and the layering only acts as a strain marker. The rock volume possesses high mean ductility (Figure 6.1). Layers become folded passively without actually being flexed or bent. There are two end-member processes leading to passive folding: (1) passive slip within the volume by means of axial-plane cleavage or (2) passive flow of rock without mesoscopic axial plane cleavage (Donath and Parker, 1964; Davis, 1984). Passive folding is commonly observed in metamorphic rocks or salt, glacial ice and water-saturated sediments that possess uniform ductile properties. Folds that don't fit into either flexural folding or passive folding can be classified as quasi-flexural folding and correspond to disharmonic folds (Figure 6.1) (Hatcher, 1990).

In the scale of a sedimentary basin characterized by layering and predominantly brittle behavior, both compressional and tensional stresses can generate folding, which is generally accompanied by faulting. Compressional stresses commonly lead to folding by means of contractional fault-related folding processes that are associated with thrust and/or reverse faults. Three main mechanisms are defined in the folding process: (1) Upward propagation of faults; i.e. fault-propagation folding, (2) Passage of hanging wall over the fault bends; i.e. fault-bend folding and (3) displacement gradient along bedding-parallel folds; i.e. the detachment folding (e.g., Suppe, 1983; Suppe and Medwedeff, 1990; Shaw *et al.*, 2005). These processes are briefly illustrated in Figure 6.2. Several sub-classes are defined to represent variations from these general cases, such as tri-shear fault-propagation folding (Erslev, 1991), shear fault-bend folding (Suppe *et al.*, 2005) and

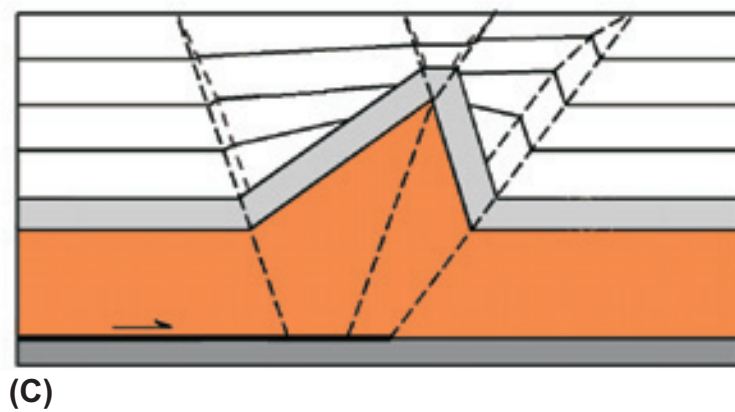
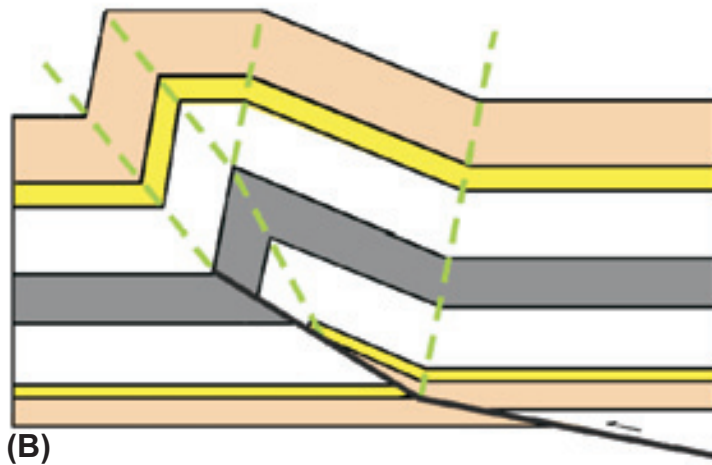
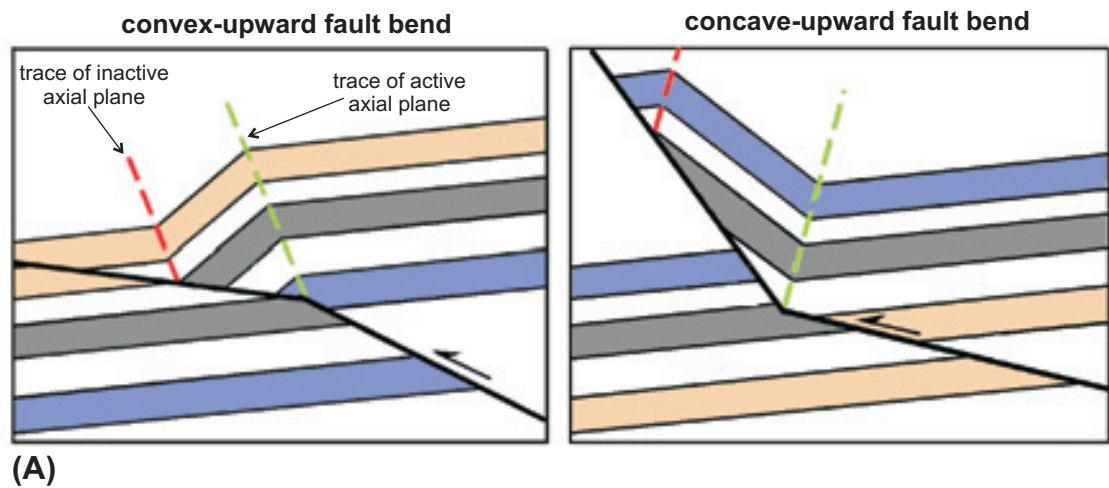


Figure 6.2. Contractional fault-related folding is achieved by means of three major processes: **(A)** fault-bend folding, **(B)** fault-propagation folding and **(C)** detachment folding. From Shaw *et al.* (2005).

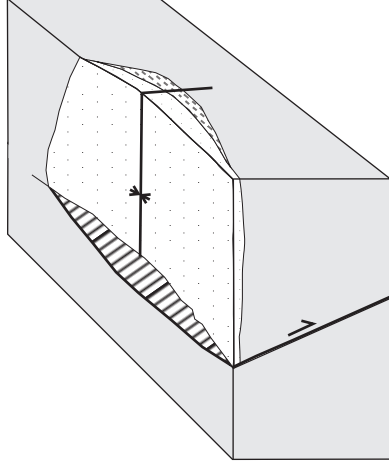
folding related to structural wedges (Medwedeff, 1989). Hinge-line orientation of these folds generally trend parallel or sub-parallel to the associated fault strike and orthogonal to the regional direction of compression. Folds can develop both as asymmetrical structures, indicating the direction of vergence and as symmetrical structures. Less commonly, folding under compressional stress can also take place across zones of transpression along strike-slip faults. Folds in these zones are generally oriented orthogonal or sub-orthogonal to the controlling fault and oblique to the regional direction of compression. Yet, many local factors may influence the fold orientation forming under compressional stresses.

Folds can also form under tensional stresses in relation to normal faults. Normal fault-related folds were simply classified as longitudinal and transverse folds based on their hinge-line orientations (Schlische, 1995). Longitudinal folds have hinge lines that are oriented parallel or sub-parallel to the strike of the associated normal fault system. Transverse folds are those that have perpendicular or sub-perpendicular fold hinges with respect to associated normal fault system. Although these two-end members are the most common mode of occurrences, folds of oblique orientations also exist (Janecke *et al.*, 1998).

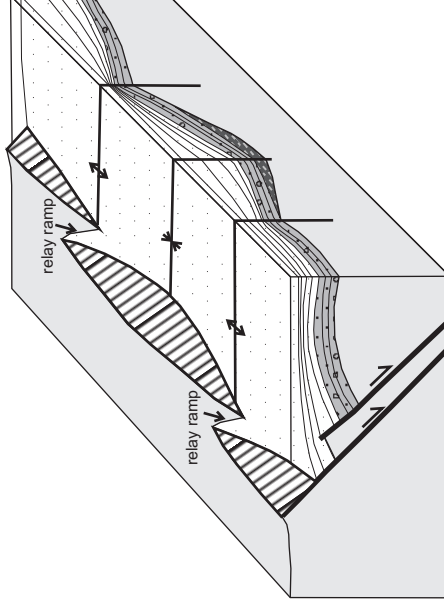
Available literature describes more than a dozen of processes that result in folding in extensional tectonic settings (Schlische, 1995; Janecke *et al.*, 1998). However, synthesis of these processes may lead to three major mechanisms that seem to be most influential in sedimentary basin scale (Figure 6.3). Indeed, these mechanisms are very similar to contractional counterparts and can be listed as: (1) upward propagation of faults; i.e. extensional fault-propagation folding; (2) passage of hanging wall above fault bends; i.e. extensional fault-bend folding and (3) displacement gradients both parallel and orthogonal to the fault strike; i.e. displacement gradient folding. These mechanisms are briefly illustrated in Figure 6.3.

Fault-propagation folds or drag folds are the results of fault growth in up-dip and along-strike directions (Figure 6.3A). Initially, the region in front of a fault tip is flexed into a monocline, which later cut and offset by the propagating fault. The result is a syncline in the hanging wall and an anticline in the footwall. Reverse drag folds represent opposite geometry to fault propagation folds in a way that synclines form in the hanging wall and anticline form in the footwall (Figure 6.3B). These folds are the geometrical results of displacement gradients within the hanging wall

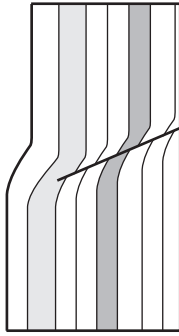
(D) Displacement gradient folding (single fault)



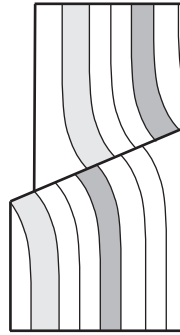
(E) Displacement gradient folding (multiple faults)



(A) Fault propagation folding



(B) Reverse drag folding



(C) Fault bend folding

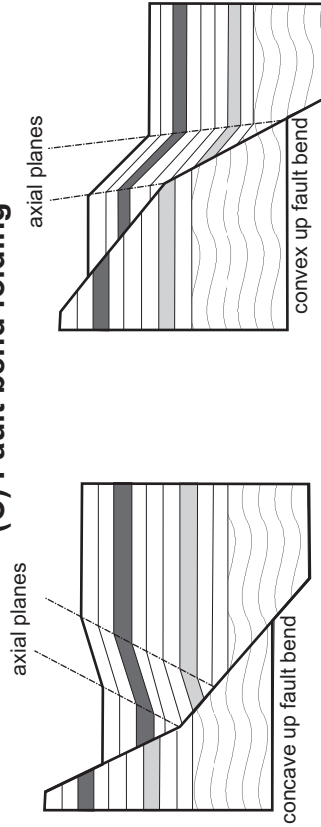


Figure 6.3. More than a dozen mechanisms were described as the cause of folding in extensional settings (e.g., Schlische, 1995; Janecke *et al.*, 1998). Among these mechanisms, the figure illustrates the most common ones. **(A)**, **(B)** and **(C)** are longitudinal folds (left column). **(D)** and **(E)** are transverse folds (right column). Folds of oblique orientations are also defined in the literature (e.g., Janecke *et al.*, 1998), but their occurrence are relatively rare.

and footwall blocks perpendicular or sub-perpendicular to the fault strike. In other words, the maximum displacement arising at the fault surface gradually decreases away from the fault both towards hanging wall and footwall to result in folding.

As in the case of contractional faults, fault bends on normal folds are very efficient ways of folding of the hanging-wall strata (6.3C). As hanging wall passes over a fault bend, a void is potentially created between the hanging wall and the fault plane. The location of the void could be above or below the fault bend depending on the convex up or concave up nature of the fault, respectively. Thus, the hanging wall collapses to fill in the potential gap and become folded (Xiao and Suppe, 1992). Fault-bend folds forming above a convex-up fault bends are traditionally called as rollover folds (Hamblin, 1965; Groshong, 1989, 1994; Dula, 1991; Xiao and Suppe, 1992). These structures were described in Chapter 5 in detail (Figures 5.9 and 5.10).

Fault-propagation folds, reverse drag folds and fault-bend folds commonly form with axial planes oriented parallel to the controlling normal fault and fall into the longitudinal fold class. Transverse folds form the other class and are predominantly controlled by lateral variation of the displacement along the fault surface. Relatively recent research in normal fault systems thought us that the cumulative displacement, which is zero at the fault tips (displacement minima), gradually increases from the fault tips towards the central zone of maximum displacement (Figure 6.4) (e.g., Dawers *et al.*, 1993; Clark and Cox, 1996; Peacock and Sanders, 1996; Cowie and Shipton, 1998; Steward, 2001). This has some implications on the hanging-wall block. If you consider a single isolated normal fault, a displacement profile characterized by maximum displacement at the center and zero displacement at the tips of the fault (i.e., Figure 6.4) would deform the hanging-wall block to form a broad syncline (Figure 6.3D). Normal faults commonly comprise isolated segments, and they progressively evolve through the linkage of these segments (see Chapter 4). This introduces multiple displacement minimums and maximums to the common hanging-wall block to form series of anticlines and synclines oriented transverse to the fault systems' trend (Figure 6.3E). Synclines will form at the displacement maximums and anticlines will form at the displacement minimums (Figure 6.3E).

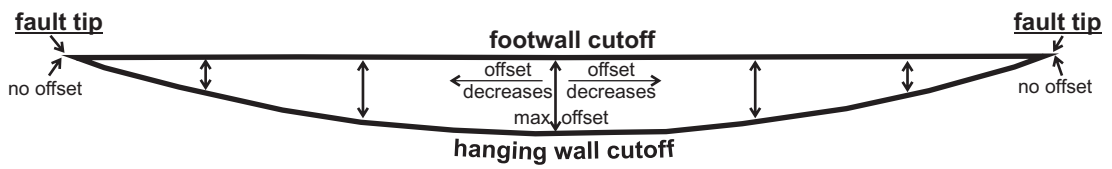


Figure 6.4. Typical displacement profile across a normal fault. Maximum displacement is achieved at the center of the fault plane. Displacement gradually decreases towards the fault tips and finally demises.

6.2. Outcrop Observations: Actual Data

In the study area, the most intensive folding is observable within outcrop exposures of the Alaşehir formation to the SW of Osmaniye (Figure 6.5). A road cut located at this area exposes numerous folds, reverse faults and normal faults that are jointly responsible for the deformation of this unit. Some of the normal faults exposed along this section control the exposure limits of the formation and can be illustrated on geological maps of conventional scale (Figure 6.5). However, folds and reverse/thrust faults along the same section are smaller-scale structures and require more detailed and larger-scale mapping approaches. Therefore, a detailed sketch cross-section was constructed along the road cut section to document the characteristics of observed deformation features (Figure 6.6).

When the road-cut section in Figure 6.6 is examined carefully, one can easily recognize that folding and reverse/thrust faulting are associated in most of the cases. Although some folds appear to lack associated faults, outcrop observations resolves many smaller-scale faults that cannot be illustrated even in the scale of the road-cut cross-section. Figure 6.7 depicts that forelimb of an asymmetrical anticline that is intensely deformed by small-scale reverse/thrust faulting. Note that faults of the forelimb are not planar but curved features in a way conformable to north-vergent character of the fold. It is likely that these faults shaping the forelimb of the anticline are also influenced by folding process; thus indicating that folding and faulting were synchronous events. The observed relations among the folds and reverse faults clearly suggest that deformation pattern comprising these structures is contractional in origin.

Lithology of the Alaşehir formation along the road-cut section is composed of thin-bedded and laminated bitumous paper shales alternating with thin sandstone and siltstone beds, typical to the Zeytinçay member (Chapter 2). This facies allow frequent bedding plane measurements throughout the section to portray the deformation accurately. Although the attitude of bedding planes varies a lot along the section due to intense folding and tilting caused by faulting, approximately E–W-striking bedding with dips towards south and north dominate the general distribution (Figure 6.8A). It is also interesting that along the road-cut section, there is a strong component of north vergence among the structures. Accordingly, most of the observed folds are asymmetrical; some are even overturned to indicate this direction of vergence (Figure 6.6). The reverse/thrust faults, on the other hand, are also

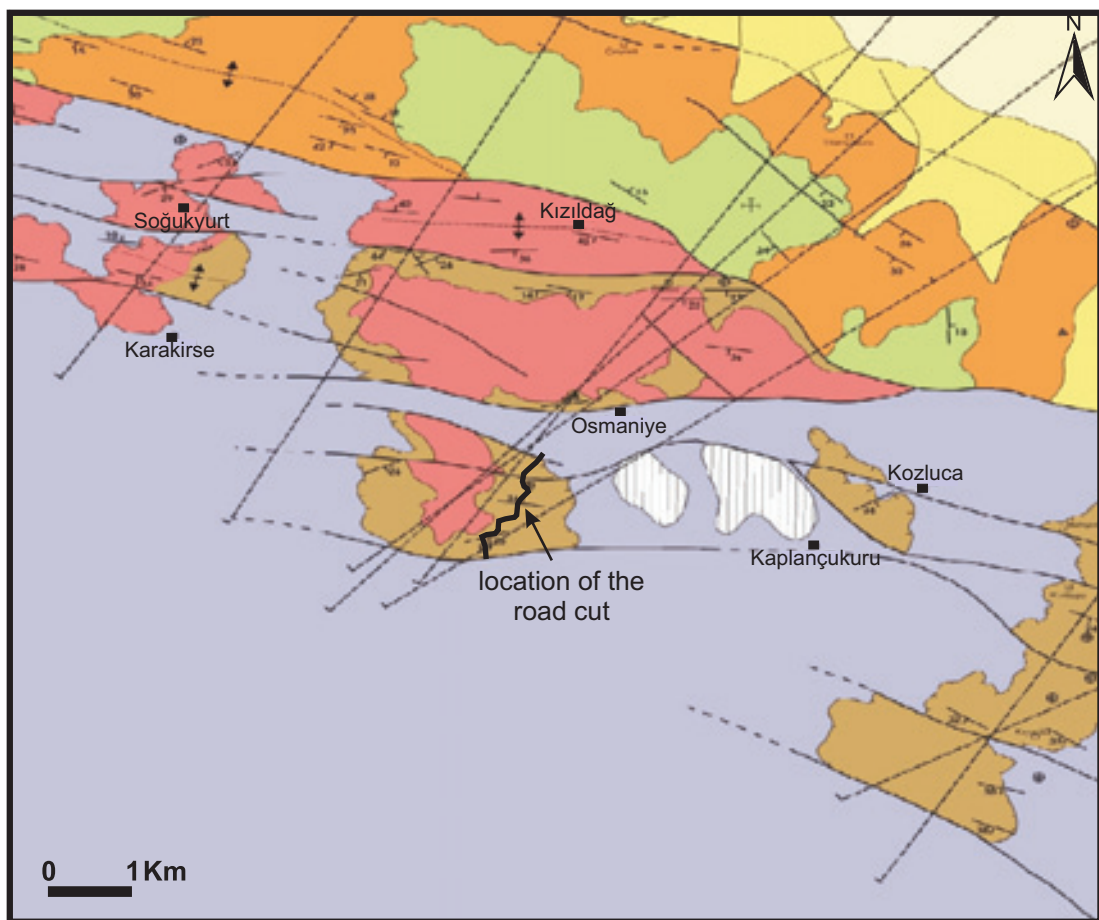


Figure 6.5. Location map of the road cut that is mapped for contractional folds and faults in detail. The section is slightly longer than 1.5 km and cuts through the Alaşehir formation. This map was extracted from Figure 5.23 and one should refer to Figure 5.23 for the explanations of the map.

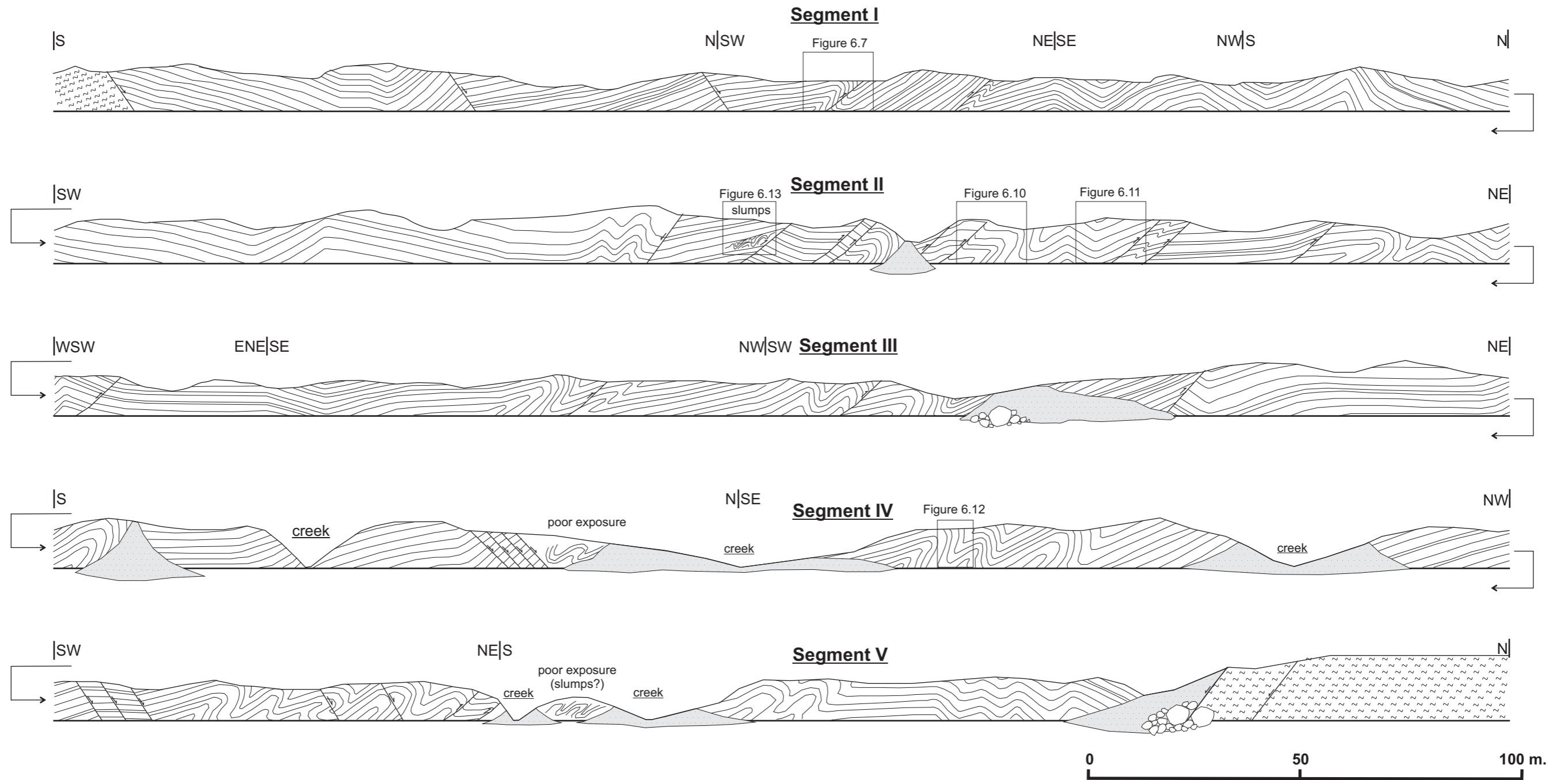
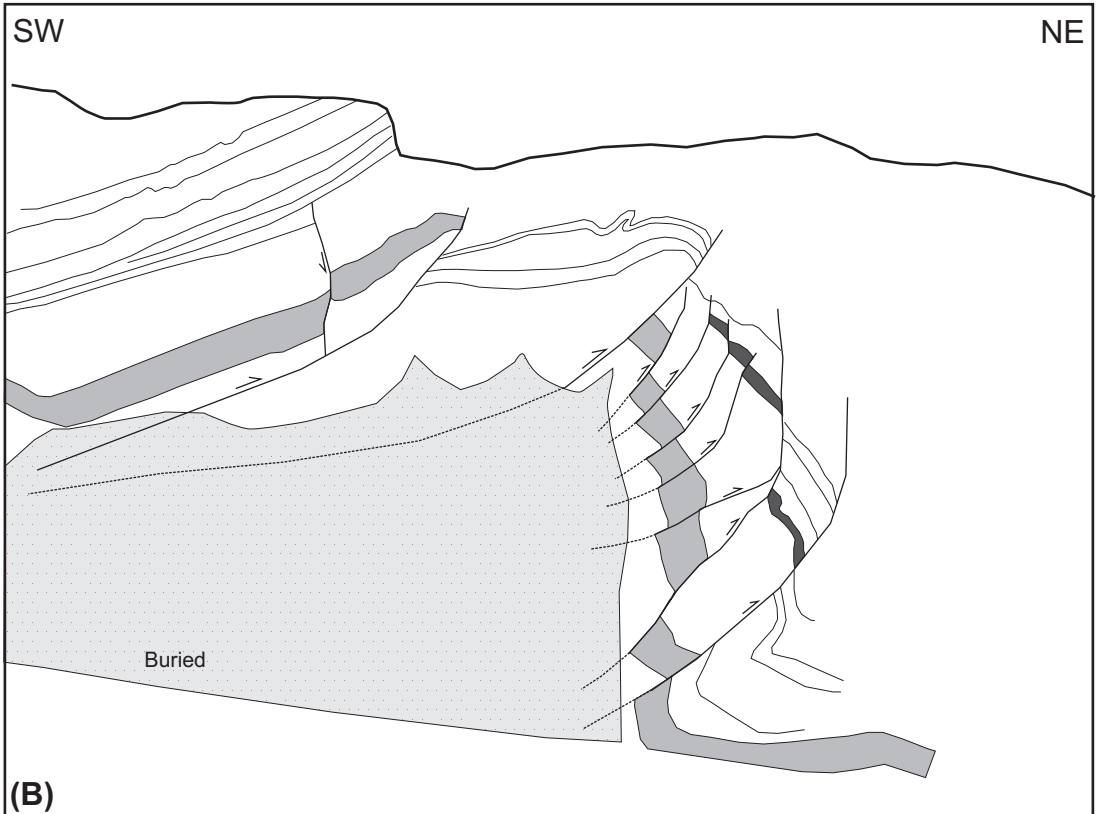


Figure 6.6. Road cut cross-section constructed to illustrate deformation pattern of the Alaşehir formation to the SW of Osmaniye. See Figure 6.1 for the location of the section. The road-cut section is slightly over 1.5 km in length and exposes deformation pattern that is controlled by folding, reverse faulting and normal faulting. It is clearly evident on this section that, in most cases the folding is associated with reverse faulting and indicate the contractional nature of deformation. The fact that normal faults cut and offset fold axes is also obvious along Segment V of the section. This suggests that some of the normal faults is related to a deformation phase that is superimposed on to the contractional deformation. There is a consistent north vergence during the contractional deformation.



(A)



(B)

Figure 6.7. Outcrop photograph (A) and basic interpretation (B) to illustrate complex deformation patterns observed along the road-cut cross-section. Note that folding is associated with intense small-scale faulting across the fore limb of the asymmetrical anticline. The faults are not planar but curved features suggesting that they may also be influenced by folding process. See Figure 6.6 for the location of the photograph. The man in the picture is 188-cm-tall.

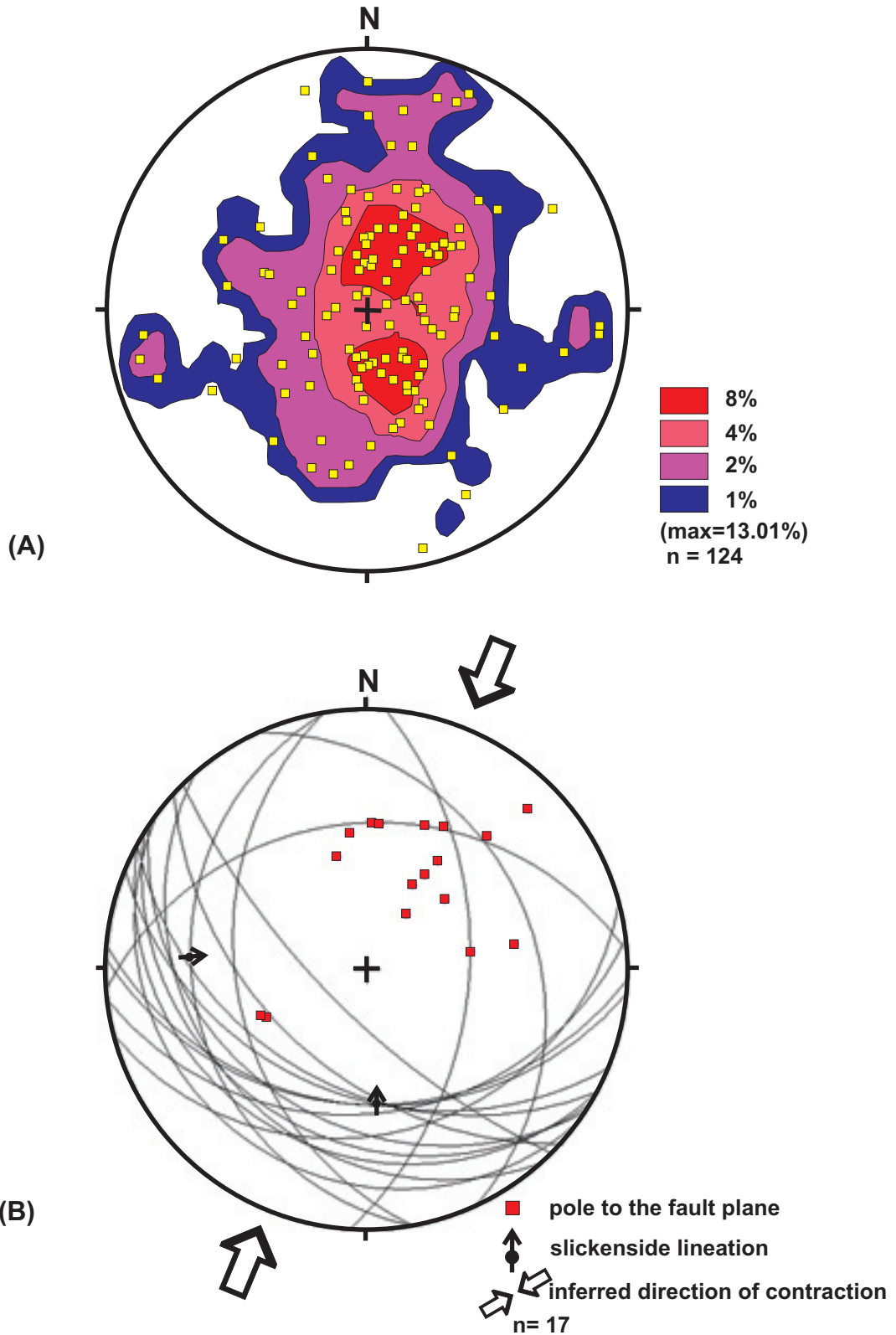


Figure 6.8. (A) Stereoplot illustrating bedding orientation along the road-cut section. Poles to the bedding plane are plotted over the density contours depicting concentration of bedding at two main attitudes. (B) Fault data acquired from reverse faults along the road cut section. Faults mostly dip towards S-SW. Rare slickenside lineations indicate dip-slip movements on the fault planes.

conformable with this vergence direction. Excluding few exceptions, all the faults dip southward with magnitudes commonly less than 45° (Figure 6.8B).

Unfortunately, the lithology of the Alaşehir formation comprising thin-bedded and laminated sediments are not suitable to allow measurement of slickenside lineation for the kinematic analysis of fault data since these surfaces are easily weathered. Yet, measured fault orientations suggest approximately NNE–SSW-oriented compression direction. Few measured fault slip data shows predominantly dip-slip movements on the fault planes (Figure 6.8B). It is interesting that the estimated direction of compression is very similar to the computed direction of extension forming the normal faults of Gediz Graben (Figure 3.26).

Folds along the section are variable in character. They generally trend E–W with plunges less than 20° (Figure 6.9). The dominant plunge direction is to west, although plunges to NW, NE and SSW also exist (Figure 6.9A). Folds are mostly asymmetrical and vary from tight folds with angular hinges to broad folds with broad curved hinges (Figures 6.7, 6.10, 6.11 and 6.12). Folding is predominantly controlled by flexural-folding mechanism and most of the folds possess parallel fold properties.

The road-cut cross-section also revealed a relation to constrain relative timing of contractional and extensional deformations along the road-cut section. In the Segment V of the cross-section in Figure 6.6, some of the normal faults evidently cut and displace axial planes of some folds. This suggests that at least some of the normal faults postdate the formation of folds along this section; i.e., the observed contractional deformation has taken place before the currently active extension of the Graben.

Deposition of the Alaşehir formation was constraint within a lacustrine basin that had a fault-controlled steep southern margin (Chapter 2). This steep margin not only provided suitable conditions to trigger the turbidity currents, but also influenced the stability of the sediments deposited over the slopes. Unavoidably, slope failures have taken place and resulted in slumps and soft-sediment deformation that is incorporated with the sedimentation (Figures 6.6 and 6.13). The observed slumps are north vergent as well, indicating mass-wasting process from southern margin towards the north. This brings along another argument that whether the observed contractional deformations are related to compressive stresses, or they are actually slumps formed during the deposition of the formation?

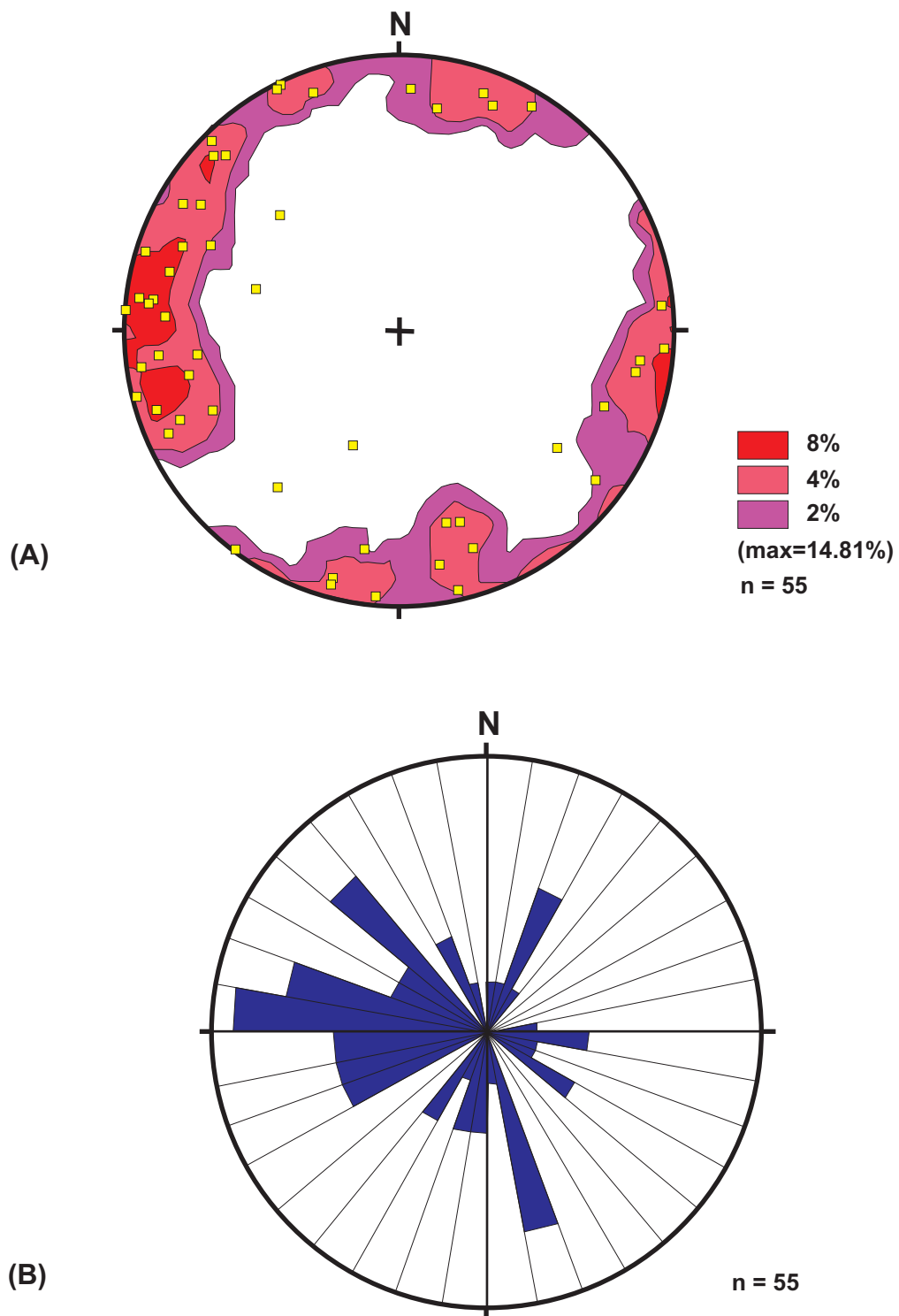


Figure 6.9. (A) Stereoplote depicting hinge-line orientations of folds with contours illustrating the density distribution. (B) Rose diagram showing the orientation of fold hinge lines. Both (A) and (B) reveal that the most dominant fold orientation is approximately E-W, although folds oriented ~N-S are also significant in numbers.

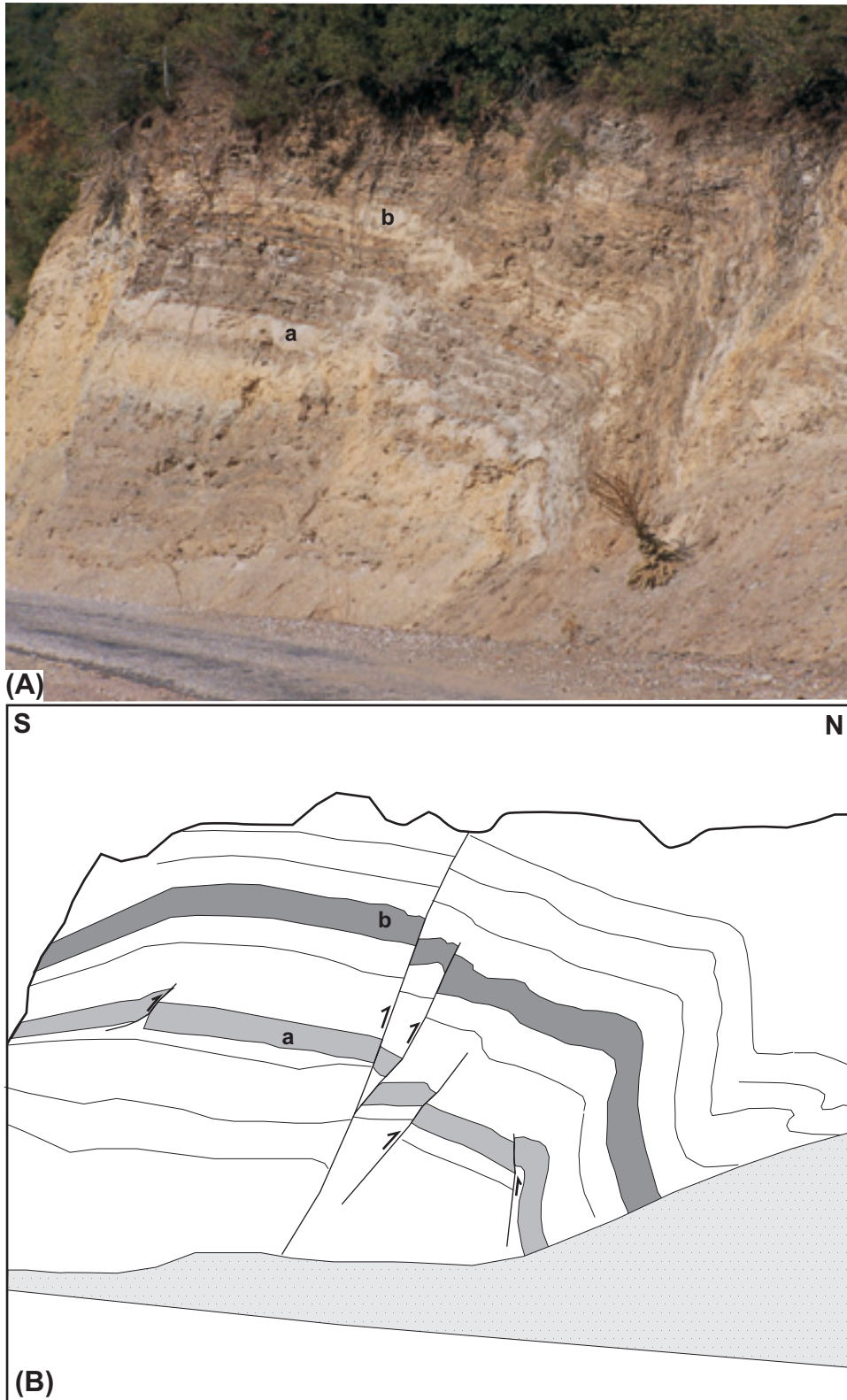
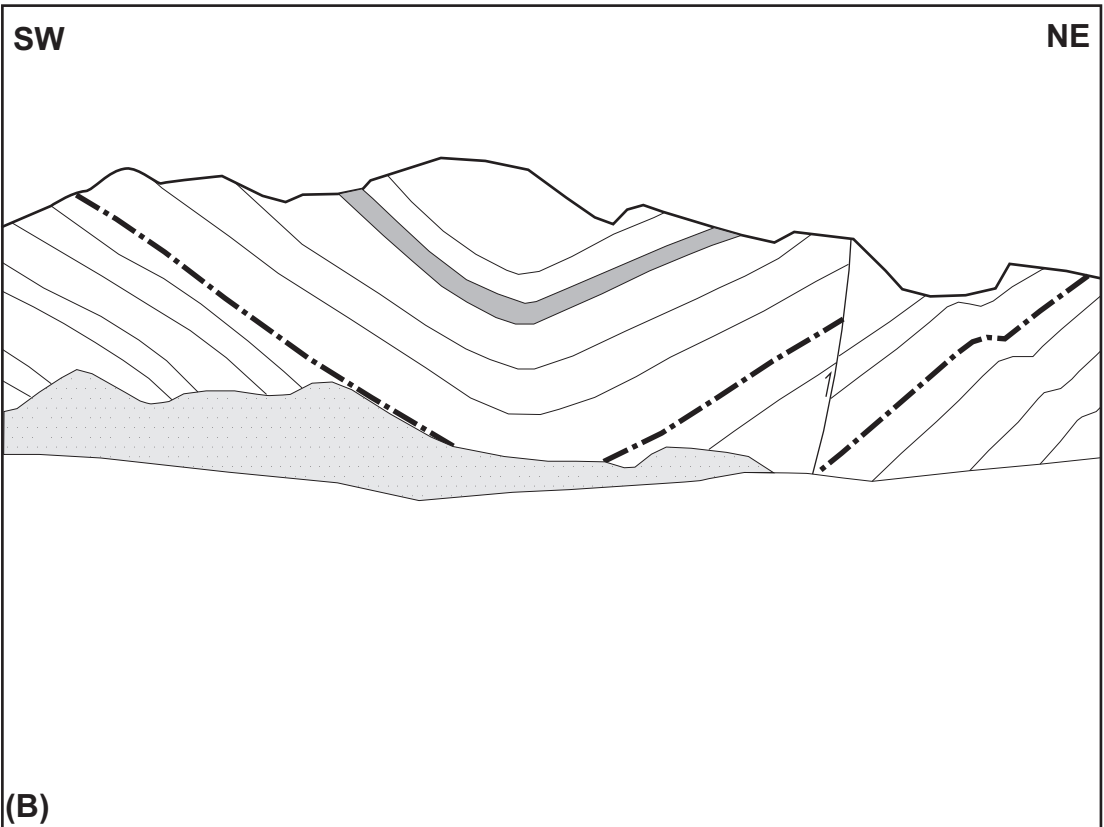


Figure 6.10. Outcrop photograph (A) and its sketch (B) showing an asymmetrical anticline that exposed along the road-cut section. The entire section is dominated by paper shales with some sandstone intercalations (gray beds). Note that shale beds and sandstone beds deformed in slightly different ways due to varying rigidity. While shale beds become folded by flexural slip, sandstone layers respond by reverse/thrust faulting. See Figure 6.2 for the location of the photograph. The exposure surface is ~12-m-high.



(A)



(B)

Figure 6.11. Outcrop photograph (A) and basic interpretation (B) showing a broad symmetrical syncline that form on the hanging wall of a reverse fault. The apparent offset on the fault plane is about 2.5 m. See Figure 6.2 for the location of the photograph. The man on the picture is 180-cm-tall.



Figure 6.12. Outcrop photograph (A) and basic interpretation (B) showing a tight chevron syncline with plunge direction to the observer. See Figure 6.2 for the location of the photograph.

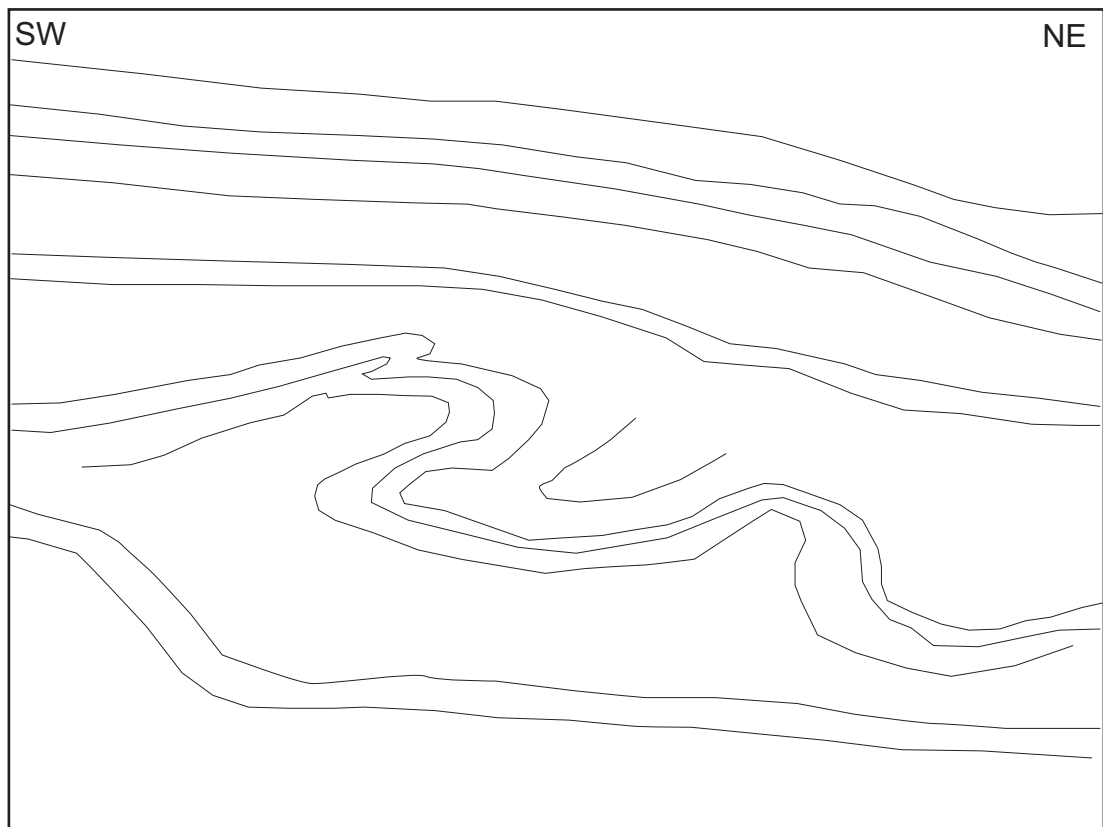
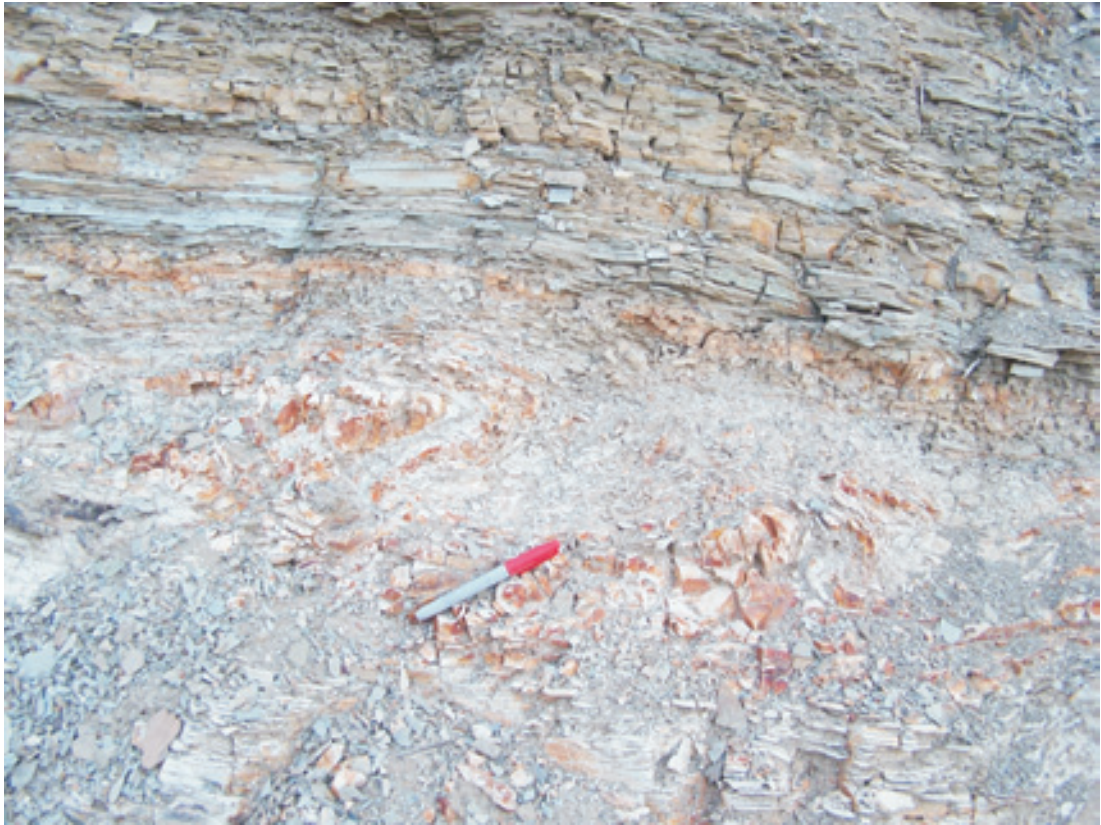


Figure 6.13. Outcrop photograph illustrating the slump features within the Alaşehir formation. Note that the folded volume of rock is constrained in between the undisturbed layering. Vergence is towards NE. See Figure 6.2 for the location of the photograph. The pen in the picture is 15-cm-long.

Slumps are easy to identify if they are smaller than the scale of observation. The key issue is to find the undisturbed sedimentary layering above and below the folded and sometime faulted slump volume (Figure 6.13). If these relations cannot be resolved on the outcrops due to larger sizes of the deformed volumes (i.e. the feature is larger than the available observation area), identification of slumps become difficult. The reason for this is the fact that deformation patterns observed within the slump volumes are also contractional, similar to those formed by regional compressive stresses. Unfortunately, the risk of misidentifying some of the slump structures as the contractional deformation is valid for the road-cut section, which allows observations along maximum 5-6 m high exposures. However, deformation styles observed in some of the folds are not very conformable the with slump processes (Figures 6.7, 6.10, 6.11 and 6.12). For example, deformation in Figure 6.7 is dominated by many small-scale thrust faults on the forelimb of the anticline. This style is probably too brittle to form with semi consolidated slump structures. The symmetrical broad fold in Figure 6.10 and chevron fold in Figure 6.12 are difficult geometries to form through the slump processes as well.

6.3. Subsurface Interpretations

Folds are also observable in seismic data throughout the basin-fill sediments of the Gediz Graben. As the dip of master graben-bounding normal fault (southern margin-bounding structure) decreases at depth through a distinct fault-bend, an extensional fault-bend fold or rollover fold has formed in the hanging-wall strata which is imaged very well on some sections (e.g., Figure 5.16). Beside this basin-size structure, smaller-scale folds associated with normal faults are also observable in transverse cross-sections (Figures 5.32, 5.33 and 6.14). In fact, all the interpreted folds across the seismic coverage are related to the normal faults and no indication of contractional folding and faulting can be resolved on these seismic sections. Remember that the scale of folding and thrust/reverse faulting observed within the outcrops of Alaşehir formation was relatively small compared to the extensional structures. Consequently, much larger scale approach than the conventional mapping scale was utilized to document these structures (Figure 6.6). This scale issue could be also valid for the subsurface data, which fail to image comparable structures due to resolution limitations of the seismic data.

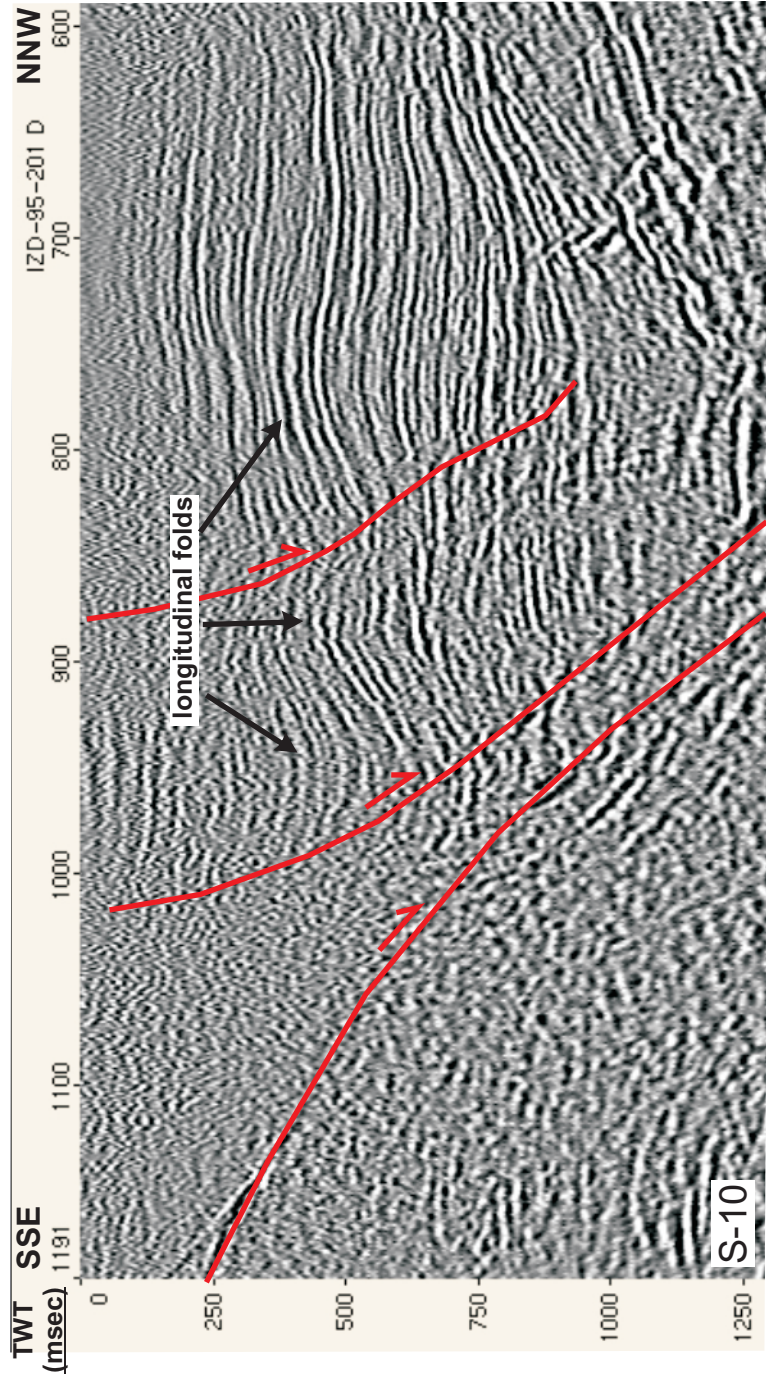


Figure 6.14. Part of seismic section S-10 illustrating small-scale longitudinal folds forming in association to normal faults. See Figure 5.1 for the location of the section.

If the structural contour maps of stratigraphic horizons are investigated, transverse anticlines and synclines catches attention as the most prominent structures shaping the graben fill (Figures 6.15 – see also Figures 5.26, 5.28 and 5.30). These structures can easily be recognized on longitudinal seismic sections oriented parallel to the graben trend (Figures 5.23, 5.36, 5.37 and 6.15). In fact, the cross section based on the interpretation of seismic section S-16 in Figure 6.15 portrays the geometry of the transverse folds better than the any other longitudinal section. This cross section is based on the closest seismic section to the southern margin structure of the graben and represents the parts of the graben that is most strongly influenced by the displacement gradient along the master structure (Figure 5.1). Stratigraphic units in this section were differentiated based on their deposition time with respect to folding (Figure 6.15). The brown-colored unit nonconformably overlies the basement metamorphic rocks and is deposited before the folding. This unit correlates to the Alaşehir formation and therefore, it constitutes the pre-growth strata. On the other hand, the overlying growth strata were differentiated into two units as: (i) the lower unit comprising the Çaltılık and Gediz formations and (ii) the upper unit made up of Plio–Quaternary deposits.

In the theory of contractional fault-related folds, kink-band migration and limb-rotation are invoked as the two main mechanisms of folding (Shaw *et al.*, 2005). For folds that develop purely by kink-band migration, fault limbs widen through time but maintain a constant dip (Figure 6.16) (Suppe *et al.*, 1992). The fold limb is bounded by active-axial surface and inactive-axial surface for the pre-growth strata and active-axial surface and growth-axial surface for the growth strata. The active- and inactive-axial surfaces mark the syncline and anticline, respectively (Figure 6.16). In limb-rotation mechanism, the fold limb preserves fixed hinge points defined by inactive axial surfaces through the folding process (Shaw *et al.*, 2005). However, the dip of the limb increases gradually as the folding progress (Figure 6.16). That results in older strata of the limb dip more steeply than the younger strata with apparent fanning down-dip the limb.

It can be recognized on the Figure 6.17 that kink-bend like folded strata have developed on the limbs of the transverse folds. While these kink bends have constant widths throughout the pre-growth strata, their widths decrease within the growth strata to form growth triangles very similar to those formed by kink-bend migration mechanism in Figure 6.16. The width of the limb for each growth horizon represents

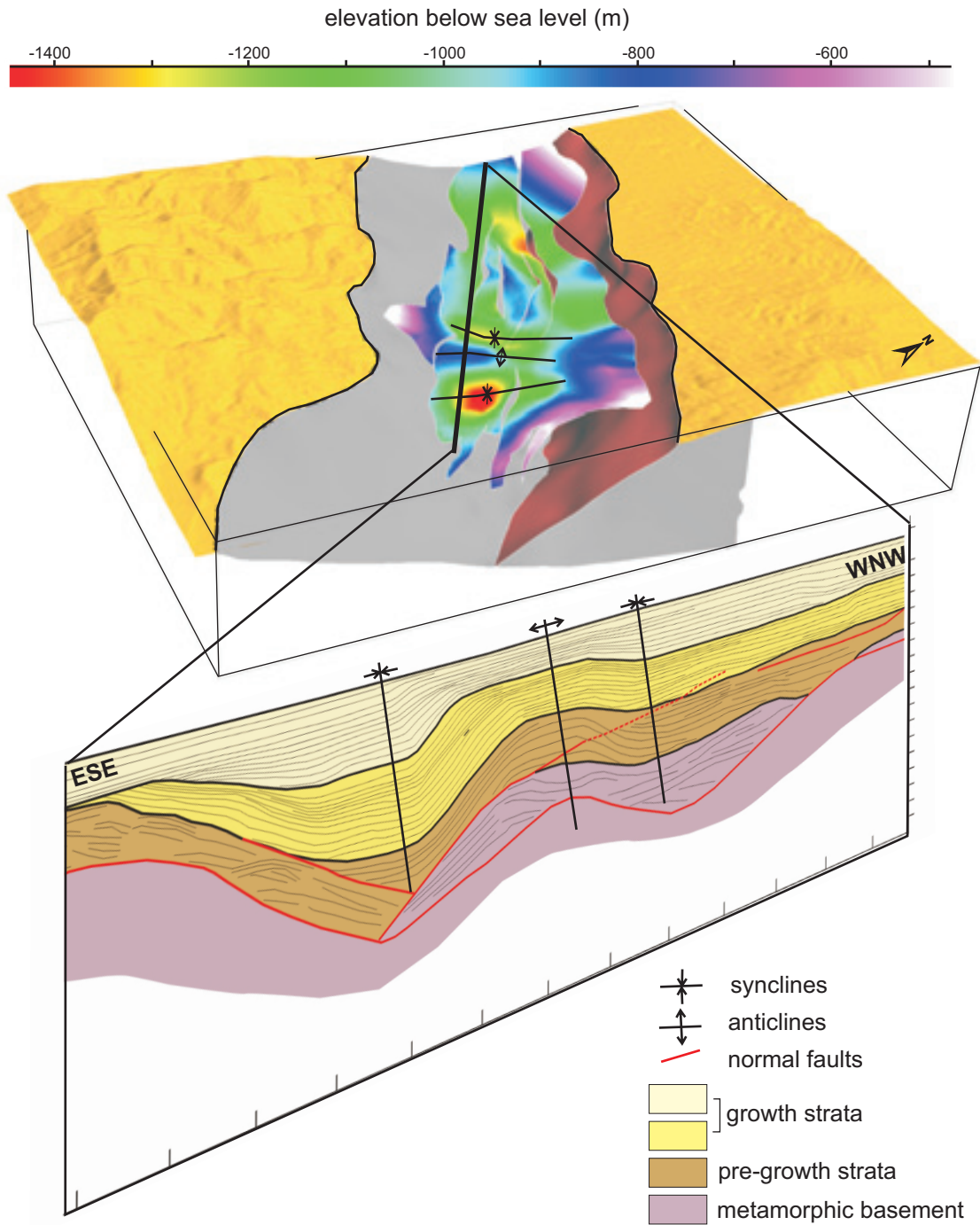


Figure 6.15. Figure depicting the transverse anticlines and synclines in the Gediz Graben. Structural contour maps of the stratigraphic horizons and the constructed longitudinal cross-section reveal the dominance of the transverse folds in the deformation of the graben fill.

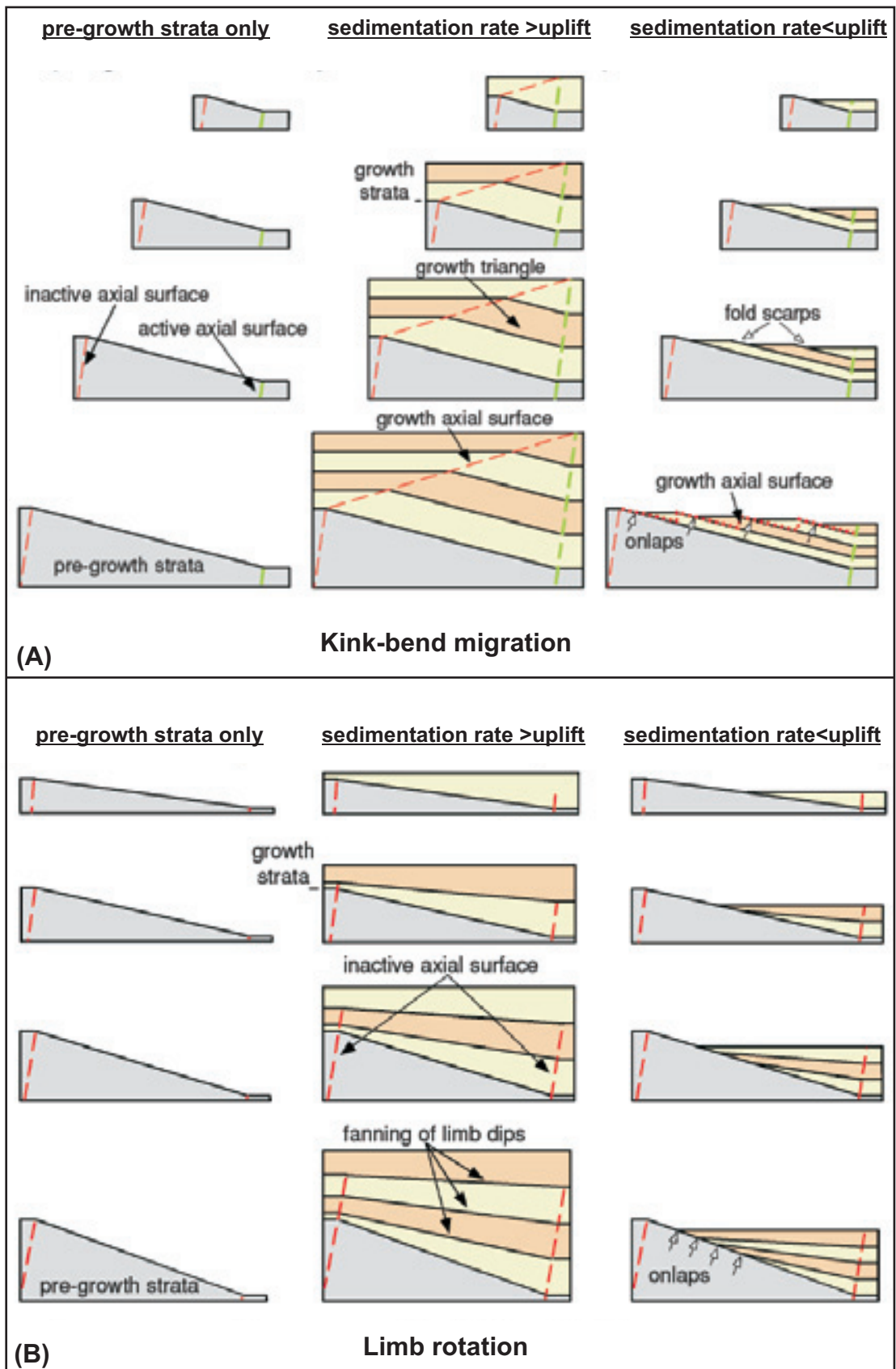


Figure 6.16. Two different ways of folding in contractional fault related folds. **(A)** Kink-bend migration, **(B)** Limb rotation. Figures depict both folding of pre-growth strata and growth strata for sedimentation rate being larger and smaller than the rate of uplift. From Shaw *et al.* (2005).

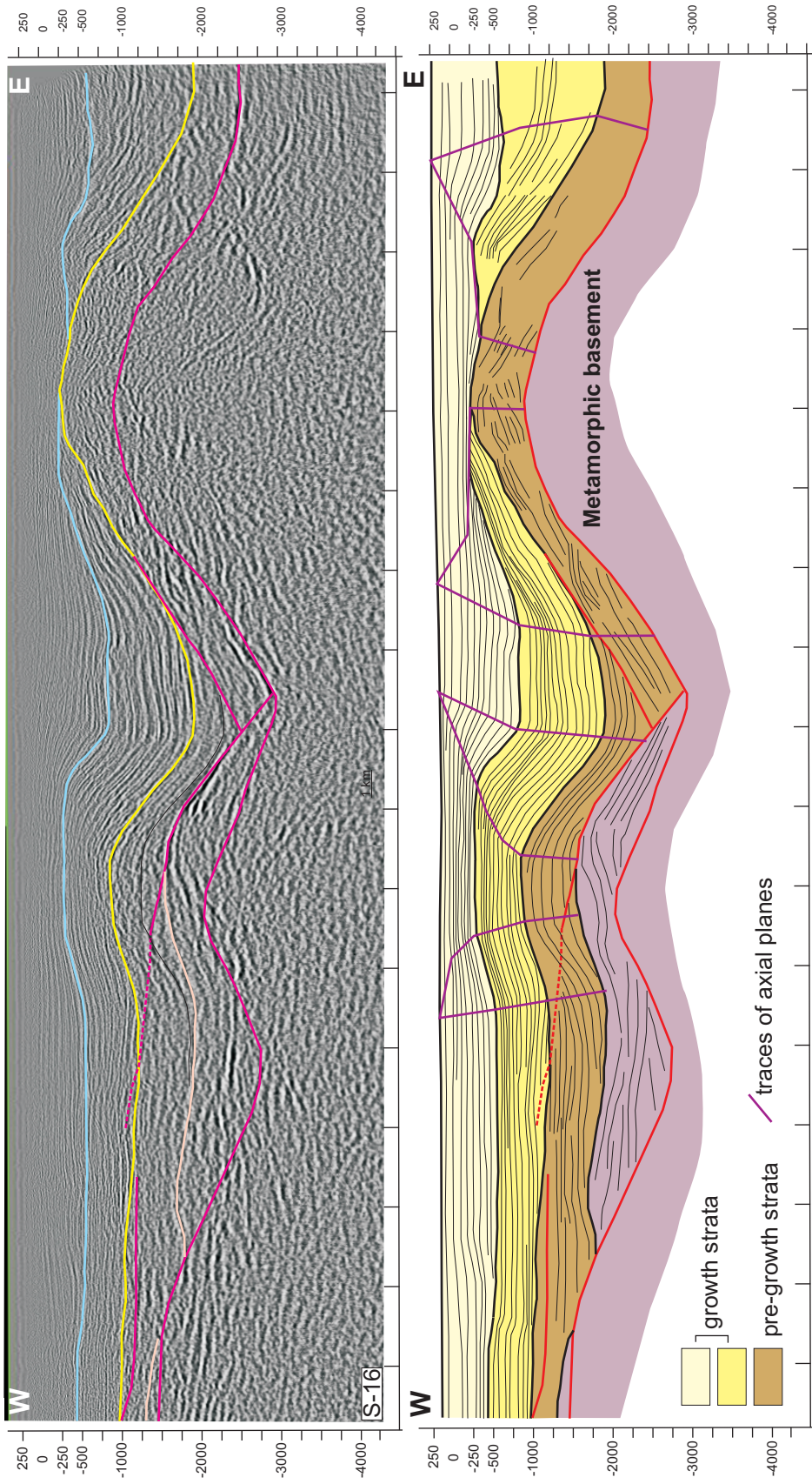


Figure 6.17. Interpretation of the seismic section S-16 in the Gediz Graben. S-16 is oriented parallel to the graben trend and is the closest section to the southern margin-bounding structure. The stratigraphic units are separated to illustrate strata deposited before folding (pre-growth) and strata deposited during folding (growth). Dip domain boundaries marks the change of dip on the folds. See Figure 5.1 for the location of the section.

the amount of fold growth since the deposition of that marker (Shaw *et al.*, 2005). Consequently, the younger horizons have smaller widths than the older horizon to form narrowing upward fold limbs constraint by growth triangles (Figure 6.17). The traces of axial planes tied to synclines appear as more regular surfaces with tendency to be a straight line. Those tied to anticlines are clearly diverted into the growth axial surfaces within the growth strata. Although kink-bend migration characterized by constant bed dips on the fold limbs is probably the dominant mechanism of folding, minor amount of down dip increase in thickness can still be observed for some of the stratigraphic levels (Figure 6.17). This suggests that folding process was predominantly governed by kink-bend migration but also influenced by limb rotation as well. The process of limb rotation is more evident in the upper growth strata (Figure 6.17).

While the thickness distribution of the pre-growth strata is independent from folding process, the lower package of the growth strata illustrates clear lateral thickness change in relation to folding. This is manifested by increased thickness over the core of synclines and decreased thickness over the core of anticlines. Furthermore, at the top of eastern anticline, the lower growth strata do not exist but an apparent angular unconformity between the lower and upper growth packages (Figure 6.17). This relation is probably caused by the sedimentation rate being less than the rate of anticlinal uplift during the deposition of the lower growth strata. This resulted in non-deposition of the lower growth package at the top of anticline in a way similar to Figure 6.16A.

6.3.1. Forward Modeling of Transverse Folding

A forward modeling effort was carried out to assess if the observed transverse folding in the graben can be produced by variable subsidence of the basin? The variable subsidence was caused by the originally segmented nature of the southern margin structure that introduced multiple displacement minimums and maximums in to the basin fill. With accumulating extensional strain, the segments will join together to form a single fault, which result in more uniform subsidence of the graben block.

Two different profiles representing the cumulative subsidence of the graben were extracted in Figure 6.18. Although the compaction of sediments also adds some accommodation space to the basin subsidence, it is ignored as an approximation in

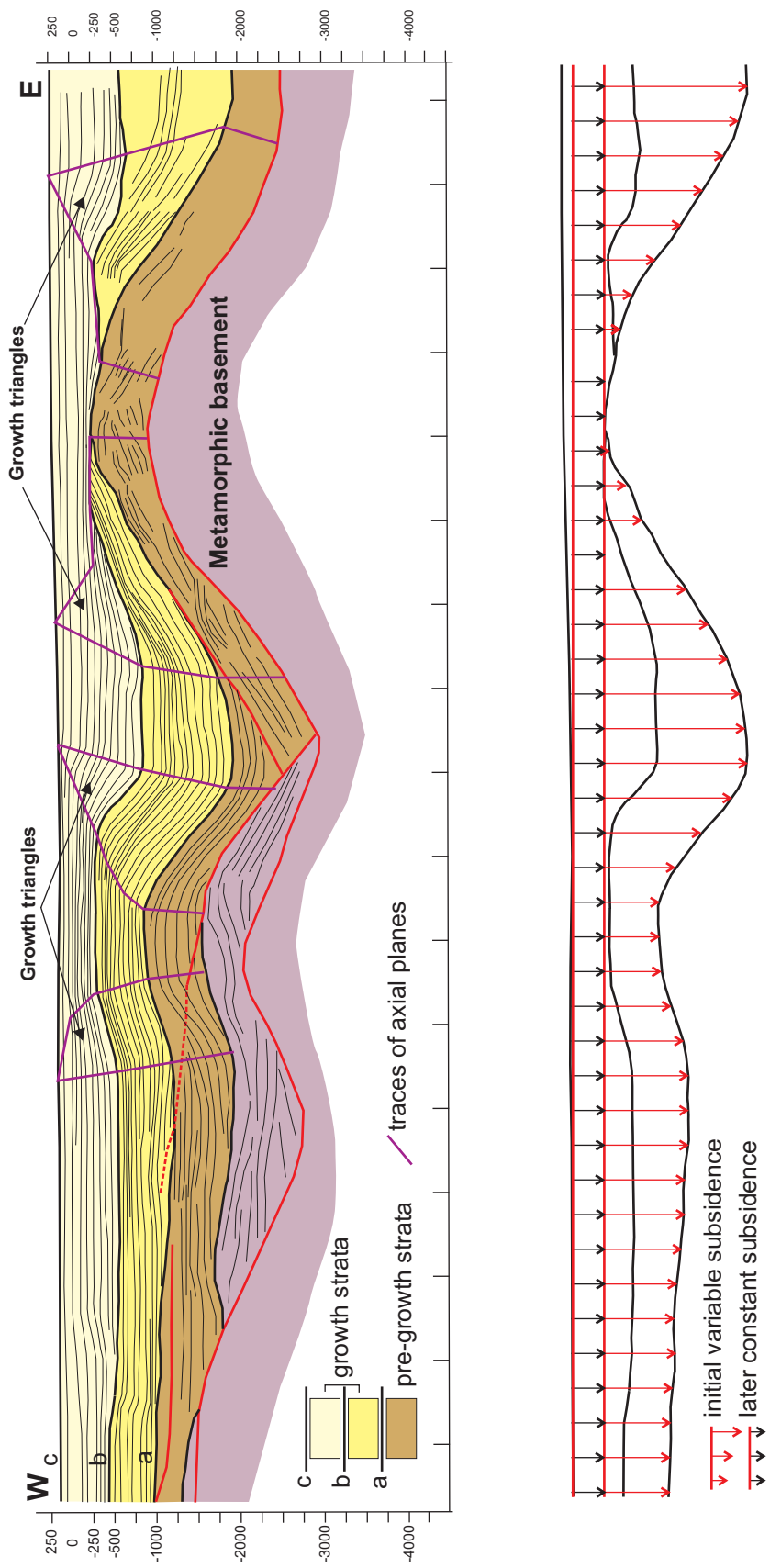


Figure 6.18. The extracted subsidence profiles. The basin probably exposed variable subsidence starting after the deposition of pre-growth strata (horizon a) and lasting until the end of first growth strata (horizon b). The variable subsidence profile was extracted based on the local angular unconformity at the top of eastern anticline until the horizon a. The constant subsidence profile fills in the gap between the ground surface and local unconformity.

the subsidence profiles. The initial variable subsidence profile represents the earlier stages in the graben evolution, which is characterized by segmented boundary fault causing different rates of subsidence along the graben basin with multiple displacement minimums and maximums. Representing the displacement minimums, the two anticlines correlate very well with the along-strike bends of the southern margin-bounding structure. At least three separate segments can be inferred based on the location of these anticlines (Figures 6.15 and 6.18). The three synclines, which border the anticlines, with distinct thickening of the growth strata correspond to displacement maximums on inferred segments (Figure 6.18). The profile was constructed based on the vertical distance between the top horizon of the pre growth strata (horizon a), and the apparent local angular unconformity formed between the lower and upper growth strata packages at the crest of eastern anticline (horizon b). As discussed in the previous section, the angular unconformity here does not represent a regional event causing exposure and erosion of the lower growth package, as it cannot be correlated with any other part of the basin. Instead, it probably indicates a lack of deposition at the crest of anticline during the folding process. Marking a displacement minimum, the crest of anticline can be used as a datum to refer the relative subsidence of the graben block (Figure 6.18).

The constant subsidence curve accounts for the accommodation generated above the horizon b and complete the cumulative subsidence of the basin (Figure 6.18). Although the subsidence during the deposition of the upper growth strata was still variable as indicated by the growth triangles extending up to the surface, lack of reference point to estimate the variation will lead to assume a constant subsidence as an approximation.

The modeling was carried out by applying the subsidence profiles to the pre-growth strata incrementally. As the folding of pre-growth strata was constructed, deposition of the growth strata kept up with folding according to simplified axial traces (Figure 6.19). Initially, variable subsidence profile was used as the measure of subsidence at steps of 25%, 75% and 100% of the total (Figure 6.19B, C and D). This constructed the geometry of the lower growth strata with no deposition at the crest of the anticline. Then, the constant subsidence profile was applied to complete the cumulative subsidence of the basin. With the deposition of the upper growth strata, the entire basin geometry was constructed. In fact, this constructed geometry (Figure 6.19E) mimics very closely the true geometry of the basin fill (Figures 6.17

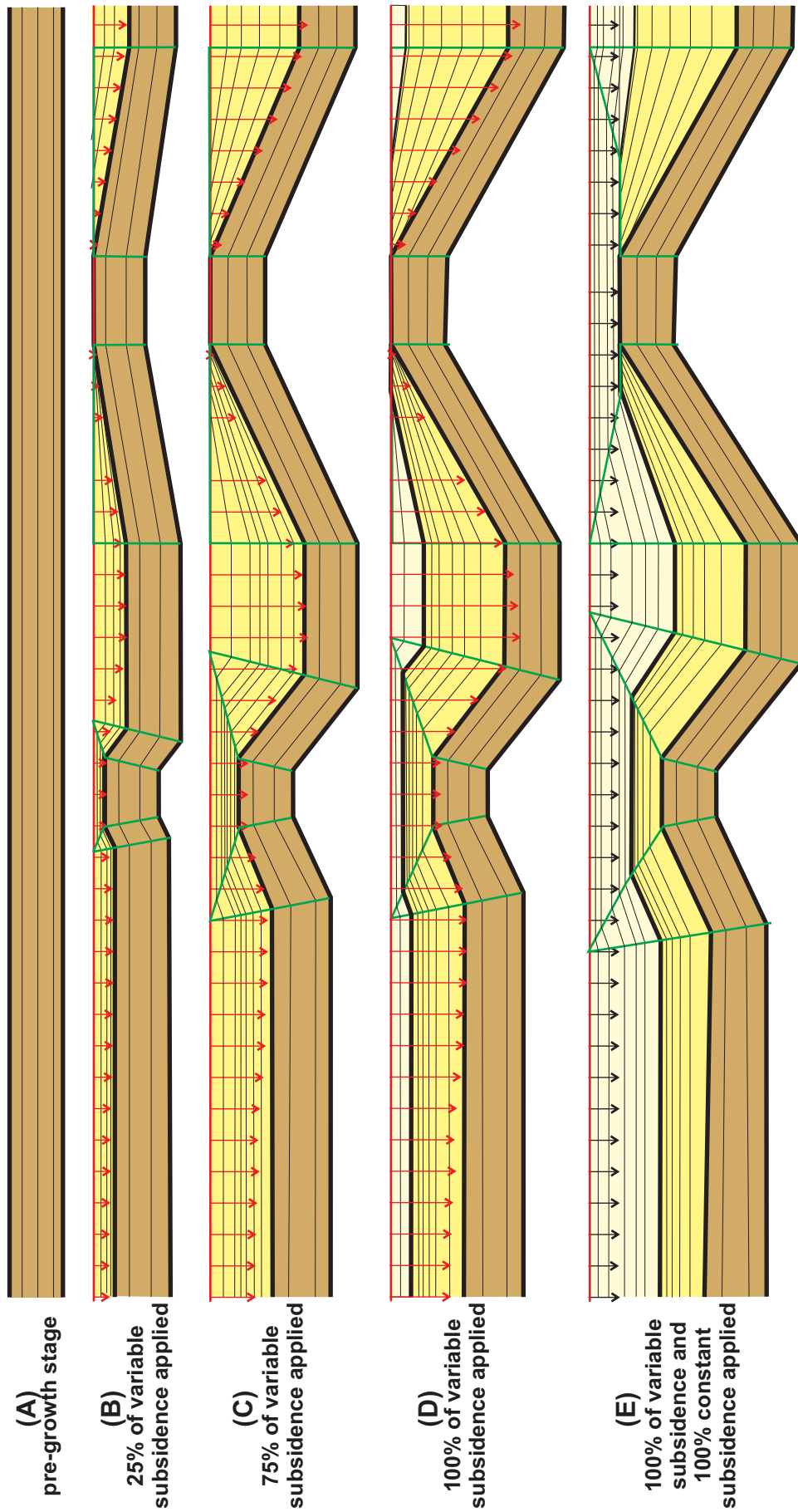


Figure 6.19. Modeling of the transverse anticlines in the Gediz Graben. (A) Pre-growth stage. (B) 25% of the variable subsidence is applied. (C) 75% of the variable subsidence is applied. (D) 100% of the variable subsidence is applied. (E) Both variable and constant components of the subsidence are applied. Note the similarity of the constructed geometry to that of actual case in Figure 6.15.

and 6.18). In the constructed forward model, the geometry of fold-limbs and discrete dip domains look very similar to the actual cross-section. Even the local angular unconformity observed at the crest of the eastern anticline was constructed successfully. The modeling effort confirms that the folded geometry of the graben fill, which is characterized by transverse folds oriented orthogonal to the southern margin-bounding structure, is caused by the variation of the subsidence along to graben trend. This variation is probably controlled by the variation of total displacement along the southern margin-bounding fault of the Gediz Graben.

6.4. Discussion

Folds certainly take part within the deformation pattern of the Gediz Graben. They are observable on the surface exposures and can be imaged with subsurface methods. Although folds of both contractional and extensional origin were identified in the Gediz Graben, those of contractional origin appears to be restricted into certain formations of the graben fill, and consequently into certain areas. In fact, the Alaşehir formation is the only lithostratigraphic unit that is deformed by the contractional deformation. As this formation displays limited spatial distribution due to its depositional realm, evidence of the contractional deformation is consequently become limited both in time and space. The most straightforward geological explanation to this situation is to consider a phase of contractional deformation that postdate the deposition of the Alaşehir formation but predate all other lithostratigraphic units that constitute the graben fill. Yet, extreme caution is needed before accepting this explanation, mainly because of two reasons. First of all, not a single evidence of contractional deformation was observed from the seismic sections, which portrays the general deformation characteristics of the basin fill sufficiently. One can argue that the exposed contractional structures are small as observed in the road-cut section and therefore fall below the resolution limits of the seismic data. However, if a regional event is considered as the cause of a contractional deformation, basin scale evidence of this similar to the extensional structures must exist.

The second point is the fact that even within the Alaşehir formation, the intensity of contractional deformation varies. In fact, similar structures cannot be identified so easily throughout the exposure of the formation to the east of the road-cut section. The fact that some of the contractional structures represent intense brittle

deformation and cannot be created by soft sedimentary deformation (e.g., slumps) is evident by outcrop observations. Therefore, limited spatial distribution of this deformation even within the Alaşehir formation may suggest if the contractional deformation is a local phenomenon and controlled by the local complexities! Unfortunately, this study was not able to document concrete evidence to state whether there is a regional compressional phase in western Anatolia or not. The recent literature following to the pioneering work of Koçyiğit et al. (1999a) provides many evidences for the existence of a short phase of compression during Late Miocene–Early Pliocene in the southwestern Anatolia (Bozkurt, 2000; Bozkurt and Rojay, 2005; Bozkurt and Sözbilir, 2006; Koçyiğit and Özacar, 2003; Baccetto et al., 2005; Kaya et al., 2004, 2007; Rojay et al., 2005; Westaway et al., 2005). If the observed contractional deformation pattern is considered to be related with this regional phase, one should also expect to see related evidences within Miocene deposits of Çaltılık and Gediz formations as well. Nevertheless, lack of evidences for the phase of regional compression in this study does not eliminate the viability of the regional phase of compression. In a very recent study, Koçyiğit (2005) documented evidences for this phase in the Denizli graben, which is located at the eastern end of the Gediz Graben, only tens of kilometers away from the study area.

Extensional folds are widespread within the graben fill and can be observed within all of the stratigraphic units in association to normal faults. They form both in longitudinal and transverse orientations with respect to the graben trend. Together with the normal faults, the transverse folds are important elements of deformation within the graben fill.

CHAPTER 7

CONCLUSIONS:

GEOLOGICAL EVOLUTION OF THE GEDIZ GRABEN

7.1. Structural Evolution

The margins and margin-bounding structures of the Gediz Graben are dynamic in geometry and extend, which vary significantly through the evolution of the graben. Currently, the graben is fault-bounded on both southern and northern margins (Figure 2.3), although the southern margin structure is more active in terms of total offset and period of activity. Indeed, the graben has evolved as a half graben through the entire Miocene period with the activity of only southern margin-bounding structure (Figures 5.32 and 5.33). Then, it became a graben with the initiation of northern margin-bounding structure during the Pliocene to Quaternary interval (Figures 5.32 and 5.33). This gives the graben a general asymmetrical shape in favor of southern margin, which evolved to a more mature structural stage relative to the northern margin.

Around the Alaşehir subbasin, the southern margin of the Gediz Graben is structurally complicated by two groups of faults: (i) high-angle normal faults and (ii) presently low-angle normal fault (the detachment fault) (Figure 2.3). The high-angle faults form a graben-facing step-like pattern along the southern margin with younging direction to the basin; i.e., faults get younger towards north (Figures 5.32 and 5.33). To the south of the master graben-bounding fault, these high-angle faults apparently cut and offset the presently low-angle normal fault (Figures 5.24, 5.32 and 5.33). Although this cross-cutting relationship is referred as one of the main indications of episodic extension in the region by two distinct structural styles (Bozkurt and Mittwede, 2005 and references therein), formation of this relationship in the continuum of deformation is a solid probability. This requires; (i) footwall rebound due to unloading (e.g., Spencer, 1984); (ii) rotation of the dip of the

detachment to a low-angle from an original high-angle by rolling hinge process (e.g., Hamilton, 1988; Wernicke and Axen, 1988; Buck, 1988, 1991); (iii) abandonment of the presently low-angle fault with formation of new high-angle faults, which are more favorable to accommodate the extension, (e.g., Sibson, 1985; Forsyth, 1992; Buck, 1993); and (iv) chopping off the abandoned, inactive low-angle normal fault by active high-angle normal faults at the footwall of the MGBF. As illustrated schematically in Figure 5.35, evolution in the continuum of deformation depends on a dynamic southern margin that develops through geometrical variation of the margin-bounding structures.

Similar to the dip-section geometrical evolution mentioned above, along-strike geometries of the normal faults also vary with time in the continuum of deformation. This variation apparently follows a certain path of evolution, which starts from an immature fault system comprising short, overlapping, multiple segments. Along the southern margin of the graben, the northernmost fault system, currently bounding the modern graben floor is an example to an immature and segmented stage (Figure 5.24). With time and accumulated extension, this fault system is expected to evolve to a more mature stage as exemplified by MGBF, which comprises single fault plane with along-strike undulations (Figures 5.13B and 5.24). Fault system maturation progresses along with formation and evolution of relay ramps through several processes. As interpreted at the Akçapınar relay ramp (Figure 4.5), these processes includes; (i) along-strike propagation of isolated fault segments to form fault overlap zones (Figure 4.2A); (ii) initiation of interaction between the overlapping segments to form a relay ramp (Figure 4.2B); (iii) accumulation of ductile strain at the ramp area by rotation and fault parallel extension (Figure 4.3); and (iv) breaching of the ramp area by fracturing and faulting to form a single fault with along-strike bend (Figure 4.2C, D and E). All these processes are locally observable in Gediz Graben and are associated with a change in structural style at the ramp area (Figure 4.11). Accordingly, stress field also varies from fault-perpendicular extension to fault-parallel extension (Figure 4.11).

The hanging-wall deformation of normal faults provides important clues to the nature of extensional regime in the Gediz Graben. Analysis of the data acquired from faults observed in the Plio-Quaternary deposits suggest that the stress regime driving the current faulting is conformable with approximately N–S-oriented extension with subvertical σ_1 , subhorizontal and E–W-trending σ_2 and subhorizontal

and N–S-trending σ_3 axes (Figure 3.19A). Low ϕ -ratio (Figure 3.19A) suggests that the direction of extension is not well defined, which resulted in simultaneous formation of the faults in multiple strike orientations (Figure 3.11 and 3.12). Analysis of the faults observed within the Neogene deposits also revealed a very similar stress regime and fault pattern to that of Plio-Quaternary deposits (Figure 3.22A). Comparison of fault pattern, stress field and ϕ -ratios between faults observed within the Plio-Quaternary and Neogene deposits provide no evidence of multiple stress fields to indicate a change in the tectonic regime. The entire extensional history of the graben is governed by the ~N–S-oriented extension (Figures 3.25 and 3.26). Minor spatial variation is evident and could be attributed to the local causes such as stress field anomalies at the relay ramps (Figure 4.13).

In the Gediz Graben, the only exception to ~N–S-oriented extension-related deformation pattern is documented by surface observations within the Alaşehir formation. Representing a contractional deformation, this exceptional pattern is characterized by thrust/reverse faults and consistently north-vergent folds that are conformable with ~N–S-oriented compressive stress field (Figures 6.8 and 6.9). The deformation evidently postdates the deposition of the Alaşehir formation and predates some of the extensional structures (Figure 6.6). This relation recalls the episodic extension model, which separates the extension in southwestern Anatolia into earlier phase (1st phase – Miocene) and later phase (2nd phase – Pliocene\Quaternary) of extension separated by a short phase of N–S contraction (Late Miocene –Early Pliocene) (e.g., Koçyiğit et al., 1999; Bozkurt, 2000; Bozkurt and Rojay, 2005; Bozkurt and Sözbilir, 2006; Koçyiğit and Özacar, 2003; Baccetto et al., 2005; Kaya et al., 2004, 2007; Rojay et al., 2005; Westaway et al., 2005; Koçyiğit, 2005). Nevertheless, some hesitations arise to fully support this intervening contractional phase with the data from the Gediz Graben because: (i) the scale of contractional structures is below the conventional mapping scale; (ii) no basin-scale contractional structures were imaged by the seismic data; (iii) the observed deformation is local and was not identified within the other Miocene deposits of Çaltılık and Gediz formations; and (iv) its spatial distribution is not consistent even within the Alaşehir formation. All these hesitations suggest that the observed contractional deformation may be a local phenomenon in the Gediz Graben. Yet, concrete evidences of the regional intervening contractional phase documented from the close surrounding of the Gediz Graben shouldn't be disregarded (e.g., Bozkurt

and Rojay, 2005; Koçyiğit, 2005; Bozkurt and Sözbilir, 2006). It might be possible that, this contractional phase was compensated by the high rates of extension in the Gediz Graben that was rather experienced a tectonic quiescence during this period.

7.2. Stratigraphic Evolution

Seven different lithostratigraphic formations were defined to represent the fill of the graben (Figures 2.2 and 2.3). These units were deposited in alluvial, fluvial and lacustrine depositional systems each of which is represented by characteristic facies associations contained by the formations (Figures 2.4, 2.6, 2.8 and 2.10). Within the same time frame, these facies associations grades into each other spatially as a function of distance to the graben-bounding normal fault systems. Alluvial deposits with coarse-grained facies dominates the vicinity of the graben-bounding structures and rapidly grades into finer fractions of fluvial and/or lacustrine systems away from the graben margins (Figures 2.4, 2.6, 2.8 and 2.10). This depositional architecture repeated itself at least three times during the Miocene and resulted in deposition of Alaşehir, Çaltılık and Gediz formations (Figures 2.2 and 2.3). All the three formations depicts distinct thickness and grain size decrease from south to north to emphasize the dominating activity of the southern margin-bounding structure of the graben (Figures 2.11, 2.13, 5.32 and 5.33). However, during this Miocene evolution of the graben, the relative abundance of alluvial/fluvial vs. lacustrine processes have changed in a way that earlier times has dominated by lacustrine systems (e.g., depositional period of Alaşehir formation in Figure 2.4) that gradually shrank in size (e.g, depositional period of Çaltılık formation in Figure 2.6) and finally occupied entirely by alluvial and/or fluvial deposits (e.g. depositional period of Gediz formation in Figure 2.6). Indeed, this trend, which starts with lacustrine deposits and changes up-section to coarse grained fluvial sediments, is not specific to the Gediz Graben but it has been reported from the number of similar basins and computer-based simulations of the continental rifts (Lambiase, 1990; Schlische, 1993; Lambiase and Bosworth, 1995; Jansen et al., 1995; Contreras et al., 1997; Contreras and Scholz, 2001; Schlische and Withjack, 2007). This large-scale stratigraphic transition is controlled primarily by the decrease of basin capacity (or accommodation space) with respect to sediment supply. Activity of the graben bounding structures controlled the basin capacity whereas sediment supply determines how much of this capacity is filled. Lacustrine systems are favorable

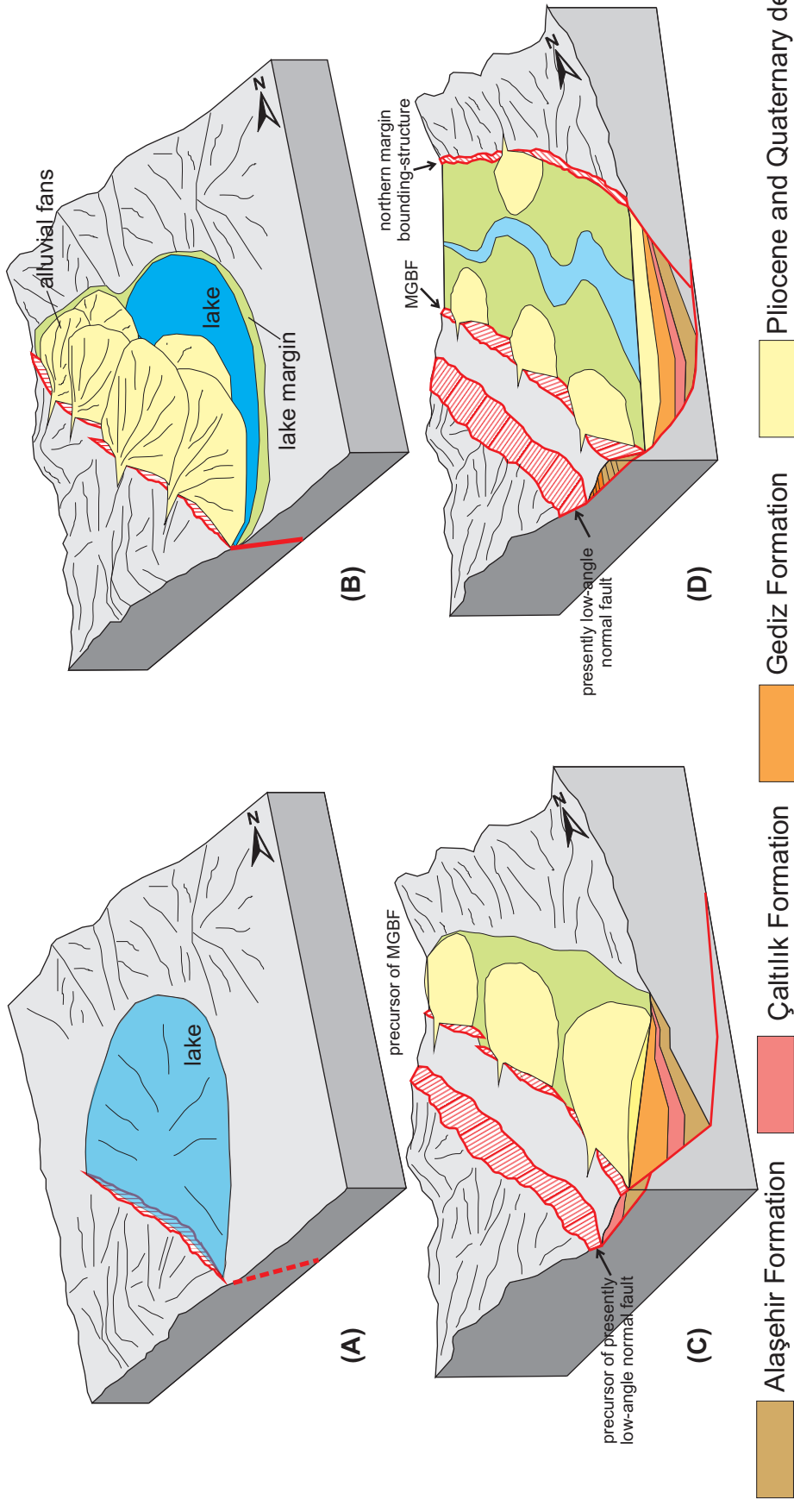


Figure 7.1. Schematic diagrams depicting geological evolution of the Alaşehir subbasin of the Gediz graben. This evolution incorporates change of structural and stratigraphic architecture of the graben. (A) Depositional period of Alaşehir formation. Note the thickness distribution of the formation in Figure 5.25. (B) Depositional period of Çaltılık formation. Note the thickness distribution of the formation in Figure 5.27. (C) Depositional period of Gediz formation. Note the thickness distribution of the formation in Figure 5.29. (D) Depositional period of Kaletepe and Bintepele formation and Quaternary alluvium (Pliocene-Quaternary). Note the thickness distribution of the formations in Figure 5.31.

when the capacity exceeds the sediment supply. During the earlier phase of extension in the Gediz graben, the accumulated tensional strain was low as the relief between the horst and graben blocks. This low relief was favorable for relatively low amount of sediment influx from the horst to graben block and resulted in basin capacity being greater than the sediment supply. This has formed the lacustrine basin of the Alaşehir formation (Figure 7.1A). Accumulated extensional strain, however, has increased the relief between the horst and graben blocks and resulted in increased amount of erosion of the horst block and increased rate of deposition in the graben. This has increased the sediment supply compared to the basin capacity. Consequently, the lacustrine basin gradually filled up during the deposition of the Çaltılık formation (Figure 7-1B). The alluvial and fluvial depositional systems finally became dominant during the deposition of Gediz formation, as they are more compatible with the increased rate of sediment supply (Figure 7.1C).

The Miocene depositional architecture mentioned above was altered slightly during the Pliocene to Quaternary interval, although the trend of general lacustrine to fluvial transition continued by the dominance of axial fluvial system (Figure 7.1-D). Kaletepe and Bintepele formations and unconsolidated Quaternary alluvium represent the deposits of this period (Figures 2.2 and 2.3). The main reason of the change in depositional architecture is the fact that the northern margin-bounding structure has formed and brought along more uniformly partitioned subsidence of the graben block on the northern and southern margins (Figures 5.32 and 5.33). Thus, sediment influx to the graben becomes bipolar and sourced from both margins. The sediment derived from southern horst block deposited the Kaletepe formation along the southern margin while the sediment derived from northern horst block deposited the Bintepele formation along the northern margin (Figure 2.3). The exposures of the both formations are composed of facies associations that can be interpreted to represent alluvial fan environment (Tables 2.7 and 2.8). Similar to Miocene depositional systems, these formations probably grades into finer fractions towards the basin center away from the southern and northern margins, respectively. It is likely that, an axial fluvial system represent the basinward continuation of both Kaletepe and Bintepele formations at the depocenter of the basin and grades upward into the Quaternary alluvium deposits.

Seismic sections from the graben revealed an existence of two distinct surfaces defined by onlap or truncation of the reflections (e.g., Figure 2.14). These

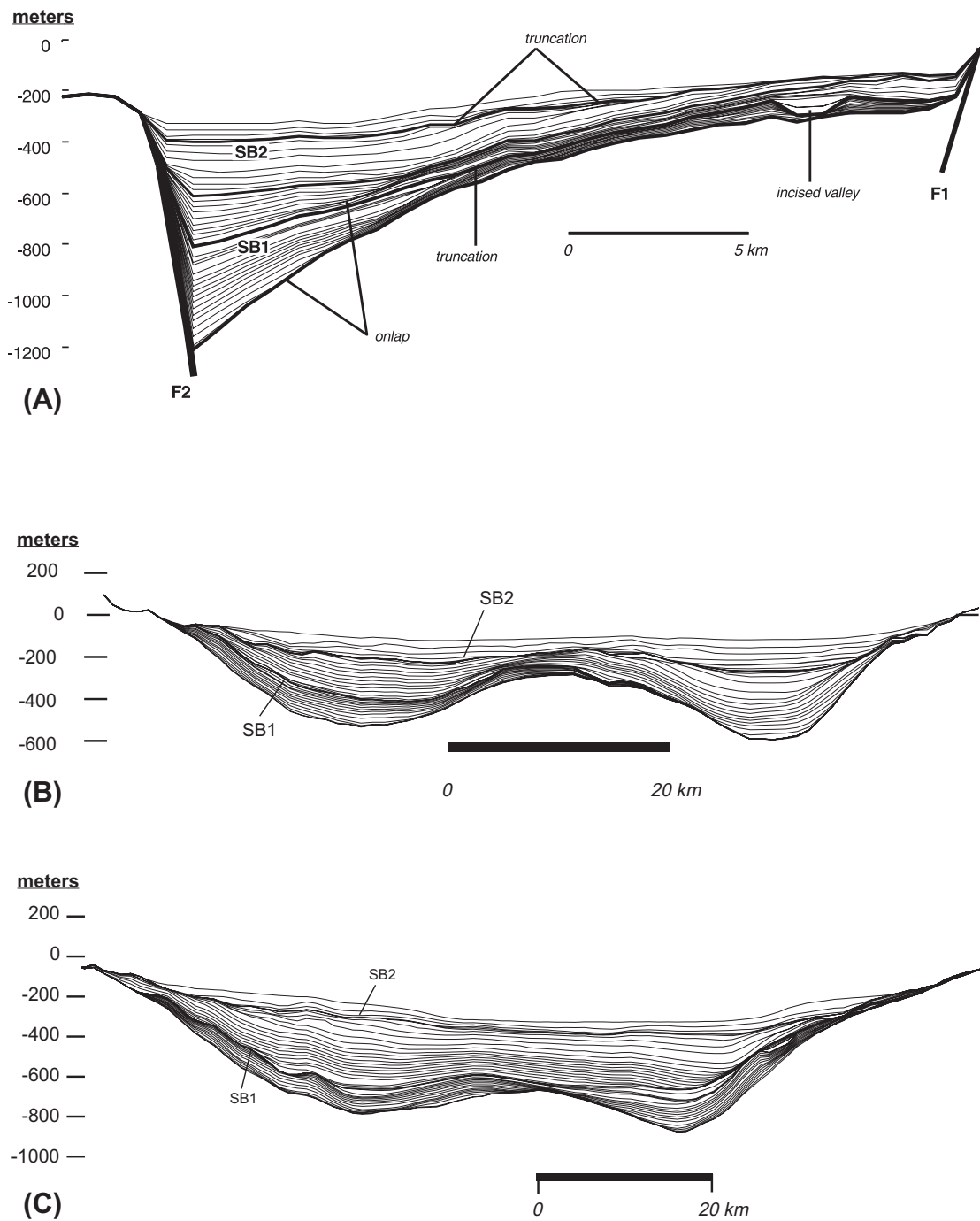


Figure 7.2. Computer-based model of continental rift stratigraphy controlled by segmented bounding structure. SB1 and SB2 are the sequence bounding unconformities that formed by simply changing the climatic conditions during continuous deposition. (A) illustrates a transverse section with respect to graben orientation. Note the onlaps and truncations that are also observed in Figure 2.14. (B) and (C) illustrates the along strike sections of the graben. The discrete depocenters separated by saddle-like anticlines are produced by originally segmented nature of the graben-bounding structure. Note the similarity of these sections to Figures 5.23, 5.32, 5.33, 5.36 and 5.37 in gross geometry and pattern of stratification. From Contreras and Scholz (2001).

bounding surfaces can be traced across the entire Alaşehir subbasin. Similar type of bounding surfaces or unconformities is important feature of the stratigraphy of the continental rift basins (Figure 7.2). Olsen (1997), for example, subdivided the synrift strata of central Atlantic rift basins into four packages based on these surfaces and named them as tectonostratigraphic packages. The bounding surfaces observed within the rift basins could represent time gaps as unconformities or they can be produced by a change in the dynamics of the depositional system during continuous deposition (Olsen, 1997; Contreras and Scholz, 2001; Schlische and Withjack, 2007). Therefore, it is not yet clear if these unconformities reflect regional events such as changes in the tectonic regime or they are related to local processes. An example to local processes could be the strain localization as distributed extension on many smaller faults is localized onto few large ones (Gupta et al., 1998). In a computer modeling effort of rift stratigraphy, Contreras and Scholz (2001) have generated these unconformities by simply changing the climatic conditions during a continuous deposition, which affected the sediment supply to the basin (Figure 7.2).

For the Gediz graben, it is not yet clear if the observed bounding (unconformity) surfaces (Figure 2.14) represent time gaps as no precise age data is available to date the stratigraphic packages at this resolution. It is also very speculative to regard these stratigraphic packages as evidence to regional tectonic events (Yazman et al., 1998; Yılmaz et al., 2000) because the graben fill has significant lateral variations in terms of the number of stratigraphic packages and intervening bounding (unconformity) surfaces. This variation is clearly illustrated in Figure 5.23 between the Alaşehir and Salihli subbasins. It is very likely that, formation of these surfaces is local phenomenon that is related to dynamics of the graben margin evolution, which includes, but not limited to strain localization, shift of main sediment entry points to the graben and climatic changes.

Angular unconformities are observable between the Gediz formation, Kaletepe formations and Quaternary alluvium along the southern margin of the Gediz graben (Figure 2.2). When these unconformities are extended to the fill of the buried graben block, they are all contained within the uppermost seismic stratigraphic unit III (Figure 2.2 and 2.15). The unit III represents a continuous deposition following the Gediz formation without any distinct bounding surface that may correlate with the exposed angular unconformities. This may indicate that the observed unconformities are local and basin margin features that form because of the

rotation and tilting of strata due to activity of the graben-bounding structures. Nevertheless, a faint angular relation defined by a downlap surface is observable in cross-section G-G' (Figure 5.33) at the northern margin of the graben, where Bintepeleer formation is deposited over the Gediz formation as an evidence to initiated activity of the northern margin structure.

7.3. Basin Evolution

Gediz graben shares many similarities with continental rift basins from different parts of the world in terms of stratigraphic and structural architecture (e.g., Lambiase, 1990; Schlische, 1993; Lambiase and Bosworth, 1995; Jansen et al., 1995; Contreras et al., 1997; Olsen, 1997; Contreras and Scholz, 2001; Schlische and Withjack, 2007). This architecture has been complicated by along-strike variations of the graben, which comprises discrete depocenters and relatively isolated subbasins, separated by saddle like transverse anticlines (Figures 5.23, 5.36 and 5.37). Computer simulations of the rift stratigraphy also produce similar along strike variations given that the entire continental rift basin was evolved from a multisegmented graben (Figure 7.2B and C) (Contreras and Scholz, 2001).

The difference in the age and number of sedimentary units deposited in the discrete subbasins suggest that all these along-strike variations are related to the diachronous evolution of the Gediz Graben. Indeed, this evolution of the graben is related to the evolution of the southern margin-bounding structure that initially had very limited along-strike extend (Figure 7.1A). The Alaşehir formation was deposited in front of this initial fault (Figure 7.1A), and consequently has limited distribution in the graben with a well-defined depocenter (Figure 5.25). The graben's evolution was continued by formation of a new, isolated segment to the west of the initial fault (Figure 7.1B). Two discrete depocenters of the Çaltılık formation in Figure 5.27 provide good evidence for the two-segment nature of the bounding-fault at this stage (Figure 7.1B). During the deposition of the Gediz formation, the two segments were already joined and the graben margin migrated towards north by forming the MGBF, which abandoned the presently low-angle normal fault behind (Figure 7.1C). Although, the thickness distribution of the Gediz formation provides limited evidences to the originally segmented nature of the MGBF, well-defined transverse anticlines probably suggest that it was segmented (Figures 5.30 and 6.17). In the last stage of the graben evolution, presently low-angle normal fault and MGBF

has evolved to their current configuration and the northern margin-bounding structure has initiated (Figure 7.1D). The fact that presently low-angle, inactive normal fault is chopped off by active faults and a new fault system is currently forming north of the MGBF is not illustrated in Figure 7.1D. The thickness distribution of the Plio-Quaternary deposits in Figure 5.31 emphasizes an axially oriented depocenter at this stage that is conformable with an axial fluvial system and more symmetrical subsidence of the Gediz Graben.

Diachronous evolution of the Gediz Graben with spatial and temporal variation of its geometry is more obvious if both Alaşehir and Salihli subbasins are considered (Figure 5.23). The Alaşehir subbasin has probably started earlier than the Salihli subbasin, which can be interpreted based on the lack of Alaşehir formation in the Salihli subbasin (Figure 7.3A). Salihli subbasin was initiated later with the depositional period of the Çaltılık formation (Figure 7.3B). During the entire Miocene, the two subbasins were evolved as isolated half grabens (Figure 7.3B and C). With the Pliocene to Quaternary depositional period, the two subbasins were joined and the northern margin-bounding structure has formed (Figure 7.3D). Thus, the current configuration of the Gediz Graben was established.

The independent evolution of the two subbasins with one being older than the other has also some influences on the structural style of the border faults (Figure 7.3D). The presently low-angle and inactive normal fault that is chopped off by active high-angle normal faults is a structural style specific to only Alaşehir subbasin. Although the presently low-angle normal fault is also observable in the Salihli subbasin, there is no such cross-cutting relationship. This may suggest that, the low angle normal fault is still active in the Salihli subbasin (Figure 7.3D). Forming earlier, the Alaşehir subbasin has probably experienced more extensional strain and therefore, established more mature structural configuration at the southern margin relative to Salihli subbasin. Indeed, the low-angle normal faults observed in the two subbasins are probably different structures that form at different times (Figure 7.3). Kinematical incompatibility of the two subbasins can be accommodated by a transfer fault that formed in between the subbasins (Figure 7.3).

The entire evolution history of the Gediz Graben is conformable with the N–S-oriented extension. Even though the extension is episodic with earlier and later phases of extension, the graben behaved well to keep up with its evolutionary path in a continuous manner due to the fact that the direction of extension has not changed.

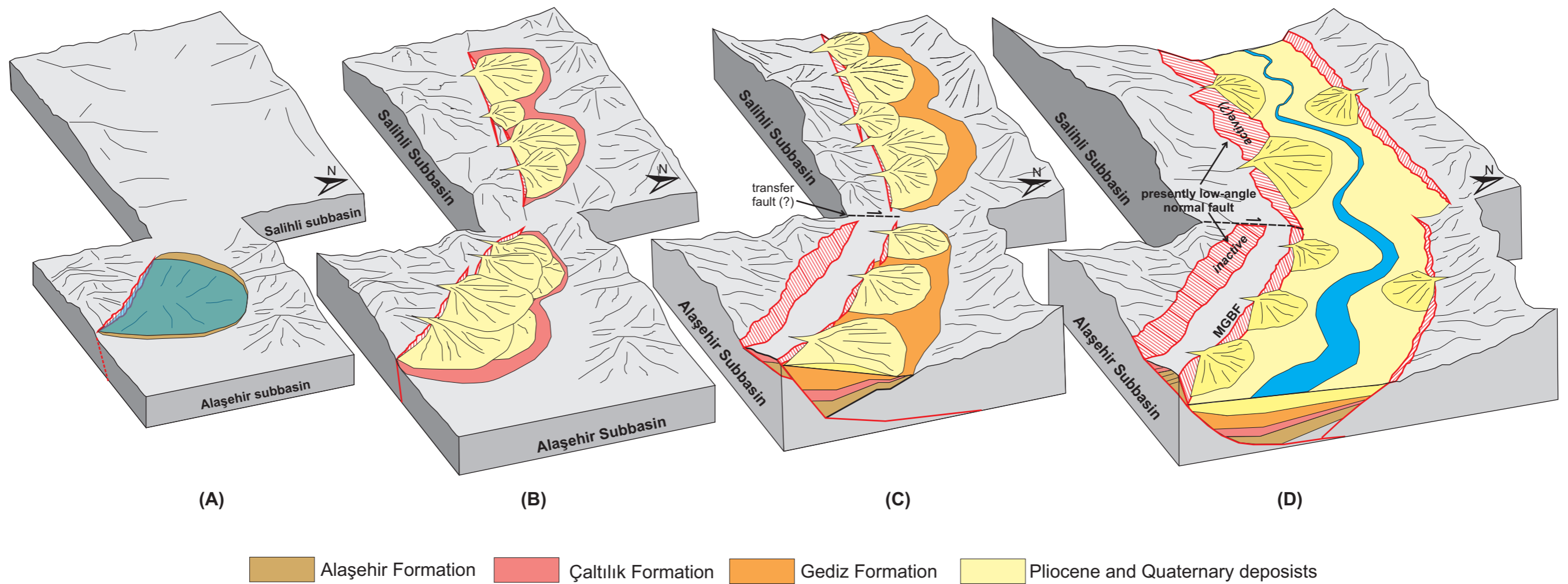


Figure 7.3. Geological evolution of the Gediz Graben. The evolution of the graben is diachronous and includes temporal and spatial variation of the graben's geometry. **(A)** Depositional period of Alaşehir formation (Miocene). **(B)** Depositional period of Çaltılık formation (Miocene). **(C)** Depositional period of Gediz formation (Miocene). **(D)** Depositional period of Kaletepe and Bintepele formations and Quaternary alluvium (Pliocene-Quaternary). Although, the graben is a continuous geomorphologic feature today, including both Alaşehir and Salihli subbasins, the two subbasins were isolated during most of the graben's history. The graben has reached its current configuration during **(D)** with the initiation of northern margin-bounding structure.

This evolutionary path was also benefited from the lack of contractional deformation in the graben that differentiates the earlier and later phases of extension. Yet, a minor change in the evolution of the graben requires some attention. Although the Gediz Graben has evolved as a half graben during the entire Miocene, it became a full graben during Pliocene to Quaternary interval with the initiated activity of the northern margin-bounding structure (Figure 7.3D). This time frame is conformable with the two-stage episodic-extension models proposed by the southwestern Anatolia (e.g., Koçyiğit et al., 1999; Bozkurt, 2000; Bozkurt and Rojay, 2005; Bozkurt and Sözbilir, 2006; Koçyiğit and Özacar, 2003; Baccetto et al., 2005; Kaya et al., 2004, 2007; Rojay et al., 2005; Westaway et al., 2005; Koçyiğit, 2005). Therefore, the change in graben's geometry from a half graben to a full graben might be potentially related with the earlier and later phases of extension. Any change in the dynamics of the extension related to the change in the phase, can drive this geometrical variation of the graben.

REFERENCES

- Acocella, V., Morvillo, P., and Funicello, R., 2005, What control relay ramps and transfer faults within rift zones? Insight from analogue models: *Journal of Structural Geology*, v. 27, p. 397–408.
- Al-Challabi, M., 1994, Seismic velocities – a critique: *First Break*, v. 12, p. 589-596.
- Altunel, E., 1999, Geological and geomorphological observations in relation to 20 September 1899 Menderes earthquake, western Turkey: *Journal of Geological Society London*, v. 156, p. 241-246.
- Ambraseys, N.N., 1988, Engineering seismology: *Earthquake Engineering and Structural Dynamics*, v. 17, p. 1–105.
- Ambraseys, N.N., and Jackson, J.A., 1998, Faulting associated with historical and recent earthquakes in the eastern Mediterranean region: *Geophysical Journal International*, v.133, p. 390-406.
- Anderson, E.M., 1951, *The dynamics of faulting and dyke formation with applications to Britain*: Oliver & Boyd, Edinburg, 206 p.
- Andres, M.H., and Schlische, R.W., 1994, Overlapping faults, intrabasin highs and the growth of normal faults: *Journal of Geology*, v. 102, p. 165-180.
- Angelier, J., 1975, Sur l'analyse de mesures recueillies dans des sites failles: l'utilite d'une confrontation entre les methods dynamiques et cinematiques: *Comptes Rendus de l'Académie des Sciences, Paris, Serie D 281*, p. 1805–1808.
- Angelier, J., 1979, Determination of mean principal direction of stress for a given fault population: *Tectonophysics*, v.56, p. T17-T26.
- Angelier, J., 1984, Tectonic analysis of fault slip data sets: *Journal of Geophysical Research*, v. 89, p. 5835-5848.
- Angelier, J., 1990, Inversion of field data in fault tectonics to obtain the regional stress. III. A new rapid direct inversion method by analytical means: *Geophysical Journal International*, v. 103, p. 363–376.
- Angelier, J., 1994, Fault slip analysis and paleostress reconstruction, in P.L. Hancock, ed., *Continental Deformation*: Pergamon Press, Oxford, p. 53–100.
- Angelier, J., and Gougel, J., 1979, Sur une methods simple de determination des axes principaux des contraintes pur unepopulation de failles: *C.R. Acad. Sci., Paris*, v. D288, p. 307-310.
- Angelier, J., Tarantola, A., Valette, B., and Manuassis, S., 1982, Inversion of field data in fault tectonics to obtain the regional stress – 1, Single phase fault populations: a new method of computing the stress tensor: *Geophysical Journal of Royal and Astronomical Society*, v. 69, p. 607–621.
- Arminjo, R., Carey, E., and Cisternas, A., 1982, The inverse problem in microtectonics and the separation of tectonic phases: *Tectonophysics*, v. 82, p. 145-160.
- Arpat, E., and Bingöl, E., 1969, The rift system in western Turkey: through on its developments: *MTA Bulletin*, v. 79, p. 1–9 [in Turkish with English Abstract].
- Asquith, G., and Gibson, C., 1982, *Basic well log analysis for geologists*, AAPG Methods in Exploration Series #3: AAPG, Tulsa, Oklahoma, 216 p.

- Asquith, G., and Krygowski, D., 2004, Basic well log analysis: AAPG Methods in Exploration Series # 16, AAPG, Tulsa, Oklahoma, 244 p.
- Axen, G.J., and Bartley, J. M., 1997, Field tests of rolling hinges: Existence, mechanical types, and implications for extensional tectonics: *Journal of Geophysical Research*, v. 102, p. 20515-20538.
- Beccaletto, L., and Steiner, C., 2005, Evidence of two-stage extensional tectonics from the northern edge of the Edremit Graben, NW Turkey: *Geodinamica Acta*, v. 18, p. 283–297.
- Ballard, D.H., 1981, Generalizing the Hough transform to detect arbitrary shapes: *Pattern Recognition*, v. 13, p. 111-122.
- Barka, A.A., and Hancock, P.L., 1984, Neotectonic deformation patterns in the convex-northwards arc of the North Anatolian fault, in J.G. Dixon and A.H.F. Robertson, eds., *The Geological Evolution of the Eastern Mediterranean: Geological Society of London Special Publication*, p. 763-773.
- Barka, A.A., and Kadinsky-Cade, K., 1988, Strike-slip fault geometry in Turkey and its influence on earthquake activity: *Tectonics*, v. 7, p. 663-84.
- Bates, C.C., 1953, Rational theory of delta formation: *American Association of Petroleum Geologists Bulletin*, v. 37, p. 2119-2161.
- Benda, L., 1971, Principles of palynologic subdivision of the Turkish Neogene: *Newsletters of Stratigraphy*, v. 1, p. 23-26.
- Benda, L., and Meulenkamp, J. E., 1979, Biostratigraphic correlations in the Eastern Mediterranean Neogene: 5. Calibration of sporomorph associations, marine microfossils and mammal zones, marine and continental stages and radiometric scale: VII. International Congress of Mediterranean Neogene, Athens, 61-70.
- Benda, L., and Meulenkamp, J.E., 1990, Biostratigraphic correlation in the Eastern Mediterranean Neogene, 9. Sporomorph associations and event stratigraphy of the Eastern Mediterranean: *Newsl. Stratigr.*, v. 23, p. 1-10.
- Bishop, A.W., 1966, The strength of solids as engineering materials: *Geotechnique*, v.16, p. 91-130.
- Boggs, S., 1987, Principles of sedimentology and stratigraphy: Merrill Publishing Company, Columbus, Ohio, 784 p.
- Bott, M.H.P., 1959, The mechanism of oblique slip faulting: *Geological Magazine*, v. 96, p. 109-117.
- Bouma, A.H., 1962, Sedimentology of some flysch deposits: Elsevier, Amsterdam, 168 p.
- Bozkurt, E., 2000, Late Alpine evolution of central Menderes massif, western Anatolia, Turkey: *International Journal of Earth Sciences*, DOI 10.1007/s005310000141, v. 89, p. 728-744
- Bozkurt, E., 2001, Neotectonics of Turkey – a synthesis: *Geodinamica Acta*, v. 14, p. 3-30
- Bozkurt, E., 2002, Discussion on the extensional folding in the Alaşehir (Gediz) Graben, western Turkey: *Journal of Geological Society London*, v. 159, p. 105-109.
- Bozkurt, E., 2003, Origin of NE trending basins in western Turkey: *Geodinamica Acta* , v. 16, p. 61–81
- Bozkurt, E., 2004, Granitoid rocks of the southern Menderes Massif (southwest Turkey): field evidence for Tertiary magmatism in an extensional shear zone: *International Journal of Earth Sciences*, v. 93, p. 52–71.
- Bozkurt, E., and Park, R.G., 1994, Southern Menderes Massif: an incipient metamorphic core complex in western Anatolia, Turkey: *Journal of Geological Society London*, v. 151, p. 213-216

- Bozkurt, E., and Park, R.G., 1997, Microstructures of deformed grains in the augen gneisses of southern Menderes Massif and their tectonic significance: *Geol. Rundschau*, v. 86, p. 103-119.
- Bozkurt, E., and Oberhänsli, R., 2001, Menderes Massif (western Turkey): structural, metamorphic and magmatic evolution – a synthesis: *International Journal of Earth Sciences*, v. 89, p. 679–708.
- Bozkurt, E., and Sözbilir, H., 2004, Tectonic evolution of the Gediz Graben: field evidence for an episodic, two-stage extension in western Turkey: *Geological Magazine*, v. 141, p. 63–79.
- Bozkurt, E., and Sözbilir, H., 2006, Evolution of the Large-scale Active Manisa Fault, Southwest Turkey: Implications on Fault Development and Regional Tectonics: *Geodinamica Acta*, v. 19, p. 427-453.
- Bozkurt, E., and Mittwede, S.K., 2005, Introduction: Evolution of Neogene extensional tectonics of western Turkey: *Geodinamica Acta*, v. 18, p.153–165.
- Bozkurt, E., and Rojay, B., 2005, Episodic, two-stage Neogene extension and short-term intervening compression in western Anatolia: field evidence from the Kiraz basin and Bozdağ horst: *Geodinamica Acta*, v. 18, p. 299–316.
- Bozkurt, E., and Sözbilir, H., 2006, Evolution of the large-scale active Manisa fault, southwest Turkey: Implications on fault development and regional tectonics: *Geodinamica Acta*, v. 19, p. 427-453.
- Buck, W. R., 1988, Flexural rotation of normal faults: *Tectonics*, v. 7, p. 959-973.
- Buck, W. R., 1991, Modes of continental lithospheric extension: *Journal of Geophysical Research*, v. 96, p. 20161-178.
- Buck, W.R., 1993, Effect of lithospheric thickness on the formation of high- and low-angle normal faults: *Geology*, v.21, p. 933-936.
- Cant, D.J., 1982, Fluvial facies models and their applications, *in* P.A. Scholle, D. Spearing, eds., *Sandstone depositional environments: American Association of Petroleum Geologists Memori 31*, p. 115-139.
- Cant, D.J., 1992, Subsurface facies analysis, *in* R.G. Walker, N.P. James, eds., *Facies models – response to sea level change: Geological Association of Canada, St. John’s, New Foundland*, p. 27-47.
- Carey, E., and Brunier, B., 1974, Analyse théorique et numérique d’une modèle mécanique élémentaire appliqué a l’étude d’une population des failles: *Comptes Rendus de l’Académie des Sciences, Paris, Serie D 279*, p. 891–894.
- Cartwright, J.A., Thrudgill, B.D., and Mansfield, C.S., 1995, Fault growth by segment linkage: an explanation of scatter in maximum displacement and trace length data from Canyonlands grabens of SE Utah: *Journal of Structural Geology*, v. 17, p. 1319-1326.
- Cashman, P.H., and Ellis, M.A., 1994, Fault interaction may generate multiple slip vectors on a single fault surface: *Geology*, v.22, p. 1123-1126.
- Castagna, J., 1995, Problem, puzzles and pitfalls: Exploration questions and answers: *The Leading Edge*, May 1995, p. 320.
- Castagna, J., 1996, Exploration questions and answers: The sequel: *The Leading Edge*, January 2005, p. 43-45.
- Cihan, M., Saraç, G., and Gökçe, O., 2003, Insights into biaxial extensional tectonics: An example from the Sandıklı Graben, West Anatolia Turkey: *Geological Journal*, v. 38, p. 47-66.
- Childs, C., Watterson, J., and Walsh, J. J., 1995, Fault overlap zones within developing normal fault systems: *Journal of the Geological Society London*, v. 152, p. 535–549.

- Clark, R. M., and Cox, S. J. D., 1996, A modern regression approach to determining fault displacement-length scaling relations: *Journal of Structural Geology*, v. 18, p.147-152.
- Cohen, H.A., Dart, C.J., Akyüz, H.S., and Barka, A.A., 1995, Syn-rift sedimentation and structural development of Gediz and Büyük Menderes graben, western Turkey: *Journal of Geological Society London*, v. 152, p. 629–638.
- Coletta, B., LeQuellec, P., Letousey, J., and Moretti, I., 1988, Longitudinal evolution of Sues rift structure (Egypt): *Tectonophysics*, v. 153, p. 221-233.
- Collins, A.S., and Robertson, A.H.F., 1998, Process of Late Cretaceous to Late Miocene episodic thrust sheet translation in the Lycian Taurides, SW Turkey: *Journal of Geological Society London*, v.155, p.759-772.
- Collinson, J.D., 1996, Alluvial Sediments, *in* H.G. Reading, ed., *Sedimentary environments: Processes, facies and stratigraphy*: Blackwell Science, Oxford, p. 37-83.
- Contreras, J.C., Scholz, H., and King, J.C.P., 1997, A model of rift basin evolution constrained by first order stratigraphic observations: *Journal of Geophysical Research*, v. 102, p. 7673-7690.
- Contreras, J.C., and Scholz, H., 2001, Evolution of stratigraphic sequences in multisegmented continental rift basins: Comparison of computer models with the basins of the East Africa rift system: *American Association of Petroleum Geologists Bulletin*, v. 85, p. 156-1581.
- Coşkun, B., 1997, Oil and gas fields—transfer zone relationships, Thrace Basin, NW Turkey: *Marine and Petroleum Geology*, v. 14, p. 401–416.
- Cowie, P.A., and Scholz, C.H., 1992, Physical explanation for the displacement-length relationships of faults using a post-yield fracture mechanics model: *Journal of Structural Geology*, v.14, p. 1133-1148.
- Cowie, P. A., and Shipton, Z. K., 1998, Fault tip displacement gradients and process zone dimensions: *Journal of Structural Geology*, v. 20, p. 983-997.
- Çiftçi, N.B., and Bozkurt, E., 2007, Anomalous stress field and active breaching in relay ramps: A field example from Gediz Graben, SW Turkey: *Geological Magazine*, in press.
- Çiftçi, N.B., Temel, R.Ö., and Terzioğlu, N., 2004, Neogene stratigraphy and hydrocarbon system of the region surrounding the gulf of Edremit, NW Anatolia, Turkey: *Turkish Association of Petroleum Geologists Bulletin*, v. 16, p. 81-104 [in Turkish with English abstract].
- Dart., C., Cohen, H.A., Akyüz, H.S., and Barka, A., 1995, Basinward migration of rift-border faults: Implications for facies distribution and preservation potential: *Geology*, v. 23, p. 69-72.
- Davidson, L.M., and Park, R.G., 1978, Late Nadssugtoqidian stress orientation derived from deformed granodioritic dykes, north of Greenland: *Journal of Geological Society London*, v. 135, p. 283-289.
- Davis, G.H., 1984, *Structural geology of rocks and regions*: John Wiley & Sons Inc., Canada, 492 p.
- Davis, G.H., and Reynolds, S.J., 1996, *Structural geology of rocks and regions*: John Wiley & Sons Inc., 525 p.
- Dawers, N. H., Anders, M. H., and Scholz, C. H., 1993, Growth of normal faults: displacement length scaling: *Geology*, v. 21, p. 1107-1110.
- Dawers, N.A., and Anders, M.H., 1995, Displacement-length scaling and fault linkage: *Journal of Structural Geology*, v.17, p. 607-614.

- Deniz, O., Sözbilir, H., and Bozkurt, E., 2002, Menderes Masifi ile Alt-Orta Miyosen tortul istif arasındaki dokanak ilişkisinin niteliği ve tektonik önemi, Alaşehir ilçesi güneyinden arazi verileri: 55th Turkish Geological Congress, Ankara, p. 59-61 [in Turkish].
- Dewey, J.F., 1988, Extensional collapse of orogens: *Tectonics*, v.7, p. 1123-1139
- Dewey, J.F., Şengör, A.M.C., 1979, Aegean and surrounding regions: Complex multiple and continuum tectonics in a convergent zone: *Geological Society of America Bulletin*, v. 90, p. 84-92
- Dix, C.H., 1955, Seismic velocities from surface measurements: *Geophysics*, v. 20, p. 68-86.
- Doglioni, C., Agostini, S., Crespi, M., Innocenti, F., Manetti, P., Riguzzi, F., and Savaşçın, Y., 2002, On the extension in western Anatolia and the Aegean Sea: *Journal of Virtual Explorer*, v. 8, p. 169-183.
- Donath, F.A., and Parker, R.B., 1964, Folds and folding: *Geological Society of America Bulletin*, v. 75, p. 45-62.
- Dula, W.F., 1991, Geometric models for listric normal faults and rollover folds: *American Association of Petroleum Geologists Bulletin*, v. 75, p. 1609-1625.
- Ediger, V.Ş., Batı, Z., and Yazman, M., 1996, Paleopalynology of possible hydrocarbon source rocks of the Alaşehir-Turgutlu area in the Gediz Graben (western Anatolia): *Turkish Association of Petroleum Geologists*, v. 8, p. 94-112.
- Emre, T., 1996, Geology and tectonics of Gediz graben: *Turkish Journal of Earth Sciences*, v. 5, p. 171-185 [in Turkish with English abstract].
- Emre, T., and Sözbilir, H., 1997, Field evidence for metamorphic core complex, detachment faulting and accommodation faults in the Gediz and Büyük Menderes grabens (western Turkey): *International Earth Sciences Colloquium on the Aegean Region, IESCA-95*, v. I, p. 73-94.
- Ercan, E., Satır, M., Sevin, A., and Türkecan, A., 1997, Batı Anadoludaki Tersiyer ve Kuvaterner yaşlı volkanik kayalarda yeni yapılan radiometrik yaş ölçümlerinin yorumu: *MTA Bulletin*, v. 119, p. 103-112 [in Turkish with an English abstract].
- Erslev, E.A., 1991, Trishear fault-propagation folding: *Geology*, v. 19, p. 617-620.
- Etchecopar, A., Vasseur, G., and Daignieres, M., 1981, An inverse problem in microtectonics for the determination of stress tensors from fault striation analysis: *Journal of Structural Geology*, v. 3, p. 51-65.
- Etris., E.L., Crabtree, N.J., Dewar, J., and Pickford, S., 2001, True depth conversion: More than a pretty picture: *CSEG Recorder*, November 2001, p. 11-22.
- Eyidoğan, H., and Jackson, J.A., 1985, A seismological study of normal faulting in the Demirci, Alaşehir and Gediz earthquake of 1960-1970 in western Turkey: implications for the nature and geometry of deformation in the continental crust: *Geophysical Journal of royal Astronomy Society*, v. 81, p. 569-607.
- Ferrill, D.A., Morris, A.P., 2001, Displacement gradient and deformation in normal fault systems: *Journal of Structural Geology*, v. 23, p. 619-638.
- Ferrill, D.A., Stamatakos, J.A., and Sims, D., 1999, Normal fault corrugation: Implication for growth and seismicity of active normal faults: *Journal of Structural Geology*, v. 21, p. 1027-1038.
- Ferrill, D.A., Morris, A.P., Stamatakos, J.A., and Sims, D.W., 2000, Crossing conjugate normal faults: *American Association of Petroleum Geologists Bulletin*, v. 84, p. 1543-1559.
- Fleuty, M.J., 1964, The description of folds: *Geological Association Proceedings*, v. 75, p. 461-492.

- Forsyth, D.W., 1992, Finite extension and low angle normal faulting: *Geology*, v.20, p. 27-30.
- Fossen, H., and Gabrielsen, R.H., 1996, Experimental modeling of extensional fault systems by use of plaster: *Journal of Structural Geology*, v. 18, p. 673.
- Fouch, T.D., and Dean, W.E., 1982, Lacustrine environments, in P.A. Scholle, D. Spearing, eds., *Sandstone depositional environments: American Association of Petroleum Geologists Memoir 31*, p. 87-115.
- Gawthorpe, R.L., and Hurst, J.M., 1993, Transfer zones in extensional basins: their structural style and influence on drainage development and stratigraphy: *Journal of the Geological Society London*, v. 150, p. 1132–1137.
- Genç, C., Altunkaynak, Ş., Karacık, Z., Yazman, M., and Yılmaz, Y., 2001, The Çubukdağ graben, south of İzmir: its tectonic significance in the Neogene geological evolution of the western Anatolia: *Geodinamica Acta*, v. 14, p. 45–56.
- Gephart, J.W., and Forsyth, D.W., 1984, An improved method for determining the regional stress tensor using earthquake focal mechanism data: an application to San Fernando earthquake sequence: *Journal of Geophysical Research*, v. B89, p. 9305-9320.
- Gessner, K., Ring, U., Christopher, J., Hetzel, R., Passchier, C.W., and Güngör, T., 2001, An active bivergent rolling hinge detachment system: central Menderes metamorphic core complex in western Turkey: *Geological Magazine*, v. 139, p. 15-26.
- Gibbs, A.D., 1983, Balanced cross-section construction from seismic sections in areas of extensional tectonics: *Journal of Structural Geology*, v. 5, p. 153-160.
- Gibbs, A.D., 1984, Structural evolution of extensional basin margins: *Journal of the Geological Society London*, v. 141, p. 609–620.
- Graue, K., 1992, Extensional tectonics in the northernmost North Sea: rifting, uplift, erosion and footwall collapse in Late Jurassic to Early Cretaceous times, in A.M. Spencer, ed., *Generation, accumulation and production of Europe's hydrocarbons: Springer, Berlin*, p. 23-34.
- Griffiths, P.S., 1980, Box-fault systems and ramps: a typical association of structures from the eastern shoulder of the Kenya rift: *Geological Magazine*, v. 117, p. 579-586.
- Groshong, R.H., 1989, Half-graben structures: Balanced models of extensional fault-bend folds: *Geological Society of America Bulletin*, v. 101, p. 96-105.
- Groshong, R.H., 1994, Area balance, depth to detachment, and strain in extension: *Tectonics*, v. 13, p. 1488-1497.
- Gupta, S., Cowie, P.A., Dawers, N.H., and Underhill, J.R., 1998, A mechanism to explain rift basin subsidence and stratigraphic patterns through fault array evolution: *Geology*, v.26, p. 595-598.
- Guy, H.P., Simons, D.B., and Richardson, E.V., 1966, Summary of alluvial channel data from flume experiments, 1956–1961: *US Geological Survey Professional Paper 462-I*, 96 p.
- Gürsoy, H., Piper, J. D. A., and Tatar, O., 2003, Neotectonic deformation in the western sector of tectonic escape in Anatolia: Palaeomagnetic study of the Afyon region, Central Turkey: *Tectonophysics*, v. 374, p. 57-59.
- Hamblin, W.K., 1965, Origin of reverse drag on the downthrown side of normal faults: *Geological Society of America Bulletin*, v. 76, p. 1145-1164.
- Harding, T.P., 1984, Graben hydrocarbon occurrences and structural style: *American Association of Petroleum Geologists Bulletin*, v. 68, p. 579-586.
- Hamilton, W.B., 1988, Detachment faulting in the Death Valley region, California and Nevada: *U.S. Geological Survey Bulletin*, v.1790, p. 51-85.

- Harding, T. P., 1984, Graben hydrocarbon occurrences and structural style: American Association of Petroleum Geologists Bulletin, v. 68, p. 333-362.
- Harms, J.C., and Fahnestock, R.K., 1965, Stratification, bed forms and flow phenomena (with examples from Rio Grande), in G.V. Middleton, ed., Primary sedimentary structures and their hydrodynamic interpretations: SEPM Special Publication 12, p. 84-155.
- Hassani R., Jongmans D. and Chery J., 1997, Study of plate deformation and stress in subduction processes using two-dimensional numerical models: Journal of Geophysical Research, v. 102, p. 17951-17965.
- Hatcher, R.D., 1990, Structural geology – principles, concepts and problems: Macmillan Publishing Company, New York, 531 p.
- Hetzl, R., Passchier, C.W., Ring, U., and Dora, O.Ö., 1995, Bivergent extension in orogenic belts: the Menderes massif (southwestern Turkey): Geology, v.23, p.455-458.
- Horsfield, W.T., 1980, Contemporaneous movement along crossing conjugate normal faults: Journal of Structural Geology, v. 2, p. 305-310.
- Huang, Q., 1988, Computer based method to separate heterogeneous sets of fault slip data into subsets: Journal of Structural Geology, v. 10, p. 297–299.
- Huang, Q., and Angelier, J., 1987, Les systemes de failles conjugees: Une methode d'identification, de separation et de calcul des axes de contrainte: C.r. heabd. Seanc. Acad. Sci., Paris, v. 304, p. 465-458.
- Hudleston, P.J., 1973, Fold morphology and some geometrical implications of theories of fold development: Tectonophysics, v. 16, p. 1-46.
- Hurley, N.F., and Peters, M., 1999, Lecture notes: Formation evaluation and well log analysis, Colorado School of Mines.
- Imber, J., Tuckwell G.W., Childs, C., Walsh, J.J., Manzocchi, T., Heath, A.E., Bonson, C. G., and Strand, J., 2004, Three-dimensional distinct element modeling of relay growth and breaching along normal faults: Journal of Structural Geology, v. 26, p. 1897-1911.
- İşik, V., Tekeli, O., and Seyitoglu, G., 2003, Ductile-brittle transition along the Alaşehir detachment fault and its structural relationship with the Simav detachment fault, Menderes Massif, western Turkey: Tectonophysics, v. 374, p. 1-18.
- İnci, U., 1998, Lignite and carbonate deposition in Middle Lignite succession of the Soma formation, Soma coalfield, western Turkey: International Journal of Coal Geology, v. 37, p. 287-313.
- İnci, U., 2002, Depositional evolution of Miocene coal successions in the Soma coalfield, western Turkey: International Journal of Coal Geology, v. 51, p. 1-29.
- İztan, H., and Yazman, M., 1991, Geology and hydrocarbon potential of the Alaşehir (Manisa) area, western Turkey: in Proceedings of the International Earth Sciences Congress on Aegean regions, İzmir, p. 327-338.
- İztan, H., Yazman, M.K., and Harput, B.O., 1991, Alaşehir (Manisa) bölgesinin jeolojisi ve hidrokarbon olanakları, TPAO Exploration Group, unpublished technical report, 83 p [in Turkish].
- Jackson, M.P.A., and Galloway, W.E., 1984, Structural and depositional styles of Gulf Coast Tertiary continental margin: Application to hydrocarbon exploration: AAPG Continuing Education Course Notes Series, v. 25, 226 p.
- Jackson, J.A., and McKenzie, D.P., 1984, Active tectonics of the Alpine-Himalayan Belt between western Turkey and Pakistan: Geophysical Journal of Royal Astronomy Society, v. 7, p. 185-264.

- Jackson, J.A., and McKenzie, D.P., 1988, The relationship between plate motions and seismic moment tensors and rates of active deformation in the Mediterranean and Middle East: *Geophysical Journal*, v. 93, p. 45-73.
- Janecke, S.U., Vandenburg, C.J., and Blankenau, J.J., 1998, Geometry, mechanisms and significance of extensional folds from examples in the Rocky Mountain Basin and Range province, U.S.A.: *Journal of Structural Geology*, v. 20, p. 841-856.
- Jansen M.E., Stephenson, R.A., Cloethingh, S., 1995, Temporal and spatial correlations between changes in plate motions and the evolution of rifted basins in Africa: *Geological Society of America Bulletin*, v. 107, p. 1317-1332.
- Jolivet L., Daniel J.M., Truffert C., and Goffé B., 1994, Exhumation of deep crustal metamorphic rocks and crustal extension in arc and back-arc regions: *Lithos*, v. 33, p. 3-30.
- Kaya, O., 1979, Ortadoğu Ege çöküntüsünün (Neojen) stratigrafisi ve tektoniği (Stratigraphy and tectonics of the Neogene central-east Aegean depression): *Geological Society of Turkey Bulletin*, v. 22, p. 35–58 (in Turkish with English abstract).
- Kaya, O., 1981, Miocene reference sections for the coastal parts of west Anatolia: *Newsletters Stratigraphy*, v. 10, p. 164–191.
- Kaya, O., Ünay, E., Saraç, G., Eichhorn, S., Hassenrück, S., Knappe, A., Pekdeğer, A., and Mayda, S., 2004, Halitpaşa transpressive zone: implications for an Early Pliocene compressional phase in central western Anatolia, Turkey: *Turkish Journal of Earth Sciences*, v. 13, p. 1–13.
- Kaya, O., Ünay, E., Göktaş, F., and Saraç, G., 2007, Early Miocene stratigraphy of Central West Anatolia, Turkey: implications for the tectonic evolution of the Eastern Aegean area: *Geological Journal*, v. 49, p. 85-109.
- Khalil S.M., and McClay K.R., 2002, Extensional fault-related folding, northwestern Red Sea, Egypt: *Journal of Structural Geology*, v. 24, p. 743-762.
- Kissel, C., Laj, C., Poisson, A., and Görür, N., 2003, Palaeomagnetic reconstruction of the Cenozoic evolution of the Eastern Mediterranean: *Tectonophysics*, v. 362, p. 199-217.
- Koçyiğit, A., 1988, Basic geological characteristics and total offset of the North Anatolian Fault Zone in Suşehri area, NE Turkey: *METU Pure Appl. Sci.*, v. 22, p. 43-68.
- Koçyiğit, A., 1989, Suşehri basin: an active fault-wedge basin on the North Anatolian Fault Zone, Turkey: *Tectonophysics*, v. 167, p. 13-29.
- Koçyiğit, A., 2005, The Denizli graben-horst system and the eastern limit of western Anatolian continental extension: basin fill, structure, deformational mode, throw amount and episodic evolutionary history: *Geodinamica Acta*, v. 18, p. 167-208.
- Koçyiğit, A., Yusufoglu, H., and Bozkurt, E., 1999a, Evidence from the Gediz graben for episodic two-stage extension in western Turkey: *Journal of the Geological Society London*, v. 156, p. 605–616.
- Koçyiğit, A., Yusufoglu, H., and Bozkurt, E., 1999b, Reply to ‘Discussion on evidence from the Gediz graben for episodic two-stage extension in western Turkey: *Journal of the Geological Society London*, v. 156, p. 1240–1242.
- Koçyiğit, A., Ünay, E., Saraç, G., 2000, Episodic graben formation and extensional neotectonic regime in west Central Anatolia and the Isparta Angle: a case study in the Ak,ehir-Afyon graben, Turkey, *in* E. Bozkurt, J.A. Winchester, J.D.A. Piper eds., *Tectonics and Magmatism in Turkey and the Surrounding Area: Geological Society of London, Special Publication*, v. 173, p. 405-21.
- Koçyiğit, A., and Özacar, A., 2003, Extensional neotectonic regime through the NE edge of the Outer Isparta Angle, SW Turkey: new evidence field and seismic data: *Turkish*

- Journal of Earth Sciences, v. 12, p. 67–90.
- Lambiase, J.J., 1990, A model for tectonic control of lacustrine stratigraphic sequences in continental rift basins, *in* B. Katz, ed., Lacustrine exploration: case studies and modern analogues: American Association of Petroleum Geologists Memoir 50, p. 265-276.
- Lambiase, J.J., and Bosworth, W., 1995, Structural controls on sedimentation in structural basins, *in* J.J. Lambiase, ed., Hydrocarbon habitat in rift basins: Geological Society Special Publication 88, p. 117-144.
- Larsen, P.H., 1988, Relay structures in a Lower Permian basement involved extension system, East Greenland: Journal of Structural Geology, v. 10, p. 3–8.
- Le Pichon, X., and Angelier, J., 1979, The Hellenic arc and trench system: a key to the evolution of eastern Mediterranean area: Tectonophysics, v. 60, p. 1-42
- Le Pichon, X., and Angelier, J., 1981, The Aegean Sea: Philos. Trans. R. Soc. London Ser., A. 300, p. 357-372
- Le Pichon, X., Chamot-Rooke, C., Lallemand, S., Noomen, R., and Veis, G., 1995, Geodetic determination of the kinematics of central Greece with respect to Europe: implications for eastern Mediterranean tectonics: Journal of Geophysical Research, v. 100, p. 12675-12690
- Lenk, O., Türkezer, A., Ergintav, S., Kurt, A.İ., and Belgen, A., 2003, Monitoring the kinematics of Anatolia using permanent GPS network stations: Turkish Journal of Earth Science, v. 12, p. 55–66.
- Lezzar, K.E., Tiercelin, J.J., Le Turdu, C., Cohen, A.S., Reynolds, D.J., Le Gall, B., and Scholz, C.A., 2002, Control on normal fault interaction on the distribution of major Neogene sedimentary depocenter, Lake Tanganyika, East Africa rift: American Association of Petroleum Geologists Bulletin, v. 86, p. 1027–1059.
- Lips, A.L.W., Cassard, D., Sözbilir, H., and Yılmaz, Y., 2001, Multistage exhumation of the Menderes Massif, western Anatolia (Turkey): International Journal of Earth Sciences, v. 89, p. 781-792
- Lisle, R.J., 1989, A simple construction for shear stress: Journal of Structural Geology, v. 11, p. 493-495.
- Lisle, R.J., Tobore, O., and Arlegui, L., 2001, A stress inversion method requiring only fault slip sense: Journal of Geophysical Research, v. 106, p. 2281-2289.
- Mantovani E., Viti M., Babbucci, D., Tamburelli, C., and Albarello, D., 2001, Back-arc extension: which driving mechanism?, *in* M.W. Jessell, ed., General Contributions: 2001: Journal of Virtual Explorer, v. 3, p. 17-45.
- Mantovani, E., Albarello, D., Babbucci, D., Tamburelli, C. and Viti, M., 2002, Trench arc-back arc systems in the Mediterranean area: examples of extrusion tectonics, *in* G. Rosenbaum and G.S. Lister, eds., Reconstruction of the evolution of the Alpine-Himalayan orogeny: Journal of the Virtual Explorer, v. 8, p. 131-147.
- Marrett, R., and Allmendinger, R.W., 1990, Kinematic analysis of fault slip data: Journal of Structural Geology, v. 12, p. 973-986.
- Mauk, J.L., and Burruss, R.C., 2002, Water washing of Proterozoic oil in the Midcontinent rift system: American Association of Petroleum Geologists Bulletin, v. 86, p. 1113–1127.
- McBride, E.F., Shepard, R.G., and Crawley, R.A., 1975, Origin of parallel, near horizontal laminae by migration of bedforms in a small flume: Journal of Sedimentary Petrology, v. 45, p. 132-139.
- McClay, K.R., Dooley, T., Whitehouse, P., and Mills, M., 2002, 4-D evolution of rift systems: Insights from scaled physical models, AAPG Bulletin, v. 86, p. 935–959.

- McClusky, S., Balassanian, S., Barka, A.A., Demir, C., Ergintav, S., Georgiev, I., Gürkan, O., Hamburger, M., Hurst, K., Kahle, H.G., Kastens, K., Kekelidze, G., King, R., Kotzev, V., Lenk, O., Mahmoud, S., Mishin, A., Nadariya, M., Ouzounis, A., Paradissis, D., Peter, Y., Prilepin, M., Reilinger, R.E., Sanlı İ., Seeger, H., Tealeb, A., Toksöz, M.N., and Veis, G., 2000, Global Positioning System constraints on plate kinematics and dynamics in the Eastern Mediterranean and Caucasus: *Journal of Geophysical Research*, v. 105, p. 5695–5720.
- Mcdonald, G.A., 1957, Faults and monoclines on Kilauea Volcano, Hawaii: *Bulletin of the Geological Society of America*, v. 68, p. 269–271.
- McKenzie, D.P., 1978a, Some remarks on the development of sedimentary basins: *Earth Planet Science Letters*, v.40, p.25-32
- McKenzie, D.P., 1978b, Active tectonics of the Alpine-Himalayan belt: the Aegean Sea and surrounding regions: *Geophysical Journal of Royal Astronomy Society*, v. 55, p. 217-254
- McLead, A.E., Underhill, J.R., Davies, S.J., and Dawersi N.H., 2002, The influence of fault array evolution on synrift sedimentation patterns: Controls on deposition in the Strathspey-Brent-Statfjord half graben, northern North Sea: *American Association of Petroleum Geologists Bulletin*, v. 86, p. 1061–1093.
- Medwedeff, D.A., 1989, Growth fault-bend folding at southeast Lost Hills, San Joaquin Valley, California: *American Association of Petroleum Geologists Bulletin*, v. 73, p. 54-67.
- Mercier, J.L., 1981, Extensional-compressional tectonics associated with the Aegean arc: comparison with the Andean Cordillera of south Peru – north Bolivia: *Philos. Trans. R. Soc. London Ser., A.*, v. 300, p. 337-355
- Meulenkamp, J.E., Wortel, M.J.R., Van Vamel, W.A., Spakman, W., and Hoogerduynstrating, E., 1988, On the Hellenic subduction zone and the geodynamic evolution of Crete since the late middle Miocene: *Tectonophysics*, v. 146, p. 203-215
- Meulenkamp, J.E., Van Der Zwan, G.J., and Van Wamel, W.A., 1994, On the late Miocene to recent vertical motions in the Cretan segment of the Hellenic arc: *Tectonophysics*, v. 234, p. 53-72
- Miall, A.D., 1985, Architectural element analysis: A new method of facies analysis applied to fluvial deposits: *Earth Science Reviews*, v. 22, p. 261-308.
- Miall, A.D., 1992, Alluvial deposits, *in* R.G. Walker, N.P. James, eds., *Facies models – response to sea level change*: Geological Association of Canada, St. John's, New Foundland, p. 119-143.
- Miall, A.D., 1996, *The geology of fluvial deposits: Sedimentary facies, basin analysis and petroleum geology*: Springer, New York, 525 p.
- Moretti, I., and Colleta, B., 1987, Spatial and temporal evolution of the Suez rift subsidence: *Journal of Geodynamics*, v. 7, p. 151-168.
- Moretti, I., and Colleta, B., 1988, Fault block tilting: the Gebel Zeit example, gulf of Suez: *Journal of Structural Geology*, v. 10, p. 9-20.
- Morris, A.P., Ferrill, D.A., and Henderson, D.B., 1996, Slip tendency analysis of fault reactivation: *Geology*, v.24, p. 275-278.
- Morley, C.K., 1988, Variable extension in lake Tanganyika: *Tectonics*, v. 7, p. 785–801.
- Morley, C.K., 1995, Developments in the structural geology of rifts over the last decade and their impact on hydrocarbon exploration, *in* J.J. Lambiase, ed., *Hydrocarbon habitat in rift basins*: Geological Society Special Publication 80, p. 1-32.
- Morley, C.K., 2002, Evolution of large normal faults: Evidence from seismic reflection data: *American Association of Petroleum Geologists Bulletin*, v. 86, p. 961-978.

- Morley, C. K., Nelson, R. A., Patton, T. L., and Munn, S. G., 1990, Transfer zone in the East African rift system and their relevance to hydrocarbon exploration in rifts: American Association of Petroleum Geologists Bulletin, v. 74, p. 1234-1253
- Nemec, W., and Steel, R.J., 1984, Alluvial and coastal conglomerates: Their significant features and some comment on gravelly mass-flow deposits, in E.H. Koster and R.J. Steel, eds., Sedimentology of Gravels and Conglomerates: Canadian Society of Petroleum Geologists Memoir 10, p. 1-31.
- Nilsen, T.H., 1982, Alluvial fan deposits, in P.A. Scholle, D. Spearing, eds., Sandstone depositional environments: American Association of Petroleum Geologists Memoir 31, p. 49-87.
- Nicol, A., Walsh, J.J., Watterson, J., Bretan, P.G., 1995, Three dimensional geometry and growth of conjugate normal faults: Journal of Structural Geology, v. 17, p. 847-862.
- Oddone, F., and Massonnat, G., 1992, Volume loss and deformation around conjugate fractures: comparison between natural examples and analogue experiments: Journal of Structural Geology, v. 14, p. 963-972.
- Olsen, P.E., 1997, Stratigraphic record of the early Mesozoic breakup of Pangea in the Laurasia-Gondwana rift system: Annual Reviews of Earth and Planetary Science, v. 25, p. 337-401.
- Oral, M.B., Reilinger, R.E., Toksöz, M.N., Kong, R.W., Barka, A.A., Kınık, İ., and Lenk, O., 1995, Global positioning system offers evidence of plate motions in Eastern Mediterranean: EOS Transac., n.76 (9).
- Orife, T., Arlegui, L., and Lisle, R.J., 2002, DIPSLIP: a QuickBasic stress inversion program for analyzing sets of faults without slip lineations: Computers and Geosciences, v. 28, p. 775-781.
- Okay, A.I., and Satır, M., 2000, Coeval plutonism and metamorphism in a latest Oligocene metamorphic core complex in northwest Turkey: Geological Magazine, v. 137, p. 495-516.
- Okay, A.I., and Tüysüz, O., 1999, Tethyan sutures of northern Turkey, in B. Durand, L. Jolivet, L. Horvath, M. Serranne, eds., The Mediterranean basins: Tertiary extension within the Alpine orogen: Geological Society of London Special Publication, v. 156, p. 475-515.
- Özer, S., and Sözbilir, H., 2003, Presence and tectonic significance of Cretaceous rudist species in the so-called Permo-Carboniferous Göktepe Formation, central Menderes Massif, western Turkey: International Journal of Earth Sciences, v. 92, p. 397-404.
- Peacock, D.C.P., 2003, Scaling of transfer zones in British Isles: Journal of Structural Geology, v. 25, p. 1561-1567.
- Peacock, D.C.P., 1991, Displacement and segment linkage in strike-slip fault zones: Journal of Structural Geology, v. 13, p. 1025-1035.
- Peacock, D.C.P., and Sanderson, D.J., 1991, Displacements, segment linkage and relay ramps in normal fault zones: Journal of Structural Geology, v. 13, p. 721-733.
- Peacock, D.C.P., and Sanderson, D.J., 1994, Geometry and development of relay ramps in normal fault systems: American Association of Petroleum Geologists Bulletin, v. 78, p. 147-165.
- Peacock, D.C.P., and Sanderson, D.J., 1996, Effects of propagation rate on displacement variations along faults: Journal of Structural Geology, v. 18, p. 311-320.
- Peacock, D.C.P., Knipe, R.J., and Sanderson, D.J., 2000, Glossary of normal faults: Journal of Structural Geology, v. 22, p. 291-305.
- Perissoratis, C., and Conispoliatis, N., 2003, The impacts of sea-level changes during latest Pleistocene and Holocene times on the morphology of the Ionian and Aegean seas (SE Alpine Europe): Marine Geology, v.196, p. 145-156.

- Piper, J. D. A., Gürsoy, H., Tatar, O., İşseven, T., Koçyiğit, A., 2002, Palaeomagnetic evidence for the Gondwanic origin of the Taurides and rotation of the Isparta Agle, southern Turkey: *Geological Journal*, v. 37, p. 317-336.
- Pollard, D.D., and Segal, P., 1987, Theoretical displacements and stresses near fractures in rock: with applications to faults, joints, veins, dikes and solution surfaces, in B.D. Atkinson, ed., *Fracture Mechanics of Rock*: Academic Press, London, p. 277-349.
- Pollard, D.D., Saltzer, S.D., and Rubin, A.M., 1993, Stress inversion methods: are they based on faulty assumptions?: *Journal of Structural Geology*, v. 15, p. 1045–1054.
- Prosser, S., 1993, Rift-related linked depositional systems and their seismic expressions, in G.D. Williams and A. Dobb, eds., *Tectonics and seismic sequence stratigraphy*: Geological Society Special Publication 71, p. 117-144.
- Purvis, M., and Robertson, A.H.F., 2004, A pulsed extension model for the Neogene–Recent E–W-trending Alaşehir Graben and the NE–SW-trending Selendi and Gördes basins, western Turkey: *Tectonophysics*, v. 391, p. 171–201.
- Purvis, M., and Robertson, A.H.F., 2005, Sedimentation of the Neogene-Recent Alasehir (Gediz) continental graben system used to test alternative tectonic models for western (Aegean) Turkey: *Sedimentary Geology*, v. 173, p. 373–408.
- Purvis, M., Robertson, A., and Pringle, M., 2005, Ar40-Ar39 dating of biotite and sanidine in tuffaceous sediments and related intrusive rocks: Implications for the Early Miocene evolution of the Gördes and Selendi basins, W Turkey: *Geodinamica Acta*, v. 18, p. 239–253.
- Ramsay, J.G., 1967, *Folding and fracturing of rocks*: McGraw-Hill Book Company, New York, 560 p.
- Ramsay, J.G., and Lisle, R.J., 2000, *Modern structural geology – Volume 3: Applications of continuum mechanics in structural geology*: Elsevier Academic Press, London, 1061 p.
- Ramsay, J.G., and Hubber, M.I., 1987, *The techniques of modern structural geology – Volume 2: Folds and fractures*: Academic Press Inc., London, 700 p.
- Reches, Z., 1987, Determination of the tectonic stress tensor from slip along faults that obey the Coulomb criterion: *Tectonics*, v. 6, p. 849-861.
- Reilinger, R.E., McClusky, S.C., Oral, M.B., King, W., and Toksöz, M.N., 1997, GPS measurements of present day crustal movements in the Arabian-Africa-Eurasia plate collision zone: *Journal of Geophysical Research*, v. 102, p. 9983-9999.
- Richardson-Bunbury, J.M., 1996, The Kula volcanic field, western Turkey: the development of a Holocene alkali basalt province and the adjacent normal-faulting graben: *Geological Magazine*, v.133, p. 275-283.
- Ring, U., Gessner, K., Güngör, T., and Passchier, C.W., 1999, The Menderes Massif of western Turkey and the Cycladic Massif in the Aegean-do they really correlate: *Journal of Geological Society London*, v.156, p. 3-6.
- Rojay, B., Toprak, V., Demirci, C., and Süzen, L., 2005, Plio-Quaternary evolution of the Küçük Menderes Graben Southwestern Anatolia, Turkey: *Geodinamica Acta*, v. 18, p. 317–331.
- Rotstein Y., 1984, Counterclockwise rotation of Anatolian block: *Tectonophysics*, v. 108, p.71-91.
- Sarıca, N., 2000, The Plio-Pleistocene age of Büyük Menderes and Gediz grabens and their tectonic significance on N-S extensional tectonics in west Anatolia: mammalian evidence from the continental deposits: *Geological Journal*, v. 35, p. 1-24.
- Schlische, R. W., 1991, Half-graben filling models: implications for the evolution of continental extensional basins: *Basin Research*, v. 3, p. 123–141.

- Schlische, R. W., 1992, Structural and stratigraphic development of the Newark extensional basin, eastern North America: implications for the growth of the basin and its bounding structures: *Geological Society of America Bulletin*, v. 104, p. 1246–1263.
- Schlische, R.W., 1993, Anatomy and evolution of the Triassic-Jurassic continental rift system, eastern North America: *Tectonics*, v. 12, p. 1026-1042.
- Schlische, R.W., 1995, Geometry and origin of fault-related folds in extensional settings: *American Association of Petroleum Geologist Bulletin*, v. 79, p. 1661-1678.
- Schlische, R.W., and Withjack, M.O., 2007, Rift basin architecture and evolution: <http://www.ldeo.columbia.edu/~polsen/nbcp/breakupintro.html>
- Schlische, R. W., and M. H. Anders, 1996, Stratigraphic effects and tectonic implications of the growth of normal faults and extensional basins, in K. K. Beratan, ed., *Reconstructing the structural history of Basin and Range extension using sedimentology and stratigraphy: Geological Society of America Special Paper 303*.
- Seyitoğlu, G., and Scott, B.C., 1991, Late Cenozoic crustal extension and basin formation in west Turkey: *Geology Magazine*, v.28, p. 155-166.
- Seyitoğlu, G., and Scott, B., 1992, The age of the Büyük Menderes Graben (west Turkey) and its tectonic implications: *Geological Magazine*, v. 129, p. 239–42.
- Seyitoğlu, G. and Scott, B.C. 1996. The age of Alaşehir Graben (west Turkey) and its tectonic implications: *Geology Journal*, v. 31, p. 1–11.
- Seyitoğlu, G., Çemen, I., and Tekeli , O., 2000, Extensional folding in the Alaşehir Gediz graben, western Turkey. *Journal of the Geological Society, London*, v. 157, p. 1097–1100.
- Seyitoğlu, G., Tekeli, O., Çemen, İ., Şen, Ş., and Işık, V., 2002, The role of flexural rotation/rolling hinge model in the tectonic evolution of the Alaşehir graben, western Turkey: *Geology Magazine*, v. 139, p. 15-26.
- Shaw, J.H., Hook, S.C., and Sitohang, E.P., 1997, Extensional fault-bend folding and synrift deposition: An example from the central Sumatra Basin, Indonesia: *American Association of Petroleum Geologists Bulletin*, v. 81, p. 367-379.
- Shaw, J.H., Connors, C., and Suppe, J., 2005, Seismic interpretation of contractional fault-related folds: *An AAPG Seismic Atlas, Studies in Geology #53*, 156 p.
- Sibson, R.H., 1985, A note on fault reactivation: *Journal of Structural Geology*, v. 7, p. 751-754.
- Soliva, R., and Benedicto, A., 2004, A linkage criterion for segmented normal faults: *Journal of Structural Geology*, v. 26, p. 2251–2267.
- Soliva, R., and Benedicto, A., 2005, Geometry, scaling relations and spacing of vertically restricted normal faults: *Journal of Structural Geology*, v. 27, p. 317–325.
- Sözbilir, H., 2001, Geometry of macroscopic structures with their relations to the extensional tectonics: field evidence from the Gediz detachment, western Turkey: *Turkish Journal of Earth Sciences*, v. 10, p. 51-67.
- Sözbilir, H. 2002, Geometry and origin of folding in the Neogene sediments of the Gediz Graben, western Anatolia, Turkey: *Geodinamica Acta*, v. 15, p. 277–288.
- Spencer, J.E., 1984, The role of tectonic denudation in the warping and uplift of low-angle normal faults: *Geology*, v.12, p. 95-98.
- Steward, A., 2001, Displacement distributions on extensional faults: Implications for fault stretch, linkage and seal: *American Association of Petroleum Geologists Bulletin*, v. 85, p. 587-599.
- Stow, D. A. W., Reading, H. G., Collinson, J. D., 1996, Deep seas, *in* H.G. Reading, ed., *Sedimentary environments: Processes, facies and stratigraphy*: Blackwell Science, Oxford, p. 395-453.

- Suppe, J., 1983, Geometry and kinematics of fault-bend folding: *American Journal of Science*, v. 283, p. 684-721.
- Suppe, J., and Medwedeff, D.A., 1990, Geometry and kinematics of fault-propagation folding: *Ecolg. Geol. Helv.*, v. 83, p. 409-454.
- Suppe, J., Chou, G.T., and Hook, S.C., 1992, Rates of folding and faulting determined from growth strata, *in* K.R. McClay, ed., *Thrust tectonics*: Chapman and Hall, London, p. 105-121.
- Şengör, A.M.C., 1979, The North Anatolian transform fault: its age, offset and tectonic significance: *Journal of Geological Society London*, v. 136, p. 269–282.
- Şengör, A.M.C., 1987, Cross faults and differential stretching of hanging walls in regions of low angle normal faulting: examples from western Turkey, *in* M.P. Coward, J.F. Dewey, and P.L. Hancock, eds., *Continental Extensional Tectonics: geological Society Special Publication*, v. 28, p. 575-589
- Şengör, A.M.C., 1993, Some current problems on the tectonic evolution of the Mediterranean during the Cainozoic, *in* E. Boschi, E. Mantovani, and A. Morelli eds., *Recent evolution and seismicity of the Mediterranean region*: Kluwer Academic Publishers, p. 1-51
- Şengör, A.M.C., and Yılmaz, Y., 1981, Tethyan evolution of Turkey: A plate tectonic approach: *Tectonophysics*, v. 75, p. 181-241.
- Şengör, A.M.C., Görür, N., and Şaroğlu, F., 1985, Strike slip faulting and related basin formation in zones of tectonic escape: Turkey as a case study, *in* K. Biddle, N. Christie-Blick, eds., *Strike Slip Deformation, Basin Formation and Sedimentation*: SEPM Special Publication, v.37, p.227-264
- Talbot, M.R., and Allen, P.A., 1996, Lakes, *in* H.G. Reading, ed., *Sedimentary environments: Processes, facies and stratigraphy*: Blackwell Science, Oxford, p. 83-125.
- Taymaz, T., 1993, The source parameters of the Çubukdağ (W Turkey) earthquake of 1986 October 11: *Geophysical Journal International*, v.113, p. 260-267.
- Taymaz, T., Jackson, J.A., and McKenzie, D.P., 1991, Active tectonics of north and central Aegean Sea: *Geophysical Journal International*, v.113, p. 433-490.
- Temiz, H., Gürsoy, H., and Tatar, O., 1998, Kinematics of Late Pliocene–Quaternary normal faulting in the southeastern end of the Gediz Graben: *International Geology Reviews*, v. 40, p. 638-646.
- Thomson, S.N., Stockhert, B., and Brix, M.N., 1998, Thermochronology of the high-pressure metamorphic rocks of Crete, Greece: implications for the speed of tectonic processes: *Geology*, v. 26, p. 259-262
- Trudgill, B.D., 2002, Structural controls on drainage development in the Canyonlands grabens of southeast Utah: *Americal Association of Petroleum Geologists Bulletin*, v. 86, p. 1095–1112.
- Trudgill, B. D., and Cartwright, J. A., 1994, Relay ramp forms and normal fault linkages, Canyonlands National Park, Utah: *Bulletin of the Geological Society of America*, v. 106, p. 1143-1157.
- Twiss, R.J., and Moores, E.M., 1992, *Structural Geology*: Freeman and Co.
- Twiss, R.J., and Unruh, J.R., 1998, Analysis of fault slip inversions; do they constrain stress or strain rate?: *Journal of Geophysical Research*, v. 103, p. 12205-12222.
- Walker, R.G., 1992, Turbidites and submarine fans, *in* R.G. Walker, N.P. James, eds., *Facies models – response to sea level change*: Geological Association of Canada, St. John's, New Foundland, p. 239-265.
- Wallace, R.E., 1951, Geometry of shearing stress and relation to faulting: *Journal of Structural Geology*, v. 13, p. 118-130.

- Walsh, J.J., and Watterson, J., 1988, Analysis of the relationship between displacements and dimensions of faults: *Journal of Structural Geology*, v.10, p. 239-247.
- Walsh, J.J., and Watterson, J., 1991, Geometric and kinematic coherence and scale effects in normal fault systems, in A.M. Roberts, G. Yielding, and B. Freeman, eds., *The Geometry of Normal Faults: Geological Society, London, Special Publications*, v. 56, p. 193–203.
- Watterson, J.A., Nicol, A., Walsh, J.J., and Meier, D., 1998, Strains at the intersections of synchronous conjugate normal faults: *Journal of Structural Geology*, v. 20, p. 363-370.
- Wernicke, B., and Axen, G.J., 1988, On the role of isostasy in evolution of normal fault systems: *Geology*, v. 16, p. 848-851.
- Westaway, R., 1994, Evidence for dynamic coupling of surface processes with isostatic compensation in the lower crust during active extension of western Turkey: *Journal of Geophysical Research*, v. 99, p. 20203–20223.
- Westaway, R., Guillou, H., Yurtmen, S., Demir, T., Scaillet, S., and Rowbotham, G., 2005, Constraints on the timing and regional conditions at the start of the present phase of crustal extension in western Turkey, from observations in and around the Denizli region: *Geodinamica Acta*, v. 18, p. 209–238.
- White, N.J., Jackson, J., and McKenzie, D.P., 1986, The relationship between the geometry of normal faults and that of the sedimentary layers in the hanging-walls: *Journal of Structural Geology*, v. 8, p. 897-909.
- Withjack, M.O., Islam, Q.T., and La Pointe, P.R., 1995, Normal faults and their hanging-wall deformations: an experimental study: *American Association of Petroleum Geologists Bulletin*, v. 79, p. 1-18.
- Woods, E.P., 1992, Vulcan Subbasin fault style-implications for hydrocarbon migration and entrapment: *The APEA Journal*, v. 32, p. 138-158.
- Woodside, J.M., Mascle, J., Zitter, T.A.C., Limonov, A.F., Ergün, M., Volkonskaia, A., and shipboard scientists of the PRISMED II Expedition, 2002, The Florence Rise, the western bend of the Cyprus arc: *Marine Geology*, v. 185, p. 177-194.
- Xiao, H., and Suppe, J., 1988, Origin of rollover: *Geological Society of America Abstracts with Programs*, v. 20, p. A109.
- Xiao, H., and Suppe, J., 1989, Role of compaction in the listric shape of growth normal faults: *American Association of Petroleum Geologists Bulletin*, v. 73, p. 777-786.
- Xiao, H., and Suppe, J., 1992, Origin of rollover: *American Association of Petroleum Geologists Bulletin*, v.76, p. 509-529.
- Yamaji, A., 2000, The multiple inverse method: a new technique to separate stresses from heterogeneous fault-slip data: *Journal of Structural geology*, v. 22, p. 441-452.
- Yamaji, A., Sato, K., and Otsubo, M., 2005, Multiple Inverse Method software package – User’s Guide: Division of Earth and Planetary Sciences, Kyoto University, 16 p.
- Yazman, M.K., and İztan, H., 1990, Alaşehir’in (Manisa) jeolojisi ve petrol olanakları, TPAO Exploration Group, unpublished technical report, 18 p [in Turkish].
- Yazman, M.K., Güven, A., Ermiş, Y., Yılmaz, M., Özdemir, İ., Akçay, Y., Gönülalan, U., Tekeli, Ö., Aydemir, V., Sayılı, A., Batı, Z., İztan, H., and Korucu, Ö., 1998, Alaşehir Grabeni'nin ve Alaşehir-1 prospektinin değerlendirme raporu, TPAO Exploration Group, unpublished technical report, 142 p [in Turkish].
- Yılmaz, Y., and Karacık, Z., 2001, Geology of the northern side of gulf of Edremit and its tectonic significance for the development of Aegean grabens: *Geodinamica Acta*, v. 14, p. 31-43.
- Yılmaz, Y., Genç, S.C., Gürer, Ö.F., Bozcu, M., Yılmaz, K., Karacık, Z., Altunkaynak, Ş., and Elmas, A., 2000, When did western Anatolian grabens begin to develop, in E.

- Bozkurt, J.A. Winchester, and J.D.A. Piper, eds., Tectonics and magmatism in Turkey and the surrounding area: Geological Society London Special Publication, v. 173, p. 353-384
- Yılmaz, O., 2001, Seismic Data Analysis: Processing, Inversion and Interpretation of Seismic Data (Vols. 1 & 2): Society of Exploration Geophysicists, Tulsa Oklahoma, 2027 p.
- Younes, A.I., and McClay, K., 2002, Development of accommodation zones in the Gulf of Suez–Red Sea rift, Egypt: American Association of Petroleum Geologists Bulletin, v. 86, p. 1003–1026.
- Young, M.J., Gawthorpe, R.L., and Sharp, I.R., 2002, Architecture and evolution of syn-rift clastic depositional systems towards the tip of a major fault segment, Suez Rift, Egypt: Basin Research, v. 14, p. 1–23.
- Yusufoğlu, H., 1996, Northern Margin of the Gediz Graben: Age and evolution, west Turkey: Turkish Journal of Earth Sciences, v. 5, p. 11-23.
- Yusufoğlu, H., 2002, Discussion on the extensional folding in the Alaşehir (Gediz) Graben, western Turkey, J. Geo. Soc., London, v. 159, p. 105-109.
- Zanchi, A., Kissle, C., and Tapırdamaz, C., 1993, Late Cenozoic and Quaternary brittle continental deformation in western Turkey: Bull. Soc. Geol. France, v. 165, p. 507-517.
- Zitter, T.A.C., Huguen, C., Woodside, J.M., 2005, Geology of mud volcanoes in the eastern Mediterranean from combined sidescan sonar and submersible surveys: Deep-Sea Research I, v. 52, p. 457–475.

APPENDIX I

MEASURED STRATIGRAPHIC SECTIONS

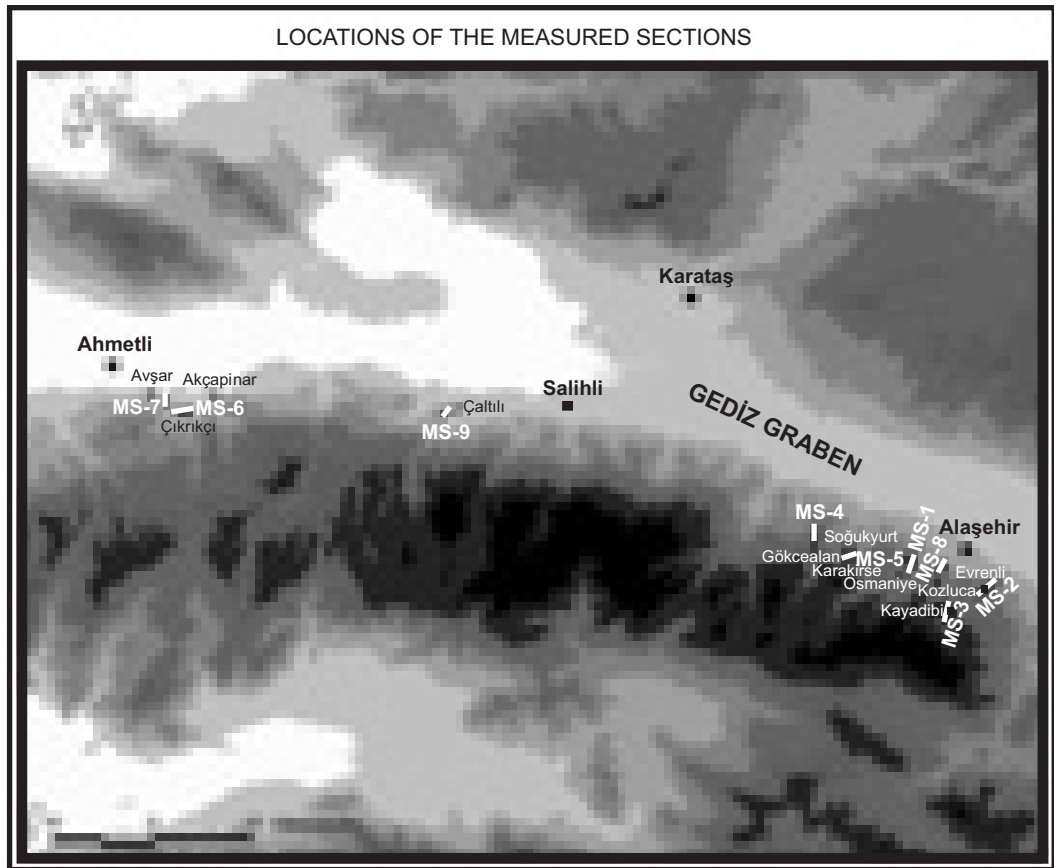


Figure AI.1. Locations of the measured stratigraphic sections (MS) along the southern margin of the Gediz Graben. There are nine measured sections from MS-1 to MS-9. See Figures AI.3 to AI.6 for the details of the sections. Chapter 2 discusses geological meaning of the observed lithofacies and their variations.

EXPLANATIONS




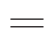










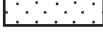

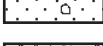

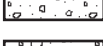

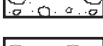












LITHOLOGY	SEDIMENTARY STRUCTURES
 Chert	 Lamination
 Limestone	 Well bedded
 Claystone	 Poorly bedded
 Marl	 Massive - Non bedded
 Siltstone	 Normally graded bedding
 Mudstone	 Inversely graded bedding
 Coal	 Planar cross bedding
 Sandstone	 Troughy cross bedding
 Pebbly Sandstone	 Foreset cross bedding
 Gravelstone	 Convolute lamination - bedding
 Conglomerates	 Erosive base
 Metamorphics	 Ripple marks
OTHERS	 Pebble imbrication
 No outcrop	 Flame structures
 Broken Section	 Rip-up clasts
 Fault	 Shear planes
	 Concretions
	 Organic remnants

Figure AI.2. Explanations of the patterns and symbols that are used to illustrate the measured stratigraphic sections in Figures AI.3 to AI.6.

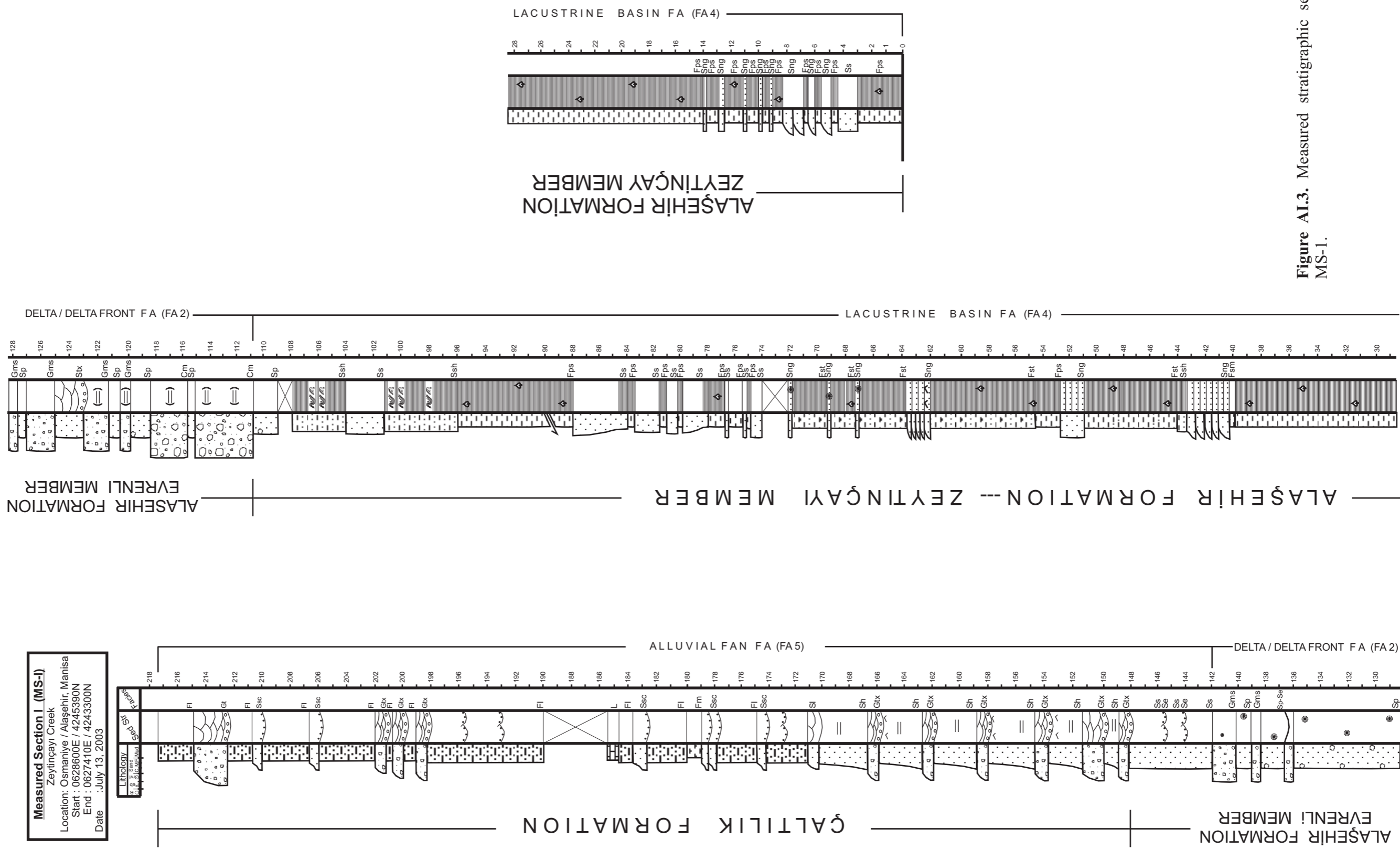


Figure AI.3. Measured stratigraphic section MS-1.

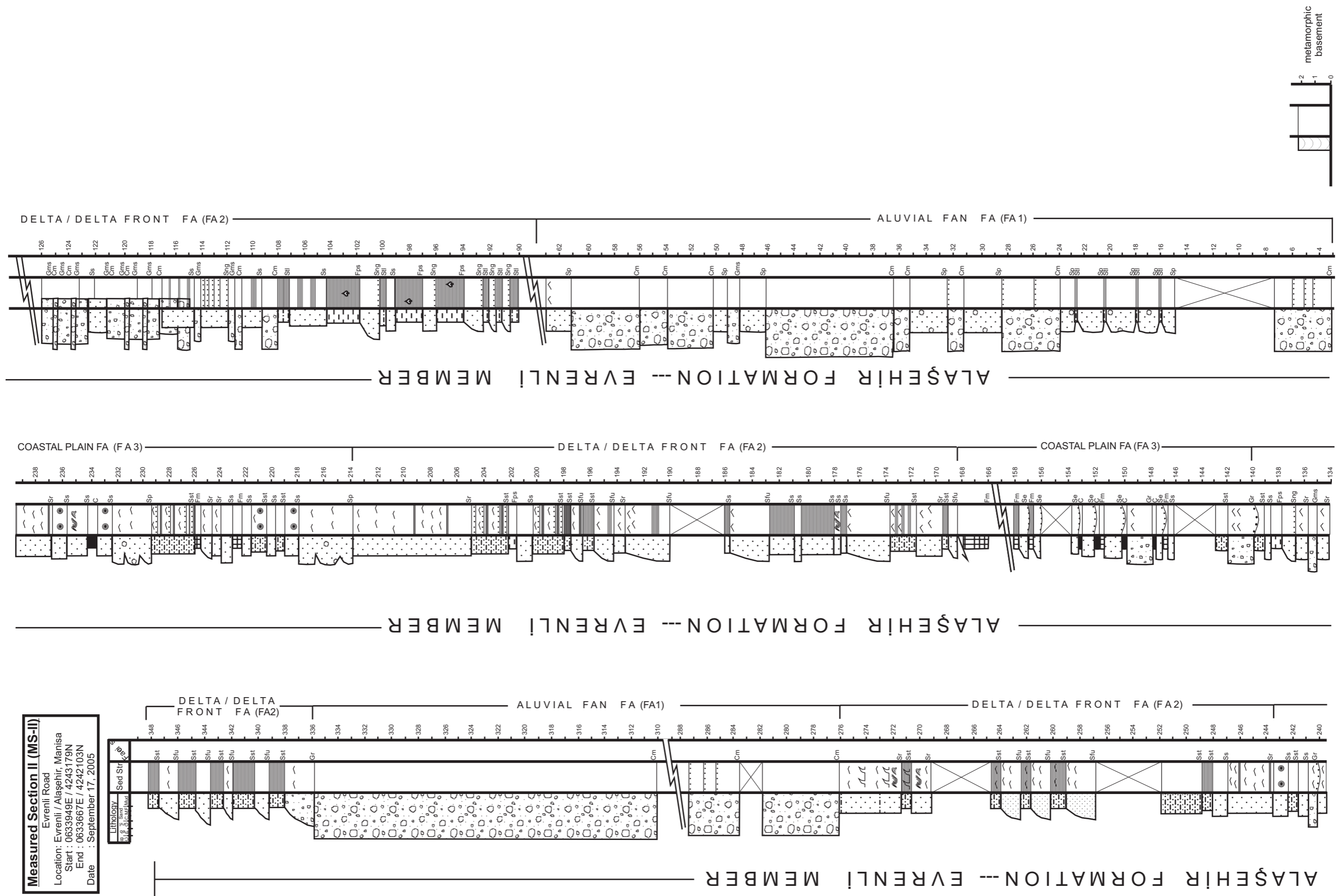
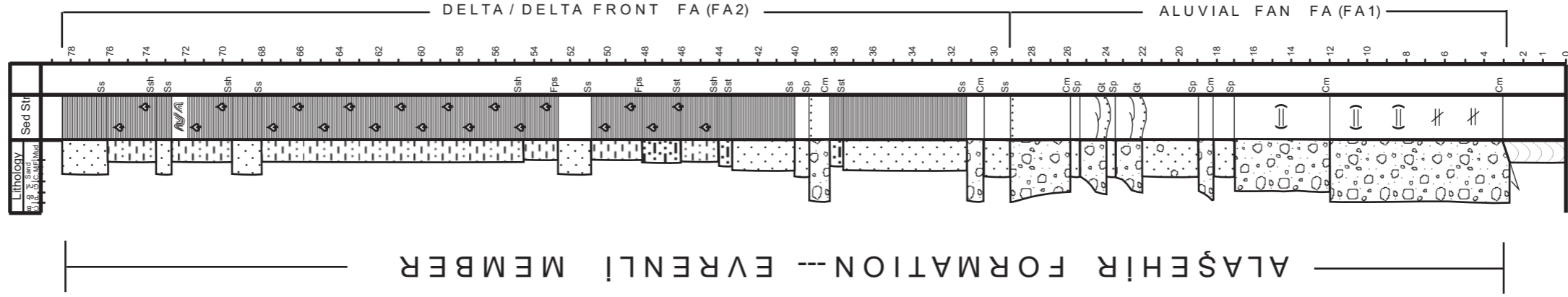
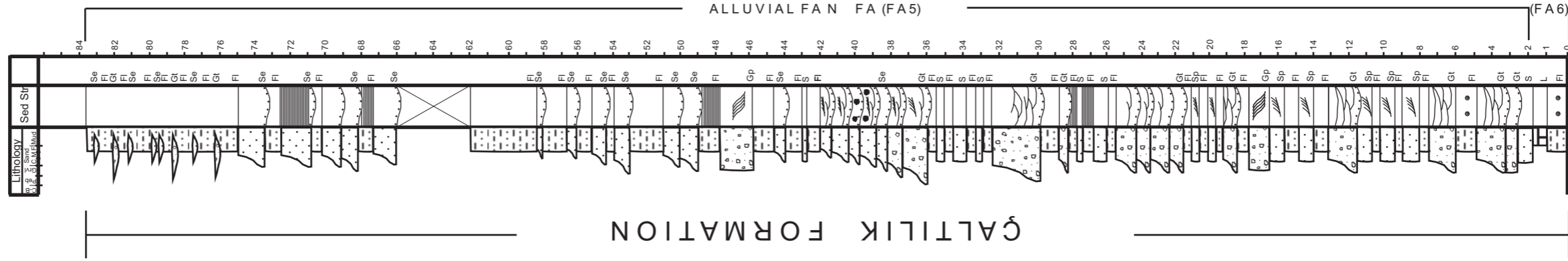


Figure AI.4. Measured stratigraphic section MS-2.

Measured Section III (MS-III)
 Kayadibi Village
 Location: Kayadibi / Alaşehir, Manisa
 Start : 0630893E / 4239272N
 End : 0630704E / 4239132N
 Date : September 9, 2005



Measured Section IV (MS-IV)
 Gökçealan Road
 Location: Gökçealan / Alaşehir, Manisa
 Start : 0620619E / 4247809N
 End : 0620780E / 4247531N
 Date : September 8, 2005



Measured Section V (MS-V)
 Karakirse Soðukyurt Village
 Location: Karakirse / Alaşehir, Manisa
 Start : 0620619E / 4247809N
 End : 0620780E / 4247531N
 Date : September 8, 2005

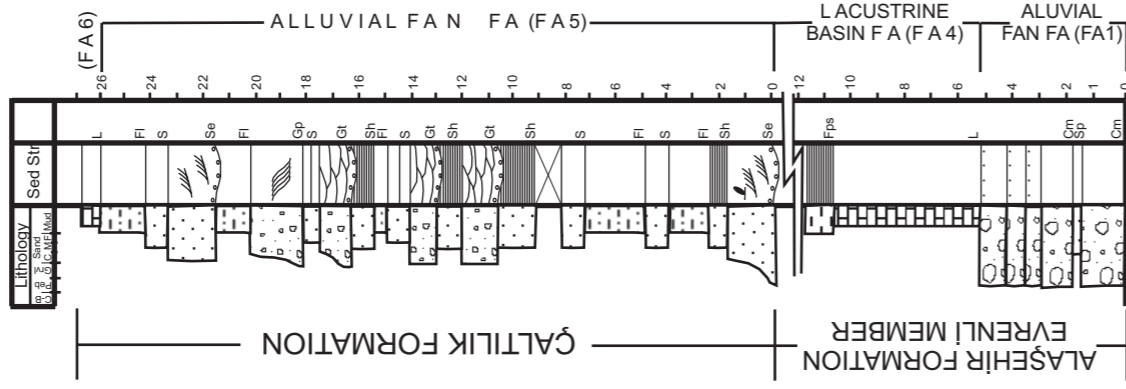
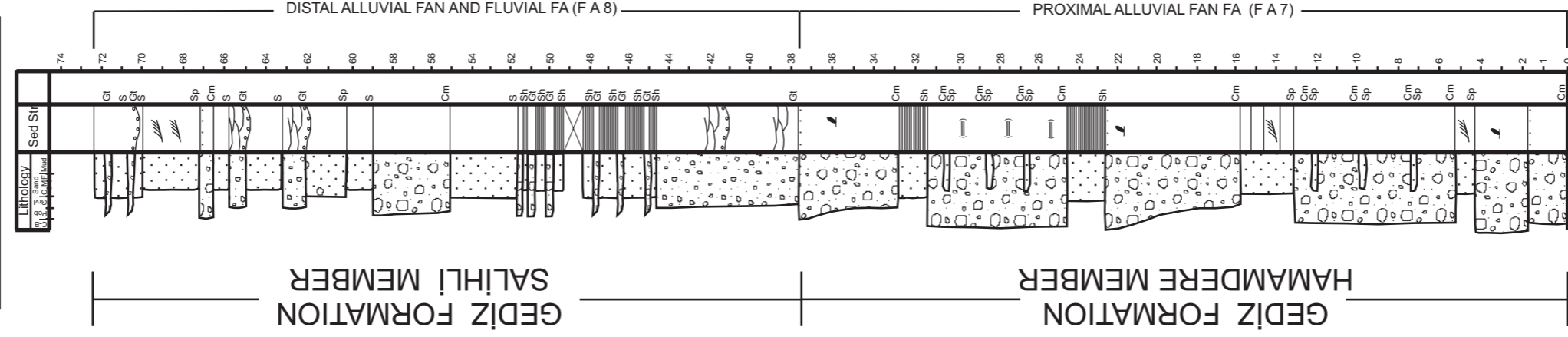
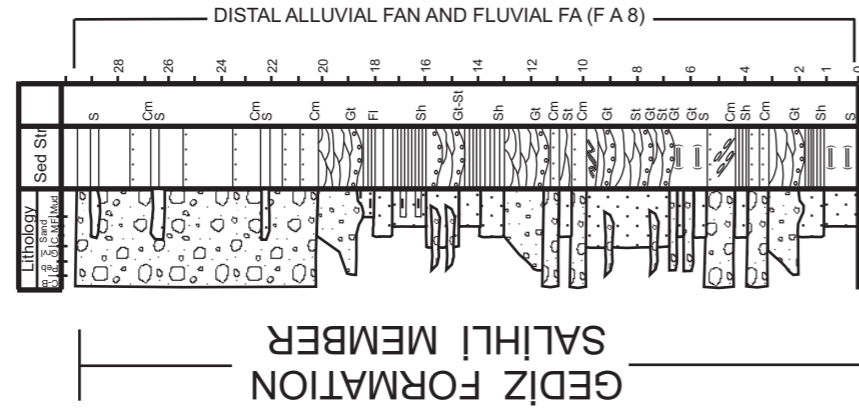


Figure A1.5. Measured stratigraphic sections MS-3, MS-4 and MS-5.

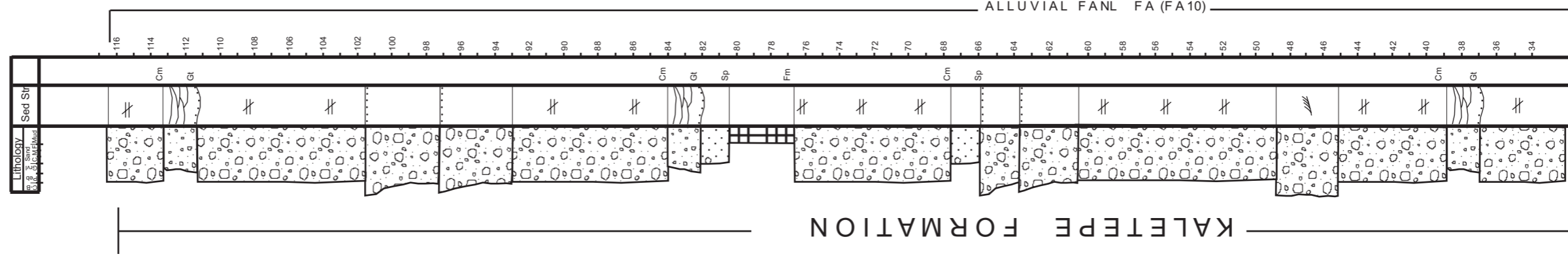
Measured Section VI (MS-VI)
 Boztepe
 Location: Çikrikci / Akcapınar, Manisa
 Start : 0571101E / 4259072N
 End : 0570539E / 4258789N
 Date : September 4, 2005



Measured Section VII (MS-VII)
 Derbent
 Location: Akcapınar, Manisa
 Start : 0569616E / 4259693N
 End : 0569475E / 4260050N
 Date : September 4, 2005



Measured Section VIII (MS-VIII)
 Kozluca Road
 Location: Kozluca / Alaşehir, Manisa
 Start : 0629994E / 4244389N
 End : 0630105E / 4243993N
 Date : September 8, 2005



Measured Section IX (MS-IX)
 Çaltılı
 Location: Sart, Manisa
 0592427E / 4258884N
 Date : September 5, 2005

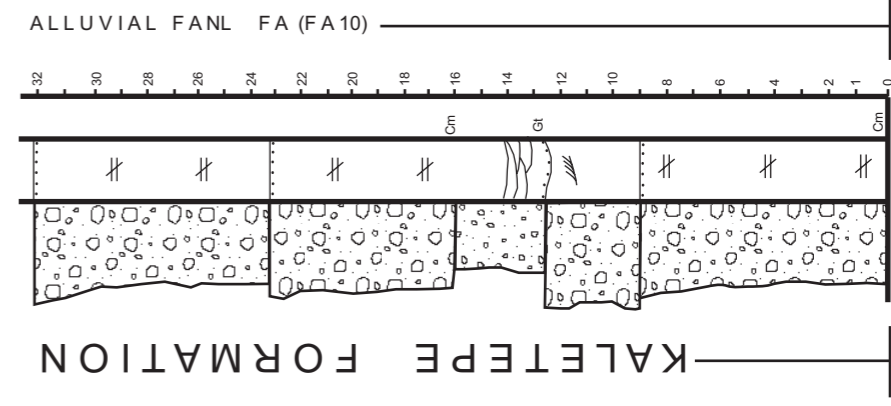
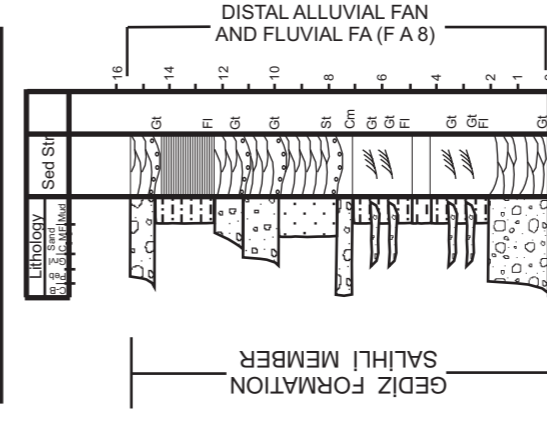


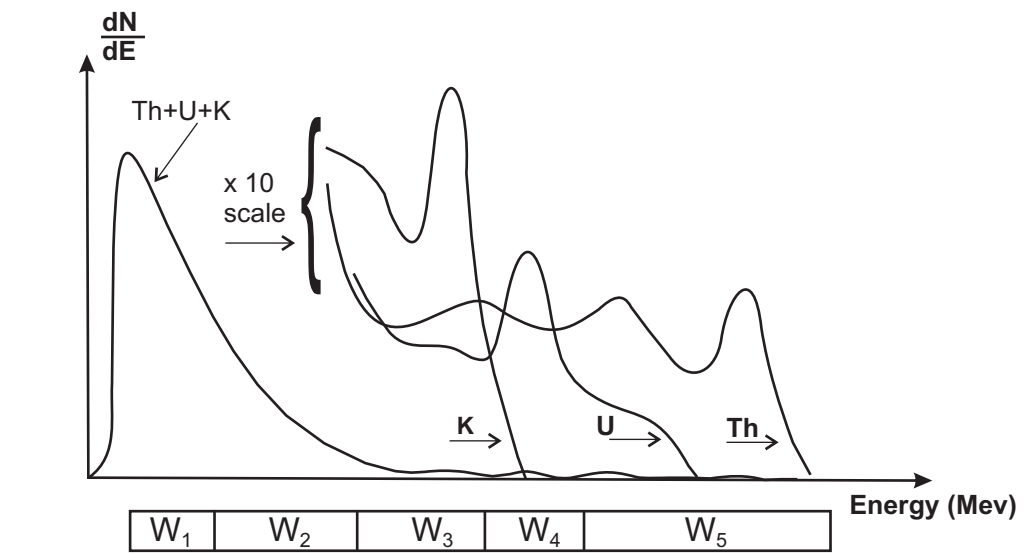
Figure A1.6. Measured stratigraphic sections MS-6, MS-7, MS-8 and MS-9.

APPENDIX II

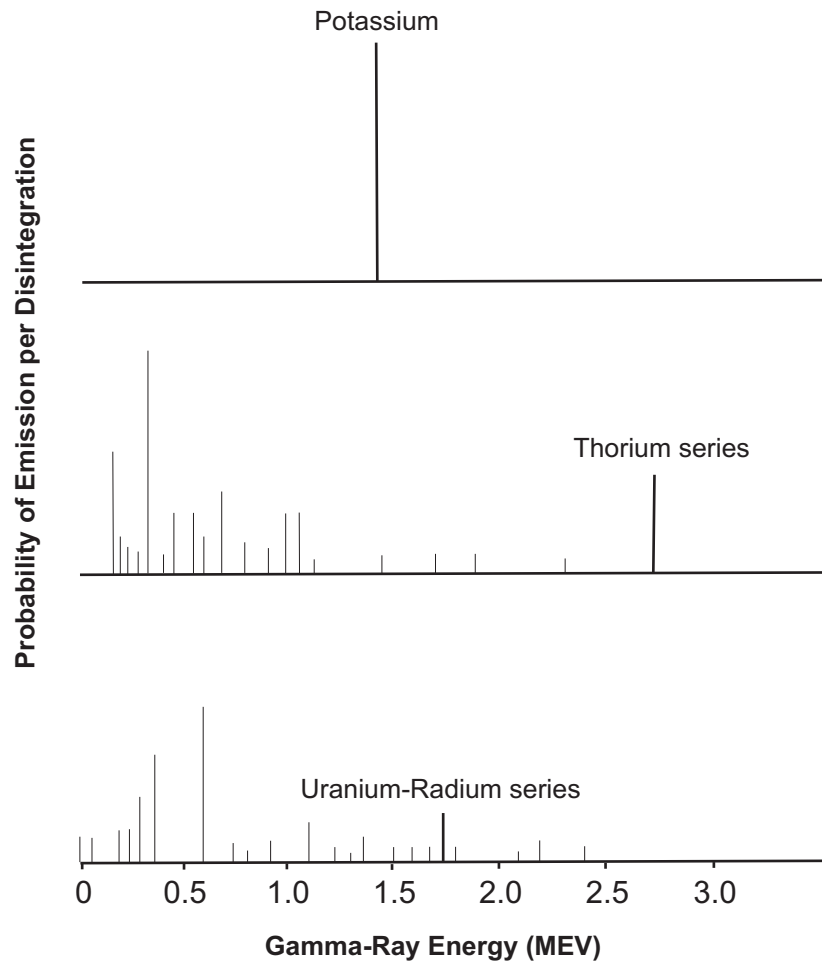
PRINCIPALS OF GAMMA RAY LOGS

The Gamma Ray Log is one of the most useful and versatile surveys available in boreholes. It was introduced commercially in 1939 by Well Surveys Inc. (WSI), and was exclusively acquired by Lane-Wells (eventually Lane-Wells absorbed WSI). Gamma Ray (GR) tool measures the natural gamma ray emission from the subsurface formations penetrated by the wells (Asquith and Gibson, 1982; Asquith and Krygowski, 2004). The natural gamma ray emissions are sourced by three main elements in nature: (i) uranium, (ii) thorium and (iii) potassium. While uranium 235, uranium 238 and thorium 232 decay to stable lead isotopes by a long chain of daughter products, potassium, K40, decays to argon. Each types of decay are characterized by a gamma ray of specific energy level (wavelength) and that the frequency of each energy decay is different (counts per time) (Figure AII.1). So, the tool is based on the count of how many GR has the formation produced in a unit time. Spectral GR tool, which is a variety of GR tools, also counts how many GR has produced from each energy level and allows determination of the type of radioactive source among uranium, thorium and potassium. All these counts are subject to statistical variations. As a result, a relatively quick GR count gives a poor estimate of the actual count rate while a long count yields a more accurate estimate. This makes the logging speed a very critical parameter.

Traditionally, two types of GR detectors have been used in the tool: (i) Geiger-Mueller and (ii) scintillation detectors. Today, almost all the GR tools are equipped with scintillation detectors (Figure AII.2). A scintillation detector contains a sodium-iodide (NaI) scintillation crystal. When a GR strikes to this crystal, a single photon of light is emitted. Then this tiny flash of light strikes a photo cathode made from cesium-antimony or silver magnesium. Each photon, after they hit to photo cathode, releases a spray of electron. These electrons are accelerated in an electric



(A)



(B)

Figure AII.1. Main basis of Gamma Ray tools. (A) Gamma ray spectra. The vertical axis represent number of GRs. (B) The cumulative and individual GR curves of potassium, thorium and uranium responses on a sodium iodide scintillation crystal. Source: Schlumberger.

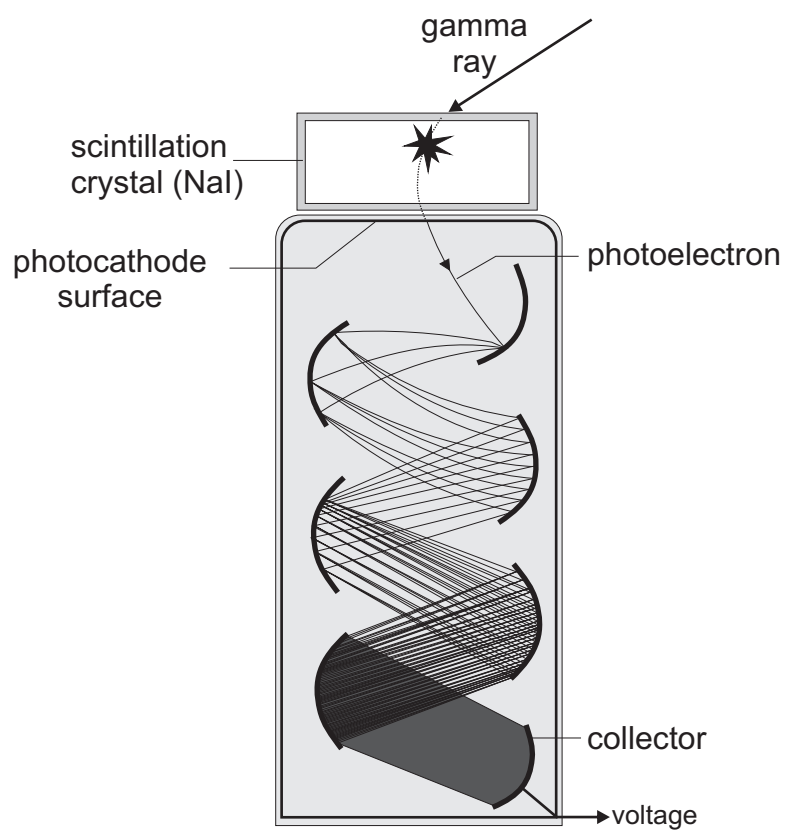


Figure AII.2. Scintillation detector with photomultiplier tube to detect gamma ray emission. Almost all the modern gamma ray tools employs this device to measure natural gamma ray radiation of the geological formations.

field to strike another electrode in order to form bigger shower of electron. This process repeated several times and finally a collector conducts a small current through a measure resistor to give voltage pulse to indicate that a GR struck to the scintillation crystal (Figure AII.2). The system has very short dead time and can recognize many counts per second without becoming swamped by signals. The units of the measurements are in API.

Mud-free sandstones and carbonates have low concentrations of radioactive materials (Table 1). As a result they give low GR readings. As the silt and clay content increases in the formation, GR response increases because of the increased concentration of radioactive materials in silt and clay. However, clean sandstones (mud-free) may also produce high GR response if sandstone contains potassium feldspars, micas, glauconite and uranium-rich ground waters. Spectral GR tool, which identifies the source radioactive material in the formation, can help with the distinction. The main applications of GR logs can be listed as follows:

- Correlation between wells (Figure AII.3)
- Shale volume content
- Identification of evaporates (potassium salts)
- Uranium prospecting
- Net/Gross sand ratios in sand-shale alternations.
- Environment of deposition (Figure AII.4)

Because GRs can pass through steel borehole casings, it can be applied both in open and cased holes. A variety of GR tool is also developed for outcrop readings, which improves surface to surface and surface to subsurface correlations significantly.

Table AII.1. Natural gamma ray measurements of some geological minerals and formations (Hurley and Peters, 1999).

	Type	Composition	GR Deflection (API units)
Minerals	Calcite	CaCO ₃	0
	Dolomite	CaMg(CO ₃) ₂	0
	Quartz	SiO ₂	0
Lithologies	Limestone		5 – 10
	Dolomite		10 – 20
	Sandstone		10 – 30
	Shale		80 – 140
Evaporites	Halite	NaCl	0
	Anhydrite	CaSO ₄	0
	Sylvite	KCl	500
	Polyhalite	K ₂ SO ₄ , MgSO ₄ , 2CaSO ₄ , 2H ₂ O	180

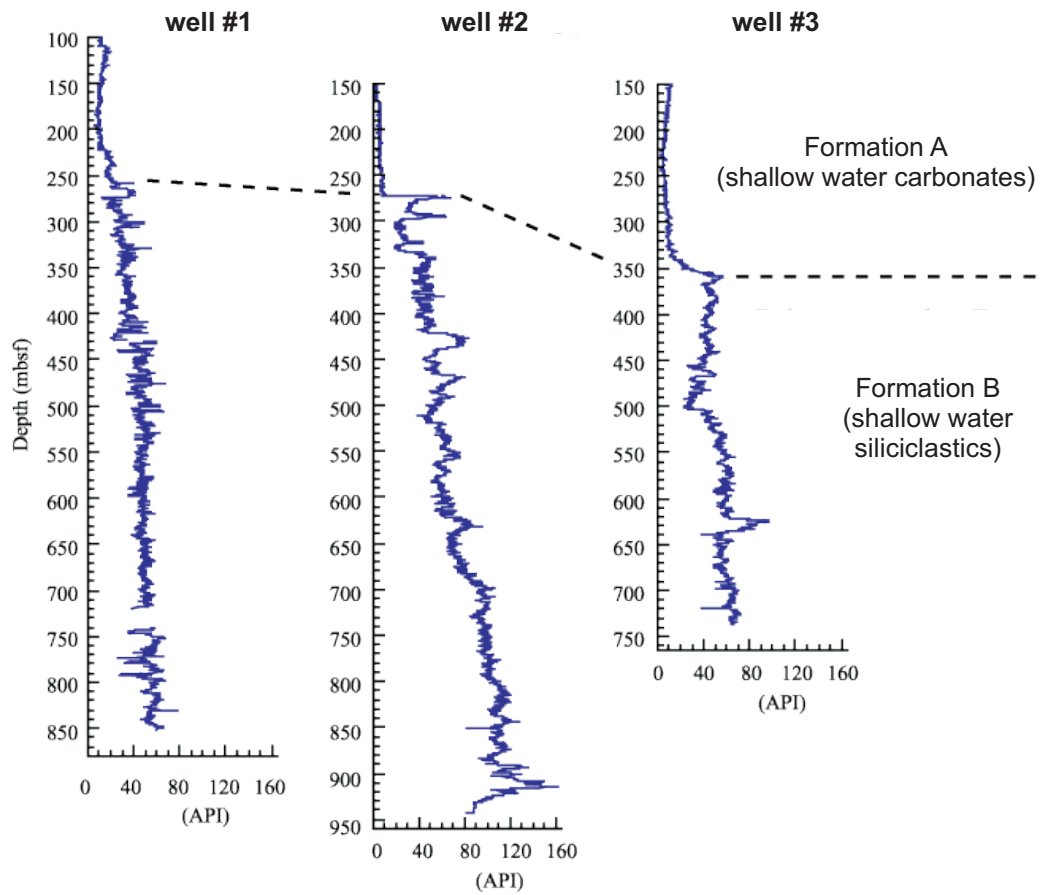


Figure AII.3. An example to use of gamma ray logs in correlation of lithostratigraphic formations.

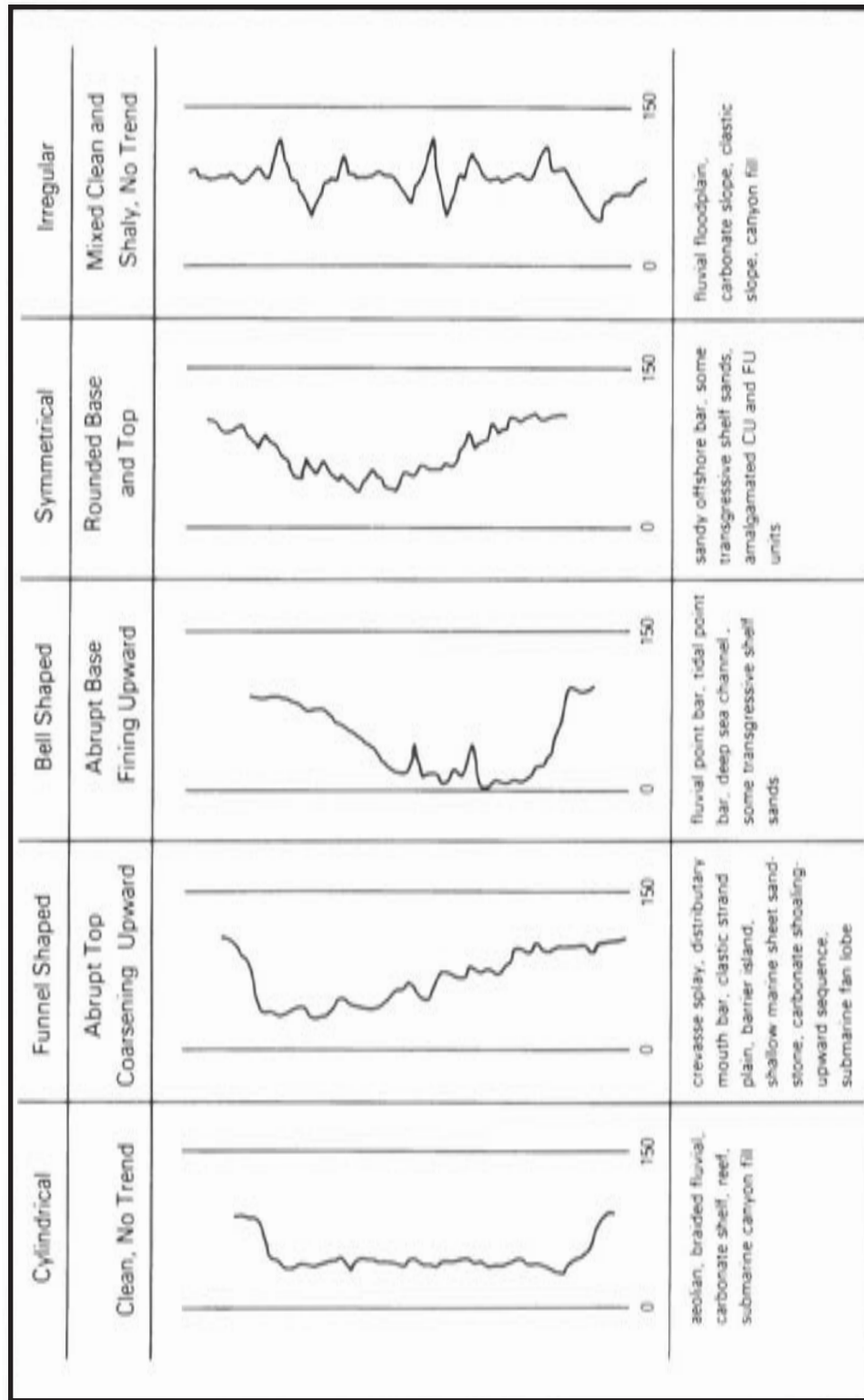


Figure AII.4. The most common GR-log curve shapes which can be utilized for facies analysis and environmental interpretation. The main limitation to facies analysis by this approach is the absence of other supporting data.

APPENDIX III

PALEOSTRESS RECONSTRUCTION

Faults form in response to tectonic stresses predominantly under brittle conditions. Estimation of these tectonic stresses, which is basically defined by three principal stress directions σ_1 , σ_2 and σ_3 , is a common effort for structural geologists to better understand the nature of deformation. It has been recognized for a long time that there is a relation between the orientation of a fault plane and the principal stress axes (Anderson, 1951). Further constraint to orientation of stress axes is provided by fault striations that imply the unit movement vector of hanging wall with respect to footwall block (Wallace, 1951; Bott, 1959). Inverse techniques that utilize orientation of fault planes and associated striations to calculate the orientation of principal stress axes have found widespread applications and known as paleostress inversion or fault-slip analysis.

Numerous methods and improvements were presented to solve the inverse problem. These methods include but not limited to Carey and Brunier (1974), Angelier (1984), Etchecopar *et al.* (1981), Armijo *et al.* (1982), Angelier (1990 and 1994), and Yamaji (2000). Solution of the inverse problem is based on several important assumptions (Ramsey and Lisle, 2000):

- (1) Given that the applied stress is sufficiently high, formation of a new fault or reactivation of a pre-existing plane of weakness takes place. In both cases, it is assumed that the slip occurs in a direction parallel to maximum resolved shear stress on the plane of movement (Wallace-Bott hypothesis Wallace, 1951; Bott, 1959).
- (2) Stress field is assumed to be homogenous within the rock volume influenced by faulting.

- (3) The slip is independent on each fault plane. The movement on one fault has no influence on the slip direction of adjacent faults.

The validity of these assumptions has been a matter of debate by numerous studies. Parallelism of resolved shear stress and fault slip was criticized if the Wallace-Bott hypothesis really holds in nature (Reches, 1987; Marret and Allmendinger, 1990; Pollard *et al.*, 1993). It was pointed out that fault interaction results in deviation (Pollard *et al.*, 1993; Cashman and Ellis, 1994). On the other hand, Twiss and Unruh (1998) proved that Wallace-Bott hypothesis is valid if fault block rotations are negligible and if strain and stress are linearly related. Furthermore, Angelier (1994) emphasized the internal consistency of the results obtained by inverse solutions to support validity of the basic assumptions.

Theoretical Background

The theoretical background of stress inversion methods was revived by Ramsey and Lisle (2000) and Angelier (1994) in great detail. The information given here is predominantly based on these two references.

Consider a plane defined within an orthogonal coordinate axes x , y and z which corresponds to principal stress axes σ_1 , σ_2 and σ_3 , respectively (Figure AIII.1A). The orientation of the plane can be defined by means of three angles (α , β , γ) that the plane's normal vector makes with each principal stress axes. The cosines of these angles are called as the direction cosines of the plane's normal, l , m and n .

$$l = \cos \alpha ; m = \cos \beta ; n = \cos \gamma$$

The orientation of any line in space can be described by its direction cosines and are related by the following equation:

$$l^2 + m^2 + n^2 = 1$$

The stress vector σ acting on the plane has three orthogonal components σ_x , σ_y and σ_z . σ_x act in the x -direction which is parallel σ_1 -direction; σ_y act in the y -direction which is parallel σ_2 -direction; and σ_z act in the z -direction which is parallel σ_3 -

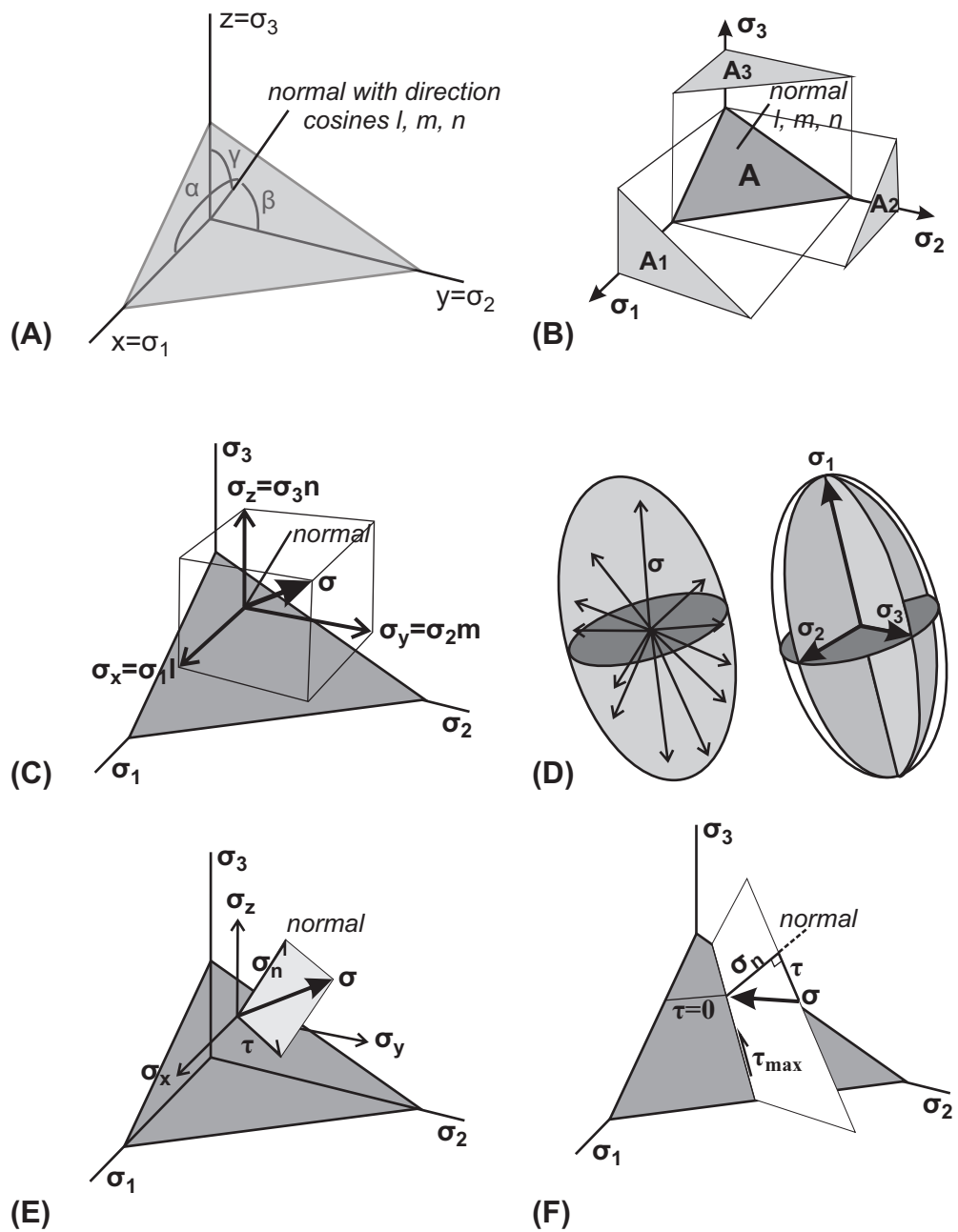


Figure AIII.1. (A) A plane can be defined in a Cartesian coordinate system with its unit vector, which have direction cosines l, m and n . Note that x, y and z axes of Cartesian coordinate system corresponds with principal stress axes. (B) Projected areas A_1, A_2 and A_3 of the plane A . (C) Reduced values σ_x, σ_y and σ_z are based on A_1, A_2 and A_3 . (D) The stress ellipsoid. (E) The shear stress component (τ) and normal stress component (σ_n) of a stress (σ) acting parallel and perpendicular to the plane. (F) The slip on the plane is parallel to the maximum shear stress (τ_{max}). From Ramsey and Lisle (2000).

direction. The magnitudes of σ_x , σ_y and σ_z are equal to reduced magnitudes of σ_1 , σ_2 and σ_3 , respectively which takes into account the projected area of the plane, A_1 , A_2 and A_3 , orthogonal to σ_1 , σ_2 and σ_3 (Figure AIII.1B and C).

$$\sigma_x = \sigma_1 (A_1/A) = \sigma_1 l$$

$$\sigma_y = \sigma_2 (A_2/A) = \sigma_2 m$$

$$\sigma_z = \sigma_3 (A_3/A) = \sigma_3 n$$

By Pythagoras theorem, the magnitude of stress vector σ is equal to;

$$\sigma = (\sigma_x^2 + \sigma_y^2 + \sigma_z^2)^{1/2} = (\sigma_1^2 l^2 + \sigma_2^2 m^2 + \sigma_3^2 n^2)^{1/2}$$

and direction cosines l_σ , m_σ and n_σ of σ are;

$$l_\sigma = \sigma_x/\sigma; m_\sigma = \sigma_y/\sigma; n_\sigma = \sigma_z/\sigma$$

Therefore, any plane of given orientation has an associated stress vector. In the utilized Cartesian coordinate system where x, y and z coincides with σ_1 , σ_2 and σ_3 , the ends of stress vector acting on planes of all potential orientations lie on an ellipsoidal surface, namely the stress ellipsoid (Figure AIII.1D). This ellipsoid can be described by following equation.

$$x^2/\sigma_1^2 + y^2/\sigma_2^2 + z^2/\sigma_3^2 = 1$$

The stress vector acting on each plane can be resolved into two components: (1) The normal stress component in the direction orthogonal to the plane and (2) The shear stress component acting parallel to the plane (Figure AIII.1E). The normal stress component σ_n is equal to cumulative of σ_x , σ_y and σ_z in the direction of planes normal.

$$\sigma_n = \sigma_x l + \sigma_y m + \sigma_z n = \sigma_1 l^2 + \sigma_2 m^2 + \sigma_3 n^2 \quad [1]$$

The magnitude of the shear stress can be found by Pythagoras relation in Figure AIII.1E.

$$\tau^2 = \sigma^2 - \sigma_n^2 = \sigma_1^2 l^2 + \sigma_2^2 m^2 + \sigma_3^2 n^2 - (\sigma_1 l^2 + \sigma_2 m^2 + \sigma_3 n^2)^2$$

This formula simplifies to,

$$\tau^2 = (\sigma_1 - \sigma_2)^2 l^2 m^2 + (\sigma_2 - \sigma_3)^2 m^2 n^2 + (\sigma_3 - \sigma_1)^2 n^2 l^2 \quad [2]$$

This equation clearly illustrates the factors that control the level of shear stress arising on a plane. The differences of the magnitudes of principal stresses are very significant factor controlling the consequential shear stress. It is clearly evident that under hydrostatic state of stress ($\sigma_1 = \sigma_2 = \sigma_3$), no shear stress is produced on the plane. It is also evident that the orientation of the plane defined by direction cosines l , m and n is also influential on shear stress magnitude. If two of the direction cosines are zero, which may occur for any plane orthogonal to principal stress axes, shear stress will be zero again.

As the main agent driving the slip on the fault plane is the shear stress, it become critical to know its direction. This direction is the projection of σ on to the plane (Figure AIII.1F). Lets consider a line on this plane having zero shear stress ($\tau=0$). This line is perpendicular to both the stress vector (σ) and the planes normal. Gasson (1983) show that the direction ratios of a line that is perpendicular to the known lines with direction ratios (l_1, m_1, n_1) and (l_2, m_2, n_2) is equal to:

$$(m_1 n_2 - n_1 m_2, n_1 l_2 - l_1 n_2, l_1 m_2 - m_1 l_2)$$

As the direction ratio of σ is $(\sigma_1 l, \sigma_2 m, \sigma_3 n)$ and the plane's normal is (l, m, n) , the direction ratio of the $\tau = 0$ line would be as follow:

$$(mn(\sigma_2 - \sigma_3), ln(\sigma_3 - \sigma_1), ml(\sigma_1 - \sigma_2))$$

If we introduce the stress shape ration $\phi = (\sigma_2 - \sigma_3)/(\sigma_1 - \sigma_3)$ and divide all with $(\sigma_1 - \sigma_3)$, the direction ratios of the line with zero shear stress become as follows:

$$mn\phi, -nl, lm(1 - \phi)$$

As the direction of maximum shear stress is perpendicular to both the $\tau = 0$ line and the plane's normal its direction ratios can be computed as follows:

$$l(m^2\phi - m^2 - n^2), m(l^2 - l^2\phi - n^2\phi), n(m^2\phi + l^2)$$

This equation can be considered as the main base of the fault slip analysis. It clearly shows that the shear stress direction on a fault plane is related to the orientation of principal stresses described by means of l , m and n and the stress ratio ϕ .

Stress Tensor

The stress ellipsoid in Figure AIII.1D can be described entirely by a stress tensor \vec{T} containing six independent variables:

$$\vec{T} = \begin{bmatrix} a & d & f \\ d & b & e \\ f & e & c \end{bmatrix}$$

In the Cartesian coordinate system defined above, the coordinate axes were selected to coincide with the principal stress axes. Thus, the stress tensor \vec{T} has much simpler form composed of three variables instead of six.

$$\vec{T} = \begin{bmatrix} \sigma_1 & 0 & 0 \\ 0 & \sigma_2 & 0 \\ 0 & 0 & \sigma_3 \end{bmatrix}$$

The eliminated three variables correspond to orientation of the three principal stress axes, σ_1 , σ_2 and σ_3 . In a general rectangular coordinate system defined by x , y and z -axis, three perpendicular unit vectors can define the orientation of these principal stress axes.

$$\begin{bmatrix} x_1 \\ y_1 \\ z_1 \end{bmatrix}, \begin{bmatrix} x_2 \\ y_2 \\ z_2 \end{bmatrix} \text{ and } \begin{bmatrix} x_3 \\ y_3 \\ z_3 \end{bmatrix}$$

The stress tensors defined in general Cartesian coordinate system is related to the tensor defined by coordinate axis that coincide the principal stress axes by the following equation. This equation is simply matricial expression of a tensor rotation.

$$\vec{T} = \begin{bmatrix} a & d & f \\ d & b & e \\ f & e & c \end{bmatrix} = \begin{bmatrix} x_1 & x_2 & x_3 \\ y_1 & y_2 & y_3 \\ z_1 & z_2 & z_3 \end{bmatrix} \bullet \begin{bmatrix} \sigma_1 & 0 & 0 \\ 0 & \sigma_2 & 0 \\ 0 & 0 & \sigma_3 \end{bmatrix} \bullet \begin{bmatrix} x_1 & y_1 & z_1 \\ x_2 & y_2 & z_2 \\ x_3 & y_3 & z_3 \end{bmatrix} \quad [3]$$

As defined in the previous section, the stress vector σ on a plane is characterized by its unit vector \vec{n} . Thus, the x, y and z components of σ on that plane can be found by following matrix equation.

$$\vec{\sigma} = \vec{T} \bullet \vec{n}$$

$$\begin{bmatrix} \sigma_x \\ \sigma_y \\ \sigma_z \end{bmatrix} = \begin{bmatrix} a & d & f \\ d & b & e \\ f & e & c \end{bmatrix} \bullet \begin{bmatrix} x \\ y \\ z \end{bmatrix}$$

The modulus of normal stress σ_n is given by scalar products of stress vector by the unit normal vector.

$$|\sigma_n| = \vec{\sigma} \bullet \vec{n} = x\sigma_x + y\sigma_y + z\sigma_z$$

The normal stress vector is obtained by following equation which is the matrix form of the equation [1].

$$\sigma_n = |\sigma_n| \vec{n}$$

$$\begin{bmatrix} \bar{\sigma}_{nx} \\ \bar{\sigma}_{ny} \\ \bar{\sigma}_{nz} \end{bmatrix} = |\bar{\sigma}_n| \begin{bmatrix} x \\ y \\ z \end{bmatrix}$$

If the stress vector and normal stress vector are known, one can easily derive the shear stress vector $\vec{\tau}$ based on the following relation. This relation is the matrix form of the equation [2].

$$\begin{aligned} \vec{\sigma} &= \bar{\sigma}_n + \vec{\tau} \\ \vec{\tau} &= \vec{\sigma} - \bar{\sigma}_n \\ \begin{bmatrix} \tau_x \\ \tau_y \\ \tau_z \end{bmatrix} &= \begin{bmatrix} \sigma_x \\ \sigma_y \\ \sigma_z \end{bmatrix} - \begin{bmatrix} \bar{\sigma}_{nx} \\ \bar{\sigma}_{ny} \\ \bar{\sigma}_{nz} \end{bmatrix} \end{aligned}$$

Lets go back to stress tensor in the system of principal axes:

$$\vec{T} = \begin{bmatrix} \sigma_1 & 0 & 0 \\ 0 & \sigma_2 & 0 \\ 0 & 0 & \sigma_3 \end{bmatrix}$$

Adding an isotropic stress field defined by $t = -\sigma_3$ and multiplying the tensor by the positive constant $k=1/(\sigma_1-\sigma_3)$ will not change the direction and sense of shear stresses but modifies the tensor into the following form:

$$\begin{bmatrix} 1 & 0 & 0 \\ 0 & \phi & 0 \\ 0 & 0 & 0 \end{bmatrix}$$

The regular stress tensor \vec{T} containing six independent variables in equation [3] cannot be solved in the absence of data to constrain the magnitudes of principal stresses σ_1 , σ_2 and σ_3 . Unfortunately, these data cannot be acquired by mere field observations because nothing is recorded on the rocks in terms of principal stress magnitudes. The fault slip data only refers the orientation and direction of shear

stresses, which is related to orientation, and direction of principal stresses. As a result, the complete stress tensor in equation [3] is modified into the reduced stress tensor (\vec{T}^*), which is defined as:

$$\vec{T}^* = \begin{bmatrix} x_1 & x_2 & x_3 \\ y_1 & y_2 & y_3 \\ z_1 & z_2 & z_3 \end{bmatrix} \bullet \begin{bmatrix} 1 & 0 & 0 \\ 0 & \phi & 0 \\ 0 & 0 & 0 \end{bmatrix} \bullet \begin{bmatrix} x_1 & y_1 & z_1 \\ x_2 & y_2 & z_2 \\ x_3 & y_3 & z_3 \end{bmatrix} \quad [4]$$

This reduced stress tensor, which depends on the orientation of principal stress axes and the stress shape ratio ϕ , contains only four independent variables and can be solved based on the fault slip data acquired by field observations.

Angelier's Method of Slip Inversion

If the stress tensor and fault orientation is known in an area, one can easily compute the orientation of the resolved shear stress on a fault plane of known attitude. Representing the direct solution, the computed shear stress on the fault plane is parallel to the fault slip according to the Wallace-Bott hypothesis. Nevertheless, we are not able to make observations regarding to the stress tensor, but we can only observe attitude of a fault plane and the orientation of a fault striations in the field. As a result we need an inverse solution to determine the reduced stress tensor which includes only the orientation of principal stress axes and the ration of ϕ .

One of the most frequently used slip inversion methodology has been presented by Angelier (1990; 1994) and utilized in this study. As most of the proposed inverse solutions, Angelier's method adopts a least square criterion as well. Thus, the minimization function S can be written as follows;

$$Sm = \sum_{k=1}^{k=K} w_k (F_{mk})^2 \quad [5]$$

where w_k represent the weight of the datum number k and F_k is a function, which express the deviation of this datum. $F_k = 0$ indicates a perfect fit between the datum and the average stress tensor and increasing F_k indicates an increasing misfit.

Different misfit criteria F_m were adopted based predominantly on the relations between the actual unit slip vector, \vec{s} , and the computed shear stress, $\vec{\tau}$.

$$F_1 = (\vec{s}, \vec{\tau})$$

$$F_2 = \sin\left(\frac{(\vec{s}, \vec{\tau})}{2}\right)$$

$$F_3 = \tan(\vec{s}, \vec{\tau}) \text{ for an angle } < 45^\circ$$

$$F_3 = 1 \text{ for an angle } > 45^\circ$$

$$F_4 = |\lambda \vec{s} \bullet \vec{\tau}|^2, \text{ where } \lambda \text{ is related to the value of largest possible shear stress.}$$

The earlier methods of solving the inverse problem are based on the search approach, which uses different values of four variables in reduced stress tensor [4]. In this procedure, computation continues with smaller and smaller numerical intervals until a satisfactory solution is obtained (Carey and Brunier, 1974). A quite different method of solution was proposed by Angelier and Gougel (1979) and Angelier (1990). This method consists of setting the partial derivatives of sum Sm to zero [5]. Thus, extreme limits of Sm , particularly the minimum value, can be computed by analytical means. This technique allows faster computation of the inverse solution in contrast to iterative search-based techniques, which requires much longer computing.

Two parameters were defined as the quality estimators of the inverse solution. They are called as RUP, which varies from 0 to 200%, and ANG, which varies from 0° to 180° (Angelier, 1994) (Figure AIII.2B and C). The ANG is simply based on the misfit angle between the actual slip vector measured on the fault plane and computed resolved shear stress (Figure AIII.2A and B). The RUP, on the other hand, depends both on the misfit angle and the relative shear stress magnitude (Figure AIII.2B). These two parameters are useful not only to check the validity of inverse solution but also to investigate the heterogeneities in data sets. These heterogeneities could be related to multiple stress regimes that have influenced area.

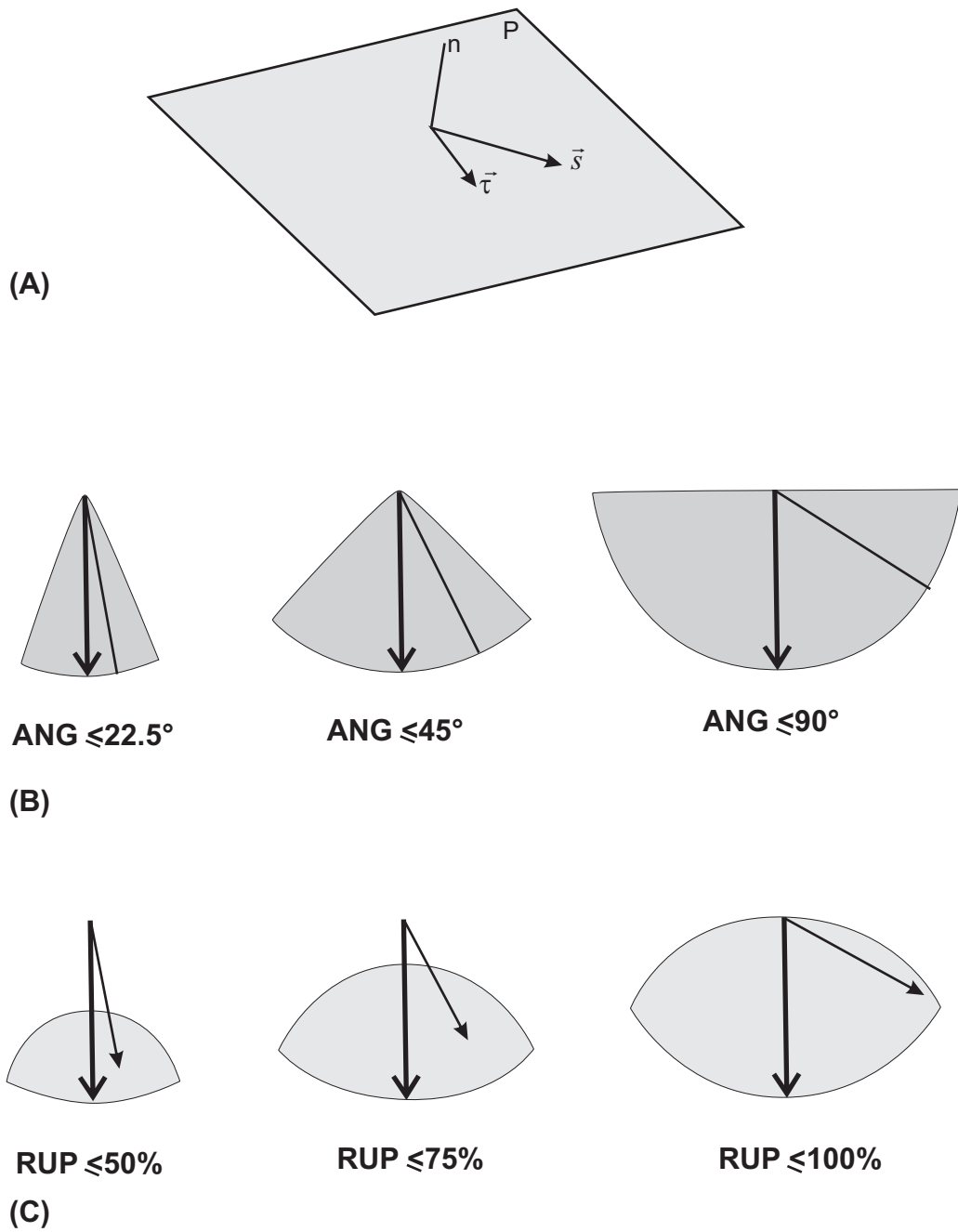


Figure AIII.2. (A) Different misfit criteria F_m were predominantly based on the relations between the actual unit slip vector, s , and the computed shear stress (τ). The parameters ANG (B) and RUP (C) are defined as quality estimators and influenced by the angular relations between s and τ . From Angelier (1994).

Multiple Inverse Method

Multiple inverse method (MIM) is a numerical technique to separate stresses from heterogeneous data set (Yamaji *et al.*, 2005; Yamaji, 2000). The method is based on the generalized Hough transform of stress inversion (Ballard, 1981).

A point in four-dimensional parameters space represents the stress determined by inversion methodology. The four-dimensional parameter space includes principal stress orientations represented by three Euler angles and the stress ratio of ϕ . The MIM employs computational grid distributed within this parameter space. The method first makes k-element subset from N faults. The number of subsets is ${}_N C_k$. Then, the classical inversion method defined above is applied to all subsets. This will compute a great number of optimal stresses each of which are represented by a point in the parameter space. Clusters of these points are consequently point out the significant stresses (Yamaji *et al.*, 2005; Yamaji, 2000).

A Stress Inversion Method Based only on Fault Slip Sense

Stress inversion procedure provides good estimates of reduced stress tensor [4] given that the slip vectors can be estimated based on slickenside lineations. In many instances, however, faults may lack striations or it might be difficult or impossible to collect such data from the observed or interpreted (by subsurface methods) fault planes. In these cases, fault plane attitude can easily be identified but associated slip vector indicators could be absent. Yet, the displacement of bedding or any other key markers may help to judge the sense of movement.

The standard methods of inversion cannot deal with data having this kind of missing information. A method proposed by Lisle *et al.* (2001), solves the inverse problem using the attitude of the fault plane and sense of fault's dip slip component (Figure AIII.3A). In general, the relation between sense of separation and slip is not a simple one. In unfolded sedimentary layers, however, separation and slip are related if: (i) offset beds are horizontal (Figure AIII.3A), (ii) the fault and the dipping beds have the same strike.

The theoretical information given below is from the Lisle *et al.* (2001). According to this study, the geometrical relationship among the slip and the fault's unit normal vector can be displayed by representation quadric (Lisle, 1989). This

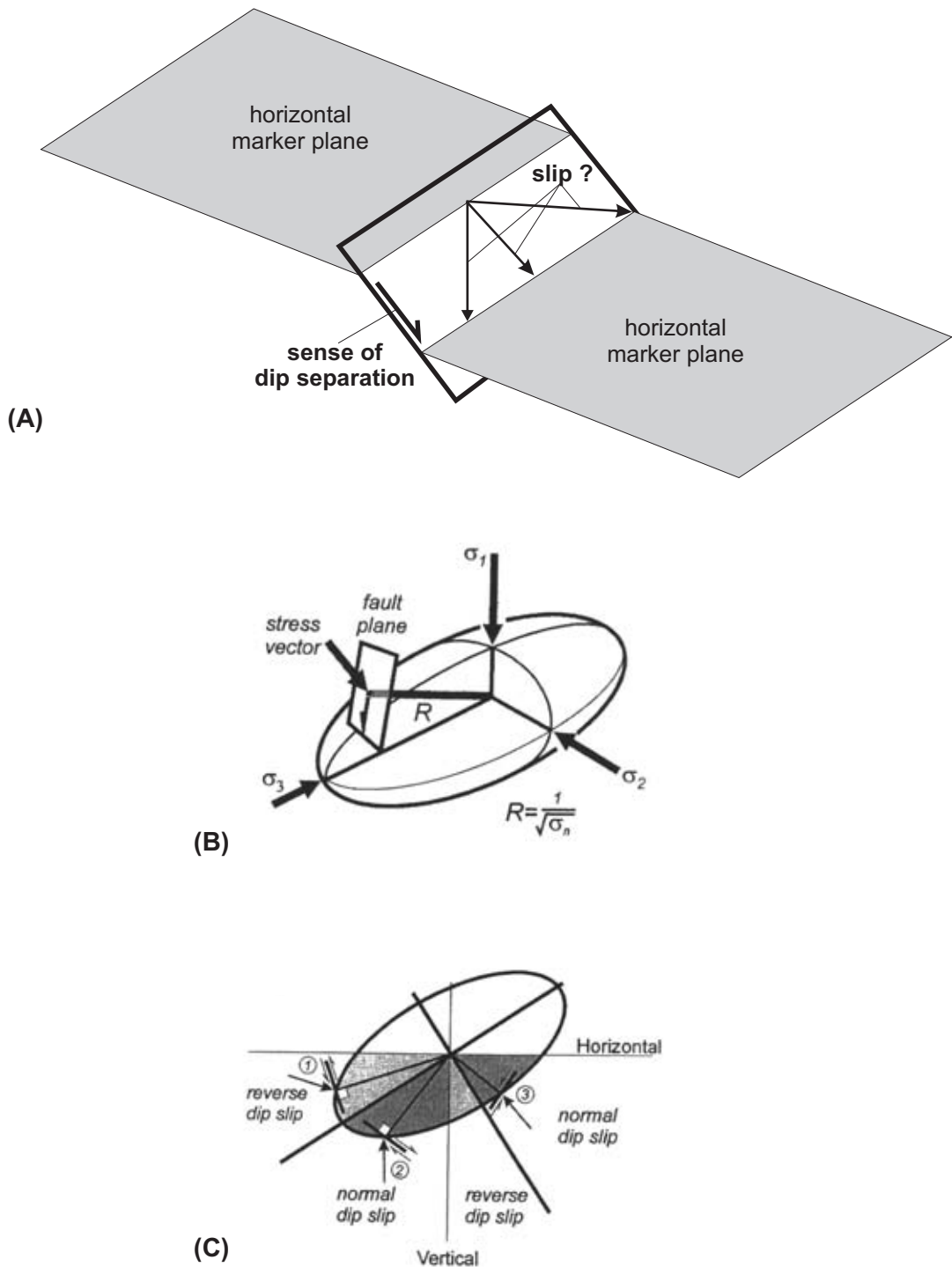


Figure AIII.3. (A) The dip separation, which is the offset of key marker in a fault's down dip direction. Although the actual slip vector can not be determined from the dip separation, the sense of dip slip component can be determined. (B) The stress quadric represents the relationship between the orientation of a fault plane and the stress vector acting on the plane. The magnitude of normal stress acting on the fault plane is related to the length of radius by $\sigma_n = 1/R^2$. (C) The determination of dip slip sense of faults. The diagram depicts the vertical cross-section through the stress quadric. From Lisle *et al.* (2001).

quadric surface, which is not to be confused with stress ellipsoid, is described by the following equation:

$$\sigma_1 x^2 + \sigma_2 y^2 + \sigma_3 z^2 = \pm 1$$

This surface is ellipsoid only if the all principal stress values have the same sign. As we are dealing with shear stress, which is unaffected by the hydrostatic component of the stress tensor, adding an arbitrary constant to each principal stress can form the ellipsoid surface of the quadric. The principal axes of the quadric are parallel to the principal stress axes. Their lengths are equal to:

$$1/\sqrt{\sigma_3} \geq 1/\sqrt{\sigma_2} \geq 1/\sqrt{\sigma_1}$$

The radius R of the quadric is given by (Figure AIII.3B):

$$R = 1/\sqrt{\sigma_n} \quad [6]$$

where σ_n (equation [1]) is the magnitude of normal stress acting on a plane whose normal is parallel to that radius. This geometrical relation is useful to portray the angular relationship between the normal of a plane (\vec{n}) and the direction of associated stress vector $\vec{\sigma}$. To find the direction of $\vec{\sigma}$ corresponding to given direction of \vec{n} , a radius to the ellipsoid is drawn parallel to \vec{n} . A normal to the ellipsoid surface, which is drawn at the point where this radius meets with the surface of the ellipsoid, is parallel to the direction of $\vec{\sigma}$.

Figure AIII.3C illustrates a cross-section of the stress quadric for a particular stress tensor. The radii of ellipse correspond to normal vectors of a family of planes having a strike perpendicular to cross-section plane. This radius-normal property allows the stress vector to be determined for any plane in this family. In 3-D space, the stress vectors associated with this family of planes are commonly not included within the vertical section plane. Their projections shown in Figure AIII.3C are sufficient to determine the sense of dip slip component of $\vec{\sigma}$.

Sense of dip slip is related to the rate of change of R with respect to dip angle of the fault (δ) (Figure AIII.4A). For normal faults:

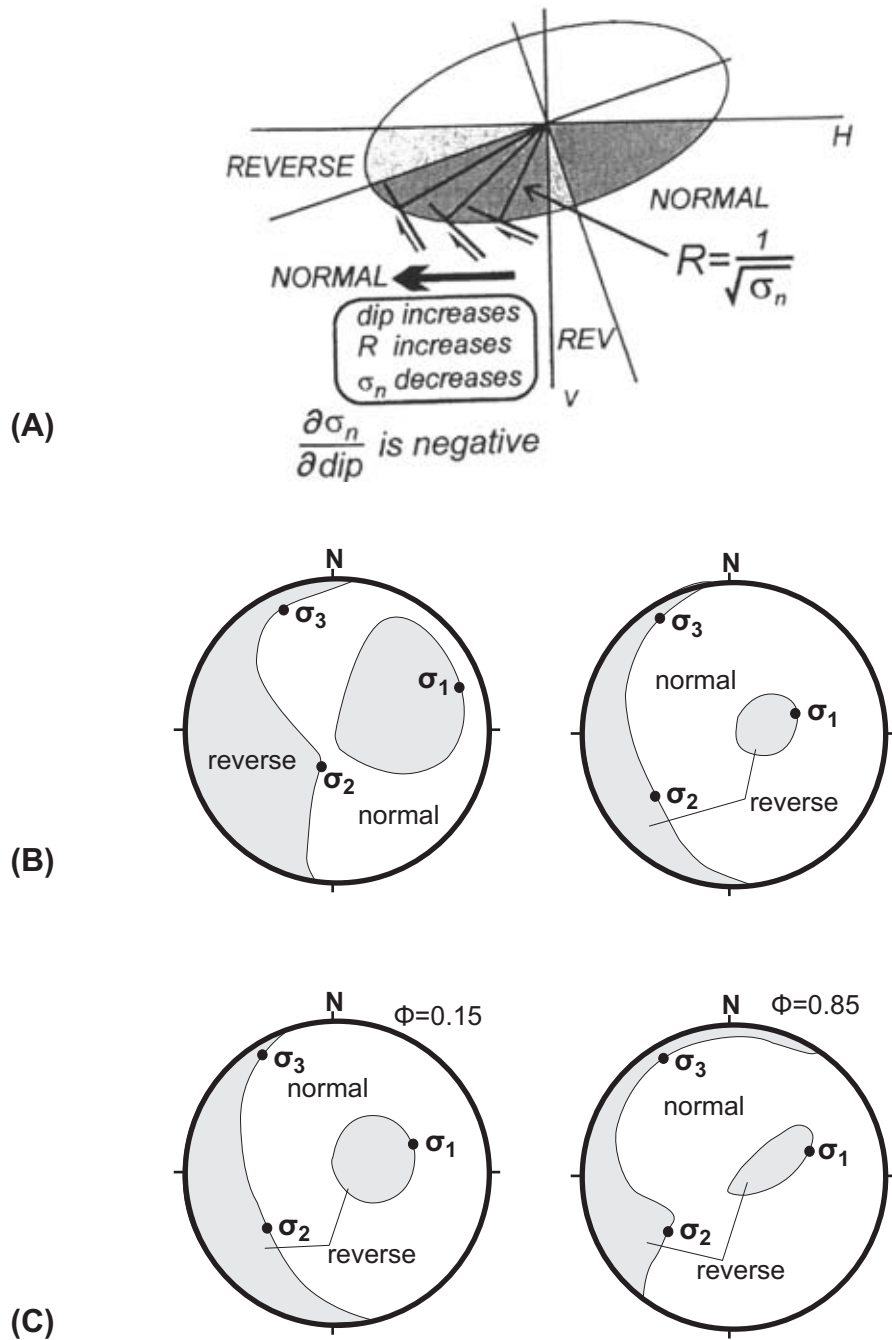


Figure AIII.4. (A) Determination of sense of normal stress variation with dip of the fault plane. Normal faults are characterized by decrease in normal stress with increase in dip. Opposite is true for reverse faults. (B) and (C) depicts the slip sense curves (SSCs) in relation to the stress tensor. SSCs form the boundaries of fault plane poles of normal and reverse faults. Both the principal stress orientations (B) and the stress ratio Φ (C) influences the distribution of SSCs. From Lisle *et al.* (2001).

$$\frac{\partial R}{\partial \delta} > 0 \quad \text{and therefore according to [6]} \quad \frac{\partial \sigma_n}{\partial \delta} < 0 \quad [7].$$

Similarly for the reverse faults:

$$\frac{\partial \sigma_n}{\partial \delta} > 0 [8]$$

Given that the stress tensor and the fault plane attitude are known, computation of slip sense can be done by numerical evaluation of derivative $\frac{\partial \sigma_n}{\partial \delta}$.

First, the normal stress magnitude σ_n is calculated on the fault plane based on the equation [1]. Next, the normal stress is also determined for a plane that has slightly steeper angle of dip than the fault plane. If this second plane has lower normal stress than the fault plane, the slip sense of the fault plane is determined as normal according to equation [7]. In contrast, if the steeper plane has higher normal stress than the fault plane, the slip sense of the fault is determined as reverse according to [8]. For two faults that have the same strike and are perpendicular to each other, the sense of dip slip will be same.

Based on the theory of normal solution given above, boundary curves between the normal and reverse faults can be computed for a given stress tensor (Figure AIII.4B). These boundary curves are named as slip-sense curves, SSCs (Lisle *et al.*, 2001). Indeed, these curves define the boundaries between the opposing dip senses. In the inverse solution, the attempt is to establish the stress tensor from the geometry of SSCs, as first realized by Davidson and Park (1978). The method of Lisle *et al.* (2001) relies on systematic computer-based search for the stress tensors compatible with the observed faults and the senses they exhibit. For any trial tensor, the sense of dip-slip can be predicted for each measured faults based on the theory given above. The method compares normal stresses on the actual fault data and on the imaginary fault data that have slightly greater dip. The goodness of fit is expressed based on the match of the trial stress tensor to the fault sense data. In order to find the best-fit tensor, a large number of (thousands) trial tensors are employed with varying principal stress orientations and the ratio of ϕ . It is a time consuming process requiring long computation times. A program called DIPSLIP.BAS (Orife *et al.*, 2002) is dedicated for this computation.

CURRICULUM VITAE

PERSONEL INFORMATION

Surname, Name : Çiftçi, Bozkurt N.
Nationality : Turkish (TC)
Date and Place of Birth : 5. March. 1973, Bolu
Address : TPAO Genel Müdürlüğü
Mustafa Kemal Mah 2.Cad No:86
06520, Söğütözü, Ankara / TURKEY
Phone :+90 312 207 2185
+90 533 621 3313
Fax :+90 312 286 9049
e-mail : bciftci@tpao.gov.tr

EDUCATION

<u>Degree</u>	<u>Institution</u>	<u>Year of Graduation</u>
M.Sc. in Geology	Colorado School of Mines, Golden, CO, USA	2001
B.Sc. in Geological Eng.	Middle East Technical University, Ankara, Turkey	1996

WORK EXPERIENCE

<u>Year</u>	<u>Place</u>	<u>Enrollment</u>
2001-Present	Türkiye Petrolleri AO, Ankara / Turkey	Project Geologist
Jan-April 2006	Harvard University, Cambridge, MA / USA	Visiting Scholar
Jan-Feb 2001	Gas Research Institute, Houston, TX / USA	Consultant
1996-1999	Dardanel Madencilik A.Ş., Ankara / Turkey	Field Geologist

PROFFESIONAL INTERESTS

Structural geology, 3-D geological modeling, geological field studies, petroleum system analysis, clastic sedimentology, GPS-DGPS applications.

AFFILIATIONS

Turkish Association of Petroleum Geologists
American Association of Petroleum Geologists
Chamber of Geological Engineers – Turkey
METU Alumni Society

PUBLICATIONS

- Ciftci, B.N., and Bozkurt, E., 2007, Anomalous stress field and active breaching at relay ramps: A field example from Gediz graben, SW Turkey: Geological Magazine, in press.
- Ciftci, B.N., Temel, R.O., and Terzioğlu, N., 2005, Neogene stratigraphy and hydrocarbon system of the region surrounding the gulf of Edremit, NW Anatolia, Turkey: Turkish Association of Petroleum Geologists Bulletin, v. 16, p. 81-104.
- Ciftci, B.N., Aviantara, A.A., Hurley, N.F., Kerr, D.R., 2004, Outcrop-based three-dimensional modeling of the Tensleep Sandstone at Alkali Creek, Bighorn Basin, Wyoming: in Grammer, G. M., Harris P. M., Eberli, G. P. eds., Integration of Outcrop and Modern Analogs in Reservoir Modeling: American Association of Petroleum Geologists Memoir 80, p. 235-259.
- Temel, O.R., and Ciftci, B.N., 2002, Stratigraphy and depositional environments of Tertiary sediments in Gelibolu Peninsula and Islands of Gökçeada and Bozcaada (Northern Aegean Region, Turkey): Turkish Association of Petroleum Geologists Bulletin, v. 14, p. 17-42.